# Biomaterial Modulation for Diagnostic and Therapeutic Benefit in Catheter-Associated Urinary Tract Infection

A thesis submitted to Cardiff University for the degree of Doctor of Philosophy

2021

Katrina Duggan

School of Dentistry

Ysgoloriaethau Sgiliau Economi Gwybodaeth
Knowledge Economy Skills Scholarships

UNDEB EWROPEAIDD
EUROPEAN UNION

Llywodraeth Cymru
Welsh Government

**Cronfa Gymdeithasol Ewrop**
**European Social Fund**

*Knowledge Economy Skills Scholarships (KESS 2) is a pan-Wales higher level skills initiative led by Bangor University on behalf of the HE sector in Wales. It is part funded by the Welsh Government's European Social Fund (ESF) convergence programme for West Wales and the Valleys.*

# Acknowledgments

Many people have helped me throughout my PhD journey and made it an enjoyable experience but my greatest thanks go to Prof. David Williams for the endless support and encouragement, truly the greatest supervisor!

I am also incredibly grateful to KESS and Prof. Mark Waters, Technovent Ltd, for funding the project and to Mark for all of his help with the silicone work. My time spent at Technovent was always enjoyable and I was always made to feel so welcome by Izzy, Ioan, Jo & James. Thanks for all the help and the endless mugs of tea and coffee.

The 3D printing work would not have been possible without the generous help of Prof. Trevor Coward and Erinc Erkel at Kings College, London who worked tirelessly until the formulation had been perfected.

I'm also grateful to my supervisors in the School of Chemistry, Prof. Ian Fallis and his student Sion Edwards for designing and producing the novel antimicrobial and sensor compounds, and Dr Alison Paul for the help with the HPLC work.

Thanks also go to by Dr Chiara Morozzi, Dr Michaela Serpi and Dr Fabrizio Pertusati from the School of Pharmacy for producing the antimicrobial compound 1771 and helping with the antimicrobial assessments.

The support of the departments 'Tech team' was also greatly appreciated: Wendy Rowe for the SEM work, Fiona Gagg for sending countless parcel of silicone to London and Alan Lloyd-Jones for dealing with the endless stream of artificial urine waste.

The entire PhD experienced was greatly enhanced by sharing an office with such a great group of friends. Thanks to Emma, Megan, Jordanna, Elen, Richard and Dan for all of the fun times and starting 'Caterpillar Cake Club'.

Thanks to my mum, dad, mother & father-in-law for being so supportive. Thanks also to Jo, Colin & Kelly for helping with childcare and school pick-ups over the years.

Lastly thanks to my husband Jaime and children Holly and Tom for the encouragement and support. I know you're all proud

# Table of Contents

Acknowledgements.....iii
List of Figures.....xii
List of Tables.....xxi
Abbreviations.....xxiv
Summary.....xxvii
Chapter 1 – Introduction and Literature Review.....1
1.1 Healthcare acquired infections.....2
1.2 Microbial biofilms.....3
1.2.1 Biofilm structure and composition.....4
1.2.2 Biofilm Formation.....6
1.2.2.1 Adherence of planktonic bacteria to surfaces.....6
1.2.2.2 Biofilm maturation.....8
1.2.2.3 Detachment of the biofilm cells.....9
1.2.3 Quorum sensing.....9
1.2.4 Antimicrobial resistance.....11
1.3 Catheter-associated urinary tract infections (CAUTIs).....13
1.3.1 The urinary catheter.....13
1.3.2 Epidemiology.....16
1.3.3 Mechanisms of bladder contamination in the catheterised patient.....16
1.3.4 Symptomatic features of CAUTIs.....17
1.3.5 CAUTI diagnosis.....18
1.3.6 Microorganisms commonly associated with CAUTIs.....19
1.3.6.1 Urease producing microorganisms.....20
1.4 Biofilm prevention and eradication.....24
1.4.1 Antimicrobial urinary catheters.....24
1.4.1.1 Surface coatings to prevent microbial attachment.....26
1.4.1.1.1Hydrogels.....26
1.4.1.1.2 Polytetrafluoroethylene (PTFE).....27
1.4.1.1.3 Polyzwitterions.....27
1.4.1.1.4 Polyethylene glycol (PEG).....29
1.4.1.1.5 Enzymes.....29
1.4.1.2 Biocidal coatings.....30

1.4.1.2.1 Silver coated silicone.....30
1.4.1.2.2 Antibiotic coatings.....31
1.4.1.2.3 Other antimicrobial agents.....32
1.4.1.2.4 Natural compounds.....33
1.4.1.3 Modifications to surface topography.....34
1.5 Detection of catheter-associated urinary tract infections.....35
1.5.1 Bromothymol blue-based detection systems.....35
1.5.2 pH responsive catheter coatings as detection systems.....37
1.6 Summary.....39
1.7 Project aims and objectives.....40
Chapter 2 – *In-Vitro* Assessment of Antimicrobial Compounds.....41
2.1 Introduction.....42
2.1.1 Triclosan and triclosan derivatives.....43
2.1.2 Silver NHC complexes and imidazolium salts.....45
2.1.3 Poly-L-lysine.....48
2.1.4 Bioflavonoids.....48
2.1.5 Caprylic acid..... 49
2.1.6 Compound 1771.....49
2.1.7 Aims.....52
2.2 Materials & Methods.....53
2.2.1 Microbiological culture media.....53
2.2.2 Microorganisms.....53
2.2.3 Preparation of test antimicrobial compounds.....55
2.2.4 Determination of minimum inhibitory concentrations (MICs).....58
2.2.5 Determination of minimum biocidal concentrations.....59
2.2.6 Minimum biofilm eradication concentration.....59
2.2.7 Quantification of virulence gene expression following antimicrobial treatment.....59
2.2.7.1 RNA extraction.....60
2.2.7.2 Reverse transcription of RNA to cDNA.....61
2.2.7.3 Primer preparation.....61
2.3.7.4 Quantitative polymerase chain reaction.....65
2.3.7.5 Statistical analysis.....65
2.3 Results.....66

2.3.1 Minimum inhibitory concentrations.....66
2.3.2 Minimum biocidal concentrations.....69
2.3.3 Quantification of selected *Escherichia coli* virulence gene expression.....72
2.3.4 Quantification of *Staphylococcus aureus* virulence gene expression.....72
2.3.5 Quantification of *Candida albicans* virulence gene expression.....72
2.5 Discussion.....81
Chapter 3 – Antimicrobial Silicone Development.....88
3.1 Introduction.....89
3.1.1 Implantable medical devices.....89
3.1.2 Silicone medical devices.....89
3.1.3 Chemical composition of silicone polymers.....90
3.1.4 Silicone classes.....91
3.1.5 Aims.....93
3.2 Materials & Methods.....94
3.2.1 Silicone preparation.....94
3.2.2 Preparation of silicones bulk-loaded with triclosan, triclosan acetate or novel imidazolium compounds.....96
3.2.3 Preparation of silicone dip-coated with 1% (w/w) triclosan and 1% (w/w) triclosan acetate containing polymers.....96
3.2.4 Preparation of a 1% w/w [HL2] Br coated silicone.....97
3.2.5 Determination of tensile strength and elongation of prepared silicone.....97
3.2.5.1 Sample preparation.....97
3.2.5.2 Testing procedure to determine tensile strength and elongation of silicone specimens.....98
3.2.6 Determination of tear strength of prepared silicone.....99
3.2.6.1 Sample preparation.....99
3.2.6.2 Testing procedure to measure tear strength of silicone.....99
3.2.7 Long-term release of antimicrobial compounds from silicone elastomers.....100

3.2.7.1 Repeated zone of inhibition assays.....100
3.2.7.2 Measurement of antimicrobial compound release using HPLC.....100
3.2.7.2.1 Preparation of artificial urine (AU).....100
3.2.7.2.2 High-performance liquid chromatography (HPLC) apparatus.....101
3.2.7.2.3 HPLC calibration standard solutions of triclosan and triclosan acetate.....101
3.2.8 Antimicrobial activity of novel silicone formulations.....102
3.2.8.1 Zone of inhibition assay.....102
3.2.8.2 Propidium iodide (PI) staining of microorganisms adhered to silicone.....102
3.2.8.3 Colony forming unit (CFU) determination of microorganisms adhered to silicone.....103
3.3 Results.....104
3.3.1 Development of antimicrobial silicone formulations.....104
3.3.2 Mechanical properties of silicones following antimicrobial incorporation.....107
3.3.3 Long-term release of antimicrobial compounds from silicone elastomers.....109
3.3.3.1 Repeated zone of inhibition assays.....109
3.3.3.2 Measurement of antimicrobial compound release using HPLC.....109
3.3.4 Antimicrobial activity of novel silicone formulations.....113
3.3.4.1 Zone of inhibition assays.....113
3.3.4.2 Enumeration of microorganisms recovered from silicone.....116
3.3.4.3 Quantification of dead cells on antimicrobial silicone surfaces.....125
3.4 Discussion.....152
3.5 Conclusions.....157
Chapter 4 – Development of a 3D Printable Antimicrobial Silicone.....159
4.1 Introduction.....161
4.1.1 Medical devices.....161
4.1.2 Fabrication of silicone medical devices using 3D printing.....162

4.1.3 3D printing antimicrobial polymers.....163
4.1.4 Aims.....165
4.2 Materials & Methods.....166
4.2.1 Development of a 3D printable antimicrobial silicone.....166
4.2.2 3D printing silicone.....169
4.2.2.1 Overview of the 3D printer.....169
4.2.2.2 x-y-z gantry robot.....169
4.2.2.3 Material delivery system.....170
4.2.2.4 3D printing specimens to determine mechanical properties....172
4.2.3 Determining the mechanical properties of 3D printed silicone specimens.....172
4.2.4 Antimicrobial properties of 3D printed silicone.....173
4.3 Results.....174
4.3.1 Development of 3D printed antimicrobial silicone.....174
4.3.2 Mechanical properties 3D printed silicone.....176
4.3.3 Antimicrobial properties of 3D printed silicone loaded with 1% triclosan.....176
4.4 Discussion.....179
4.5 Conclusions.....181
Chapter 5 – Development of a 3D Printable Antimicrobial Silicone.....182
5.1 Introduction.....183
5.1.1 Detection of *Escherichia coli* based on β-D-glucuronidase and β-galactosidase activity.....184
5.1.2 Detection of urease positive bacteria using pH sensors.....186
5.1.3 Detection of *Pseudomonas aeruginosa* through cytochrome oxidase activity.....187
5.1.4 Detection of microorganisms by metabolic activity using tetrazolium compounds.....188
5.1.5 Detection of microorganisms by dehydrogenase enzymic action and resazurin.....189
5.1.6 Aims.....190
5.2 Materials & Methods.....192
5.2.1 Preparation of artificial urine (AU).....192
5.2.2 Preparation of sensor reagents.....192

5.2.3 Microorganisms.....194
5.2.4 Evaluation of sensor compounds against planktonic microorganisms.....195
5.2.4.1 Determining sensor sensitivity against number of viable bacteria.....195
5.2.4.2 Determination of sensitivity of sensor molecules against planktonic bacteria.....195
5.2.4.3 Determination of absorbance thresholds for sensor molecules.....197
5.2.5 Evaluation of candidate sensor compounds in a filter paper model.....197
5.2.5.1 Evaluation of 4-methylumbelliferyl-b-D- glucuronide (MUG) and chlorophenol Red-β-D-galactopyranoside (CPRG) as filter paper sensor materials.....198
5.2.5.2 Evaluation of 4-methylumbelliferyl-b-D-glucuronide (MUG) in a dual-species infection model.....198
5.2.5.3 Evaluation of tetramethyl-p-phenylenediamine dihydrochloride (Kovacs reagent) as a Pseudomonas aeruginosa sensor molecule.....198
5.2.5.4 Evaluation of additional candidate sensor molecules absorbed on to filter paper discs.....198
5.2.6 Evaluation of candidate sensor molecules incorporated into polymers.....199
5.2.6.1 Bromothymol blue (BTB) sensor production.....199
5.2.6.2 Production of a porous bromothymol blue (BTB-P) silicone material.....200
5.2.6.3 Production of chlorophenol red-b-D-galactopyranoside (CPRG) and resazurin sensor materials.....200
5.2.6.4 Production of a resazurin polyurethane foam sensor Material.....200
5.2.6.5 Evaluation of polymer sensor materials in an in-vitro

batch model.....201
5.3 Results.....202
5.3.1 Evaluation of sensor compounds against planktonic microorganisms.....202
5.3.1.1 Evaluation of chlorophenol red β-galactopyranoside (CPRG) as a sensor for coliform bacteria.....202
5.3.1.2 Detection of *E. coli* using 4-methylumbelliferyl-ß-D-glucuronide substrate.....216
5.3.1.3 Evaluation of bromothymol blue (BTB) as a sensor molecule to detect urease positive bacteria.....221
5.3.1.4 Evaluation of tetrazolium compounds to detect viable bacteria..... ..221
5.3.1.5 Evaluation of resazurin to detect viable bacteria.....226
5.3.1.6 Comparison of sensitivity and specificity of the evaluated sensor molecules.....226
5.3.2 Evaluation of candidate sensor compounds in a filter paper model.....229
5.3.2.1 Evaluation of 4-methylumbelliferyl-b-D-glucuronide (MUG) and chlorophenol Red-β-D-galactopyranoside (CPRG) as filter paper sensor materials.....229
5.3.2.2 Evaluation of 4-methylumbelliferyl-b-D-glucuronide (MUG) in a dual-species infection model.232
5.3.2.3 Evaluation of tetramethyl-p-phenylenediamine dihydrochloride (Kovac's reagent) as a *Pseudomonas aeruginosa* sensor molecule.....232
5.3.2.4 Evaluation of MUG, tetrazolium compounds and Kovac's reagent absorbed on to filter paper discs.....235
5.3.3 Evaluation of candidate sensor molecules incorporated into polymers.....237
5.3.4 Evaluation of polymer sensor materials in an *in-vitro* batch model.....237
5.4 Discussion.....239
5.5 Conclusions.....244

Chapter 6 – Assessment of Novel Biomaterials Using an In-Vitro Bladder Model....246
6.1 Introduction....246
6.1.1 Design of the *in-vitro* bladder model....247
6.1.2 Aims....249
6.2 Materials & Methods....250
6.2.1 Production of bulk-loaded antimicrobial cylinders....250
6.2.2 Production of antimicrobial dip-coated catheters....250
6.2.3 Assessment of bulk-loaded antimicrobial cylinders and dip-coated catheters to prevent ascending *Proteus mirabilis* infection using an *in-vitro* bladder model....250
6.2.4 Determination of pH of AU collected from *in vitro* bladder model....252
6.2.5 Scanning electron microscopy of dip-coated catheters....252
6.2.6 XRMA analysis of crystalline biofilm....252
6.2.7 Performance of bromothymol blue sensor materials and resazurin in a *Proteus mirabilis* inoculated *in vitro* bladder model....252
6.2.8 Resazurin as an indicator for bladder infection in catheterised models....253
6.3 Results....254
6.3.1 Assessment of bulk-loaded antimicrobial cylinders and dip-coated catheters to prevent ascending *Proteus mirabilis* infection in an *in-vitro* bladder model....254
6.3.2 BTB sensor materials and resazurin for *Proteus mirabilis* detection *in vitro* bladder model....261
6.4 Discussion....271
6.5 Conclusions....276
Chapter 7 – General Discussion....278
7.1 General Discussion....279
7.2 Conclusions....288
References....290
Appendix....315

# List of Figures


| | | Page |
|---|---|---|
| **Figure 1.1** | Biofilm formation on various surfaces | 3 |
| **Figure 1.2** | A typical biofilm structure | 4 |
| **Figure 1.3** | The phases of biofilm formation | 7 |
| **Figure 1.4** | Quorum sensing mechanisms of Gram-negative and Gram-positive bacteria | 10 |
| **Figure 1.5** | Persister cells within biofilm populations | 13 |
| **Figure 1.6** | Schematic of an inflated Foley catheter within a bladder | 14 |
| **Figure 1.7** | (A) Schematic of a silicone Foley catheter (B) catheter tip showing the eye-hole and inflated retention balloon (C) cross-sectional diagram of a Foley catheter showing the inlet channel for inflation of the retention balloon and the urine drainage channel. | 15 |
| **Figure 1.8** | Blockage of a urinary catheter by struvite and apatite due to *P. mirabilis* infection | 21 |
| **Figure 1.9** | The general life cycle of motile cells of bacteria as they swarm on surfaces | 23 |
| **Figure 1.10** | Antimicrobial mechanisms | 26 |
| **Figure 1.11** | Zwitterionic mechanisms of antifouling | 28 |
| **Figure 1.12** | Nano-cone patterned surfaces disrupt bacterial cell membranes | 35 |
| **Figure 1.13** | Schematic diagram of the duel-layered catheter coating developed by Milo *et al*. | 37 |
| **Figure 1.14** | Production of a fluorescent-coloured urine within the drainage bag of an *in-vitro* bladder model through release of carboxyfluorescein dye, in response to *P. mirabilis* infection | 38 |
| **Figure 2.1.1** | The chemical structure of triclosan | 44 |
| **Figure 2.1.2** | Mechanisms of antimicrobial action of triclosan and silver ions on bacteria | 47 |
| **Figure 2.1.3** | A) General structure of LTA; B) Chemical structure of Type I LTA; C) Structure of compound 1771 | 51 |

| | | |
|---|---|---|
| **Figure 2.3.1** | **1** The effect of triclosan on *Escherichia coli* virulence gene expression | 73 |
| **Figure 2.3.2** | The effect of $[HL]^2$ BR on *Escherichia coli* virulence gene expression | 74 |
| **Figure 2.3.3** | The effect of triclosan on *Staphylococcus aureus* virulence gene expression | 75 |
| **Figure 2.3.4** | The effect of $[HL]^2$ BR on *Staphylococcus aureus* virulence gene expression | 76 |
| **Figure 2.3.5** | The effect of triclosan on *Candida albicans* virulence gene expression | 78 |
| **Figure 2.3.6** | The effect of $[HL]^2$ BR on *Candida albicans* virulence gene expression | 80 |
| **Figure 3.1.1** | The chemical structure of silicone polymers | 90 |
| **Figure 3.1.2** | Diagrammatic representation of cross-linked silicone polymers | 91 |
| **Figure 3.1.3** | The composition and structure of silicone elastomers | 92 |
| **Figure 3.2.1** | Schematic representation of dumbbell shaped moulds used to produce silicones to determine tensile strength and elongation | 97 |
| **Figure 3.2.2** | Diagrammatic representation of measurements used to determine elongation of silicone specimens | 98 |
| **Figure 3.2.3** | Dimensions of specimens used to determine tear strength of prepared silicone | 99 |
| **Figure 3.3.1** | Mechanical properties of novel silicone formulations | 108 |
| **Figure 3.3.2** | Zones of inhibition on agar plates with *Staphylococcus aureus* NSM 7, using silicone coupons bulk-loaded with 1% (w/w) triclosan (T2) or 1% (w/w) triclosan acetate (TA-2), or dip-coated with a 1% (w/w) triclosan (T2-DC), 1% (w/w) triclosan acetate formulation (TA-2-DC) or coated with acetoxy silicone containing 1% (w/w) $[HL^2]$ Br) | 111 |
| **Figure 3.3.3** | Triclosan release from bulk-loaded silicone elastomers over 6 weeks | 112 |
| **Figure 3.3.4** | Zones of inhibition generated by formulated silicones | 115 |

| | | |
|---|---|---|
| **Figure 3.3.5** | Colony forming units of CAUTI causing microorganisms recovered following 24 h adherence to control silicone (S2) and silicone bulk-loaded with 1% (w/w) triclosan (T2) | 118 |
| **Figure 3.3.6** | Colony forming units of CAUTI causing microorganisms recovered following 24 h adherence to control silicone (S2) and silicone bulk-loaded with 1% (w/w) triclosan acetate (TA-2) | 120 |
| **Figure 3.3.7** | Colony forming units of CAUTI causing microorganisms recovered following 24 h adherence to dip-coated silicones | 122 |
| **Figure 3.3.8** | Colony forming units of CAUTI causing microorganisms recovered following 24 h adherence to silicone dip-coated with acetoxy silicone without antimicrobial compound (S2_A) and silicone dip-coated with acetoxy silicone containing 1% (w/w) [$HL^2$] Br (A_[$HL^2$]Br) | 124 |
| **Figure 3.3.9** | Propidium iodide stained (dead) microorganisms adhered to silicone | 128 |
| **Figure 3.3.10** | Representative images of dead *Escherichia coli* NCTC 12923 and *Staphylococcus aureus* NSM 7 cells | 129 |
| **Figure 3.3.11** | Representative images of dead *Klebsiella pneumoniae* P6 wk2 and *Serratia marcescens* NSM 51 cells upon silicone bulk-loaded with 1% (w/w) triclosan (T2) or without antimicrobial (S2) | 130 |
| **Figure 3.3.12** | Representative images of dead *Providencia stuartii* NSM 58 and *Proteus mirabilis* 12 RTB cells upon silicone bulk-loaded with 1% (w/w) triclosan (T2) or without antimicrobial (S2) | 131 |
| **Figure 3.3.13** | Representative images of dead *Candida albicans* ATTC 90028 and *Pseudomonas aeruginosa* NCTC 10662 cells silicone bulk-loaded with 1% (w/w) triclosan (T2) or without antimicrobial (S2) | 132 |
| **Figure 3.3.14** | Propidium iodide stained (dead) microorganisms adhered to silicone | 134 |

**Figure 3.3.15** Representative images of dead *Escherichia coli* NCTC 12923 and *Staphylococcus aureus* NSM 7 cells on silicone bulk-loaded with 1% (w/w) triclosan acetate (TA-2) or without antimicrobial (S2) 135

**Figure 3.3.16** Representative images of dead *Klebsiella pneumoniae* P6 wk2 and *Serratia marcescens* NSM 51 cells on silicone bulk-loaded with 1% (w/w) triclosan acetate (TA-2) or without antimicrobial (S2) 136

**Figure 3.3.17** Representative images of dead *Providencia stuartii* NSM 58 and *Proteus mirabilis* 12 RTB cells on silicone bulk-loaded with 1% (w/w) triclosan acetate (TA-2) or without antimicrobial (S2) 137

**Figure 3.3.18** Representative images of dead *Candida albicans* ATCC 90028 and *Pseudomonas aeruginosa* NCTC 10662 cells on silicone bulk-loaded with 1% (w/w) triclosan acetate (TA-2) or without antimicrobial (S2) 138

**Figure 3.3.19** Propidium iodide stained (dead) microorganisms adhered to silicone 140

**Figure 3.3.20** Representative images of dead *Escherichia coli* NCTC 12923 and *Staphylococcus* NSM 7 cells on silicone dip coated with 1% (w/w) triclosan (T2-DC), 1% (w/w) triclosan acetate (TA-2-DC) or dip-coated with silicone without antimicrobial (S2-DC) 141

**Figure 3.3.21** Representative images of dead *Klebsiella pneumoniae* P6 wk2 and *Serratia marcescens* NSM 51 cells on silicone dip coated with 1% (w/w) triclosan (T2-DC), 1% (w/w) triclosan acetate (TA-2-DC) or dip-coated with silicone without antimicrobial (S2-DC) 142

**Figure 3.3.22** Representative images of dead *Providencia stuartii* NSM 58 and *Proteus mirabilis* 12 RTB cells on silicone dip coated with 1% (w/w) triclosan (T2-DC), 1% (w/w) triclosan acetate (TA-2-DC) or dip-coated with silicone without antimicrobial (S2-DC) 143

**Figure 3.3.23** Representative images of dead *Candida albicans* ATCC 90028 and *Pseudomonas aeruginosa* NCTC 10662 cells on silicone dip coated with 1% (w/w) triclosan (T2-DC), 1% (w/w) triclosan acetate (TA-2-DC) or dip-coated with silicone without antimicrobial (S2-DC) 144

**Figure 3.3.24** Dead microorganisms adhered to silicone rubber dip coated with acetoxy silicone containing 1% (w/w) [$HL^2$] Br (A_[$HL^2$] Br) or dip-coated with acetoxy silicone without antimicrobial compound (S2_A) 146

**Figure 3.3.25** **25** Representative images of dead *Escherichia coli* NCTC 12923 and *Staphylococcus aureus* NSM 7 cells on silicone dip coated with acetoxy silicone containing 1% (w/w) [$HL^2$] Br (A_[$HL^2$] Br) or dip-coated with acetoxy silicone without antimicrobial (S2_A) 147

**Figure 3.3.26** Representative images of dead *Klebsiella pneumoniae* P6 wk 2 and *Serratia marcescens* NSM 51 on silicone dip coated with acetoxy silicone containing 1% (w/w) [$HL^2$] Br (A_[$HL^2$] Br) or dip-coated with acetoxy silicone without antimicrobial (S2_A) 148

**Figure 3.3.27** Representative images of dead *Providencia stuartii* NSM 58 and *Proteus mirabilis* 12 RTB on silicone dip coated with acetoxy silicone containing 1% (w/w) [$HL^2$] Br (A_[$HL^2$] Br) or dip-coated with acetoxy silicone without antimicrobial (S2_A) 149

**Figure 3.3.28** Representative images of dead *Candida albicans* ATCC 90028 and *Pseudomonas aeruginosa* NCTC 10662 on silicone dip coated with acetoxy silicone containing 1% (w/w) [$HL^2$] Br (A_[$HL^2$] Br) or dip-coated with acetoxy silicone without antimicrobial (S2_A) 150

**Figure 4.2.1** Printer cartoon including gantry and material delivery system 169

**Figure 4.2.2** The gantry robot 170

**Figure 4.2.3** The gantry with printer head 170

| | | |
|---|---|---|
| **Figure 4.2.4** | The mixing chamber depicting two inlets for part A and part B silicone and the mixing chamber | 171 |
| **Figure 4.2.5** | 3D printed specimens for determination of mechanical properties | 172 |
| **Figure 4.3.1** | Mechanical properties of silicone formulations. | 177 |
| **Figure 4.3.2** | Zones of inhibition against common CAUTI pathogens produced by 3D printed silicone elastomers. | 178 |
| **Figure 5.1.1** | Schematic representation *of E. coli* β-glucuronidase activity on the methylumbelliferyl-β-D-glucuronide (MUG) | 184 |
| **Figure 5.1.2** | Schematic representation of *E. coli* β-D-galactosidase activity with chlorophenol red-β-D-galactopyranoside (CPRG) | 185 |
| **Figure 5.1.3** | The structure of bromothymol blue in its acid and base forms | 186 |
| **Figure 5.1.4** | Oxidation of tetramethyl-p-phenylenediamine dihydrochloride to indophenol (Würster's blue) | 187 |
| **Figure 5.1.5** | Illustration of a positive (A) and negative (B) reaction between Kovac's reagent and *Pseudomonas aeruginosa* | 188 |
| **Figure 5.1.6** | Reduction of 3-(4,5-dimethylthiazol-2-yl)-2,5-diphenyltetrazolium bromide (MTT) by cellular reductase enzymes | 189 |
| **Figure 5.1.7** | Cellular reduction of resazurin | 190 |
| **Figure 5.3.1** | Growth of test species monitored at absorbance 600 nm over 24 h | 204 |
| **Figure 5.3.2** | Correlation curves of colony forming units (CFU) against optical density at 600 nm for 4 *Escherichia coli* strains | 205 |
| **Figure 5.3.3** | Correlation curves of colony forming units (CFU) against optical density at 600 nm for *Escherichia coli* NCTC 12923, *Klebsiella pneumoniae* p6 wk2 and *Proteus mirabilis* 12 RTB | 206 |

| | | |
|---|---|---|
| **Figure 5.3.4** | Evaluation of chlorophenol red β-galactopyranoside for detection of test bacteria based on ß-galactosidase production | 209 |
| **Figure 5.3.5** | Evaluation of chlorophenol red β-galactopyranoside for detection of test bacteria based on ß-galactosidase production | 210 |
| **Figure 5.3.6** | Evaluation of CPRG for detection of test bacteria based on ß-galactosidase production | 211 |
| **Figure 5.3.7** | Evaluation of chlorophenol red β-galactopyranoside for detection of test bacteria based on ß-galactosidase production | 212 |
| **Figure 5.3.8** | Evaluation of chlorophenol red β-galactopyranoside for detection of *Escherichia coli* using ß-galactosidase activity | 213 |
| **Figure 5.3.9** | Evaluation of chlorophenol red β-galactopyranoside for detection of *Escherichia coli* using ß-galactosidase activity | 214 |
| **Figure 5.3.10** | Evaluation of chlorophenol red β-galactopyranoside for detection of *Escherichia coli* using ß-galactosidase activity | 215 |
| **Figure 5.3.11** | Detection of *Escherichia coli* through ß -glucuronidase activity on 4-methylumbelliferyl-ß-D-glucuronide substrate | 217 |
| **Figure 5.3.12** | Detection of *Escherichia coli* through ß -glucuronidase activity on 4-methylumbelliferyl-ß-D-glucuronide substrate | 218 |
| **Figure 5.3.13** | Detection of *Escherichia coli* through ß -glucuronidase activity on 4-methylumbelliferyl-ß-D-glucuronide substrate | 219 |
| **Figure 5.3.14** | Reactions between 8 CAUTI causing microorganisms with the substrates CPRG (2mM) and MUG (2mM) | 220 |
| **Figure 5.3.15** | Detection of *Proteus mirabilis* 12 RTB using bromothymol blue (BTB) | 223 |

| | | |
|---|---|---|
| **Figure 5.3.16** | Detection of *Escherichia coli* NCTC 12923 and *Escherichia coli* 9 with MTT at a final concentration of 0.1 mM | 224 |
| **Figure 5.3.17** | Detection of coloured formazan products formed by reduction of the novel tetrazolium compounds triphenyl-tetrazolium phosphate (TTP), 2,6-difluro-triphenyl-tetrazolium phosphate (2,6-diFTTP) and 2,6-dichloro-triphenyl-tetrazolium phosphate (2,6-diClTTP) by *Proteus mirabilis* 12 RTB and *Escherichia coli* NCTC 12923 | 225 |
| **Figure 5.3.18** | Exploiting the ability of metabolically active *Proteus mirabilis* 12RTB and *Escherichia coli* NCTC 12923 to reduce resazurin for use as a microbial sensor molecule | 228 |
| **Figure 5.3.19** | Detection of *Escherichia coli* using a filter paper sensor impregnated with 2 mM MUG | 230 |
| **Figure 5.3.20** | Detection of *Escherichia coli* with a CPRG filter paper sensor material | 231 |
| **Figure 5.3.21** | Detection of *Escherichia coli* in a dual species test using a MUG filter paper sensor material | 233 |
| **Figure 5.3.22** | Reactions of CAUTI bacteria with filter papers soaked with 1% w/v Kovac's reagent (tetramethyl-p-phenylenediamine dihydrochloride | 234 |
| **Figure 5.3.23** | Detection of CAUTI causing microorganisms with filter paper sensors. | 236 |
| **Figure 5.3.24** | Detection of *Proteus mirabilis* with bromothymol blue (BTB) silicone sensor materials and a resazurin polyurethane foam | 238 |
| **Figure 6.1** | Schematic representation of the *in-vitro* bladder model | 248 |
| **Figure 6.3.1** | Effect of bulk-loaded antimicrobial inserts on AU pH in an *in-vitro* bladder model of ascending *Proteus mirabilis* infection | 255 |
| **Figure 6.3.2** | Effect of antimicrobial dip-coated catheters on AU pH in an *in-vitro* bladder model of ascending *Proteus mirabilis* infection | 257 |

| | | |
|---|---|---|
| **Figure 6.3.3** | Representative scanning electron micrographs and corresponding XRMA of Foley catheter sections taken from a *Proteus mirabilis* encrusted catheter used in an *in-vitro* bladder model of ascending infection | 260 |
| **Figure 6.6.4.** | pH of AU collected from the bladder chamber and drainage bags of the *in vitro* bladder model inoculated ± *Proteus mirabilis* 12 RTB | 262 |
| **Figure 6.3.5** | CFUs of *Proteus mirabilis* in AU collected from the bladder chambers and drainage bags of *in vitro* bladder models | 264 |
| **Figure 6.3.6** | Standard bromothymol blue sensor material (BTB) and porous bromothymol blue sensor material (BTB-P) 48h post inoculation of the *in-vitro* bladder model with *Proteus mirabilis* | 267 |
| **Figure 6.3.7** | Resazurin stained AU collected in drainage bags from an *in vitro* bladder model at intervals between 1h and 24h | 269 |
| **Figure 6.3.8** | Scanning electron micrographs of urinary catheters removed from an *in vitro* bladder model 48 h post inoculation | 270 |

# List of Tables


| | | Page |
|---|---|---|
| **Table 1.1** | Medical devices and bacteria commonly associated with biofilm formation on their surfaces | 2 |
| **Table 1.2** | Summary of biofilm EPS composition | 6 |
| **Table 1.3** | Examples of bacterial biofilm resistance mechanisms | 11 |
| **Table 1.4** | Types of catheter use and frequency of urinary infection in catheterised populations | 16 |
| **Table 1.5** | Microbiologic diagnosis of urinary infection associated with catheter usage | 18 |
| **Table 1.6** | Microorganisms isolated from the urine of patients undergoing long-term catheterisation | 19 |
| **Table 1.7** | Composition of some commercially available Foley catheters | 25 |
| **Table 2.1** | Compounds selected for the prophylactic management of CAUTIs | 43 |
| **Table 2.2.1** | Microorganism strains and corresponding agar used in cultures | 54 |
| **Table 2.2.2** | Chemical structures of triclosan and triclosan esters | 56 |
| **Table 2.2.3** | Chemical structures of novel imidazolium (A-C) and novel silver (D-F) compounds. | 57 |
| **Table 2.2.4** | Chemical structures of commercially available compounds evaluated | 58 |
| **Table 2.2.5** | Primer sequences of *Escherichia coli* virulence genes | 62 |
| **Table 2.2.6** | Primer sequences of *Candida albicans* virulence genes | 63 |
| **Table 2.2.7** | Primer sequences of *Staphylococcus aureus* virulence genes | 64 |
| **Table 2.3.2** | Minimum inhibitory concentrations (MICs) | 68 |
| **Table 2.3.3** | Minimum biocidal concentrations (MBCs) | 71 |
| **Table 3.1** | Key properties of silicone rubbers | 90 |
| **Table 3.2.1** | Formulation of silicone bases for silicones S1 and S2 | 95 |
| **Table 3.2.2** | Formulation of platinum catalyst concentrates for silicones S1 and S2 | 95 |
| **Table 3.2.3** | Formulation of part A for silicones S1 and S2 | 95 |

| | | |
|---|---|---|
| **Table 3.2.4** | Formulation of part B for silicones S1 and S2 | 95 |
| **Table 3.3.1** | Curing scores of novel silicone formulations (S1 and S2) bulk-loaded with antimicrobial compounds | 105 |
| **Table 3.3.2** | Curing scores of silicone formulations bulk-loaded with 1% (w/w) [$HL^2$] BR using heat activated platinum cyclovinylmethylsiloxane catalyst | 105 |
| **Table 3.3.3** | Curing scores of silicone formulations bulk-loaded with 1% (w/w) [$HL^2$] BR using room temperature activated platinum cyclovinylmethylsiloxane catalyst | 106 |
| **Table 3.3.4** | Curing scores of silicone formulations without antimicrobial compounds using 2.72% (w/w) cross-linker and 0.5% (w/w) heat activated or room temperature activated platinum cyclovinylmethylsiloxane catalyst | 106 |
| **Table 3.3.5** | Summary of significance of antimicrobial activity of novel silicone formulations against 8 microorganisms | 151 |
| **Table 4.1** | Advantages and disadvantages of methods to manufacture silicone medical devices | 162 |
| **Table 4.2.1** | Composition of silicone formulations 3D-S1 – 3D-S7 for use in 3D printing applications | 167 |
| **Table 4.2.2** | Composition of silicone formulations 3D-S8 – 3D-S10 for 3D printing applications using platinum retarder stock at 2.5% (w/w) | 167 |
| **Table 4.2.3** | Composition of silicone formulation 3D-S11 for 3D printing applications using platinum retarder stock at 2.5% (w/w) | 168 |
| **Table 4.2.4** | Composition of silicone formulation 3D-S12 for 3D printing applications using platinum retarder stock at 2.5% (w/w) | 168 |
| **Table 4.3.1** | Work times and cure times of silicone formulations developed for use in 3D printing applications | 175 |
| **Table 5.2.1** | Chemical structures of candidate sensor molecules | 193 |
| **Table 5.2.2** | Microorganisms used to evaluate sensor molecules | 194 |
| **Table 5.3.1** | Colony forming units (CFU)/ml of bacteria at the time of detection using selected sensor compounds | 207 |

| | | |
|---|---|---|
| **Table 5.3.2** | Summary of candidate sensor molecules and their detection of planktonic microorganisms, detection in filter paper and detection in polymers | 208 |
| **Table 6.3.1** | Time (days) for ascending *Proteus mirabilis* to reach the bladder using bulk-loaded antimicrobial silicone inserts to prevent migration | 254 |
| **Table 6.3.2** | Time (days) for ascending *Proteus mirabilis* to reach the bladder utilising antimicrobial dip-coated catheters to prevent migration | 256 |
| **Table 6.3.3** | Comparison of the times taken for the porous bromothymol blue sensor material (BTB-P), standard bromothymol blue sensor (BTB) material and resazurin added to the drainage bag to signal the presence of *P. mirabilis* infection | 266 |

# List of Abbreviations

| | |
|---|---|
| ε-PL | Poly-L-lysine |
| $[HL]^2BR$ | 3-hexadecyl-1-isopropyl-1H-imidazole-3-ium bromide |
| 2,6-diClTTP | 2,6-dichloro-triphenyl-tetrazolium phosphate |
| 2,6-diFTTP | 2,6-difluro-triphenyl-tetrazolium phosphate |
| *A. baumannii* | *Acinetobacter baumannii* |
| Act 1 | Actin 1 |
| AHL | Acyl Homoserine Lactone |
| AI-2 | Auto-Inducer 2 |
| AIP | Auto-Inducing Peptide |
| ALS | Agglutinin-Like Sequence |
| AMR | Antimicrobial Resistance |
| ANOVA | Analysis of Variance |
| ASTM | American Society for Testing and Materials |
| ATCC | American Type Culture Collection |
| AU | Artificial Urine |
| BTB | Bromothymol Blue |
| *C. albicans* | *Candida albicans* |
| *C. difficile* | *Clostridium difficile* |
| CAASB | Catheter Associated Asymptomatic Bacteriuria |
| CAUTI | Catheter-Associated Urinary Tract Infection |
| CDC | Centre for Disease Control and Prevention |
| CDH | Cellobiose Dehydrogenase |
| CF | Cystic Fibrosis |
| CFU | Colony forming unit |
| CLED | Cysteine Lactose Electrolyte-Deficient |
| Compound 1771 | [2-oxo-2-(5-phenyl-1,3,4-oxadiazol-2-ylamino) ethyl-2-naphtho[2,1-*b*] furan-1-ylacetate] |
| CPRG | Chlorophenol Red β-Galactopyranoside |
| CR | Chlorophenol Red |
| CRBSI | Catheter-Related Blood Stream Infections |
| CTAB | Cetyltrimethylammonium Bromide |
| DLVO | Derjaguin-Landau-Verwey-Overbeek |
| DMSO | Dimethyl Sulphoxide |
| DNase I | Deoxyribonuclease I |
| *E. coli* | *Escherichia coli* |
| *E. faecium* | *Enterococcus faecium* |
| EDNA | Extracellular DNA |
| ENR | Enoyl-acyl carrier protein reductase |
| EPA1 | Epithelial Adhesin 1 |
| EPS | Extracellular Polymeric Substances |
| ESKAPE | *Enterococcus faecium*, *Staphylococcus aureus*, K*lebsiella pneumoniae*, *Acinetobacter baumannii*, *Pseudomonas aeruginosa* and *Enterobacter* species |
| FDA | The Food and Drug Administration |
| FI | Fluorescent intensity |

| | |
|---|---|
| Fnb B | Fibronectin Binding Protein B |
| GAL | β-Galactosidase |
| GHS | Glycoside Hydrolase |
| GUD | β--Glucuronidase |
| Gyr B | DNA gyrase B |
| HCAI | Healthcare Acquired Infection |
| HIP | High Persister |
| HPLC | High Pressure Liquid Chromatography |
| HTV | High Temperature Vulcanising |
| HWP 1 | Hyphal Wall Protein 1 |
| ICA | Intercellular Adhesin |
| ISO | International Organisation for Standardisation |
| *K. pneumoniae* | *Klebsiella pneumoniae* |
| LPS | Lipopolysaccharide |
| LTA | Lipoteichoic acid |
| LTAS | Lipoteichoic Acid Synthase |
| LW | Lifshitz Van der Waals |
| MBC | Minimum Biocidal Concentration |
| MBEC | Minimum Biofilm Eradication Concentration |
| MHB | Mueller-Hinton Broth |
| MHRA | Medical and Healthcare products Regulatory Agency |
| MIC | Minimum Inhibitory Concentration |
| MRSA | Methicillin-Resistant *Staphylococcus aureus* |
| MTT | 3-(4,5-dimethylthiazol-2-yl)-2,5-diphenyltetrazolium bromide |
| MUG | Methylumbelliferyl-β-D-Glucuronide |
| NCTC | National Collection of Type Cultures |
| NHC | *N*-Heterocyclic Carbene |
| NICE | The National Institute for Health and Care Excellence |
| OTC | Over-The Counter |
| *P. aeruginosa* | *Pseudomonas aeruginosa* |
| *P. mirabilis* | *Proteus mirabilis* |
| *P. rettgeri* | *Providencia rettgeri* |
| *P. stuartii* | *Providencia stuartii* |
| *P. vulgaris* | *Proteus vulgaris* |
| PDMS | polydimethylsiloxane |
| PEG | Polyethylene Glycol |
| $pH_n$ | Nucleation pH |
| PIA | Polysaccharide Intercellular Adhesin |
| PLD | Phospholipase D |
| PTFE | Polytetrafluoroethylene |
| QS | Quorum Sensing |
| RTV | Room Temperature Vulcanising |
| *S. aureus* | *Staphylococcus aureus* |
| *S. marcescens* | *Serratia marcescens* |
| SAP | Secreted Aspartyl Proteinase |
| SEM | Scanning Electron Microscopy |
| SPA | Sparfloxacin |

| | |
|---|---|
| TSA | Tryptone Soya Agar |
| TTO | Tea-Tree Oil |
| TTP | Triphenyl-Tetrazolium Phosphate |
| UTI | Urinary Tract Infection |
| VAP | Ventilator-Associated Pneumonia |
| VRE | Vancomycin Resistant Enterococci |
| VTEC | Verotoxin producing *E. coli* |
| WHO | World Health Organization |
| XRMA | X-ray Micro Analysis |
| ZOI | Zone Of Inhibition |

## Summary

Catheter-associated urinary tract infections (CAUTIs) are associated with urinary catheters biofilms. The overarching aim of this research was to identify biocidal agents that when incorporated into silicone elastomers inhibited such biofilm formation.

In solution and when incorporated into the silicone matrix, triclosan and triclosan acetate exhibited broad-spectrum activity against planktonic cultures. Both agents inhibited *S. aureus*, *K. pneumoniae*, *P. stuartii* and *P. mirabilis*, whilst triclosan also had inhibited *Escherichia coli* and *Candida albicans*. *Serratia marcescens* and *Pseudomonas aeruginosa* were resistant. Mechanical properties of silicone were not negatively affected by incorporation of these antimicrobials, and elongation strength was increased. This would be advantageous for a urinary catheter as significant forces may be applied during device removal or by an attached drainage bag.

Additionally, triclosan and triclosan acetate were released from bulk-loaded silicone over 12 weeks, with the latter providing the highest sustained release rate.

A 3D printable silicone elastomer containing 1% triclosan was developed with superior mechanical properties, compared to compression moulded silicone, and inhibited growth of *P. mirabilis*, *E. coli* and *S. aureus*.

Dip-coating Foley catheters in a silicone formulation containing 0.2% triclosan or triclosan acetate prevented catheter blockage by *P. mirabilis* in an *in-vitro* bladder model of CAUTI.

A 1% coating of the novel imidazolium compound 3-hexadecyl-1-isopropyl-1H-imidazole-3-ium bromide ([$HL^2$] Br) in silicone reduced growth of *S. aureus* and *C. albicans*.

A panel of signalling molecules were evaluated to determine their activity and sensitivity against numerous CAUTI causing pathogens with the most promising compounds, namely bromothymol blue (BTB) and resazurin selected for incorporation into biomaterials. The aim was to develop biomaterial sensors to signal early CAUTI and thus, facilitate improved management.

A silicone sensor incorporating (BTB) changed colour from yellow to dark blue in the presence of ammonium ions generated by urease positive bacteria. Increasing the surface area of this sensor reduced the signalling time of *P. mirabilis* infection in an *in-vitro* bladder model by 3 h, compared with the original BTB sensor.

To create a universal microbial sensor material, a range of chemicals were evaluated, and resazurin, commonly used to determine cell viability, provided the best signalling

response to infection. Incorporation this agent into a biomaterial was unsuccessful, but its addition to the drainage bag in the *in vitro* bladder model signalled *P. mirabilis* infection with similar sensitivity to the BTB sensor. It is anticipated that resazurin could be used to detect multiple microbes and thus be a valuable diagnostic agent in CAUTI.

# Chapter 1

## Introduction and Literature Review

## 1.1 Healthcare acquired infections

Healthcare acquired infections (HCAIs) are infections that develop while receiving treatment in a hospital or other healthcare setting, such as in a nursing home. A HCAI is one that occurs 48 h after hospital admission or within 30 days of receiving healthcare (Bougnoux et al. 2008)(Haque et al. 2018).

HCAIs occur in 7-10% of hospital admissions and are an increasing global problem (Khan et al. 2017a). Frequently, indwelling medical devices, such as endotracheal tubes, central venous catheters, urinary catheters and prosthetic heart valves contribute to HCAIs through supporting the formation of bacterial biofilms upon their surfaces (Table 1.1) (Behnia et al. 2014; Jamal et al. 2015; Gominet et al. 2017; Karkee et al. 2018). Infections arising from these medical devices include ventilator-associated pneumonia (VAP), catheter-related blood stream infections (CRBSI), catheter-associated urinary tract infections (CAUTIs) and endocarditis. Such device-related infections are a financial burden to health-care services and contribute to increased patient morbidity and mortality. In 2016/2017 an estimated 653,000 adult inpatients in NHS general and teaching hospitals in England acquired an HCAI, with an attributable cost of £2.1 billion (Guest et al. 2020).

**Table 1.1** Medical devices and bacteria commonly associated with biofilm formation on their surfaces

| **Medical Device** | **Biofilm-forming bacteria** | **References** |
|---|---|---|
| Urinary catheter | *Proteus mirabilis*, *E. coli*, *S. marcescens*, *P. stuartii*, *P. aeruginosa*, *S. aureus* | (Karkee et al. 2018) |
| Endotracheal tube | *P. aeruginosa*, *K. pneumoniae*, *S. aureus*, *Citrobacter* species, *Stenotrophomonas maltophilia* | (Behnia et al. 2014) |
| Dental implants | Gram-positive *cocci*, Gram-negative anaerobic oral bacteria, *Actinomyces* spp. | (Veerachamy et al. 2014) |
| Orthopaedic implants | *P. aeruginosa*, *S. aureus*, *S. epidermidis*, *E. coli* | (Arciola et al. 2015) |
| Central venous catheter | Coagulase-negative *staphylococci*, *S. aureus*, *S. epidermidis*, Gram-negative Bacilli | (Gominet et al. 2017) |
| Mechanical heart valves | *S. epidermidis*, Gram-negative Bacilli, *S. aureus*, *Streptococcus* species, *Enterococcus* species | (Jamal et al. 2015) |

## 1.2 Microbial biofilms

Biofilms are defined as matrix enclosed bacterial populations that are adherent to each other and/or to surfaces or interfaces and the vast majority of bacteria are found in biofilms (Costerton et al. 1995).

Biofilms can occur on biotic or abiotic surfaces and are commonly observed in natural aquatic environments, such as on substrata in lakes and riverbeds (Besemer 2015). In the clinical setting, biofilms are present on the surfaces of teeth (dental plaque), indwelling medical devices, prosthesis or within wounds (Figure 1.1) and account for 80% of microbial infections within the body (Veerachamy et al. 2014). However, attachment to a surface is not necessary, and biofilms can also be found floating on liquid surfaces. A study by Hsu *et al* demonstrated that *Legionella pneumophila* was detected in greater quantities in free-floating biofilms in natural springs than in attached biofilms (Hsu et al. 2011).

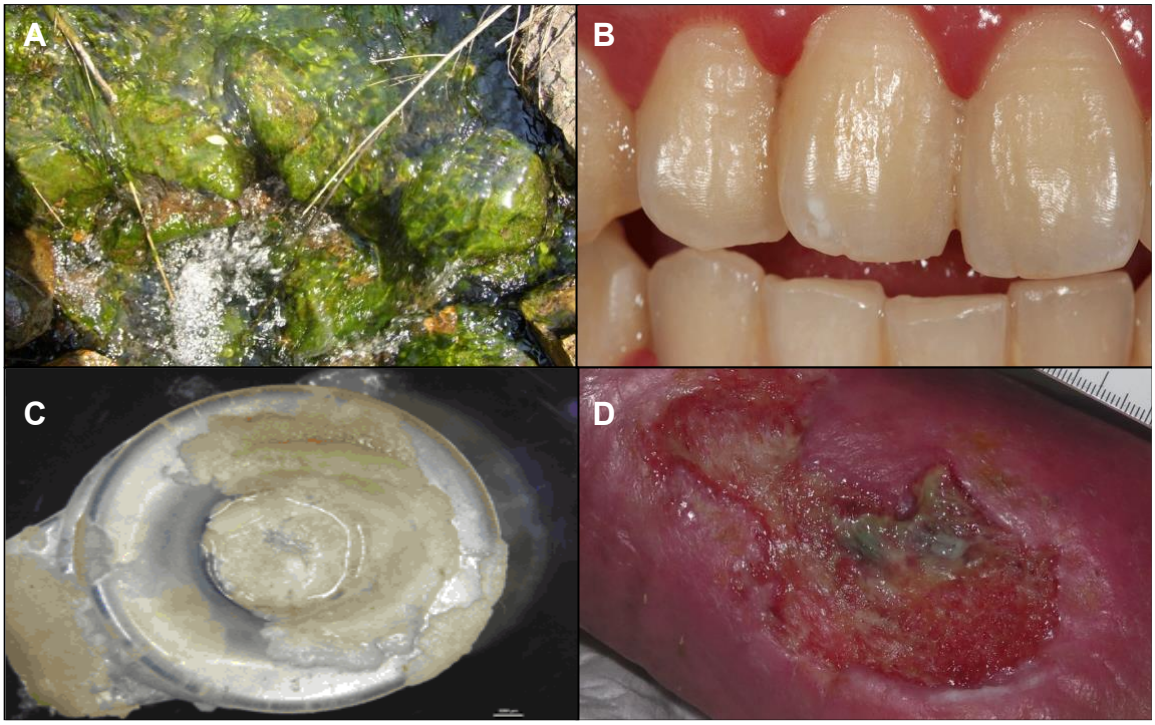


**Figure 1.1** Biofilm formation on various surfaces: (A) rocks in riverbeds, credit U.S Geological Survey (B) oral biofilms, credit Watanyou, Isostock photo (C) biofilm formation on a voice box prosthesis (Reproduced from Timmermans *et al.*, 2016 with permission from John Wiley & Sons) (D) biofilm within a wound, credit Dr Elena Conde

### 1.2.1 Biofilm structure and composition

A biofilm fundamentally consists of 3 layers, namely a conditioning film that coats the tissue or material surface, a base film containing microbes and an outer surface film that releases planktonic microorganisms into the surrounding area (Figure 1.2) (Veerachamy et al. 2014). The microbes within these sessile communities are genotypically and phenotypically distinct from their planktonic counterparts.

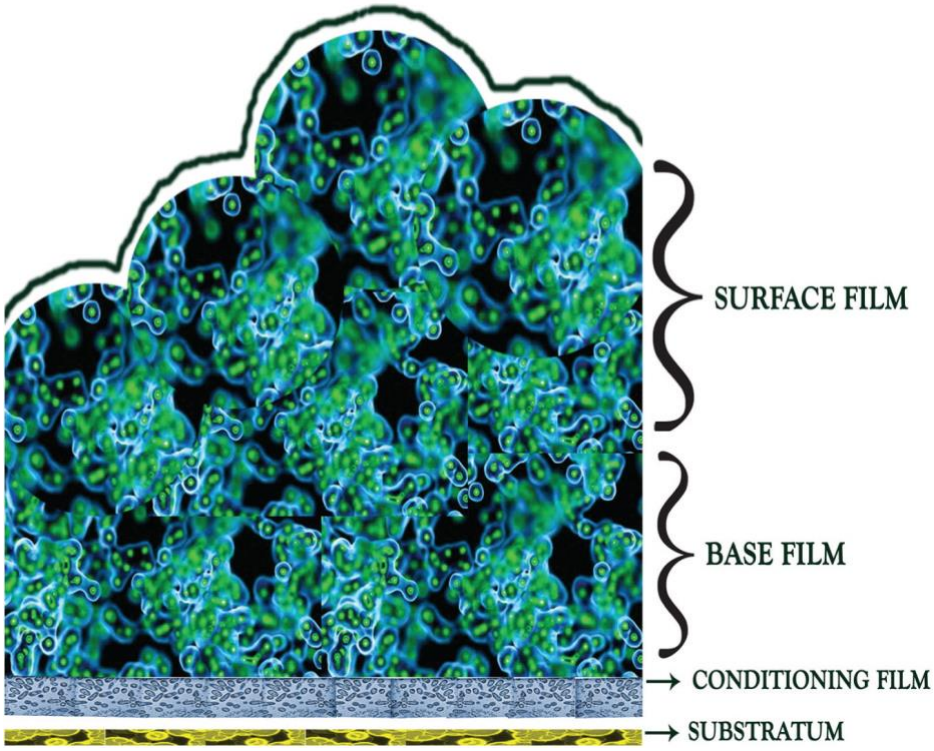


**Figure 1.2** A typical biofilm structure consisting of a conditioning film coating the substratum, a base film containing the bulk of the microbes and a surface film, where microbes can be released into the surrounding environment (Reproduced with permission from Veerachamy *et al.*, 2014)

Biofilms are highly organised 3D structures, with a network of water channels that allow for transportation of macromolecules and nutrients from the external environment to central regions of the structure, and also between areas of the biofilm. These channels also facilitate removal of waste products.

Planktonic or 'free swimming' bacteria can irreversibly attach to surfaces of medical devices including silicone or latex catheters and once attached, these microorganisms divide, form microcolonies and produce extracellular polymeric

substances (EPS) (Donlan 2001). EPS contribute to an insoluble, structured, ‘slimy’ matrix secreted by bacteria that encapsulates the cells.

The physical and chemical properties of EPS differ depending on the producing microorganism, the surrounding environment and available nutrients. Whilst EPS often consists largely of polysaccharides, the net charge of components will depend upon the ions present. Gram-negative bacteria produce polyanionic or neutral polysaccharides with uronic acids, such as glucuronic acid, galacturonic acid and mannuronic acid conferring negative charges (Donlan and Costerton 2002). Magnesium and calcium ions are also present and maintain the structural integrity of the biofilm by holding the polymers together (Vasudevan 2014). *Staphylococcus* species, including coagulase negative *Staphylococcus,* have biofilms consisting of cationic components, including teichoic acid and proteins (Donlan and Costerton 2002).

An important virulence factor in *Staphylococcus* biofilms is the polysaccharide intercellular adhesin (PIA), composed of β-1,6-linked N-acetylglucosamine and encoded by the *ica* operon. Biofilms of *S. aureus* and *S. epidermidis* are frequently recovered from implantable medical devices and studies of *ica* deficient mutants show growth attenuation (Cramton et al. 1999; Fluckiger et al. 2005), highlighting the role of PIA in *Staphylococcus* biofilms.

EPS often conveys a number of advantages to the underlying microbial cells. Charged EPS components can bind external nutrients required for cell growth and survival, and aid in cell dispersal from the biofilm. EPS may act as a protective barrier against external forces, as well as antimicrobials (Veerachamy et al. 2014). A significant proportion of the biofilm is composed of water (up to 97%), which promotes hydrogen bonding between the microbial cells enclosed within it (Jamal et al. 2015). Along with microbial cells and polysaccharides, small amounts of other components including proteins, lipids, DNA, RNA and ions are also present (Table 1.2).

**Table 1.2** Summary of biofilm EPS composition (adapted from Jamal *et al.*, 2015)

| Component | Percentage of matrix | Function | References |
|---|---|---|---|
| Water | Up to 97% | Promotes hydrogen bonding, dispersal of nutrients | (Jamal et al. 2015) |
| Microbial cells | 2-5 % | Proliferate | (Vasudevan 2014) |
| Polysaccharides | 1-2% | Adhesion, protection, structural integrity | (Limoli et al. 2015) |
| Proteins | <1-2% (includes enzymes) | Cell attachment, stability, degradation of matrix components | (Fong and Yildiz 2015) |
| DNA and RNA | <1-2% | Initial attachment, early biofilm formation | (Harmsen et al. 2010) |
| Ions | Bound and free | Cell attachment, structural stability | (Wang et al. 2019) |

Mixed species biofilms are normally encountered on environmentally exposed surfaces, whilst single species biofilms occur most frequently on surfaces of medical implants (O'Toole et al. 2000). Of note, is that as the duration of catheter use increases, multiple microorganisms become more frequently isolated (Holá et al. 2010).

### 1.2.2 Biofilm Formation

The microbiological composition of biofilms is dynamic, involving the continuous acquisition and loss of organisms. Biofilm formation occurs in distinct phases as detailed below.

#### 1.2.2.1 Adherence of planktonic bacteria to surfaces

Microbial adherence occurs in two sequential stages, referred to as reversible and irreversible attachment. Reversible attachment occurs immediately after planktonic bacteria are delivered to the solid surface via liquid flow or active motility (step 1, Figure 1.3). The surface is usually 'conditioned' by adsorption of various solutes and these components provide different surface properties to an unconditioned surface (Van Houdt and Michiels 2005). In the case of urinary catheters, a conditioning film consisting of components from the host urine are deposited, and these include proteins, electrolytes and other organic molecules (Trautner and Darouiche 2004). This film alters the surface of the catheter and can

neutralise any anti-adhesive properties (Gristina 1987). The first microorganisms to attach to surfaces are termed as primary colonisers and initial adherence of planktonic bacteria to the conditioning film is usually through hydrophobic or electrostatic interactions and weak Lifshitz Van der Waals (LW) forces between the bacterial cell surface and the substratum.

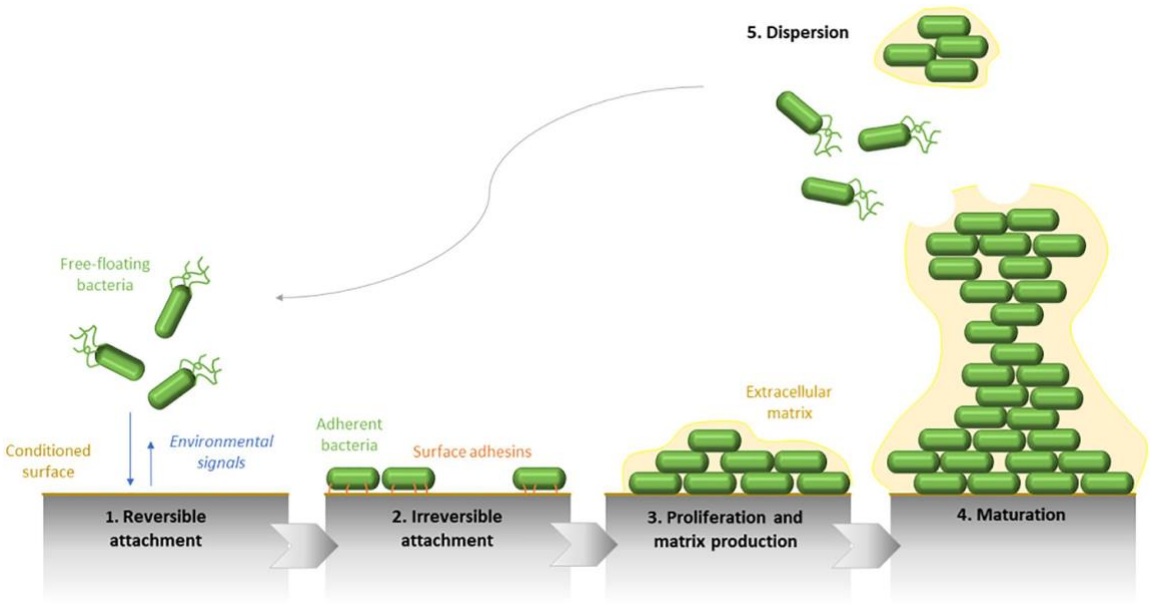


**Figure 1.3** The phases of biofilm formation © 2020 Olivares, Badel-Berchoux, Provot, Prévost, Bernardi and Jehl. Reproduced with permission (Olivares *et al.*, 2020)

Reversible attachment typically occurs soon after initial contact with the surface and can be influenced by surface properties of the substratum, with rougher and/or more hydrophobic surfaces lending themselves more favourably to attachment than smoother, more hydrophilic surfaces. Environmental factors, such as pH and temperature, can also influence these forces (Vasudevan 2014).

A number of models have been developed to predict bacterial attachment to surfaces, with the Derjaguin-Landau-Verwey-Overbeek (DLVO) and the extended DLVO models being the most widely recognised. The DLVO model determines the overall interaction energy between a microbial cell and a surface using electrostatic interactions (EL and LW forces as a function of the separation distance between the cell and the surface). EL are long-range forces between microbial cells and a surface and are influenced by a number of factors including

cell surface charge, substratum surface charge and the ionic strength of a liquid medium. However, numerous studies have concluded that the DVLO theory cannot be universally applied to all bacterial attachment situations and an extended DLVO model that takes hydrogen bonding and osmotic interactions into account was developed (Wang et al. 2015).

Irreversible attachment occurs via covalent interactions between surface receptors and adhesins on the surfaces of microorganisms (step 2, Figure 1.3). Type I fimbria, curli and conjugative pili play important roles in irreversible attachment of bacteria (Vasudevan 2014).

Type I fimbria are filamentous adhesins that occur on both pathogenic and commensal organisms. In the case of *E. coli*, between 100 and 500 fimbria are expressed on a bacterial cell surface and studies have shown an association between their presence and the virulence of the microorganism (Kaper et al. 2004). Fimbriae appear to play a role in both the early and later stages of biofilm formation.

Curli are thin, external proteinaceous appendages expressed by members of the *Enterobacteriaceae* family, including *E. coli*, *Shigella*, *Citrobacter* and *Enterobacter*. Curli adhere to extracellular matrix proteins, such as fibronectin, laminin and plasminogen, and contribute to the irreversible binding of microorganisms to surfaces. Curli also plays a role in cell to cell interactions (Vasudevan 2014).

#### 1.2.2.2 Biofilm maturation

Following growth and division of primary colonisers, microcolonies develop and merge to form a layer of cells covering the substratum (Figure 1.3). As the layers of cells expand, mushroom-shaped macro-colonies (or stacks) surrounded by water channels are formed (step 4, Figure 1.3). The dispersal of nutrients and signalling molecules via these channels aid biofilm survival (Dufour et al. 2012).

The biofilm maturation phase is also characterised by the self-production of EPS. In response to mechanical stress, EPS production can be increased to provide a strengthened structural matrix (Flemming and Wingender 2010).

#### 1.2.2.3 Detachment of the biofilm cells

Cells may 'slough away' from the established biofilm due to a number of factors, including limited nutrient supply (Figure 1.3). Single bacterial cells are able to revert back to the planktonic state, becoming motile and released to seek out a fresh nutrient supply (O'Toole et al. 2000).

Detachment can be divided into both active and passive mechanisms. Active detachment mechanisms are initiated by the bacterial cells, such as enzymatic degradation of the biofilm matrix and quorum sensing (QS) (Soto 2013). Overexpression of alginate lyase may contribute to an increased detachment rate in the clinically resistant microorganism, *P. aeruginosa*, representing an active detachment mechanism. Detachment by external forces, such as fluid shear, abrasion and human intervention, represent passive detachment mechanisms (Soto 2013).

### 1.2.3 Quorum sensing

A method of intercellular communication, termed quorum sensing (QS), occurs in biofilms. QS is defined as a cell-density dependent, bacterial intercellular signalling mechanism that enables bacteria to co-ordinate group behaviour (Dufour et al. 2012). QS was first described in *Vibrio fischeri*, a bioluminescent marine bacterium that exists in symbiotic relationships with marine animals. In exchange for nutrients, the bacteria generate bioluminescence to attract prey, avoid predators and find mates. However, bioluminescence only occurs once the bacteria have reached a critical density, controlled by QS. The ability of bacteria to communicate and behave as a group is advantageous, aiding host colonisation, biofilm development, defence against competitors and adaptation to changing environments (Li and Tian 2012).

Cells are able to communicate with one another using diffusible signal molecules (auto inducers) released by bacteria. Using this mechanism, bacteria can regulate gene expression to respond to variations in population density, and thus coordinate behaviour to elicit appropriate responses (Dufour et al. 2012).

Both intra and inter-species QS communication methods exist. Intra-species communication between Gram-negative bacteria usually uses acyl homoserine lactones (AHLs) as auto-inducers that are produced by AHL synthases, while small oligopeptides, auto-inducing peptides (AIPs), mediate communication

between Gram-positive bacteria (Figure 1.4). AHLs diffuse across the cell membrane and increase in concentration in proportion to cell density (Li and Tian 2012). Within Gram-positive bacteria, AIPs are produced as pro-peptides within the intracellular compartment, processed by endopeptidases and subsequently secreted from the cell as mature AIPs (Ivanova et al. 2013).

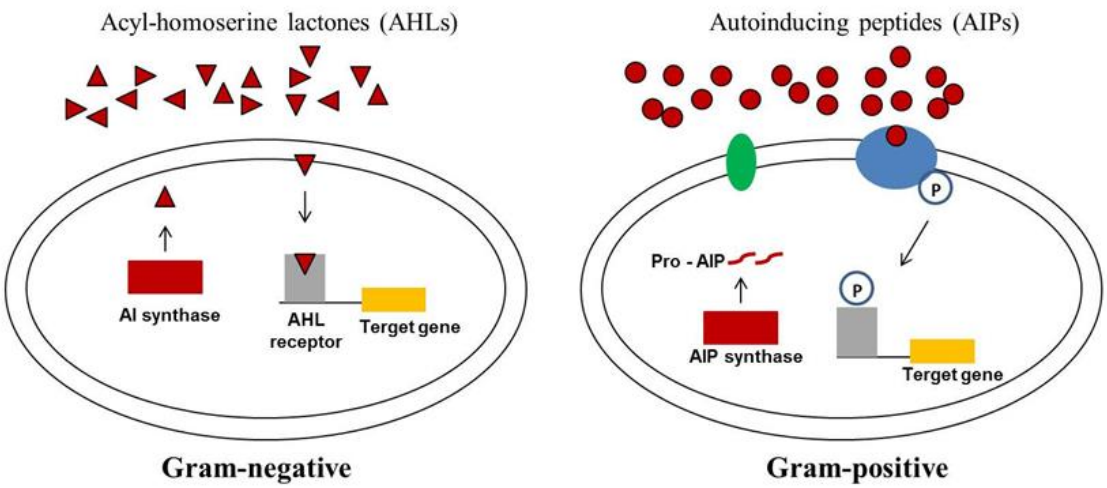


**Figure 1.4** Quorum sensing mechanisms of Gram-negative and Gram-positive bacteria. Gram-negative bacteria secrete AHLs (red triangles), which initiate responses to cells upon reaching a critical concentration threshold. Activation of the AHL receptor induces QS regulated gene expression. Gram positive bacteria produce mature AIPs (red circles), that interact with transmembrane receptors to activate gene expression via autophosphorylation of the transcriptional regulator (Ivanova et al. 2013)

Auto-inducer 2 (AI-2), a furanosyl borate diester, is a QS molecule for inter-species communication. The gene encoding AI-2, *lux S*, occurs in a wide variety of Gram-negative and Gram-positive bacteria and is therefore often regarded as a universal signalling molecule for inter-species communication.

Activities linked to QS have been implicated in the virulence and pathogenic potential of bacteria (Dong et al. 2001; Lin et al. 2003). Therefore, understanding and inhibiting QS could lead to the development of new antimicrobial therapies.

### 1.2.4 Antimicrobial resistance

Biofilm embedded microorganisms have increased resistance to antimicrobials, with studies showing such cells to be up to 1000-fold more resistant than their planktonic counterparts, due to numerous mechanisms (Potera 2010). Common resistance mechanisms of bacterial biofilms are listed in Table 1.3.

**Table 1.3** Examples of bacterial biofilm resistance mechanisms

| Resistance mechanism | Description and Examples | References |
|---|---|---|
| Extracellular polymeric substance (EPS) | • Delays or prevents diffusion of antimicrobials<br>• Binds cationic substances due to negative charge<br>• Binds positively charged antibiotics | (Davenport et al. 2014) |
| Efflux pumps | • Decreased accumulation of antimicrobials e.g., ACRAB-TolC pump in *E. coli* | (Piddock 2006; Soto 2013) |
| Transmission of resistance genes | • Conjunctive pili can aid horizontal gene transfer<br>• Transfer of drug-resistant plasmids | (Madsen et al. 2012; Król et al. 2013) |
| Persister cells | • Dormant cells survive antibiotic attack and repopulate e.g., infections associated with cystic fibrosis | (Lewis 2010) |

The EPS matrix can physically hinder diffusion of antimicrobial compounds through the biofilm to limit access to cells, or diffusion can be delayed resulting in the time taken for antibiotic diffusion to be longer than the treatment time. The negatively charged EPS matrix is also able to bind cationic heavy metals and positively charged antibiotics, such as aminoglycosides, to prevent or delay penetration through the biofilm. Uncharged antibiotics, such as β-lactams, will remain unbound and are able to diffuse more rapidly through the biofilm (Davenport et al. 2014). Antibiotics that are able to diffuse may also be inactivated due to pH changes within the biofilm structure (Thomas et al. 2012). Importantly, the EPS layer can also prevent large components of the host immune system from reaching microbes within the biofilm. The EPS components are able to protect

microbes against phagocytosis, protect from cationic antimicrobial peptides and prevent recognition by antibodies (de Vor et al. 2020).

Transmission of resistance genes between biofilm cells can occur via plasmids and transposons, and represents an additional benefit of biofilms for resistance as the microorganisms are located in close proximity to each other (Król et al. 2013). Conjunctive pili, also known as 'sex pili', are hair-like appendages of 6-7 nm diameter and can aid horizontal gene transfer between bacteria. Pili of a donor bacterium can 'catch' a recipient cell, form a pore and subsequently form a conjugation bridge to allow the transfer of DNA from the donor to recipient. Although the genes that form pili are often those transferred, other genes can be co-transferred allowing for genetic traits to be disseminated throughout a bacterial population. Genes involved in antibiotic resistance may be transferred throughout a biofilm using this method (Madsen et al. 2012). Conjugation is possible between bacteria of different species and the cell-to-cell contacts aid in stabilisation of the biofilm.

Antimicrobial resistance (AMR) of biofilms may also be aided by increased expression of efflux pumps, and this is a key mechanism employed by Gram-negative bacteria. Clinical isolates of *E. coli* have been shown to overexpress a well-characterised efflux pump (ACRAB-TolC system), that exports chloramphenicol, fluoroquinolones, fusidic acid, rifampicin and tetracycline amongst others. The genes encoding this efflux pump are upregulated during exposure to certain antibiotics (Soto 2013). Such efflux pumps also have an important role in biofilm formation, and aid colonisation and persistence of bacteria within the host (Piddock 2006).

In biofilms, it is evident that there are subpopulations of cells that prevent complete eradication by antibiotic compounds (Figure 1.5). These 'persister cells' are dormant, non-dividing variants of regular microbial cells and are key players in recalcitrance of chronic infections, such as cystic fibrosis (CF). In CF infections, high antibiotic doses may be administered periodically, allowing selection of high persister (*hip*) mutants (Lewis 2010). Along with components of the immune system, antibiotic therapy is able to eradicate the majority of the bacterial population, but persister cells survive due to antibiotic compounds requiring active cells to target. Once the level of antibiotic is lowered, persister cells are able to repopulate the biofilm and the infection can be re-established (Lewis 2010).

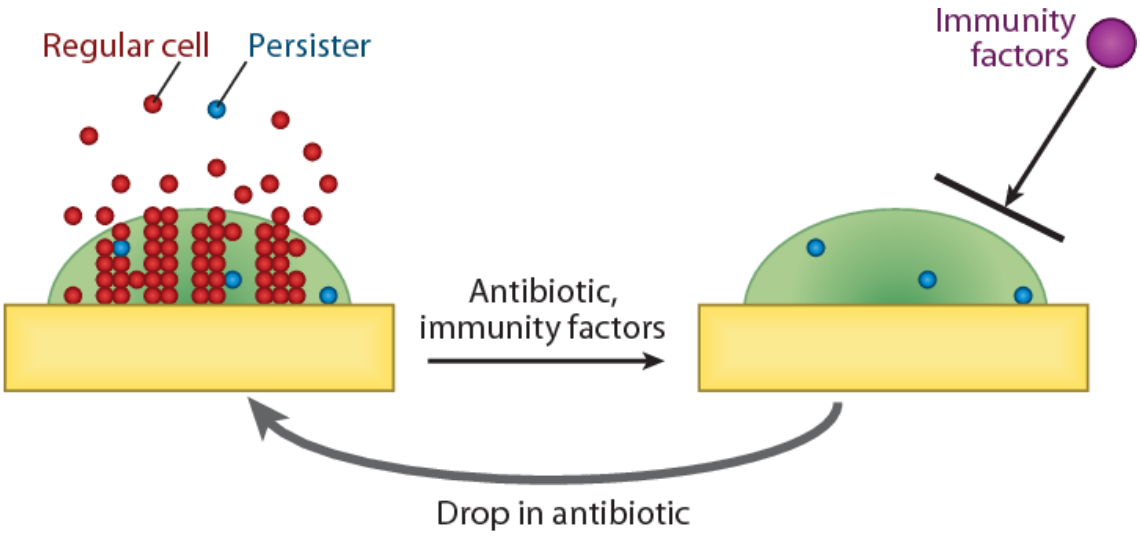


**Figure 1.5** Persister cells within biofilm populations allow microbes to repopulate and re-establish infections following eradication of regular cells by antibiotic treatment and the host immune system (Reproduced with permission from Lewis, 2010)

### 1.3 Catheter-associated urinary tract infections (CAUTIs)

In healthcare settings, reliance on in-dwelling urinary catheters in immobile or otherwise incontinent patients is a primary cause for large numbers of catheter-associated urinary tract infections (CAUTIs), resulting in a significant economic burden to the NHS in the UK. CAUTIs are associated with increased mortality and length of hospital stay in critically ill patients. A study of device-associated infection rates in Ecuadorian intensive care units showed CAUTIs to contribute to 9.2 excess hospital days and 17.6% crude mortality (Salgado Yepez et al. 2017). The financial burden to the NHS through additional bed days and treatment costs associated with CAUTIs has been estimated at £99 million per annum and £1,968 per episode of infection (Loveday et al. 2014).

#### 1.3.1 The urinary catheter

Urinary catheters have been used since 1500 BC to alleviate urinary retention. Early versions were of rigid design and only used for intermittent catheterisation. The invention of a flexible latex catheter by Frederic Foley in the 1930s permitted urinary catheters to remain *in-situ* for long periods to aid management of

incontinence and the problem of urinary retention. To overcome cytotoxicity issues associated with latex Foley catheters, silicone elastomers were subsequently used to coat the latex catheters. Currently, most catheters are made entirely of silicone elastomers with hydrophilic coatings to reduce friction during insertion (Feneley et al. 2015) (Figure 1.6).

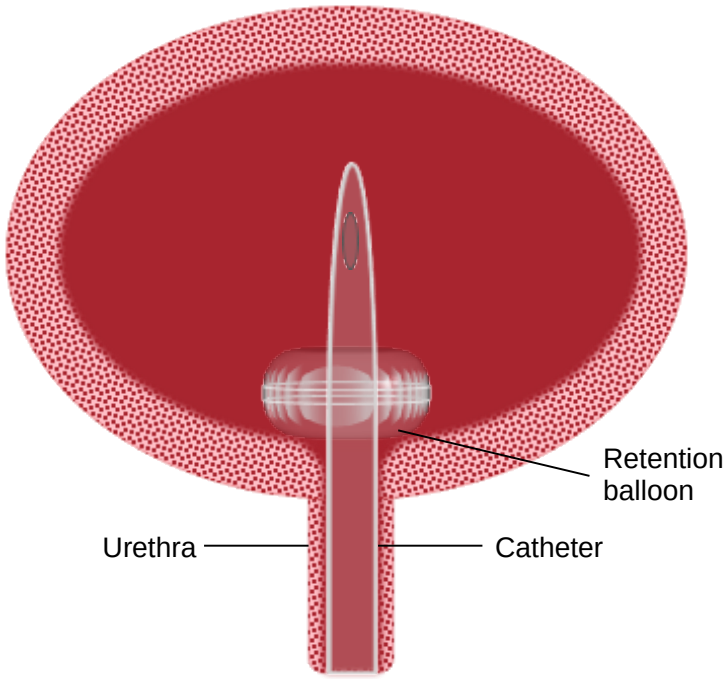


**Figure 1.6** Schematic of an inflated Foley catheter within a bladder

The sterile flexible latex or silicone tube is aseptically inserted into the bladder, via the urethra, and the retention balloon is inflated via the inlet port using a fixed volume of sterile liquid (Figure 1.7). The balloon holds the catheter in place to prevent movement of the device and leakage of urine. The bladder retains urine until reaching a level above the catheter eye-hole, when drainage of urine occurs via the catheter lumen to a drainage bag. However, the volume of urine below the catheter eye-hole is retained, leading to difficulties in complete eradication of any infection. Within this system, the flow of urine is unable to provide the required mechanical forces to flush away microorganisms in the catheter lumen, leading to establishment of bacterial biofilms along the device.

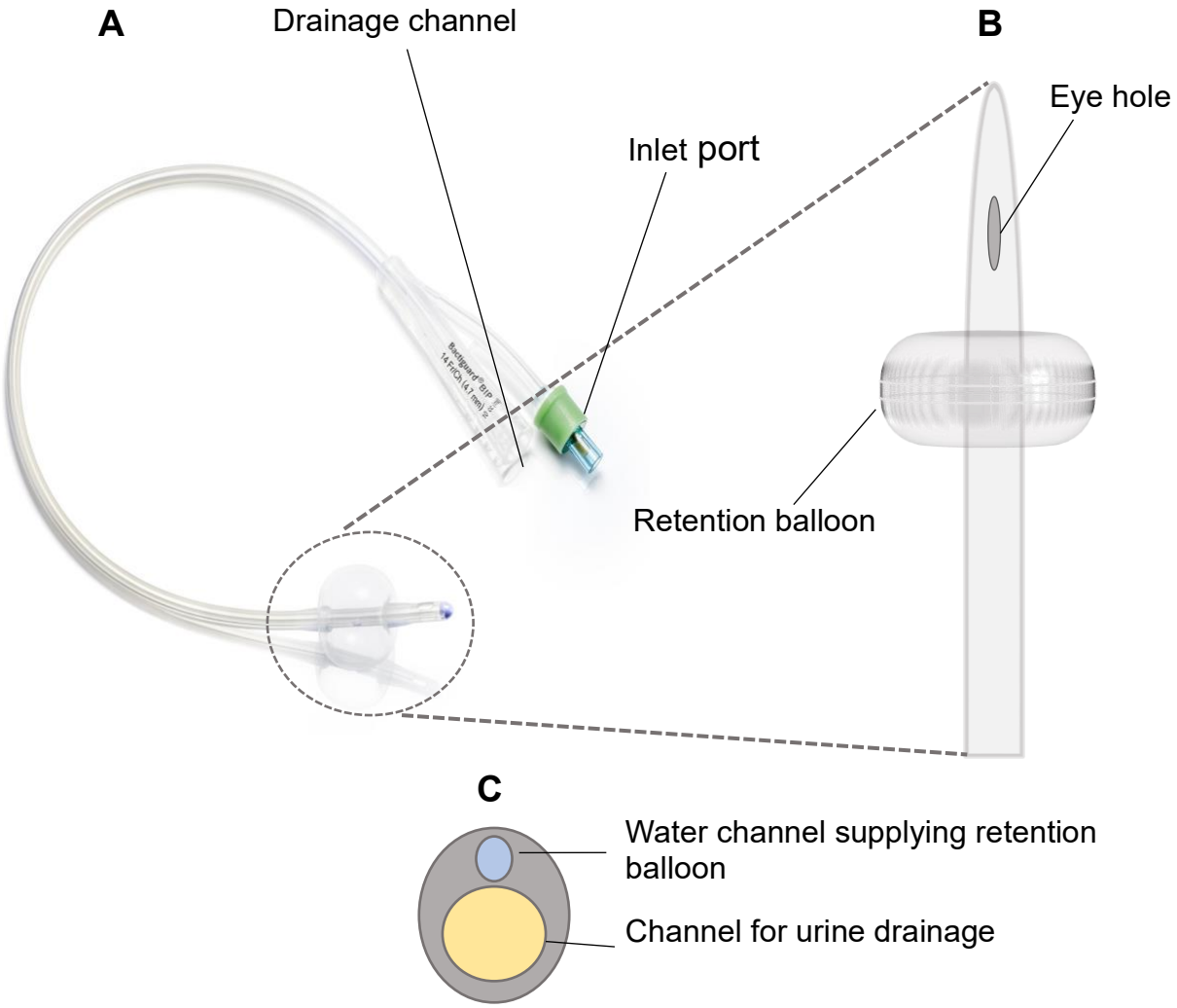


**Figure 1.7** (A) Schematic of a silicone Foley catheter (B) catheter tip showing the eye-hole and inflated retention balloon (C) cross-sectional diagram of a Foley catheter showing the inlet channel for inflation of the retention balloon and the urine drainage channel

Urinary catheters may be short term indwelling, long term indwelling or intermittent (Table 1.4). Short term catheterisation is defined as the use of a catheter for a period of less than 30 days and long term when periods extend beyond this. Intermittent catheterisation is where catheters do not remain *in situ,* but are used multiple times daily to drain the bladder and are often self-administered (Nicolle 2015).

**Table 1.4** Types of catheter use and frequency of urinary infection in catheterised populations

| Catheter | Usual Population | Infection Rate |
|---|---|---|
| **Indwelling Urethral** | | |
| **Short term** | Medical facilities<br>Urine output monitoring<br>Postsurgical<br>Acute urinary retention | 5% per day Women > men |
| **Long term** | Long-term care: 5%–10% of residents<br>Chronic urinary retention – men<br>Incontinence – women | 100% prevalence |
| **Intermittent catheter** | Neurogenic bladder<br>Spinal cord injury<br>Multiple sclerosis<br>Other impaired bladder emptying | 1%–3% per catheterisation |

### 1.3.2 Epidemiology

Approximately 40% of HCAIs are attributed to UTIs, with 80% of these relating to catheter use (Maki and Tambyah 2001). In intensive care settings, 97% of all UTIs are associated with a urinary catheter (Richards et al. 1999). It is also estimated that indwelling catheters are placed in 25% of all hospital patients (Haley et al. 1985). A study of 35,904 patients found that 85% of surgical patients had an indwelling catheter, with 50% of these remaining beyond 48 h (Wald *et al.*, 2008). A reported 5.4 - 7.5% of nursing home residents across the USA and Europe have long-term indwelling catheters *in-situ*, often for relief of urinary retention, with an increased usage in men compared to women. A study of 166 nursing home residents with indwelling urinary catheters, recorded a total of 17,525 catheter days, averaging 105 days per resident (Davis 2019).

### 1.3.3 Mechanisms of bladder contamination in the catheterised patient

Urinary catheters facilitate entry of bacteria into the bladder in a number of ways, via extra- or intra-luminal routes. It is estimated that 66% of CAUTIs originate from extra-luminal contamination, with 34% occurring intra-luminally (Tambyah et al. 1999).

Contamination of the bladder may occur during catheter insertion, often from microbial species from the perineum and urethral meatus, and these are likely to be of faecal origin (Daifuku and Stamm 1984). The microorganisms ascend along

the external surface of the catheter and into the bladder (Tambyah et al. 1999). Intraluminal contamination occurs through ascent of microorganisms from contaminated drainage bags or catheters. The junction between the catheter and drainage bag, along with the drainage port of the drainage bag, are entry points for microorganisms. Once in the bladder, microorganisms proliferate in the retained volume of urine, leading to the establishment of a catheter-associated urinary tract infection.

A shorter urethra in females, compared to males, is thought to account for increased CAUTI prevalence in women. A study of 200 patients with indwelling urinary catheters admitted to the medical care unit, gynaecology ward or surgical intensive care unit in an Indian hospital, showed increased CAUTI incidence amongst female (42.23%) compared to male (23.63%) patients (Dund, Durani and Ninama, 2015).

### 1.3.4 Symptomatic features of CAUTIs

A long-term indwelling catheter is a significant factor in development of both symptomatic and asymptomatic UTIs. CAUTI is a symptomatic UTI established with a current or recently removed in-dwelling catheter. Catheter-associated asymptomatic bacteriuria (CAASB) is the term used to describe urine containing significant numbers of bacteria, without symptoms of infection. Although CAASB is more common than CAUTI, the term CAUTI is often adopted to describe any positive urine culture associated with catheter use (Hooton *et al.*, 2010).

UTIs are classed either as complicated or uncomplicated. An uncomplicated UTI typically occurs in an otherwise healthy individual, without any structural or neurological abnormalities of the urinary system. Uncomplicated UTIs can be lower (bladder, termed cystitis) or upper (kidney, termed pyelonephritis) infections (Hooton, 2012). Factors that compromise the urinary tract or alter the host defence mechanisms that lead to UTIs, are complicated UTIs. These factors include urinary obstruction, urinary retention due to neurological disease, renal failure, renal transplantation, immunosuppression, pregnancy and the presence of an indwelling catheter (Lichtenberger and Hooton, 2008). In the USA, 70-80% of complicated UTIs are attributed to indwelling catheter usage (Lo *et al.*, 2014).

Symptoms of CAUTIs include fever, suprapubic tenderness, flank tenderness, tachycardia and delirium. In the elderly, some common symptoms may be absent,

due to the inability of the immune system to elicit an effective response to infection. Such patients may present with behavioural changes, such as agitation, confusion/delirium, dizziness and loss of appetite. Blood in the urine (haematuria), foul smelling, discoloured or cloudy urine and catheter obstruction are also indicators of catheter associated infection (Davis 2019).

In cases where a CAUTI goes undiagnosed or measures to prevent advancement of the infection are unsuccessful, sepsis and eventually death may occur. Between 2016-1017, 1,467 deaths were directly attributed to CAUTIs across English NHS Trusts (Smith et al. 2019).

### 1.3.5 CAUTI diagnosis

Diagnosis of CAUTIs requires collection and culture of urine, performed in an aseptic manner and before commencement of antimicrobial therapy. Collection of urine can occur at the time of catheterisation for patients who require intermittent catheterisation, or directly after the placement of a new device for patients with long-term, indwelling catheters.

Asymptomatic patients with bacterial counts of $\geq 10^5$ colony forming units (CFU)/ml can be diagnosed with a CAUTI. In instances where patients present with lower urinary tract symptoms, a count of $\geq 10^2$ CFU/ml is the threshold for positive diagnosis. This figure is elevated to $\geq 10^4$ CFU/ml for patients presenting with systemic symptoms (Table 1.5, Nicolle, 2015).

**Table 1.5** Microbiologic diagnosis of urinary infection associated with catheter usage (Nicolle 2015)

| **Clinical Presentation** | **Bacteria count** |
|---|---|
| **Asymptomatic** | $\geq 10^5$ CFU/ml single |
| **Symptomatic**<br>Lower tract symptoms[a]<br>Systemic symptoms | <br>$\geq 10^2$ CFU/ml<br>$\geq 10^4$ CFU/ml |
| [a] Usually subjects with intermittent catheterisation. | |

### 1.3.6 Microorganisms commonly associated with CAUTIs

Microorganisms that make up the intestinal microflora are largely responsible for CAUTIs and mostly consist of Gram-negative bacterial species. The most prevalent of these, *E. coli* accounts for 30-40% of all bacteria isolated from the urine of catheterised patients (Table 1.6). Other bacterial genera commonly isolated include *Klebsiella*, *Proteus*, *Enterobacter* and *Enterococcus*. A comparison of 4 studies showed that *Klebsiella* species were the second most prevalent bacteria isolated from urine cultures in 3 of the studies and had a detection rate of 13 - 21.8% across all 4 studies (Table 1.6).

**Table 1.6** Microorganisms isolated from the urine of patients undergoing long-term catheterisation

| | | **Study** | | | |
|---|---|---|---|---|---|
| | | (Dund JV, Durani K, Ninama RD 2015) | (Mahmoud Ahmed Abdallah et al. 2011) | (Karkee et al. 2018) | (Bagchi, Jaitly 2013) |
| **Microorganism** | **Gram -ve/+ve** | **% of bacterial isolates** | | | |
| ***E. coli*** | - | 40.06 | 23 | 35.30 | 34.85 |
| ***Klebsiella*** | - | 21.80 | 13 | 17.65 | 19.70 |
| ***Pseudomonas*** | - | 10.93 | 10 | 11.67 | 12.12 |
| ***Enterococcus*** | + | 7.81 | 17 | 17.65 | 6.06 |
| ***Proteus*** | - | 6.25 | 10 | 5.89 | 3.03 |
| ***Staphylococcus aureus*** | + | 4.68 | 10 | 5.89 | 4.55 |
| ***Acinetobacter*** | - | 7.81 | - | - | - |
| ***Enterobacter*** | - | - | - | 5.89 | - |
| **Coagulase -ve *Streptococcus*** | - | - | 10 | - | - |

Species that persist in the environment or colonise the skin are also commonly isolated from the urine of patients undergoing long-term catheterisation. Such bacterial genera include *Pseudomonas*, *Providencia*, *Serratia* and *Staphylococcus* including coagulase-negative *Staphylococcus* and *Acinetobacter*.

From the list of bacteria associated with CAUTI, it is evident that many are ESKAPE pathogens (*Enterococcus faecium*, *Staphylococcus aureus*, K*lebsiella pneumoniae*, *Acinetobacter baumannii*, *Pseudomonas aeruginosa* and *Enterobacter* species). ESKAPE are a group of bacteria that are highly resistant to antibiotics and globally are leading causes of HCAIs, with high incidences of morbidity and mortality (Santajit and Indrawattana 2016).

*Candida*, a commensal yeast found on the skin, in the oral cavity and digestive tract, has also been implicated in CAUTIs. A study of catheterised patients in a French ICU showed the mean onset of candiduria was 17 days, with the organism deemed a late coloniser (Bougnoux et al. 2008) . However, in 2015, the Centre for Disease Control and Prevention (CDC) excluded candiduria from the definition of CAUTIs (Saran et al. 2018).

Although *Proteus* species are not the leading cause of UTIs, due to its high urease activity *P. mirabilis* is almost solely responsible for catheter encrustation and blockage in patients with long-term, indwelling catheters (Stickler et al. 1993).

#### 1.3.6.1 Urease producing microorganisms

*Proteus mirabilis* is a urease producing bacteria and responsible for over 80% of catheter obstructions in long-term indwelling catheters (Jacobsen et al., 2008). Other urease producing species isolated from catheter biofilms, include *P. aeruginosa*, *K. pneumoniae*, *M. morganii*, other *Proteus* species (*e.g., P. vulgaris)*, certain species of *Providencia*, some strains of *S. aureus* and coagulase-negative *Staphylococci* (Jordan and Nicolle, 2014).

In the case of urinary catheter biofilms containing urease positive microorganisms, urease-mediated hydrolysis of urea leads to generation of ammonia (Stickler and Morgan, 2008). Urease produced by *P. mirabilis* is extremely efficient and generates ammonia faster than other species (Jones and Mobley, 1987).

$$(NH_2)2CO + 3H_2O \xrightarrow{\textbf{UREASE}} CO_2 + 2NH_4OH$$

Urinary pH rises due to ammonia presence, and this creates conditions that allow microcrystalline structures of hydroxylated calcium phosphate (apatite) and long

rectangular crystals of magnesium ammonium phosphate (struvite) to develop (Jacobsen and Shirtliff, 2011). The crystalline biofilm encrusts and blocks the catheter lumen and eye-hole (Figure 1.8), leading to urinary retention and ultimately reflux of infected urine to the upper urinary tract, causing serious clinical complications such as pyelonephritis, septicaemia and shock (Stickler, 2008).

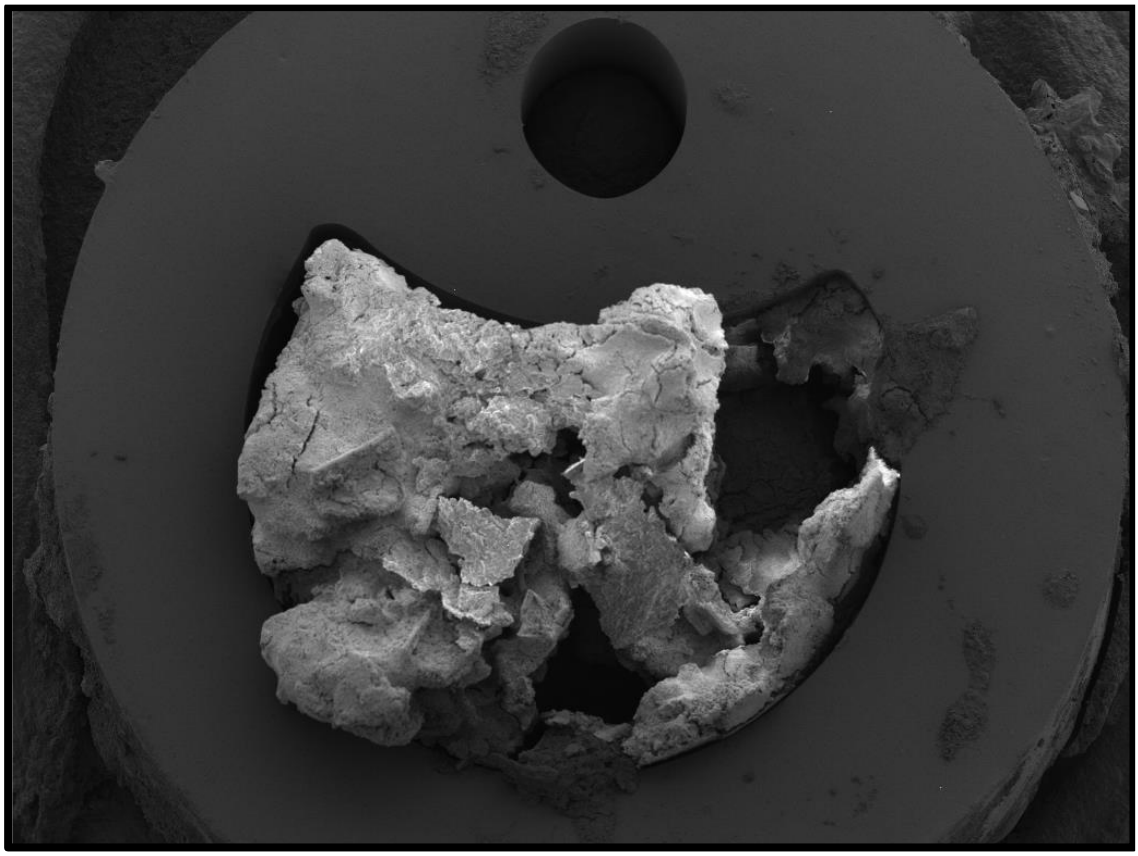

**Figure 1.8** Blockage of a urinary catheter by struvite and apatite due to *P. mirabilis* infection

The pH at which the salts crystallise is termed the nucleation pH ($pH_{(n)}$) and attempts have been made to manipulate it in numerous ways. Using an *in-vitro* bladder model, Stickler *et al* diluted artificial urine with water, whilst also increasing the flow rate through the bladder chamber leading to an increase in $pH_{(n)}$ from 6.7 to 7.5. This approach delayed encrustation and blockage of the urinary catheter to 110-137 h from 19-31 h. Additionally, supplementation of the artificial urine with 1.5 mg/ml citrate increased the $pH_{(n)}$ to 8.3-9.1 allowing the urine to drain freely for 7 days (Stickler and Morgan 2006).

*Proteus mirabilis* is a late coloniser of urinary catheters, and patients undergoing short-term catheterisation are often unaffected by catheter blockage (Matsukawa

et al., 2005). As the duration of catheterisation increases, the greater the likelihood of isolating *P. mirabilis* from the urine and catheter biofilm.

Almost a third of all urinary tract stones are attributed to *P. mirabilis* infection, with 62% of patients with recurrent *P. mirabilis* catheter encrustation developing bladder stones (Sabbubba et al., 2004). Mathur *et al*., 2005 isolated genotypically identical *P. mirabilis* from catheter biofilms and faecal matter of the same patients, revealing the faecal microflora from the gastrointestinal tract was the likely source of *P. mirabilis* contamination.

Whist the ability of *P. mirabilis* to cause encrustation of urinary catheters is linked to urease production, it also possesses other virulence attributes to promote infection. These include an ability to initially colonise and travel over the catheter surface through swarming motility. Small swimming bacilli arrange themselves into multicellular, elongated rafts of hyperflagellated swarmer cells that are able to migrate across surfaces of inert medical devices, including urinary catheters and into the bladder, an important step in the pathogenesis of CAUTIs (Figure 1.9). These swarmer cells also produce more urease than their single cellular counterparts, further promoting the encrustation of urinary catheters (Jordan and Nicolle 2014).

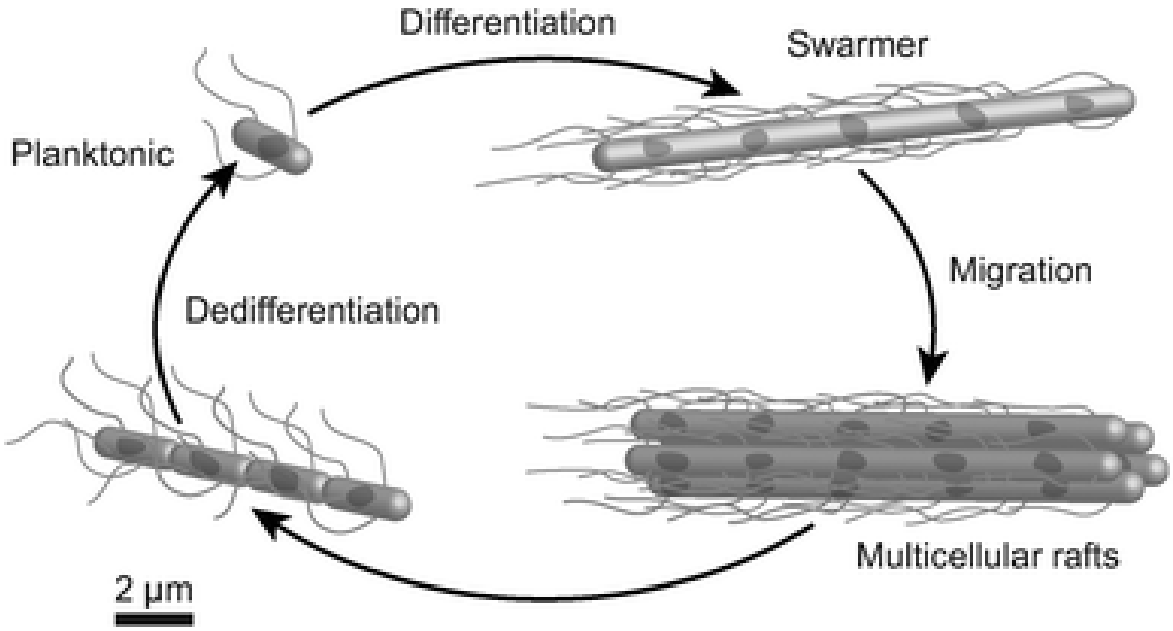


**Figure 1.9** The general life cycle of motile cells of bacteria as they swarm on surfaces. The length of the flagella (in relation to the length of cells) and the number of flagella per swarmer cell has been reduced for clarity. The spots depict the bacterial chromosome. The scale bar is an approximate estimate of dimensions, (Copeland and Weibel 2009)

Progression of planktonic cells to swarmer cells involves cellular elongation into multinucleated filaments and an increase in the density of flagella on cell surfaces (Figure 1.9). A cell density threshold is believed to exist, beyond which the cells are able to move collectively. Experimental data suggests a threshold of $1 \times 10^3$ $/\mu m^{-2}$ is required for *P. mirabilis* cells to differentiate into the swarmer phenotype. The water content of the substrate is also believed to be a factor in the initiation of swarming motility. Multicellular rafts are then able to move rapidly across a surface to seek out fresh nutrient supplies, before separation into single filaments and ultimately back to the planktonic phenotype. The addition of water to a swarmer colony appears to promote this change with dispersion of single cells back into the fluid (Copeland and Weibel 2009).

## 1.4 Biofilm prevention and eradication

For medical devices, biofilm eradication and prevention strategies are currently aimed at inhibiting initial colonisation of devices, minimising microbial cell attachment to the device, promoting penetration of the biofilm matrix to kill associated cells and finally, where possible, device removal. Future treatments may be directed at inhibition of genes involved in cell attachment and biofilm formation (Donlan and Costerton 2002). A review of current strategies to prevent biofilm or eradicate urinary catheter biofilms is provided below.

### 1.4.1 Antimicrobial urinary catheters

The inert and biocompatible properties of silicone have led it to become the material of choice for urinary catheter manufacture. Silicone rubber is also an attractive surface for colonisation by microorganisms and the prevention of biofilm formation on such surfaces is a challenge faced by healthcare providers and scientists. The relative ease of modifying silicone surfaces with antimicrobial coatings has enabled the development of commercially available catheters with antimicrobial properties (Table 1.7). Such surfaces commonly use methods to prevent fouling of the silicone surface or the release of biocidal agents (Figure 1.10) (Singha, Locklin and Handa, 2017). However, these catheters have challenges and disadvantages associated with their use, as described below.

**Table 1.7** Composition of some commercially available Foley catheters

| **Material** | **Coating** | **Product name** | **Company** | **Studies investigating usage** |
|---|---|---|---|---|
| Latex | Silver alloy /hydrogel | BARDEX® I.C | BARD Medical | (Morris et al. 1997; Verleyen et al. 1999) |
| Silicone | | BARD® All Silicone | BARD Medical | (Morris et al. 1997; Sabbuba et al. 2002) |
| Latex | Hydrogel | BIOCATH® | BARD Medical | (Morris et al. 1997; Sabbuba et al. 2002) |
| Silicone | Hydrogel | BARD® LUBRI-SIL® | BARD Medical | (Srinivasan et al. 2006) |
| Latex | Silicone elastomer | | BARD Medical | (Sabbuba et al. 2002) |
| Latex | Polytetrafluoroethylene | BARDEX® | BARD Medical | (Pickard et al. 2012) |
| Silicone | Silver/ hydrogel | Dover™ | Covidien | (Sabbuba et al. 2002) |

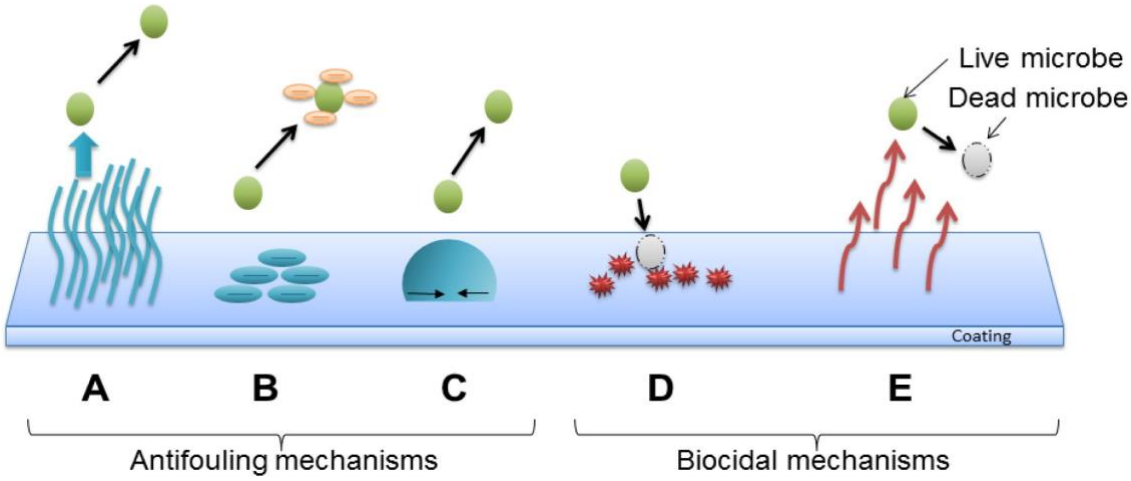


**Figure 1.10** Antimicrobial mechanisms: (A) Exclusion steric repulsion, (B) Polymer surface coatings act as a physical barrier to prevent cell attachment, (C) Low surface energy to reduce microbial adhesion, (D) Release of biocidal agents to kill microbes, (E) Contact-active: microbes are killed upon contact with the surface (Reproduced from Singha, Locklin and Handa, 2017 with permission from Elsevier)

#### 1.4.1.1 Surface coatings to prevent microbial attachment

A number of antifouling coatings have been developed aimed at preventing the initial attachment events of microorganisms to device surfaces and these are discussed below.

##### 1.4.1.1.1.Hydrogels

Hydrogels are insoluble, hydrophilic polymers with the capacity to swell and retain water up to 99% of its total volume. Such hydrogels also display solid-like properties, which imparts mechanical strength. Once swollen, a hydrogel-coated catheter forms a hydration layer upon the catheter surface, increasing hydrophilicity and creating a barrier to non-specific protein adsorption.

Clinical trials of hydrogel-coated catheters have yielded mixed results. A trial of catheterised men with a mean catheterisation duration of 2.2 days, compared siliconised latex, pure silicone and hydrogel-coated silicone catheters. The hydrogel-coated catheters reduced catheter encrustation, whilst pure silicone

catheters completely prevented encrustation and showed the lowest incidence of urethral inflammation (Talja et al. 1990).

An additional study by Chene *et al* found no difference in the occurrence of healthcare associated CAUTI between those catheterised with silicone-coated and hydrogel-coated catheters (Chene et al. 1990). Using an *in-vitro* bladder model of *P. mirabilis* infection, hydrogel coated catheters were found to increase the rate of catheter encrustation and blockage (Kazmierska et al. 2010).

#### 1.4.1.1.2 Polytetrafluoroethylene (PTFE)

Due to its 'non-stick' properties, PTFE, also known as Teflon®, is used extensively as a coating in a variety of applications, including for cookware. For this reason, manufacturers have developed urinary catheters coated with Teflon® to try and prevent bacterial adhesion, however many clinical trials have concluded that other coatings are superior to Teflon®. A study comparing hydrogel-coated, Teflon®-coated and all silicone catheters concluded that the hydrogel-coated catheters were superior at preventing bacterial attachment and reducing mucosal irritation (Murakami et al. 1993). Additionally, a clinical trial testing the capacity of numerous catheters to reduce biofilm formation and prevent blockage over a 14 day period concluded that an all-silicone catheter out-performed catheters manufactured from latex or those coated with silicone or Teflon® (Kunin et al. 1987).

#### 1.4.1.1.3 Polyzwitterions

Polyzwitterions exert their antifouling action through steric and electrostatic repulsion. Catheters coated with polyzwitterions have equal positive and negative charges, and hydrogen bonds formed between the groups on the zwitterion and water molecules at the coating interface results in the formation of a hydration layer. These layers prevent the formation of conditioning films and therefore, bacterial adhesion events are inhibited (Figure 1.11) (Singha et al. 2017).

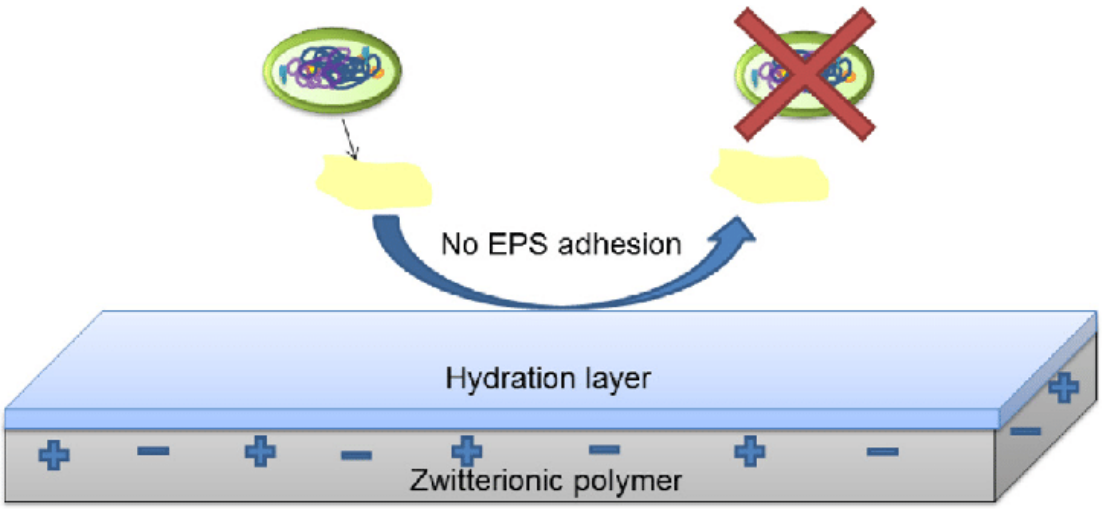


**Figure 1.11** Zwitterionic mechanisms of antifouling. Electrostatic hydrogen bonds between the water molecules and zwitterions forms a hydration layer that prevents attachment of the extracellular polymeric substance produced by microbial cells, thus inhibiting microbial adhesion. (Reproduced from Singha, Locklin and Handa, 2017 with permission from Elsevier)

Phosphorylcholine, sulfobetaines and carboxy-betaine groups bound to polymethacrylate, or polyacrylamide backbones are the most commonly studied zwitterions. In 2002, Stickler *et al* used an *in-vitro* bladder model of *P. mirabilis* infection to study the efficacy of silicone and latex catheters coated with zwitterionic polymers (2-methacryloloxyethylphosphorylcholine co-polymerised with long-chain alkyl methacrylate's). Bacterial attachment, biofilm formation and encrustation were not prevented on either device.

Additional studies of phosphorylcholine (PC) coated polymers have demonstrated increased resistance to adhesion and biofilm formation by *E. coli* and reduced encrustation by *P. mirabilis,* using an artificial urine medium (Russell and Stratford 2000). A clinical trial of PC-coated urinary catheters and ureteral stents reported reduced encrustation of ureteral stents, but not urinary catheters, suggesting encrustation events may differ between devices (Stickler et al. 2002).

The stability of the hydration layer is a key factor in producing polyzwitterionic coatings, as a breached layer could allow adherence of proteins, and ultimately bacteria, to the device surface. Increasing the stability of the layer beyond the typical lifetime of a catheter (typically 1 month) is an important area of future research.

#### 1.4.1.1.4 Polyethylene glycol (PEG)

PEG-coated surfaces have excellent protein repellent properties. The brush layers within the PEG structure effectively blocks long-range attractive forces between the surface and microbial cells and provides repulsive steric forces.

A number of studies have shown PEG was able to reduce protein and microbial adhesion. In 2007, Sankar and Rajalakshmi formulated a latex polymer with a thin PEG hydrogel coating, significantly reducing protein adhesion, compared to the latex control material. Added to this, a PEG-coated polyurethane was formulated and showed reduced adhesion of *E. coli*. The adhesion of *Staphylococcus epidermidis* was also investigated during this study, but the material did not reduce the attachment of this microbe (Sankar and Rajalakshmi 2007).

#### 1.4.1.1.5 Enzymes

A number of enzymes have been investigated as surface coatings to disrupt pathways in biofilm formation. A silicone catheter coating of $\alpha$-amylase and acylase was shown to reduce *in-vitro P. aeruginosa* biofilm formation by over 40%, *S. aureus* biofilms by over 30%, and mixed cultures (*P. aeruginosa* and *E. coli*) by over 50%, whilst planktonic growth remained unaffected. Additionally, biofilm growth was delayed up to 7 days in an animal model. $\alpha$-amylase disrupts assembly of EPS, whilst small molecules involved in QS are degraded by acylase (Ivanova et al. 2015).

Another enzyme used to inhibit biofilm formation is cellobiose dehydrogenase (CDH). This enzyme is able to produce hydrogen peroxide by using oligosaccharides as electron donors. Immobilising CDH on the surface of silicone has been shown to release hydrogen peroxide for over 16 days and prevent *S. aureus* biofilm formation.

An additional study of *S. aureus* biofilm formation on CDH-coated silicone showed that production of 18 $\mu$M of hydrogen peroxide within a 2 h period significantly reduced bacterial viability and attachment (Lipovsky et al. 2015).

A crucial component of the biofilm structure and architecture is its EPS, as this aids resistance against antimicrobial compounds and the host immune system. An enzyme that cleaves glycosidic bonds of EPS components, glycoside hydrolase (Ghs), has been investigated as a potential antibiofilm agent. Numerous studies

have shown that *P. aeruginosa* biofilm formation can be disrupted or prevented by the addition of Ghs to cultures or pre-formed biofilms (Baker et al. 2016; Asker et al. 2018).

A major structural and functional component of the biofilm matrix is extracellular DNA (eDNA), so enzymes capable of eDNA degradation have been studied as antibiofilm agents. Deoxyribonuclease I (DNase I) has been shown to exhibit antibiofilm activity against a variety of Gram-negative and Gram-positive species. In flow cell culture systems, *P. aeruginosa* biofilm formation was inhibited by the addition of DNase I at the time of inoculation, yet pre-formed biofilms were resistant or partially resistant to detachment. Early biofilms (12-60 h) were dissolved by DNase I treatment, but more established biofilms (84 h old) were resistant (Whitchurch et al. 2002).

Ghanwate *et al* coated urinary catheters with DNase and prolonged *P. aeruginosa* biofilm formation from 2 to 5 days compared to uncoated versions (Ghanwate et al. 2014). DNase I is thought to prevent initial bacterial attachment events through degradation of cell surface associated nucleic acids that act as surface adhesins. Detachment of newly formed biofilms is thought to be through degradation of eDNA. Additional adhesins may however be present in mature biofilms and these are, therefore, resistant to DNase-mediated detachment.

#### 1.4.1.2 Biocidal coatings

Numerous biocidal agents have been investigated as urinary catheter coatings or incorporated into the bulk of the catheter material. Such materials may exert their actions through release of the biocide into the external environment or the biocidal mechanism may be exerted upon microbial contact. Examples of these are discussed below.

##### 1.4.1.2.1 Silver coated silicone

Silver is microbicidal at low concentrations and has the advantage of being approved by The Food and Drug administration (FDA) as a coating. Pure silver coatings, silver alloy coatings, silver containing polymers and silver nanoparticle containing silicone have all been investigated for use as antimicrobial agents in urinary catheters (Singha, Locklin and Handa, 2017).

Studies of pure silver coatings revealed that the coating deteriorated and released silver ions too rapidly in aqueous environments (Singha, Locklin and Handa, 2017). To overcome this problem, silver nanoparticles incorporated into the silicone material have allowed more controlled release, overcoming any potential cytotoxicity issues in patients (Knetsch and Koole, 2011).

In a study comparing silver alloy and nitrofurazone (an antibiotic) coated catheters, the latter was found to be more effective in preventing bacterial adherence and biofilm formation against 11 CAUTI causing microorganisms (Johnson, Johnston and Kuskowski, 2012).

In a multi-centre randomised control study comparing silver alloy coated catheters with nitrofurazone-impregnated catheters in short-term catheterised patients (<14 days), higher rates of patient discomfort were recorded with use of the antibiotic catheter (Pickard *et al.*, 2012). Due to cost effectiveness, The U.S Food and Drug Administration (FDA) approval and superior patient comfort over antibiotic coated catheters, a market for silver alloy coated catheters remains. Silver hydrogel coatings have also shown promise as catheter coatings in a number of studies but require further cytotoxicity studies to be undertaken prior to advancement to commercial products (Lederer *et a.*, 2014).

#### 1.4.1.2.2 Antibiotic coatings

Frequently used antibiotics for use as urinary catheter coatings include nitrofurazone, sparfloxacin, rifampicin and minocycline, amongst others (Johnson et al. 2012; Kowalczuk et al. 2012; Salvarci et al. 2015). Commercially available nitrofural impregnated catheters have also been widely studied. Nitrofurazone was found to temporarily inhibit DNA replication, but removal of the agent led to resumption of the replication process (Ona, Courcelle and Courcelle, 2009). Comparison of nitrofurazone catheters with silver-alloy coated catheters concluded that the former were superior in preventing planktonic growth, biofilm formation and were more cost effective (Johnson, Johnston and Kuskowski, 2012; Kilonzo *et al.*, 2014).

Studies have associated nitrofurazone catheters with patient discomfort (Pickard *et al.*, 2012), whilst nitrofurazone has also been linked to the development of ovarian and mammary tumours in animal subjects (Hiraku *et al.*, 2004). For this reason, the FDA prohibited nitrofurazone use as a drug and also prevented it from

being used in food products. Nitrofurazone impregnated catheters were removed from the market in 2012 due to limited evidence to support their effectiveness.

Sparfloxacin (SPA) inhibits DNA gyrase, which is involved in bacterial DNA replication. As with nitrofural, SPA treated catheters showed superior ability in preventing growth of planktonic bacteria and preventing biofilm growth, compared with silver-alloy coated catheters. Broad-spectrum antimicrobial activity was maintained for 6 months (Kowalczuk *et al.*, 2012).

Minocycline-rifampicin (MR) impregnated silicone catheters prevent *P. mirabilis* colonisation. However, antimicrobial efficacy was not observed against *E. coli* and *P. aeruginosa* (Salvarci, Koroglu and Gurpinar, 2015). Fisher *et al.*, 2015 impregnated rifampicin, sparfloxacin and triclosan combinations into urinary catheters, leading to broad spectrum antibiofilm activity against *P. mirabilis*, *S. aureus* and *E. coli*. Zones of inhibition assays revealed that the antibiotic impregnated catheter material was able to continue to produce inhibition zones for more than 100 days, compared to 2 days for silver-alloy and nitrofural containing material (Fisher et al. 2015).

The emerging problem of bacterial resistance to antibiotics provides a hurdle to be overcome in the development of new commercially available antibiotic catheters. Resistance of CAUTI causing pathogens to antibiotics used in catheter coatings would not only render the product ineffective but could lead to the emergence of highly resistant organisms, with consequences beyond those of catheter-related infections.

#### 1.4.1.2.3 Other antimicrobial agents

Many other antimicrobial agents have been used as surface coatings or for bulk loading of urinary catheters. These agents include chlorhexidine, triclosan, antimicrobial peptides, bacteriophages, nitric oxide, liposomes and naturally occurring compounds (Singha, Locklin and Handa, 2017).

Triclosan is a widely used, broad spectrum antimicrobial compound and frequently employed in personal care products, such as soaps and toothpastes, household items including laundry detergents, and medical devices (Fang *et al.*, 2010). At low concentrations, triclosan is bacteriostatic through inhibition of enoyl-acyl carrier protein reductase (ENR), a bacterial enzyme involved in fatty acid

synthesis. At high concentrations, biocidal effects are observed due to disruption of bacterial cell membranes (Levy *et al.*, 1999).

Incorporation of triclosan into the retention balloons of urinary catheters reduced *E. coli, K. pneumoniae*, *S. aureus* and *P. mirabilis* biofilm formation and significantly lowered planktonic cell numbers of *P. stuartii*, and *Enterococcus faecalis* (Jones *et al.*, 2006). A German clinical trial also investigated the use of triclosan (Farco-Fill®) as a liquid to inflate the balloons of catheters in patients with chronic indwelling suprapubic catheters. The study showed a statistically significant extension in catheter in-dwelling time, a reduction of pain during catheter changes and reduction of catheter encrustation (Sperling et al. 2014). Previous studies at the School of Dentistry, Cardiff University reported that a dip-coated silicone containing 0.2% (w/v) triclosan prevented catheter encrustation by *P. mirabilis* in all but one of the test catheters. Long-term antimicrobial activity of the material was evident for 11 weeks (Jordan *et al.*, 2015). However, a separate study exposing *P. mirabilis* to triclosan on agar plates, resulted in selection of mutants with up to 300-fold reduction in triclosan susceptibility as observed by an increase in MIC value (Stickler and Jones, 2008).

Concerns have been raised over the safety of triclosan, due to reports of mammalian cell toxicity and carcinogenicity, endocrine disruption, development of bacterial resistance and increased antimicrobial resistance against antibiotics (Fang *et al.*, 2010; Singha, Locklin and Handa, 2017).

In 2017, the FDA ruled that sufficient evidence existed to support the use of triclosan in some consumer products, whilst no evidence exists to support its use in over-the counter (OTC) antiseptic products. A final rule was issued stating that use of triclosan in such products would only be possible with a pre-market review.

#### 1.4.1.2.4 Natural compounds

Due to the increasing prevalence of antibiotic resistance, the use of naturally occurring biocides has been investigated for use in urinary catheters to prevent biofilm formation.

In 2014, Malic *et al* investigated the susceptibility of *P. mirabilis* and other CAUTI causing bacteria to several essential oils, namely tea-tree oil (TTO), terpinen-4-ol, cineole and eugenol. The study concluded that terpinene-4-ol and eugenol inhibited growth and swarming activity of planktonic *P. mirabilis*, but a later study

investigating silicones impregnated with these naturally derived agents failed to demonstrate antimicrobial activity (Jordan et al. 2015).

Natural polymers, such as hyaluronic acid and heparin, have shown potential as antiadhesive surface coatings (Tenke et al. 2004). Recently, an extracellular polymer produced by a marine cyanobacterium has been used as a surface coating (CyanoCoating) and demonstrated antiadhesive properties against a range of bacteria, including *S. aureus*, *S. epidermidis*, *P. aeruginosa* and *E. coli* (Costa et al. 2019). When applied as a coating to urinary catheters, biofilm formation was significantly impaired for *E. coli*, *P. mirabilis* and *C. albicans* and the catheter was less prone to encrustation (Costa et al. 2020).

Polysaccharides from other marine sources, including chitosan, alginate, agarose and ulvan have also shown potential to be used as antiadhesive surface coatings (Junter et al. 2016; D'Almeida et al. 2017).

#### 1.4.1.3 Modifications to surface topography

Surfaces that do not rely on additional chemistries or antimicrobial agents to prevent biofilm formation have been investigated for use in urinary catheters. The topography of a surface plays an important role in microbial attachment and efforts to mimic surfaces that are antimicrobial in nature have been investigated to reduce biofilm formation. Shark skin has been found to be naturally resistant to microbial attachment, due to its nanoscale texture, so Sharklet® (Sharklet Technologies, Colorado, USA), a material with a microscopic diamond shaped repeating pattern was developed as an antifouling material.

A study by Reddy *et al* compared colonisation of uropathogenic *E. coli* on Sharklet® micropatterned silicones against smooth silicone surfaces (Reddy et al. 2011). Both colonisation and migration of *E. coli* were reduced on the micropatterned surfaces.

Additional modifications to material surfaces to prevent microbial colonisation include fabrication of nano-cone arrays onto polystyrene and nano-pillar structures onto polymethylmethacrylate films. The nano-cones displayed bactericidal activity against *E. coli* and *Klebsiella pneumoniae* (Hazell et al. 2018), whilst nanopillar structures on polymethylmethacrylate films caused death of *E.coli* following direct contact with the surfaces (Dickson et al. 2015). The exact bactericidal mechanisms of these structures have yet to be fully elucidated but it is believed that disruption

of bacterial cell membranes by nanopillar structures play a pivotal role (Figure 1.12).

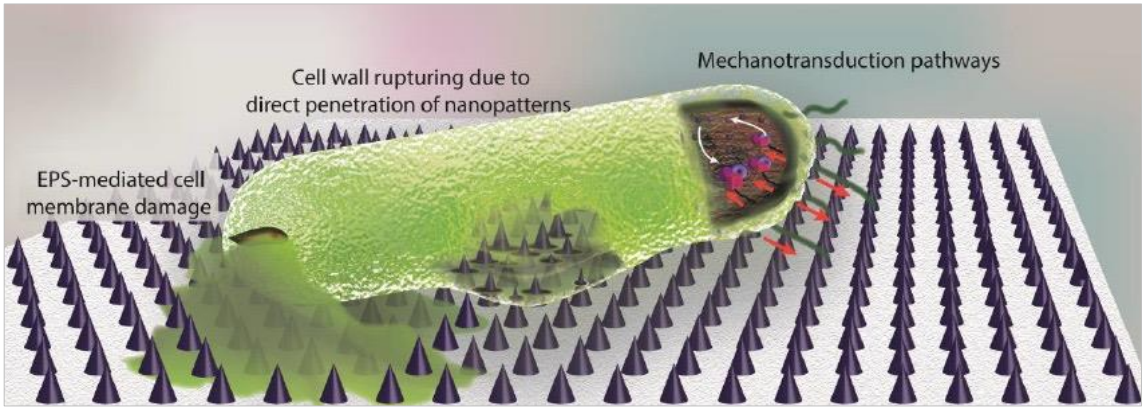


**Figure 1.12** Nano-cone patterned surfaces disrupt bacterial cell membranes (Reproduced from Modaresifar *et al.*, 2019 with permission from Elsevier)

### 1.5 Detection of catheter-associated urinary tract infections

Although prevention of biofilm formation on medical devices through functionalisation of their surfaces could lead to reduced incidence of CAUTIs, early detection of infections represents another tool in CAUTI management and to inform clinicians on treatment strategies. To date, limited detection systems exist that allow early diagnosis of CAUTIs and those that have been developed are primarily aimed at detecting urease producing bacteria.

#### 1.5.1 Bromothymol blue-based detection systems

As discussed in Section 1.3.6.1, encrustation and blockage of urinary catheters is driven by urease producing bacteria that are able to form crystalline salts through urease-mediated hydrolysis of urea. The resulting increase in urinary pH through generation of ammonium ions has been exploited in a number of detection systems.

In 2006, Stickler *et al* produced a cellulose acetate-based sensor material that had the pH responsive bromothymol blue (BTB) compound covalently bound to it. At pH below 6.5, BTB exhibits a yellow colour that gradually changes to blue-black as the pH increases above 8.0. Using an *in-vitro* bladder model of CAUTI, the sensor successfully detected an increase in urinary pH following inoculation of the bladder with *P. mirabilis*. Uninoculated urine had a pH of 6.1 and under these

conditions the bromothymol blue sensor was yellow. Elevated pH above 8, which typically occurs in cases of *P. mirabilis* infection resulted in the development of a dark blue sensor colour. Placement of the sensor at two different locations within the bladder model (in-line between the catheter and the drainage bag, and within the drainage bag) showed that *P. mirabilis* infection was detected earlier when the sensor was placed in the drainage bag and the signal was also stronger. This sensor material was able to signal *P. mirabilis* infection an average of 43 h prior to catheter blockage, when located within the drainage bag (Stickler *et al.*, 2006).

Clinical assessment of this sensor material was undertaken on 20 catheterised patients over an 8 week period (Stickler *et al.*, 2006). The material was located in drainage bags and was changed weekly. Microbiological analysis of patients' urine showed that all but 5 developed *P. mirabilis* infection over the course of the study, and the material remained unresponsive in those 5 patients. The material successfully signalled *P. mirabilis* infection in the other patients, with mean signalling occurring 12 days before blockage occurred.

Although promising, commercial development of the cellulose acetate-BTB sensor proved difficult on a large scale. Therefore, Malic *et al* adapted the sensor and incorporated BTB into silicone using a hydrophilic filler (Malic et al. 2012).

The silicone sensor was placed at the catheter and drainage bag junction, where urine from the bladder of the *in-vitro* model would pass over the surface. Bladders that had been inoculated with weak urease producing bacteria, namely *K. pneumoniae* and *S, aureus*, did not initiate a colour change of the sensor despite the pH increasing from 6.1 to 6.76 and 6.6, respectively. Bladders inoculated with strains of *P. mirabilis*, *P. vulgaris* and *Providencia rettgeri* all led to catheter encrustation and blockage. The sensor successfully signalled infection in all instances, with detection occurring between 12 and 19 h before catheter blockage.

A clinical trial of the BTB silicone sensor revealed that the sensor changed colour from yellow to blue-black in response to infection by *P. mirabilis*, *Providencia* and *Morganella* species in 6 out of 7 infected patients (Long et al. 2014). The pH of urine that caused the colour change was reported between 5.5 and 9.0 with a mean of 7.6 and the mean number of catheterised days before blockage occurred was 23. The sensor typically changed colour between 24 and 48 h after catheter insertion.

Patient questionnaires revealed that almost half of participants experienced leakage around the sensor junction, but instances were infrequent and resolved quickly. It was also reported that most participants would recommend the sensor if the time between the sensor changing colour and catheter blockage was shorter (Long et al. 2014).

### 1.5.2 pH responsive catheter coatings as detection systems

Another system to detect *P. mirabilis* infection in catheterised patients has been developed (Milo et al. 2016). A pH responsive catheter coating consisting of a lower hydrogel (polyvinyl alcohol) layer with a carboxyfluorescein dye and an upper pH responsive layer (EUDRGADIT S100®) that dissolved upon elevation of urinary pH above 7, released a fluorescent dye in the lower layer, where it accumulated in the drainage bags of *in-vitro* bladder systems (Figure 1.13).

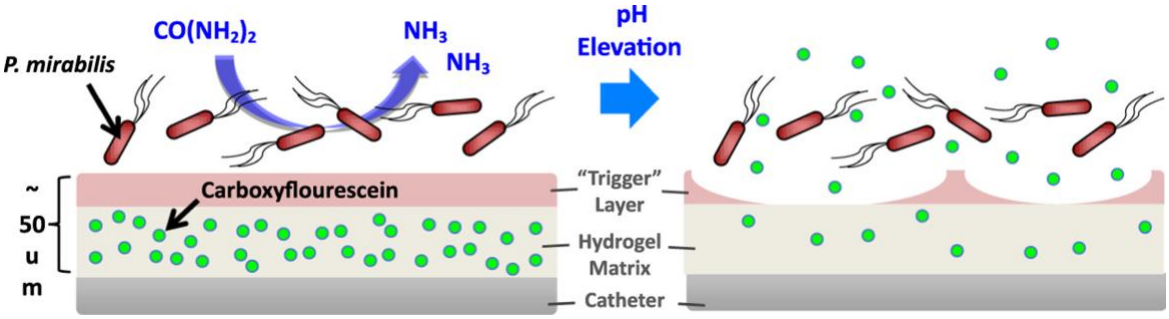


**Figure 1.13** Schematic diagram of the duel-layered catheter coating developed by Milo *et al*. An elevation in urinary pH caused by *P. mirabilis* degrades the upper trigger layer to release the carboxyfluorescein dye contained below it (Milo et al. 2016). Reproduced under terms of the Creative Commons CC-BY license.

This system provided advanced warning of *P. mirabilis* infection, signalling infection 10-12 h before catheter blockage occurred. To enable a greater concentration of the fluorescent dye to be visualised in the drainage bag, Milo *et al*, used the same technology to produce a sensor 'lozenge" (Milo et al. 2018a). The lozenge consisted of a cylindrical hydrogel layer containing the fluorescent dye surrounded by the pH sensitive trigger layer, EUDRAGIT S100® (figure 1.14). Placement of the lozenge directly in the drainage bag had a number of advantages over the previous catheter coated system. It allowed higher levels of dye to be released and visualised in the drainage bag, whilst also avoiding potential

cytotoxicity effects of the compounds upon the urethra. This sensor system detected *P. mirabilis* infection 14.5 h before catheter blockage occurred.

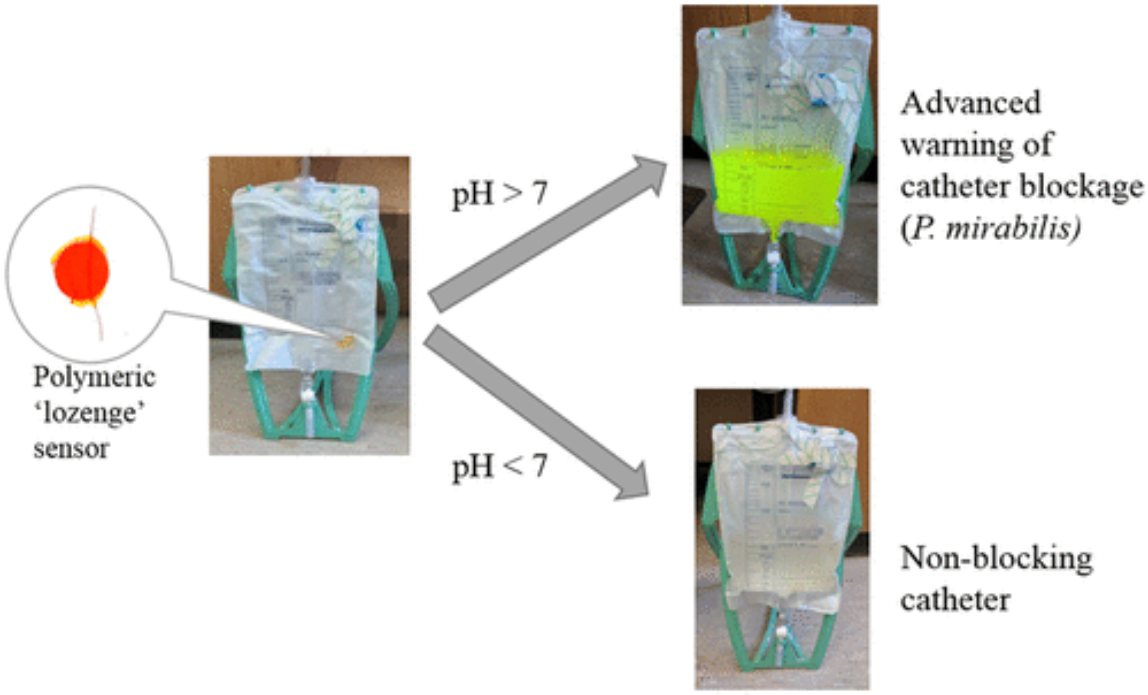


**Figure 1.14** Production of a fluorescent coloured urine within the drainage bag of an *in-vitro* bladder model through release of carboxyfluorescein dye, in response to *P. mirabilis* infection (Milo et al. 2018b). Reproduced with permission from ACS Publications.

An additional sensor system that responds to an increase in urinary pH upon production of ammonia by urease producing organisms has also been reported (Surender et al. 2017). Europium III, a reactive fluorophore has its red fluorescence quenched at elevated pH levels. The 'switching off' mode could potentially signal infection by urease positive bacteria. This system has yet to be tested in laboratory models of CAUTI infection and still represents a proof-of-concept.

## 1.6 Summary

Infections associated with urinary catheter use are major contributors to HCAIs. Biofilm formation on medical device surfaces are largely resistant to compounds that eradicate planktonic bacteria and despite efforts to reduce biofilm formation, the problem of CAUTI remains. Modifications to surface structure and coating surfaces with numerous antimicrobial/antibiotic agents have had some success *in-vitro,* but not all have translated to commercially viable products and a market still exists for the production of a urinary catheter that is resistant to biofilm formation and is able to prevent CAUTI in patients with long-term, in-dwelling catheters.

Few methods currently exist to detect CAUTIs in catheterised patients, with diagnosis often occurring once patients have become symptomatic or catheters have blocked. Efforts to produce sensor systems for the early detection of infection have focused on urease positive microorganisms (typically *P. mirabilis*), through pH responsive mechanisms. Whilst infections with *Proteus* species are almost entirely responsible for encrustation and blockage of urinary catheters, a number of other microorganisms are more prevalent in CAUTIs and go undetected by these sensors.

Methods to detect non-urease producing microorganisms may prove to be valuable tools to aid early diagnosis of CAUTI with potential for earlier treatment regimens to be implemented, thus reducing incidences of severe complications linked to CAUTI.

## 1.7 Project aims and objectives

The overarching aims of this research can broadly be divided into two sections. The first part of the study will focus on the prevention of biofilm formation of CAUTI causing organisms on silicone surfaces. Identification of antimicrobial compounds with broad spectrum activity against numerous CAUTI causing microorganisms and incorporation of candidate compounds into silicone polymers will be undertaken.

Secondly, detection of microorganisms responsible for CAUTIs will be investigated through identification of molecules that elicit a colour change in response to infection. Incorporation of responsive compounds into silicone polymers will be investigated for use a sensor detection tools.

The aims of each experimental chapter were to:

Chapter 2: Investigate antimicrobial compounds that demonstrate broad spectrum activity against a panel of CAUTI causing microorganisms.

Chapter 3: Incorporate candidate antimicrobial compounds into silicone elastomers and evaluate release kinetics of these compounds from the materials produced. Antimicrobial activity of the silicone materials will also be assessed.

Chapter 4: Generate an antimicrobial silicone formulation with desirable physical properties to enable production of 3D printed structures.

Chapter 5: Identify and evaluate molecules that signal the presence of CAUTI causing microorganisms. Incorporation of lead compounds into silicone elastomers will follow.

Chapter 6: Evaluate antimicrobial silicone formulations and sensor materials using an *in-vitro* bladder model of CAUTI.

# Chapter 2

## *In-Vitro* Assessment of Antimicrobial Compounds

## 2.1 Introduction

Antimicrobial resistance (AMR) is a threat to global health and the World Health Organisation (WHO) has declared it to be one of the top 10 global public health threats facing humanity (WHO, 2016). The overuse of antimicrobial therapies has allowed microorganisms to develop resistance mechanisms to such drugs that allow them to evade their biocidal actions (Table 1.3).

Bacteria commonly associated with CAUTIs have developed resistance to frequently used antibiotics. Ciprofloxacin is often used to treat urinary tract infections (UTIs) and catheter associated urinary tract infections (CAUTIs). However, resistance of *Escherichia coli* and *Klebsiella pneumoniae* to ciprofloxacin has been reported between 8.4-92.9% and 4.1-79.4%, respectively (WHO, 2016). Colistin is often the last remaining treatment option for carbapenem resistant Enterobacteriaceae, such as *E. coli* and *K. pneumoniae*, but the resistance of these species to colistin leaves no effective treatment options available (WHO, 2016).

The most highly virulent and multidrug resistant (MDR) bacterial pathogens have been given the acronym ESKAPE (*Enterococcus faecium, Staphylococcus aureus, K. pneumoniae, Acinetobacter baumannii, Pseudomonas aeruginosa* and *Enterobacter* species) and the WHO has encouraged pharmaceutical companies to prioritise development of antimicrobial therapies against these species to avert a global healthcare crisis (Breijyeh et al. 2020; WHO 2020).

All ESKAPE pathogens have been implicated in CAUTI pathogenesis (Hernandez et al. 2017; Khan et al. 2017b; Sosa Hernández et al. 2019) and current treatment of CAUTIs often happens once a urinary catheter has become blocked (Jacobsen and Shirtliff 2011), or the patient develops associated symptoms such as fever, delirium or even sepsis (Davis 2019). Treatment options are then limited to catheter replacement and administration of systemic antibiotics (National Institute for Health and Care Excellence 2018), which are often ineffective due to the developed resistance mechanisms of the pathogens to the drugs (Breijyeh et al. 2020).

Prevention of bacterial proliferation and biofilm formation on catheter surfaces through use of prophylactic drugs could avert such crisis management situations. Ideally, such drugs would have multiple cellular targets to prevent development of

resistance. A number of synthetically derived and naturally occurring compounds have been identified (Table 2.1), as potential prophylactic agents for the management of CAUTIs and their mechanisms of actions are described below.

**Table 2.1.** Compounds selected for the prophylactic management of CAUTIs

| Compounds | Biocide class | Chemical basis | Bacterial targets/resistance mechanisms | References |
|---|---|---|---|---|
| **Triclosan and triclosan esters** | Synthetic | Phenyl ether | ENR, cell membrane, efflux pumps | (Poole 2004; Fang et al. 2010) |
| **Silver *N*-Heterocyclic carbenes's and imidazolium salts** | Synthetic | Cyclic carbene with 2 neighbouring nitrogen atoms | Cell wall, plasma membrane, bacterial DNA | (Ricco and Assadian 2011; Johnson et al. 2017) |
| **ε-poly-L-lysine** | Naturally occurring | Polypeptide | Membrane phospholipids | (Hyldgaard et al. 2014) |
| **Citrox®** | Naturally occurring | Bioflavonoid preparation/ polyphenols | DNA gyrase, cytoplasmic membrane, cell metabolism | (Ohemeng et al. 1993; Tsuchiya and Iinuma 2000) |
| **Caprylic acid/ Octanoic acid** | Naturally occurring | Saturated fatty acid | Cell membrane, cytoplasm | (Shilling et al. 2013) |
| **Compound 1771** | Synthetic | Phenol and oxadiazole rings | Lipoteichoic acid synthase (LtaS) | (Richter et al. 2013; Paganelli et al. 2017) |

### 2.1.1 Triclosan and triclosan derivatives

Triclosan, a phenyl ether with broad-spectrum antimicrobial activity (Figure 2.1.1), has been widely used in a number of household items, including laundry detergents, hand soaps and toothpastes and also as an antimicrobial agent in medical devices and hospital settings (Fang et al. 2010).

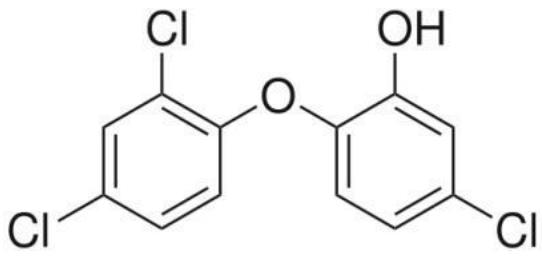


**Figure 2.1.1** The chemical structure of triclosan

The compound is readily absorbed and distributed within the human body, with rapid metabolism and secretion into the urine (Sandborgh-Englund et al. 2006). Concerns have been raised over the use of triclosan with reports that the compound induces proliferation of cultured breast cancer cells (Henry and Fair 2013). However, such proliferation may be reduced in the presence of estradiol (Gee et al. 2008). A review regarding the cancer risk associated with triclosan concluded that “epidemiologic studies of risk associated with various concentrations and durations of exposure to triclosan are needed, as well as studies to characterize human exposure to triclosan through varying use of triclosan-containing consumer products and other routes of exposure” (Dinwiddie et al. 2014).

Earlier studies also revealed that products containing triclosan up to 1% were not dermal irritants (Kanetoshi et al. 1992), whilst reviews of oral safety studies determined that triclosan was not an oral toxicant (Bhargava and Leonard 1996).

In 2016, the U.S. Food and Drug administration (FDA) issued a final rule banning sale of over-the-counter antiseptic wash products containing triclosan. Triclosan’s use in hand sanitisers and products used in healthcare settings is still permitted (McNamara and Levy 2016).

Triclosan has a dual mechanism of antimicrobial action depending on concentration. At sub-lethal concentrations, triclosan inhibits fatty acid synthesis by binding to the enoyl-acyl carrier protein reductase (ENR) (Figure 2.1.2), although some bacterial strains including those of *Pseudomonas aeruginosa* possess a triclosan resistant ENR. Resistance of *P. aeruginosa* to triclosan can also be attributed to the presence of multi-drug efflux pumps (Poole 2004). At low

doses, triclosan exhibits bacteriostatic effects, whilst it gains bactericidal activity at higher doses by targeting multiple cellular components, including the cell membrane (Fang et al. 2010). The reported minimum inhibitory concentrations (MICs) and minimum biocidal concentrations of triclosan (MBCs) varies between and within species. MICs of triclosan against *Staphylococcus aureus* of between 0.025-4 μg/ml and MBCs between 0.25-32 μg/ml have been reported (Kampf and Kramer 2004). For 368 strains of *E. coli*, triclosan MICs values of between 0.015–128 μg/ml and MBC values between 0.015–512 μg/ml have been recorded (Morrissey et al. 2014).

Esterified triclosan derivatives are also antimicrobial (Shulong 1999) and patents for use of such derivatives as antimicrobial coatings of fabrics exist (Shulong 1999). It has been claimed that hydrolysis of triclosan esters (including triclosan acetate and triclosan benzoate) to triclosan occurs in aqueous environments, confers antimicrobial properties to the fabric. Additionally, triclosan esters have been shown to impart greater substantivity to fabrics than triclosan (Shulong 1999), allowing a slower rate of release.

### 2.1.2 Silver NHC complexes and imidazolium salts

*N*-heterocyclic carbenes (NHCs) have been used as carrier ligands for transition metals for use in biological applications, including antibacterial and antitumor effects (Youngs et al. 2008; Wright et al. 2012). Previous research using silver-NHC (Ag (I)-NHC) complexes as potential antibacterial compounds has revealed these chemicals as being efficient at inhibiting Gram-negative bacterial species, including *E. coli* and *P. aeruginosa* (Melaiye et al. 2004; Patil et al. 2011), Gram-positive species, including *S. aureus* (Patil et al. 2011), and the fungus, *Candida albicans* (Browne et al. 2014). Imidazolium salts are precursor molecules to NHCs, and have also been investigated for antimicrobial potential (Gök et al. 2014). Imidazolium salts exhibit antimicrobial effects against both Gram-negative and Gram-positive bacteria, although reduced susceptibility has been reported relative to their silver conjugated NHC counterparts (Gök et al. 2014).

The antibacterial properties of silver are well documented, with benefits including reduced incidence of bacterial resistance and fewer toxic effects reported for eukaryotic cells. The numerous antimicrobial mechanisms of action of silver ions are illustrated in Figure 2.1.2. Briefly, silver ions penetrate the bacterial cell wall

and plasma membrane, inactivating membrane bound proteins through binding to thiol groups in cysteine rich proteins (Ricco and Assadian 2011). Silver ions also prevent DNA replication by binding to bacterial DNA, prevent ribosomes from translating messenger RNA and also activate cytochrome b (Ricco and Assadian 2011). Given the potential of such agents, a component of this research was to evaluate susceptibility of CAUTI causing microorganisms against novel Ag (I)-NHC compounds and associated precursor imidazolium salts.

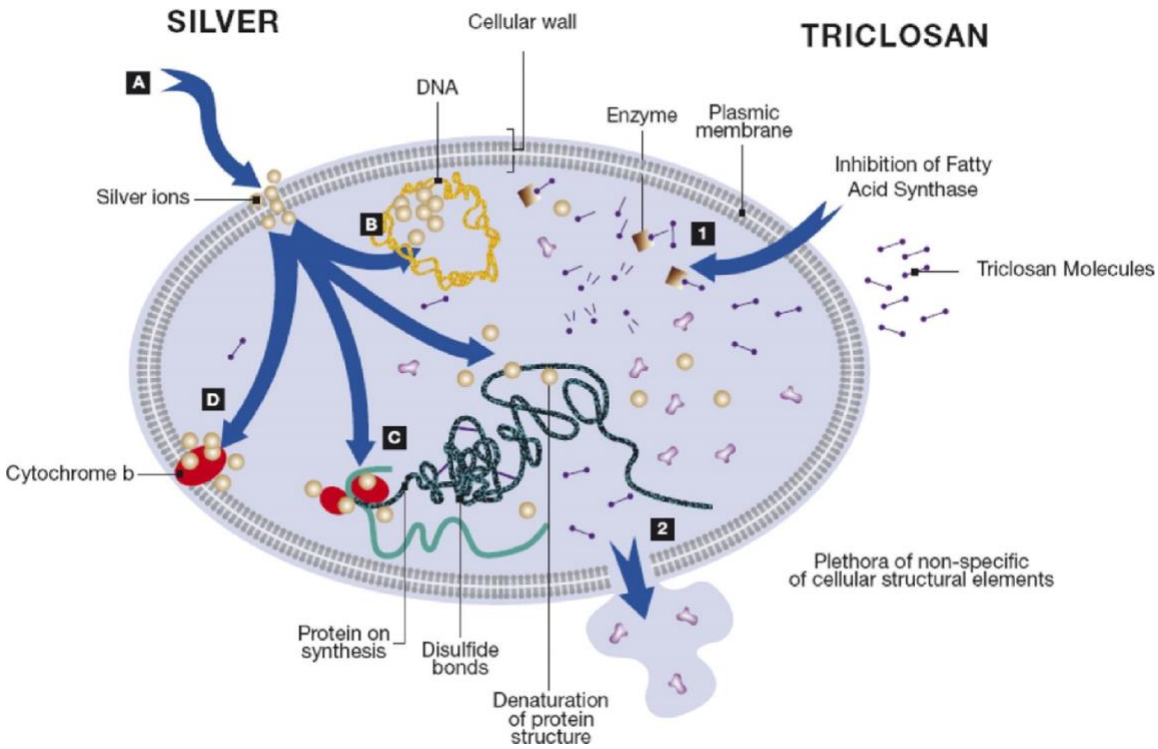


**Figure 2.1.2** Mechanisms of antimicrobial action of triclosan and silver ions on bacteria. (1) triclosan molecules bind to enoyl-acyl carrier protein reductase (ENR) of bacteria, encoded by the Fab I gene, preventing fatty acid synthesis. (A) silver ions penetrate bacterial cell walls and bind to the phospholipid bilayer of the cytoplasmic membrane. (C) Silver ions interfere with the ability of ribosomes to transcribe messenger RNA. (D) Silver ions bind to sulfhydryl groups of cytochrome b (Ricco and Assadian 2011)

### 2.1.3 Poly-L-lysine

Poly-L-lysine (ε-PL) is a naturally occurring peptide that has been widely studied as an antimicrobial agent against Gram-negative and Gram-positive bacteria (Shima et al. 2012). ε-PL has been shown to prevent *E. coli* contamination within the food industry (Hyldgaard et al. 2014), where it binds to *E. coli* lipopolysaccharide (LPS) and induces cell morphological alteration. It has been hypothesised that ε-PL destabilises membranes by interacting with negatively charged phospholipid head groups, causing membrane folding and formation of vesicles and micelles (Hyldgaard et al. 2014). The use of poly-L-lysine to prevent CAUTIs has not previously been reported, so its efficacy against common CAUTI causing pathogens was investigated as part of this study.

### 2.1.4 Bioflavonoids

There is an increasing awareness by the public concerning the merits of natural antimicrobial agents, which are often perceived as offering benefits devoid of harmful side effects towards the patient. Often natural agents are comprised of a complex mixture of compounds and thus offer numerous mechanisms of action. This in turn, makes it difficult for microorganisms to rapidly develop resistance mechanisms. One commercially available natural antimicrobial is Citrox® (Curaden AG, Kriens, Switzerland), which is a complex bioflavonoid preparation that has previously been used to control microbial colonisation in a wide range of applications. Citrox® has been shown to increase the shelf-life of vacuum packed poultry products (Vardaka et al. 2016; Yehia et al. 2019) and has been investigated as an aerosol to reduce contamination of surfaces in nosocomial settings (Galvin et al. 2012). More recently, dental surgeons have recommended Citrox® in combination with cyclodextrin to be investigated to prevent infection and progression of SARS-CoV-2 (Covid-19) (Batista et al. 2020).

Citrox® has clear antimicrobial effects against oral biofilms, including *C. albicans* and bacteria, such as *Porphyromonas gingivalis* and *Streptococcus gordonii* (Hooper et al. 2011). Viability of *in vitro Staphylococcus aureus* biofilms was successfully reduced by over 97% using 1% (v/v) Citrox® (Hogan et al. 2016). Furthermore the growth of Gram-negative bacteria, including *E. coli* and *Salmonella enterica* is inhibited by Citrox® (Vardaka et al. 2016). The broad

spectrum antimicrobial activity, along with absence of reported host cell toxicity (Hogan et al. 2016), makes Citrox® an attractive agent to be explored for the management of CAUTIs.

### 2.1.5 Caprylic acid

Fatty acids, including caprylic acid, have shown antimicrobial properties against a number of bacteria, including *E. coli* and *Clostridium difficile* (Skřivanová et al. 2009; Shilling et al. 2013). Addition of caprylic acid to *E. coli* contaminated food preparations of young rabbits reduced the output of faecal coliforms (Skřivanová et al. 2009), whilst a study into virgin coconut oil concluded that presence of caprylic acid in the oil played inhibited *C. difficile* (Shilling et al. 2013).

A study by Vargas-Cruz et al used an *in vitro* model to study the efficacy of a novel double-balloon Foley catheter (Vargas-Cruz et al. 2019). The device enabled a portion of extraluminal catheter, located within the periurethral space between the bladder junction and the meatus to be irrigated with an antimicrobial solution containing polygalactouronic acid and caprylic acid. The irrigated section of extraluminal surface resisted colonisation by numerous pathogens, including *E. coli*, *K. pneumoniae*, *P. aeruginosa*, *Proteus mirabilis*, *Enterococcus faecalis* and *C. albicans*. In contrast, the non-irrigated sections developed biofilms within 24 h. Therefore, caprylic acid was considered to have broad spectrum activity and its assessment as a potential antimicrobial compound against CAUTI causing microorganisms was warranted.

### 2.1.6 Compound 1771

*Staphylococcus aureus*, including methicillin-resistant *S. aureus* (MRSA*)* and vancomycin resistant *S. aureus,* are often isolated from the urine and catheters of long-term catheterised patients (Vinoth. et al. 2017). Although less commonly isolated from catheterised patients, other Gram-positive species, including *Enterococcus* species, contribute to CAUTIs and are difficult to eradicate. Indeed, vancomycin resistant enterococci (VRE) can be leading causes of nosocomial infection (Orsi and Ciorba 2013). The antibiotics, daptomycin and linezolid, are licenced to treat systemic multidrug resistant *S. aureus* and *E. faecium* infections (Micek 2007; Rosa et al. 2014). However, rapid resistance can develop to these

drugs (Mangili et al. 2005; Fossati et al. 2010). As such, the development of new effective antimicrobials to combat these species is urgently required.

Preventing biosynthesis of the key cell wall polymer, lipoteichoic acid (LTA), in Gram-positive bacteria has become a focus for drug manufacturers (Percy and Gründling 2014; Gale and Brown 2015). LTA is a polymer containing alditolphosphate and is linked to the bacterial cell membrane via a lipid anchor (Figure 2.1.3A). Whilst 5 sub-classes of LTAs exist, type I LTAs are most commonly encountered in *S. aureus*, and have been studied in the greatest detail (Percy and Gründling 2014). Type I LTAs are formed from simple, unbranched polyglycerol phosphate backbones with D-alanine and sugar residues (Figure 2.1.3B) (Schneewind and Missiakas 2014). LTA plays an essential role in bacterial cell growth, membrane homeostasis and virulence (Percy and Gründling 2014).

The chemical [2-oxo-2-(5-phenyl-1,3,4-oxadiazol-2-ylamino) ethyl-2-naphtho[2,1-*b*] furan-1-ylacetate], termed compound 1771 (Figure 2.1.3C) has the ability to inhibit lipoteichoic acid synthase (LtaS) which is the enzyme involved in LTA biosynthesis. Compound 1771 has been shown to be active against *S. aureus* and *E. faecium in vitro* and *in vivo* (Richter et al. 2013; Paganelli et al. 2017). It is, however, difficult to chemically synthesise and researchers in the School of Pharmacy (Dr Fabrizio Pertusati and Dr Michaela Serpi; School of Pharmacy, Cardiff University), have sought a simpler and more cost-effective means of production. This newly synthesised version of compound 1771 was assessed for its antimicrobial efficacy a range of CAUTI causing microorganisms.

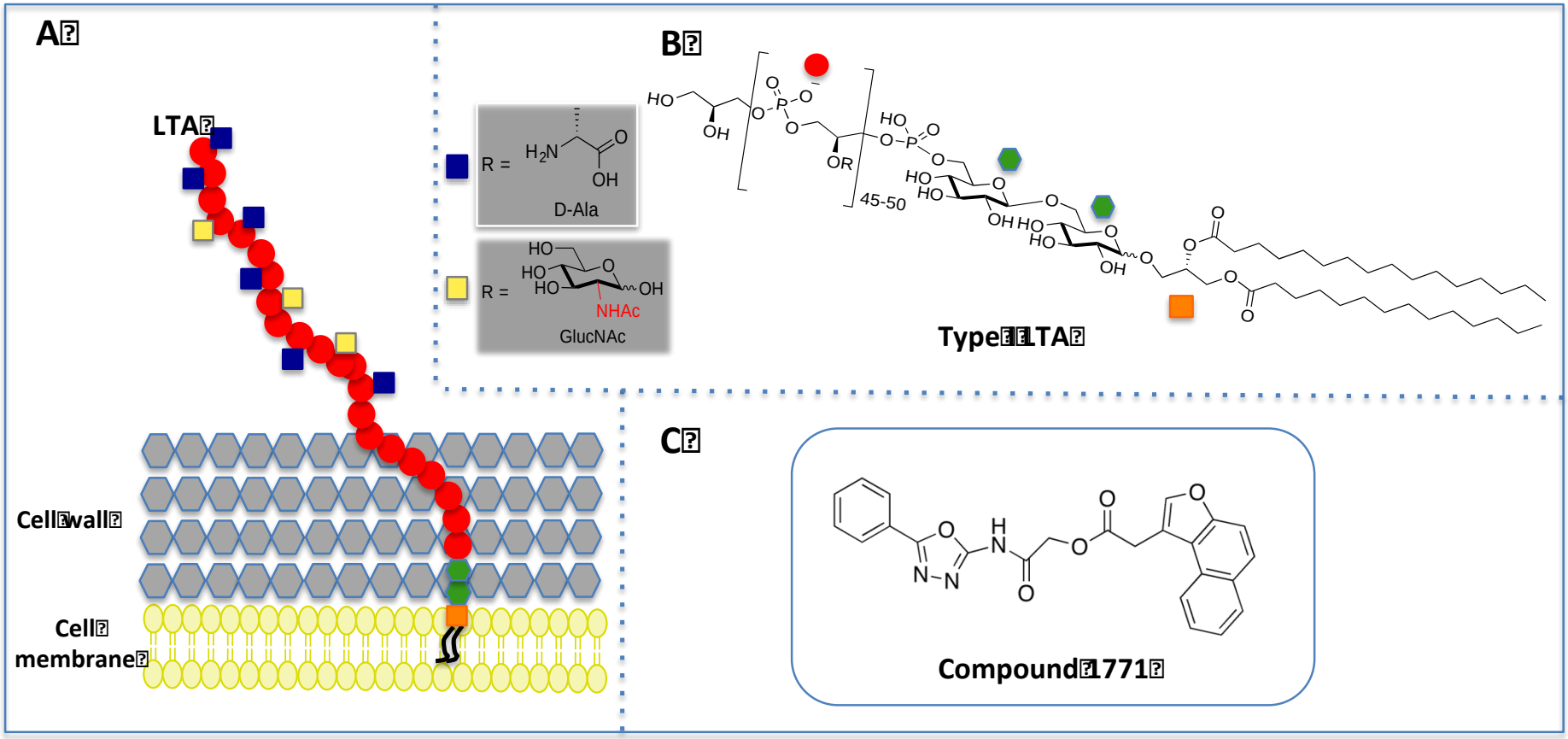


**Figure 2.1.3.** A) General structure of LTA; B) Chemical structure of Type I LTA; C) Structure of compound 1771 (Morozzi, et al . 2020)

### 2.1.7 Aims

CAUTIs are, at present, poorly managed, and often this is done retrospectively by crisis management following occurrence of infection. Prophylactic use of traditional antibiotics would be ill-advised given the increasing incidence of antimicrobial resistance (AMR). The aim of this research was therefore to evaluate a range of alternative antimicrobials, that would be less likely to promote AMR, for their effectiveness in the treatment of CAUTI causing microorganisms. Based on the spectrum of activity, sensitivity and impact on virulence gene expression, candidate compounds would then be identified for further study and progression into an antimicrobial biomaterial (Chapters 3 and 4).

A number of antimicrobials were assessed and included novel agents sourced from the School of Chemistry (Cardiff University) and also commercially available compounds, currently used to inhibit biofilms of clinical relevance away from the urinary tract. Specific aims of the Chapter were:

- To determine the antimicrobial activity of the chosen compounds against selected planktonic bacteria (clinical isolates and reference strains), using established methods to measure minimum inhibitory concentrations (MICs) and minimum biocidal concentrations (MBCs).

- To determine the antibiofilm activity of the compounds and expressed as minimum biofilm eradication concentrations (MBECs). The method for this has previously been reported and published by the research group (Hooper et al. 2011).

- To establish the expression of a panel of virulence associated genes for selected microorganisms, following sub-inhibitory antimicrobial exposure.

## 2.2 Materials & Methods

### 2.2.1 Microbiological culture media

All dehydrated media was obtained from Oxoid (Basingstoke, UK), unless otherwise stated.

- Cysteine Lactose Electrolyte-Deficient (CLED) agar was prepared according to the manufacturer's instructions in deionised water, autoclaved at 121°C for 15 min, before being cooled to 60°C using a water bath and aseptically dispensed into petri dishes. CLED agar was used to support growth of *P. mirabilis* and prevent colony swarming.
- Tryptone Soya Agar (TSA) was dissolved in deionised water, as described by the manufacturer, autoclaved at 121°C for 15 min and aseptically dispensed into petri dishes. TSA was used to support the growth of *Candida albicans*.
- Blood agar base was prepared according to the manufacturer's instructions in deionised water and sterilised by autoclaving at 121°C for 15 min, before cooling to 60°C in a water bath. Defibrinated horse blood (5% v/v) (Gibco, UK) was then aseptically added, mixed prior to dispensing into petri dishes.
- Mueller-Hinton broth (MHB) was dissolved in deionised water according to the manufacture and decanted into 100 ml volumes before sterilisation by autoclaving at 121°C for 15 min. 100 ml aliquots were stored at room temperature until required.

### 2.2.2 Microorganisms

Table 2.2.1 presents the bacterial strains associated with urinary tract infections that were used in these studies. The *Enterococcus faecium* strains were obtained from patients within various wards of The University Hospital of Wales, Cardiff.

**Table 2.2.1** Microorganism strains and corresponding agar used in cultures

| Microorganism | Origin | Reference | Agar |
|---|---|---|---|
| *Escherichia coli* NCTC 12923 | Reference strain | - | Blood |
| *Klebsiella pneumoniae* P6 wk2 | Indwelling catheter of long-term catheterised patients | | Blood |
| *Providencia stuartii* NSM 58 | Indwelling catheter of long-term catheterised patients | (Jones et al. 2006b) | Blood |
| *Pseudomonas aeruginosa* NCTC 10662 | Reference strain | - | Blood |
| *Serratia marcescens* NSM 51 | Urine or catheter of long-term catheterised patients | (Sabbuba et al. 2002) | Blood |
| *Proteus mirabilis* 12 RTB | Indwelling catheter of long-term catheterised patients | | CLED |
| *Candida albicans* ATCC 90028 | Reference strain | - | TSA |
| *Staphylococcus aureus* NSM 7 | Urine or catheter of long-term catheterised patients | (Broomfield 2007) | Blood |
| *Staphylococcus aureus* NSM 49 | Urine or catheter of long-term catheterised patients | (Sabbuba et al. 2002) | Blood |
| *Staphylococcus aureus* NSM 5 | Indwelling catheter of long-term catheterised patients | (Jones et al. 2006b) | Blood |
| *Staphylococcus aureus* P10 6/9 | Indwelling catheter of long-term catheterised patients | (Broomfield et al. 2009) | Blood |
| *Enterococcus faecium* Q11 (VRE) | Patients from wards of Welsh hospitals | (Kuriyama et al. 2003) | Blood |
| *Enterococcus faecium* Q41 (VRE) | Patients from wards of Welsh hospitals | (Kuriyama et al. 2003) | Blood |
| *Enterococcus faecium* M49 (VRE) | Patients from wards of Welsh hospitals | (Kuriyama et al. 2003) | Blood |

NCTC, National Collection of Type Cultures
ATCC, American Type Culture Collection
VRE, Vancomycin resistant *Enterococcus*

### 2.2.3 Preparation of test antimicrobial compounds

The chemical structures of the compounds assessed in this Chapter are displayed in Tables 2.2.2, 2.2.3 and 2.2.4.

Triclosan (Irgasan, Sigma; 10,000 μg/mL), and the three triclosan esters (Table 2.2) were prepared in 100% dimethyl sulphoxide (DMSO). Serial dilutions were performed to create working stocks of 5000, 2500, 1250, 625, 312.5 and 156.25 μg/mL in 100% DMSO. Each stock was diluted 1:50 in sterile Muller-Hinton broth (MHB, Sigma) to achieve drug concentrations ranging from 1.56 to 200 μg/mL in 2% (v/v) DMSO.

Poly-L-lysine (Sigma) and novel imidazole (compounds A-C) and silver (compounds D-F) compounds (provided by the School of Chemistry, Cardiff University) (table 2.3) were dissolved in sterile water and 1% (w/v) DMSO, respectively, and prepared as described above. 100% caprylic acid was dissolved to 48% (v/v) in 100% ethanol, before further dilution in MHB to achieve a 12% solution.

Citrox® MDC30 (Curaden, Switzerland) was provided as a 2% v/v solution and was further diluted with MHB to create working stocks at between 0.0078 and 1% v/v.

Commercial compound 1771 was obtained from Enamine Ltd, Kiev, Ukraine, and a newly synthesised version was also created by collaborators at School of Pharmacy, Cardiff University. Both compounds were prepared as a 10,000 μg/mL solution in 100% DMSO and further diluted to 200 10,000 μg/mL with MHB. Working stocks between 1.56 and 100 μg/mL were prepared by serial dilutions with MHB.

**Table 2.2.2** Chemical structures of triclosan and triclosan esters.

| **Compound** | **Structure** |
|---|---|
| Triclosan | 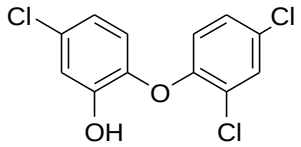 |
| Triclosan acetate | 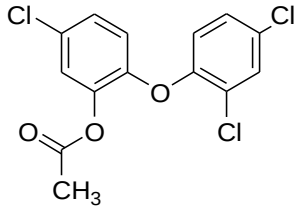 |
| Triclosan laurate | 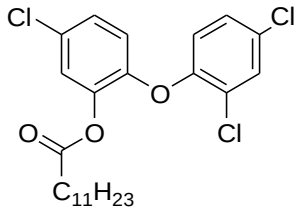 |
| Triclosan benzoate | 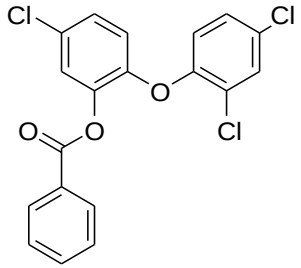 |

**Table 2.2.3** Chemical structures of novel imidazolium (A-C) and novel silver (D-F) compounds

| **Compound** | **Structure** |
|---|---|
| **A**<br>3-hexadecyl-1-methyl-1H-imidazole-3-ium bromide | 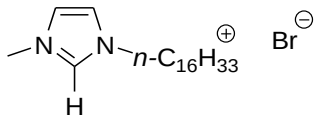 |
| **B**<br>1-(2,3-dihydroxypropyl)-3-hexadecyl-1H-imidazole-3-ium bromide | 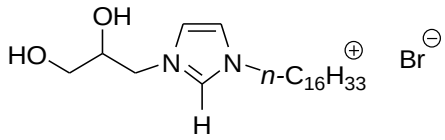 |
| **C**<br>3-hexadecyl-1-isopropyl-1H-imidazole-3-ium bromide | 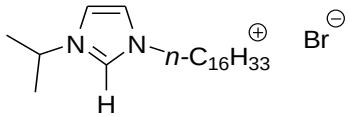 |
| **D**<br>(1-hexadecyl-3-methylimidazol-2-ylidene)silver(I) bromide | 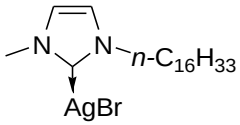 |
| **E**<br>(1-(2,3-dihydroxypropyl)-3-hexadecylimidazol-2-ylidene)silver(I) bromide | 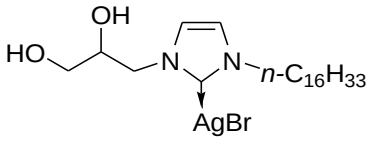 |
| **F**<br>(1-hexadecyl-3-isopropylimidazol-2-ylidene)silver(I) | 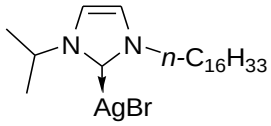 |

**Table 2.2.4** Chemical Structures of commercially available compounds evaluated

| **Compound** | **Structure** |
|---|---|
| Epsilon Poly-L-lysine | 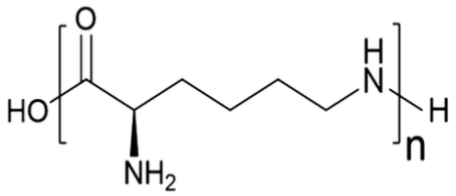 |
| Compound 1771<br><br>[2-oxo-2-(5-phenyl-1,3,4-oxadiazol-2-ylamino)ethyl-2-naphtho[2,1-*b*]furan-1-ylacetate] | 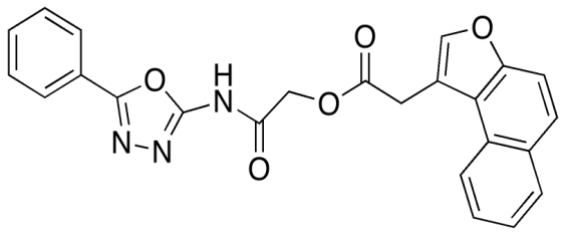 |

### 2.2.4 Determination of minimum inhibitory concentrations (MICs)

Briefly, the optical density of a 16-24 h bacterial culture in Muller-Hinton broth (MHB) was determined and adjusted to a 0.5 McFarlane standard by addition of culture medium. The bacterial suspension (100 μl) was added to the wells of a 96-well plate. A 100-μl volume of the compound to be assessed was added to the bacterial suspension, mixed by pipetting, and incubated at 37°C for 24 h. The compound was added at two-fold the final working concentration to account for dilution. Bacteria only control wells contained 200 μl of bacterial suspension only, and media only control wells contained 200 μl of MHB. All tests were repeated in triplicate and bacterial growth was determined by measuring the change in OD at 620 nm. Percentage inhibition was calculated using the following equation:

$$\%\ inhibition = \frac{sample\ OD\ (620\ nm) - media\ control\ OD\ (620\ nm)}{bacteria\ only\ control\ OD\ (620\ nm)} \times 100$$

The concentration of compound resulting in 80% or more inhibition in bacterial growth was recorded as the MIC.

### 2.2.5 Determination of minimum biocidal concentrations

Following determination of the MIC, the entire 200 μl volume of the incubated bacteria/drug suspension was transferred to 2 ml of fresh MHB (in triplicate) and incubated at 37°C for 24 h. Negative and positive control samples were also prepared. The concentration where no visible growth was evident after incubation was recorded as the minimum biocidal concentration (MBC).

### 2.2.6 Minimum biofilm eradication concentration

The OD (620 nm) of 16-24 h bacterial cultures was read and adjusted with MHB to a 0.5 McFarlane standard. A 100 μl volume of the suspension was added to wells of a 96-well microtiter plate and incubated at 37°C for 24 h. Planktonic bacteria were removed by removal of the culture media and the subsequent addition and removal of sterile phosphate buffered saline (PBS). This washing step was repeated 3 times. A 100 μl volume of the test compound was then added to each well. Following overnight incubation at 37°C, the culture medium was removed by pipetting, and 100 μl of fresh MHB added. The biofilm was disrupted by repeated pipetting in the fresh culture medium. The OD at 620 nm was recorded, and the plate incubated for a further 24 h period. The OD at 620 nm was then measured and the MBEC recorded as the concentration of compound that inhibited bacterial proliferation at >80% compared with bacteria only controls not exposed to the compound. Wells containing MHB only were also set up. Percentage inhibition was calculated using:

$$\%\ inhibition = \frac{sample\ OD\ (620\ nm) - media\ control\ OD\ (620\ nm)}{bacteria\ only\ control\ OD\ (620\ nm)} \times 100$$

### 2.2.7 Quantification of virulence gene expression following antimicrobial treatment

Microorganisms were sub-cultured from a single colony grown on appropriate agar into liquid broth and cultured for 16-24 h at 37°C. Cultures were diluted to 0.2 OD

$_{600nm}$ with MHB and a 250 μl volume was added to 250 μl of test compound at double the required concentration and incubated for 2 h at 37°C on an orbital shaker. The final concentrations were at sub-inhibitory concentrations. Cultures without test compound were also set up as controls.

Following incubation, the cultures were stabilised by the addition of double volume of RNA protect (Qiagen) to each inoculum. Cultures were vortexed, incubated at room temperature for 5 min and spun at 5000 x g for 10 min. Supernatants were decanted and the remaining pellets were stored at -80 °C.

#### 2.2.7.1 RNA extraction

RNA extraction was performed using the RNeasy Mini Kit (Qiagen). Centrifugation steps were performed at 8000 x g unless otherwise stated.

In the case of *E. coli*, 100 μl Tris EDTA buffer (10mM Tris.HCl, 1 mM EDTA, pH 8.0) containing lysozyme (10mg/ml) was added to thawed pellets and incubated at room temperature for 10 min, with vortex mixing every 2 min. For *S. aureus*, 200 μl of lysostaphin (100 μg/ml in Tris EDTA buffer) was added to each pellet, vortexed and incubated at 37 °C for 20 min. *C. albicans* pellets were treated with 100 μl of lyticase (100 units/ml in TE buffer) and incubated at 37°C for 1 h, with vortex mixing at 20 min intervals.

Three hundred and fifty μl of RLT buffer containing 1% (v/v) β-mercaptoethanol was added and vortex mixed for 10 s. Samples were transferred to sterile microcentrifuge tubes containing 1/3 glass lysis beads of mixed diameter and vortex mixed for 15 s. A 500 μl volume of phenol: chloroform: isoamyl alcohol (25:24:1) was added to each sample, vortexed for 1 min and centrifuged for 5 min. The upper aqueous phase was transferred to new microcentrifuge tube containing 700 μl of 100% molecular biology grade ethanol. The samples were placed at –20 °C for 15 min to allow protein precipitation to occur. The resulting lysates were transferred to spin columns and centrifuged for 1 min. The flow through was discarded and any excess lysate was added to the spin column and centrifuged.

The spin column membrane was washed by the addition of 350 μl buffer RW1 and subsequent centrifugation for 15 s. The flow-through was discarded. Residual DNA was removed by the direct application of 80 μl of pre-prepared DNase I (Qiagen) to the column membrane. Following a 20 min incubation step at room

temperature, the membrane was washed with 350 μl buffer RW1, incubated for 5 min at room temperature, centrifuged for 15 s and the flow-through discarded.

A 500 μl volume of RPE buffer was added to the RNeasy Spin Columns and the columns were centrifuged for 15 s and the flow-through discarded. A further 500 μl of buffer RPE was added as a wash step with centrifugation for 2 min.

The RNeasy Spin Columns were placed in new collection tubes and 35 μl of RNase-free water (Qiagen) was added directly to the membrane. Tubes were centrifuged for 1 min and the resulting eluent was reapplied to the membrane and re-centrifuged. The eluted RNA was immediately placed on ice for immediate RNA quantification or stored at - 80 °C if required at a later timepoint.

RNA quantification was carried out using the NanoVue Plus instrument (GE Healthcare), according to the manufacturer's instructions. Quality of RNA was assessed by obtaining the A260/A280 and A260/A230 ratios. Values between 1.8 and 2.0 were acceptable for A260/A280 and between 2.0 and 2.2 for A260/A230.

#### 2.2.7.2 Reverse transcription of RNA to cDNA

All reagents for reverse transcription of RNA to cDNA were obtained from Promega (Southampton, UK), unless otherwise stated.

Five hundred ng of RNA was added to 1 μl of random primers and made up to a total volume of 13 μl with nuclease-free water. Samples were heated to 70 °C for 5 min to allow annealing of the random primers to occur and cooled to 4 °C for 5 min using a benchtop thermocycler. A master mix containing 5 μl MMLV buffer, 5 μl dNTP mix (10 mM), 1 μl RNase inhibitor and 1 μl reverse transcriptase per reaction was made. Twelve μl of master mix was added to the RNA and random primer sample, mixed by pipetting, heated to 37 °C for 1 h and cooled to 4 °C in the benchtop thermal cycler. The generated cDNA samples were stored at – 20 °C until required.

#### 2.2.7.3 Primer preparation

Lyophilised primers (MWG Biotech, Germany) (Tables 2.2.5, 2.2.6 & 2.2.7) were reconstituted in nuclease-free water to achieve stock concentrations of 100 pmol/μl. Working stocks of 10 μM were prepared with nuclease-free water.

**Table 2.2.5** Primer sequences of *Escherichia coli* virulence genes (reported in Yang et al. 2016)

| Target Gene | Primer sequence (5'-3') | Functions of encoded products |
|---|---|---|
| ***16* s** | F - CAAGGGCACAACCTCCAAAT<br>R - GTGTAGCGGTGAAATGCGTAGAG | Structural role. Defines the positions of ribosomal proteins. |
| ***fim H*** | F - TTTGCGACAGACCAACAACT<br>R - GACATCACGAGCAGAAGCAT | Adhesin. Mediates bacterial attachment. |
| ***uvr Y*** | F - TCAGACAAACTGGCAAATGG<br>R - CTATTCAGGGCAGCGTTACA | Controls transcription of adhesins. |
| ***csr A*** | F - CCTGGATACGCTGGTAGAT<br>R - TCGTCGAGTTGGTGAGAC | RNA binding protein. Repressor of biofilm formation and activator of biofilm dispersal. |

**Table 2.2.**6 Primer sequences of *Candida albicans* virulence genes (reported in Morse et al. 2019)

| Target Gene | Primer sequence (5'-3') | Functions of encoded products |
|---|---|---|
| **Actin 1** ***(act 1)*** | F - TGCTGAACGTATGCAAAAGG<br>R - TGAACAATGGATGGACCAGA | Structural integrity of the cytoskeleton |
| **Hyphal wall protein 1** ***(hwp 1)*** | F - TCTACTGCTCCAGCCACTGA<br>R - CCAGCAGGAATTGTTTCCAT | Glycoprotein located on the cell surface. A substrate of mammalian transglutaminase |
| **Epithelial adhesin 1** ***(epa 1)*** | F - ATGTGGCTCTGGGTTTTACG<br>R - TGGTCCGTATGGGCTAGGTA | Mediates interaction with host cells. |
| **Secreted aspartyl proteinase 4** ***(sap 4)*** | F – GTCAATGTCAACGCTGGTGTCC<br>R - ATTCCGAAGCAGGAACGGTGTCC | Nutrient acquisition, invasion, tissue damage. |
| **Secreted aspartyl proteinase 6** ***(sap 6)*** | F – AAAATGGCGTGGTGACAGAGGT<br>R - CGTTGGCTTGGAAACCAATACC | Nutrient acquisition, invasion, tissue damage. |
| **Agglutinin-like sequence 1** ***(als 1)*** | F – CCCAACTTGGAATGCTGTTT<br>R – TTTCAAAGCGTCGTTCACAG | Adhesin formed from glycoproteins and located on the cell surface. |
| **Agglutinin-like sequence 3** ***(als 3)*** | F – CTGGACCACCAGGAAACACT<br>R – GGTGGAGCGGTGACAGTAGT | Adhesin formed from glycoproteins and located on the cell surface. |
| **Phospholipase D** ***(pld 1)*** | F - GCCAAGAGAGCAAGGGTTAGCA<br>R – CGGATTCGTCATCCATTTCTCC | Hydrolyses phospholipids to signalling products. Important role in growth, development, stress response and dimorphic transition. |

**Table 2.2.7 Primer** sequences of *Staphylococcus aureus* virulence genes

| Target Gene | Primer sequence (5'-3') | Functions of encoded products | Reference |
|---|---|---|---|
| ***16* s** | F- GGGACCCGCACAAGCGGTGG<br>R- GGGTTGCGCTCGTTGCGGGA | Structural role. Defines the positions of ribosomal proteins. | (Atshan et al. 2013) |
| **Fibronectin binding protein B *(fnb B)*** | F- ACGCTCAAGGCGACGGCAAAG<br>R- ACCTTCTGCATGACCTTCTGCACCT | Adhesion to cells and internalisation by cells. | (Atshan et al. 2013) |
| **Intercellular adhesin *B* *(ica B)*** | F- ATACCGGCGACTGGGTTTAT<br>R- TTGCAAATCGTGGGTATGTGT | Mediates production of polysaccharide intercellular adhesin (PIA). | (Atshan et al. 2013) |
| **Intercellular adhesin C *(ica C)*** | F- CTTGGGTATTTGCACGCATT<br>R- GCAATATCATGCCGACACCT | Mediates production of polysaccharide intercellular adhesin (PIA). | (Atshan et al. 2013) |
| **Intercellular adhesin D *(ica D)*** | F- ACCCAACGCTAAAATCATCG<br>R- GCGAAAATGCCCATAGTTTC | Mediates production of polysaccharide intercellular adhesin (PIA). | (Atshan et al. 2013) |
| ***fts Z*** | F- ATCCAAATCGGTGAAAAATTAACAC<br>R- CCATGTCTGCACCTTGGATTG | Cell division protein. | (Duquenne et al. 2010) |
| **DNA gyrase B *(gyr B)*** | F- CCAGGTAAATTAGCCGATTGC<br>R- AAATCGCCTGCGTTCTAGAG | Subunit of DNA gyrase. Involved in DNA supercoiling. | (Rudkin et al. 2012) |

#### 2.3.7.4 Quantitative polymerase chain reaction

cDNA was diluted 1:10 using nuclease free-water. A master mix containing 10 μl of 2 x Precision Fast Master Mix (Primer Design, Southampton, UK), 2 μl forward primer, 2 μl reverse primer and 1 μl nuclease free water per reaction was made. 15 μl of master mix was added to 5 μl of diluted cDNA in a 96-well QPCR plate (Primer Design). Each sample was set up in duplicate. The following program was run on the QuantStudio 6 Flex Real Time PCR system (Applied Biosystems): 95 °C for 2 min, followed by 40 cycles of 95 °C for 5 s, 60 °C for 20 s. A post amplification melt curve step was run following completion of the cycles consisting of 95 °C for 15 s, 60 °C for 1 min and 95 °C for 15 s. The software automatically determined the amplification threshold for each sample. Virulence gene expression of treated cultures were calculated relative to non-treated controls and normalised to an endogenous control gene. Analysis of relative gene expression was calculated using the ΔΔCt method (Livak and Schmittgen 2001).

#### 2.3.7.5 Statistical analysis

Statistical analysis was performed using GraphPad Prism version 6.0c (GraphPad, CA, USA). One-way ANOVA followed by Dunnett's multiple comparisons test was used to calculate P values at the 95% confidence interval.

## 2.3 Results

### 2.3.1 Minimum inhibitory concentrations

A summary of the antimicrobial activity of tested compounds is presented in Table 2.3.1. Triclosan MIC values were 0.78 μg/ml for 6 out of the 8 microorganisms tested. *Serratia marcescens* and *P. aeruginosa* were resistant to triclosan at all the tested concentrations. Compound A was highly effective at inhibiting *S. aureus*, with an MIC value of 0.78 μg/ml recorded. Higher MICs (100 μg/ml) were evident for *E. coli, K. pneumoniae* and *S. marcescens*. *Proteus mirabilis*, *P. stuartii* or *P. aeruginosa* were all resistant to compound A.

At a low concentration (3.125 μg/ml), compound B was inhibitory to planktonic growth of *S. aureus but* was ineffective against the other microorganisms. An MIC of 1.58 μg/ml was similarly obtained for compound C against *S. aureus*. Higher MIC values of 50 μg/ml were evident for *E. coli*, *P. mirabilis* and *S. marcescens*.

For compound C, MIC values against *K. pneumoniae* and *P. aeruginosa* were 100 μg/ml, and no inhibition was evident against *P. stuartii*.

An MIC of 50 μg/ml for compound D against *P. aeruginosa* was recorded. *Escherichia coli*, *S. aureus*, *P. mirabilis*, *K. pneumoniae* demanded higher concentrations (100 μg/ml) to inhibit planktonic growth. Compound D did not inhibit *S. marc*escens.

Compound E was only effective at inhibiting growth of *Candida albicans,* with an MIC value of 3.125 μg/ml.

Compound F was inhibitory at a concentration of 100 μg/ml against *E. coli*, *P. mirabilis*, *K. pneumoniae*, *P. stuartii*, *S. marcescens* and the usually resistant *P. aeruginosa*. Lower MIC values (25 μg/ml) were obtained against *C. albicans* and *S. aureus*.

Triclosan acetate was effective at inhibiting 7 of the 8 organisms tested, with *S. marcescens* presenting as the resistant organism. Interestingly, *P. aeruginosa* was inhibited at a concentration of 0.78 μg/ml, whilst it was resistant to triclosan at all concentrations. A low concentration of 0.024 μg/ml was required to inhibit the growth of the Gram-positive bacteria, *Staphylococcus aureus*. *Klebsiella pneumoniae* was inhibited at a low triclosan acetate concentration (0.39 μg/ml), whilst double the concentration was required to inhibit *E. coli*, *P. mirabilis* and *P. stuartii*. *Serratia marcescens* was resistant to triclosan acetate.

The triclosan ester, triclosan laurate, was effective at inhibiting the growth of *E. coli*, *P. mirabilis* and *K. pneumoniae* at 100 μg/ml, whilst 50 μg/ml inhibited *P. stuartii*. A concentration of 12.5 μg/ml was sufficient to inhibit *S. aureus*. *Candida albicans*, *S. marcescens* and *P. aeruginosa* were resistant to triclosan laurate.

*Staphylococcus aureus* was inhibited by the triclosan ester, triclosan benzoate at a concentration of 0.78 μg/ml, whilst all other organisms were resistant.

*Proteus mirabilis*, *P. stuartii* and *S. marcescens* were resistant to the polymer, poly-L-lysine at the concentrations tested, but *S. aureus* and *P. aeruginosa* were effectively inhibited at a concentration of 25 μg/ml. A higher concentration of 50 μg/ml was sufficient to inhibit the growth of *E. coli*. A further increase to 100 μg/ml led to inhibition of *K. pneumoniae* and *C. albicans*.

A 1% (v/v) solution of caprylic acid inhibited growth of *C. albicans* and *P. stuartii,* whilst 3% caprylic acid effectively inhibited the often-resistant bacteria, *S. marcescens* and *P. aeruginosa*. All other microorganisms were resistant at the concentrations tested.

The bioflavonoid product, Citrox®, was able to inhibit the growth of *S. aureus* at 0.25% (v/v). Doubling the concentration led to the inhibition of *C. albicans*, *P. mirabilis* and *P. stuartii*. A further increase to 1% led to inhibition of *E. coli*, *S. marcescens* and *P. aeruginosa*. No inhibition was evident against *K. pneumoniae*.

The commercial and synthesised versions of compound 1771 produced identical MICs against the strains of *S. aureus* and *E. faecium*. All values were 3.125 – 6.25μg/ml.

**Table 2.3.2** Minimum inhibitory concentrations (MICs). Thirteen compounds were tested against a panel of 8 CAUTI causing microorganisms. Two versions of compound 1771 were tested against 3 strains of 2 species of Gram-positive bacteria. Values represent the mode of three independent experiments

| MIC µg/ml | *Candida albicans* ATCC 90028 | *Escherichia coli* NCTC 12923 | *Staphylococcus aureus* NSM 7 | *Proteus mirabilis* 12 RTB | *Klebsiella pneumoniae* P6 wk2 | *Providencia stuartii* NSM 58 | *Serratia marcescens* NSM 51 | *Pseudomonas aeruginosa* NCTC 10662 | *Staphylococcus aureus* NSM 5 | *Staphylococcus aureus* NSM 49 | *Staphylococcus aureus* P10 6/9 | *Enterococcus faecium* Q41 | *Enterococcus faecium* Q11 | *Enterococcus faecium* M49 |
|---|---|---|---|---|---|---|---|---|---|---|---|---|---|---|
| **Triclosan** | 3.125 | 0.39 | 0.39 | 0.39 | 0.78 | 0.39 | > 100 | > 100 | NT | NT | NT | NT | NT | NT |
| **Triclosan acetate** | 12.5 | 0.78 | 0.024 | 0.78 | 0.39 | 0.78 | > 100 | 0.78 | NT | NT | NT | NT | NT | NT |
| **Triclosan laurate** | > 100 | 100 | 12.5 | 100 | 100 | 50 | > 100 | > 100 | NT | NT | NT | NT | NT | NT |
| **Triclosan benzoate** | > 100 | > 100 | 0.78 | > 100 | > 100 | > 100 | > 100 | > 100 | NT | NT | NT | NT | NT | NT |
| **3-hexadecyl-1-methyl-1H-imidazole-3-ium bromide (A)** | 6.25 | 100 | 0.78 | > 100 | 100 | > 100 | 100 | > 100 | NT | NT | NT | NT | NT | NT |
| **1-(2,3-dihydroxypropyl)-3-hexadecyl-1H-imidazole-3-ium bromide (B)** | 1.58 | > 100 | 3.125 | > 100 | > 100 | > 100 | > 100 | > 100 | NT | NT | NT | NT | NT | NT |
| **3-hexadecyl-1-isopropyl-1H-imidazole-3-ium bromide (C)** | 3.125 | 50 | 1.58 | 50 | 100 | > 100 | 50 | 100 | NT | NT | NT | NT | NT | NT |
| **1-hexadecyl-3-methylimidazol-2-ylidene) silver(I) bromide (D)** | 3.125 | 100 | 100 | 100 | 100 | 100 | > 100 | 50 | NT | NT | NT | NT | NT | NT |
| **1-(2,3-dihydroxypropyl)-3-hexadecylimidazol-2-ylidene) silver(I) bromide (E)** | 3.125 | > 100 | > 100 | > 100 | > 100 | > 100 | > 100 | > 100 | NT | NT | NT | NT | NT | NT |
| **(1-hexadecyl-3-isopropylimidazol-2-ylidene) silver(I) bromide (F)** | 25 | 100 | 25 | 100 | 100 | 100 | 100 | 100 | NT | NT | NT | NT | NT | NT |
| **Poly-L-lysine** | 100 | 50 | 25 | > 100 | 100 | > 100 | > 100 | 25 | NT | NT | NT | NT | NT | NT |
| **Caprylic Acid (% v/v)** | 1.5 | > 6 | > 6 | > 6 | > 6 | 1.5 | 3 | 3 | NT | NT | NT | NT | NT | NT |
| **Citrox (% v/v)** | 0.5 | 1 | 0.25 | 0.5 | > 1 | 0.5 | 1 | 1 | NT | NT | NT | NT | NT | NT |
| **Compound 1771 (Commercial)** | NT | NT | NT | NT | NT | NT | NT | NT | 3.125 | 6.25 | 6.25 | 3.125 | 3.125 | 6.25 |
| **Compound 1771 (Synthesised)** | NT | NT | NT | NT | NT | NT | NT | NT | 3.125 | 6.25 | 6.25 | 3.125 | 3.125 | 6.25 |

NT = Not Tested

### 2.3.2 Minimum biocidal concentrations

A summary of bactericidal activity of the compounds tested is presented in Table 2.3.2. Triclosan was not biocidal for any of the microorganisms tested. Compound A was only biocidal against *E. coli, K. pneumoniae* and *S. marcescens* at the highest concentration tested (100 μg/ml). Compound C was biocidal against *S. aureus* at 3.125 μg/ml and 50 μg/ml was biocidal against *E. coli* and *P. mirabilis*. Biocidal activity was observed with compound C at 100 μg/ml against *K. pneumoniae* and *S. marcescens*, but there was no activity against *P. stuartii* or *P. aeruginosa*. Compound D was biocidal against *E. coli* at 50 μg/ml, whilst 100 μg/ml elicited biocidal activity against *P. mirabilis*, *K. pneumoniae* and *P. aeruginosa*. Compound D was not biocidal against *S. aureus*, *P. stuartii* or *P. aeruginosa*. Compounds B and E were ineffective in producing biocidal action against any of the pathogens tested.

An MBC of 100 μg/ml was obtained against 6 out of 8 microorganisms for compound F. An MBC of 200 μg/ml was obtained against *Staphylococcus aureus,* whist *P. stuartii* was resistant.

Although triclosan proved not to have any biocidal activity against any of the CAUTI causing organisms at the concentrations tested, its derivative triclosan acetate was biocidal against *S. aureus* at a low concentration of 0.195 μg/ml. Increasing the concentration of triclosan acetate to 0.78 μg/ml enabled destruction of *E. coli*, *P. mirabilis*, *K. pneumoniae* and *P. stuartii*. At concentrations up to 200 μg/ml, *C. albicans*, *S. marcescens* and *P. aeruginosa* were resistant to the biocidal actions of triclosan acetate.

Triclosan laurate and triclosan benzoate only exerted biocidal activity against *Staphylococcus aureus* at 100 μg/ml and 1.58 μg/ml, respectively.

A minimum biocidal concentration of 100 μg/ml of poly-L-lysine was obtained for all microorganisms, with the exception of *Klebsiella pneumoniae* and *Serratia marcescens,* which were resistant at the concentrations tested.

Caprylic acid demonstrated biocidal activity against *Candida albicans*, *P. stuartii* and *S. marcescens* at 1.5, 3 & 6% respectively. Biocidal activity was not detected against the remaining 5 bacteria.

A 1% solution of Citrox® was sufficient to elicit biocidal activity against *Pseudomonas aeruginosa.* Such activity was not demonstrated in the remaining organisms.

Minimum biocidal concentrations between 50 and 100 μg/ml were obtained for both versions of compound 1771 against *S. aureus* and *E. faecium.*

No minimum biofilm eradication concentrations (MBECs) were obtained for any of the compounds tested against any microorganism, although it should be noted that MBEC assays were not performed using compound 1771.

**Table 2.3.3** Minimum biocidal concentrations (MBCs). Thirteen compounds were tested against a panel of 8 CAUTI causing microorganisms. Two versions of compound 1771 were tested against 3 strains of 2 species of Gram-positive bacteria. Values represent the mode of three independent experiments

| MBC µg/ml | *Candida albicans* ATCC 90028 | *Escherichia coli* NCTC 12923 | *Staphylococcus aureus* NSM 7 | *Proteus mirabilis* 12 RTB | *Klebsiella pneumoniae* P6 wk2 | *Providencia stuartii* NSM 58 | *Serratia marcescens* NSM 51 | *Pseudomonas aeruginosa* NCTC 10662 | *Staphylococcus aureus* NSM 5 | *Staphylococcus aureus* NSM 49 | *Staphylococcus aureus* P10 6/9 | *Enterococcus faecium* Q41 | *Enterococcus faecium* Q11 | *Enterococcus faecium* M49 |
|---|---|---|---|---|---|---|---|---|---|---|---|---|---|---|
| **Triclosan** | > 200 | > 200 | > 200 | > 200 | > 200 | > 200 | > 200 | > 200 | NT | NT | NT | NT | NT | NT |
| **Triclosan acetate** | > 200 | 0.78 | 0.195 | 0.78 | 0.78 | 0.78 | > 200 | > 200 | NT | NT | NT | NT | NT | NT |
| **Triclosan laurate** | > 200 | > 200 | 100 | > 200 | > 200 | > 200 | > 200 | > 200 | NT | NT | NT | NT | NT | NT |
| **Triclosan benzoate** | > 200 | > 200 | 1.58 | > 200 | > 200 | > 200 | > 200 | > 200 | NT | NT | NT | NT | NT | NT |
| **3-hexadecyl-1-methyl-1H-imidazole-3-ium bromide (A)** | > 200 | 100 | > 200 | > 200 | 100 | > 200 | 100 | > 200 | NT | NT | NT | NT | NT | NT |
| **1-(2,3-dihydroxypropyl)-3-hexadecyl-1H-imidazole-3-ium bromide (B)** | > 200 | > 200 | > 200 | > 200 | > 200 | > 200 | > 200 | > 200 | NT | NT | NT | NT | NT | NT |
| **3-hexadecyl-1-isopropyl-1H-imidazole-3-ium bromide (C)** | > 200 | 50 | 3.125 | 50 | 100 | > 200 | 100 | > 200 | NT | NT | NT | NT | NT | NT |
| **1-hexadecyl-3-methylimidazol-2-ylidene)silver(I) bromide (D)** | > 200 | 50 | > 200 | 100 | 100 | > 200 | > 200 | 100 | NT | NT | NT | NT | NT | NT |
| **1-(2,3-dihydroxypropyl)-3-hexadecylimidazol-2-ylidene)silver(I) bromide (E)** | > 200 | > 200 | > 200 | > 200 | > 200 | > 200 | > 200 | > 200 | NT | NT | NT | NT | NT | NT |
| **(1-hexadecyl-3-isopropylimidazol-2-ylidene)silver(I) bromide (F)** | 100 | 100 | 50 | 100 | 100 | > 200 | 100 | 100 | NT | NT | NT | NT | NT | NT |
| **Poly-L-lysine** | 100 | 100 | 100 | 100 | > 200 | 100 | > 200 | 100 | NT | NT | NT | NT | NT | NT |
| **Caprylic Acid (% v/v)** | 1.5 | > 6 | > 6 | > 6 | > 6 | 3 | 6 | > 6 | NT | NT | NT | NT | NT | NT |
| **Citrox (% v/v)** | > 1 | > 1 | > 1 | > 1 | > 1 | > 1 | > 1 | 1 | NT | NT | NT | NT | NT | NT |
| **Compound 1771 (Commercial)** | NT | NT | NT | NT | NT | NT | NT | NT | 50 | 100 | 100 | 50 | 100 | 100 |
| **Compound 1771 (Synthesised)** | NT | NT | NT | NT | NT | NT | NT | NT | 50 | 100 | 100 | 50 | 100 | 100 |

NT = Not Tested

### 2.3.3 Quantification of selected *Escherichia coli* virulence gene expression

Virulence genes associated with uropathogenic strains of *Escherichia coli* were assessed to quantify changes in expression levels relative to non- treated controls, following exposure to triclosan and compound C ([HL]$^2$Br ), (Figures 2.3.1 and 2.3.2). *Fim H* expression was unaltered, following exposure to all concentrations of triclosan and [HL]$^2$BR tested, ($P>0.05$). Genes involved in the carbon storage regulatory system, c*sr A* and *uvr Y*, were also unaffected by triclosan and [HL]$^2$BR treatment at the concentrations tested ($P>0.05$).

### 2.3.4 Quantification of *Staphylococcus aureus* virulence gene expression

A host of virulence factors assist in the colonisation of *Staphylococcus aureus* on a variety of biotic and abiotic surfaces. The expression of the adhesin, fibronectin-binding protein B (*fnb*) was unaltered following treatment with triclosan and [HL]$^2$BR at all concentrations, relative to untreated cells ($P>0.05$), (Figures. 2.3.3 and 2.3.4). Expression of the gene encoding fts Z, a key protein involved in cell division of *S. aureus*, also remained unaltered, following treatment with triclosan and [HL]$^2$BR ($P>0.05$). Expression levels of other virulence genes associated with *S. aureus* pathogenesis, DNA gyrase B (*gyr B*) and the intercellular adhesin B, C & D genes (*ica B, ica C* & *ica D*) remained unchanged, following triclosan and [HL]$^2$BR treatment, relative to untreated *S. aureus* ($P>0.05$).

### 2.3.5 Quantification of *Candida albicans* virulence gene expression

The relative expression of a selection of *Candida albicans* virulence genes, following exposure to sub-MIC levels of triclosan and the novel imidazolium compound [HL]$^2$BR, in comparison to non-treated cultures were quantified and are summarised in Figures 2.3.5 and 2.3.6.

Epithelial adhesin 1 (*epa 1*), agglutinin-like sequence 1 & 3 (*als 1* & *3*), hyphal wall protein 1 (*hwp 1*), secreted aspartyl proteinases 4 & 6 (sap 4 & 6) and phospholipase D 1 (*pld 1*) gene expression remained unchanged ($P>0.05$), following exposure to both triclosan and [HL]$^2$BR at all concentrations tested.

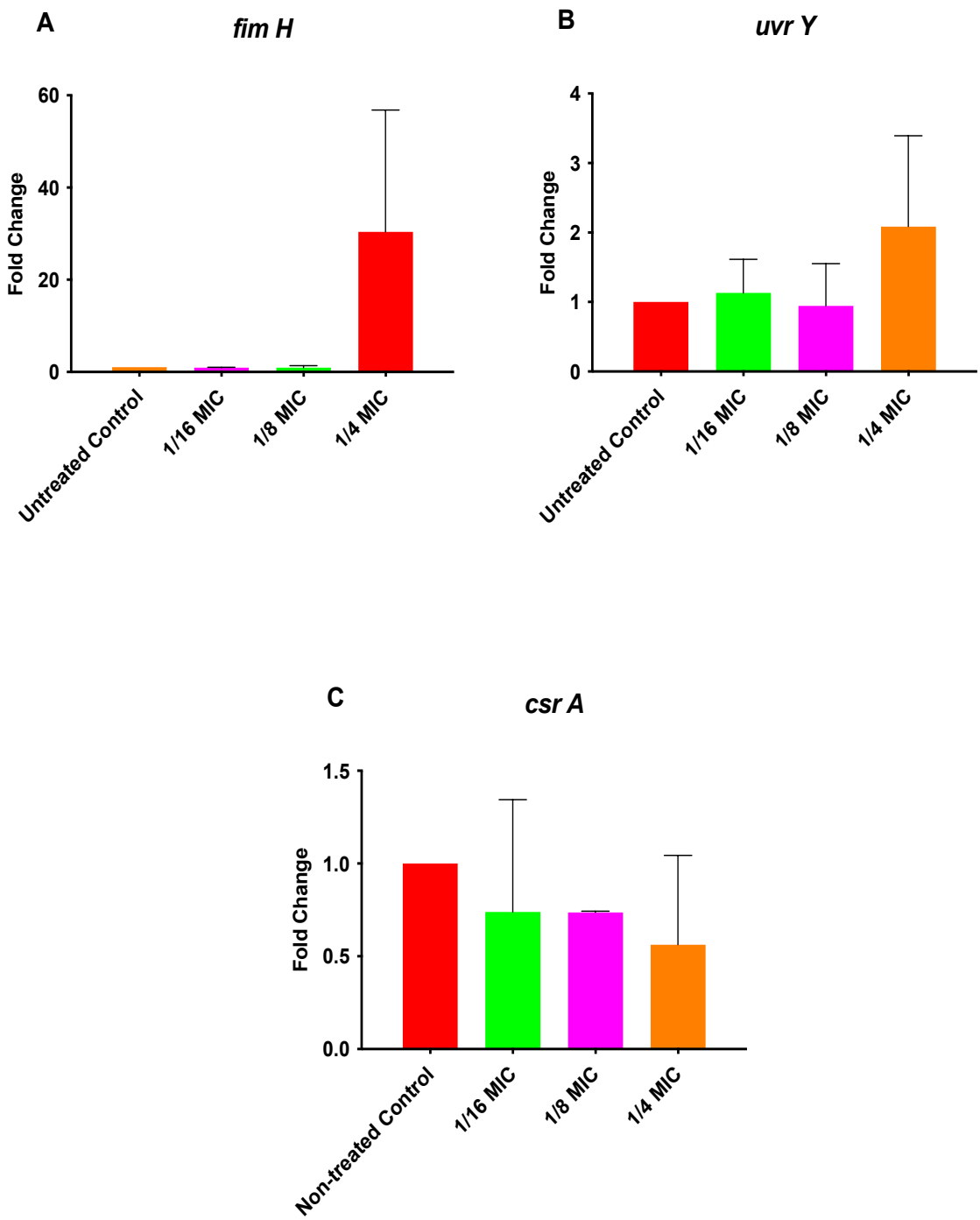


**Figure 2.3.1** The effect of triclosan on *Escherichia coli* virulence gene expression. Changes in expression following treatment with triclosan at 1/4 to 1/16 of the MIC concentration. Expression changes calculated relative to the housekeeping gene *16S* and normalised to non-treated controls. $^{\Delta\Delta}$Ct method was used for analysis. Data expressed as mean of 3 replicates. Error bars represent SD. *** $P<0.001$

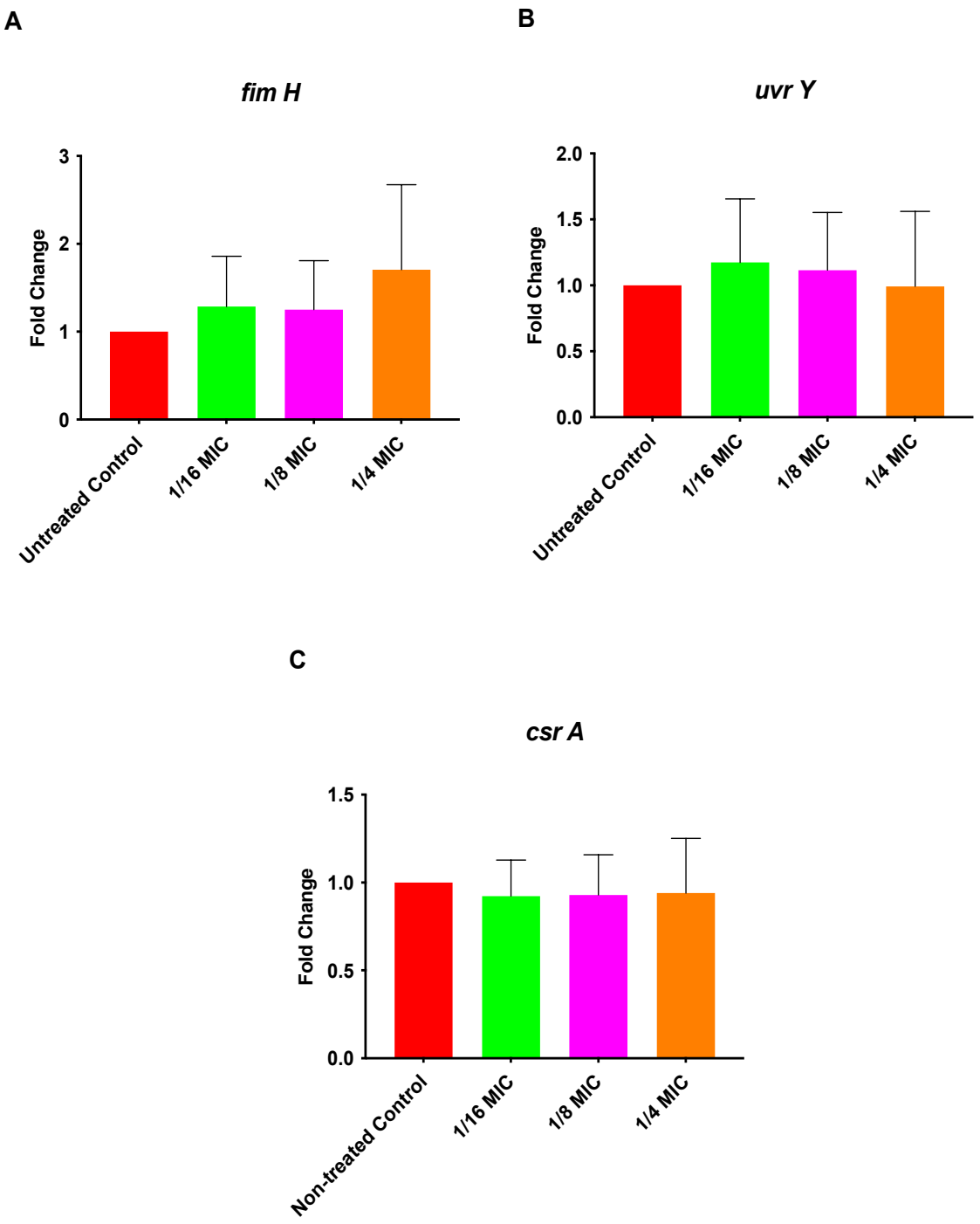


**Figure 2.3.2** The effect of $[HL]^2$ BR on *Escherichia coli* virulence gene expression. Changes in expression following treatment with $[HL]^2$ BR at 1/4 to 1/16 of the MIC concentration. Expression changes calculated relative to the housekeeping gene *16S* and normalised to non-treated controls. $^{\Delta\Delta}$Ct method was used for analysis. Data expressed as mean of 3 replicates. Error bars represent SD. *** $P<0.001$

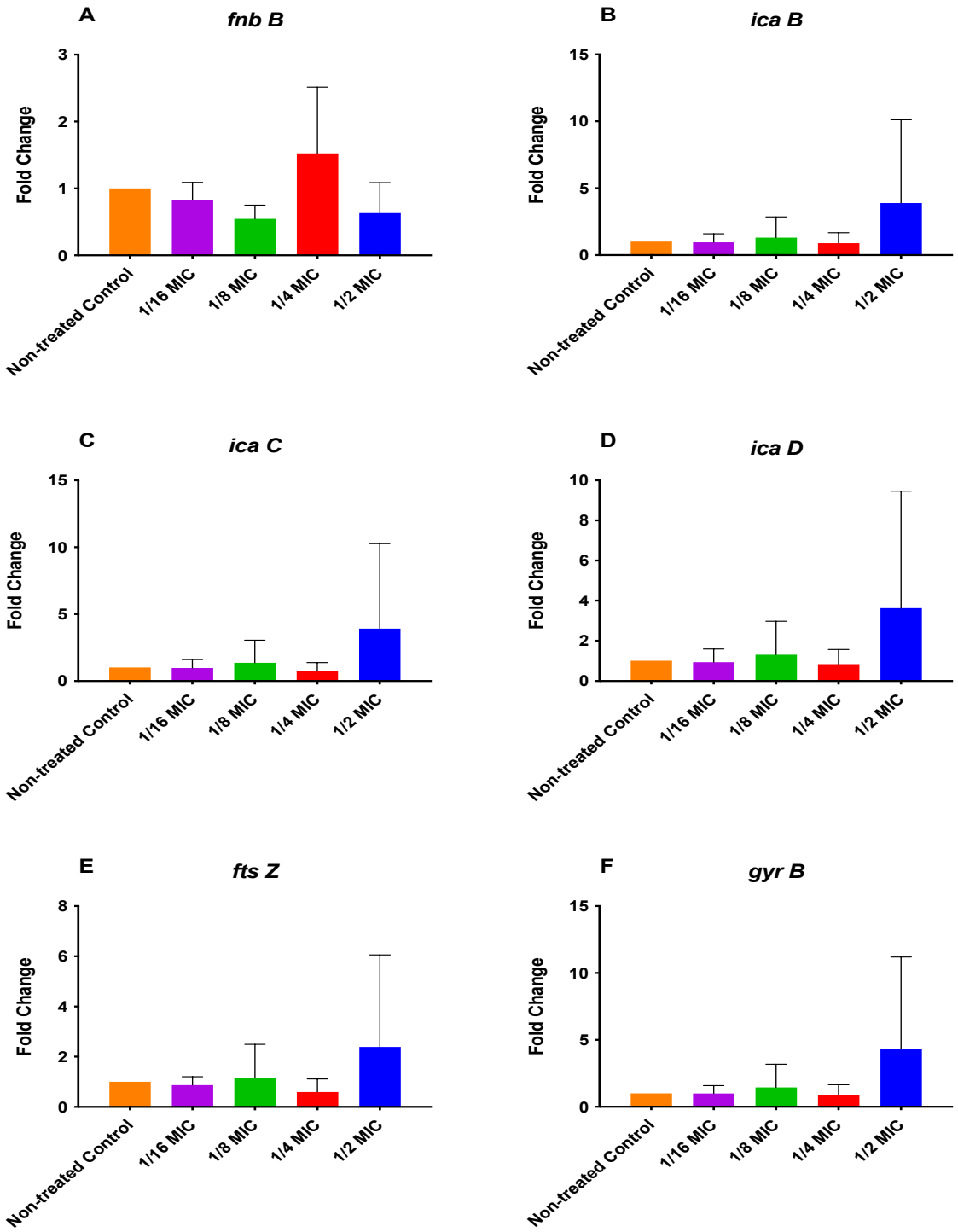


**Figure 2.3.3** The effect of triclosan on *Staphylococcus aureus* virulence gene expression. Changes in expression following treatment with triclosan at 1/4 to 1/16 of the MIC concentration. Expression changes calculated relative to the housekeeping gene *16S* and normalised to non-treated controls. $^{\Delta\Delta}$Ct method was used for analysis. Data expressed as mean of 3 replicates. Error bars represent SD

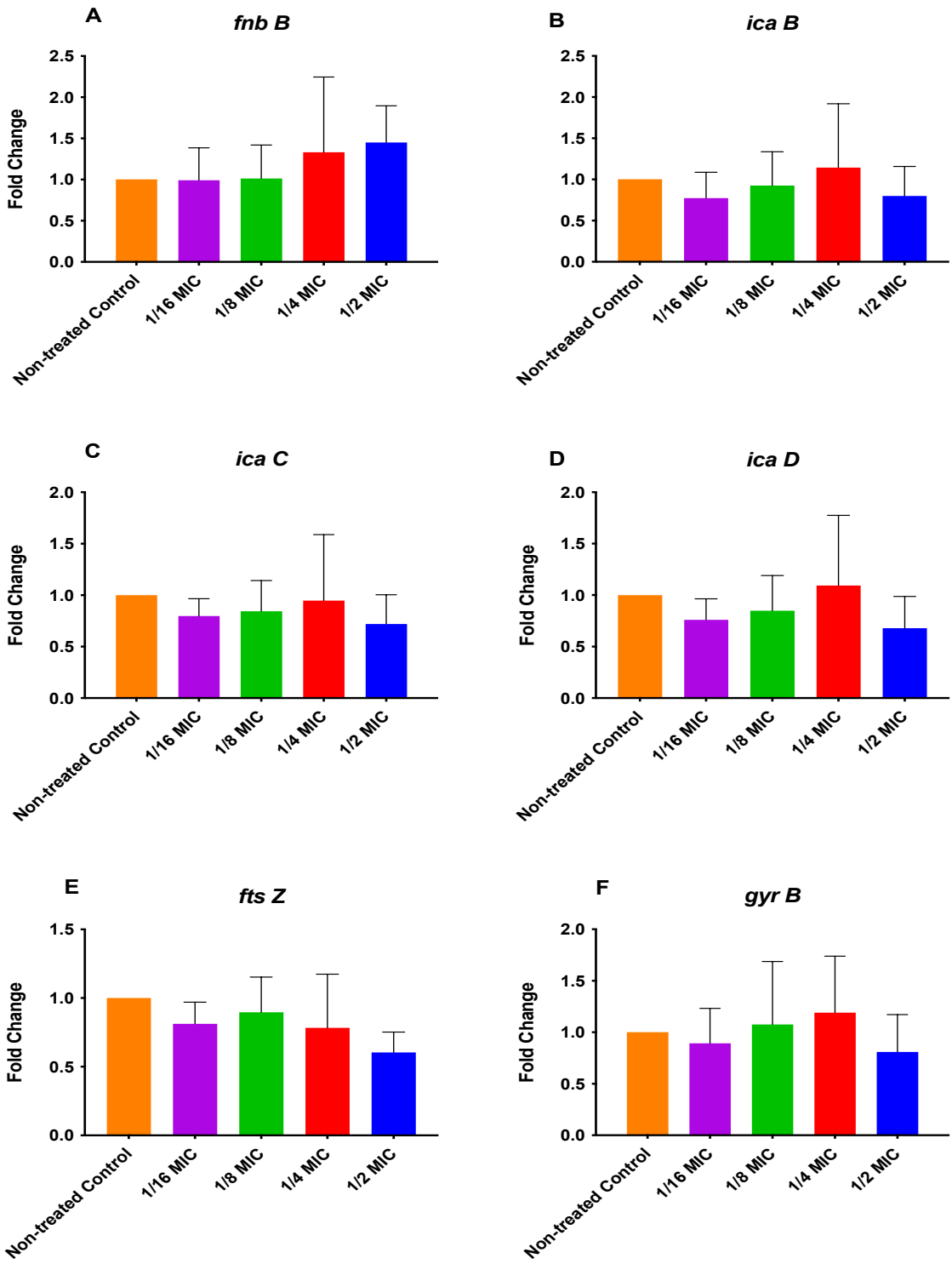


**Figure 2.3.4** The effect of $[HL]^2$ BR on *Staphylococcus aureus* virulence gene expression. Changes in expression following treatment with $[HL]^2$ BR at 1/4 to 1/16 of the MIC concentration. Expression changes calculated relative to the housekeeping gene *16S* and normalised to non-treated controls. $^{\Delta\Delta}$Ct method was used for analysis. Data expressed as mean of 3 replicates. Error bars represent SD

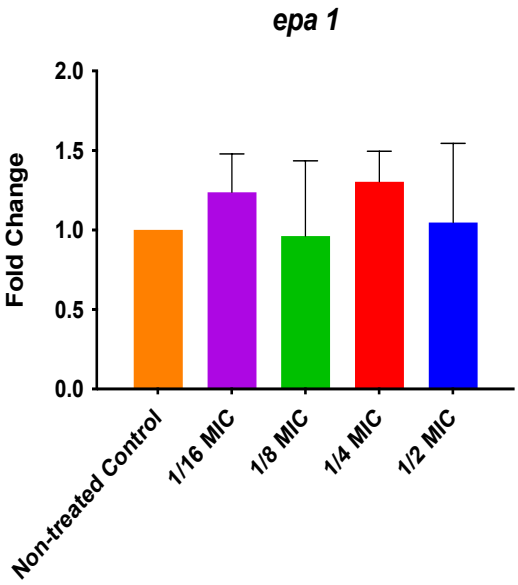
epa 1
Fold Change
2.0
1.5
1.0
0.5
0.0
Non-treated Control
1/16 MIC
1/8 MIC
1/4 MIC
1/2 MIC

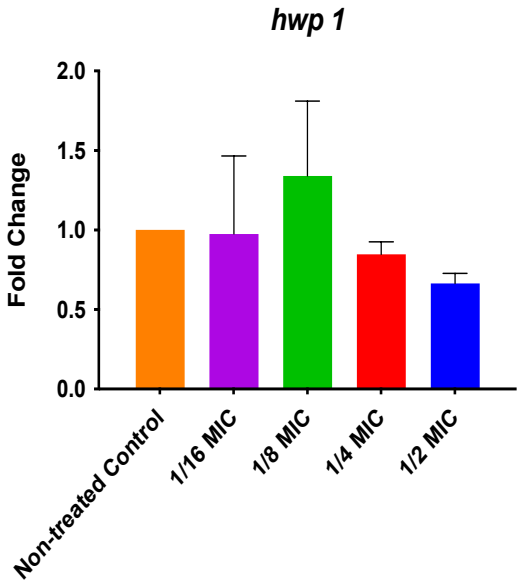
hwp 1
Fold Change
2.0
1.5
1.0
0.5
0.0
Non-treated Control
1/16 MIC
1/8 MIC
1/4 MIC
1/2 MIC

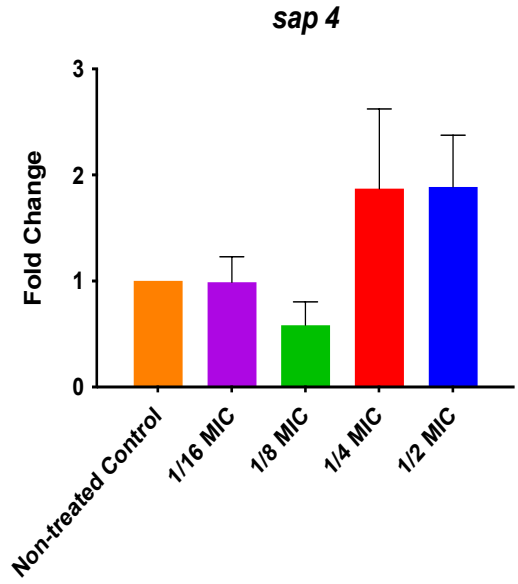
sap 4
Fold Change
3
2
1
0
Non-treated Control
1/16 MIC
1/8 MIC
1/4 MIC
1/2 MIC

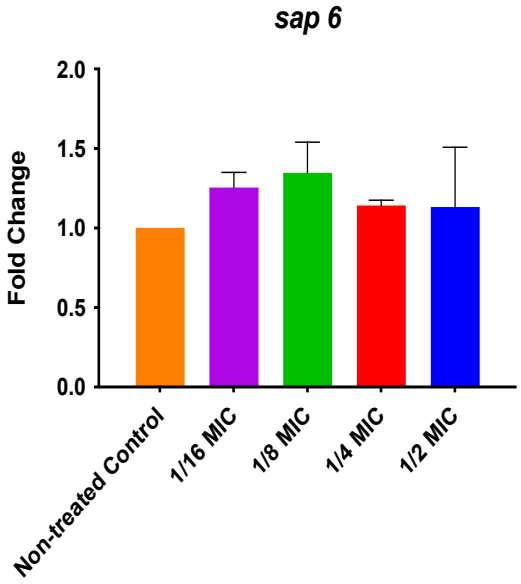
sap 6
Fold Change
2.0
1.5
1.0
0.5
0.0
Non-treated Control
1/16 MIC
1/8 MIC
1/4 MIC
1/2 MIC

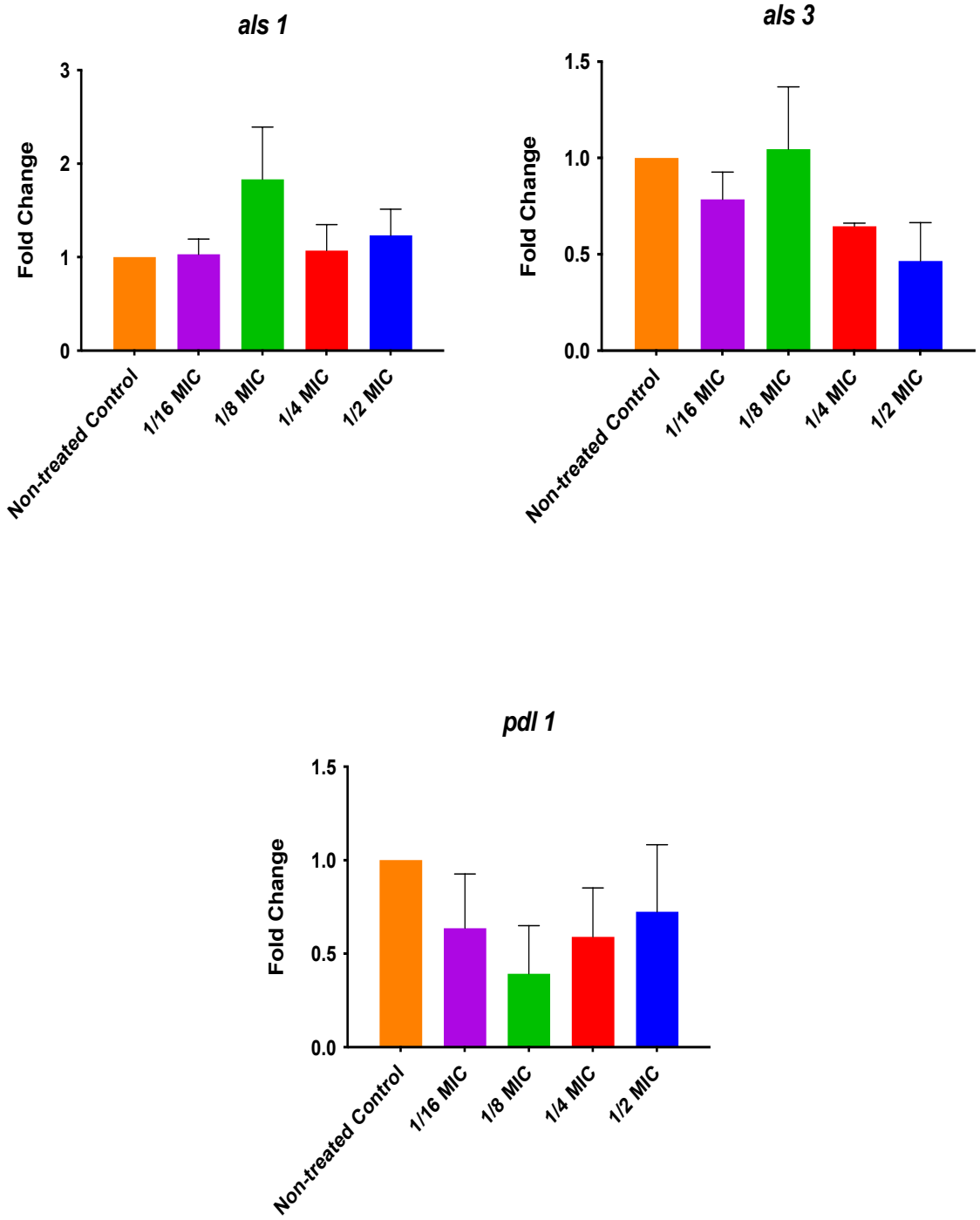


**Figure 2.3.5** The effect of triclosan on *Candida albicans* virulence gene expression. Changes in expression following treatment with triclosan at 1/4 to 1/16 of the MIC concentration. Expression changes calculated relative to the housekeeping gene *actin 1* and normalised to non-treated controls. $^{\Delta\Delta}$Ct method was used for analysis. Data expressed as mean of 3 replicates. Error bars represent SD

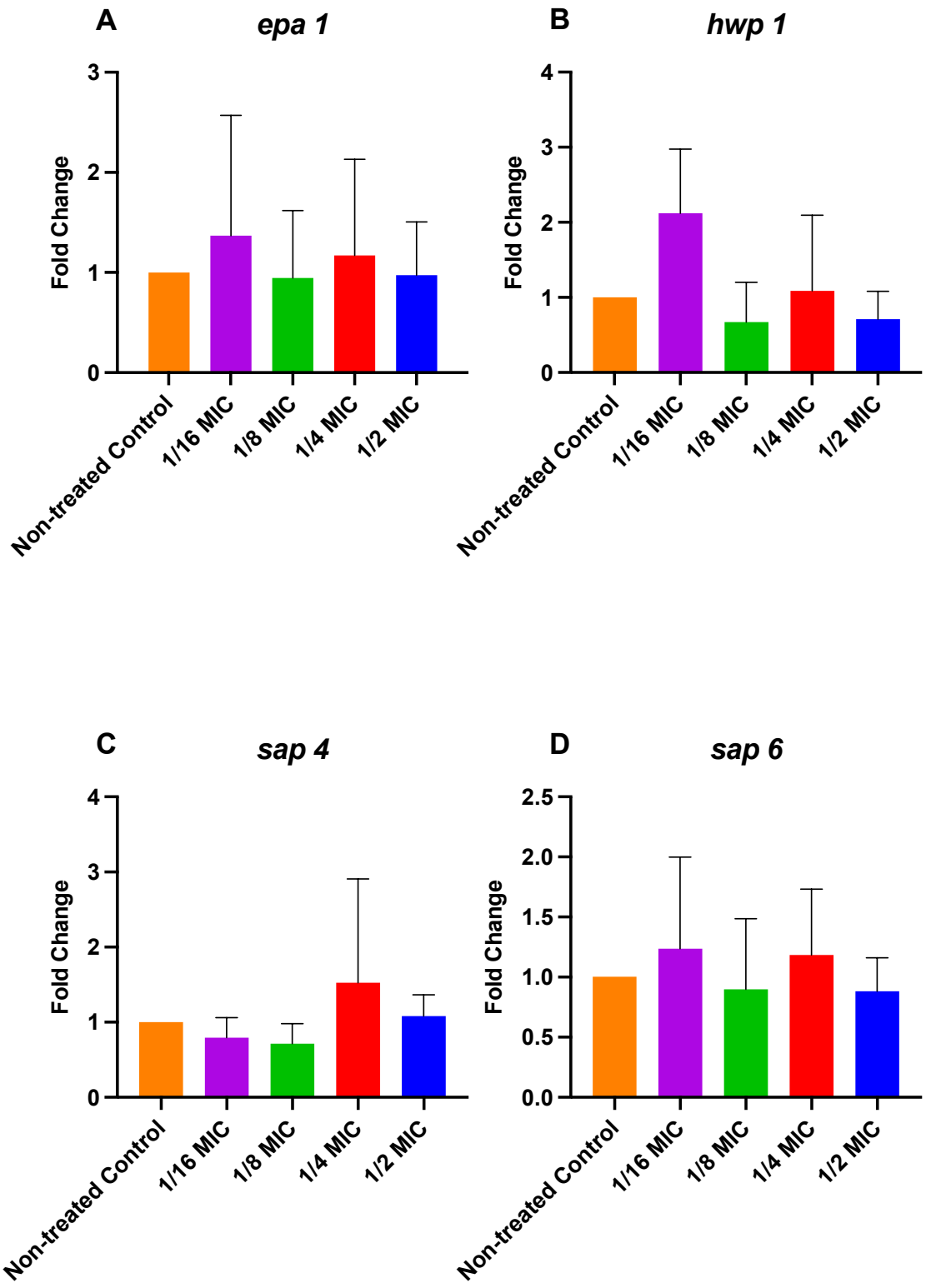
A
epa 1
Fold Change
0
1
2
3
Non-treated Control
1/16 MIC
1/8 MIC
1/4 MIC
1/2 MIC
B
hwp 1
Fold Change
0
1
2
3
4
Non-treated Control
1/16 MIC
1/8 MIC
1/4 MIC
1/2 MIC
C
sap 4
Fold Change
0
1
2
3
4
Non-treated Control
1/16 MIC
1/8 MIC
1/4 MIC
1/2 MIC
D
sap 6
Fold Change
0.0
0.5
1.0
1.5
2.0
2.5
Non-treated Control
1/16 MIC
1/8 MIC
1/4 MIC
1/2 MIC

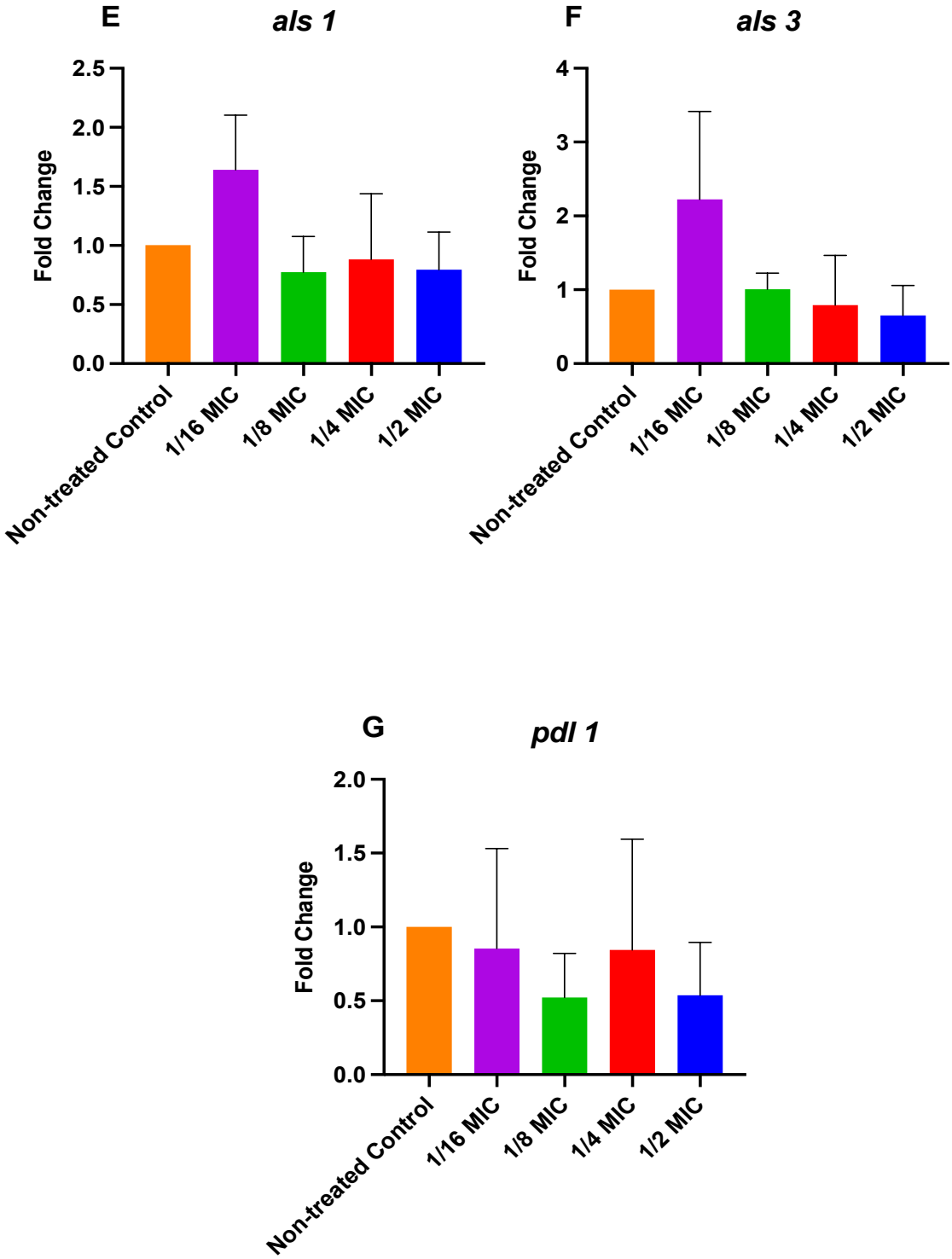


**Figure 2.3.6** The effect of $[HL]^2$ BR on *Candida albicans* virulence gene expression. Changes in expression following treatment with triclosan at 1/4 to 1/16 of the MIC concentration. Expression changes calculated relative to the housekeeping gene *actin 1* and normalised to non-treated controls. $^{\Delta\Delta}$Ct method was used for analysis. Data expressed as mean of 3 replicates. Error bars represent SD

## 2.5 Discussion

Catheter associated urinary tract infections (CAUTIs) are the most prevalent hospital acquired infections and responsible for a significant level of patient morbidity and mortality (NICE 2012). Serious complications, including pyelonephritis, bacteraemia and sepsis, can arise when there is poor management of these conditions (Hooton 2012; Smith et al. 2019). Often infections can progress undetected and may involve organisms that exhibit multidrug resistance. It is, therefore, imperative that appropriate therapeutic options are available to mitigate the impact of CAUTI.

The aims of this research were to evaluate a range of candidate antimicrobials against microorganisms frequently implicated in CAUTIs. Antimicrobials were assessed for their spectrum of activity against planktonic and biofilm growth forms, and on this basis, lead chemicals would be identified for progression for future study into biomaterial development. A range of candidate agents were selected for evaluation. A key consideration for selection included the avoidance of traditional antibiotics, which would potentiate AMR development when used prophylactically. In this respect, biocides that have several targets to induce antimicrobial effects were attractive, as these would likely have reduced incidence of AMR development. This is undoubtedly the case for triclosan, the bioflavonoid preparation of Citrox®, silver carbenes and their precursor imidazolium salts and caprylic acid, whose targets and mechanisms of resistance are listed in Chapter 2, Table 2.1 (Ohemeng et al. 1993; Tsuchiya and Iinuma 2000; Poole 2004; Fang et al. 2010; Shilling et al. 2013; Johnson et al. 2017).

The inclusion of triclosan for evaluation may appear controversial, due to widely publicised concerns regarding potential toxicity (Henry and Fair 2013). The advantages and disadvantages of using triclosan have previously been discussed in Section 2.1.1 and it was concluded that potential disadvantages would be mitigated by clinical benefit to long-term catheterised patients. At low concentrations, triclosan inhibits planktonic growth of Gram-positive bacteria, such as *S. aureus*, largely due to the absence of an outer cell membrane, allowing agents to more readily penetrate into the cell (Suller 2000). Furthermore, Gram-negative species, including *K. pneumonia*, *E. coli*, *P. mirabilis* and *P. stuartii,* are susceptible to low doses of triclosan. The MICs for these species have been

reported between 0.1 and 0.8 µg/ml (Jones *et al.*, 2006), concurring with data obtained in this study, where MICs between 0.39 and 0.78 µg/ml were obtained for the same species. As previously mentioned, (Section 1.4.1.2.3), at low concentrations (< 1µg/ml), triclosan exerts it bacteriostatic effects by inhibiting the enoyl-acyl carrier protein reductase (ENR) involved in fatty acid synthesis. High concentrations (>50 µg/ml) of triclosan lead to disruption of bacterial cell membranes. In the case of triclosan, the antimicrobial effects reported in these studies were consistent with findings from previous authors (Jones et al. 2006b; Stickler and Jones 2008; Morrissey et al. 2014). It was noticeable that *S. marcescens* and *P. aeruginosa* that are species often exhibiting high resistance to antibiotics and antiseptic agents (Jones *et al.*, 2006), were also most tolerant to triclosan. The inherent resistance of *P. aeruginosa* to triclosan can largely be attributed to a triclosan resistant ENR, Fab V, an enzyme involved in fatty acid synthesis (Huang et al. 2016). Deletion of the *Fab V* gene leads to *P. aeruginosa* being extremely sensitive to triclosan (Zhu et al. 2010). In addition, resistance by *P. aeruginosa* may also arise through spontaneous mutations, acquisition of resistance genes, and multidrug efflux systems (Poole 2004). Additionally, outbreaks of *S. marcescens* infections in hospitals have been linked to triclosan soaps (Barry et al. 1984). Resistance mechanisms of *S. marcescens* to many antimicrobials is again associated with expression of efflux pumps and the low permeability of the outer membrane (Haifei Yang 2012).

Biocidal activity of triclosan was not apparent in this research. Tiwari et al determined the MIC and MBEC values of triclosan against common uropathogens and found biocidal values between 800 and 3200 µg/ml, some 3 to 1800-fold higher than MICs (Tiwari and Ghnawate 2017). The current study used a maximum concentration of 200 µg/ml and on reflection higher triclosan concentrations could have been used.

Three esterified derivatives of triclosan, namely triclosan laurate, triclosan benzoate and triclosan acetate were included in this study. The rationale for evaluating these agents was that for downstream applications using biomaterials, improved release profiles may be encountered based on different diffusion and release properties of these chemicals. It was apparent that both triclosan laurate and triclosan benzoate did not offer any advantages, in terms of antimicrobial function compared with triclosan. However, triclosan acetate had an MIC of 0.024

µg/ml against *S. aureus* that was 16-fold lower than triclosan. Furthermore, *P. aeruginosa* was inhibited by a relatively low concentration of triclosan acetate, despite being resistant to triclosan. Triclosan acetate was biocidal for 5 out of the 8 tested organisms, which was not seen with triclosan. It is hypothesised that the lipophilic nature of triclosan acetate enhances diffusion across bacterial plasma membranes, increasing triclosan bioavailability following hydrolysis of triclosan acetate (Shulong 1999). A patent application for use of triclosan acetate as an antimicrobial fabric coating, highlighted its lipophilic properties as a factor that facilitated diffusion into fibres (Shulong 1999). This agent has not previously been used in the treatment of CAUTIs and would be a novel agent to incorporate into a urinary catheter.

A comparatively new class of antimicrobials are imidazolium salts and their silver NHC derivatives. Previous studies have found higher inhibition of planktonic bacteria using Ag-NHCs, compared with their parent compounds (Gök et al. 2014; Wagers et al. 2014). In this study, such an effect was also encountered, with the Ag-NHCs (compounds D-F) having a broader spectrum of antimicrobial activity than the imidazolium salts (compounds A-C). A broader spectrum of antimicrobial activity occurred with 3-hexadecyl-1-isopropyl-1H-imidazole-3-ium bromide ($[HL]^2Br$, compound C), compared with 3-hexadecyl-1-methyl-1H-imidazole-3-ium bromide (compounds A) and 1-(2,3-dihydroxypropyl)-3-hexadecyl-1H-imidazole-3-ium bromide (compound B). It was hypothesised that the propyl side group of compound C increased the polarity of this molecule, which coupled with its large non-polar alkyl side chain, resulted in an amphoteric molecule that was able to act as a surfactant to aid disruption of bacterial cell membranes. Chemical modification of 3-hexadecyl-1-isopropyl-1H-imidazole-3-ium bromide (C) to Ag(I)-NHC (1-hexadecyl-3-isopropylimidazol-2-ylidene) silver(I) bromide, (compound F), was found to further increase inhibition of planktonic microorganisms, with 7 of 8 species being susceptible. Despite this wider spectrum of activity, MICs of susceptible organisms were not reduced.

It was hypothesised that delivery of silver ions to bacteria via surfactant-like compounds would increase inhibition and biocidal activity of the compound. This was true for the compounds in this study, with increased bactericidal activity of compounds A and C when converted to their retrospective silver-NHCs (compounds D and F). Compound 1-(2,3-dihydroxypropyl)-3-hexadecyl-1H-

imidazole-3-ium bromide (compound B) and its derivative (1-(2,3-dihydroxypropyl)-3-hexadecylimidazol-2-ylidene) silver(I) bromide (compound E) did not exhibit biocidal activity against any of the CAUTI causing microorganisms. Importantly, compounds A, C and F inhibited planktonic growth and had biocidal effects against *S. marcescens*, albeit at high concentrations. Inhibition of *P. aeruginosa* by compounds C, D and F was also encountered, whilst the biocidal activity of compounds D and F against *P. aeruginosa* were significant findings.

Notable results for other assessed compounds included the bacteriostatic and bactericidal action of ε-poly-L-lysine and Citrox® against *P. aeruginosa*, whilst ε-PL was also biocidal against 5 other species. MICs with ε-PL ranged between 25-100 μg/ml, correlating with findings of other studies (Shima et al. 2012; Hyldgaard et al. 2014). Previous work has investigated synergy between poly-L-lysine and other antimicrobials (Amrouche et al. 2010). PL showed synergism with an antimicrobial peptide, subtilosin against *Listeria monocytogenes* (Amrouche et al. 2010). Future projects may investigate synergistic effects between ε-PL and some of the most promising novel compounds.

Ultimately, a key aim of this PhD was to use novel compounds within a urinary catheter system to inhibit growth of CAUTI causing species. An important consideration was, therefore, the potential diminishing available antimicrobial concentration during extended urinary catheter use, which may be *in-situ* up to 12 weeks. In such a situation, sub-lethal levels of the agent might conceivably limit its value. With this in mind, an inability of a compound to eradicate bacteria or biofilms might not necessarily negate its value in managing infection. It is possible that sub-lethal concentrations of an agent could impact on bacterial activity and associated gene expression. An evaluation of targeted gene expression by test bacteria following exposure to sub-lethal concentrations of the antimicrobials was, therefore, undertaken.

Adherence of *E. coli* can be mediated through type I fimbriae. Such structures facilitate D-mannose specific adhesion and are associated with virulence in the urinary tract and may be associated with adherence of *E. coli* to extraluminal catheter surfaces (Schembri et al. 2002). The *fim H* gene regulates fimbral length and its expression has been shown to increase 4-fold in the presence of triclosan

(Yu et al. 2012), suggesting a possible protective mechanism of *E. coli* against the compound.

In contrast, a different antimicrobial compound extracted from garlic, allicin, caused downregulation of *fim H* in *E. coli* biofilms, in response to increased concentrations (Yang et al. 2016). No statistically significant differences in *fim H* expression were, however, observed in the current study following exposure to triclosan, contradicting the study by Yu et al (Yu et al. 2012).

Expression of *E. coli* virulence genes that are involved in biofilm formation and carbon storage, *Uvr Y* and *Csr A*, were also not affected by exposure to sub-MIC levels of triclosan and $[HL]^2Br$. Similarly, no effect on expression of *S. aureus* and *C. albicans* virulence genes were found following treatment of planktonic cultures with triclosan and the novel imidazolium salt, $[HL]^2Br$.

Jang et al conducted a genome wide transcriptional analysis to elucidate the cellular response of *S. aureus* to triclosan (Jang et al. 2008b). Following 60 min exposure to triclosan, 707 genes of the 2892 within the entire genome showed statistically significant differences in expression, with 122 of these showing > 2-fold change. Of these, genes involved in fatty acid synthesis, metabolism and carbohydrate transport were downregulated following triclosan exposure, whilst there was upregulation of multidrug resistance genes, and genes associated with metabolism and transcription (Jang et al. 2008b). The study showed that *ica A*, a gene that leads to production of polysaccharide intercellular adhesin (PIA) and poly-n-succinayl-beta-1,6 glucosamine (PNSG) were downregulated, following triclosan exposure.

Although the present study only quantified expression of the *ica* B, C and D genes, ica A, D, B and C are encoded by a single operon and the same expression pattern is expected to occur in all 4 genes. In the present study the *ica* B, C and D genes of *S. aureus* appeared to be upregulated at the highest concentration of triclosan used, contradicting the study from Jang et al. Whilst the differences were not statistically significant, it can be hypothesised that prolonged exposure to these compounds may lead to biofilm formation as a protective response. It is also important to note that different concentrations of triclosan were used in the studies and the bacteria were exposed for different time periods.

A further study by the same group investigated the effects of sub-lethal doses of another compound orthophenylphenol (OPP) on *S. aureus* virulence gene

expression and revealed aberrant expression of the intracellular adhesins *ica* A, D and B (Jang et al. 2008a). Downregulation of gene expression occurred following a 20 min exposure time and these same genes were upregulated when exposure was increased to 60 min. The response of *S. aureus* to prolonged exposure to the compound may also be attributed to a protective mechanism. These results suggest that the *ica* operon is an important virulence mechanism in *S. aureus* biofilm formation and antimicrobial compounds that can modulate its expression may prevent associated disease and pathogenesis.

Ideally, a microarray analysis system could be used in the future to generate a wider screen of genes to assess impact of these antimicrobials. Unfortunately, this was not possible in the current project given available time and resources. It is anticipated that changes in virulence gene expression would occur, following antimicrobial treatment of developing or pre-formed biofilms on biotic or abiotic surfaces. RNA could be extracted from biofilms attached to antimicrobial silicones developed in subsequent chapters, to determine if sub-inhibitory treatment would affect the expression of virulence genes involved in biofilm formation.

Lipoteichoic acid is a cell wall polymer of Gram-positive bacteria that consists of 1,3- polyglycerol-phosphate linked to glycolipid. LTA synthase (LtaS) polymerises polyglycerol-phosphate from phosphatidylglycerol and this reaction is thought to be essential for the growth of Gram-positive bacteria (Richter et al. 2013). A compound termed 1771 has shown promise in abrogating the growth of two Gram-positive bacteria, *S. aureus* and *E. faecium,* in their planktonic states (Richter et al. 2013; Paganelli et al. 2017) and its mechanism of action has been elucidated. Compound 1771 blocks phosphatidylglycerol binding to LtaS, thus preventing formation of LTA and preventing growth (Paganelli et al. 2017).

Commercially available and ‘in-house’ synthesised versions of compound 1771 generated equivalent MIC and MBC values against three strains of *S. aureus* and *E. faecium*. Paganelli had previously obtained MIC values for this compound against multiple strains of *E. faecium* and achieved values between 0.5 and 32 μg/ml and the values from this present study are consistent with these (Paganelli et al. 2017).

Although compound 1771 has a narrow spectrum of activity, susceptible species still account for significant numbers of CAUTIs. *Enterococcus* species that include *E. faecium* have been reported to account for 27-30 % of CAUTIs in hospital

intensive care units (Harshan et al. 2019), whilst another study attributed 6% of CAUTIs to coagulase negative *Staphylococcus aureus* (Bagchi, Jaitly 2013). The use of compound 1771 to prophylactically manage such infections would provide another tool in the fight against CAUTIs. Whilst it had been demonstrated that compound 1771 is unable to prevent the growth of mature biofilms (Paganelli et al. 2017), it would be interesting to incorporate this compound into silicones to investigate release and determine its ability to prevent biofilm formation along medical devices, such as urinary catheters.

Preventing biofilm formation of vancomycin resistant *E. faecium* would enable management of CAUTIs caused by VRE and minimise the need for antibiotic administration to already highly resistant species. Unfortunately, compound 1771 was investigated at a chronologically later stage of the project and its incorporation into silicone was not possible.

To conclude, the MICs and MBCs of a broad range of compounds against microbes implicated in the pathogenesis of CAUTIs have been determined. Studies to determine MBECs were also conducted, but the concentrations of compounds used were not sufficient to eradicate pre-formed biofilms. In addition, the virulence genes of 3 microorganisms implicated in CAUTIs, namely *E. coli*, *S. aureus* and *C. albicans,* were quantified following sub-lethal exposure to triclosan and $[HL]^2$ Br, revealing no statistically significant differences between treated and untreated cultures. However, lead candidate compounds have been identified from this research that will be investigated in subsequent chapters for use in biomaterials to help manage CAUTIs. Based on their broad spectrum of activity and low MIC values compared to the other compounds assessed, triclosan, triclosan acetate, $[HL]^2$ Br (compound C) and compound E, were chosen for incorporation into silicone elastomers.

# Chapter 3

## Antimicrobial Silicone Development

## 3.1 Introduction

### 3.1.1 Implantable medical devices

In 1958, the first implantable medical device, a simple cardiac pacemaker was placed into an experimental animal (van Hemel and van der Wall, 2008), and later developed for use in human patients (Senning, 1983). Over the past 60 years, significant advancements have been made in the design and production of numerous implantable medical devices, and as such they have become important tools in modern medicine to manage and treat numerous medical conditions. Such devices include cardiac pacemakers, blood-pressure sensors and cochlear implants (Ouyang *et al.*, 2019; Naples and Ruckenstein, 2020; Song *et al.*, 2020). Implantable medical devices can be partially or wholly introduced into the body and may be *in-situ* over short (< 30 days) or long-term (> 30 days) durations (Jain, Ganesh and Venkatesh, 2018). Examples of partially implantable medical devices include endotracheal tubes, central venous catheters and urinary catheters (Trautner and Darouiche, 2004; Ryan *et al.*, 2018; Barnes *et al.*, 2019), whilst cardiac pacemakers, coronary stents and hip implants are examples of wholly introduced medical devices (Barrère *et al.*, 2008; Ouyang *et al.*, 2019; Toh *et al.*, 2021). Although significant benefits arise from the use of such medical devices, their surfaces are susceptible to colonisation by bacteria introduced from internal or external sources (Percival *et al.*, 2015). Overcoming bacterial biofilm formation upon such surfaces remains a challenge faced by healthcare providers and device manufacturers alike.

### 3.1.2 Silicone medical devices

Implantable medical devices require construction from durable, biocompatible materials, and may have to be able to withstand considerable physical forces *e.g.* prosthetic hip joints (Barrère *et al.*, 2008). Silicone rubber has become the material of choice for a diverse range of medical devices, including urinary catheters, mechanical heart valves, Swanson joints and endotracheal tubes (Shepherd, 2002; Trautner and Darouiche, 2004; Barrère *et al.*, 2008; Noly *et al.*, 2020). Silicone rubbers possess additional properties that lend them to being suitable for medical device manufacture (Table 3.1) (Heide, 1999).

**Table 3.1** Key properties of silicone rubbers

| **Property** |
|---|
| Hypoallergenic |
| Low toxicity |
| Temperature resistant (- 100°C – 300°C) |
| Low chemical reactivity |
| Abrasion resistance |
| High tear strength |
| High elongation |

### 3.1.3 Chemical composition of silicone polymers

Silicone polymers are more correctly termed polysiloxanes and consist of repeating units of silicon and oxygen (siloxane) with two organic side groups (R) attached to the silicon via C-Si bonds (Figure 3.1.1). The most widely used silicone has methyl groups attached to the backbone, termed polydimethylsiloxane (PDMS). By substituting these side groups, alteration of the properties of a silicone can be achieved (Colas, 2005).

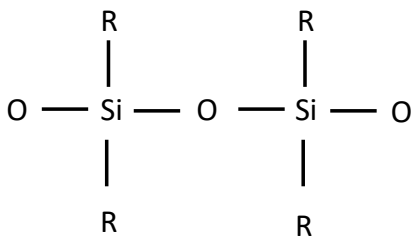


**Figure 3.1.1** The chemical structure of silicone polymers

The bonds between the silicon and the oxygen atoms are very long and flexible, allowing the backbone to move freely and produce an elastic material. Linear silicone chains can form chemical bonds with adjacent chains via a cross-linking reaction, producing a 3D network (Figure 3.1.2) (Colas, 2005).

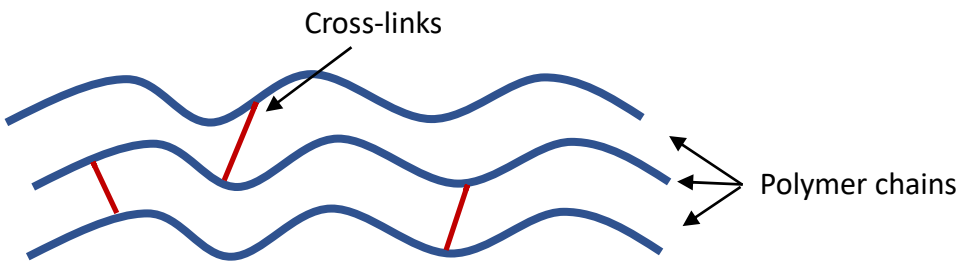


**Figure 3.1.2** Diagrammatic representation of cross-linked silicone polymers

Chemical cross-linking (curing) occurs in one of three ways 1) peroxide curing, 2) condensation curing and 3) platinum-catalysed addition curing (Heiner, Stenberg and Persson, 2003; Jurásková *et al.*, 2020; Lukin *et al.*, 2020). Whilst more expensive to produce, platinum cured silicones are the material of choice for medical grade products, due their superior tensile and tear strengths and production of clear silicones (Lewis *et al.*, 1997).

### 3.1.4 Silicone classes

The combination of chain lengths, side groups and the degree of cross-linking can produce materials with different properties. In general terms, the higher the degree of cross-linking, the more rigid the material becomes (Acharya *et al.*, 2020). Silicones can broadly be divided into four classes, depending on their structure. The first of these are silicone fluids which have short chains and a constant viscosity (Thomas, 2003). The low surface tension of silicone fluids lends them to uses as lubricants and for use in skin care products (Thomas, 2003; Aziz *et al.*, 2019). Silicone gels are based on PDMS chains, with a few cross-links between the chains, resulting in an open 3D network (Acharya *et al.*, 2020). The network can be swollen with silicone fluids or non-silicone fluids, such as mineral oil (Acharya *et al.*, 2020). Such gels are often used as shock absorbers in shoes (Matsumoto *et al.*, 1999) and postoperatively to reduce surgical scar formation (Wang *et al.*, 2020). Silicone elastomers (rubbers) have increased cross-linking between the linear chains, producing a structure similar to natural rubber, although not as strong (Kaliyathan *et al.*, 2018). Silicone rubbers are stable at both low and high temperatures (- 100°C – 300 °C) and are commonly used to manufacture medical devices, including urinary catheters (Fisher *et al.*, 2015; Kaliyathan *et al.*, 2018).

Silicone resins have a 3D structure with atoms arranged tetrahedrally around the silicon atom. The resins are highly water repellent and are used in products, such as masonry coatings, electrical insulating varnish and cosmetic products (Mayer, 1998; Maiti, 2005; Robeyns, Picard and Ganachaud, 2018).

Properties of silicone elastomers can be modified through adjustments to the ratios of the key components (Figure 3.1.3). Combinations of short, medium and long polymer chains alter the fluidity of the resulting silicone, with higher ratios of short chains leading to more fluid-like products (Mazurek, Vudayagiri and Skov, 2019). Fumed silica fillers are also used to reinforce silicone elastomers and may also act as thickening agents. These may be hydrophilic or hydrophobic in nature. The proportion of cross-linking reagent influences the elasticity and strength of the silicone elastomer (Mazurek, Vudayagiri and Skov, 2019).

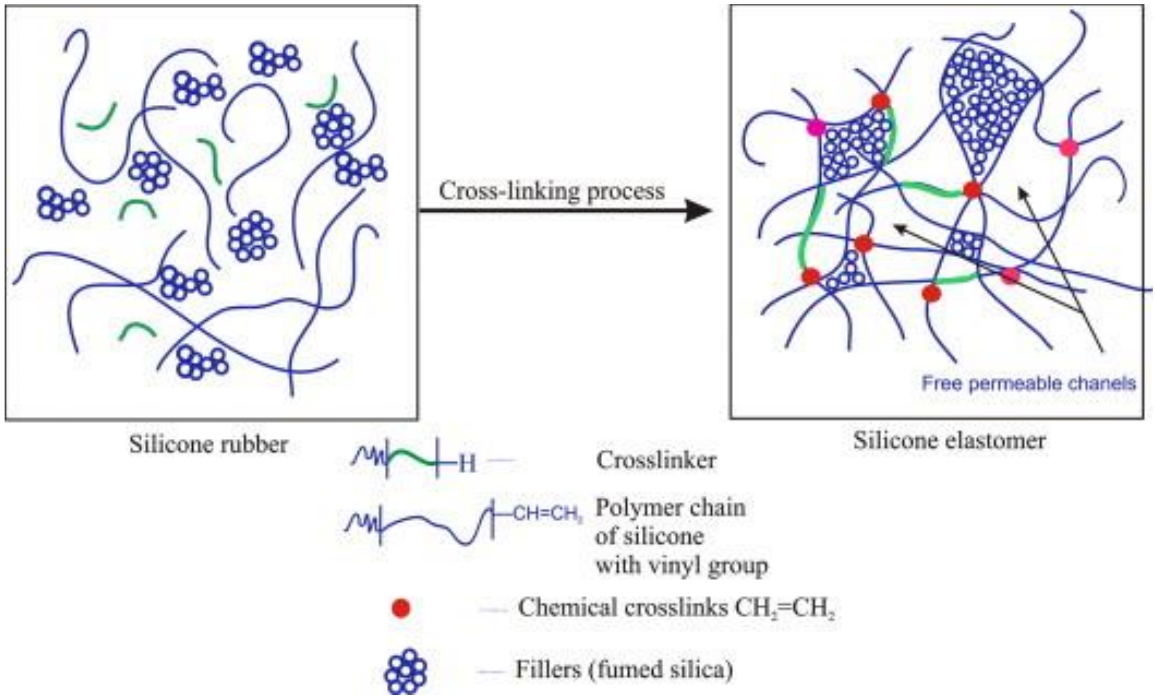


**Figure 3.1.3** The composition and structure of silicone elastomers (Mojsiewicz-Pieńkowska *et al.*, 2015)

Although the physical properties of silicone rubber lend it to being the material of choice for the manufacture of implantable medical devices, it is also susceptible to colonisation by microorganisms and subsequent biofilm formation (Donlan and Costerton, 2002). Chapter 1 described the numerous strategies that have been employed to try and prevent microbial colonisation of silicone surfaces, either through use of anti-fouling mechanisms or by release of biocidal agents (Pelling *et al.*, 2019).

The effectiveness of antimicrobial coated silicones may be limited by the deposition of conditioning films upon the surfaces (Trautner and Darouiche, 2004). In the case of urinary catheters, a conditioning film comprised of components from urine including proteins, electrolytes and other organic matter may act to mask any biocidal coating or prevent diffusion of antimicrobial compounds from the bulk of the material (Trautner and Darouiche, 2004). Some urinary catheters have a hydrogel coating upon the outside to aid insertion and this may also reduce the diffusion of antimicrobial compounds (Kazmierska *et al.*, 2010). Table 1.6 lists some commercially available Foley catheters including their composition and any hydrogel coatings. Furthermore, antimicrobials contained within the silicone may be rapidly depleted by the flow of urine over the surface (Moreira *et al.*, 2013).

### 3.1.5 Aims

The research presented in this chapter aims to incorporate a selection of candidate compounds (evaluated in Chapter 2) into silicone elastomers, to produce an antimicrobial silicone suitable for use as a urinary catheter. Candidate compounds will be bulk-loaded into the silicone polymer and/or dip coated to create a biocidal surface coating. The physical properties of the developed materials will be assessed along with determination of compound release and longevity of release. Antimicrobial properties of the developed materials will be evaluated against common CAUTI causing microorganisms.

## 3.2 Materials & Methods

### 3.2.1 Silicone preparation

A previously used silicone formulation (termed S1) was produced using a two-part system. The base formulation contained 54.36% (w/w) V46 vinyl terminated platinum divinyl tetramethyldisiloxane (VT-PDMS, Silanes and Silicones, Stockport, UK), 16.34% (w/w) V31, 5% (w/w) V21, 5% (w/w) hydrophilic filler, HDK H2000 (Wacker, Germany) and 19.44% hydrophobic filler, hexamethyldisilazane (HMDS; Silanes and Silicones, Stockport, UK; Table 3.3.1). The base was mixed using a Kenwood stand mixer for a period of 2 h at room temperature. A concentrate containing 1% (w/w) platinum-cyclovinylmethylsiloxane complex (Silanes and Silicones) and 99% (w/w) of the above base formulation (Table 3.3.2), was mixed using a Kenwood stand mixer for 1 h.

Part A formulation consisted of 90% (w/w) base formula and 10% (w/w) concentrate and was mixed for 10 min (Table 3.2.3). Part B was formulated with 90% w/w base and 10% (w/w) H301 cross-linking reagent (Table 3.2.4). Parts A and B were mixed in a 1:1 ratio in a vacuum mixer (Obodent, Vacudent) for 2 min and poured into a stainless-steel mould (100 mm × 100 mm × 2 mm), previously sprayed with a wax mould sealant and release agent (Medimould, Polymed Ltd, Cardiff, UK). The mould was clamped and incubated at 50°C for 1 h to cure.

A second formulation (S2) was produced with different ratios of polymers, fillers, cross-linker, and platinum catalyst (Tables 3.2.1 – 3.2.4). The final composition of S2, compared to S1, had 10-fold less platinum catalyst and 2-fold less cross-linking reagent. S2 also contained approximately 2-fold more HMDS filler. Parts A and B were mixed, poured into moulds, and cured, as previously described.

**Table 3.2.1** Formulation of silicone bases for silicones S1 and S2

| Reagent | Concentration (% w/w) | |
|---|---|---|
| | **S1** | **S2** |
| V46 | 54.36 | 30 |
| V31 | 16.34 | 50 |
| V21 | 5.0 | 5 |
| HDK H2000 | 4.86 | 5 |
| HMDS | 19.44 | 10 |

**Table 3.2.2** Formulation of platinum catalyst concentrates for silicones S1 and S2

| Reagent | Manufacture | Concentration (% w/w) | |
|---|---|---|---|
| | | **S1** | **S2** |
| **Base** | See Table 3.2.1 | 90 | 99 |
| **Platinum-cyclovinylmethylsiloxane** | Silanes and Silicones, Stockport, UK | 10 | 1 |

**Table 3.2.3** Formulation of part A for silicones S1 and S2

| | Concentration (% w/w) | |
|---|---|---|
| | **S1** | **S2** |
| **Base** | 90 | 90 |
| **Platinum catalyst concentrate** | 10 | 10 |

**Table 3.2.4** Formulation of part B for silicones S1 and S2

| | Concentration (%) | |
|---|---|---|
| | **S1** | **S2** |
| **Base** | 90 | 94.56 |
| **H301 cross linker** | 10 | 5.44 |

### 3.2.2 Preparation of silicones bulk-loaded with triclosan, triclosan acetate or novel imidazolium compounds

S1 and S2 silicone formulations were produced containing 1% triclosan in the final product, termed T1 and T2. Part A formulations were prepared as previously described (Table 3.2.3). Solutions of 10% (w/w) triclosan dissolved in acetone were prepared. One part of the solution was added to 4 parts of the part B solution (Table 3.3.4), prepared as described above. Evaporation of the acetone during the heat curing process resulted in 2% triclosan containing silicone formulations. Part A and part B were then mixed in a 1:1 ratio in a vacuum mixer for 2 min, before a 50°C curing period in a stainless-steel mould as previously described, resulting in a 1% (w/w) triclosan containing silicone. Triclosan acetate silicone (TA 2), (1% w/w) was also prepared from S2 silicone using this method. All silicone rubbers produced were assessed for their ability to produce a well cured silicone rubber and given a curing score of 0-5, with 0 denoting no curing and 5 denoting the production of a well cured silicone. 3-hexadecyl-1-isopropyl-1H-imidazole-3-ium bromide ([$HL^2$]Br) that had previously demonstrated antimicrobial efficacy during antimicrobial susceptibility studies was selected for incorporation into S2 silicone using this method. The use of 0.05, 0.5 and 0.75% w/w heat activated, and room temperature activated platinum catalysts was investigated along with three different concentrations of H301 cross-linking reagent (2.72, 5 and 10% w/w) to assess optimal silicone curing. The curing of the resulting silicone formulations was scored between 0 and 5, with no curing scoring 0 and fully cured silicone scoring 5.

### 3.2.3 Preparation of silicone dip-coated with 1% (w/w) triclosan and 1% (w/w) triclosan acetate containing polymers

Slabs of S2 silicone rubber were created as described in Section 3.2.1 and cut into 2cm x 5 cm strips. The part A and part B solutions containing triclosan or triclosan acetate (described in Section 3.2.2) were each mixed with the solvent Probond remover (Technovent, Bridgend, UK) in a 1:1 ratio. Part A and Part B were mixed in a 1:1 ratio to create dip coating formulations containing 1% (w/w) triclosan and 1% (w/w) triclosan acetate. The silicone rubber strips were immersed in the dip coat formulations for 5 min and hung at room temperature for 5 mins before complete curing occurred at 50°C for 1 h. Silicone coated with the triclosan and

triclosan acetate dip-coated formulations were termed T2-DC and TA-2-DC, respectively.

### 3.2.4 Preparation of a 1% w/w [HL2] Br coated silicone

[$HL^2$] Br was ground to a fine powder and added to trimethylsiloxy terminated polydimethylsiloxane silicone oil (Gelest, USA) at a final concentration of 10% (w/w). G531 acetoxy silicone (Technovent) was mixed with Probond remover in a 1:1 ratio. The solution of [$HL^2$] Br in silicone oil was mixed into the acetoxy/solvent formulation at (Technovent) at 5% of the final weight. After solvent evaporation, the final dip coat formulation contained 1% (w/w) [$HL^2$] Br.

Pre-cut silicone rubber strips that had been cut as described in Section 3.2.3, were immersed into the dip-coat formulation for 30 s and hung at room temperature to allow condensation curing to occur utilising atmospheric humidity. [HL2] Br coated silicone was termed A_[$HL^2$] Br and the S2 silicone coated with acetoxy silicone layer without antimicrobial compound, termed S2_A.

### 3.2.5 Determination of tensile strength and elongation of prepared silicone

#### 3.2.5.1 Sample preparation

Aluminium dumb-bell shaped moulds (Figure 3.3.1) were used to cut samples from the prepared silicone slabs. Six samples were prepared for each material.

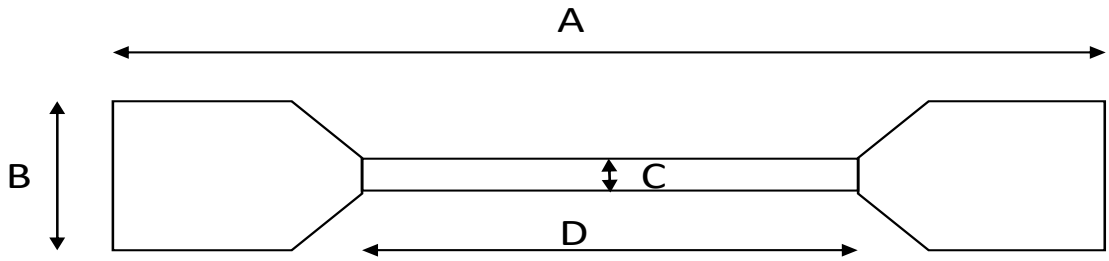


A = 75mm, B = 12.5 mm, C = 4 mm, D = 2 mm, Depth = 2.5 mm

**Figure 3.2.1** Schematic representation of dumbbell shaped moulds used to produce silicones to determine tensile strength and elongation

### 3.2.5.2 Testing procedure to determine tensile strength and elongation of silicone specimens

Dumb-bell shaped silicone samples (Section 3.2.5.1) were loaded into self-mounting grips of a tensile machine (MultiTest -*d*, Mecmesin), fitted with a 500N load cell (AFG 500N, Mecmesin), connected to a computer. The samples were pulled at a constant speed of 300 mm/min. A stress-strain curve was produced by the computer software. The load (N) and displacement (mm) were noted at the time of failure and tensile strength calculated, using the following equation:

$$\boldsymbol{T = \frac{F}{A}}$$

T= Tensile strength (N/mm$^2$)

F= Force at failure (N)

A= Cross-sectional area (mm$^2$)

Displacement of the silicone as represented in Figure 3.2.2 can be used to calculate the percentage elongation (% E), using the following equation:

$$\boldsymbol{E}\ (\%) = \frac{\boldsymbol{L_1}}{\boldsymbol{L_0}}\ \textbf{x 100}$$

E = Elongation (%)

$L_1$ = Extension at break (mm)

$L_0$ = Gauge length (mm)

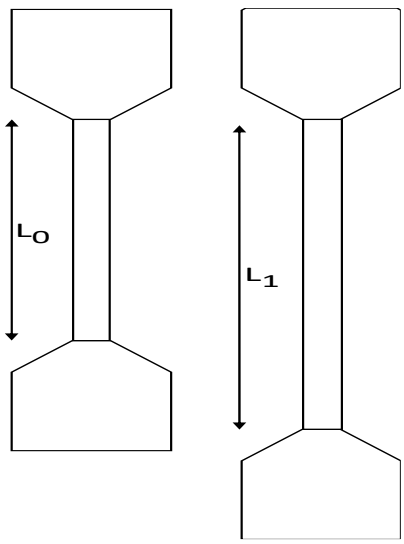


**Figure 3.2.2** Diagrammatic representation of measurements used to determine elongation of silicone specimens

### 3.2.6 Determination of tear strength of prepared silicone

#### 3.2.6.1 Sample preparation

Tear specimens (50 mm x 10 mm x 2.5 mm) were cut from previously manufactured silicone rubber slabs (100 mm x 100 mm x 2 mm) and a 4 mm cut was made, as shown in Figure 3.3.3.

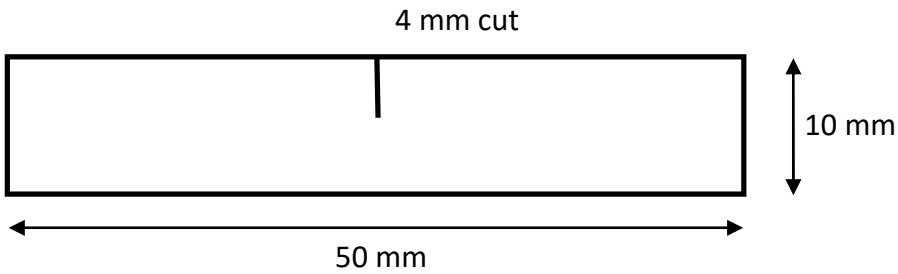


**Figure 3.2.3** Dimensions of specimens used to determine tear strength of prepared silicone

#### 3.2.6.2 Testing procedure to measure tear strength of silicone

Tear specimens (Figure 3.3.3) were loaded into the grips of the testing machine (MultiTest -*d*, Mecmesin) fitted with a 500N load cell (AFG 500N, Mecmesin), connected to a computer. The samples were pulled as described in Section 3.2.5.2. At the point of failure, the software calculated the tear resistance using the following equation:

$$\mathbf{Ts} = \frac{\mathbf{F}}{\mathbf{t}}$$

Ts = tear resistance (N/mm)

F = load at failure (N)

t = thickness of specimen (mm)

Statistical analysis of the mechanical properties of the silicone formulations were calculated using unpaired t-tests, with unequal variances by the software GraphPad Prism.

### 3.2.7 Long-term release of antimicrobial compounds from silicone elastomers

#### 3.2.7.1 Repeated zone of inhibition assays (ZOIs)

*Staphylococcus aureus* NSM 7 was sub-cultured onto agar media for 16-24 h at 37°C, before incubating in Mueller-Hinton broth (MHB) for an additional 16-24 h at 37°C. The OD at 600 nm of the cultures was subsequently measured and adjusted to an equivalent of a 0.5 MacFarlane standard (0.1 $OD_{600}$), by addition of MHB. Cotton swabs were dipped into the culture solutions and streaked across agar plates. Previously prepared 10 mm silicone coupons that had been bored out of the prepared silicone and autoclaved, were placed on to the inoculated agar plates and incubated for 24 h at 37°C. Each plate contained 3 silicone coupons without antimicrobial compound or 3 antimicrobial containing coupons. The diameter of any zones around the coupons without bacterial growth (zones of inhibitions; ZOIs) were measured and the diameter of the coupons subtracted from these measurements. The first measurement represented t=0. The coupons were removed from the agar plates and placed into 2 ml of artificial urine (AU) at pH 6.1 for 6 days. The coupons were then placed on to agars freshly inoculated with *S. aureus* and incubated for 24 h at 37°C to measure ZOIs. This process was continued for a 12-week period. Each experiment was conducted in triplicate. Statistical analysis was performed using paired t-tests, to compare zones produced by non-antimicrobial and antimicrobial containing coupons. Silicone coupons bulk-loaded with 1% w/w triclosan or triclosan acetate, silicone dip-coated with 1% w/w triclosan or triclosan acetate and silicone with an acetoxy coating containing $[HL^2]$ Br, were compared to their non-antimicrobial equivalent silicones.

#### 3.2.7.2 Measurement of antimicrobial compound release using HPLC

##### 3.2.7.2.1 Preparation of artificial urine (AU)

The following components were dissolved in 900 ml deionised water: calcium chloride (0.49 g/l), magnesium chloride hexahydrate (0.65 g/l), sodium chloride (4.6 g/l), sodium sulphate (2.3 g/l), trisodium citrate dihydrate (0.65 g/l), disodium oxalate (0.02 g/l), potassium dihydrogen phosphate (2.8 g/l), potassium chloride

(1.6 g/l), ammonium chloride (1.0 g/l), urea (25.0 g/l), and gelatin (5.0 g/l). The pH was adjusted to 6.1 with 5 M hydrochloric acid or pH 7.0 and 9.5 with 5 M sodium hydroxide. The solutions were passed through 0.2 μm vacuum filter units (Sarstedt, Germany), before addition of 100 ml autoclaved tryptone soy broth (TSB) at 10 g/l to give a final concentration of 1 g/l.

Ten-mm diameter silicone coupons (T2 and TA-2) were placed in 24-well plates and immersed in 2 ml sterile AU that had been adjusted pH 6.1, 7.0 or 9.5 before incubation at 37 °C for periods between 4 h and 12 weeks. Plates were sealed with parafilm to prevent evaporation during incubation. After the relevant time period, the AU was removed and stored in vials at -20 °C, until HPLC analysis was performed.

#### 3.2.7.2.2 High-performance liquid chromatography (HPLC) apparatus

Triclosan and triclosan acetate released into AU from silicone coupons were measured using high-performance liquid chromatography (HPLC). The HPLC apparatus consisted of an Agilent 1200 G13179B degasser, HP Agilent 1100 HPLC G1310A Isocratic Pump, HP Agilent 1100 G1313A Autosampler, HP Agilent G1314A Variable Wavelength Detector and an Agilent Eclipse Plus C18 Column (4.6 mm x 100 mm, 3.5 μm). Sample volumes of 10 μl were injected and analysed using acetonitrile and $H_2O$ in a 7:3 ratio as the mobile phase. The flow rate was set at 1 ml/min and the analytical wavelength set at 285 nm. Agilent Chemstation was used for data collection and analysis. Statistical differences between the data points at each time-point were determined using one-way ANOVA with repeated measures. Statistical differences between triclosan released from T2 and TA-2 coupons were determined using 2-tailed t-tests.

#### 3.2.7.2.3 HPLC calibration standard solutions of triclosan and triclosan acetate

Standard solutions of triclosan and triclosan acetate were prepared in DMSO at concentrations of 0, 1, 2.5, 5,10, 25, 50, 100, 250 and 500 μg/ml. HPLC was performed, as described above. The resulting peak areas obtained (*y*) were plotted against triclosan/triclosan acetate concentration (*x*).

Least squares regression analysis determined the slope and coefficient of determination ($R^2$) of the data. The equation of the regression line was used to

calculate the triclosan/triclosan acetate concentration released into AU from silicone coupons.

### 3.2.8 Antimicrobial activity of novel silicone formulations

#### 3.2.8.1 Zone of inhibition assay

Microorganisms listed in Table 2.3.1 were sub-cultured on to agar media for 16-24 h, before incubating in Mueller-Hinton broth (MHB) for 16-24 h at 37°C. The OD at 600 nm of the cultures was subsequently measured and adjusted to an equivalent of a 0.5 MacFarlane standard (0.1 $OD_{600}$), by addition of MHB. Bacteria were homogenously spread plated onto appropriate agar and ZOIs obtained, as described in Section 3.2.7.1, with the exception that repeated ZOIs over consecutive weeks were not measured. Each experiment was conducted in triplicate. Statistical analysis was performed using paired t-tests, to compare zones produced by non-antimicrobial and antimicrobial containing coupons. Silicone coupons bulk-loaded with 1% w/w triclosan or triclosan acetate, silicone dip-coated with 1% w/w triclosan or triclosan acetate and silicone with an acetoxy coating containing $[HL^2]$ Br, were compared to their non-antimicrobial equivalent silicones.

#### 3.2.8.2 Propidium iodide (PI) staining of microorganisms adhered to silicone

Coupons (5 mm diameter) were bored from 2.5 mm thick slabs of silicone bulk loaded with 1% (w/w) triclosan (T2), 1% (w/w) triclosan acetate or the silicone without antimicrobial compound S2 (control) and T2 (1% triclosan). Additional coupons were also bored from silicone that had been dip-coated with 1% (w/w) triclosan polymer, 1% (w/w) triclosan acetate polymer, a dip-coated control coupon without antimicrobial, $[HL^2]$ Br acetoxy coated silicone and the acetoxy coated control formulation. All coupons were autoclaved prior to use.

Overnight cultures of 8 CAUTI causing microorganisms (Table 2.2.1) were produced in MHB and centrifuged at 11, 000 x *g* for 5 min to form a pellet. Pellets were resuspended in 1 ml fresh culture medium and 100 μl pipetted directly on to the surface of 5 mm diameter silicone coupons that were situated in wells of a 96 well plate. The silicone coupons were incubated at 37°C for 90 min, gently washed in sterile $dH_2O$ to remove non-adhered cells and placed in 1 ml volumes of sterile

$dH_2O$ for 16 h at 37°C. The coupons were removed, blotted on tissue paper to remove excess liquid and 10 μl of PI solution (Life Technologies, 1 μl/ ml in $dH_2O$), was added to the surface of the coupons. Images were obtained using an Olympus AX70 fluorescent microscope fitted with a 550/580 nm filter cube. Five random fields of view were captured for each coupon at x 600 final magnification. Three antimicrobial containing coupons were imaged along with 3 of the corresponding non-antimicrobial control coupons. All coupons originated from separately manufactured batches.

Image analysis was performed using Image J software (NIH, USA). Briefly, images were thresholded to exclude background pixilation, converted to binary images and the software automatically calculated percentage area covered by PI stained cells. Unpaired t-tests were performed on the data sets to determine differences between biocidal activity of antimicrobial containing silicone and the non-antimicrobial silicones.

#### 3.2.8.3 Colony forming unit (CFU) determination of microorganisms adhered to silicone

Overnight cultures of 8 microorganisms (Table 2.2.1) in MHB were prepared, as previously described in Section 3.2.8.1. Ten-mm diameter coupons bored from 2 mm deep S2 and T2 silicone slabs were autoclaved and immersed in 1 ml volumes of the established overnight cultures. Following a 90 min incubation period at 37°C, the coupons were gently washed in sterile $dH_2O$ and placed in 1 ml volumes of $dH_2O$ for 16 h at 37°C.

Coupons were placed in 2 ml of fresh sterile $dH_2O$, and vortex mixed for 1 min at 3000 rev/min to remove adherent microorganisms. This approach was validated to show no statistically significant difference between recovered microorganisms on silicone coupons generated from the same silicone batch. Serial dilutions of the suspensions were prepared and 3 x 10 μl volumes spotted on to tryptone soy agar (TSA) plates or CLED agar (for *Proteus mirabilis*), as described by Miles and Misra (Miles, Misra and Irwin, 1938). Following incubation at 37°C for 16-24 h, CFUs were counted, recorded and the CFU/ml calculated based on dilution factor. Coupons from 3 separate batches of S2, T2, TA-2, T2-DC, TA-2-DC, S2_A, A_[$HL^2$] Br silicone were used. Statistical analysis was performed using unpaired t-tests or one way ANOVA.

## 3.3 Results

### 3.3.1 Development of antimicrobial silicone formulations

Incorporation of both triclosan and triclosan acetate into the bulk of the silicone matrix did not affect curing of the S1 and S2 silicone rubbers when antimicrobials were used at a final concentration of 1% (w/w) (Table 3.3.1). However, incorporating the novel imidazolium compound [$HL^2$] Br (final concentration of 1% w/w) in these silicone formulations inhibited curing (Table 3.3.1).

Effects of increasing the concentration of heat-activated platinum catalyst in increments from 0.05% to 1.0% (w/w) final concentration on the curing of silicone containing [$HL^2$] Br in the matrix was assessed. Combinations of cross-linking reagent between 2.72% and 10% (w/w) was also investigated with catalyst concentration. Although partial curing occurred when 5% (w/w) cross-linking reagent was used with platinum catalyst levels ≥ 0.5% (w/w), complete curing was not evident (Table 3.3.2). When undertaking similar experiments using a room-temperature activated platinum catalyst ≤ 0.75% (w/w) in the final formulation, incomplete curing of the silicone rubber occurred (Table 3.3.3).

In the absence of [$HL^2$] Br, complete curing occurred with heat or room temperature activated platinum catalyst at 0.5% (w/w) final concentration with 2.72% (w/w) cross-linking reagent (Table 3.3.4). This indicated that it was the [$HL^2$] Br that was inhibiting the silicone curing process.

**Table 3.3.1** Curing scores of novel silicone formulations (S1 and S2) bulk-loaded with antimicrobial compounds

| Antimicrobial compound in final formulation | Silicone formulation | |
|---|---|---|
| | **S1** | **S2** |
| **+ 1% (w/w) Triclosan** | 5 | 5 |
| **+ 1% (w/w) Triclosan acetate** | 5 | 5 |
| **+ 1% (w/w) [$HL^2$] Br** | 1 | 1 |

*Curing scores from 0-5 where 0 represents uncured silicone and 5 represents complete curing.

**Table 3.3.2** Curing scores of silicone formulations bulk-loaded with 1% (w/w) [$HL^2$] BR using heat activated platinum cyclovinylmethylsiloxane catalyst

| % (w/w) heat activated platinum catalyst | % (w/w) H301 cross-linker | | |
|---|---|---|---|
| | **2.72** | **5.0** | **10.0** |
| **0.05** | 0 | NT | NT |
| **0.5** | 0 | 3 | 2 |
| **0.75** | NT | 3 | NT |
| **1.0** | NT | 3 | NT |

Curing scores from 0-5, where 0 represents uncured silicone and 5 represents complete curing. NT= not tested

**Table 3.3.3** Curing scores of silicone formulations bulk-loaded with 1% (w/w) [$HL^2$] BR using room temperature activated platinum cyclovinylmethylsiloxane catalyst

| % (w/w) room temp activated platinum catalyst | % (w/w) H301 cross-linker | | |
|---|---|---|---|
| | **2.72** | **5.0** | **10.0** |
| **0.05** | 0 | 0 | 0 |
| **0.5** | 1 | 2 | 2 |
| **0.75** | 2 | 2 | 2 |

*Curing scores from 0-5, where 0 represents uncured silicone and 5 represents complete curing.

**Table 3.3.4** Curing scores of silicone formulations without antimicrobial compounds using 2.72% (w/w) cross-linker and 0.5% (w/w) heat activated or room temperature activated platinum cyclovinylmethylsiloxane catalyst

| | **2.72 % (w/w) H301 cross-linker** |
|---|---|
| **0.5 % (w/w) heat activated platinum catalyst** | 5 |
| **0.5 % (w/w) room temp activated platinum catalyst** | 5 |

Curing scores from 0-5, where 0 represents uncured silicone and 5 represents complete curing.

### 3.3.2 Mechanical properties of silicones following antimicrobial incorporation

Silicone rubber prepared using the S1 formulation had lower tensile strength, compared with the S2 formulation (S2), ($P = 0.0037$). Addition of 1% triclosan (T1 and T2) and triclosan acetate (TA-2) to the bulk of the silicone did not alter tensile strength, compared with controls (Figure 3.3.1A).

Elongation assessment of silicone rubbers showed that S2 silicone had significantly reduced elongation, compared with S1 ($P < 0.0001$). Elongation of T2 and TA-2 was significantly reduced in comparison to T1 ($P < 0.0001$) (Figure 3.3.1B). However, it was notable that addition of triclosan and triclosan acetate increased elongation, compared to control silicones (T1 vs S1, $P = 0.0145$, T2 vs S2, $P = 0.0067$, TA-2 vs S2, $P = 0.0077$).

The tear resistance of S2 silicone was significantly lower than S1 ($P < 0.0001$) (Figure 3.3.1C). Silicone T2 also had lower tear resistance than T1 ($P < 0.0001$). The tear resistance of triclosan acetate containing silicone (TA-2) was similar to the triclosan containing counterpart and the non-loaded, control formulation. S2 silicone formulation was selected for future investigations, based on its superior tensile strength compared to S1. Since the dip-coated silicone formulations used S2 silicone rubber as the base, mechanical properties were not assessed as changes in mechanical properties were not expected to occur.

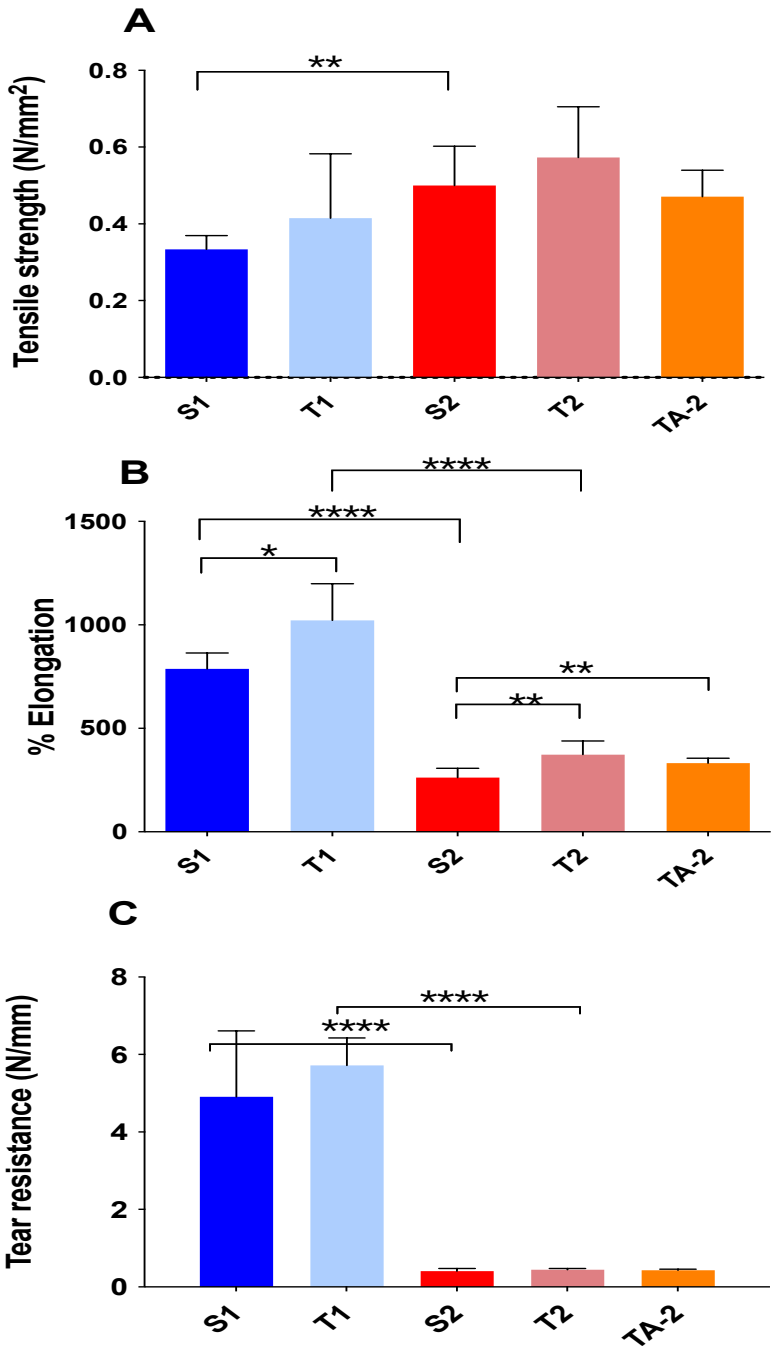


**Figure 3.3.1** Mechanical properties of novel silicone formulations. S1 and S2 represent silicone formulations without triclosan, and T1 and T2 are formulations with 1% (w/w) triclosan. TA-2 formulation was bulk-loaded with 1% (w/w) triclosan acetate. All measurements were made using a 500 N load cell pulled at 300 mm/min. (A) tensile strength of silicone specimens, (B) % elongation of silicone specimens, (C) tear resistance of silicone tear specimens. Measurements were done in triplicate for each of three independently generated batches of silicone. Error bars represent the standard deviation. Unpaired t-tests used for statistical analysis. * P<0.05, ** P<0.01, *** P< 0.001, **** P< 0.0001

### 3.3.3 Long-term release of antimicrobial compounds from silicone elastomers

#### 3.3.3.1 Repeated zone of inhibition assays

Silicone rubbers that had been bulk-loaded with antimicrobials (T2 and TA-2) generated significantly larger ZOIs than control elastomer (S2) ($P<0.0001$), with inhibition of bacterial growth evident over a 12-week period (Figure 3.3.2). Such bulk-loaded materials also produced significantly larger ZOIs than the dip-coated equivalents (T2-DC and TA-2-DC) ($P<0.0001$). Silicone rubbers bulk-loaded and dip-coated with triclosan acetate demonstrated slower and more sustained release of antimicrobial agent than the equivalent triclosan elastomers**.** ZOIs generated by the triclosan and triclosan acetate dip-coated elastomers were evident for 9 and 11 weeks, respectively. Silicone rubber coated with acetoxy silicone containing 1% w/w [$HL^2$] Br only generated ZOIs in the first week. However, the equivalent product without antimicrobial compound continued to produce ZOIs for 5 weeks.

#### 3.3.3.2 Measurement of antimicrobial compound release using HPLC

Silicone coupons bulk loaded with 1% triclosan (T2) and 1% triclosan acetate (TA-2) were immersed in artificial urine (AU) for periods between 4 h and 12 weeks, and the AU was recovered to determine triclosan and triclosan acetate concentration that had been released. Triclosan and triclosan acetate standards of known concentration were run in the HPLC instrument to generate standard curves (see Appendix I). Standard curves were used to calculate concentrations of triclosan and triclosan acetate from the solutions. Figure 3.3.3 shows the accumulation of triclosan released from T2 and TA-2 over 6 weeks. Unfortunately, due to technical issues, the AU collected at the 12-week time-point could not be analysed. Of note, triclosan acetate was not detected in AU at any timepoint when using TA-2 silicone coupons; however, triclosan was detected.

At pH 6.1, AU that contained T2 silicone led to accumulation of triclosan between 4 h and 168 h (7 days). Slightly less triclosan was detected at 14 days, but the concentration gradually increased for 6 weeks.

The equivalent AU samples at pH 6.1 containing TA-2 silicone, released significantly ($P = 0.0085$) less triclosan that the T2 silicone. Release of triclosan from TA-2 was pH dependent, with release increasing as pH increased from 6.1

to 7.0 and 9.5. However, statistical significance was not observed between samples across the pH range. The concentration of triclosan detected was highest at 7 days, and then rapidly decreased regardless of pH of AU.

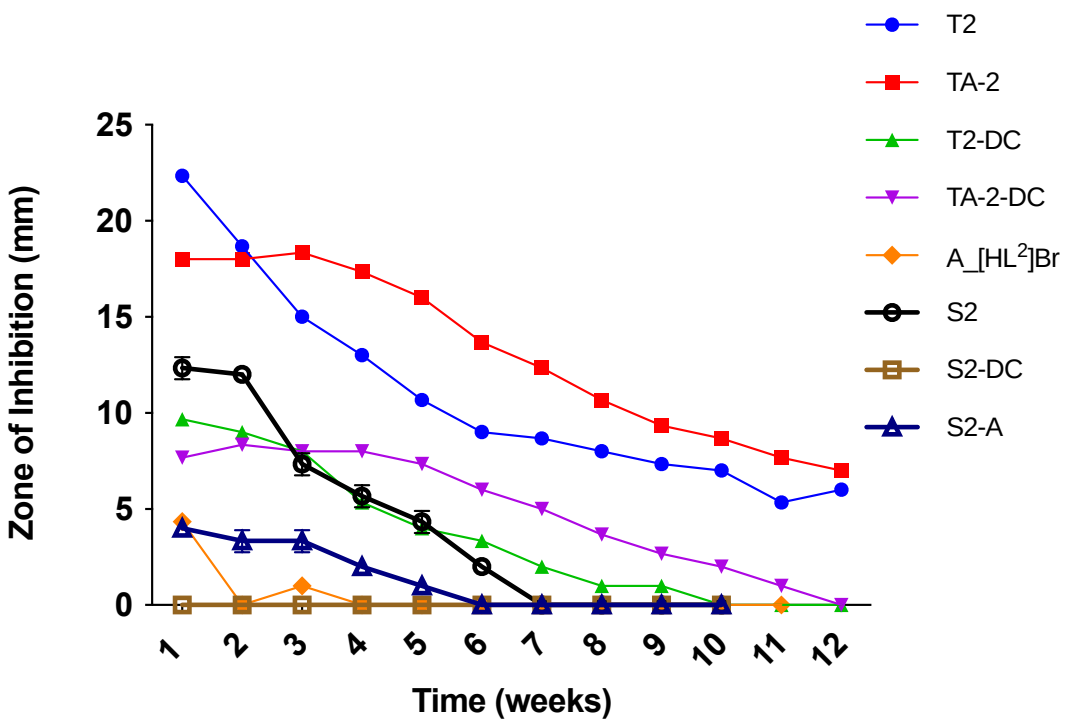


**Figure 3.3.2** Zones of inhibition on agar plates with *Staphylococcus aureus* NSM 7, using silicone coupons bulk-loaded with 1% (w/w) triclosan (T2) or 1% (w/w) triclosan acetate (TA-2), or dip-coated with a 1% (w/w) triclosan (T2-DC), 1% (w/w) triclosan acetate formulation (TA-2-DC) or coated with acetoxy silicone containing 1% (w/w) [$HL^2$] Br). Coupons without antimicrobial compound (S2), dip-coated control (S2-DC) and coupons coated with acetoxy silicone without antimicrobial compounds (S2_A) were used as controls. Silicone coupons were placed on to freshly inoculated *S. aureus* plates every 7 days and zones of inhibition were measured over 12 weeks. Means of zones produced by 3 coupons were plotted with error bars representing SD. Statistical analysis was performed using paired t-tests

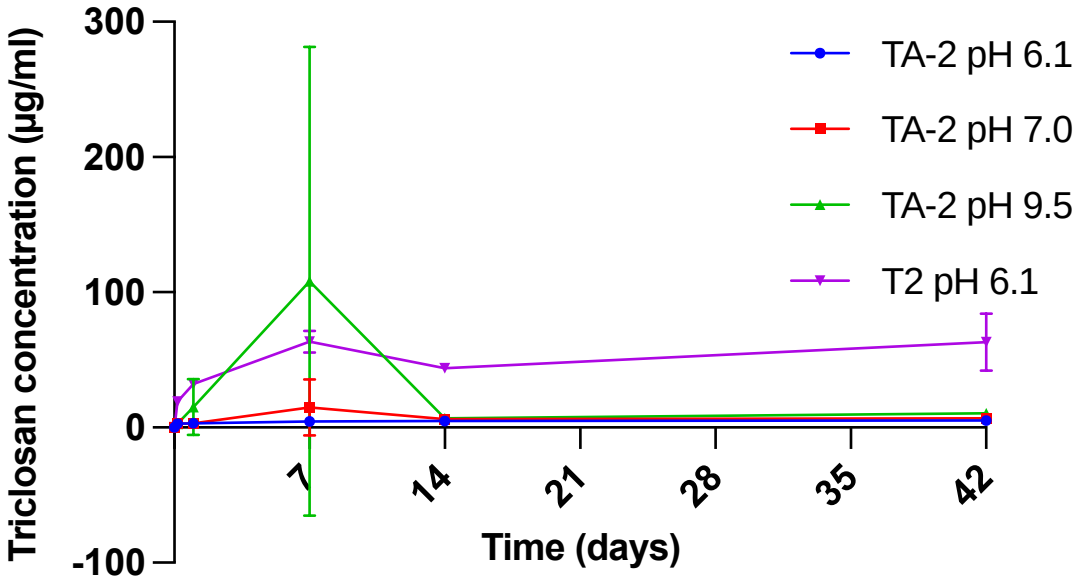


**Figure3.3.3** Triclosan release from bulk-loaded silicone elastomers over 6 weeks. Triclosan released from 1% w/w bulk-loaded silicone (T2) in artificial urine at pH 6.1. and from silicone bulk-loaded with 1% w/w triclosan acetate in AU at pH 6.1, 7.0 and 9.5. Means of 3 independent experiments are depicted with error bars representing SD. Statistical analysis was performed using one-way ANOVA with repeated measures. Two-tailed t-test was used to determine statistical differences between T2 and TA-2 at pH 6.1

### 3.3.4 Antimicrobial activity of novel silicone formulations

The antimicrobial activity of silicone formulations containing antimicrobial compounds was assessed using three different methods against 8 CAUTI causing microorganisms. The results of these investigations are summarised in Table 3.3.5 with full description in sections 3.3.4.1 to 3.3.4.3.

#### 3.3.4.1 Zone of inhibition assays

Antimicrobial release and activity from formulated silicone elastomers with antimicrobial in either the material bulk (Figure 3.3.4A) or on the surface (Figures 3.3.4B and 3.3.4C) was investigated using ZOI assays. T2 silicone (1% (w/w) triclosan) was inhibitory to *E. coli*, *S. aureus*, *K. pneumoniae*, *P. stuartii*, *P. mirabilis* and *C. albicans*. No inhibition of *P. aeruginosa* or *S. marcescens* occurred with this material. In comparison, TA-2 silicone was only inhibitory to *S. aureus* (Figure 3.3.4A). The control formulation (S2) generated a very small ZOI with *E. coli*, *S. aureus*, *K. pneumoniae*, *P. stuartii and P. mirabilis*. Silicones S2 and TA-2 produced equivalent ZOIs against *E. coli*, *P. mirabilis*, *K. pneumoniae* and *P.* stuartii. *Pseudomonas aeruginosa, S. marcescens* and *C. albicans* were resistant to both antimicrobial silicone rubbers.

Silicone rubber dip coated with 1% (w/w) triclosan or 1% (w/w) triclosan acetate exhibited lower antimicrobial effects against Gram-negative bacteria and *C. albicans* than bulk-loaded counterparts (Figure 3.3.4B). Triclosan coated silicone rubbers yielded larger ZOIs against *P. stuartii* and *P. mirabilis* than controls ($P<0.01$) and smaller ZOIs than controls with *E. coli* and *K. pneumoniae* ($P<0.05$). Both triclosan and triclosan acetate coated silicones inhibited *S. aureus*. However, ZOIs produced by the triclosan coated silicone were approximately 3-fold smaller than for silicone bulk loaded with the same compound. Silicone dip-coated with the triclosan acetate was not inhibitory to *C. albicans* or the 7 Gram-negative bacterial species. Silicone rubber with a surface coating of acetoxy silicone containing 1% (w/w) [$HL^2$] Br (A_[$HL^2$] Br)) was inhibitory to *S. aureus* ($P<0.05$) and *C. albicans* ($P<0.001$) (Figure 3.3.4C). Although a small ZOI was evident with *P. aeruginosa*, it was not statistically significant when compared to the ZOI of the control coupon. Silicone with a [$HL^2$] Br acetoxy coating did not inhibit the growth of any Gram-negative bacteria investigated.

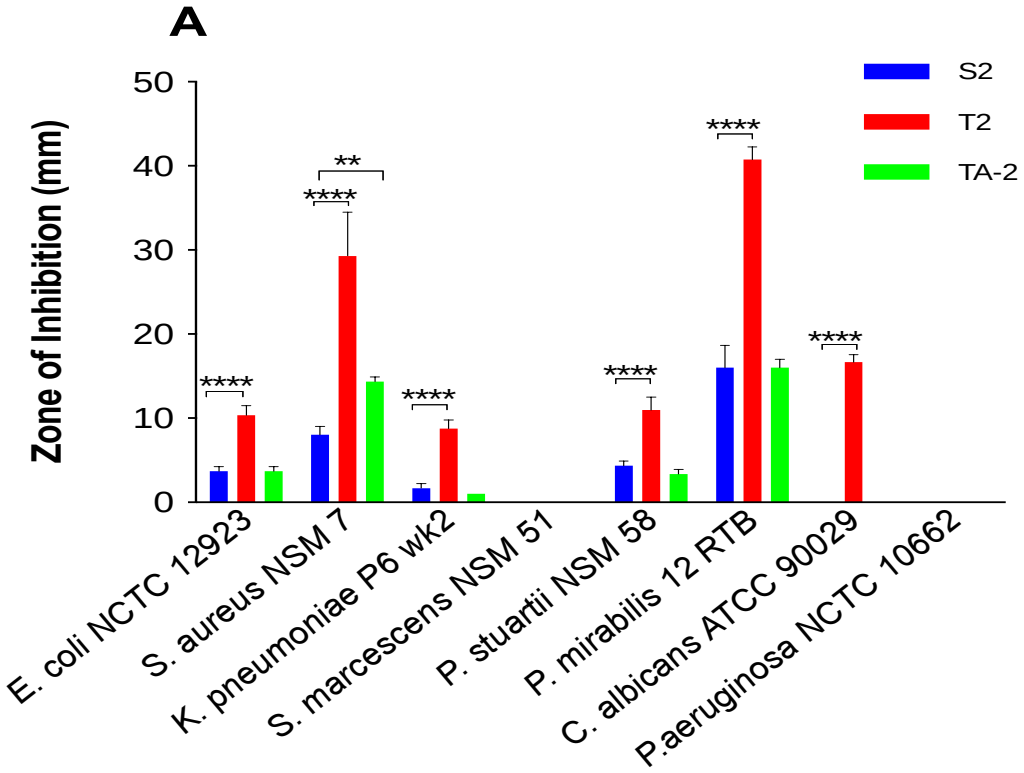
A
Zone of Inhibition (mm)
50
40
30
20
10
0
S2
T2
TA-2
****
**
****
****
****
****
****
E. coli NCTC 12923
S. aureus NSM 7
K. pneumoniae P6 wk2
S. marcescens NSM 51
P. stuartii NSM 58
P. mirabilis 12 RTB
C. albicans ATCC 90029
P.aeruginosa NCTC 10662

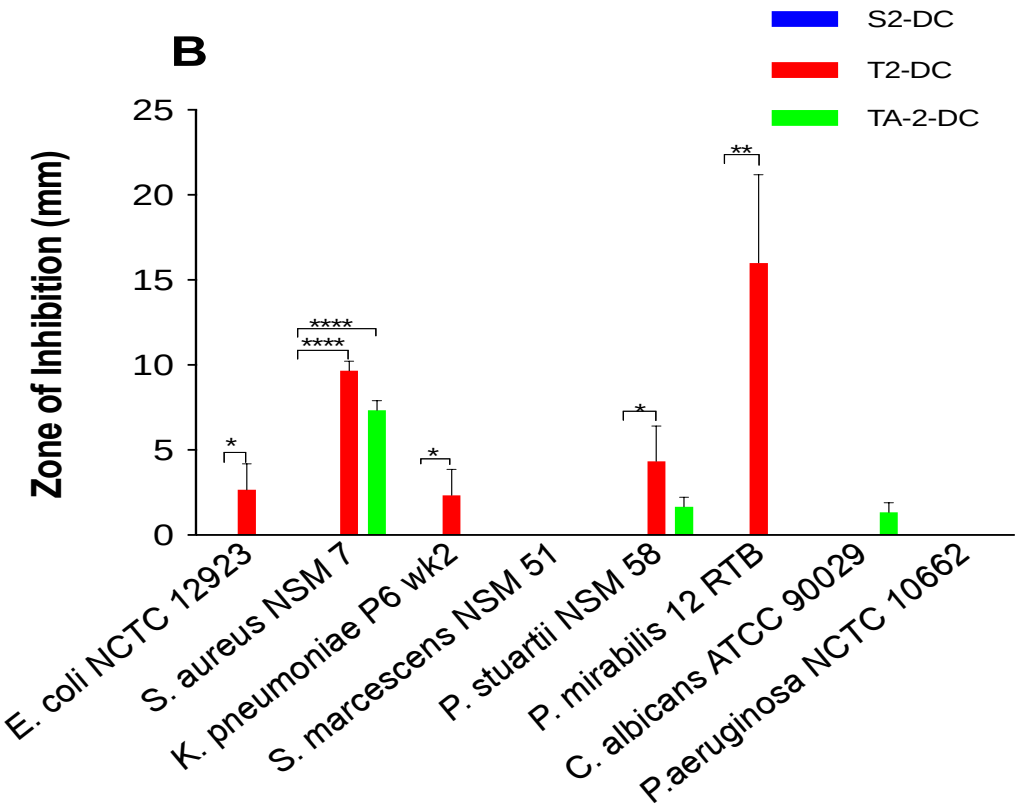
B
Zone of Inhibition (mm)
25
20
15
10
5
0
S2-DC
T2-DC
TA-2-DC
*
****
****
*
*
**
E. coli NCTC 12923
S. aureus NSM 7
K. pneumoniae P6 wk2
S. marcescens NSM 51
P. stuartii NSM 58
P. mirabilis 12 RTB
C. albicans ATCC 90029
P.aeruginosa NCTC 10662

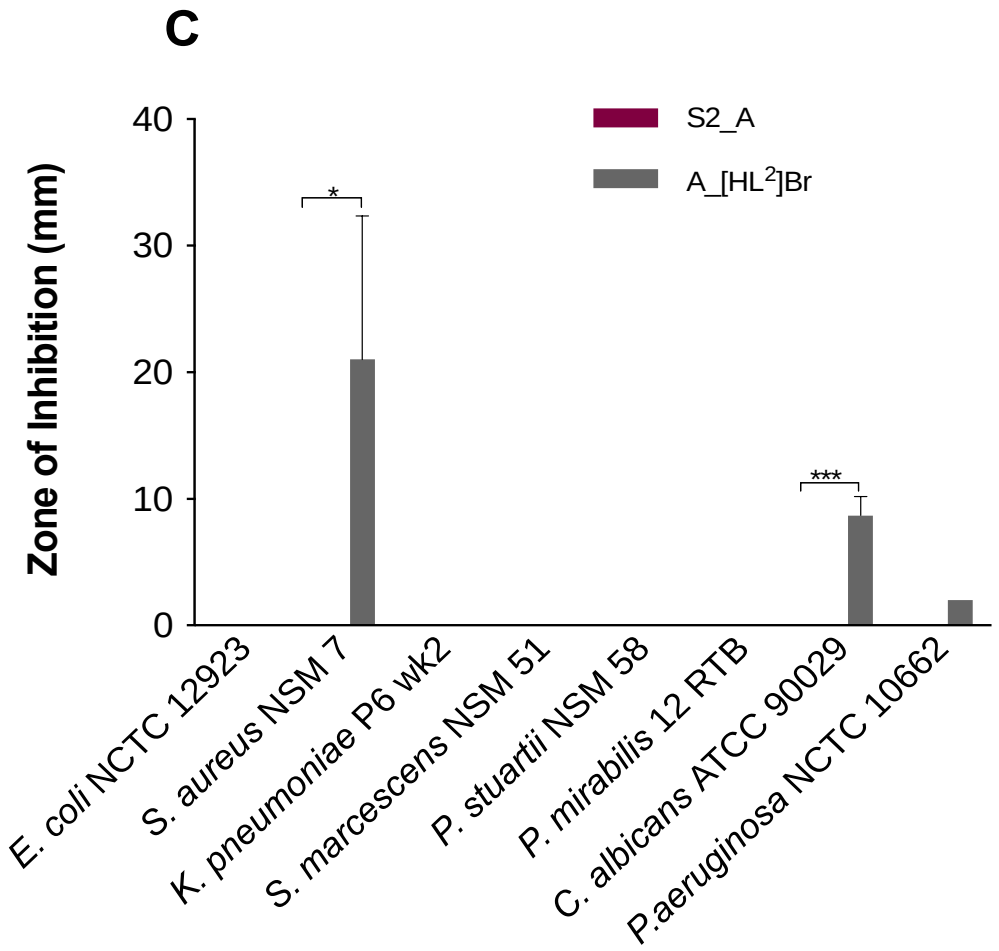


**Figure 3.3.4** Zones of inhibition generated by formulated silicones. Agar plates were prepared with 8 CAUTI causing microorganisms. Zones of inhibition following 24 h incubation with silicone coupons were measured. (A) control silicone (S2) vs 1%(w/w) bulk-loaded triclosan silicone (T2) and 1% (w/w) bulk-loaded triclosan silicone (TA-2), (B) dip-coated control silicone (S2-DC) vs 1%(w/w) triclosan dip-coated silicone (T2-DC) and 1%(w/w) triclosan acetate dip-coated silicone (TA-2-DC), (C) silicone dip-coated with an acetoxy silicone formulation with (A_[HL$^2$]Br) or without 1% (w/w) [HL$^2$]Br (S2_A). Means of 3 silicone coupons from separate batches were plotted. Error bars show standard deviation. One way ANOVA was used for statistical analysis for A and B. Unpaired t-tests used for statistical analysis of silicone in C. * P<0.05, ** P<0.01, *** P< 0.001 **** P< 0.0001

### 3.3.4.2 Enumeration of microorganisms recovered from silicone

Viable microorganisms recovered from silicone coupons after an initial adherence and incubation period, were cultured on agar medium and the number of colony forming units (CFUs) were determined. Higher CFUs of *E. coli* (P = 0.0031), *S. aureus* (P = 0.0111), *K. pneumoniae* (P< 0.0001) *P. mirabilis* (P = 0.0062) and *C. albicans* (P = 0.0351) were recovered from control silicone (S2) than from silicone bulk loaded with 1% (w/w) triclosan (T2) (Figures 3.3.5 A, B, C, F and G). Similar CFUs of *S. marcescens* and *P. aeruginosa* were recovered from S2 and T2 coupons (P>0.05) (Figures 3.3.5D and H). Although higher CFUs of *P. stuartii* were recovered from S2 compared with T2 coupons, the difference was not significant (P >0.05). In contrast, lower numbers of viable *K. pneumoniae* and *P. stuartii* cells were recovered from silicone bulk-loaded with 1% (w/w) triclosan acetate (TA-2) (P >0.05) (Figures 3.3.6C and E).

Recovery of viable of microorganisms from silicone rubber dip-coated with additional layers of silicone containing 1% (w/w) triclosan (T2-DC), 1% (w/w) triclosan acetate (TA-2-DC) or an acetoxy silicone containing 1% (w/w) [$HL^2$] Br (A_[$HL^2$] Br), were investigated using the same method and compared to formulations without antimicrobial compounds (Figures 3.3.7 and 3.3.8).

The recovery of viable *C. albicans* and 6 Gram-negative bacteria species from triclosan and triclosan acetate coated silicone were not statistically different to the control formulations (Figures 3.3.7A, C-H). However, reduced CFUs of *S. aureus* (Figure 3.3.7B) were recovered from triclosan and triclosan acetate coated silicone (P<0.01), compared to the control silicone formulation. Reduced CFUs of *K. pneumoniae*, *P. mirabilis*, *P. stuartii* and *C. albicans* were obtained from 1% (w/w) triclosan coated silicone, compared to the control, but the differences were not significant. Similarly, a 1% (w/w) triclosan acetate coating reduced the recovery of viable *K. pneumoniae*, *P. mirabilis*, and *C. albicans* from the silicone, but again the differences were not statistically significant.

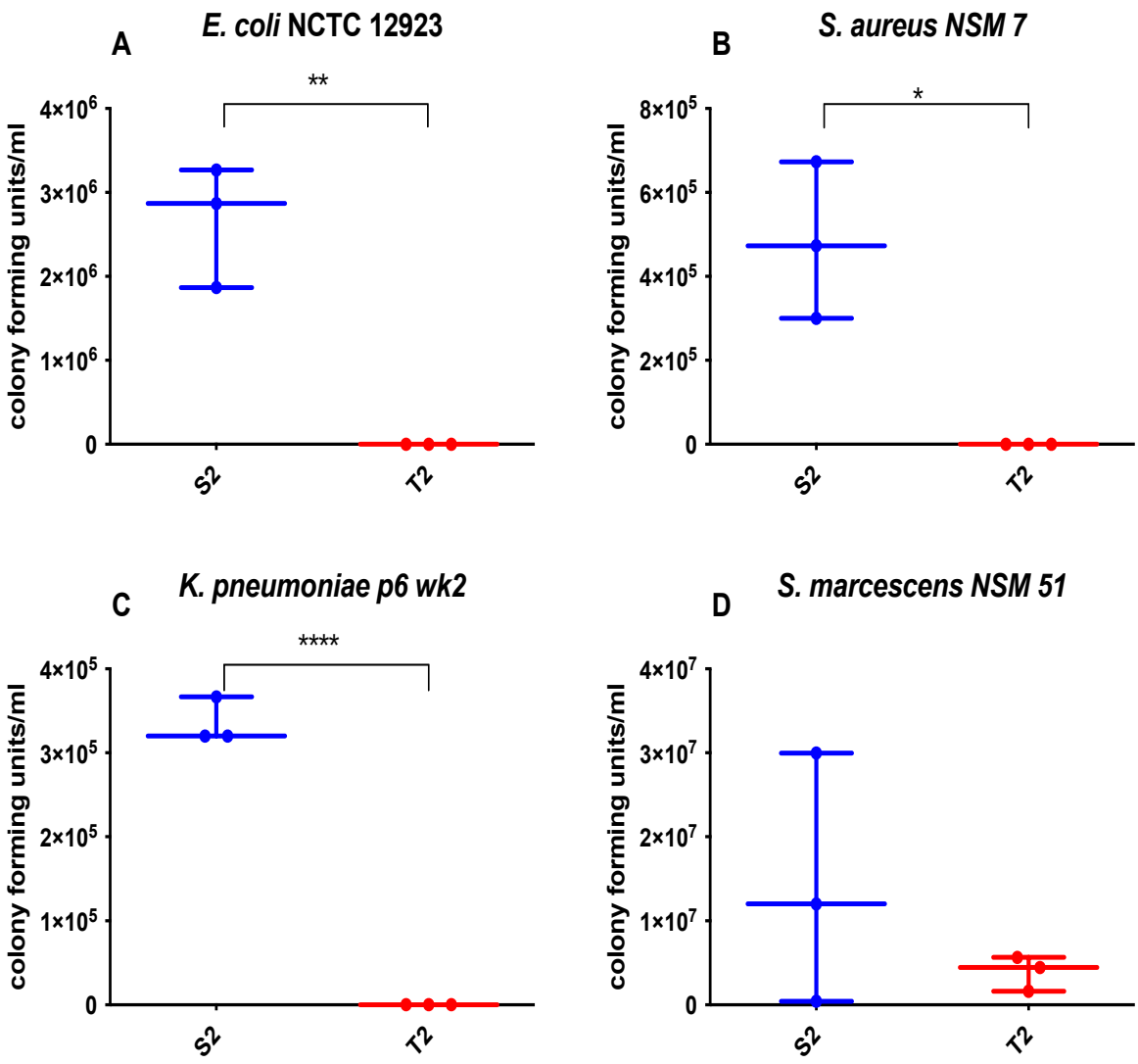
A
E. coli NCTC 12923
**
colony forming units/ml
4×10^6
3×10^6
2×10^6
1×10^6
0
S2
T2
B
S. aureus NSM 7
*
colony forming units/ml
8×10^5
6×10^5
4×10^5
2×10^5
0
S2
T2
C
K. pneumoniae p6 wk2
****
colony forming units/ml
4×10^5
3×10^5
2×10^5
1×10^5
0
S2
T2
D
S. marcescens NSM 51
colony forming units/ml
4×10^7
3×10^7
2×10^7
1×10^7
0
S2
T2

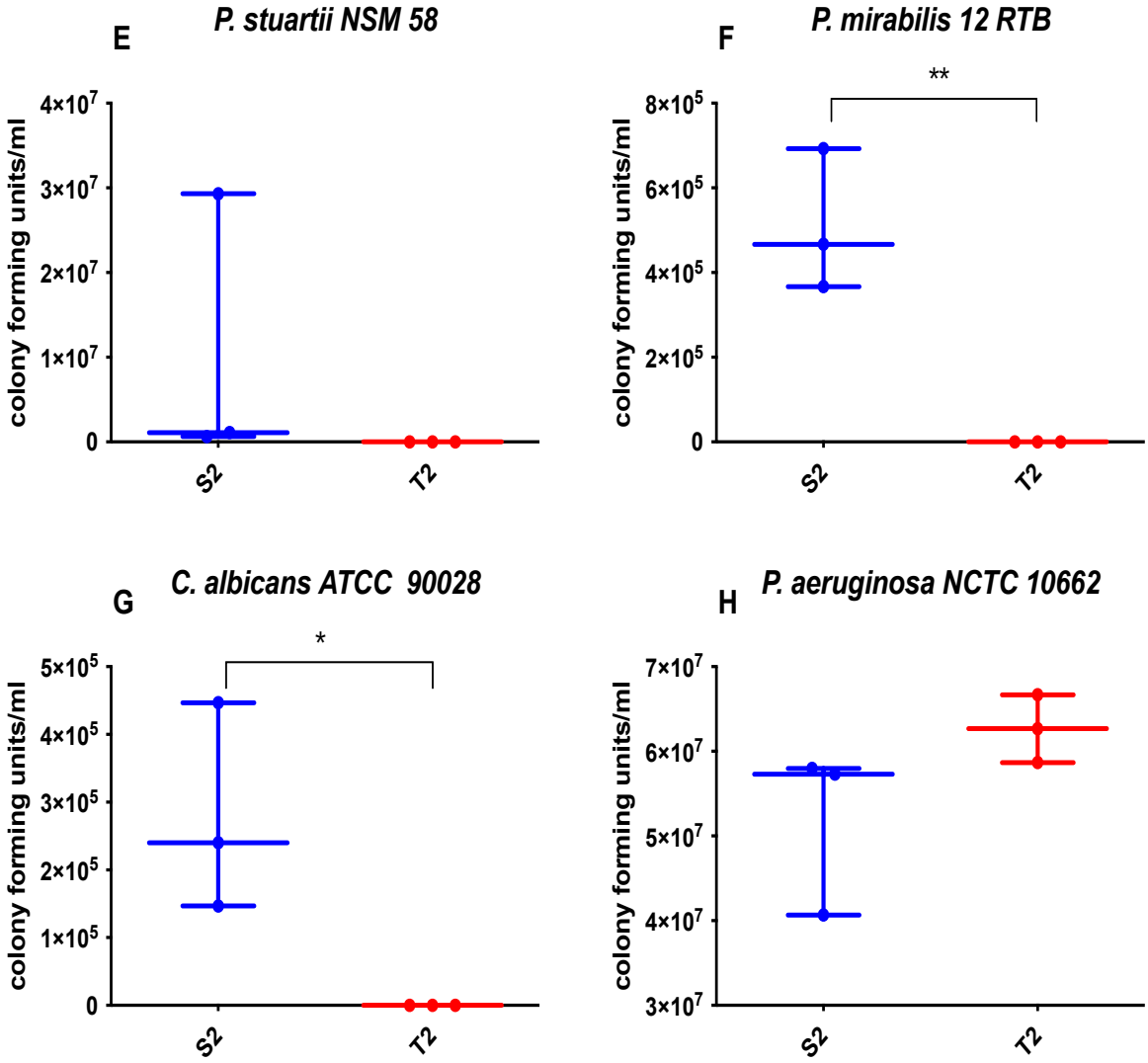


**Figure 3.3.5** Colony forming units of CAUTI causing microorganisms recovered following 24 h adherence to control silicone (S2) and silicone bulk-loaded with 1% (w/w) triclosan (T2). Data expressed as mean of three replicates with error bars representing standard deviation. Unpaired t-tests used for statistical analysis. * P<0.05, ** P<0.01, *** P< 0.001, **** P< 0.0001

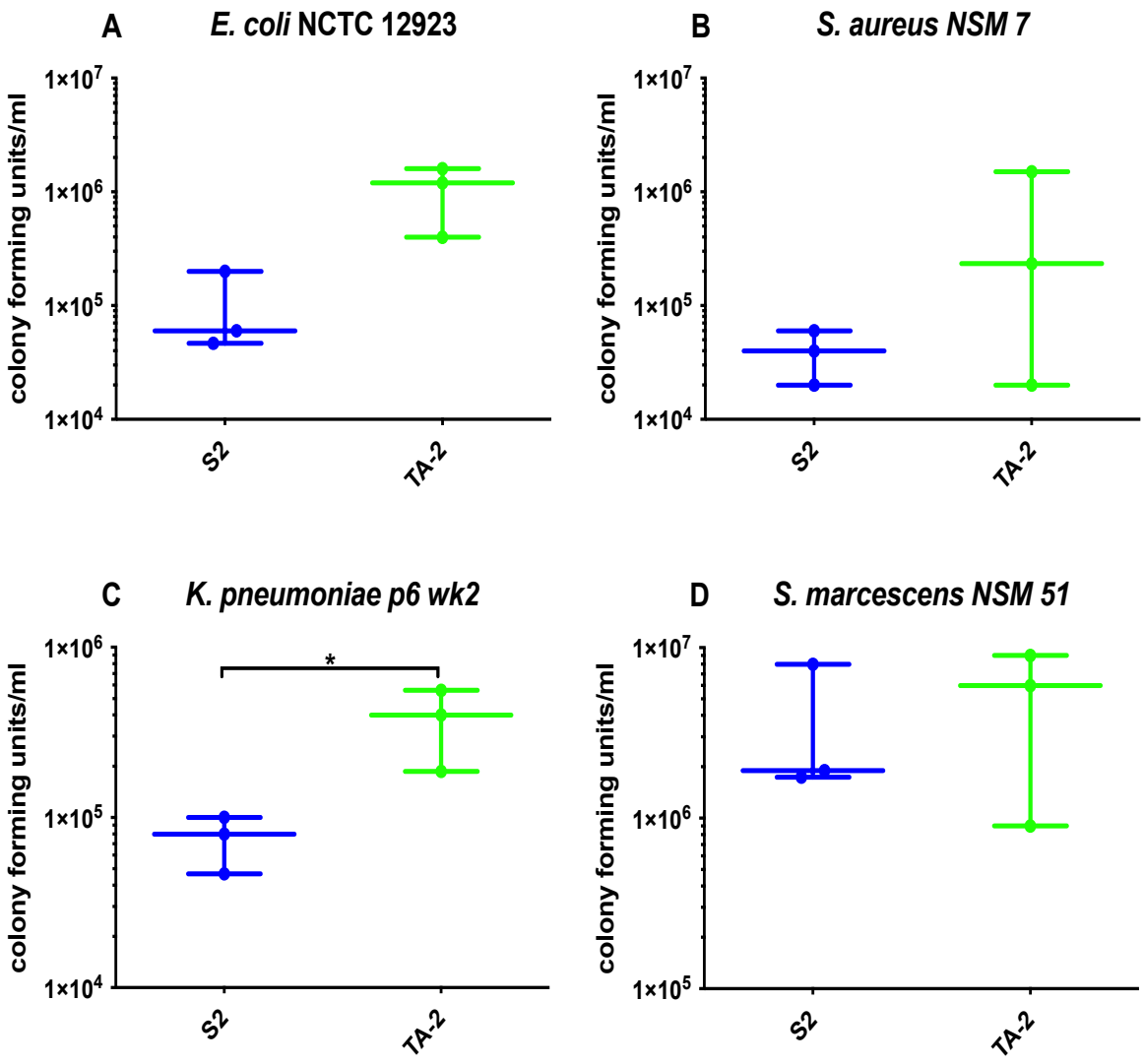
A
E. coli NCTC 12923
B
S. aureus NSM 7
C
K. pneumoniae p6 wk2
D
S. marcescens NSM 51
colony forming units/ml
1×10^7
1×10^6
1×10^5
1×10^4
S2
TA-2
*

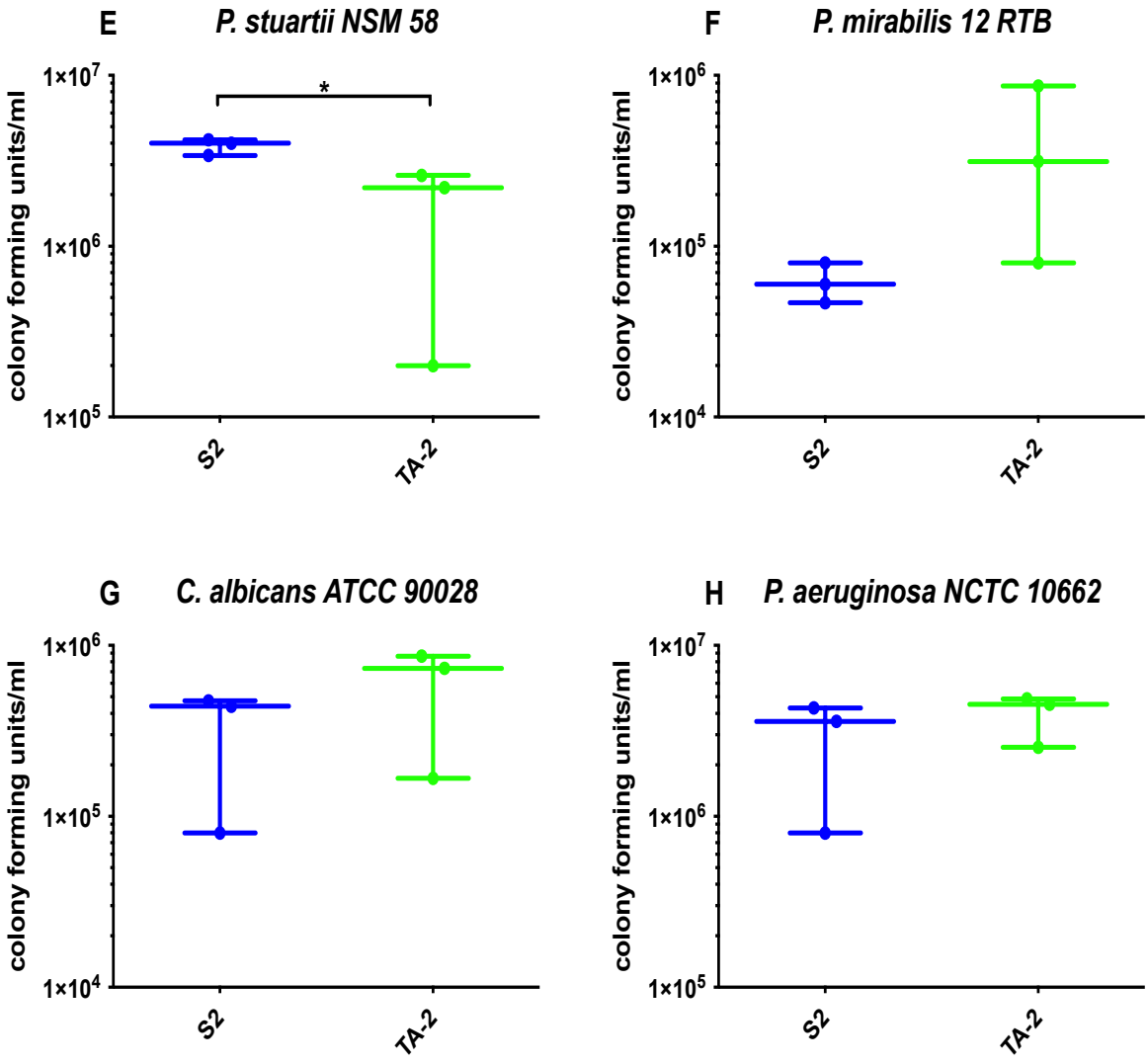


**Figure 3.3.6** Colony forming units of CAUTI causing microorganisms recovered following 24 h adherence to control silicone (S2) and silicone bulk-loaded with 1% (w/w) triclosan acetate (TA-2). Data expressed as mean of three replicates with error bars representing standard deviation. Unpaired t-tests used for statistical analysis. * $P<0.05$

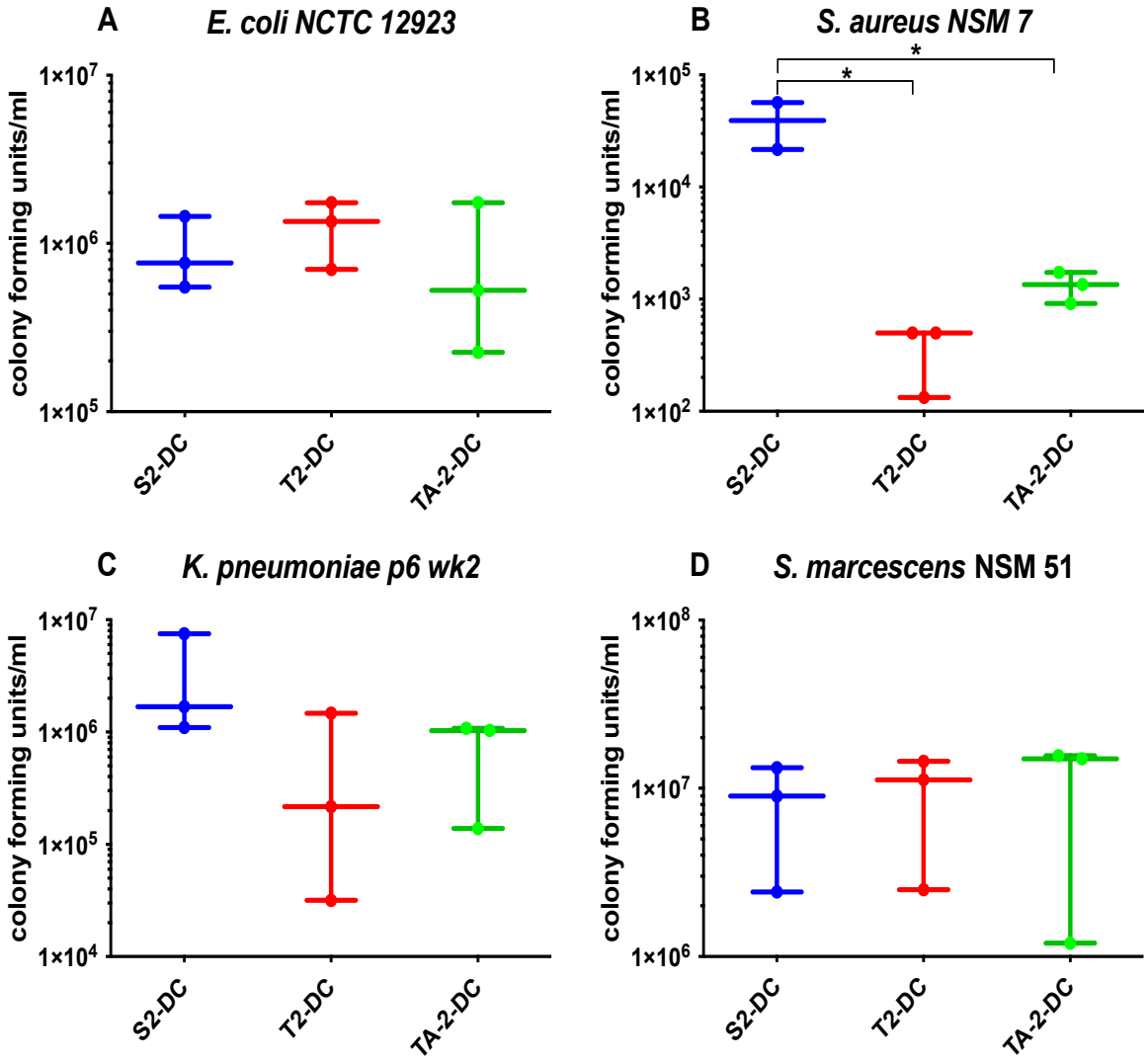
A
E. coli NCTC 12923
colony forming units/ml
1×10^7
1×10^6
1×10^5
S2-DC
T2-DC
TA-2-DC
B
S. aureus NSM 7
*
*
colony forming units/ml
1×10^5
1×10^4
1×10^3
1×10^2
S2-DC
T2-DC
TA-2-DC
C
K. pneumoniae p6 wk2
colony forming units/ml
1×10^7
1×10^6
1×10^5
1×10^4
S2-DC
T2-DC
TA-2-DC
D
S. marcescens NSM 51
colony forming units/ml
1×10^8
1×10^7
1×10^6
S2-DC
T2-DC
TA-2-DC

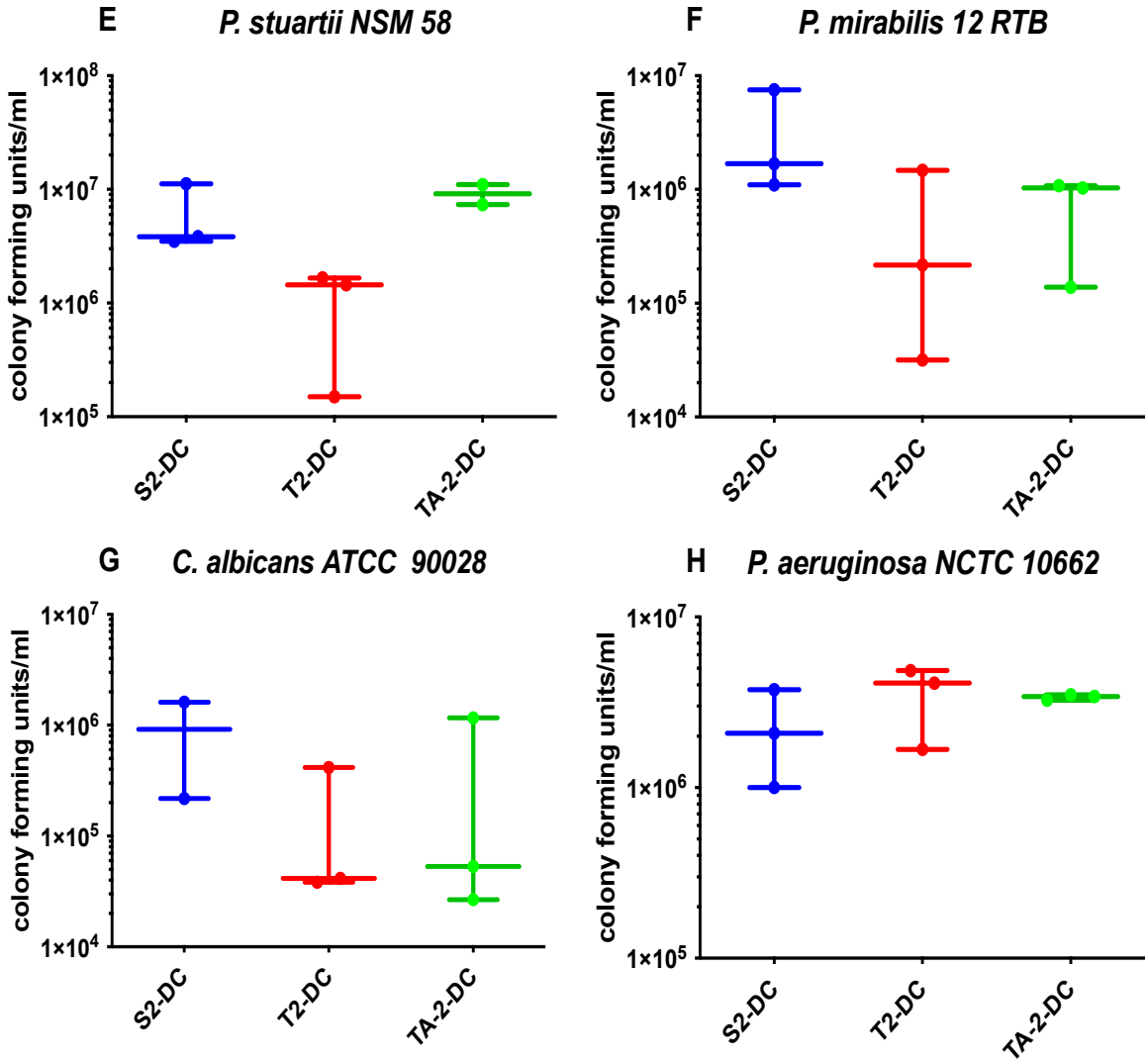


**Figure 3.3.7** Colony forming units of CAUTI causing microorganisms recovered following 24 h adherence to dip-coated silicones. Silicone without antimicrobial (S2-DC), 1% (w/w) triclosan dip-coating (T2-DC) and 1% (w/w) triclosan acetate dip-coatings (TA-2-DC) were compared. Data expressed as mean of three replicates with error bars representing standard deviation. ANOVA used for statistical analysis. * $P<0.05$

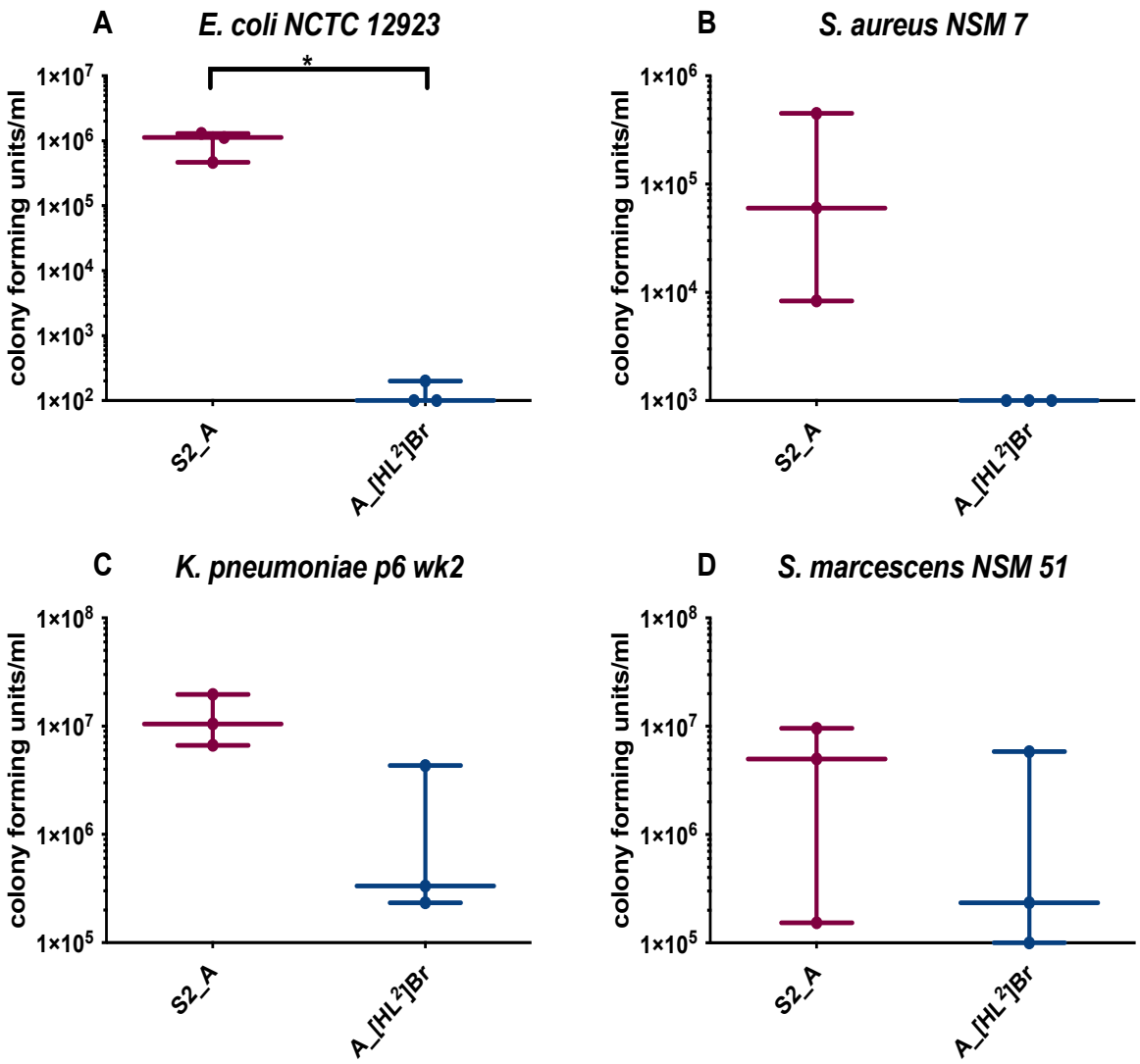
A
E. coli NCTC 12923
*
colony forming units/ml
1×10^7
1×10^6
1×10^5
1×10^4
1×10^3
1×10^2
S2_A
A_[HL2]Br
B
S. aureus NSM 7
colony forming units/ml
1×10^6
1×10^5
1×10^4
1×10^3
S2_A
A_[HL2]Br
C
K. pneumoniae p6 wk2
colony forming units/ml
1×10^8
1×10^7
1×10^6
1×10^5
S2_A
A_[HL2]Br
D
S. marcescens NSM 51
colony forming units/ml
1×10^8
1×10^7
1×10^6
1×10^5
S2_A
A_[HL2]Br

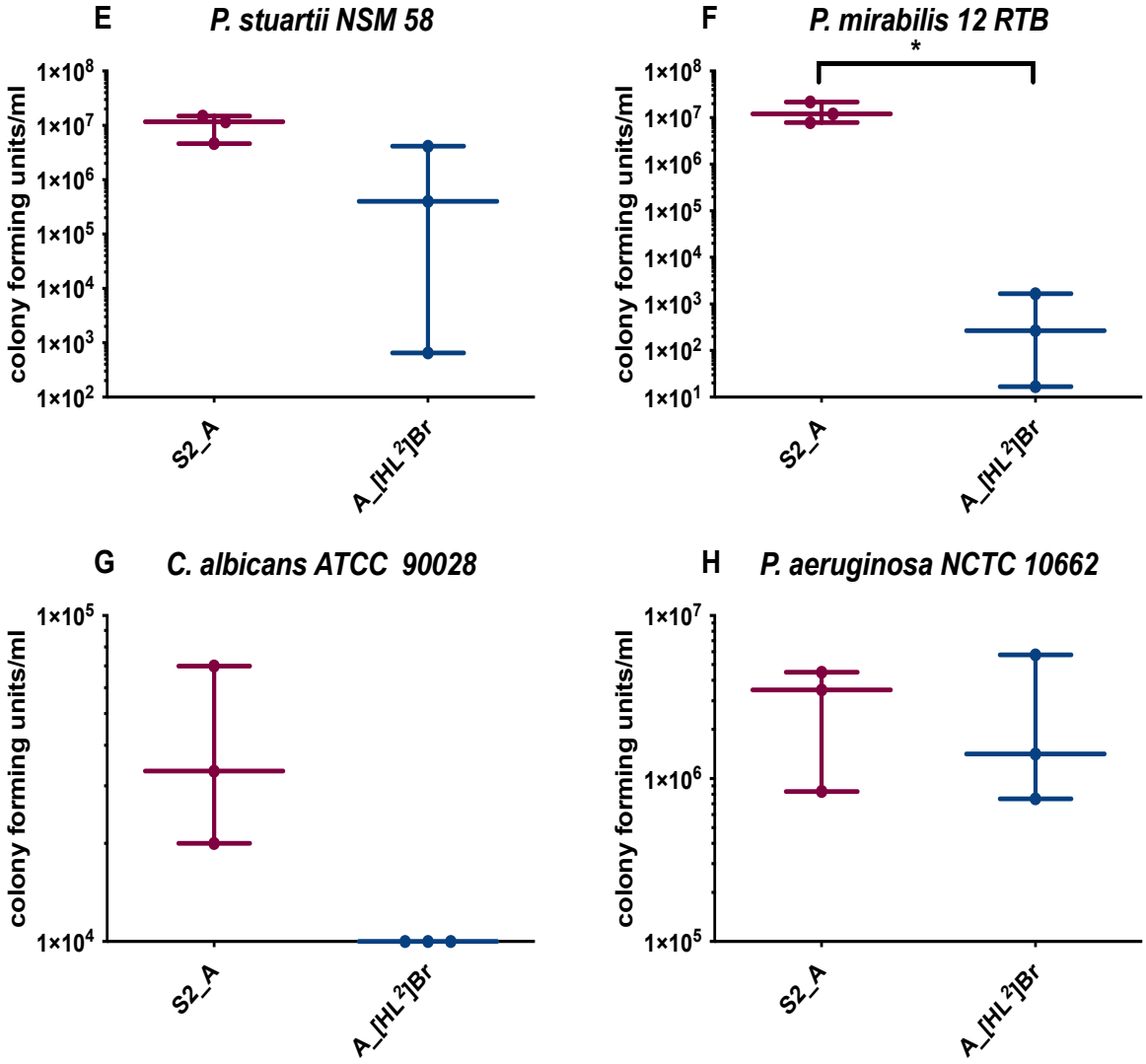


**Figure 3.3.8** Colony forming units of CAUTI causing microorganisms recovered following 24 h adherence to silicone dip-coated with acetoxy silicone without antimicrobial compound (S2_A) and silicone dip-coated with acetoxy silicone containing 1% (w/w) [$HL^2$]Br (A_[$HL^2$]Br). Data expressed as mean of three replicates with error bars representing standard deviation. Unpaired t-tests used for statistical analysis. * $P<0.05$

### 3.3.4.3 Quantification of dead cells on antimicrobial silicone surfaces

Microbes adhered to silicone coupons for 90 min were stained with propidium iodide (PI) and imaged by fluorescent microscopy to detect dead cells. PI stained cells were expressed as a percentage area of the total field of view. Biocidal formulations were compared with controls. Silicone bulk-loaded with 1% (w/w) triclosan (T2) yielded significantly higher numbers of PI-stained *E. coli, S. aureus, K. pneumoniae, P. stuartii*, and *C. albicans* ($P<0.05$) compared with (S2) (Figures 3.3.9A, B, C, E and G). The mean surface area of PI-stained *S. marcescens* (Figures 3.3.9D) cells was higher on silicone bulk loaded with triclosan, although the difference was not statistically significant. No antimicrobial effect was evident with *P. aeruginosa* (Figure 3.3.9H). Figures 3.3.10-3.3.13 depict PI-stained cells on bulk-loaded triclosan silicone coupons.

Silicone bulk-loaded with 1% (w/w) triclosan acetate (TA-2) resulted in significantly larger areas ($P<0.05$) of dead *S. aureus* (B), *K. pneumoniae* (C), *P. stuartii* (E), and *P. mirabilis* (F) compared with controls (S2) (Figure 3.3.14). No difference in PI staining was found for *E. coli* (A), *S. marcescens* (D), *C. albicans* (G) and *P. aeruginosa* (H), for triclosan acetate coated surfaces and controls. Representative images of dead cells on TA-2 surfaces are shown in Figures 3.3.15- 3.3.18.

Silicone rubber dip-coated with 1% (w/w) triclosan resulted in significantly larger areas ($P< 0.05$) of dead *K. pneumoniae,* compared to controls (Figure 3.3.19C and 3.3.21). Evaluation of the 7 additional microorganisms showed no biocidal effect of the dip-coated triclosan containing formulation. With exception of *E. coli*, 1% (w/w) triclosan acetate dip-coated formulation had equivalent areas of PI stained cells to controls. (Figures 3.3.19A and 3.3.20). Figures 3.3.20-3.3.23 are representative images of PI-stained cells on dip-coated silicone coupons.

Silicone coated with an acetoxy silicone containing 1% (w/w) $[HL^2]Br$, (A_$[HL^2]Br$) had larger areas of dead cells for 3 out of 8 microorganisms, compared with controls (S2_A) (Figure. 3.3.24). Significant differences were observed with *S. aureus* (B, $P<0.01$), *K. pneumoniae* (C, $P<0.05$) and *C. albicans* (G, $P<0.05$). Although not statistically significant, $[HL^2]Br$ coated silicone increased the mean surface area of dead *E. coli* (A), *S. marcescens* (D), *P. stuartii* (E), and *P. mirabilis* (F), compared with controls. Representative images of PI-stained cells upon acetoxy coated silicone coupons are shown in Figures 3.3.25 - 3.3.28.

Interestingly, differences in the morphology of *C. albicans* were observed on the coupons of different silicone formulations. A mixture of C*andida* in its spherical, yeast form and the more pathogenic hyphal form was observed on control silicone (S2) (Figures 3.3.13 and 3.3.18). The hyphal form was the predominant phenotype on the dip-coated controls S2-DC (Figure 3.3.23) and S2_A (Figure 3.3.28). Silicone containing triclosan, either bulk-loaded into the matrix or dip-coated, appeared to prevent transition of the yeast to hyphal phenotype, or S2 silicone promoted this transition (Figures 3.3.13 and 3.3.23). Incorporation of the novel imidazolium compound into an acetoxy coating also did not lead to a phenotypic switch (Figure 3.3.28). Significant numbers of hyphae were observed for triclosan acetate containing formulations suggesting this was less effective than triclosan in preventing transition to hyphae or better at inducing such transition (Figures 3.3.18 and 3.3.23).

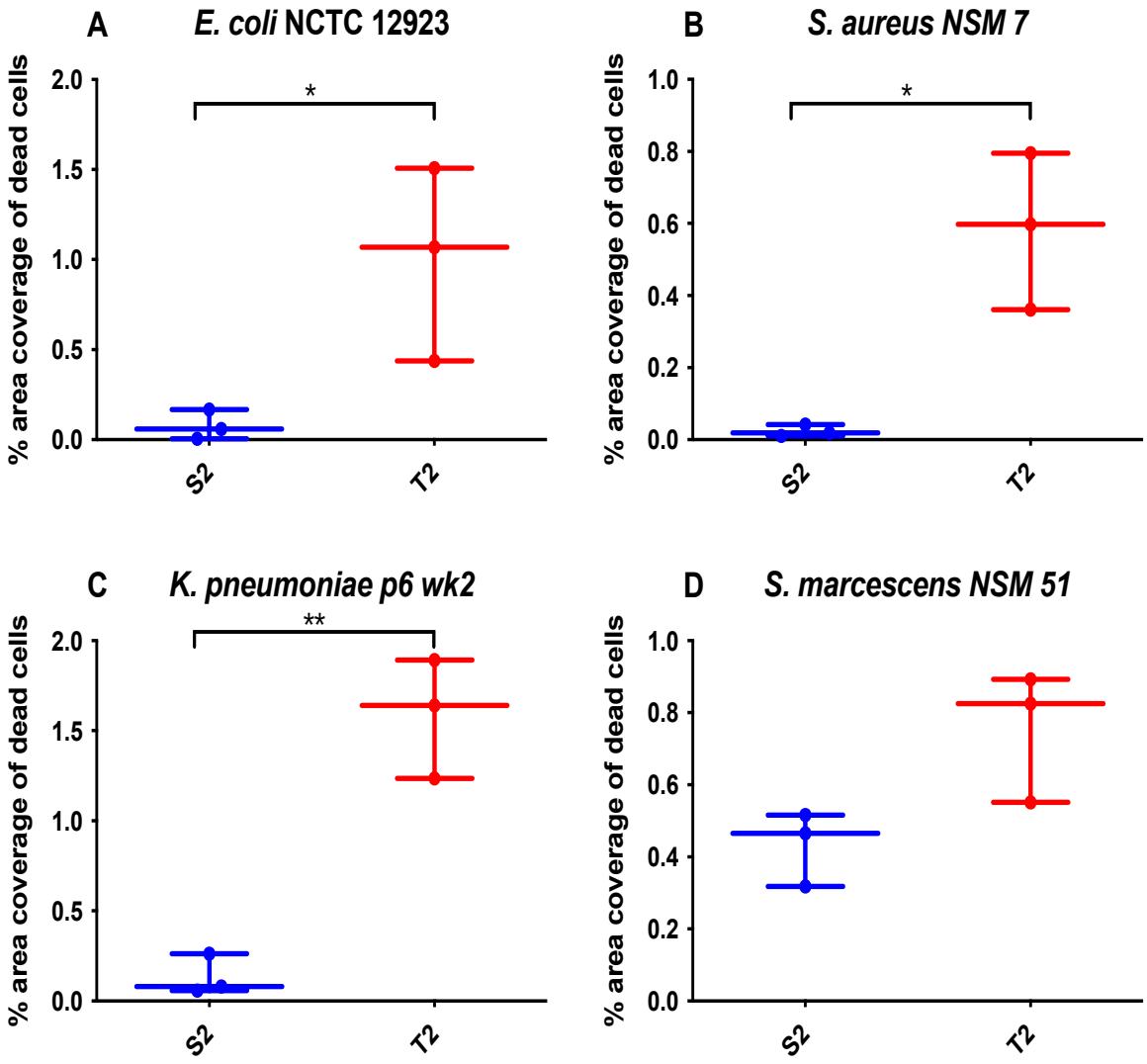
A
E. coli NCTC 12923
% area coverage of dead cells
2.0
1.5
1.0
0.5
0.0
*
S2
T2
B
S. aureus NSM 7
% area coverage of dead cells
1.0
0.8
0.6
0.4
0.2
0.0
*
S2
T2
C
K. pneumoniae p6 wk2
% area coverage of dead cells
2.0
1.5
1.0
0.5
0.0
**
S2
T2
D
S. marcescens NSM 51
% area coverage of dead cells
1.0
0.8
0.6
0.4
0.2
0.0
S2
T2

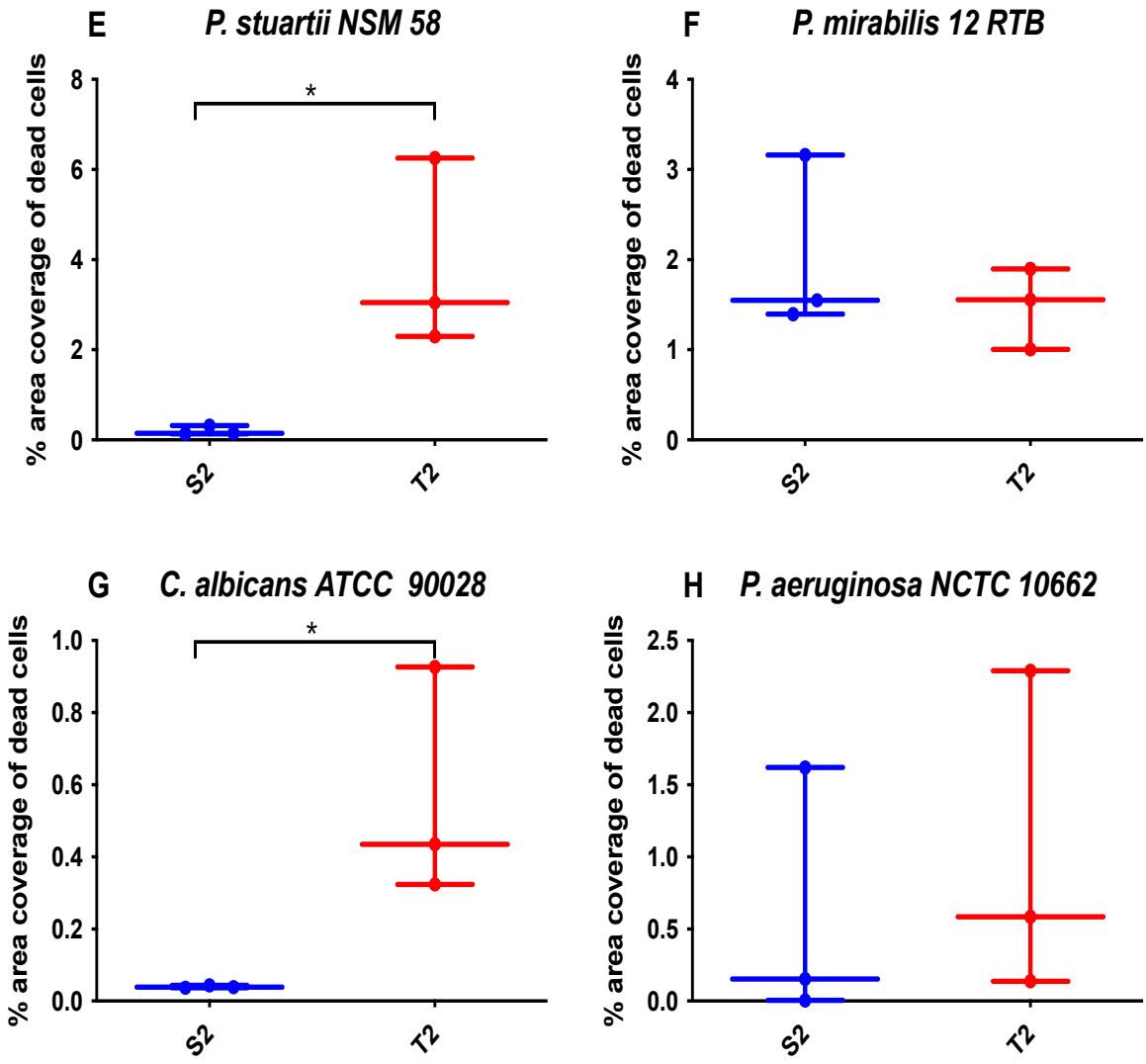


**Figure 3.3.9** Propidium iodide stained (dead) microorganisms adhered to silicone. Silicone formulations without antimicrobial compound (S2) and silicone bulk loaded with 1% (w/w) triclosan (T2) were compared. Data expressed as % area coverage of propidium iodide stained cells from 5 fields of view of 3 independently made silicone coupons. Unpaired t-tests used for statistical analysis. Error bars represent standard deviation. * P<0.05, ** P<0.01

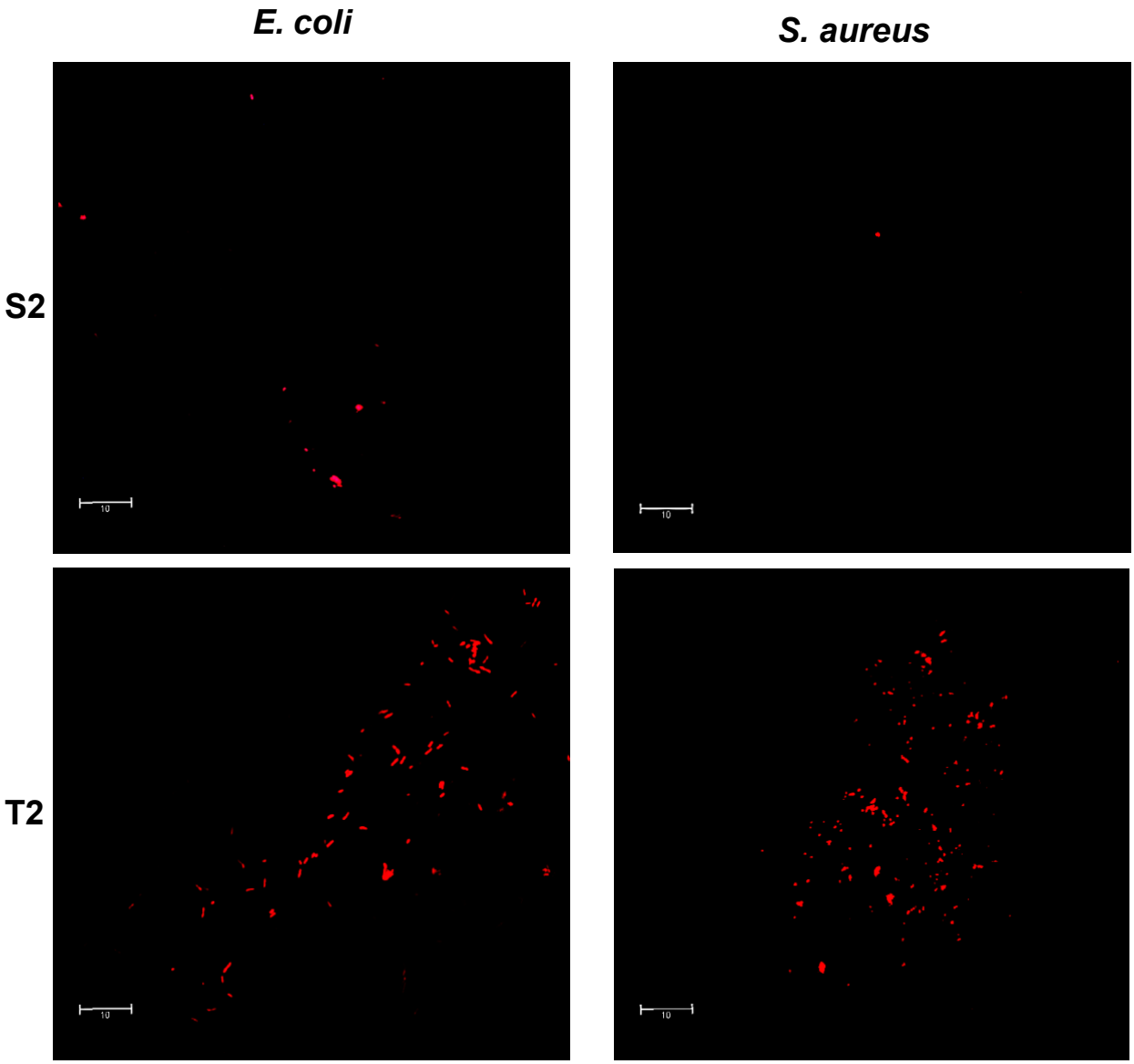


**Figure 3.3.10** Representative images of dead *Escherichia coli* NCTC 12923 and *Staphylococcus aureus* NSM 7 cells. Propidium iodide was used to stain dead cells, following 90 min adherence and incubation for 24 h at 37 °C upon silicone bulk-loaded with 1% (w/w) triclosan (T2) or without antimicrobial (S2). Scale bar represents 10 μm

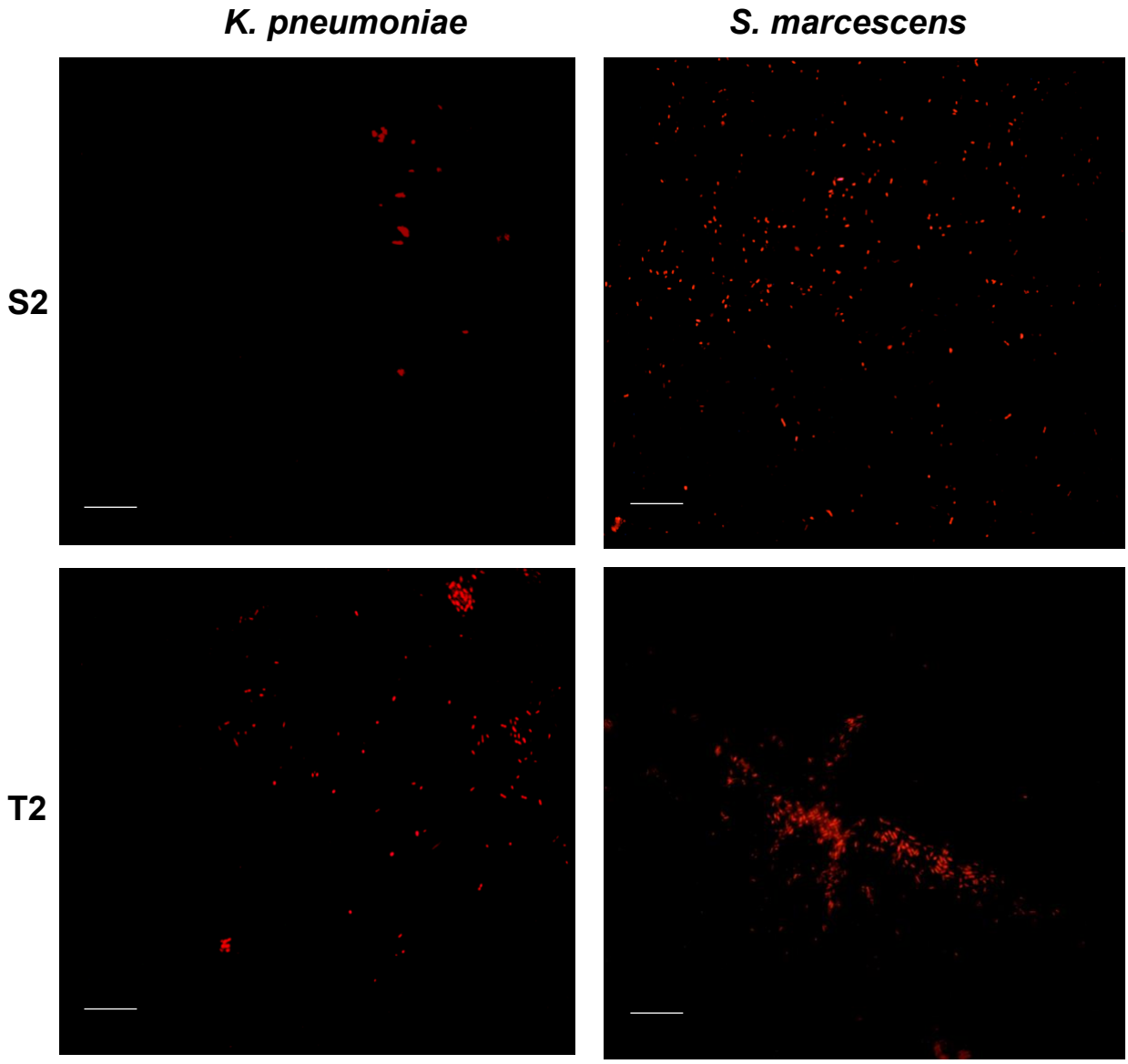


**Figure 3.3.11** Representative images of dead *Klebsiella pneumoniae* P6 wk2 and *Serratia marcescens* NSM 51 cells stained with propidium iodide, following adherence and incubation upon silicone bulk-loaded with 1% (w/w) triclosan (T2) or without antimicrobial (S2). Scale bar represents 10 μm

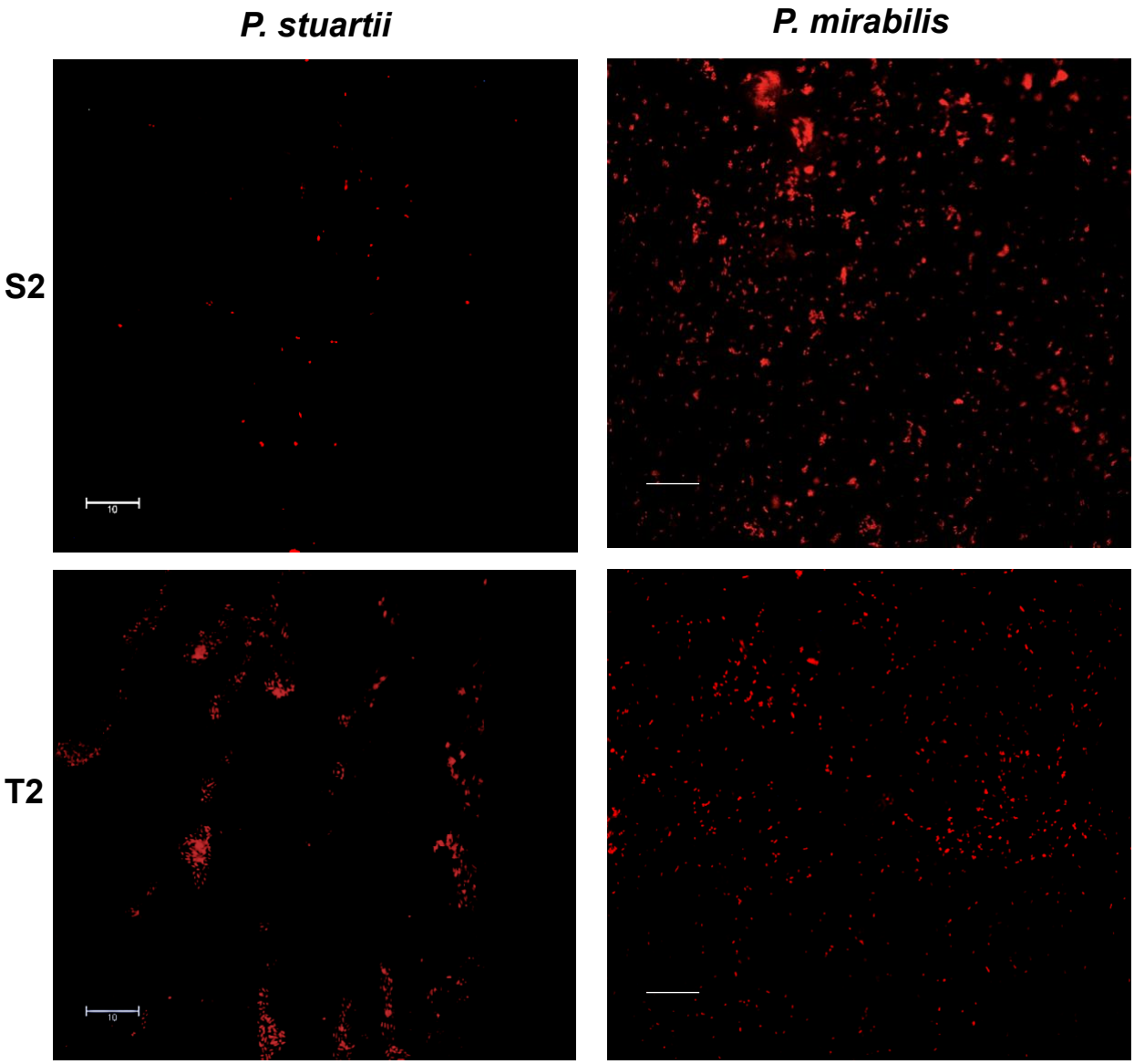


**Figure 3.3.12** Representative images of dead *Providencia stuartii* NSM 58 and *Proteus mirabilis* 12 RTB cells stained with propidium iodide, following adherence and incubation upon silicone bulk-loaded with 1% (w/w) triclosan (T2) or without antimicrobial (S2). Scale bar represents 10 μm

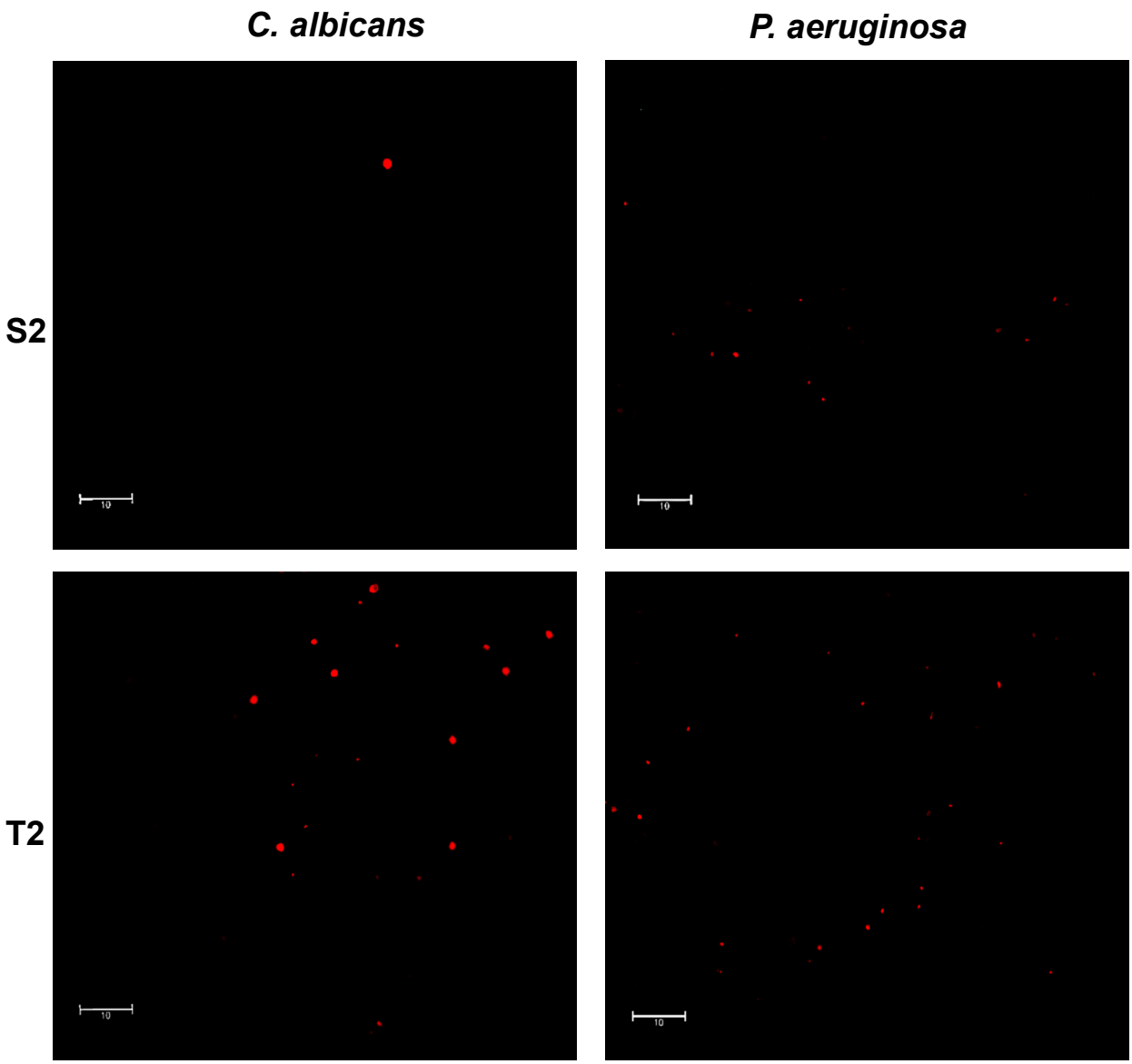


**Figure 3.3.13** Representative images of dead *Candida albicans* ATTC 90028 and *Pseudomonas aeruginosa* NCTC 10662 cells stained with propidium iodide, following adherence and incubation upon silicone bulk-loaded with 1% (w/w) triclosan (T2) or without antimicrobial (S2). Scale bar represents 10 μm

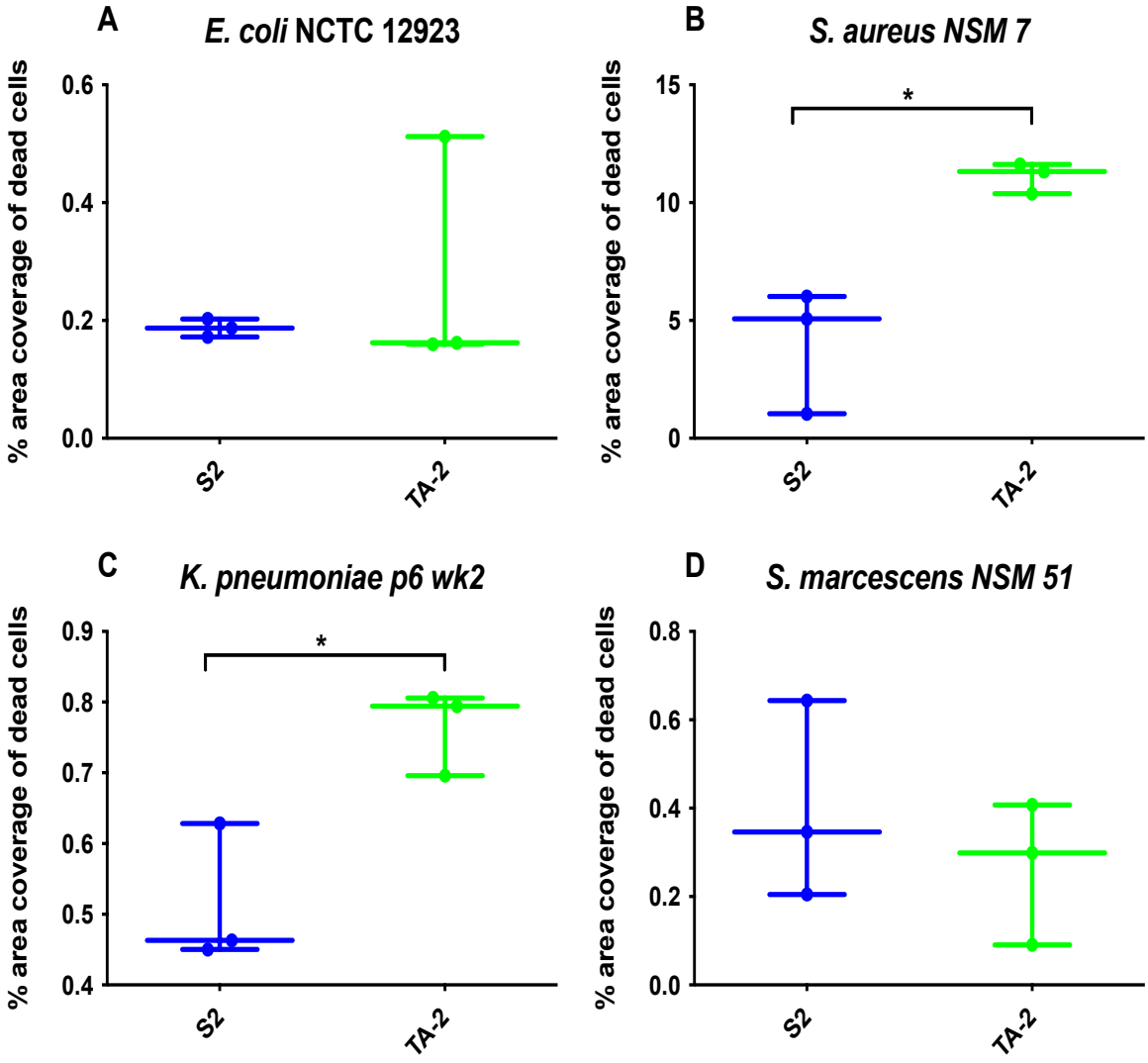
A
E. coli NCTC 12923
% area coverage of dead cells
0.6
0.4
0.2
0.0
S2
TA-2
B
S. aureus NSM 7
% area coverage of dead cells
15
10
5
0
*
S2
TA-2
C
K. pneumoniae p6 wk2
% area coverage of dead cells
0.9
0.8
0.7
0.6
0.5
0.4
*
S2
TA-2
D
S. marcescens NSM 51
% area coverage of dead cells
0.8
0.6
0.4
0.2
0.0
S2
TA-2

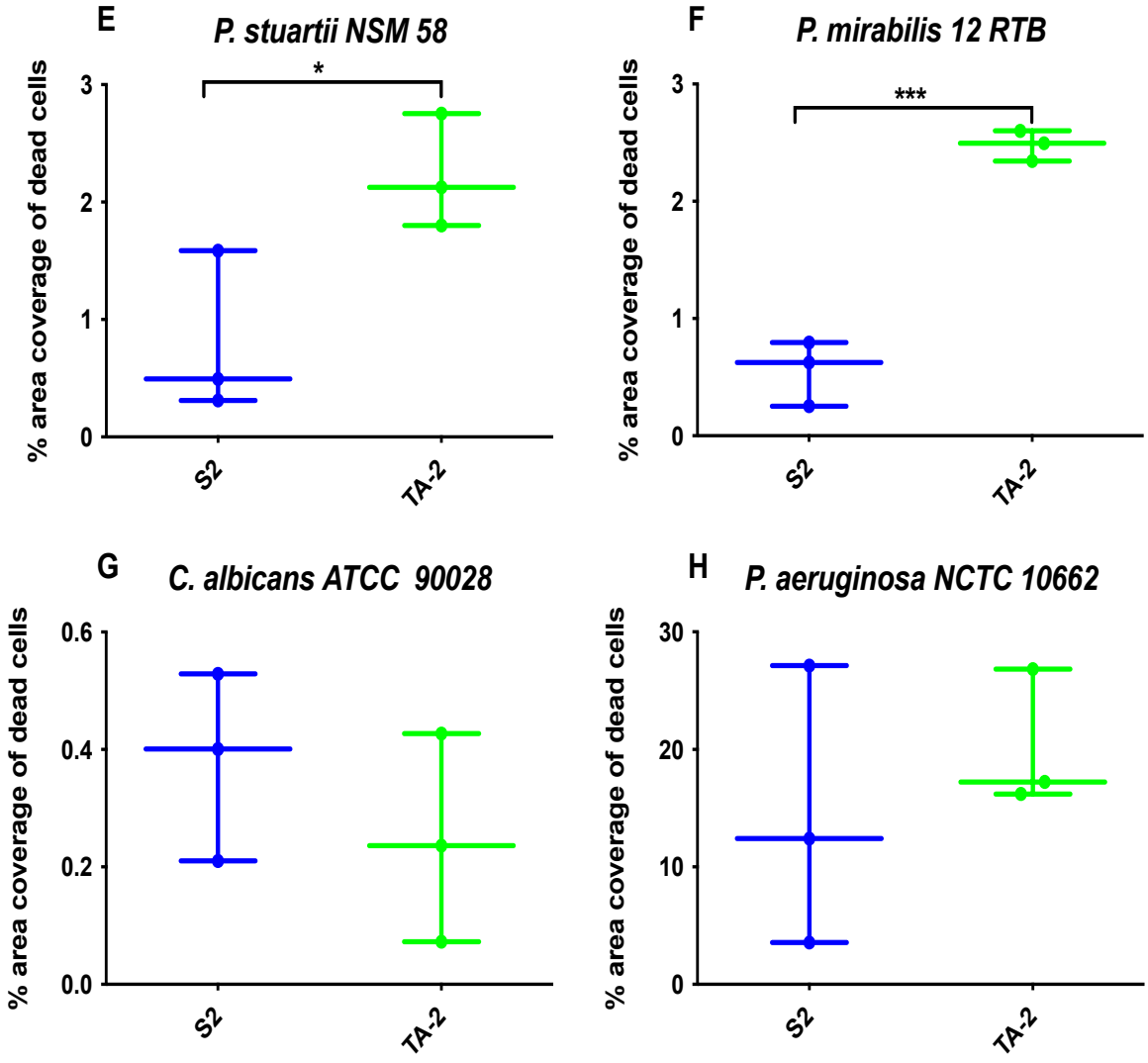


**Figure 3.3.14** Propidium iodide stained (dead) microorganisms adhered to silicone. Silicone formulations without antimicrobial compound (S2) and silicone bulk loaded with 1% (w/w) triclosan acetate (TA-2) were compared. Data expressed as % area coverage of propidium iodide stained cells from 5 fields of view of 3 independently made silicone coupons. Unpaired t-tests used for statistical analysis. Error bars represent standard deviation. * P<0.05, ** P<0.01

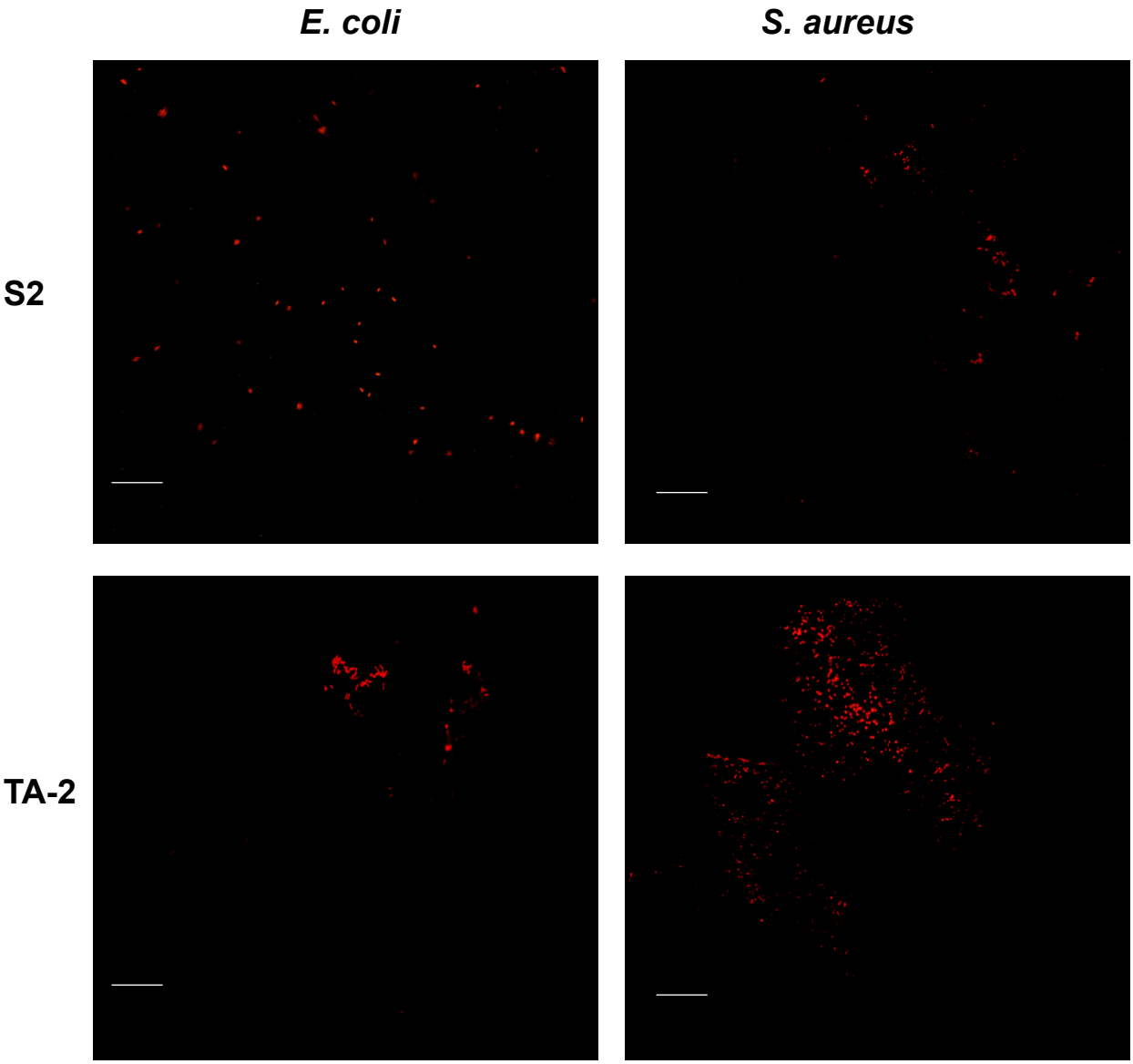


**Figure 3.3.15** Representative images of dead *Escherichia coli* NCTC 12923 and *Staphylococcus aureus* NSM 7 cells stained with propidium iodide, following adherence and incubation on silicone bulk-loaded with 1% (w/w) triclosan acetate (TA-2) or without antimicrobial (S2). Scale bar represents 10 μm

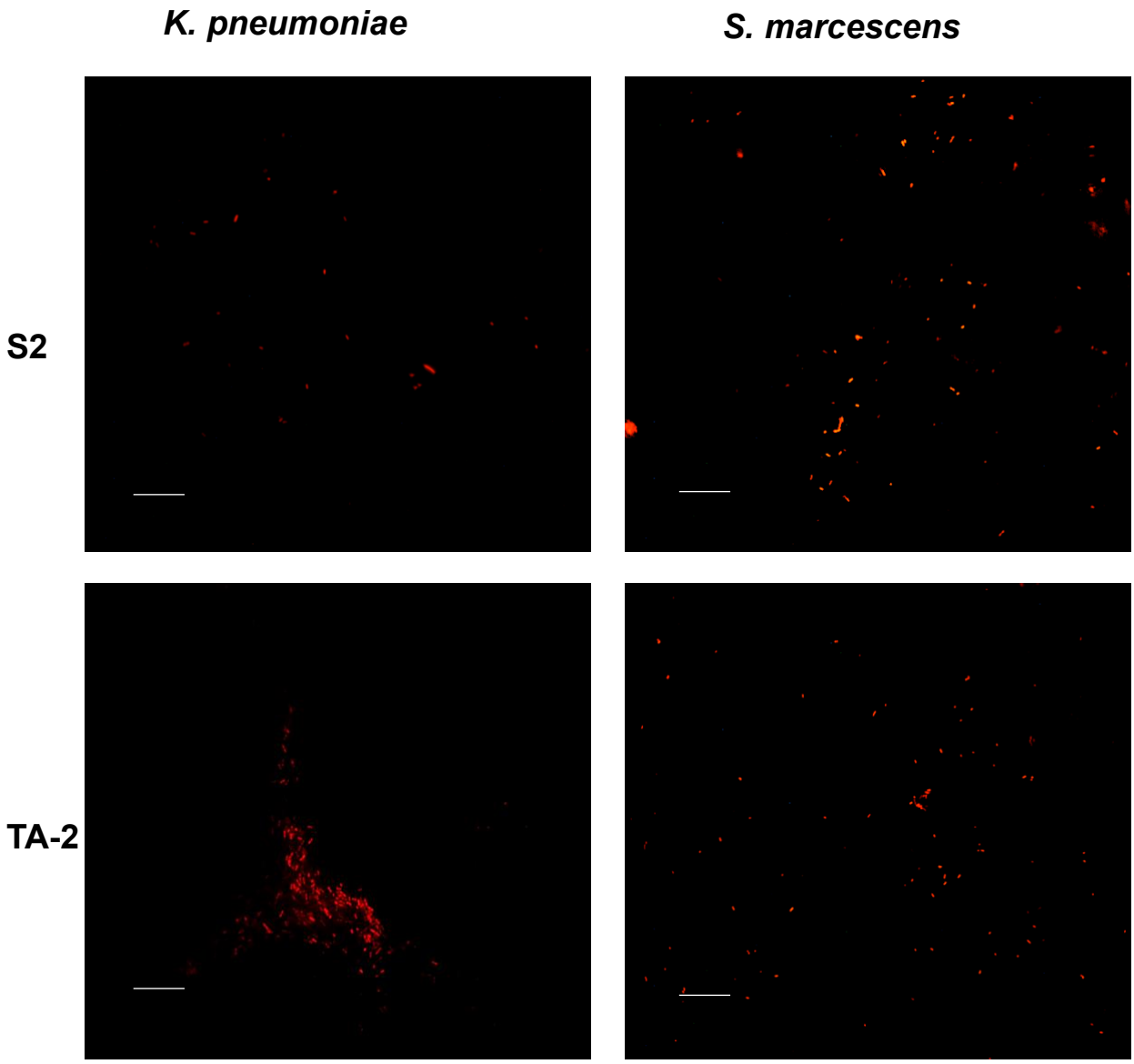


**Figure 3.3.16** Representative images of dead *Klebsiella pneumoniae* P6 wk2 and *Serratia marcescens* NSM 51 cells stained with propidium iodide, following adherence and incubation on silicone bulk-loaded with 1% (w/w) triclosan acetate (TA-2) or without antimicrobial (S2). Scale bar represents 10 μm

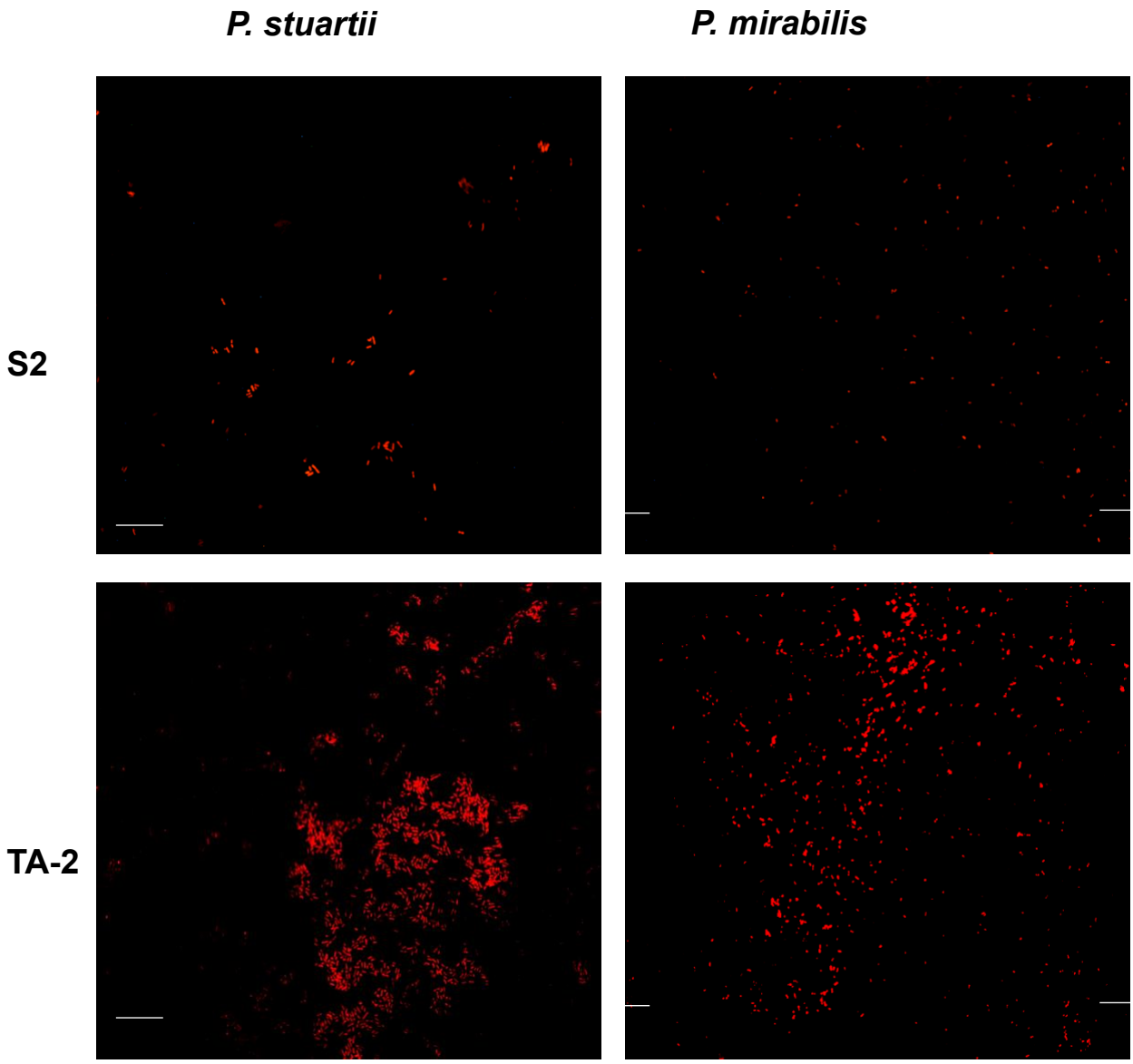


**Figure 3.3.17** Representative images of dead *Providencia stuartii* NSM 58 and *Proteus mirabilis* 12 RTB cells stained with propidium iodide, following adherence and incubation on silicone bulk-loaded with 1% (w/w) triclosan acetate (TA-2) or without antimicrobial (S2). Scale bar represents 10 μm

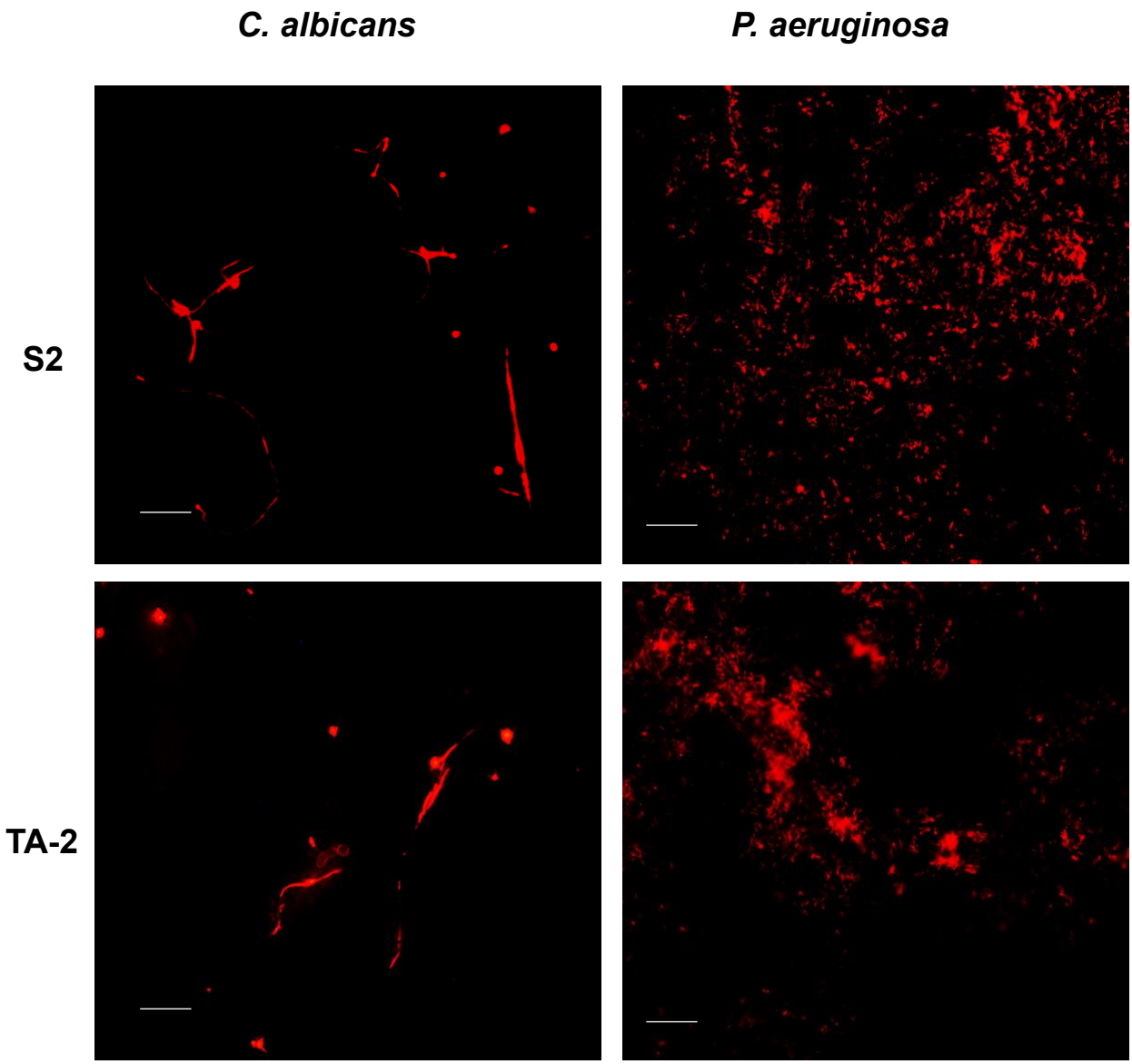


**Figure 3.3.18** Representative images of dead *Candida albicans* ATCC 90028 and *Pseudomonas aeruginosa* NCTC 10662 cells stained with propidium iodide, following adherence and incubation on silicone bulk-loaded with 1% (w/w) triclosan acetate (TA-2) or without antimicrobial (S2). Scale bar represents 10 μm

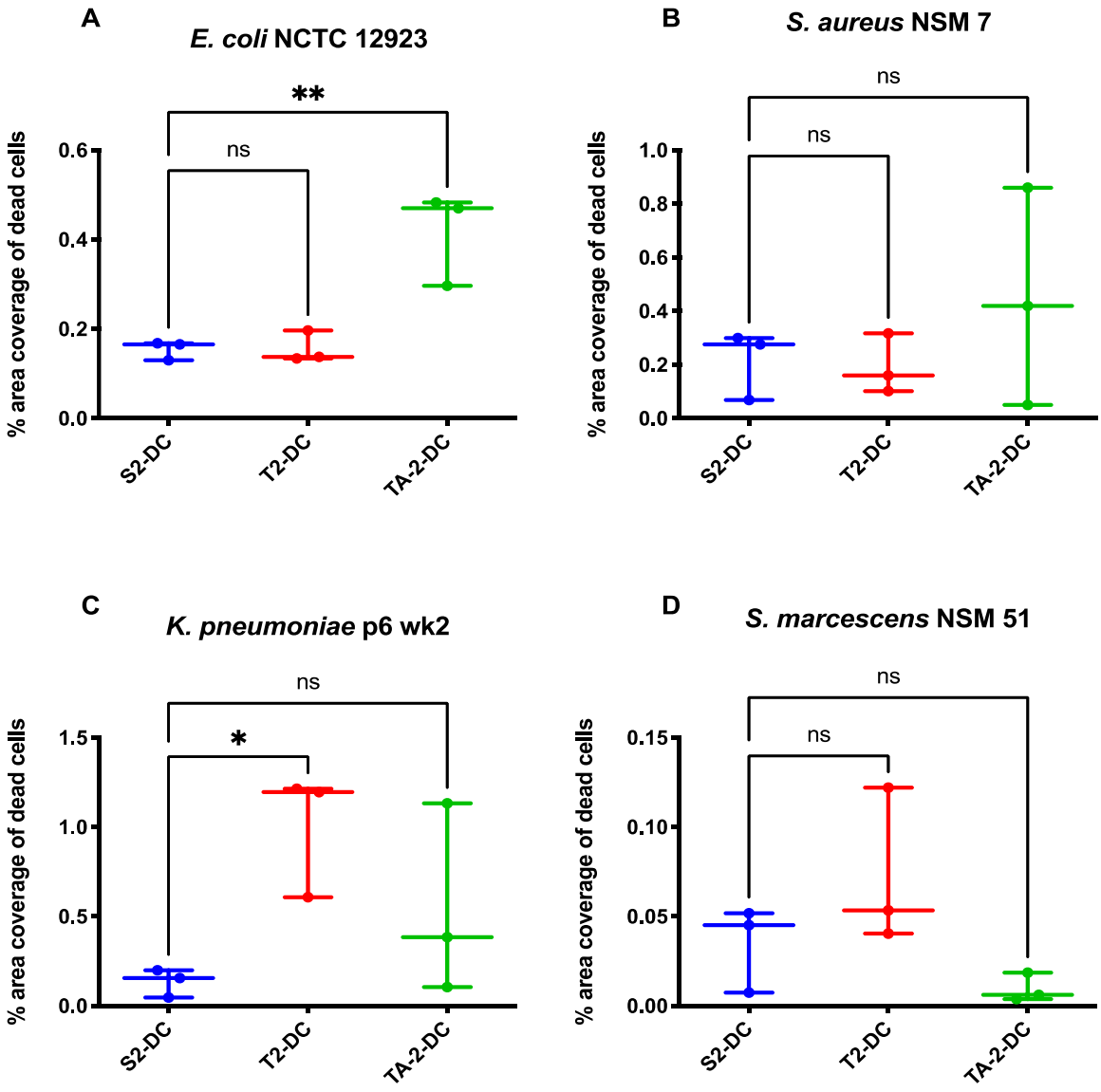
A
E. coli NCTC 12923
**
ns
% area coverage of dead cells
0.6
0.4
0.2
0.0
S2-DC
T2-DC
TA-2-DC
B
S. aureus NSM 7
ns
ns
% area coverage of dead cells
1.0
0.8
0.6
0.4
0.2
0.0
S2-DC
T2-DC
TA-2-DC
C
K. pneumoniae p6 wk2
ns
*
% area coverage of dead cells
1.5
1.0
0.5
0.0
S2-DC
T2-DC
TA-2-DC
D
S. marcescens NSM 51
ns
ns
% area coverage of dead cells
0.15
0.10
0.05
0.00
S2-DC
T2-DC
TA-2-DC

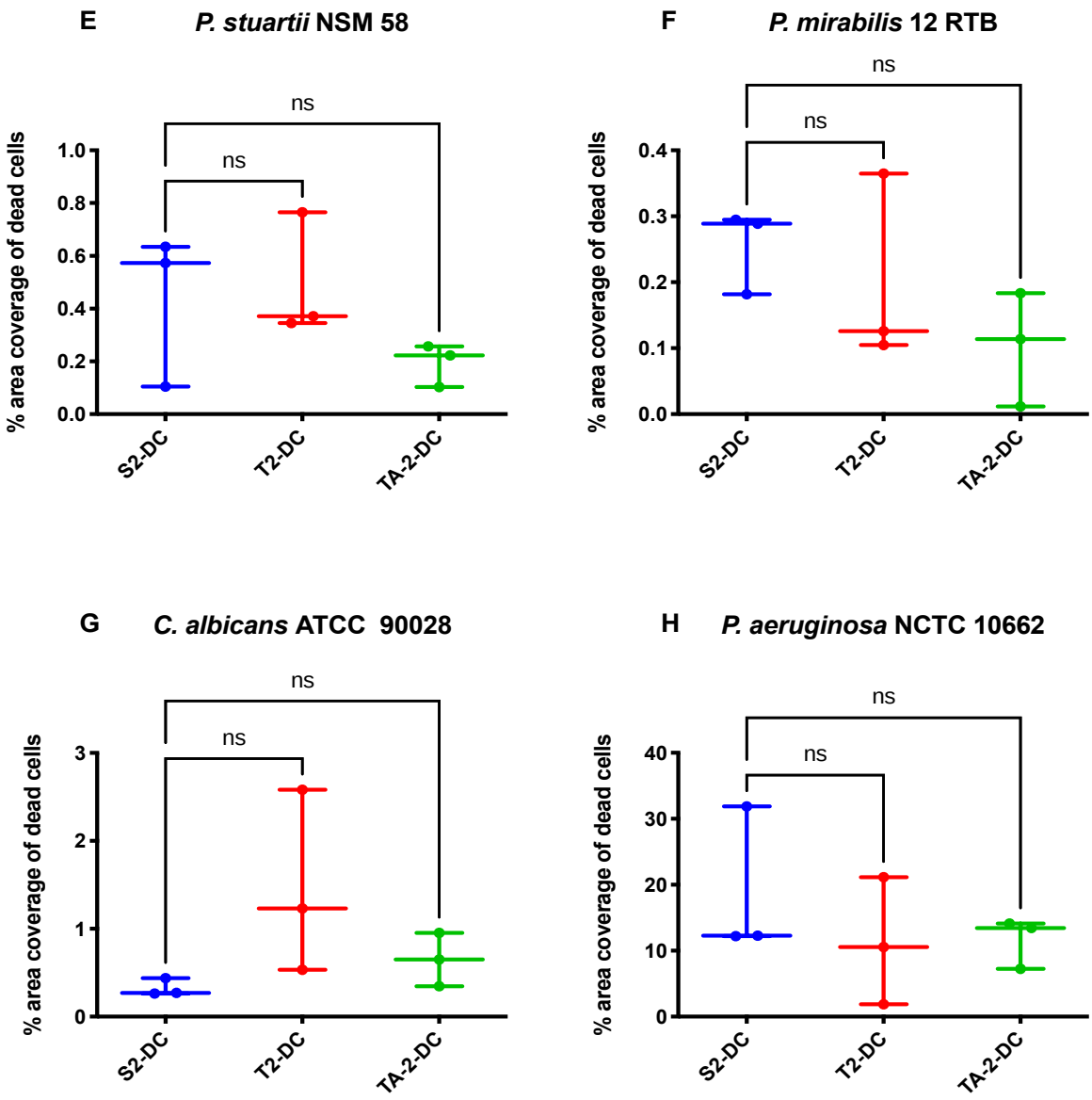


**Figure 3.3.19** Propidium iodide stained (dead) microorganisms adhered to silicone. Silicone formulations without antimicrobial compound (S2-DC), or dip coated with silicone containing 1% (w/w) triclosan (T2-DC) or 1% (w/w) triclosan acetate (TA-2-DC) were compared. Data expressed as % area coverage of propidium iodide stained cells from 5 fields of view of 3 independently made silicone coupons. One-way ANOVA with Dunnett's multiple comparisons used for statistical analysis. Error bars represent standard deviation. ** P<0.01, ns = not significant

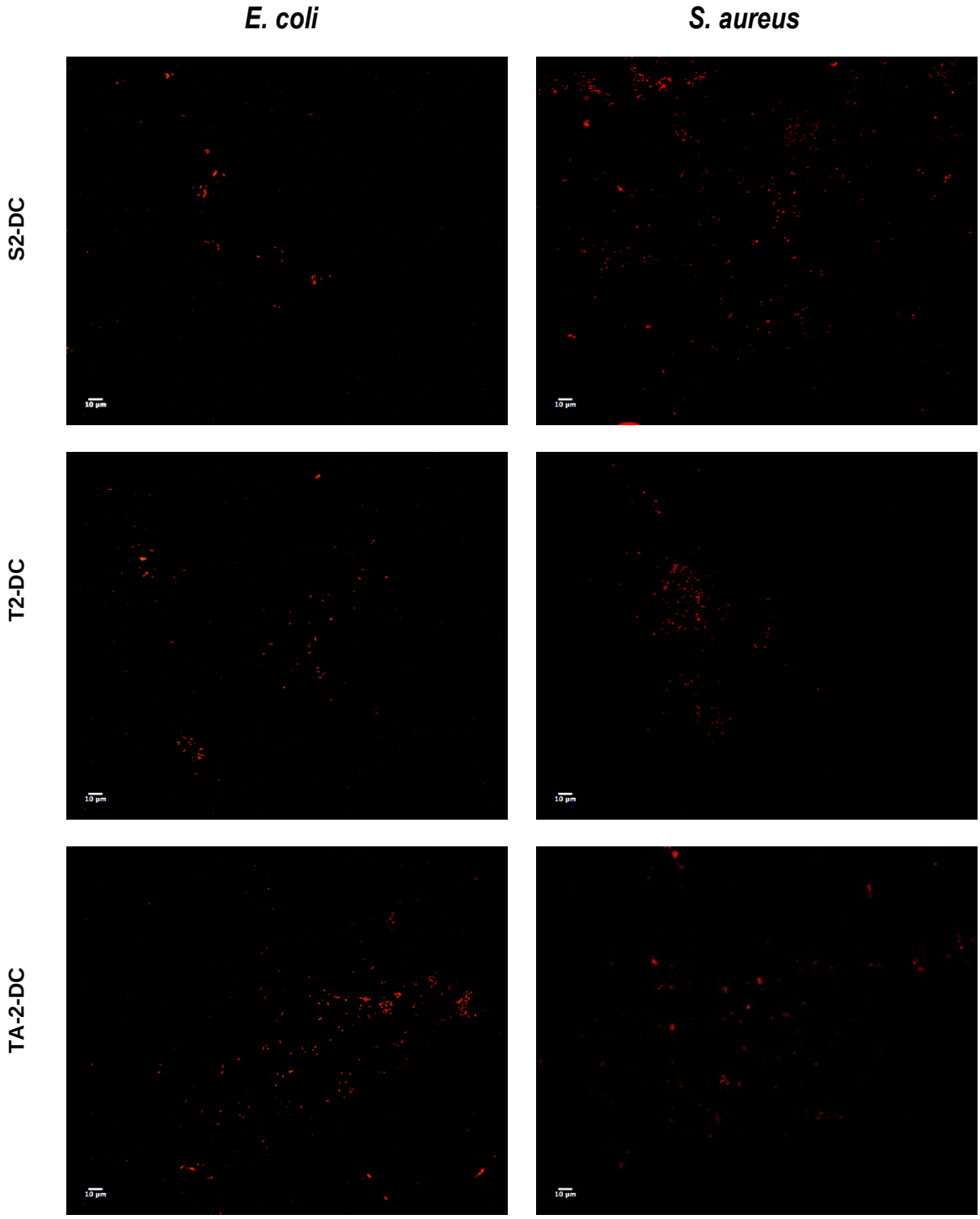


**Figure 3.3.20** Representative images of dead *Escherichia coli* NCTC 12923 and *Staphylococcus aureus* NSM 7 cells stained with propidium iodide, following adherence and incubation on silicone dip coated with 1% (w/w) triclosan (T2-DC), 1% (w/w) triclosan acetate (TA-2-DC) or dip-coated with silicone without antimicrobial (S2-DC). Scale bar represents 10 µm

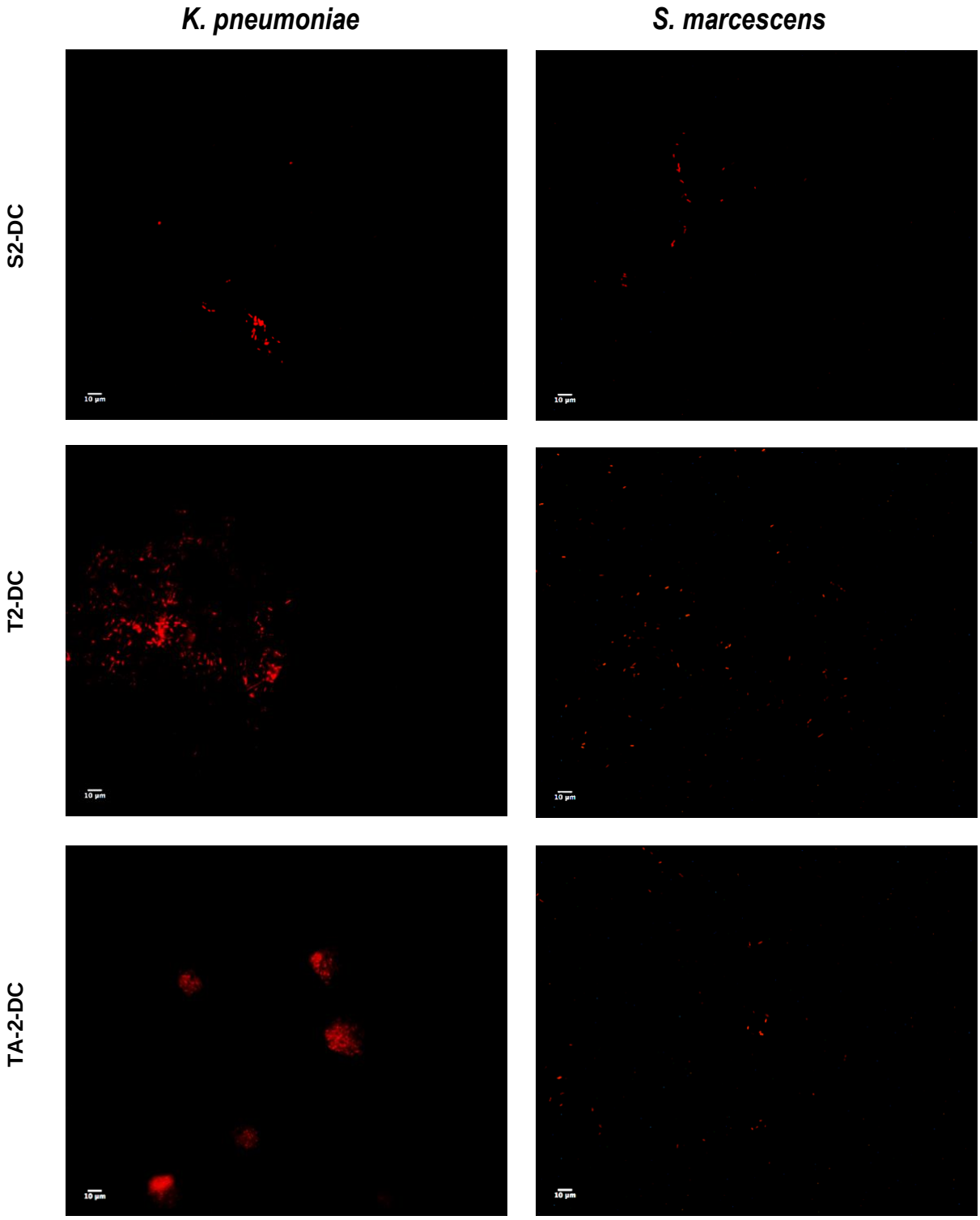


**Figure 3.3.21** Representative images of dead *Klebsiella pneumoniae* P6 wk2 and *Serratia marcescens* NSM 51 cells stained with propidium iodide, following adherence and incubation on silicone dip coated with 1% (w/w) triclosan (T2-DC), 1% (w/w) triclosan acetate (TA-2-DC) or dip-coated with silicone without antimicrobial (S2-DC). Scale bar represents 10 µm

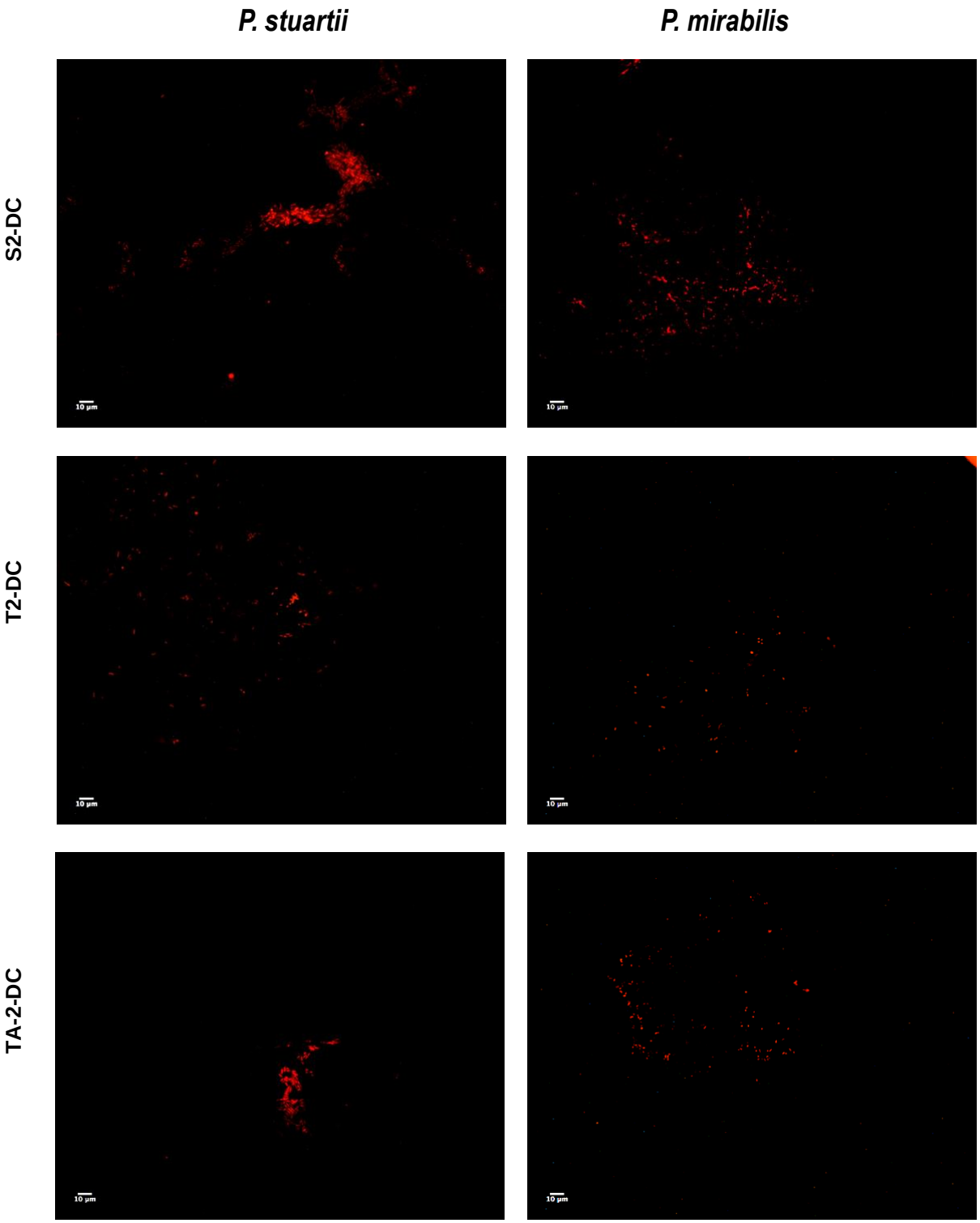


**Figure 3.3.22** Representative images of dead *Providencia stuartii* NSM 58 and *Proteus mirabilis* 12 RTB cells stained with propidium iodide, following adherence and incubation on silicone dip coated with 1% (w/w) triclosan (T2-DC), 1% (w/w) triclosan acetate (TA-2-DC) or dip-coated with silicone without antimicrobial (S2-DC). Scale bar represents 10 µm

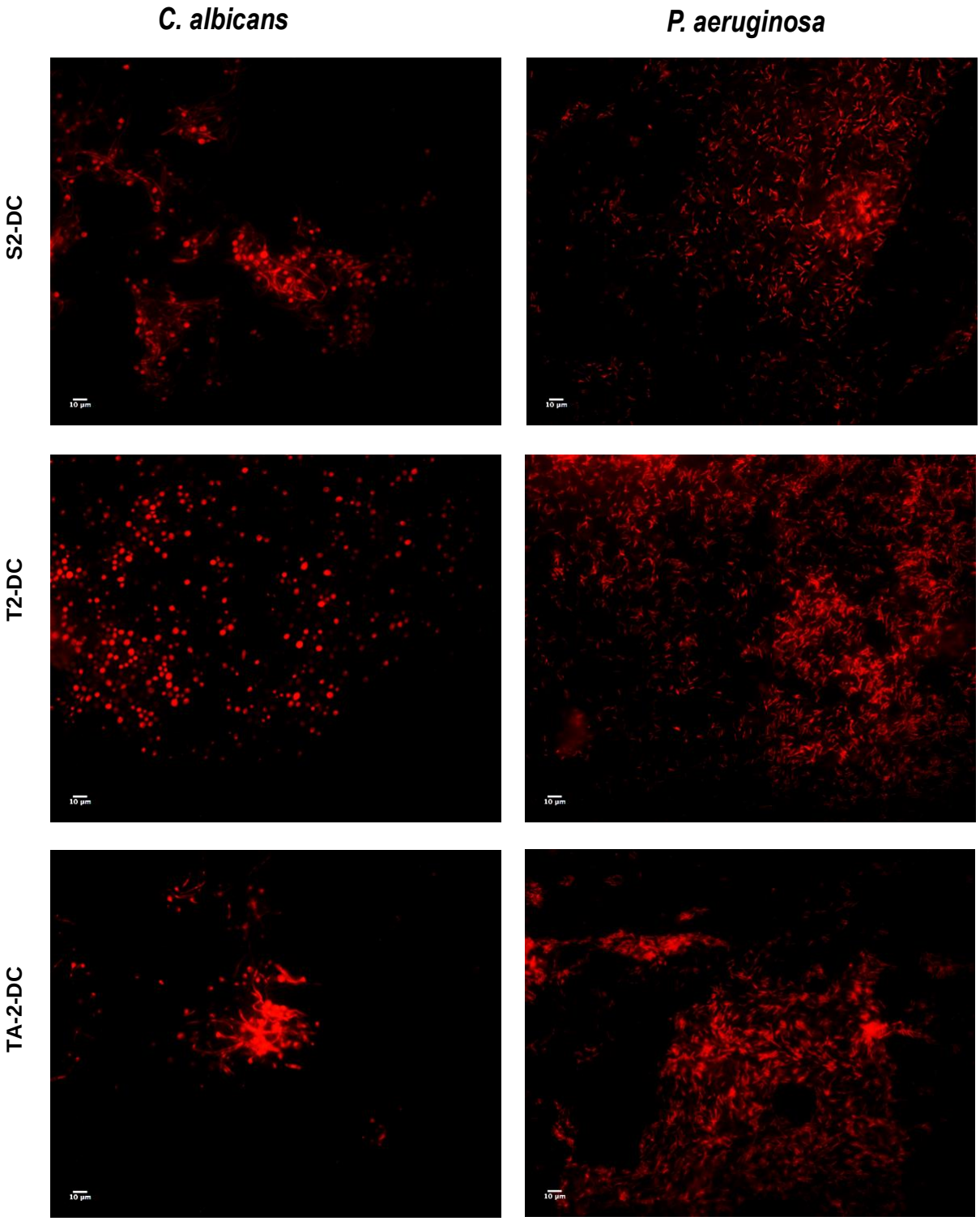


**Figure 3.3.23** Representative images of dead *Candida albicans* ATCC 90028 and *Pseudomonas aeruginosa* NCTC 10662 cells stained with propidium iodide, following adherence and incubation on silicone dip coated with 1% (w/w) triclosan (T2-DC), 1% (w/w) triclosan acetate (TA-2-DC) or dip-coated with silicone without antimicrobial (S2-DC). Scale bar represents 10 µm

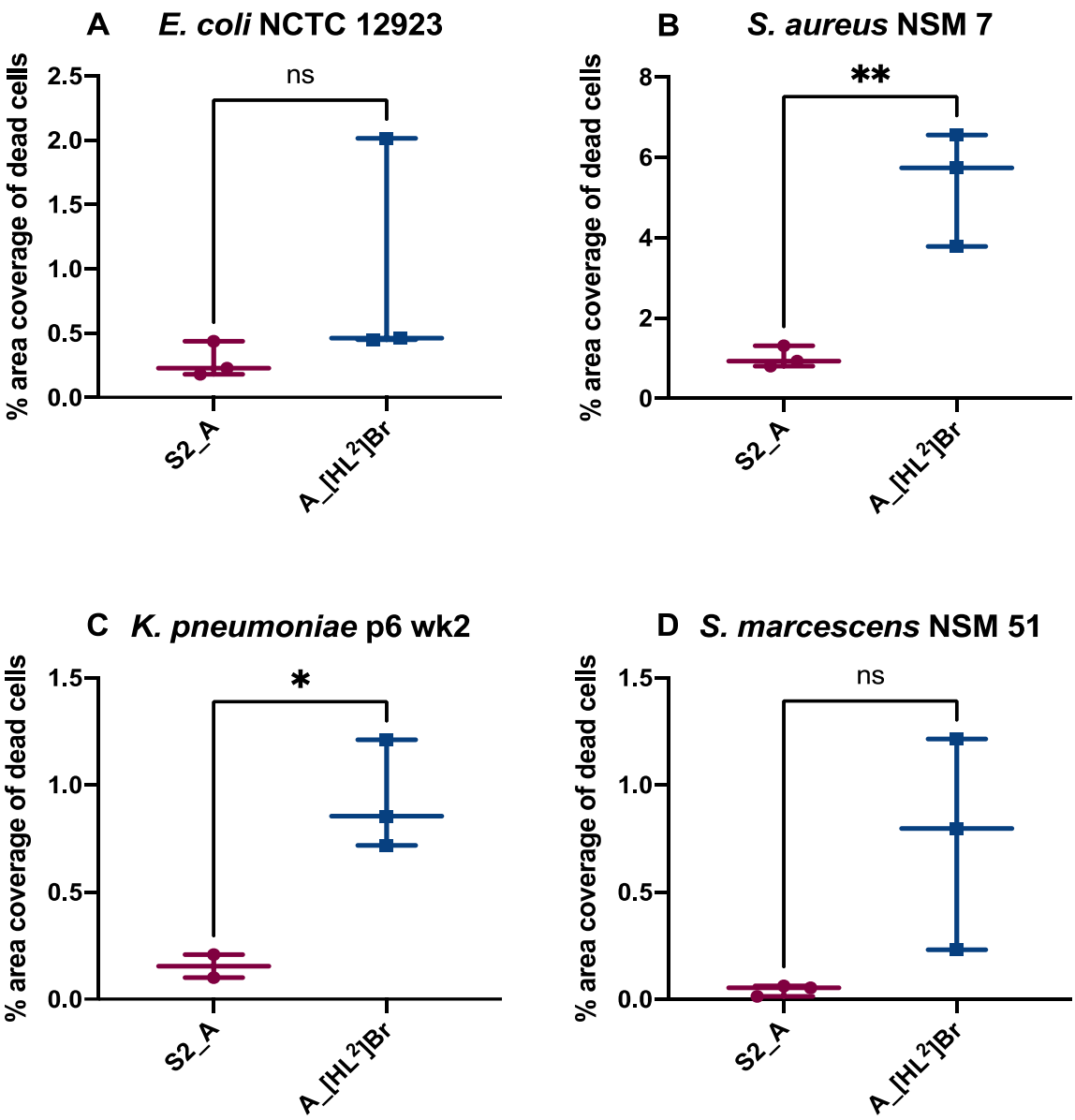
A
E. coli NCTC 12923
ns
% area coverage of dead cells
2.5
2.0
1.5
1.0
0.5
0.0
S2_A
A_[HL2]Br
B
S. aureus NSM 7
**
% area coverage of dead cells
8
6
4
2
0
S2_A
A_[HL2]Br
C
K. pneumoniae p6 wk2
*
% area coverage of dead cells
1.5
1.0
0.5
0.0
S2_A
A_[HL2]Br
D
S. marcescens NSM 51
ns
% area coverage of dead cells
1.5
1.0
0.5
0.0
S2_A
A_[HL2]Br

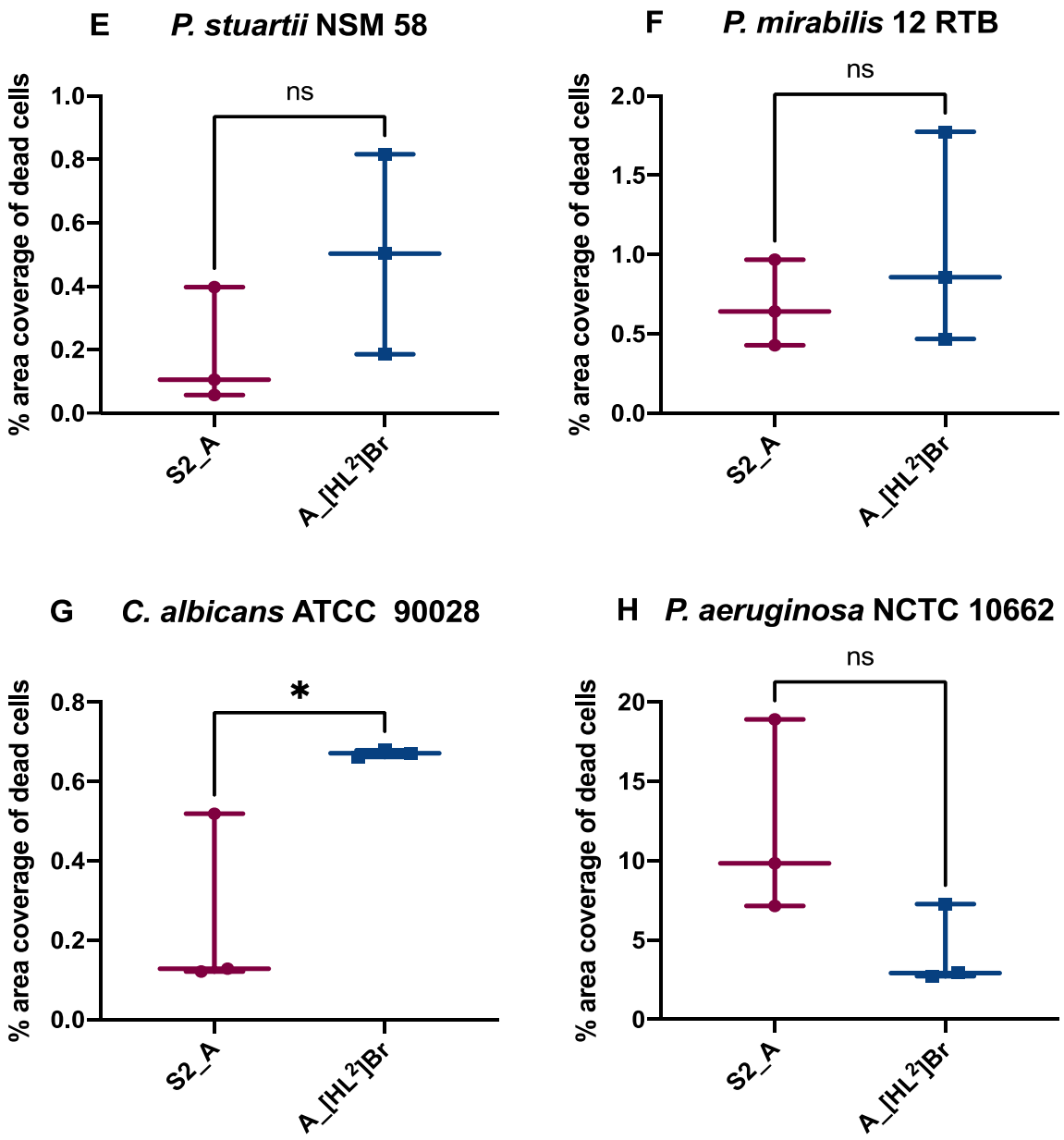


**Figure 3.3.24** Dead microorganisms adhered to silicone rubber dip coated with acetoxy silicone containing 1% (w/w) [$HL^2$] Br (A_[$HL^2$] Br) or dip-coated with acetoxy silicone without antimicrobial compound (S2_A). Data expressed as % area coverage of propidium iodide-stained cells from 5 fields of view of 3 independently made silicone coupons. Unpaired t-tests used for statistical analysis. Error bars represent standard deviation. * $P<0.05$, ** $P<0.01$, ns = not significant

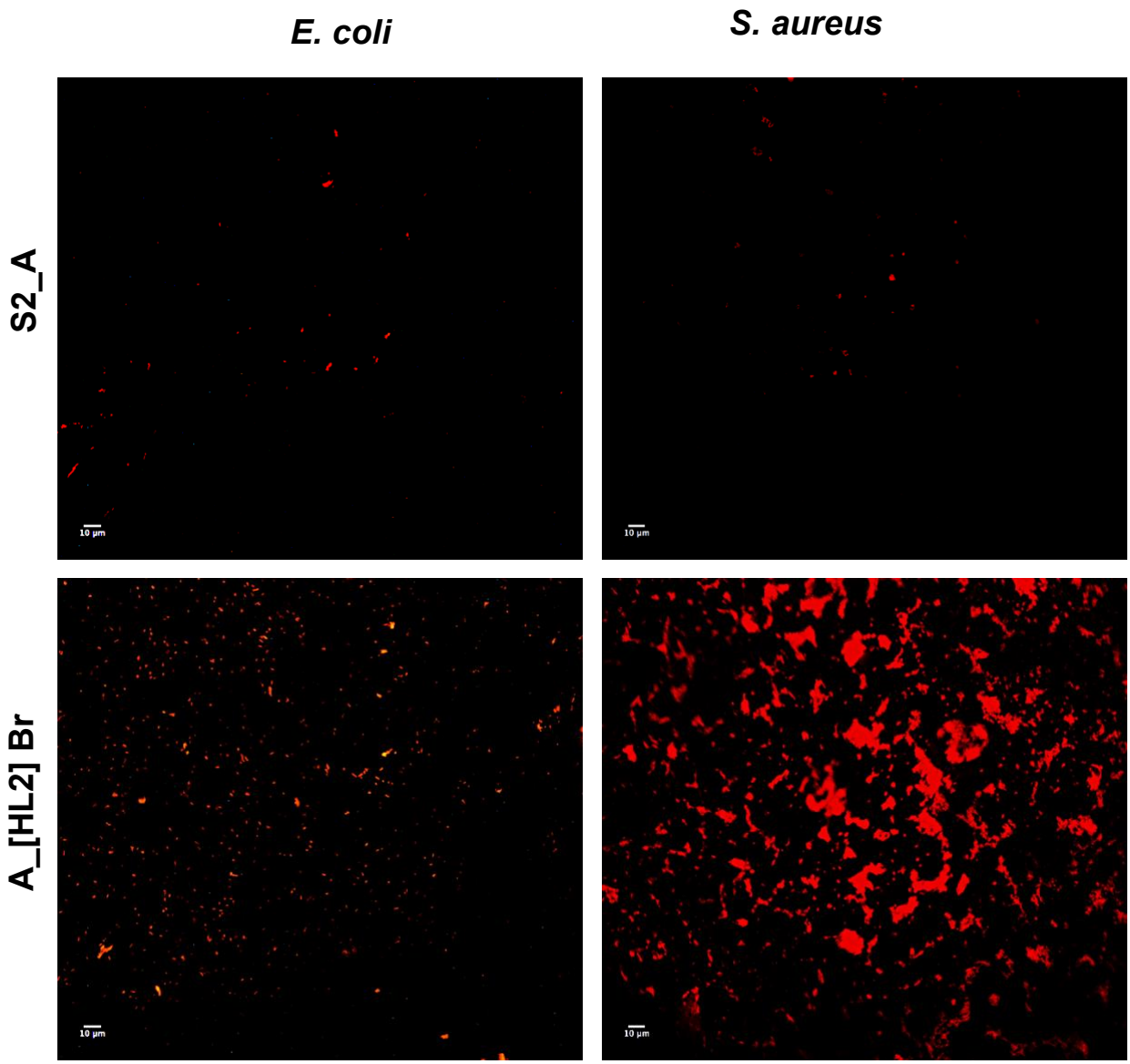


**Figure 3.3.25** Representative images of dead *Escherichia coli* NCTC 12923 and *Staphylococcus aureus* NSM 7 cells stained with propidium iodide, following adherence and incubation on silicone dip coated with acetoxy silicone containing 1% (w/w) [$HL^2$] Br (A_[$HL^2$] Br) or dip-coated with acetoxy silicone without antimicrobial (S2_A). Scale bar represents 10 µm

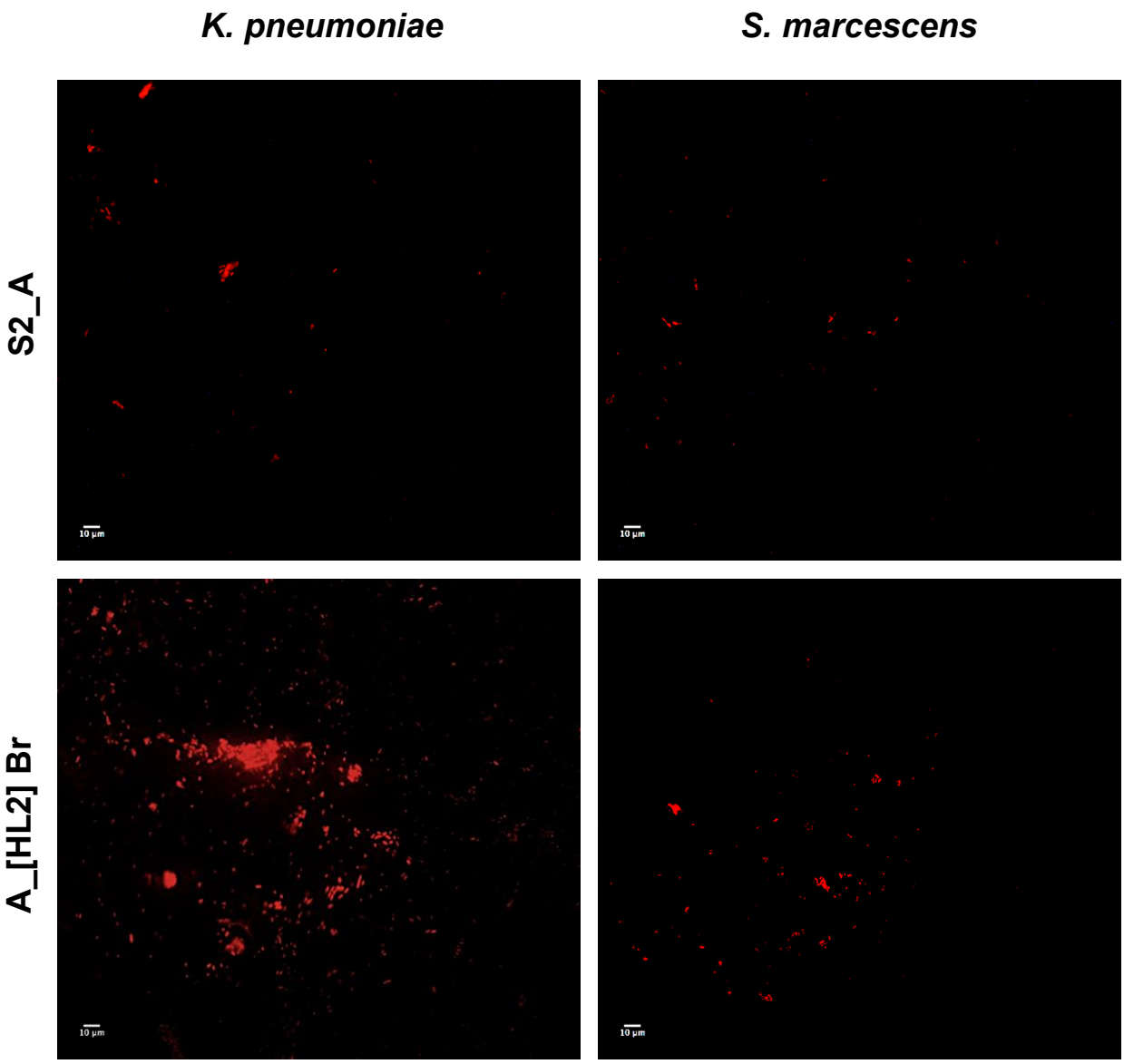


**Figure 3.3.26** Representative images of dead *Klebsiella pneumoniae* P6 wk 2 and *Serratia marcescens* NSM 51 cells stained with propidium iodide, following adherence and incubation on silicone dip coated with acetoxy silicone containing 1% (w/w) [$HL^2$] Br (A_[$HL^2$] Br) or dip-coated with acetoxy silicone without antimicrobial (S2_A). Scale bar represents 10 µm

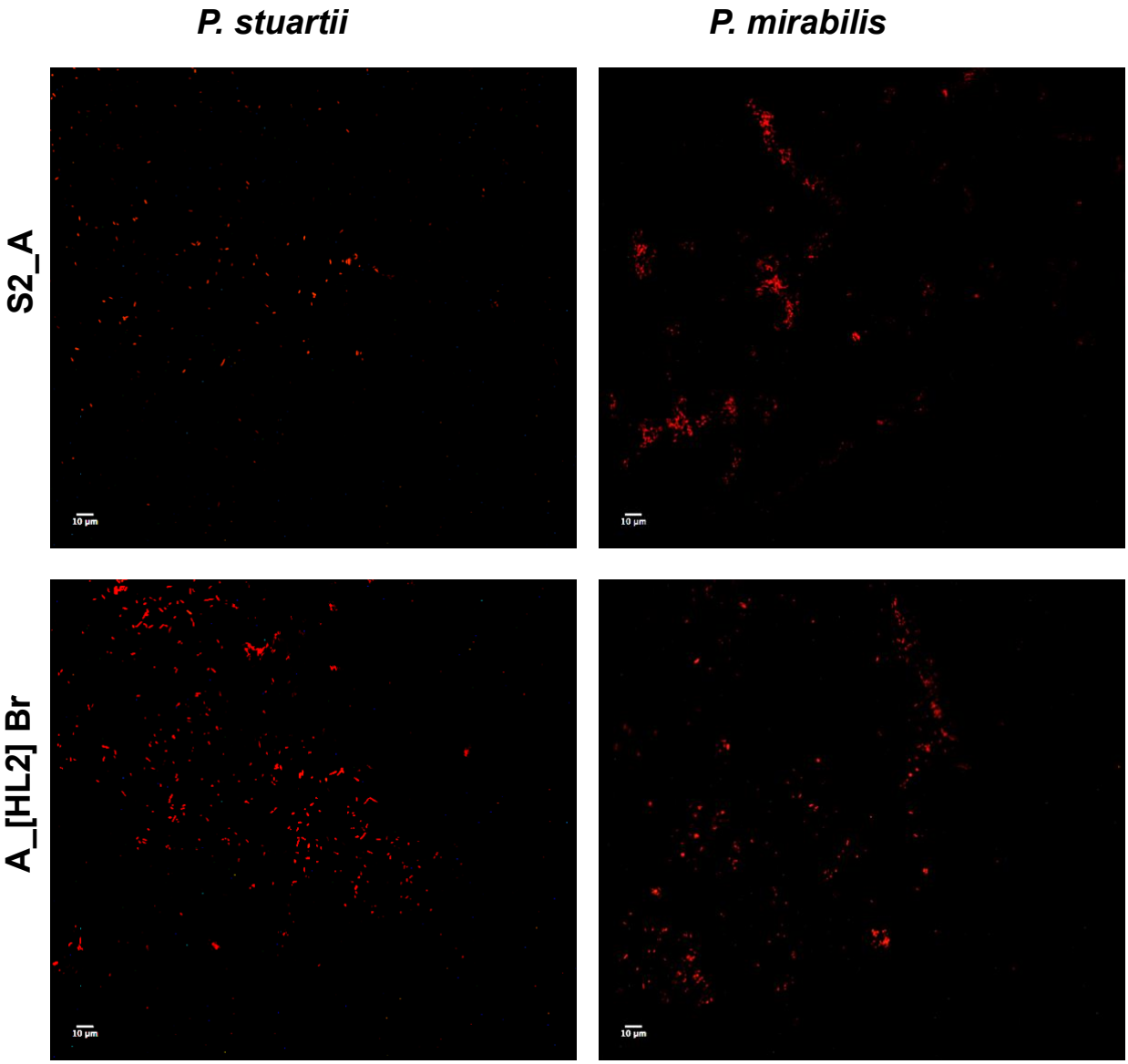


**Figure 3.3.27** Representative images of dead *Providencia stuartii* NSM 58 and *Proteus mirabilis* 12 RTB. Cells were stained with propidium iodide, following 90 min adherence and incubation for 24 h at 37 °C on silicone dip coated with acetoxy silicone containing 1% (w/w) [$HL^2$] Br (A_[$HL^2$] Br) or dip-coated with acetoxy silicone without antimicrobial (S2_A). Scale bar represents 10 µm

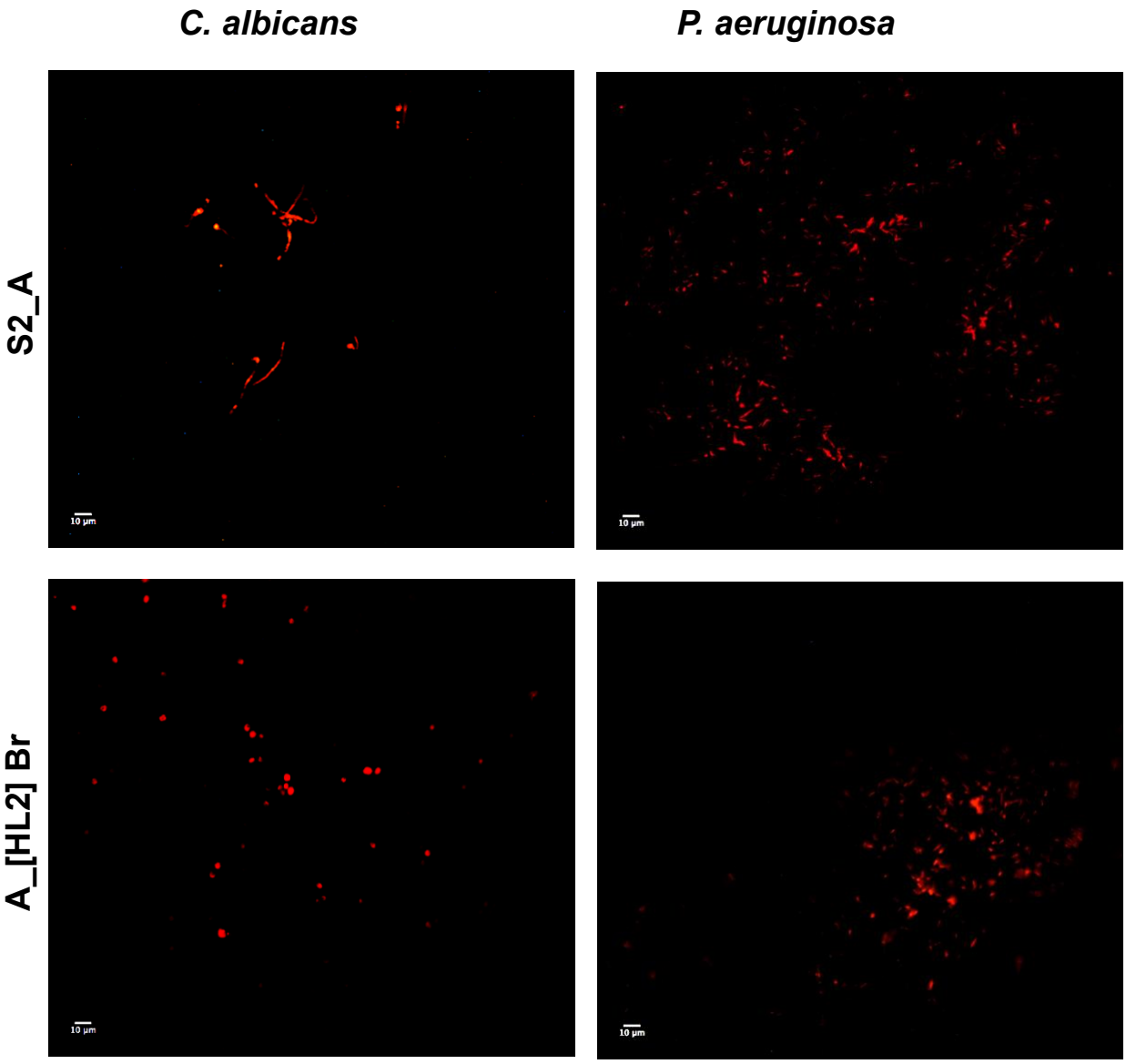


**Figure 3.3.28** Representative images of dead *Candida albicans* ATCC 90028 and *Pseudomonas aeruginosa* NCTC 10662. Cells were stained with propidium iodide, following 90 min adherence and incubation for 24 h at 37 °C on silicone dip coated with acetoxy silicone containing 1% (w/w) [$HL^2$] Br (A_[$HL^2$] Br) or dip-coated with acetoxy silicone without antimicrobial (S2_A). Scale bar represents 10 µm

**Table 3.3.5** Summary of significance of antimicrobial activity of novel silicone formulations against 8 microorganisms.

Zone of inhibition (ZOI) studies, recovery of viable colony forming units (CFUs) from silicone surfaces and staining dead cells with propidium iodide (PI) were used to determine antimicrobial activity of silicone bulk-loaded with 1% (w/w) triclosan (T2) or triclosan acetate (TA-2), silicone dip-coated with 1% (w/w) triclosan or triclosan acetate (T2-DC and TA-2-DC), and silicone dip-coated with an acetoxy layer containing 1% (w/w) [$HL^2$]BR (A_[$HL^2$]BR). Statistical significance against the appropriate control silicones were determined using appropriate tests described in section 3.2.

| | **Silicone Formulation** | | | | | | | | | | | | | | |
|---|---|---|---|---|---|---|---|---|---|---|---|---|---|---|---|
| | **T2** | | | **TA-2** | | | **T2-DC** | | | **TA-2-DC** | | | **A_[$HL^2$]BR** | | |
| **Microorganism** | **ZOI** | **CFU** | **PI staining** | **ZOI** | **CFU** | **PI staining** | **ZOI** | **CFU** | **PI staining** | **ZOI** | **CFU** | **PI staining** | **ZOI** | **CFU** | **PI staining** |
| *E. coli* NCTC 12923 | **** | ** | * | ns | ns | ns | * | ns | ns | ns | ns | ** | ns | ** | ns |
| *S. aureus* NSM 7 | **** | * | * | ** | ns | * | **** | * | ns | **** | * | ns | * | * | ** |
| *K. pneumoniae* P6 wk2 | **** | **** | ** | ns | * | * | * | ns | * | ns | ns | ns | ns | ns | * |
| *S. marcescens* NSM 51 | ns | ns | ns | ns | ns | ns | ns | ns | ns | ns | ns | ns | ns | ns | ns |
| *P. stuartii* NSM 58 | **** | ns | * | ns | * | * | * | ns | ns | ns | ns | ns | ns | ns | ns |
| *P. mirabilis* 12 RTB | **** | ** | ns | ns | ns | *** | ** | ns | ns | ns | ns | ns | ns | ns | ns |
| *C. albicans* ATCC 90028 | **** | * | * | ns | ns | ns | ns | ns | ns | ns | ns | ns | *** | ns | * |
| *P. aeruginosa* NCTC 10662 | ns | ns | ns | ns | ns | ns | ns | ns | ns | ns | ns | ns | ns | ns | ns |

* P< 0.05, **P< 0.01, * **P< 0.001, ****P< 0.0001, ns= not significant compared to control

## 3.4 Discussion

Silicone elastomers are frequently used to construct indwelling medical devices, due to their superior flexibility, biocompatibility, chemical inertness, and resistance to physical forces. Unfortunately, the surfaces of such elastomers are highly attractive to bacteria, who readily establish highly resistant biofilms that are leading causes of healthcare-acquired infections. Developing silicones that can prevent biofilm formation, either through release of biocidal agents or can prevent initial cell attachment, has attracted much investigation, yet the problem of biofilm production still exists. This Chapter aimed to incorporate the leading novel agents evaluated in Chapter 2 into silicone elastomers, to prevent biofilm formation that contribute to catheter-associated urinary tract infections (CAUTIs).

Development of a silicone formulation for use as a functional medical device material has, thus far, yielded two formulations (S1 and S2), each with different ratios of silicone polymer chains, hydrophobic and hydrophilic fillers and cross-linking reagent. Triclosan 1% (w/w) was incorporated into the bulk matrix of both of these silicone formulations (T1 and T2), whilst triclosan acetate was only bulk-loaded into S2 to produce material TA-2. Whilst triclosan and triclosan acetate were successfully bulk-loaded into silicone polymers, the imidazolium compound [$HL^2$] Br appeared to 'poison' the platinum catalyst and inhibited the silicone curing reaction. However, an alternative approach that incorporated [$HL^2$] Br into an acetoxy silicone was successfully applied as a surface coating.

Although the S2 formulation had higher tensile strength, compared with S1 formulation, the elongation and tear strength of the former was lower. A reduction in cross-linking reagent and hydrophobic filler in the S2 formulation may have been responsible for the lowered tear resistance and elongation. Furthermore, decreasing the ratio of the longest silicone polymer (V46) from 54% to 30% may have also contributed to the reduced elasticity of the material and therefore, the reduction in elongation. Longer polymer chains facilitate greater flexibility in the final material, as there are less sites for cross-linking to occur (Nakka et al. 2011). A 10-fold reduction in the platinum enzyme that catalyses the addition curing of the silicone was also a likely contributing factor to the lowered tear strength of S2 silicone.

Whilst the decreased ratio of long chain polymer may have been attributable for reduced elasticity of S2, it also enabled a more rigid material to be formed and

therefore, increased tensile strength. Due to the greater tensile strength of S2 in comparison to S1, S2 was selected as the formulation to be bulk-load with antimicrobial compounds and to serve as the base rubber for dip-coated formulations.

Whilst incorporation of 1% (w/w) triclosan and triclosan acetate into the bulk matrix of the silicone rubber had no effect on tensile or tear strength, elasticity was found to increase. This observation that tensile and tear strength was unaffected supports those of a previous study (Fisher *et al.*, 2015), where 1% triclosan was incorporated into silicone catheters via soaking the catheter in a solution of the antimicrobial agent. The study reported no differences in load, modular or tensile strength between control and triclosan impregnated catheters.

Analysis of AU that had been co-incubated with coupons of T2 and TA-2 silicone revealed that triclosan is released from both elastomers over the 6 week period evaluated. Interestingly, no TA was detected in the AU incubated with TA-2 coupons, but triclosan was detected, albeit at lesser quantities that AU incubated with T2.

The zones of inhibition produced showed that whilst triclosan silicone released its contents rapidly over the first 14 days, TA-2 silicone had a more sustained release retaining a longer ability to inhibit *S. aureus* (over 12 weeks). Silicone dip-coated with triclosan and TA containing silicone showed the same pattern, although the zones produced were smaller than their equivalent bulk-loaded formulations. Although the equivalent silicone formulation without antimicrobial compound also demonstrated inhibition of *S. aureus* over a 6-week period, the zones of inhibition produced by all bulk-loaded and dip-coated formulations were significantly larger. These observations suggest that the control silicone formulations had some level of antimicrobial activity that was enhanced by incorporation of triclosan and triclosan acetate. A possible explanation for this occurrence could be due to unevaporated acetone leaching from the silicone elastomer. Jordan et al (2015) conducted similar experiments to investigate triclosan release from a 1% (w/w) bulk-loaded silicone using *Proteus mirabilis* as the test bacteria. It was also concluded that triclosan was released over an 11-week test period, concurring with these present findings.

Determining the antimicrobial activity of the silicone formulations relied on interpreting the results from experiments using 3 separate methods. Ideally,

propidium iodide would have been used in combination with Syto 9 to stain microorganisms on the silicone coupons and obtain ratios of live to dead cells. Unfortunately, Syto 9 irreversibly bound to the surface of the silicone material, preventing visualisation of live cells. Therefore, propidium iodide staining of adherent microorganisms, along with viable cells recovered from the surfaces of silicone coupons enabled the biocidal activity of the modified silicone formulations to be assessed. ZOIs produced by the novel silicones against 8 CAUTI causing microorganisms contributed to the assessment of antimicrobial activity. Silicone bulk-loaded with triclosan was inhibitory and/or biocidal towards *E. coli*, *S. aureus*, *K. pneumoniae*, and *C. albicans*. Two of the three assays supported that the silicone also had antimicrobial activity against *P. stuartii* and *P. mirabilis*. All methods revealed *Serratia marcescens* and *P. aeruginosa* to be resistant to the bulk loaded silicones. These findings were supportive of the MIC data obtained in Chapter 2. A bulk-loaded triclosan (1% w/w) silicone rubber was also produced by Jordan et al, and similar ZOIs were reported against *P. mirabilis*, *P. stuartii* and *E.coli*, whilst resistance by *P. aeruginosa* was also noted (Jordan et al. 2015).

Silicone dip-coated with 1% (w/w) triclosan was not as effective as an antimicrobial against the chosen microorganisms. Two of the three assays showed antimicrobial activity against *S. aureus* and *K. pneumoniae*, but only ZOI studies had statistically significant differences between the control dip-coated silicone and the triclosan containing dip-coated silicone against *E. coli*, *P. stuartii* and *P. mirabilis*. Such results are not supportive of the study conducted by Jordan et al, where silicone dip-coated with 0.2% (w/w) triclosan formulation delayed encrustation of urinary catheters by *P. mirabilis* in an *in-vitro* bladder model (Jordan et al. 2015). The use of a Muller-Hinton broth instead of artificial urine combined with the different methods of evaluation may account for such discrepancies. The method employed by Jordan et al will be used to evaluate the dip-coated silicone formulations in Chapter 6, enabling a direct comparison to be made.

Silicone bulk-loaded with triclosan acetate proved to be less effective at exerting antimicrobial activity against the panel of microorganisms than that bulk-loaded with triclosan. Of the 3 methods used, two demonstrated significant differences ($P < 0.05$) between control formulations and TA-2 silicone against *S. aureus*, *K. pneumoniae* and *P. stuartii*. Similarly, the dip-coated triclosan acetate silicone only demonstrated antimicrobial activity against *S. aureus*.

It was hypothesised that antimicrobial action of an esterified derivative of triclosan, triclosan acetate (TA) from the bulk of the silicone rubber would only be facilitated at an elevated pH, due to hydrolysis of the esterified triclosan into the active triclosan component. The ZOI data for TA-2 silicone supports this hypothesis. The growth of microorganisms that were previously susceptible to TA in broth microdilution studies (Chapter 2, Table 2.1), namely *E. coli, P. mirabilis*, *K. pneumoniae*, *P. stuartii* and *C. albicans*, were not inhibited by TA containing silicone. This may be attributable to retention of the triclosan within the silicone rubber. Small amounts of triclosan release may account for the ZOIs evident against *S. aureus* from bulk-loaded and dip-coated TA formulations. This would correlate with the extremely low MIC values obtained for TA against *S. aureus* in Chapter 2 (Table 2.1).

Patents were previously granted for use of triclosan ester derivatives, including triclosan acetate, in dye baths for diffusion into textiles and provide long-lasting antimicrobial fabrics (patents US5968207A and JP3495330B2). It was stated that 'the use of triclosan merely provides an effective manner of applying and diffusing triclosan itself' (Shulong 1999). The patent describes extended antimicrobial activity of textiles incorporating triclosan acetate within the fibres than with triclosan. The improved longevity is thought to occur due to the triclosan acetate migrating to the surface of the fibres at very slow rates to provide the fabric with an antimicrobial effect.

The same mode of action is thought to impart improved longevity to the novel triclosan acetate silicone formulations over the equivalent triclosan containing silicone. These novel silicones could be of benefit for use in medical device construction, and in the case of urinary catheters, could prevent CAUTIs over the duration of use, which is typically 12 weeks for long-term catheterised patients.

Silicone coated with an acetoxy layer containing 1% (w/w) $[HL^2]Br$ was only inhibitory to *S. aureus* and *C. albicans*, correlating with the low MIC values obtained in Chapter 2. Although numerous studies exist that demonstrate the antimicrobial properties of imidazolium containing compounds in planktonic cultures (Hodyna et al. 2016; Hodyna et al. 2018), few have incorporated such compounds into silicone rubbers. However, Ghamrawi et al (Ghamrawi et al. 2020) modified silicone with imidazolium ionic liquids and such materials demonstrated antifungal activity against 8 species, supporting our findings.

The ZOIs for *S. aureus* from the acetoxy silicone without antimicrobial compound persisted for 5 weeks, in comparison to the acetoxy silicone containing [$HL^2$]Br, which only produced zones for 3 weeks. A consideration for use of acetoxy silicone is the production of acetic acid during curing, which may be responsible for the ZOIs in the control formulation, but importantly could cause biocompatibility issues when used in a medical device. For this reason, use of the [$HL^2$]Br acetoxy coating can be considered as a 'proof-of-principle', with alternative condensation cured silicones, such as neutral curing silicones, to be investigated in future.

Whilst rapid release of the [$HL^2$]Br from the acetoxy coating does not lend itself to being functional for a long-term use medical device (*in-situ* > 30 days), methods to enable bulk-loading of the silicone and slow release of the compound may be investigated in future studies. Alternative catalysts to platinum will be investigated in future product developments to enable bulk-loading of [$HL^2$]Br into a silicone elastomer, whilst incorporation of the compound into liposomes to be bulk-loaded into the silicone matrix may also be investigated.

The discovery that the both triclosan containing silicone formulations along with the dip-coated silicone containing [$HL^2$]Br inhibited transition of *C. albicans* from the yeast to hyphal phenotype is an important finding. Although both hyphal and non-hyphal phenotypes have been associated with UTIs (Fisher 2011), the production of hyphae has been shown to promote virulence (Kretschmar et al. 1999). Commercial mouthwashes containing triclosan at final concentrations of 10 and 20 % have previously been shown to inhibit germ tube formation of *C. albicans* by approximately 86% and 88% respectively. partially supporting our findings (Aroonrerk and Dhanesuan 2007). Such findings suggest that triclosan and [$HL^2$]Br containing silicones may delay or prevent candiduria and complications, such as pyelonephritis and sepsis arising from such infections (Guler et al. 2006). Due to non-*C. albicans* species becoming increasingly more in catheterised patients within hospital settings (Jain et al. 2011), future investigations should evaluate the efficacy of the developed silicones against such species.

## 3.5 Conclusions

The aims of the Chapter were to incorporate a selection of antimicrobial compounds into silicone elastomers, either through bulk-loading of the silicone matrix or applied as dip-coatings. Physical properties and antimicrobial activity of such elastomers were to be determined. Such aims were successfully fulfilled, and antimicrobial incorporation showed no detrimental effects on the physical properties of the silicone elastomers.

Overall, novel antimicrobial silicone formulations have been produced which demonstrate antimicrobial efficacy against numerous CAUTI causing microorganisms. The novel triclosan ester derivative, triclosan acetate, was successfully incorporated into the bulk matrix of silicone and also as a dip-coating. These materials had increased longevity of antimicrobial release compared to triclosan formulations. Additionally, the bulk-loaded formulations had longer antimicrobial release than their dip-coated counterparts. However, triclosan silicone formulations had broader spectra of antimicrobial activity than triclosan acetate formulations, likely due to the requirement of triclosan acetate silicone to be in a high pH environment before hydrolysis to triclosan can occur (Shulong 1999).

An additional novel silicone was created using an acetoxy silicone coating with an imidazolium compound, $[HL^2]Br$, and this formulation had antimicrobial activity against *S. aureus* and *C. albicans*. Although use of $[HL^2]Br$ coated silicone did not exert antimicrobial activity against the Gram-negative bacteria tested, such effectiveness against the Gram-positive species and yeast represented a significant finding. Given that 4-5% and 21% of all CAUTIs can be attributed to *S. aureus* and *C. albicans* respectively (Warren et al. 1982; Dund, Durani, Ninama 2015), preventing CAUTI infection by these species could contribute to improved health amongst long-term catheterised patients and reduce the financial burden associated with treatment of such infections.

The production of an entire Foley catheter manufactured from bulk-loaded triclosan and triclosan acetate silicone was not possible in this study. However, cylinders constructed of bulk-loaded antimicrobial silicone were placed between the base of a urinary catheter and the drainage bag of an *in-vitro* bladder model to assess their effectiveness at preventing ascending infection due to *Proteus mirabilis*. Additionally, Foley catheters dip-coated with triclosan and triclosan

acetate silicone formulations were assessed for effectiveness at preventing *P. mirabilis*. Such experiments are discussed fully in Chapter 6. To conclude, silicone elastomers that could lead to reduced CAUTI incidence were successfully produced.

# Chapter 4

## Development of a 3D Printable Antimicrobial Silicone

## 4.1 Introduction

### 4.1.1 Medical devices

Medical devices are products constructed to support, enhance or replace part or the whole of a biological structure (Sampath et al. 2020). Cardiac stents are examples of devices that provide structural support (Cayton et al. 2012), whereas nasogastric tubes, central venous catheters, and urinary catheters aid the transport of biological or chemical agents into, or away, from the body (Ha et al. 2016; Sanaie et al. 2017). Voice box prosthesis and orthopaedic implants are examples of medical devices that function as anatomical replacements (Grundei 1996; Xin et al. 2021). Whilst such medical devices are often highly successful in fulfilling their primary aim to restore function or deliver therapeutics, they can provide a suitable surface for the growth of infectious biofilms.

The UK medical devices industry is highly regulated and since January 2021, all medical devices marketed within the UK were required to be registered with the Medical and Healthcare products Regulatory Agency (MHRA) (MHRA 2021). The regulatory body may require materials used for medical device construction to conform to standards set by the International Organisation for Standardisation (ISO) or standards imposed by ASTM International, formerly known as the American Society for Testing and Materials (Sampath et al. 2020). Such regulations ensure the materials and final products can perform under physiological forces, are non-toxic, biocompatible, non-carcinogenic and can be sterilised (Sampath et al. 2020).

Metals, polymers, ceramics and composites are the 4 classes of material most commonly used to form biomaterials for use in medical device construction (Sampath et al. 2020). These materials can be used alone or in combination to form the vast majority of medical devices (Sampath et al. 2020). Titanium and its alloys provide biocompatibility, high strength and fracture toughness to orthopaedic and dental implants (Oldani and Dominguez 2012), whereas the flexibility provided by polyurethane elastomers make them suitable for the production of devices such as dialysis tubing, blood bags and aortic balloons (Yoda 1998). The raw materials used to produce polyurethane medical devices are not approved by The Food and Drug Administration (FDA), but approval may be granted depending on the device constructed (Sampath et al. 2020).

Due to biocompatibility, cost effectiveness, non-leaching of plasticisers and ability to withstand degradation and physical forces (Colas 2005), silicone polymers have

become the material of choice for numerous implantable medical devices, including endotracheal tubes, central venous catheters and urinary catheters (Heide 1999). Additional beneficial properties of silicone rubbers are listed in Chapter 3, Table 3.1.

A variety of methods are employed to manufacture silicone biomaterials including injection moulding, compression moulding and extrusion (Yoda 1998), and each process has associated advantages and disadvantages that are briefly summarised in Table 4.1.

**Table 4.1** Advantages and disadvantages of methods to manufacture silicone medical devices

| Manufacturing method | Advantages | Disadvantages | References |
|---|---|---|---|
| **Injection moulding** | •Complex designs.<br>•Ability to mould micro and nano scale parts.<br>•Enhanced strength through use of fillers.<br>•Integration of metal or plastic elements. | •High tooling costs.<br>•Design restrictions.<br>•Restrictions on thickness to avoid shrinkage problems. | •(Steinbichler 1987; Ikeda 2010; Bont et al. 2021) |
| **Compression moulding** | •Cost effective.<br>•Low tool costs.<br>•Flexible mould design.<br>•Good surface finish. | •Slow production rate.<br>•Only able to produce flat or moderately curved parts. | •(Wang et al. 2021) |
| **Extrusion** | •High production volumes<br>•Products have consistent cross-sections. | •Difficult to predict the size of expansion.<br>•Size variations. | •(Lambert et al. 1991; De Cubber 1998) |

### 4.1.2 Fabrication of silicone medical devices using 3D printing

Additive manufacturing, also known as 3D printing, allows structures to be constructed by sequentially building 2-dimensional (2D) layers and joining each to the layer below (FDA 2017). Manufacturers can rapidly engineer a variety of designs, including the creation of structures that are porous or that encompass complicated geometric shapes (FDA 2017).

3D printing has become a cost-effective way to produce intricate plastic moulds to be used in the manufacture of silicone moulded products. However, directly printing silicone is a relatively new method to produce medical devices, and recent developments in this field include the 3D printing of meniscus implants, customisable nasal stents, heart valves and as anatomical models to be used as medical training tools (Mills et al. 2018; Coulter et al. 2019; DeZeeuw et al. 2020; Luis et al. 2020). The 3D printing of silicone medical devices allows anatomically matched medical devices to be created and reproduced without the need for multiple fittings, as would be the case for traditional moulded prosthetics (Jindal et al. 2016).

Traditionally, silicone medical devices are produced using heat-activated platinum catalysts. However, 3D printing apparatus are typically situated at ambient temperatures, therefore catalysts must be substituted with room-temperature vulcanising (RTV) versions (Jindal et al. 2016). The drawback of using RTV catalysts in 3D printable silicone manufacturing is the rapid curing rate prevents the building of the object in the typical layer-upon-layer approach, which is often slower than the rate of curing (Jindal et al. 2018). Typically, a platinum retarder, also known as a moderator, is incorporated into the silicone formulation to decrease the rate of curing. This is achieved by inhibiting and slowing the hydrosilyation cross-linking reaction at the vinyl ends of the polydimethylsiloxane (PDMS) chains (Jindal et al. 2018).

Further modifications to the silicone formulations are also often required to increase viscosity and prevent ‘slumping’ of the printed shape. The use of thixotropic agents, often termed ‘anti-slump’ may be used for such purposes. Such agents act by changing the spatial distribution of particles, increasing interparticle attractions and increasing the entanglement density of the chains (Mewis and Wagner 2009). Temporary hydrogen bonds can be formed with silanol groups on the surfaces of filler particles and act by slowing the hydrosilylation process during cross-linking (Mewis and Wagner 2009).

### 4.1.3 3D printing antimicrobial polymers

The use of 3D printing methods to produce customisable devices has gained momentum over recent years and particularly since the emergence of the highly contagious coronavirus (SARS-CoV-2) (Zuniga and Cortes 2020). 3D printing technologies were well-positioned to manufacture a range of customisable products, including personal protective equipment (PPE) and other medical supplies (Zuniga and

Cortes 2020). Copper nanocomposites have previously been used to impart antimicrobial properties to polypropylene thermoplastics used in injection moulding and 3D printing (Palza et al. 2018; Zuniga 2018). A 3D printed antimicrobial finger prosthesis was constructed from a polylactic acid polymer containing a copper nanoparticle additive and demonstrated 98.95-99.99% effectiveness against *Staphylococcus aureus* (including methicillin-resistant *S. aureus*) and 98.95-99.99% effectiveness against *Escherichia coli* (Zuniga 2018). Though use of antimicrobial thermoplastics in 3D printable products is a developing field, incorporating antimicrobial compounds in 3D printable silicone products represents an undiscovered area. To date, STERNE, France is the only manufacturer to have a commercially available antimicrobial silicone for use in 3D printing, although, the antimicrobial component and the efficacy of the product has not been published.

A recent review of silicone biomaterials concluded that "silicone's future as a biomaterial depends on its ability to demonstrate antimicrobial properties, particularly for applications including mammary prosthesis, contact lenses and urinary catheters" (Zare et al. 2021). Jindal et al developed a 3D printable silicone formulation for production of maxillofacial prostheses (Jindal et al. 2016). A customised 3D printer was used that extruded the silicone through an unheated nozzle and printed onto an unheated print bed. The printer was designed to allow printing of 2-component silicones, and contained separate chambers for the 2 parts, storing part A containing the platinum catalyst away from the part B that contained cross-linking reagent. The instrument contained a mixing chamber to allow thorough mixing of the 2 parts prior to extrusion (Jindal et al. 2016; Jindal et al. 2018).

It is anticipated that future projects will investigate the design and production of a 3D printed antimicrobial silicone device aimed at preventing ascending infection of the catheterised urinary tract. The product will be inserted between the catheter and the drainage bag and be designed with complex geometry to provide a large antimicrobial surface area for bacteria to migrate along. 3D printing has many advantages over traditional compression moulding for this application. The computer automated design (CAD) process allows the design to be altered without the need for reproducing expensive moulds, and the design can be reproduced. Although production of the final device is beyond the scope of this project, this research chapter will provide a proof-of-concept approach to the design and evaluation of a 3D printed antimicrobial silicone.

### 4.1.4 Aims

Access to the 3D printer used by Jindal et al (2016) was permitted for this research through collaboration with Prof. Trevor Coward, Kings College London. The specific aims of this chapter were to:

- Formulate a 3D printable antimicrobial silicone that would retain its 3D shape following extrusion, and cure within set parameters.
- Formulate a 3D printable antimicrobial silicone with comparable physical properties to a moulded version.
- Demonstrate antimicrobial release and activity of the 3D printed silicone against selected pathogens.

## 4.2 Materials & Methods

### 4.2.1 Development of a 3D printable antimicrobial silicone

The previously prepared silicone bases S1 and S2 (Table 3.2.1) along with the corresponding platinum catalyst concentrate (Table 3.2.2), were produced as in Section 3.3.1, with the modification that the previously used heat temperature vulcanising (HTV) catalyst was replaced with a room temperature vulcanising version (RTV), (Silanes & Silicones, Stockport, UK). Parts A and B were produced as previously described (Section 3.3.1) and mixed in equal parts, 5g of each, to produce the final silicone rubber which was cured at room temperature. The work times and cure times of the silicone rubber were recorded.

Varying quantities of platinum retarder, also termed moderator, and thixotropic agent were added to silicone formulations, as detailed in Tables 4.2.1-4.2.4. Where indicated, the platinum retarder (1,3,5,7-tetracinyl-1,3,5,7-tetra-methylcyclotetrasiloxane, Gelest, PA, USA) was diluted with V21 silicone oil (Vinyl Terminated PDMS, 100 cst, Gelest, USA). Two thixotropic agents were trialled, M514, Technovent, UK and A-300-8 (Factor II, Inc, Arizona, USA).

Triclosan (Sigma, UK) was dissolved in acetone to create a 40% (w/w) solution, before incorporating into silicone. Tables 4.2.2-4.2.4 show the composition of silicone formulations with varying amounts of acetone. The cure times and ‘slumping’ of the formulations were assessed before the triclosan was dissolved in the acetone to create a 1% (w/w) final silicone formulation, termed 3D-T12. Parts A and B containing acetone were placed at 50ºC for 15 min to aid solvent evaporation.

2.5% (w/w) of the triclosan stock solution (40% w/w in acetone) was added to each of part A and B of the 3D-S12 formulation to create a 1% (w/w) triclosan silicone, termed 3D-T12.

**Table 4.2.1** Composition of silicone formulations 3D-S1 – 3D-S7 for use in 3D printing applications

| Formulation | Part A | | | | Part B | | | |
|---|---|---|---|---|---|---|---|---|
| | Base S2 (%w/w) | Platinum concentrate (%w/w) | Thixotropic agent * (%w/w) | Platinum retarder (%w/w) | Base S2 (%w/w) | Cross-linker (H301) (%w/w) | Thixotropic agent * (%w/w) | Platinum retarder (%w/w) |
| **3D-S1** | 89.5 | 10 | 0.5 | 0 | 94.06 | 5.44 | 0.5 | 0 |
| **3D-S2** | 86.5 | 10 | 0.5 | 3 | 91.06 | 5.44 | 0.5 | 3 |
| **10% (w/w) moderator stock in V21** | | | | | | | | |
| **3D-S3** | 86.5 | 10 | 0.5 | 3 | 91.06 | 5.44 | 0.5 | 3 |
| **3D-S4** | 86 | 10 | 3 | 1 | 90.56 | 5.44 | 3 | 1 |
| **3D-S5** | 86.5 | 10 | 3 | 0.5 | 91.06 | 5.44 | 3 | 0.5 |
| **5% (w/w) moderator stock** | | | | | | | | |
| **3D-S6** | 86.5 | 10 | 3 | 0.5 | 91.06 | 5.44 | 3 | 0.5 |
| **2.5% (w/w) moderator stock** | | | | | | | | |
| **3D-S7** | 86.5 | 10 | 3 | 0.5 | 91.06 | 5.44 | 3 | 0.5 |

* M514, Technovent, UK

**Table 4.2.2** Composition of silicone formulations 3D-S8 – 3D-S10 for 3D printing applications using platinum retarder stock at 2.5% (w/w)

| Formulation | Part A | | | | | Part B | | | | |
|---|---|---|---|---|---|---|---|---|---|---|
| | Base S2 (%w/w) | Platinum concentrate (%w/w) | Thixotropic agent * (%w/w) | Platinum retarder (%w/w) | Acetone (% w/w) | Base S2 (%w/w) | Cross-linker (H301) (%w/w) | Thixotropic agent * (%w/w) | Platinum retarder (%w/w) | Acetone (% w/w) |
| **3D-S8** | 86.5 | 10 | 3 | 0.5 | 20 | 91.06 | 5.44 | 3 | 0.5 | 20 |
| **3D-S9** | 85.5 | 10 | 4 | 0.5 | 5 | 90.06 | 5.44 | 4 | 0.5 | 5 |
| **3D-S10** | 85.5 | 10 | 4 | 0.5 | 2 | 90.06 | 5.44 | 4 | 0.5 | 2 |

* M514, Technovent, UK

**Table 4.2.3** Composition of silicone formulation 3D-S11 for 3D printing applications using platinum retarder stock at 2.5% (w/w)

| Formulation | Part A | | | | | Part B | | | | |
|---|---|---|---|---|---|---|---|---|---|---|
| | Base S1 (%w/w) | Platinum concentrate (%w/w) | Thixotropic agent * (%w/w) | Platinum retarder (%w/w) | Acetone (% w/w) | Base S1 (%w/w) | Cross-linker (H301) (%w/w) | Thixotropic agent * (%w/w) | Platinum retarder (%w/w) | Acetone (% w/w) |
| **3D-S11** | 85.5 | 10 | 4 | 0.5 | 5 | 90.06 | 5.44 | 4 | 0.5 | 5 |

* M514, Technovent, UK

**Table 4.2.4** Composition of silicone formulation 3D-S12 for 3D printing applications using platinum retarder stock at 2.5% (w/w)

| Formulation | Part A | | | | | Part B | | | | |
|---|---|---|---|---|---|---|---|---|---|---|
| | Base S1 (%w/w) | Platinum concentrate (%w/w) | Thixotropic agent † (%w/w) | Platinum retarder (%w/w) | Acetone (% w/w) | Base S1 (%w/w) | Cross-linker (H301) (%w/w) | Thixotropic agent † (%w/w) | Platinum retarder (%w/w) | Acetone (% w/w) |
| **3D-S12** | 85.6 | 10 | 4 | 0.4 | 2.5 | 90.16 | 5.44 | 4 | 0.4 | 2.5 |

† A-300-8 (Factor II, Inc, Arizona, USA)

### 4.2.2 3D printing silicone

#### 4.2.2.1 Overview of the 3D printer

The 3D printer (Figure. 4.2.1) comprised of an x-y-z gantry robot (Aerotech AGS1000 ES16232; Aerotech Inc., PA, USA), a material delivery system, a processor (A3200; Aerotech Inc.), and component design software (RoboCAD 4.2.8) (Tubío et al., 2016, Xie et al., 2006).

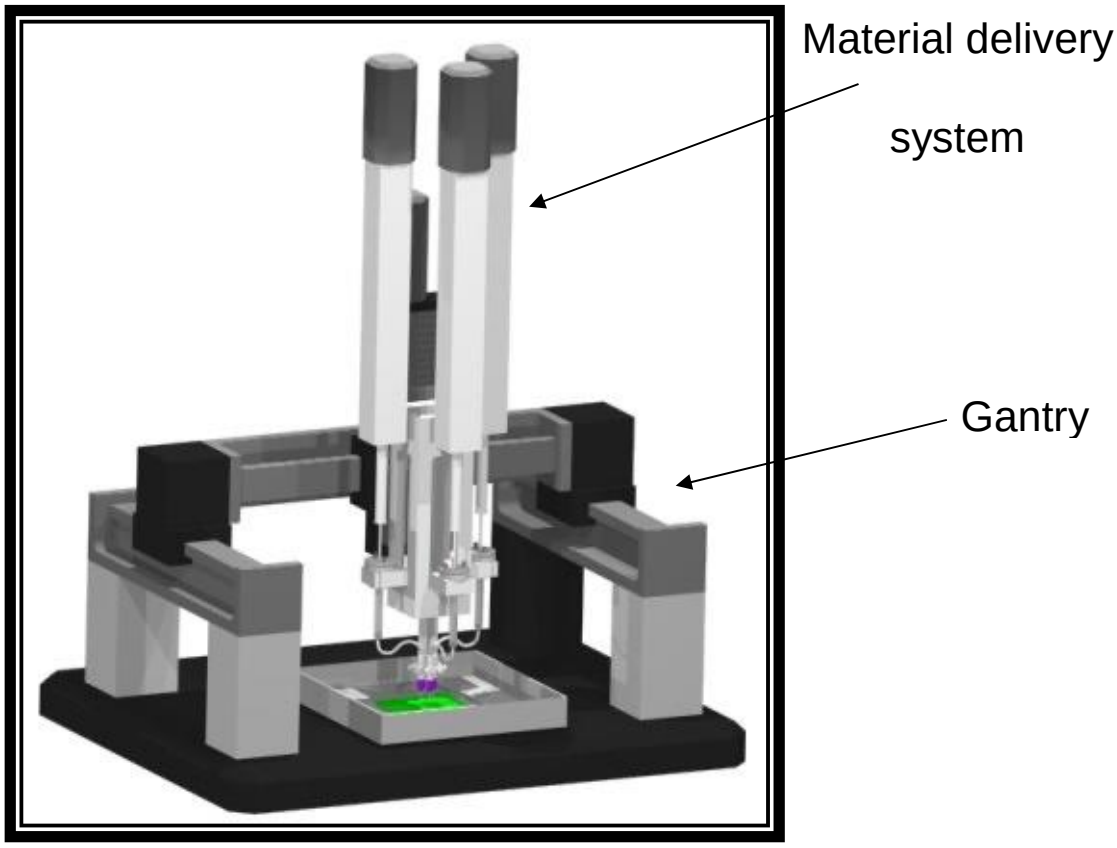


**Figure 4.2.1** Printer cartoon including gantry and material delivery system. Reproduced with permission from Jindal 2016

#### 4.2.2.2 x-y-z gantry robot

The selected commercial gantry robot (Figure. 4.2.2) had high precision in the x-y plane (0.01 μm step resolution, 0.1 μm repeatability) and precision in the z plane of around 0.1 to 1 μm. A linear speed of up to 10 mm/s could be achieved.

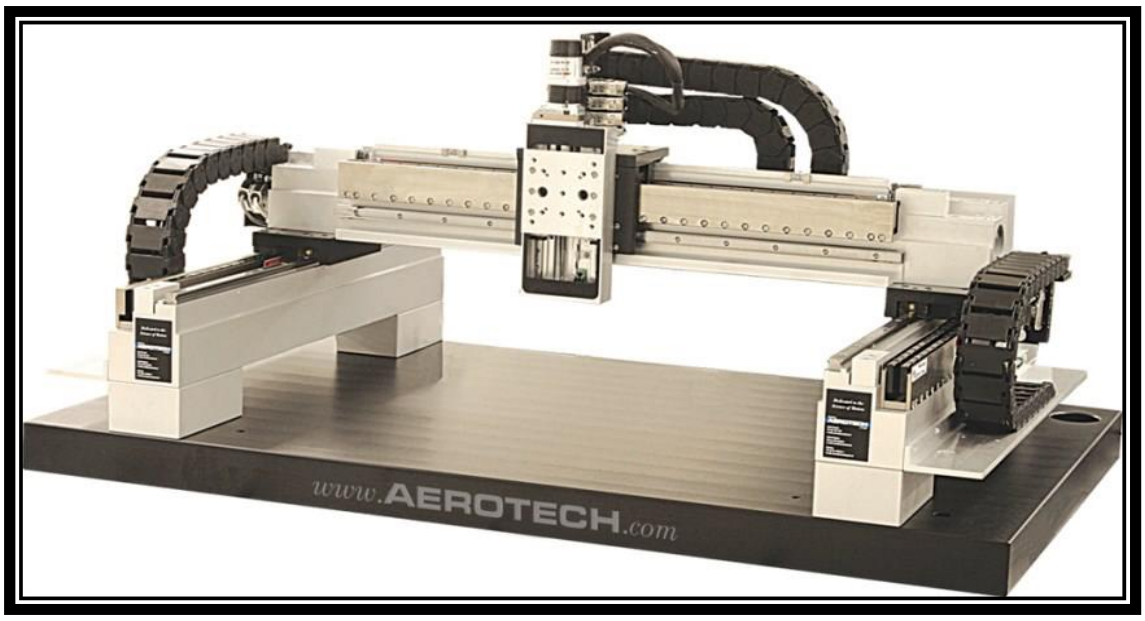


**Figure 4.2.2** The gantry robot**.** Reproduced with permission from Jindal 2016.

#### 4.2.2.3 Material delivery system

The material delivery system or print head was custom designed to print two-component silicone via a mixing chamber. The print head (Figure. 4.2.3) comprised of an array of four syringe pumps (Aerotech BMS35; Aerotech Inc.), connected to the mixing chamber via tubing. The print head delivered material directly from the syringes to a mixing chamber through a single nozzle.

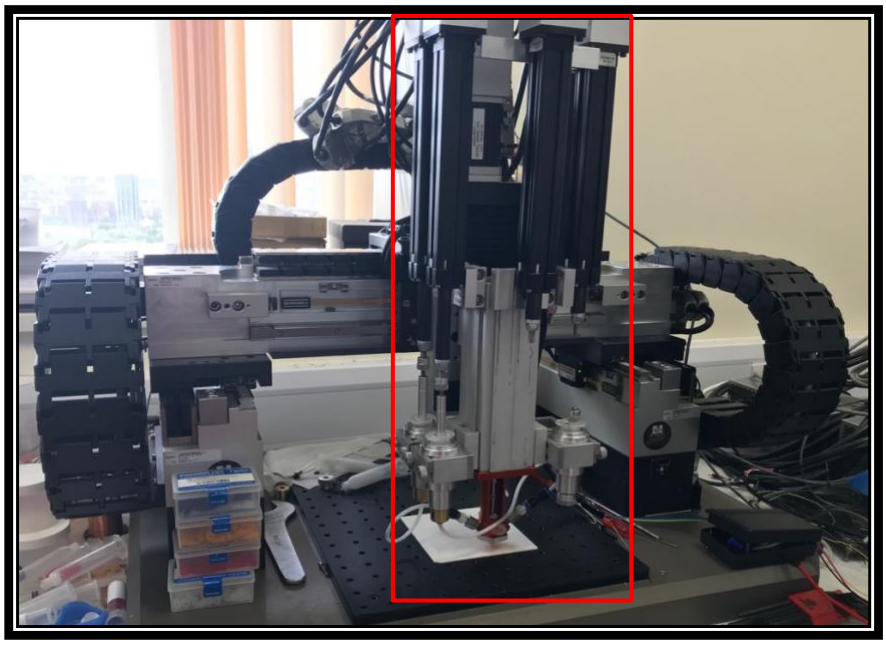

**Figure 4.2.3** The gantry with printer head (outlined in red)

The mixing chamber further incorporated a mixer body, a mixer nozzle, and a motorised mixing paddle (Figure. 4.2.4). The nozzle or printing tip diameter could be adjusted between 0.1 and 2 mm, but typically nozzles in the 0.2 to 0.5 mm diameter range were chosen for printing silicone.

The syringe pumps were brushless rotary motors with positive displacement capable of producing 445 N of thrust force on the syringe plunger, such that it was capable of creating around 4.82 MPa of pressure in a 3 ml or 5 ml syringe. Syringes are the material reservoirs. The printer had 4 syringe pumps that allowed up to 4 components to be mixed and printed, if required. The material(s) entered the mixing chamber via the 4 inputs, flowed through the check valve and then congregated towards the mixing tip (Figure. 4.2.4). At the mixing tip, the materials were mechanically mixed via a rotary shaft (100 rpm) in the middle of the chamber, then extruded through the printing tip.

Figure: 4.2.4 depicts the working mechanism of the printer, where part A and part B entered and were mixed using a motor prior to extrusion. This printer had a material printing resolution of 100–200 µm.

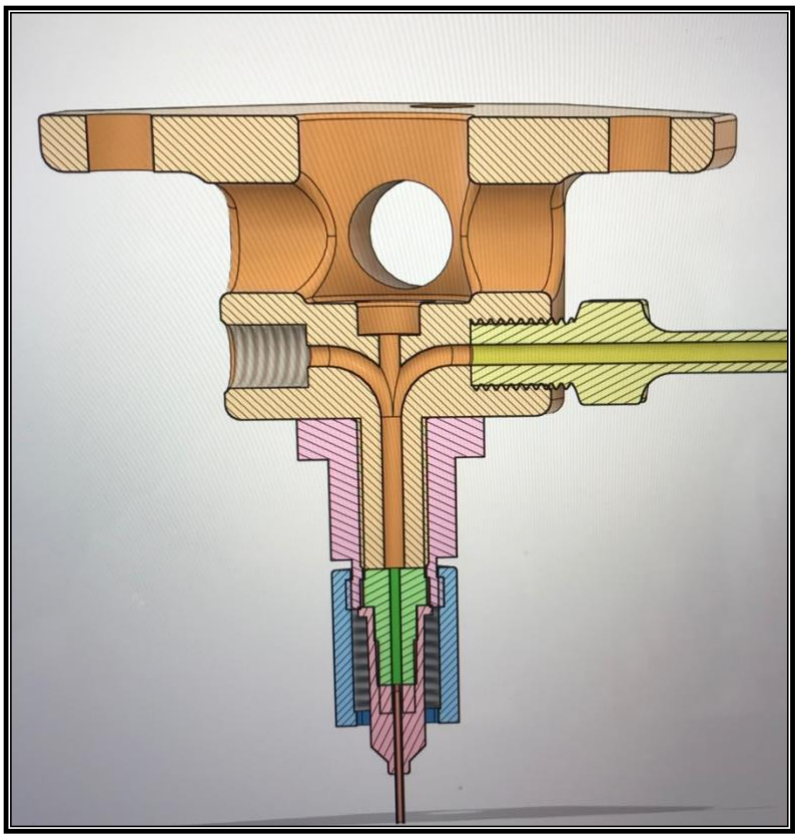

**Figure 4.2.4** The mixing chamber depicting two inlets for part A and part B silicone and the mixing chamber (green)

#### 4.2.2.4 3D printing specimens to determine mechanical properties

Part A and part B silicone were loaded into the removable syringe pump chambers using a spatula and centrifuged for 10 s at 3000 rpm (SpeedMixer Dac 150FVZ-K, Siemens, Buckinghamshire, UK), to remove air bubbles before loading the syringes into the pump chambers.

Computer aided design (CAD) files had previously been designed by researchers at Kings College, London using RoboCAD 5.10.136 software (3D Inks LLC, Oklahoma, USA), to conform to the dimensions required to perform tensile and elongation testing, according to ISO standard 37. The dimensions are illustrated in 3.2.1. Figure 4.2.5A depicts the printed specimen. Additional specimens were printed to conform to ISO standard 34-1 (Figure. 4.2.5 B), method B as illustrated in Figure 3.2.3.

The outlines of the shapes (Figure. 4.2.5) were printed before the 'rastering', or in-filling occurred. The rastering occurred in a layer-upon-layer approach with the direction of printing alternating with each layer. Each layer was 0.45 mm in height. Curing occurred at room temperature, typically within 30 min per sample.

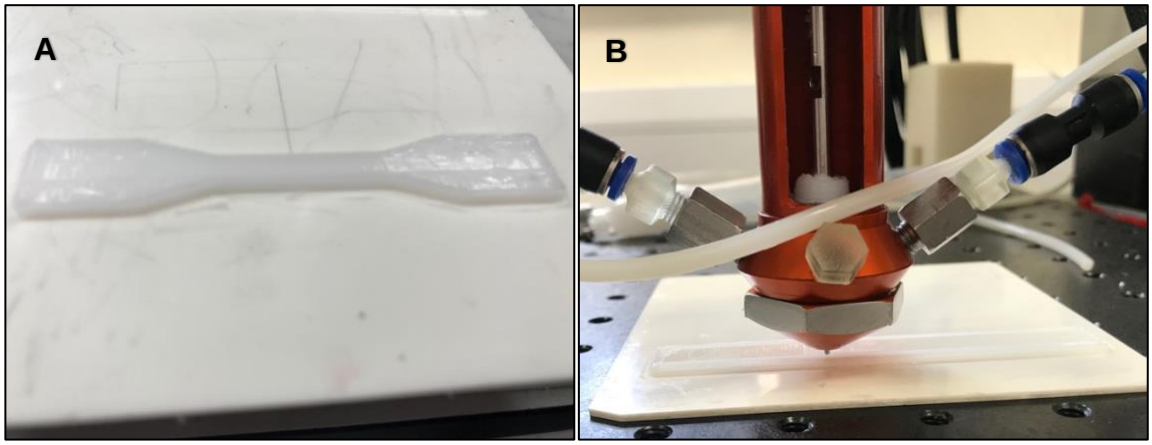


**Figure 4.2.5** 3D printed specimens for determination of mechanical properties. **A.** Dumb-bell shaped specimen used to determine tensile strength and elongation. **B.** Rectangle specimen used to measure tear resistance

### 4.2.3 Determining the mechanical properties of 3D printed silicone specimens

The 3D printed dumb-bell shaped silicone samples (Section 4.2.2.4), were loaded into self-mounting grips of a tensile machine (MultiTest -*d*, Mecmesin), fitted with a 500N load cell (AFG 500N, Mecmesin), and the tensile strength and elongation were determined, as previously described (Section 3.3.5). Tear resistance of the rectangle shaped specimens were determined, as described in Section 3.3.6. Measurements

were taken from 6 separately printed specimens from silicone with (3D-T12) and without 1% w/w triclosan (3D-S12). Statistical analyses were calculated using unpaired t-tests with unequal variances by the software GraphPad Prism.

### 4.2.4 Antimicrobial properties of 3D printed silicone

Coupons (10 mm) were bored from the remnants of the specimens following mechanical testing and sterilised by autoclaving. Antimicrobial activity of the 3D printed silicone against *Staphylococcus aureus* NSM 7, *Escherichia coli* NCTC 12923 and *P. mirabilis* 12 RTB was determined as previously described in Section 3.3.8.1. Statistical analysis was performed using paired t-tests to compare zones of inhibition produced by non-antimicrobial and antimicrobial containing coupons.

## 4.3 Results

### 4.3.1 Development of 3D printed antimicrobial silicone

The silicone base S2 developed in Chapter 3 (Table 3.2.1), was used to produce a new silicone formulation suitable for 3D printing applications. An optimal silicone for this application would be able to hold its shape when uncured, be 'workable' for longer than 10 min and cure within 20-30 min at room temperature. Table 4.3.1 shows the work and cure times of the silicone formulations produced during the development process.

The addition of a thixotropic agent to parts A and B at 0.5% (w/w), but without moderator (platinum retarder) allowed rapid curing (< 1 min) of the silicone when mixed in a 1:1 ratio. Adding 3% w/w of undiluted moderator solution to parts A and B delayed curing of the final silicone rubber to > 300 mins. Diluting the moderator to a 10% (w/w) stock solution and increasing the concentration of the thixotropic agent from 0.5% to 3% w/w (3D-S3 – 3D-S5) reduced cure time to 90 min.

To achieve a faster cure time, the moderator stock concentration was reduced to 5% w/w (3D-S6) and 2.5% w/w (3D-S7). Although the work and cure time of 3D-S7 was acceptable, the viscosity of the silicone was too low to allow 3D printing.

As acetone was required to solubilise triclosan in the final product, it was added at concentration between 2% and 20% (w/w) in parts A and B of formulations 3D-S8-3D-S10, before placing at 50ºC to allow evaporation of the solvent. The curing of 3D-S8-3D-S10 was optimal, but the viscosity was still too low and 'slumping' of the shaped material occurred during 3D printing.

To increase viscosity, base S1 (described in Section 3.2) was used. S1 had a higher concentration of long polymer chains (V46) than the S2 formulation and twice the amount of filling agent. Increasing the thixotropic agent to 4% w/w (3D-S11) allowed curing to occur in 35 min, but viscosity was not optimal. The thixotropic agent used for 3D-S2 – 3D-S11 was substituted for an alternative product (A-300-8, Factor II, USA) and used at 4% w/w. Along with 2.5% (w/w) acetone and 0.0125% moderator in the final formulation, curing was achieved in 25 min and the viscosity was optimal for 3D printing to be performed without slumping of the final shape.

A 40% (w/w) stock solution of triclosan in acetone was prepared and 2.5% added to parts A and B of 3D-S12 in substitution of the acetone component. After solvent

evaporation, a 1% (w/w) triclosan silicone (3D-T12) was created and was suitable for use in 3D printing applications.

**Table 4.3.1** Work times and cure times of silicone formulations developed for use in 3D printing applications

| Formulation | Work time (min) | Cure time (min) |
|---|---|---|
| **3D-S1** | < 0.5 | < 1 |
| **3D-S2** | > 300 | > 300 |
| **3D-S3** | 120 | 180 |
| **3D-S4** | > 60 | 120 |
| **3D-S5** | 45 | 90 |
| **3D-S6** | 30 | 60 |
| **3D-S7** | 15 | 35 |
| **3D-S8** | 15 | 35 |
| **3D-S9** | 16 | 30 |
| **3D-S10** | 15 | 25 |
| **3D-S11** | 22 | 35 |
| **3D-S12** | 15 | 25 |
| **3D-T12** | 15 | 25 |

### 4.3.2 Mechanical properties 3D printed silicone

The mechanical properties of 3D printed silicone specimens were compared to specimens that were fabricated by compression moulding, without thixotropic agent or platinum retarder. Specimens bulk-loaded with 1% triclosan and non-antimicrobial controls were produced. The tensile strength of the 3D printed specimens was significantly higher than the moulded versions ($P<0.0001$) (Figure 4.3.1A). A reduction in tensile strength was also evident following addition of 1% triclosan to the 3D printed formulation ($P<0.01$). The elongation potential of the 3D printed specimens was not affected by addition of 1% triclosan, yet significant differences were observed between the triclosan (T1) and triclosan-free (S1) specimens ($P<0.05$) (Figure 4.3.1B). Significantly greater elongation was observed in the 3D printed control (3D-S12) than the moulded control (S1). The tear resistance of the silicone specimens was not affected by addition of triclosan for either fabrication method, but the 3D printed elastomers had significantly greater tear resistance than their moulded counterparts (Figure 4.3.1 C).

### 4.3.3 Antimicrobial properties of 3D printed silicone loaded with 1% triclosan

3D printed silicone elastomers containing 1% triclosan (3D-T12) produced zones of inhibition (ZOIs) against *Escherichia coli*, *Staphylococcus aureus* and *Proteus mirabilis* (Figure 4.3.2). 3D printed elastomers without triclosan (3D-S12) did not produce ZOIs against any of the 3 bacteria. The ZOIs produced against *E. coli* by 3D-T12 were significantly larger than 3D-S12 ($P<0.001$), and greater statistical differences were achieved against *S. aureus* and *P. mirabilis* ($P<0.0001$).

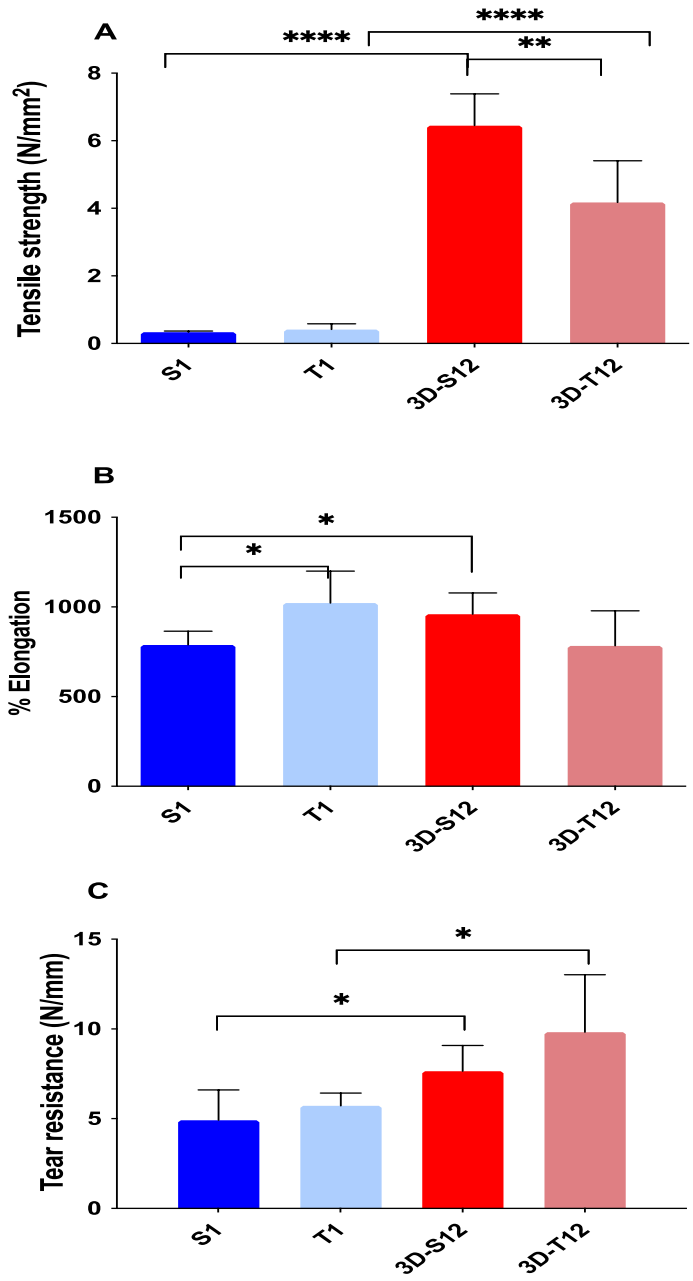


**Figure 4.3.1** Mechanical properties of silicone formulations. S1 and 3D-S12 represent silicone formulations without triclosan, and T1 and 3D-T12 are formulations with 1% (w/w) triclosan. S1 and T1 specimens were produced via compression moulding and 3D-S12 and 3D-T12 specimens were 3D printed. All measurements were made using a 500 N load cell pulled at 300 mm/min. (A) tensile strength of silicone specimens, (B) % elongation of silicone specimens, (C) tear resistance of silicone tear specimens. Measurements were performed on 6 separately produced specimens. Error bars represent the standard deviation. Unpaired t-tests used for statistical analysis. * P<0.05, ** P<0.01, *** P< 0.001, **** P< 0.0001

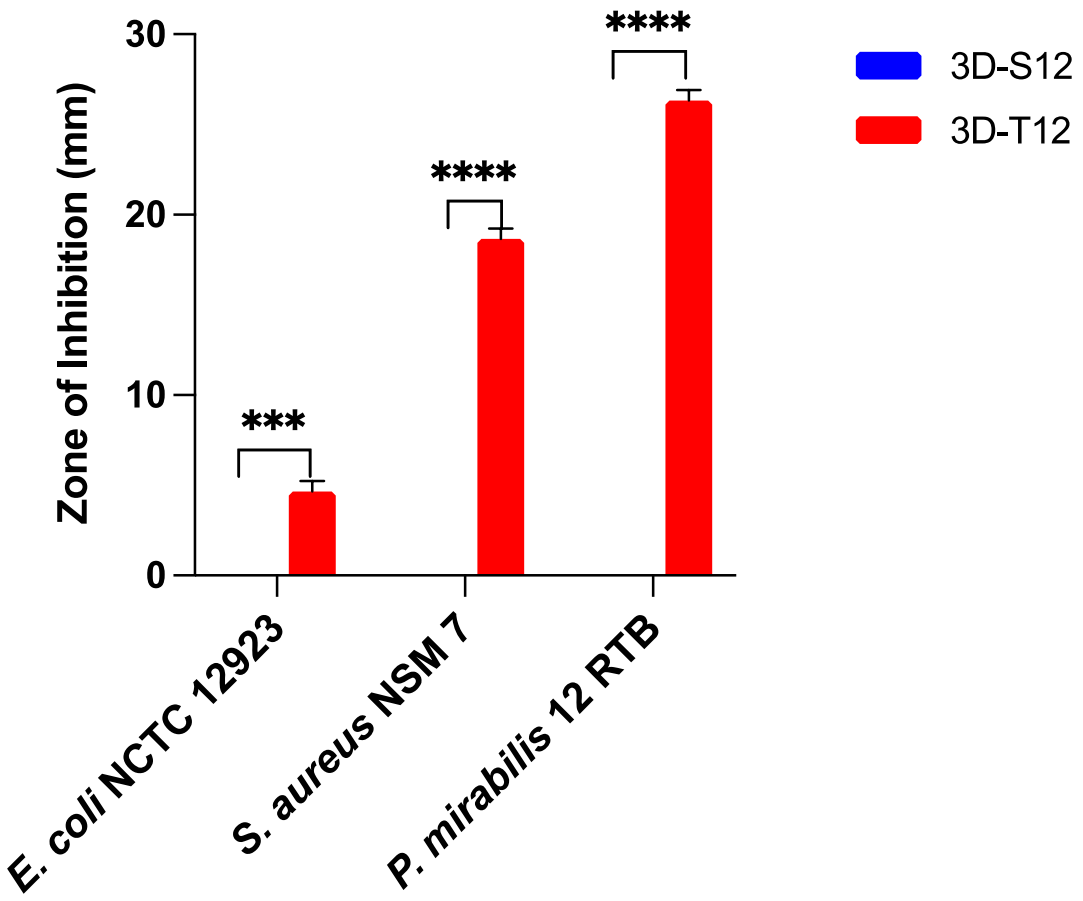


**Figure 4.3.2** Zones of inhibition against common CAUTI pathogens produced by 3D printed silicone elastomers. Agar plates were prepared with 3 CAUTI causing microorganisms. Zones of inhibition following 24 h incubation with silicone coupons were measured. Silicone coupons were bored from shapes that had been 3D printed with (3D-T12) and without 1% w/w triclosan (3D-S12). Means of 3 silicone coupons from separately printed specimens were plotted. Error bars show standard deviation. Unpaired t-tests were used for statistical analysis. * P<0.05, ** P<0.01, *** P< 0.001 **** P< 0.0001

## 4.4 Discussion

Medical devices are important tools for the management of numerous medical conditions. Often, such devices require partial or complete implantation into the body and as such, they must be constructed from durable materials that can withstand degradation and physiological forces, and are both biocompatible and easily sterilised (Sampath et al. 2020). A major drawback of medical device use is the ability of bacterial biofilms to form on their surfaces. Bacteria that colonise areas adjacent to, or near the site of device entry, can readily migrate and colonise the surfaces of devices (Behnia et al. 2014). As such, up to 50% of all healthcare-acquired infections (HCAIs) are attributed to use of indwelling medical devices (NICE 2012). Ventilator associated pneumonia (VAP), catheter-related blood stream infections (CRBSIs), and catheter-associated urinary tract infections (CAUTIs) are all examples of infections instigated by use indwelling medical devices (Behnia et al. 2014; Jamal et al. 2018; Karkee et al. 2018).

Silicone polymers are frequently used in the fabrication of medical devices, due to their biocompatibility, chemical inertness, thermal stability and numerous fabrication methods available (Colas 2005). The advantages and disadvantages of each fabrication method are listed in Table 4.1. Developing infection resistant silicone surfaces to combat device-related infections has attracted much attention in recent years, with research focussed on a few key areas; antifouling mechanisms aimed at preventing cell attachment and biocidal surfaces that release antimicrobial agents into the surrounding environment or cause cell death upon surface contact (Singha et al. 2017).

The rapid advancement of 3D printing technologies has paved the way for customisable silicone devices to be created, and recent developments in the field include nasal stents, meniscus implants and heart valves to be produced in this way (Mills et al. 2018; Coulter et al. 2019; Luis et al. 2020). The production of 3D printable antimicrobial silicones is the next logical step in the field of medical device fabrication. Customisable devices that can resist bacterial colonisation would herald a new era in medical device development.

The aim of the research presented in this Chapter was to provide a ‘proof-of-concept’ approach to 3D printing antimicrobial silicone. A 1% triclosan silicone

rubber demonstrated broad spectrum antimicrobial activity in Chapter 3, therefore producing a 3D printable version of this was the focus of this research.

The tensile strength of 3D printed silicone elastomers with and without triclosan were superior to the moulded versions and these differences could be attributed to numerous factors. The addition of a thixotropic agent to the formulation increases viscosity and changes the spatial distribution of the particles. As a result, interparticle attractions would be increased and the entanglement density of the chains increased (Jindal et al. 2018). Extruding the silicone under high pressure was also a factor that increased tensile strength in the 3D printed silicone relative to the moulded version. Previous studies have demonstrated significantly increased tensile strength of silicones fabricated via 3D printing methods, when compared to compression moulding techniques. This is believed to be due to reduced levels of air entrapment inside the silicone polymers (Ozbolat et al. 2018). A study by Bibars et al showed that addition of a thixotropic agent to three different commercially available silicones, reduced tear strength and elongation, but not tensile strength (Bibars et al. 2018). The tear resistance of the silicone elastomers 3D printed in this study actually increased and this was likely due to the fabrication method occurring under high pressure extrusion, rather than the addition of the thixotropic agent. The same explanation can be afforded to the observed increase in elongation of the 3D printed formulation without triclosan, when compared to the moulded version without thixotropic agent.

The study by Bibars et al determined the tensile strength, elongation and tear resistance of three commercially available silicones, following addition of thixotropic agent (Bibars et al. 2018). The tensile strength of the newly developed 3D-S12 and 3D-T12 were comparable to the Z004 formulation produced by Technovent, Ltd, which had the highest tensile strength of the three silicones evaluated. The elongation of the 3D printed formulations 5-fold higher than M511 (Technovent, Ltd), which had the greatest elongation of the three commercially available silicones. Regarding tear resistance, a 5-fold increase was also observed compared to the Z004.

It can be concluded that the mechanical properties of the novel 3D printed silicones were equivalent or above the standards required for commercial silicone formulations, and the addition of triclosan did not adversely affect such properties.

The 1% triclosan silicone produced via 3D printing demonstrated growth inhibition of the three bacteria evaluated, namely *Escherichia coli*, *Staphylococcus aureus* and *Proteus mirabilis* (Karkee et al. 2018). These bacteria are often isolated from urinary catheters of patients undergoing long-term catheterisation and as such, silicones that can prevent biofilm formation by these pathogens would be valuable in reducing incidence of CAUTI.

It is anticipated that future projects will aim to develop 3D printed silicone devices that can be inserted between the catheter and drainage bag. The device could be shaped as a tubing with a honeycomb-like lumen to increase the available biocidal surface area, with an aim of preventing motile bacteria, such *as P. mirabilis,* from ascending from the drainage bag to the catheter. 3D printing such a device will enable numerous designs to be explored through adaptations to computer-aided design (CAD) files, without requirement for new tooling for each design. Furthermore, fabricating devices via 3D printing has been shown to impart greater mechanical properties to the silicone than traditional moulding techniques.

## 4.5 Conclusions

A novel silicone formulation containing 1% triclosan was produced that had the desirable viscosity to be 3D printed and retain its shape until curing. Crucially, curing occurred within the desired 20-30 min window and this allowed shapes to be printed before complete curing occurred. The mechanical properties of the 3D printed shapes were equivalent or exceeded those of commercially available silicones. Importantly, the triclosan silicone inhibited growth of three CAUTI causing microorganisms, namely *E. coli*, *S. aureus* and *P. mirabilis*. It is envisaged that future applications of this 3D printed triclosan silicone will be directed at reducing CAUTI infection. The technology may also be used to create sensor materials with increased surface areas.

# Chapter 5

## Identification of Sensor Compounds to Detect Urinary Tract Infections in Catheterised Patients

## 5.1 Introduction

Urinary tract infections (UTIs) in catheterised patients, are termed catheter-associated urinary tract infections (CAUTIs), and often go undiagnosed for considerable periods of time. This allows CAUTIs to proliferate, eventually leading to patients becoming symptomatic. Such symptoms include fever, suprapubic tenderness, flank tenderness, haematuria, tachycardia and delirium (Davis, 2019). At the point when a patient displays symptoms, the infection is often well-established and difficult to eradicate using systemic antibiotics (Nicolle, 2012). In some instances, advanced CAUTIs lead to sepsis and eventually death, with 1467 reported deaths attributed to CAUTIs in English hospital trusts between 2016 and 2017 (Smith et al., 2019).

As discussed in Chapter 1, CAUTIs caused by *Proteus mirabilis* commonly involve blockage of urinary catheters through deposition of crystalline salts (D. Stickler et al., 1993). Such blockage leads to retention of infected urine and reflux of the urine to the kidneys, causing pyelonephritis, sepsis and shock (David J. Stickler, 2008). Current treatment regimens involve catheter replacement and administration of antibiotics.

The ability to detect the early stages of CAUTIs would be of considerable value, as early treatment would result in patients experiencing fewer CAUTI complications and the NHS would have reduced financial costs. Indeed direct hospital costs incurred due to CAUTI and catheter-associated blood stream infections (CABSI) between 2016-2017 were previously been estimated at £54.4 million (Smith et al., 2019).

As discussed in Chapter 1, a previous collaboration between the Microbial Diseases Research Group of Cardiff University and Technovent Ltd, led to the successful development of a silicone sensor to detect CAUTIs caused by urease positive bacteria (Malic et al., 2012). The sensor incorporated a pH sensitive compound, bromothymol blue (BTB), into the bulk matrix of a silicone device, which generated a colour change (yellow to dark blue), due to penetration of the silicone material by ammonium ions from urine infected by *P. mirabilis*. Clinical evaluation of the sensor revealed that it successfully detected *P. mirabilis*, *Providencia* and *Morganella* infections in 6 out of 7 patients, with detection occurring on average 23 days before catheter blockage (Long et al., 2014).

This current experimental chapter sought to identify additional compounds able to detect a wider range of pathogens responsible for causing CAUTIs. Selected agents were evaluated as potential sensor molecules within a polymer material. The compounds selected for evaluation are described below. Candidate sensor molecules were primarily those that had previously been described in laboratory diagnostic approaches and readily commercially available. In addition, in collaboration with the School of Chemistry, a range of novel tetrazolium compounds were evaluated.

### 5.1.1 Detection of *Escherichia coli* based on β-D-glucuronidase and β-galactosidase activity

*Escherichia coli* is the bacterium most commonly isolated from the urine and catheters of patients undergoing long-term catheterisation, with a prevalence of between 30 and 40% (Abdallah et al. 2011; Dund, Durani and Ninama 2015; Karkee et al. 2018). Early *E. coli* detection in catheterised patients would significantly reduce complications associated with advanced CAUTI infections.

Methylumbelliferyl-β-D-glucuronide (MUG) has long been used as a molecule to detect *E. coli* contamination in foods and water sources (Farnleitner et al., 2002; Villari et al., 1997). The basis of detection by MUG is the ability of an enzyme (β-glucuronidase), expressed by most *E. coli* strains to hydrolyse the MUG substrate (Figure 5.1.1).

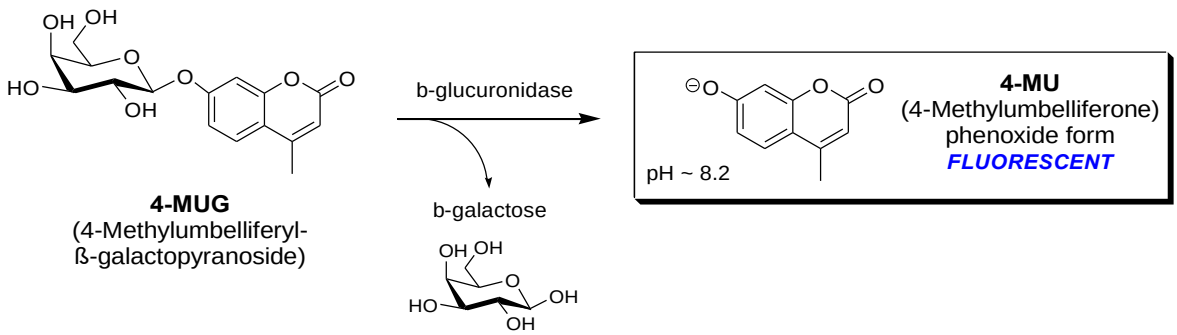


**Figure 5.1.1** Schematic representation *of E. coli* β-glucuronidase activity on the methylumbelliferyl-β-D-glucuronide (MUG)

The enzyme β-D-glucuronidase is produced by *E. coli* and other *Enterobacteriaceae* and hydrolyses MUG to yield the 4-methyl-umbelliferone moiety, which constantly fluoresces blue under long-wavelength ultraviolet light (Figure 5.1.1). Of note, is that clinically relevant verotoxin producing *E. coli* (VTEC), do not produce β-D-glucuronidase and thus, yield a negative MUG result (Thompson et al., 1990). Some strains of *Shigella* species are also able to hydrolyse MUG and give a positive result (Feng & Hartman, 1982).

MUG detection of *E. coli* was developed by Cakir *et al.*, 2001 and offers a rapid and cost-effective assay for *E. coli* detection. With this in mind, using MUG as a sensor molecule for presence of *E. coli* in urinary catheters or the attached drainage bags could prove as a useful tool in early detection of CAUTI.

An alternative molecule for potential detection of *E. coli* and other faecal coliforms including *Klebsiella pneumoniae* is chlorophenol red-β-D-galactopyranoside (CPRG). CPRG exploits the β-galactosidase activity of bacteria to hydrolyse the substrate and release the water-soluble red product, chlorophenol red (CR) (Figure 5.1.2).

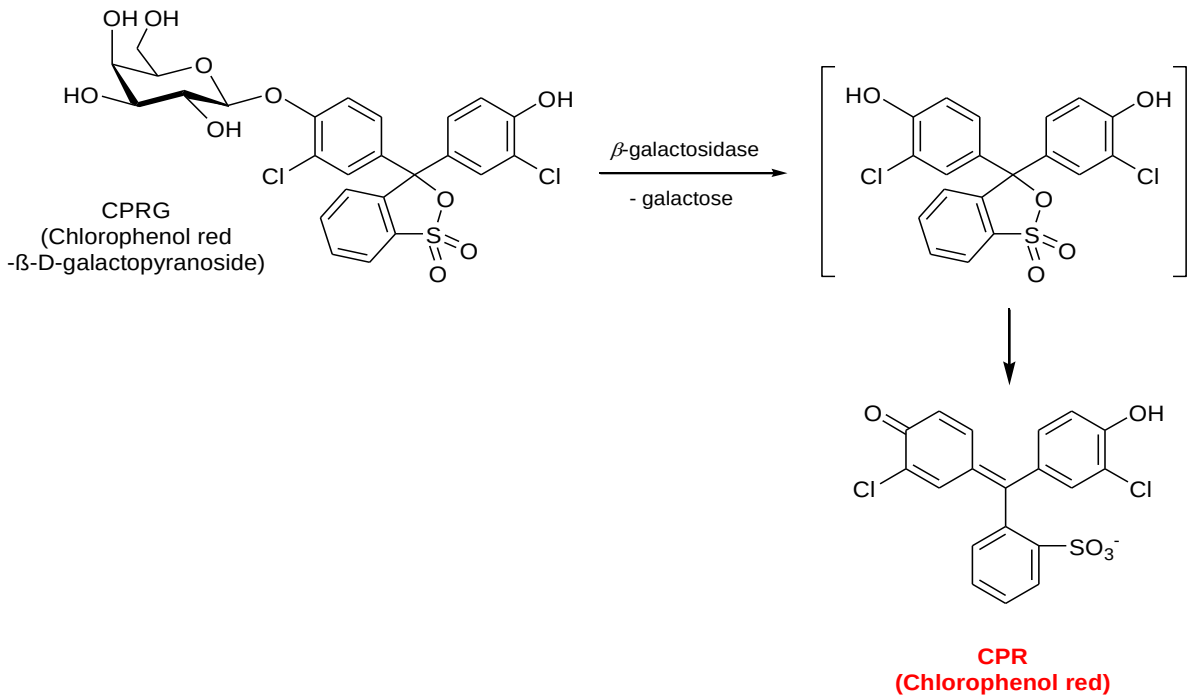


**Figure 5.1.2** Schematic representation of *E. coli* β-D-galactosidase activity with chlorophenol red-β-D-galactopyranoside (CPRG)

CPRG has been used to detect faecal contamination in water sources (Sicard et al., 2014). Wutor et al also developed a voltametric sensor to detect the electrooxidation of chlorophenol red released by the enzymatic breakdown of CPRG from bacterial coliforms (Wutor, Togo, Limson, et al., 2007). The advantage of CPRG over MUG as a sensor molecule is that with CPRG a positive reaction would be visible by eye without UV light exposure. Experiments undertaken in this Chapter will evaluate CPRG alongside MUG to determine whether either are suitable candidates for incorporation into polymer-based materials as a CAUTI sensor.

### 5.1.2 Detection of urease positive bacteria using pH sensors

Urease positive bacteria including *P. mirabilis* and *Proteus vulgaris* cause an elevated pH of urine through generation of ammonia from the enzymatic breakdown of urea. Detecting this increased pH can be achieved using the pH sensor, BTB. At pH below 6, BTB is in its acid form and appears yellow. Above pH 7.6, BTB is reduced to its basic form and turns blue (Figure 5.1.3).

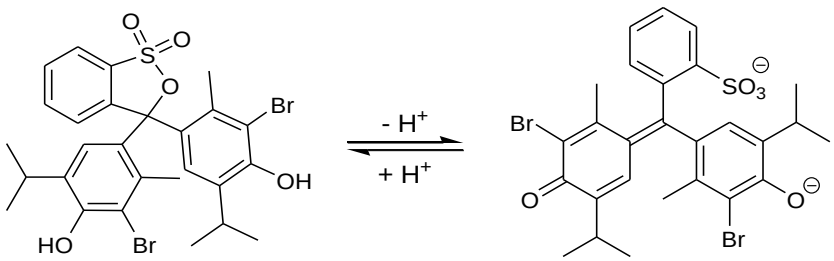


Bromothymol blue
(acid form)
Yellow below pH 6

Bromothymol blue
(base form)
Blue above pH 7.6

**Figure 5.1.3** The structure of BTB in its acid and base forms

The pH sensor BTB has previously been incorporated into a silicone polymer and developed as a sensor device to detect urease positive bacteria in the urine of catheterised patients (Malic et al., 2012).

In this Chapter, BTB will be included in the evaluation of sensor compounds as a positive control for certain urease positive bacteria. Modifications to the structure of the BTB sensor will also be investigated with an aim of reducing the time required for sensor to change colour.

### 5.1.3 Detection of *Pseudomonas aeruginosa* through cytochrome oxidase activity

The 'oxidase test' detects bacterial cytochrome oxidase, following oxidation of the substrate tetramethyl-p-phenylenediamine dihydrochloride (Kovac's reagent) to indophenol, also known as Würster's blue (Figure 5.1.4).

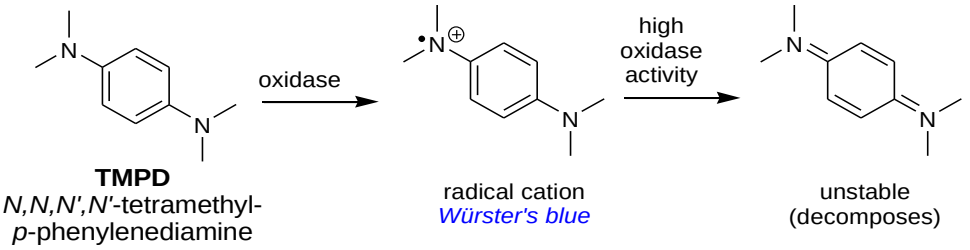


**Figure 5.1.4** Oxidation of tetramethyl-p-phenylenediamine dihydrochloride to indophenol (Würster's blue)

Indophenol is a dark purple product, with a positive test detecting species with cytochrome oxidase (*Pseudomonas*, *Neisseria*, *Vibrio*, *Brucella* and *Pasteurella* species; *Enterobacteriaceae* produce a negative result) (Figure 5.1.5).

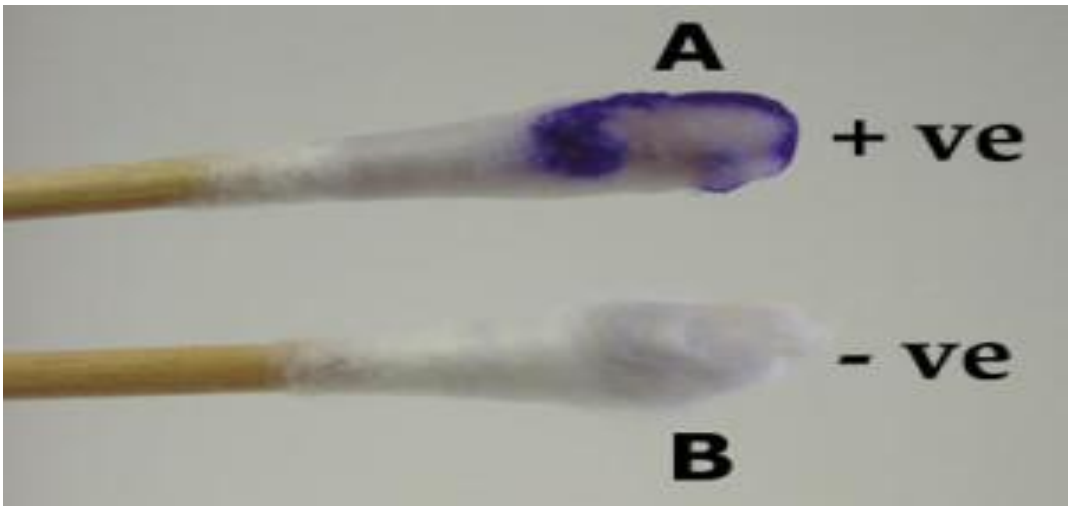


**Figure 5.1.5** Illustration of a positive (A) and negative (B) reaction between Kovac's reagent and *Pseudomonas aeruginosa*

Oxidase test strips containing dehydrated tetramethyl-p-phenylenediamine dihydrochloride are routinely used in diagnostic microbiology laboratories and are hydrated with water to prevent auto-oxidation of the substrate. Ascorbic acid (0.1%) can be added to solutions of Kovac's reagent to prevent its oxidation. Iron can catalyse oxidation of phenylenediamine and can give rise to false positives. Therefore, it is essential that platinum loops are used for the removal of bacteria from agar plates and cultures on grown on blood-free substrates (*Oxidase Test. UK Standards for Microbiology*, 2019).

### 5.1.4 Detection of microorganisms by metabolic activity using tetrazolium compounds

Tetrazolium compounds are commonly used to determine microbial metabolic activity and cell viability (Isa et al., 2014). NADPH-dependant cellular oxidoreductase enzymes reduce tetrazolium salts to insoluble coloured formazan products (Figure 5.1.6). Such products can be solubilised using acid or alcohol solutions. Possibly the most widely used tetrazolium compound is 3-(4,5-dimethylthiazol-2-yl)-2,5-diphenyltetrazolium bromide (MTT) and experiments in this Chapter will evaluate MTT alongside three novel tetrazolium compounds (produced by the School of Chemistry, Cardiff University), as bacterial sensor molecules.

A device using MTT and phenazine methosulphate to detect viable bacteria in water samples has previously been developed. However, this spectrometry device required the addition of reagents by the end user before a result can be obtained (Liao et al., 2020).

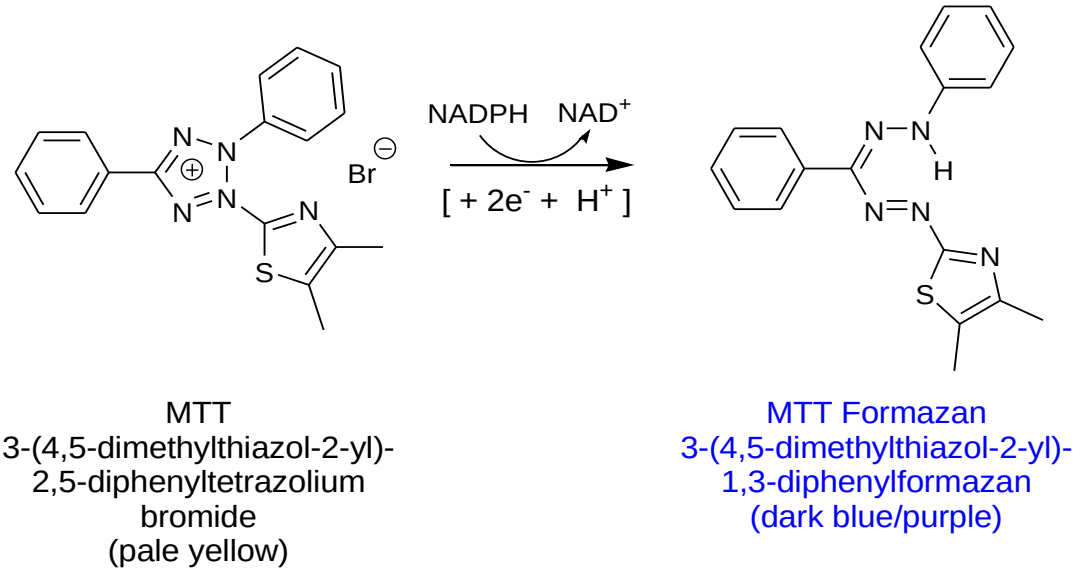


**Figure 5.1.6** Reduction of 3-(4,5-dimethylthiazol-2-yl)-2,5-diphenyltetrazolium bromide (MTT) by cellular reductase enzymes

### 5.1.5 Detection of microorganisms by dehydrogenase enzymic action and resazurin

Resazurin, commercially known as Alamar blue, is a water-soluble blue dye, which upon loss of a single oxygen atom from the activity of bacterial dehydrogenase enzymes, is converted to a pink, fluorescent resorufin, and this change is irreversible by atmospheric oxygen (Figure 5.1.7). Resorufin is further reduced to a colourless product (hydroresorufin), which can then be reversed by atmospheric oxygen. This reduction reaction readily occurs in the presence of metabolically active cells and has been extensively used to assess cell viability, growth and toxicity (Elavarasan et al., 2013; Reagent, 2004). Specific uses of resazurin include monitoring microbial contamination of milk and assessing semen quality (Carter et al., 1998; Chabo et al., 2000).

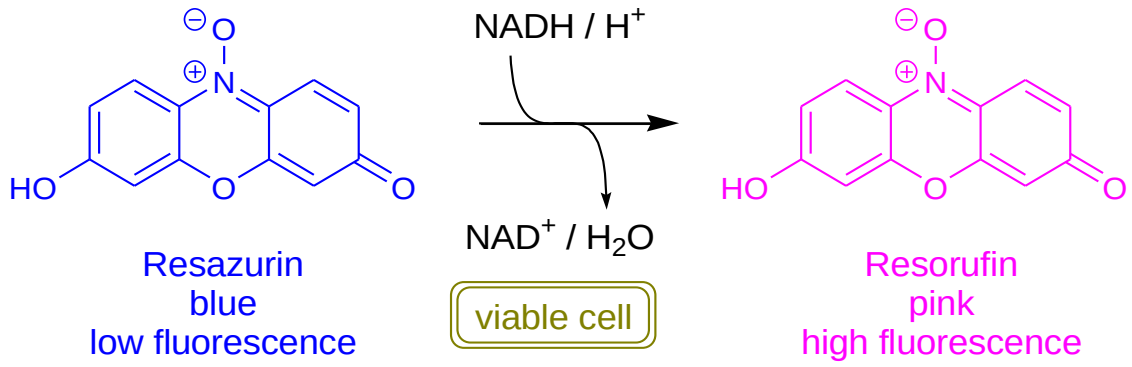


**Figure 5.1.7** Cellular reduction of resazurin

Resazurin assays correlate well with other cell viability assays, including tetrazolium-based assays using MTT. Resazurin has the advantage of low cell toxicity and the generation of water-soluble coloured products. The use of resazurin in detecting CAUTI infection has largely been limited to assessments of bacterial viability following antimicrobial treatment in *in-vitro* assays (Townsend et al., 2020).

### 5.1.6 Aims

The aim of this experimental chapter was to identify a range of chemical substrates that would allow detection of key CAUTI causing bacteria. Candidate molecules would be incorporated into suitable materials that would retain the sensing agent and facilitate microbial detection. To achieve this overarching aim, targeted experimental objectives were undertaken as outlined below.

Test compounds were initially evaluated to detect planktonic bacterial species, prior to testing sensor molecules absorbed into filter paper material. A selection of the most promising compounds would then be advanced for incorporation into silicone materials and evaluated in an *in-vitro* culture model using CAUTI causing microorganisms. Structural modifications of an existing BTB sensor would also be investigated, to determine if the time taken for the sensor to signal a urease positive infection could be reduced.

The ideal CAUTI device would allow for rapid and broad-spectrum bacterial detection, be cost effective, user friendly and allow simple interpretation of results. With the exception of BTB, none of the compounds evaluated had previously been

used to detect CAUTIs. Therefore, successful incorporation of one or more into a medical device would represent a novel development.

## 5.2 Materials & Methods

### 5.2.1 Preparation of artificial urine (AU)

The following components were dissolved in 900 ml of deionised $H_2O$ and the pH adjusted to 6.1 with 5 M hydrochloric acid (HCl): calcium chloride (0.49 g), magnesium chloride hexahydrate (0.65 g), sodium chloride (4.6 g), sodium sulphate (2.3 g), trisodium citrate dihydrate (0.65 g), disodium oxalate (0.02 g), potassium dihydrogen phosphate (2.8 g), potassium chloride (1.6 g), ammonium chloride (1.0 g), urea (25.0 g), and gelatin (5.0 g). The solution was passed through a 0.2 μm vacuum filter unit (Sarstedt, Germany) before addition of 100 ml of autoclaved tryptone soy broth (TSB; 10g/l) to give a final concentration of 1 g/l.

### 5.2.2 Preparation of sensor reagents

All compounds were obtained from Sigma, UK, unless otherwise stated. Chemical structures of the candidate sensor compounds are depicted in Table 4.2.1. 4-methylumbelliferyl-β-D-glucuronide (MUG) and chlorophenol red-β-D-galactopyranoside (CPRG) were prepared in Muller-Hinton Broth (MHB), (Oxoid, UK) at 2, 4, and 8 mM. BTB (sodium salt) was prepared as stock solutions at 0.1% and 0.5% (w/v) in MHB, containing 1% (v/v) 1 M citric acid.

The novel tetrazolium salts, triphenyl-tetrazolium phosphate (TTP), 2,6-difluro-triphenyl-tetrazolium phosphate (2,6-diFTTP) and 2,6-dichloro-triphenyl-tetrazolium phosphate (2,6-diClTTP), were obtained from the School of Chemistry, Cardiff University, and MTT (3-(4,5-dimethylthiazol-2-yl)-2,5-(diphenyltetrazolium bromide) were prepared as 10 mM stocks in acetone. MTT was prepared at 1 mM in MHB. Resazurin sodium salt (Oxoid, UK) was prepared as a 0.05% (w/v) solution in sterile distilled water. Tetramethyl-p-phenylenediamine dihydrochloride (Kovacs reagent) was prepared as a 1% (w/v) solution in distilled water. All solutions were filter sterilised using 0.2 μm syringe filter units before use and stored (protected from light) at 4$^{o}$C for up to 2 weeks.

**Table 5.2.1** Chemical structures of candidate sensor molecules

| Sensor | Structure | Sensor | Structure |
|---|---|---|---|
| MTT | 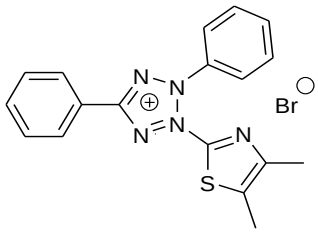 | TTP* | 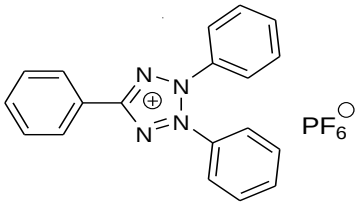 |
| 2,6-diFTTP* | 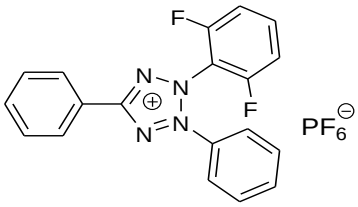 | 2,6-diClTTP* | 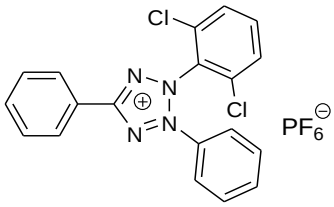 |
| Bromo-thymol blue | 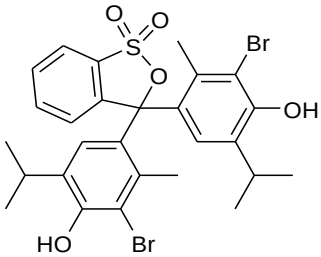 | CPRG | 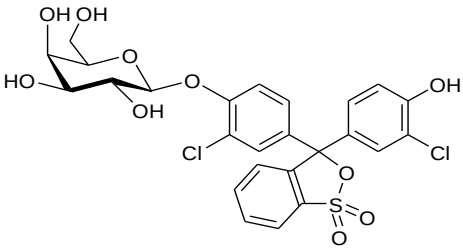 |
| Resazurin | 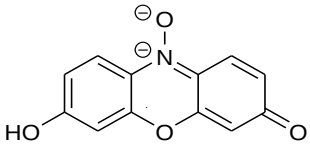 | MUG | 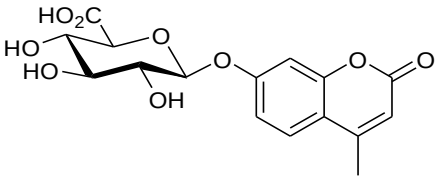 |
| Kovacs Reagent (Würsters blue) | 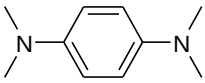 | | |

* Denotes hexafluorophosphate salt which has low water solubility

### 5.2.3 Microorganisms

The microorganisms used to evaluate sensor molecules are listed in Tables 5.2.2. Culture methods and media are described in Section 2.1.2.

**Table 5.2.2** Microorganisms used to evaluate sensor molecules

| **Microorganism (species)** | **Strain** | **Source** |
|---|---|---|
| *Proteus mirabilis* | 12 RTB | Urine or catheter of long-term catheterised patients |
| *Staphylococcus aureus* | NSM 7 | Urine or catheter of long-term catheterised patients |
| *Klebsiella pneumoniae* | P6 wk2 | Urine or catheter of long-term catheterised patients |
| *Providencia stuartii* | NSM 58 | Urine or catheter of long-term catheterised patients |
| *Pseudomonas aeruginosa* | NCTC 10662 | Type strain |
| *Serratia marcescens* | NSM 51 | Urine or catheter of long-term catheterised patients |
| *Candida albicans* | ATCC 90028 | Type strain |
| *Escherichia coli* | NCTC 12923 | Type strain |
| *Escherichia coli* | 9 | Urine, Welsh hospital wards |
| *Escherichia coli* | 16 | Urine, Welsh hospital wards |
| *Escherichia coli* | 17 | Urine, Welsh hospital wards |
| *Escherichia coli* | 18 | Urine, Welsh hospital wards |

NCTC, National Collection of Type Cultures
ATCC, American Type Culture Collection

### 5.2.4 Evaluation of sensor compounds against planktonic microorganisms

#### 5.2.4.1 Determining sensor sensitivity against viable bacteria

Overnight cultures of test bacteria were established in MHB and subsequently diluted with MHB to create microbial suspensions with OD $600_{nm}$ values between 0.01 and 1.0.

The Miles and Misra method (Miles et al., 1938), was used to determine the colony forming units (CFUs) of each culture. Further dilutions were made and 10 μl of these dilutions were spotted in triplicate onto agar plates, before incubation overnight at 37°C. CLED agar was used for *P. mirabilis* and TSA for all other bacterial species. Resulting CFUs were enumerated and calculations per ml, determined, according to dilution factor.

Three separate cultures were set up for each OD 600nm value and calibration curves with line of best fit plotted of OD 600 against CFU using GraphPad Prism. These calibration curves were then used to estimated CFUs present in a sample based on optical density at 600nm.

#### 5.2.4.2 Determination of sensitivity of sensor molecules against planktonic bacteria

Microorganisms were cultured overnight at 37°C in MHB and adjusted to a 0.5 MacFarland standard with culture medium. The inoculum was further diluted 100-fold in MHB. Microtiter plate wells containing 100 μl of inoculum and 100 μl of the test sensor molecule were mixed using a pipette. Wells containing 100 μl of inoculum and 100 μl MHB were used for bacterial growth monitoring, and further controls without bacteria were also prepared. Positive reactions between bacteria and sensor molecules were monitored by reading absorbances at hourly intervals over a 24 h period in a benchtop plate reader at 37°C (Fluostar Optima, BMG Labtech).

The production of chlorophenol red (CR) from CPRG due to β-galactosidase positive bacteria was measured by reading absorbance at 570 nm. Final CPRG concentrations of 1, 2, 4, and 8 mM were used to assess CR development induced by test microorganisms. Specificity of the bacteria able to generate CR was determined using 12 CAUTI causing microorganisms (Table 5.2.2).

Absorbance at 570 nm for wells with bacteria, but without sensor molecule, were subtracted from absorbance values of bacteria with sensor. This allowed the plotting of the subtracted absorbance value representing the enzyme-substrate reaction. Images of the microtiter plates (visual result) after 24 h were obtained using a smartphone.

Absorbance at 570 nm was also used to measure formazan production after reduction of MTT by bacteria. Final MTT concentrations of 0.1 and 0.2 mM were assessed against two test strains of bacteria, namely *P. mirabilis* 12 RTB and *E. coli* NCTC 12923. Reduction of the novel tetrazolium compounds (TTP, 2,6-diFTTP and 2,6-diClTTP) by these bacteria to formazan compounds was measured by changes in OD490 nm. Final absorbance values were adjusted for bacterial growth, as described previously.

BTB was used to detect elevated pH due to urease positive bacteria in AU, by measuring absorbance changes at 590 nm. BTB was used at final concentrations of either 0.01 or 0.05% (w/v) and *Proteus mirabilis* as the test species and *E. coli* NCTC 12923 as a control. As previously described, absorbance values were adjusted to account for bacterial growth. Reduction of resazurin to resorufin by bacteria was determined by calculating the absorbance difference between resazurin (600 nm) and resorufin (570 nm). Final resazurin concentrations of 0.005% (w/v) were used against the test strains of *P. mirabilis* 12 RTB and *E. coli* NCTC 12923.

The fluorescent MU molecule produced following cleavage of MUG by β-glucuronidase positive bacteria was detected by measuring fluorescent intensity (FI) using 340/460 nm excitation and emission filters. Final MUG concentrations of 1, 2, 4 and 8 mM were used to assess MU production by test microorganisms. The specificity of MUG detection was determined using 12 bacterial species/strains (Tables 5.2.2). Assays were performed in black microtiter plates (Thermofisher) to prevent ‘crosstalk’ between wells. Microtiter plates were visualised in a UV light viewing cabinet (365nm, Cole-Palmer) and images captured with a camera.

Bacterial growth curves were generated from the absorbance values (600 nm) of wells with bacterial cultures and without sensor molecules at hourly intervals.

The time of visible signal detection for each sensor was recorded, as well as the OD 600 nm from the bacterial growth curves. The number of CFUs present at the time of signal was estimated from previously generated calibration curves of OD 600nm against CFU/ml.

#### 5.2.4.3 Determination of absorbance thresholds for sensor molecules

Where positive reactions were achieved for bacteria with test sensor molecule, the coloured product was serially diluted 1:10 with the stock sensor solution to create a colour gradient of positive to negative reaction colour. The well where a positive reaction was visualised was noted, and the plate read at the appropriate wavelength for the sensor molecule. The absorbance value for this well was set as the detection threshold, where a positive reaction was deemed as being at or above that value.

### 5.2.5 Evaluation of candidate sensor compounds in a filter paper model

#### 5.2.5.1 Evaluation of 4-methylumbelliferyl-β-D-glucuronide (MUG) and chlorophenol Red-β-D-galactopyranoside (CPRG) as filter paper sensor materials

To assess MUG as an *E. coli* sensor within a material, 20 mm x 20 mm squares of mini-trans blot filter paper (Bio-Rad, UK) (sterilised by autoclaving), were placed into the wells of a 12-well plate. A 300 μl volume of 2 mM MUG was pipetted onto the material which was then allowed to dry for 1 h.

Bacterial suspensions of *E. coli* NCTC 12923 and *P. mirabilis* 12 RTB (negative control) were cultured overnight in MHB and adjusted to a 0.5 MacFarland standard and 300 μl of the suspensions added to the appropriate wells. Filter paper with MUG or bacteria only were set up as controls. Plates were incubated at 37 ºC for 24 h before visualisation using UV light.

Disks of mini trans-blot filter paper (Bio-Rad, UK) were cut using a hole punch (4 mm diameter) and sterilised by autoclaving. The filter paper disks were placed into individual wells of a 96-well microtiter plate, before 20 μl of CPRG (2 mM) was pipetted directly on to the filter paper and allowed to absorb. The sensor solution was allowed to dry in the filter paper for 2 h.

Overnight cultures of *E. coli* 12923 were adjusted to 0.5 MacFarland standard and serially diluted, as previously described. Twenty μl of each dilution was added to the filter paper containing the sensor molecule. A bacteria-free well was set up as a control and incubation was at 37ºC for 24 h. The filter paper disks were visualised by eye and images captured with a digital camera.

#### 5.2.5.2 Evaluation of 4-methylumbelliferyl-β-D-glucuronide (MUG) in a dual-species infection model

To determine the ability of MUG to detect *E. coli* within a mixed-species culture, a filter paper screen was established using 4 mm filter paper disks as previously described. Twenty-μl of MUG (2 mM) was pipetted directly on to the surface and allowed to dry for 2 h. Cultures of 8 microorganisms (Table 5.2.2) were prepared by overnight incubation at 37ºC in MHB and these were adjusted to a 0.5 MacFarland standard with MHB. Seven cultures were prepared containing equal volumes of *E. coli* NCTC 12923, plus one other organism known to cause catheter related infections. A 20 μl volume of each culture was pipetted on to the MUG-soaked filter paper disk. A culture of *E. coli* was also added to a MUG containing disk and a bacteria-free control was prepared. Following 24 h incubation at 37ºC, the plate was viewed under UV light and images captured using a camera.

#### 5.2.5.3 Evaluation of tetramethyl-p-phenylenediamine dihydrochloride (Kovacs reagent) as a Pseudomonas aeruginosa sensor molecule

One hundred μl of tetramethyl-p-phenylenediamine dihydrochloride was prepared as previously described (Section 5.2.2), and pipetted on to a filter paper disc. Colonies of *Pseudomonas aeruginosa*, *Klebsiella pneumoniae*, *Escherichia coli* and *Proteus mirabilis* were removed from tryptone soya agar (or CLED agar plates for *P. mirabilis*), with sterile plastic loops and spread directly on to the filter paper. A colour change from colourless to purple within 10 s was indicative of a positive test for cytochrome oxidase containing bacteria.

#### 5.2.5.4 Evaluation of additional candidate sensor molecules absorbed on to filter paper discs

Filter paper disks prepared as described in Section 5.2.5.1, were saturated with 20 μl of sensor solution and allowed to dry in the filter paper for 2 h. Sensor solutions tested were MUG (2 mM), TTP (1 mM), 2,6-diFTTP (1 mM), 2,6-diClTTP (1 mM), resazurin (0.015% w/v), Kovacs reagent (1% w/v) and MTT (1 mM).

A panel of 7 CAUTI causing bacteria and *Candida albicans* (Table 5.2.2) were cultured overnight at 37ºC in MHB and adjusted to a 0.5 MacFarland standard with MHB and further diluted ten-fold to give approximately $10^7$ CFU/ml. Twenty μl of each inoculum was pipetted on to the disks containing the sensor solutions, enabling each sensor molecule to be screened against each microorganism. Filter paper disks containing sensor solutions and 20 μl of MHB without microorganisms were set up as controls. Images were captured following incubation at 37ºC for 24 h.

### 5.2.6 Evaluation of candidate sensor molecules incorporated into polymers

#### 5.2.6.1 Bromothymol blue (BTB) sensor production

A silicone base was created using silicone polymers of varying chain lengths and a fumed silica product. Note, the exact formulation is protected under European Patent No. 1 761 162. A 10% (w/v) solution of BTB was prepared in distilled water and gently warmed whilst the solution was mixed using a magnetic stirrer ,until the BTB had completely dissolved.

Two sub-bases (A and B) were prepared using the pre-prepared silicone base. Part A required addition of a platinum catalyst (platinum cyclovinylmethylsiloxane, Silanes and Silicones, Stockport, UK), BTB solution and cetyltrimethylammonium bromide (CTAB, Sigma, UK). Part B contained silicone base, BTB solution, trimethylsiloxy-terminated-methylhydrosiloxane-dimethyl siloxane copolymer (HMS-301, Gelest, USA) cross-linker and CTAB. Both sub-bases were initially manually mixed, followed by a 3 min mixing cycle using a vacuum mixer (Obodent, Vacudent). The mixtures were fully removed from the sides of the vessels and mixed for a further 3 min with a vacuum mixer. Twenty ml of sub-base A and sub-base B were loaded into each side of a dual cartridge using syringes and a mixing nozzle attached to the end of the cartridge.

Approximately 20 ml of the mixed silicone formulation was injected into the centre of a stainless-steel mould (100 x 100 x 2 mm) that had been pre-coated with wax-release spray (Medimould, Cardiff, UK). The mould was sealed by addition of the top section and screwed into place. The material was cured for 1 h at room temperature, prior to the mould being released. The silicone material was soaked in water for 5 min followed by a 1 min wash in 100 % ethanol and a further 1 min wash in water. The material was air dried on lint-free tissue.

#### 5.2.6.2 Production of a porous bromothymol blue (BTB-P) silicone material

The BTB silicone formulation described above was used to create a porous BTB material with increased surface area. Briefly, part A and part B were added at a 1:1 ratio and double the weight of a coarse sugar (940 – 1000 μm; Sudzucker, Germany), which was rapidly mixed into the silicone and packed tightly into a mould pre-coated with wax-release spray. The top of the mould was secured firmly, and the silicone cured for 2 h at room temperature. Following removal of the material from the mould, the silicone was irrigated with warm water to dissolve the sugar crystals and washed for 2h 30 min at 90°C without detergent. The wash cycle was repeated three times and the material transferred to a bench-top steamer (Kitdget, 3 x 30 min cycles). Silicone was dried in a drying oven (Hendi) for 3 h, or until completely dry.

#### 5.2.6.3 Production of chlorophenol red-β-D-galactopyranoside (CPRG) and resazurin sensor materials

Stock solutions (1% w/v) of both CPRG and resazurin were prepared in distilled water. CPRG and resazurin materials were prepared using the silicone base used in the production of the BTB sensor. Parts A and B were prepared as described for the BTB sensor, substituting the BTB solution with either CPRG or resazurin solution. The mixing and curing protocols were as described in Chapter 3. A porous CPRG silicone sensor material was prepared using the method described in Section 5.2.6.2.

#### 5.2.6.4 Production of a resazurin polyurethane foam sensor material

A polyurethane foam containing a final resazurin concentration of 0.63% (w/w) was produced using the FlexFoam-iT ™ III System (Smooth-On, Pensylvania, USA). Briefly, a 1% (w/v) resazurin solution in water was added to FlexFoam III

part B to create a final 0.1% (w/w) resazurin part B. FlexFoam III part A was added to part B in a ratio of 5.75:10 followed by thorough manual mixing. The mixture was allowed to expand into a foam and cured at room temperature for 30 min before handling.

#### 5.2.6.5 Evaluation of polymer sensor materials in an *in-vitro* batch model

Silicone polymer coupons were cut from 2 mm deep slabs using an 8 mm diameter cork-borer. Resazurin foam was cut into roughly 8 x 8 x 6 mm cubes using a sterile scalpel.

Cultures of *P. mirabilis* 12 RTB were established in MHB and incubated for 16 h at 37 ºC before centrifugation at 4000 rev/min in a bench-top centrifuge (IEC CL10, ThermoFisher Scientific) and replacement of the broth with AU. Cultures were diluted to 0.3 $OD_{600}$ with AU, and 800 μl of culture was added to wells of a 24-well plate.

Silicone coupons or resazurin foam pieces were placed into wells containing inoculum and incubated at 37ºC. At time-points between 1 h and 24 h, the plates were removed, and images captured using a smartphone. Additional identical wells were prepared without sensor material and 10 μl of these was removed at each time-point for determination of CFUs, using the Miles and Misra method (Miles et al., 1938). The pH of the AU from these wells were recorded using a benchtop pH meter (Hanna Instruments, Bedfordshire, UK). Bacteria-free wells were set up as controls and the experiment was repeated on 3 separate occasions.

## 5.3 Results

### 5.3.1 Evaluation of sensor compounds against planktonic microorganisms

Growth of planktonic microorganisms in Muller-Hinton broth (MHB) or artificial urine (AU), was monitored by recording the optical density (OD) at 600 nm over a 24 h period (Figure 5.3.1).

The colony forming units (CFUs) present in cultures over a range of OD values were determined, as described in Section 5.2.4.1 and correlation curves of OD 600 nm against CFU/ml were plotted (Figures 5.3.1 and 5.3.2). These plots were subsequently used to estimate the CFUs of microorganisms present in cultures at the time a candidate sensor molecule produced a detectable signal. The assessments of the candidate sensor molecules performed in this Chapter are summarised in Tables 5. 3. 1 and 5.3.2.

#### 5.3.1.1 Evaluation of chlorophenol red β-galactopyranoside (CPRG) as a sensor for coliform bacteria

Detection of coliform bacteria was assessed using the candidate sensor molecule CPRG, which upon reaction with β-galactosidase, would generate the water-soluble product CR that would be visually detectable. An absorbance 570nm value of CR above 1.5 was deemed to be readily detected by eye.

All tested β-galactosidase negative species (*S. aureus*, *S. marcescens*, *P. stuartii*, *P. mirabilis*, *P. aeruginosa* and *C. albicans*) produced signals below the visible threshold at all CPRG concentrations tested (1-8 mM) (Figures 5.3.4 to 5.3.7).

*Klebsiella pneumoniae*, a β-galactosidase positive species, produced positive reactions with CPRG at all test concentrations (Figures 5.3.4). For 8 mM CPRG, the visible detection threshold for CR was achieved after 7 h. The detection time increased to 9 h when CPRG was used at 1 mM. At these detection times, it was established that *K. pneumoniae* was at a level of 9 x $10^8$ CFU/ml.

Figure 5. 3.14 shows the specificity of CPRG for several coliform bacteria, and positive reactions with *E. coli* and *K. pneumoniae*.

Five strains of *E. coli* were used to assess CPRG sensitivity (time of detection) and this varied between strains. CPRG (8 mM) was found to signal detection of *E. coli* strains between 5.5 h and 10 h (Figures 5.3.8–5.3.10). Growth and calibration curves were used to calculate CFUs at the time of detection and showed that positive signals occurred when between 2.5 x $10^8$ and 1 x $10^9$ CFU/ml were

present (Tables 5.3.1 and 5.3.2). Increasing the concentration of the CPRG from 1 to 8 mM was found to lower the detection time for 4 of the *E. coli* strains by 1-2 h. However, CPRG at 8 mM reduced detection time for *E. coli* 16 by 8 h compared with 1 mM CPRG (Figure 5.3.9).

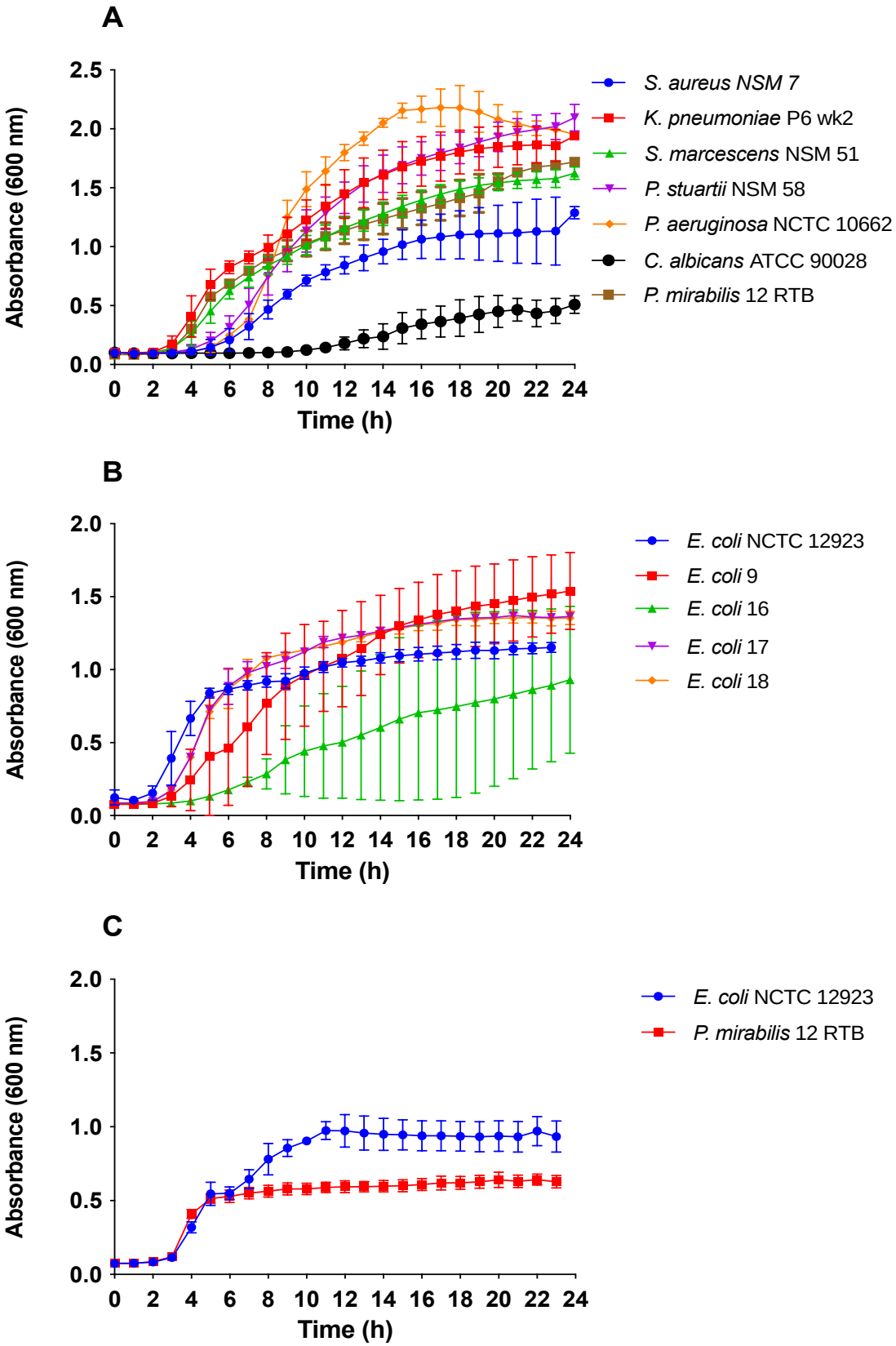


**Figure 5.3.1** Growth of test species monitored at absorbance 600 nm over 24 h. Graphs A and B represent microorganisms cultured in Muller-Hinton broth. Graph C represents bacteria grown in artificial urine. Error bars represent SD

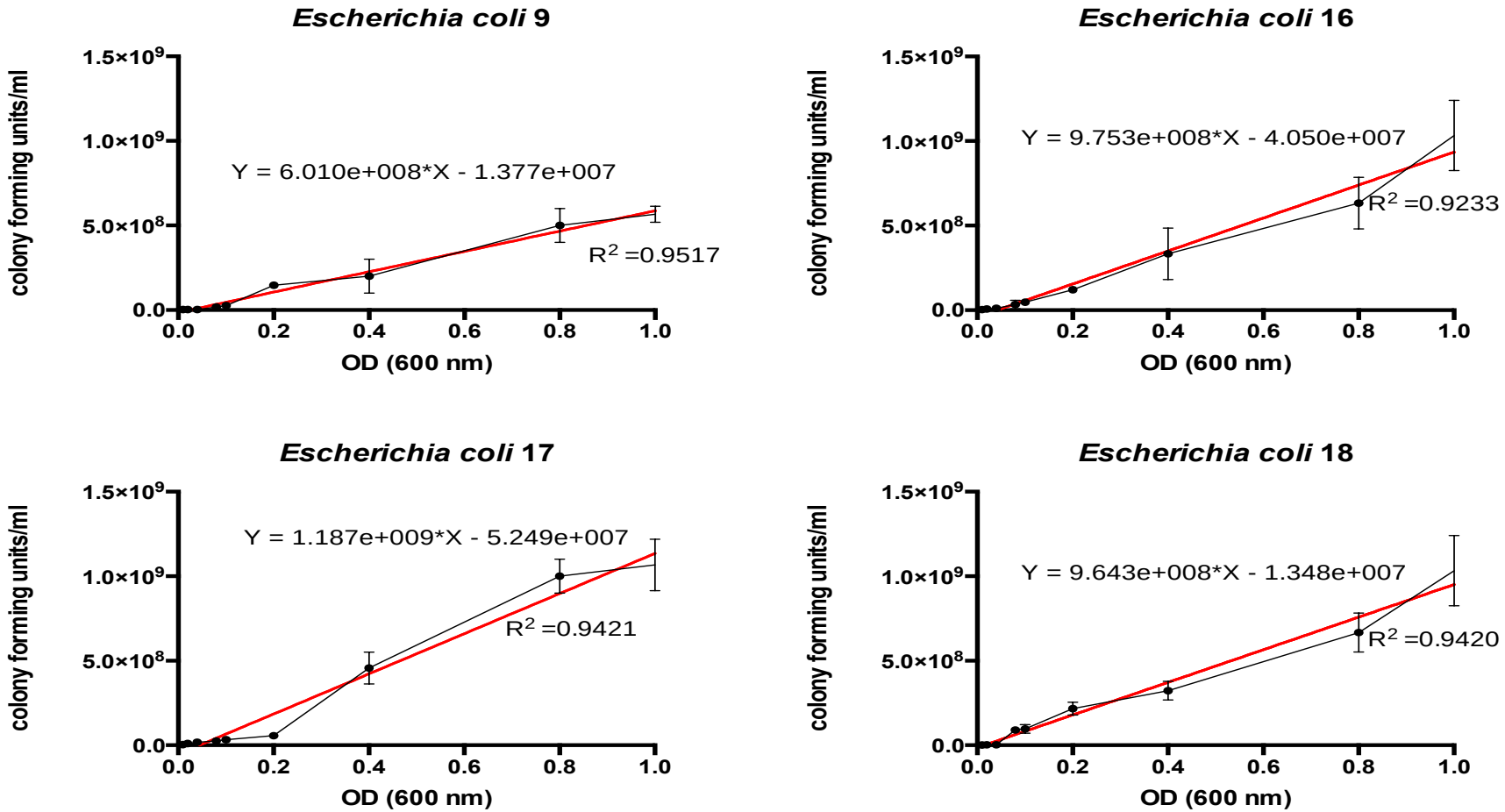


**Figure 5.3.2** Correlation curves of colony forming units (CFU) against optical density at 600 nm for 4 *Escherichia coli* strains. The plots were used to determine the CFU present in reactions between bacteria and sensor molecules based on optical density at 600 nm. Means of 3 independent experiments were plotted with error bars representing SD

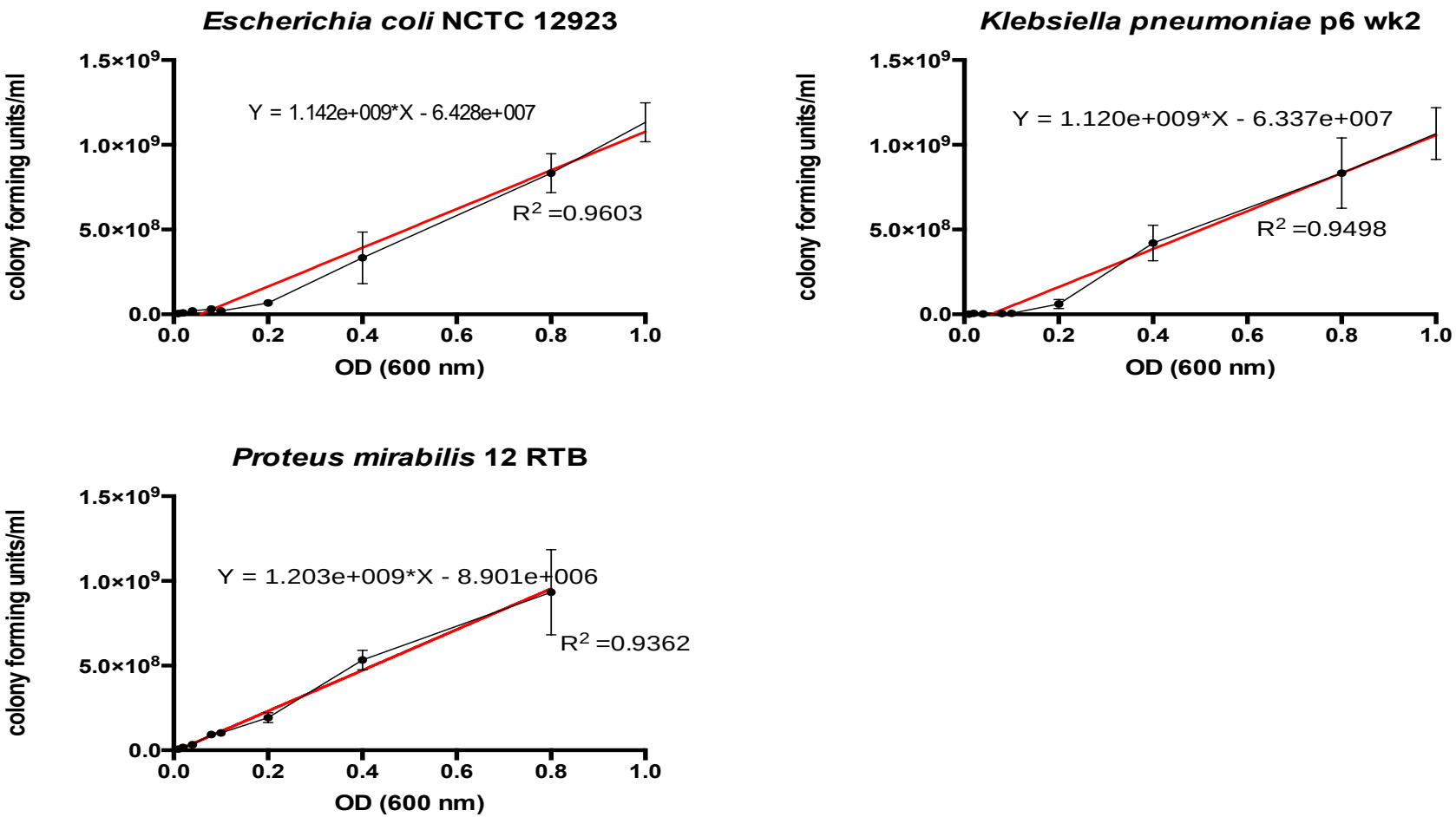


**Figure 5.3.3** Correlation curves of colony forming units (CFU) against optical density at 600 nm for *Escherichia coli* NCTC 12923, *Klebsiella pneumoniae* p6 wk2 and *Proteus mirabilis* 12 RTB. The plots were used to determine the CFU present in reactions between bacteria and sensor molecules based on the optical density at 600 nm. Means of 3 independent experiments were plotted with error bars representing SD

**Table 5.3.1** Colony forming units (CFU)/ml of bacteria at the time of detection using selected sensor compounds.

| Detection thresholds (CFU/ml) of sensor molecules | | | | | | | | |
|---|---|---|---|---|---|---|---|---|
| **Sensor molecule / Bacteria** | **CPRG[1] (8 mM)** | **MUG[2] (1mM)** | **BTB[3] (0.1% w/v)** | **Resazurin (0.005 % w/v)** | **MTT[4] (0.1 mM)** | **TTP[5] (1mM)** | **2,6-diFTTP[6] (1mM)** | **2,6-diClTTP[7] (1mM)** |
| ***E. coli* NCTC 12923** | $9.5 \times 10^8$ | $>9.5 \times 10^8$ | ND | $2.2 \times 10^8$ | $8.5 \times 10^8$ | $>1.05 \times 10^9$ | $1.05 \times 10^9$ | $>1.05 \times 10^9$ |
| ***E. coli* 9** | $2.5 \times 10^8$ | $2.2 \times 10^8$ | NT | NT | $2.7 \times 10^7$ | NT | NT | NT |
| ***E. coli* 16** | $3.5 \times 10^8$ | $8.3 \times 10^8$ | NT | NT | NT | NT | NT | NT |
| ***E. coli* 17** | $1 \times 10^9$ | $>1.1 \times 10^9$ | NT | NT | NT | NT | NT | NT |
| ***E. coli* 18** | $8.5 \times 10^8$ | $>9.5 \times 10^8$ | NT | NT | NT | NT | NT | NT |
| ***K. pneumoniae* P6 wk2** | $9 \times 10^8$ | NT | NT | NT | NT | NT | NT | NT |
| ***P. mirabilis* 12 RTB** | ND | NT | $1 \times 10^8$ | $1.8 \times 10^8$ | NT | $>9 \times 10^8$ | $>9 \times 10^8$ | $>9 \times 10^8$ |
| ***S. aureus* NSM 7** | ND | NT | NT | NT | NT | NT | NT | NT |
| ***P. stuartii* NSM 58** | ND | NT | NT | NT | NT | NT | NT | NT |
| ***S. marcescens* NSM 51** | ND | NT | NT | NT | NT | NT | NT | NT |
| ***P. aeruginosa* NCTC 10662** | ND | NT | NT | NT | NT | NT | NT | NT |
| ***C. albicans* ATCC 90028** | ND | NT | NT | NT | NT | NT | NT | NT |

ND = Not Detected, NT = Not Tested

**1**. chlorophenol red-β-D-galactopyranoside **2.** 4-methylumbelliferyl-beta-D-glucuronide **3.** Bromothymol blue
**4**. 3-(4,5-dimethylthiazol-2-yl)-2,5-(diphenyltetrazolium bromide) **5.** triphenyl-tetrazolium phosphate
**6.** 2,6-difluro-triphenyl-tetrazolium phosphate **7.** 2,6-dichloro-triphenyl-tetrazolium phosphate

**Table 5.3.2** Summary of candidate sensor molecules and their detection of planktonic microorganisms, detection in filter paper and detection in polymers*

| Candidate sensor molecule | Detected planktonic species | Sensitivity (CFU/ml) | Detection in filter paper | Detection in Silicone | Detection in polyurethane foam |
|---|---|---|---|---|---|
| **CPRG[1]** | *E. coli, K. pneumoniae* | $2.5 \times 10^8 – 1 \times 10^9$ | *E. coli* | ND | NT |
| **MUG[2]** | *E. coli* | $2.2 \times 10^8$ – >$1.1 \times 10^9$ | *E. coli* | NT | NT |
| **BTB[3]** | *P. mirabilis* | $1 \times 10^8$ | *P. mirabilis* | *P. mirabilis* | NT |
| **Resazurin** | *E. coli, P. mirabilis* | $1.8 \times 10^8 – 2.2 \times 10^8$ | *E. coli, K. pneumoniae, P. mirabilis, S. marcescens, P. stuartii, S. aureus* | ND | *P. mirabilis* |
| **Kovacs reagent[4]** | NT | NT | *P. aeruginosa* | NT | NT |
| **MTT[5]** | *E. coli* | $2.7 \times 10^7$ - $8.5 \times 10^8$ | *E. coli, K. pneumoniae, P. mirabilis, E. coli, S. marcescens, P. stuartii, S. aureus, P. aeruginosa, C. albicans* | NT | NT |
| **TTP[6]** | *E. coli, P. mirabilis* | >$9.8 \times 10^8$ | *E. coli, K. pneumoniae, P. mirabilis, S. marcescens, P. stuartii, S. aureus, P. aeruginosa* | NT | NT |
| **2,6-diFTTP[7]** | *E. coli, P. mirabilis* | >$9.8 \times 10^8$ | *E. coli, K. pneumoniae, P. mirabilis, S. marcescens, P. stuartii* | NT | NT |
| **2,6-diClTTP[8]** | *E. coli, P. mirabilis* | >$9.8 \times 10^8$ | *E. coli, K. pneumoniae, P. mirabilis, S. marcescens, P. stuartii* | NT | NT |

* Note not all species were assessed with every sensor molecule in every system.

NT= Not tested, ND= Not detected

**1**. chlorophenol red-β-D-galactopyranoside **2.** 4-methylumbelliferyl-beta-D-glucuronide **3.** Bromothymol blue **4.** tetramethyl-p-phenylenediamine dihydrochloride **5**. 3-(4,5-dimethylthiazol-2-yl)-2,5-(diphenyltetrazolium bromide) **6.** triphenyl-tetrazolium phosphate **7.** 2,6-difluro-triphenyl-tetrazolium phosphate **8.** 2,6-dichloro-triphenyl-tetrazolium phosphate

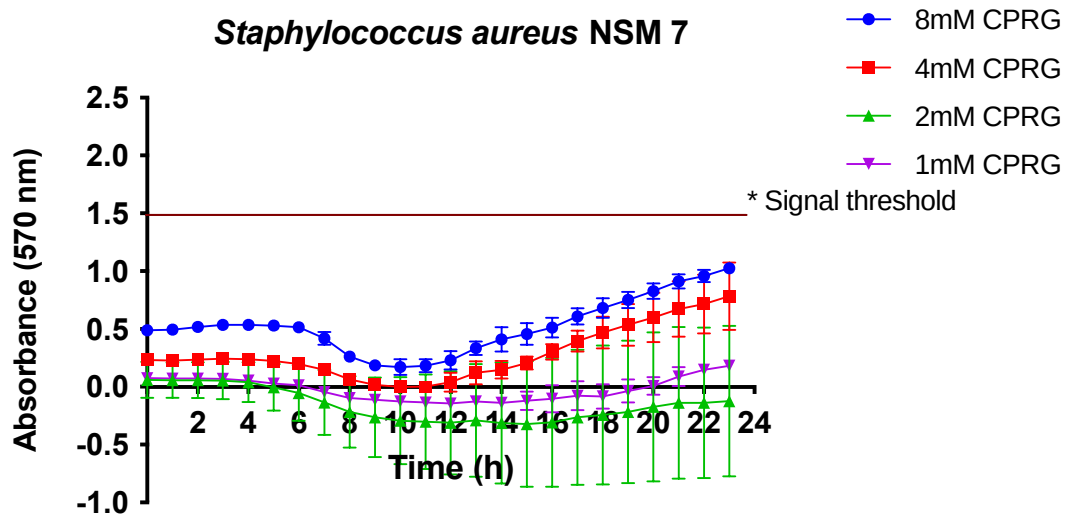


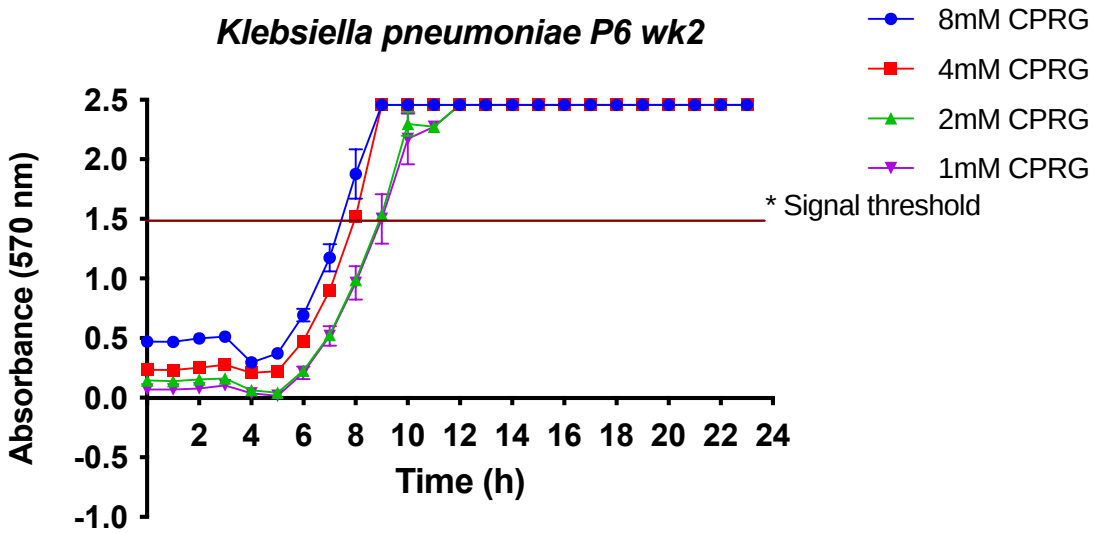


* Chlorphenol red can be visualised above $A_{570\ nm}$ values of 1.5

**Figure 5.3.4** Evaluation of chlorophenol red β-galactopyranoside for detection of test bacteria based on ß-galactosidase production. Values plotted are means from 3 independent experiments. Error bars represent SD

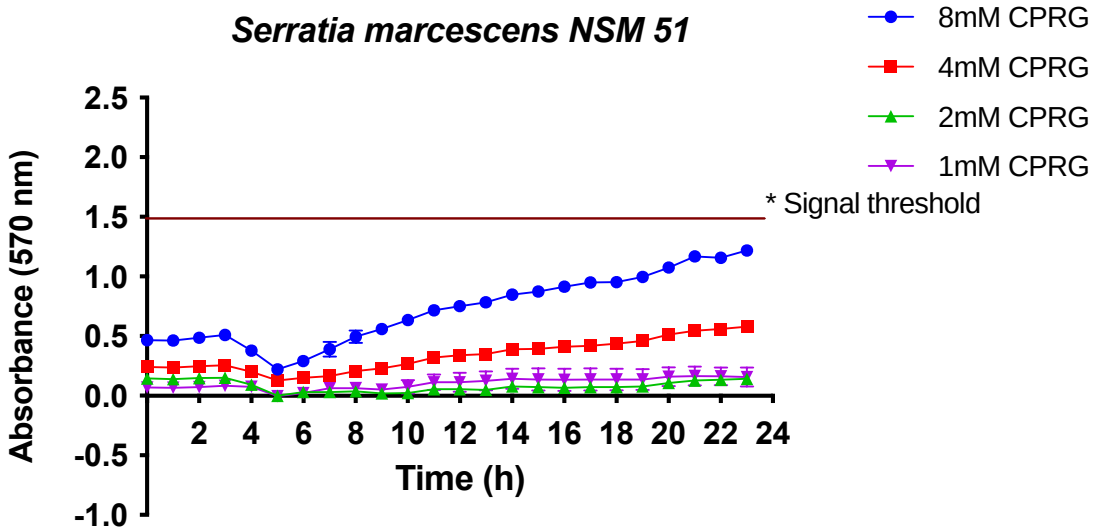


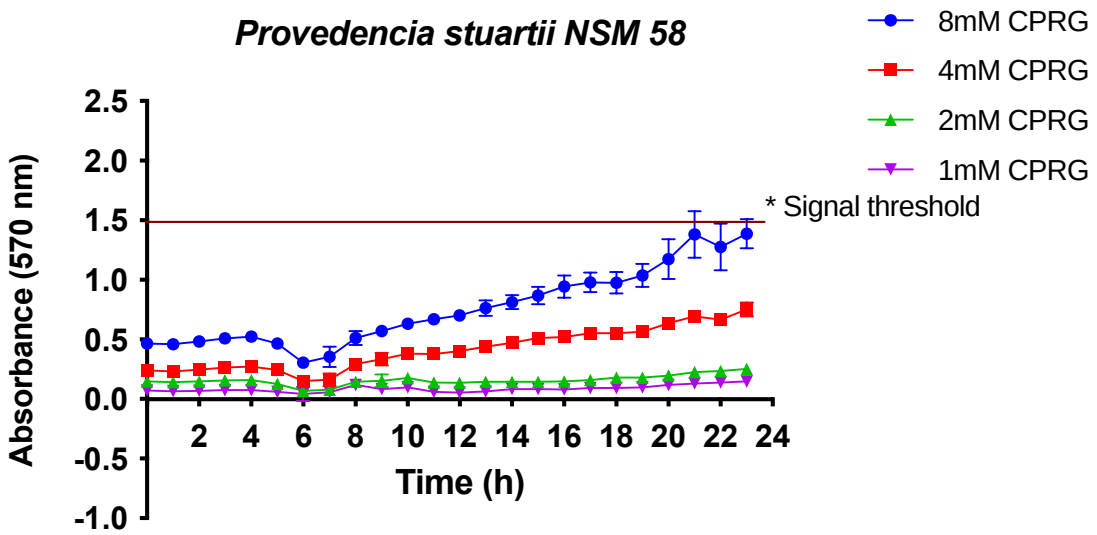


* Chlorphenol red can be visualised above $A_{570\ nm}$ values of 1.5

**Figure 5.3.5** Evaluation of chlorophenol red β-galactopyranoside for detection of test bacteria based on ß-galactosidase production. Values plotted are means from 3 independent experiments. Error bars represent SD

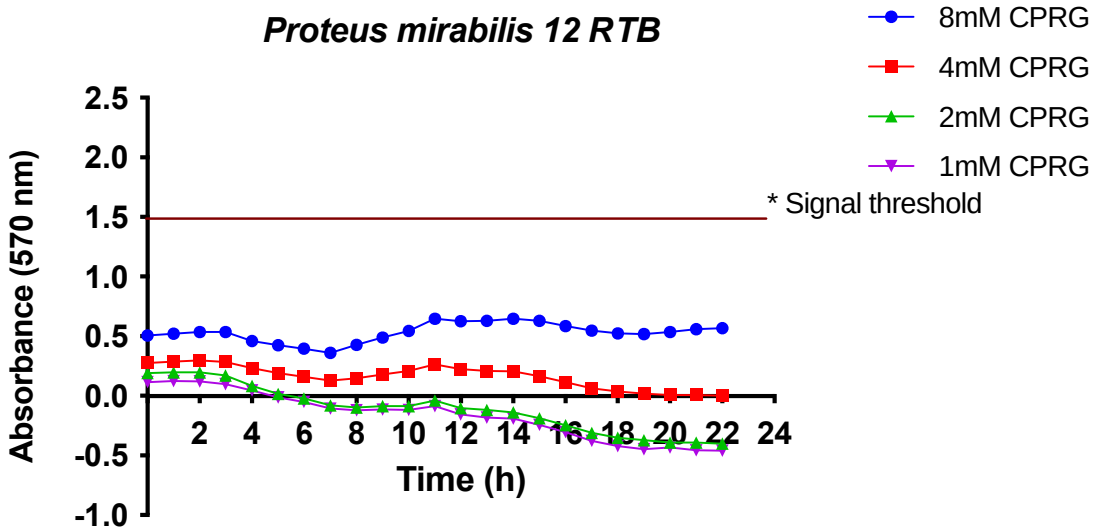


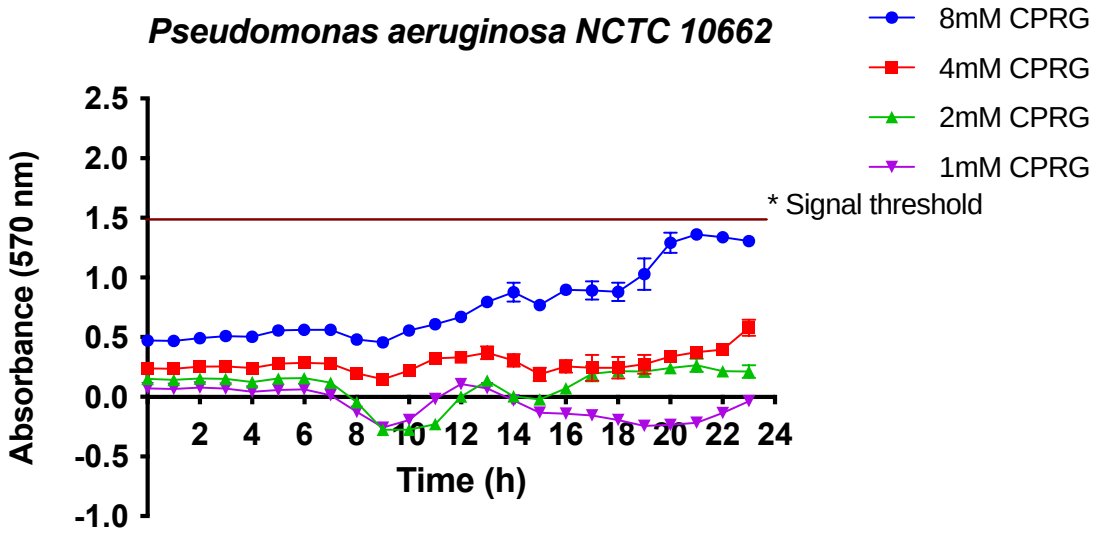


* Chlorphenol red can be visualised above $A_{570\ nm}$ values of 1.5

**Figure 5.3.6** Evaluation of CPRG for detection of test bacteria based on ß-galactosidase production. Values plotted are means from 3 independent experiments. Error bars represent SD

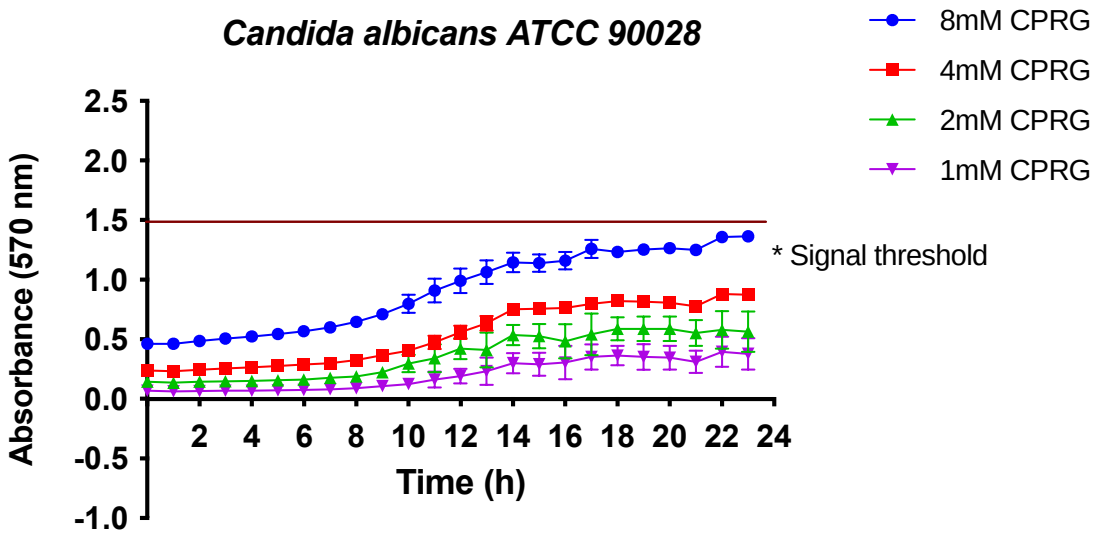


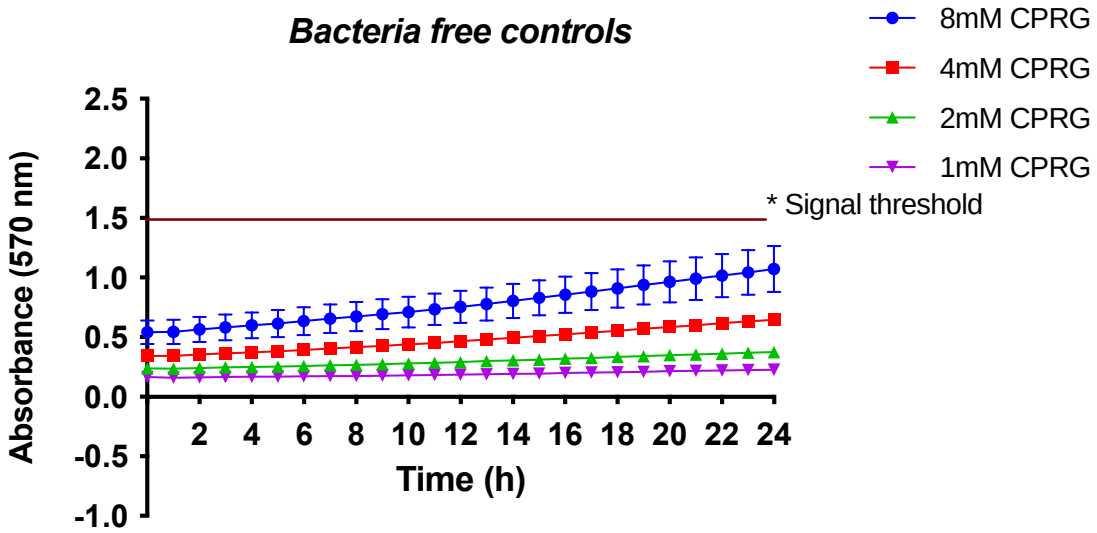


* Chlorphenol red can be visualised above $A_{570\,nm}$ values of 1.5

**Figure 5.3.7** Evaluation of chlorophenol red β-galactopyranoside for detection of test bacteria based on ß-galactosidase production. Values plotted are means from 3 independent experiments. Error bars represent SD

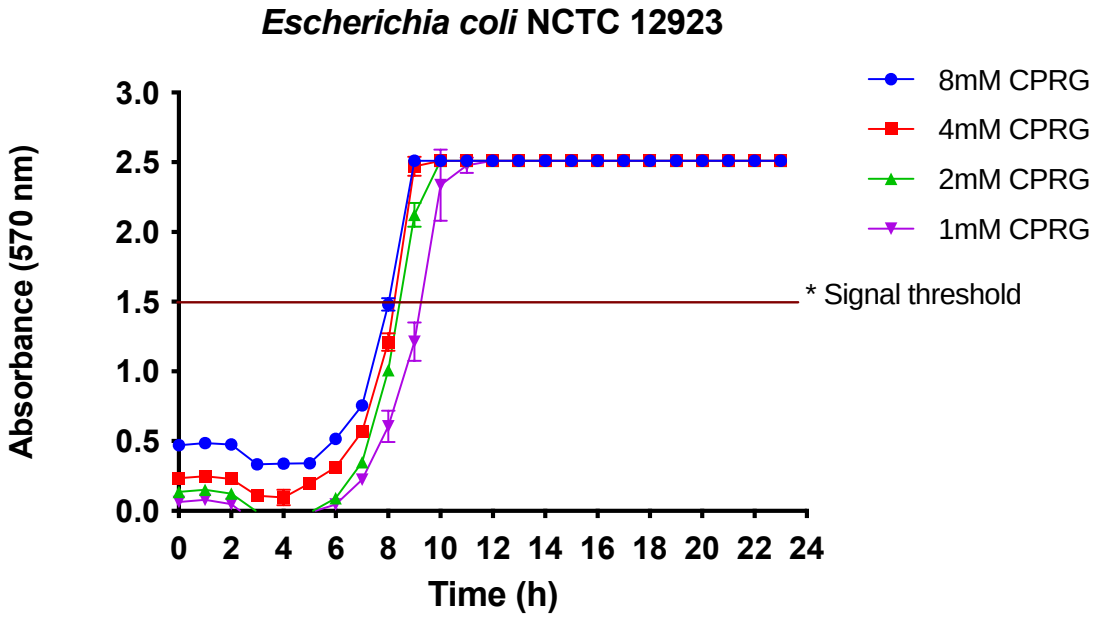


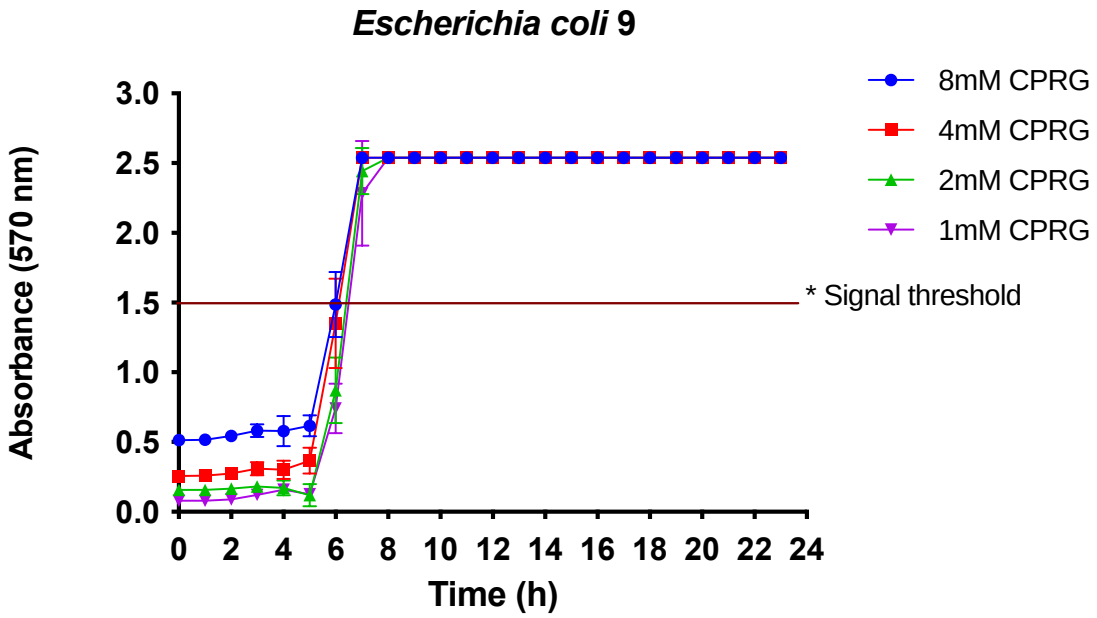


* Chlorphenol red can be visualised above $A_{570\ nm}$ values of 1.5

**Figure 5.3.8** Evaluation of chlorophenol red β-galactopyranoside for detection of *Escherichia coli* using ß-galactosidase activity. Plotted values represent means from 3 independent experiments. Error bars represent SD

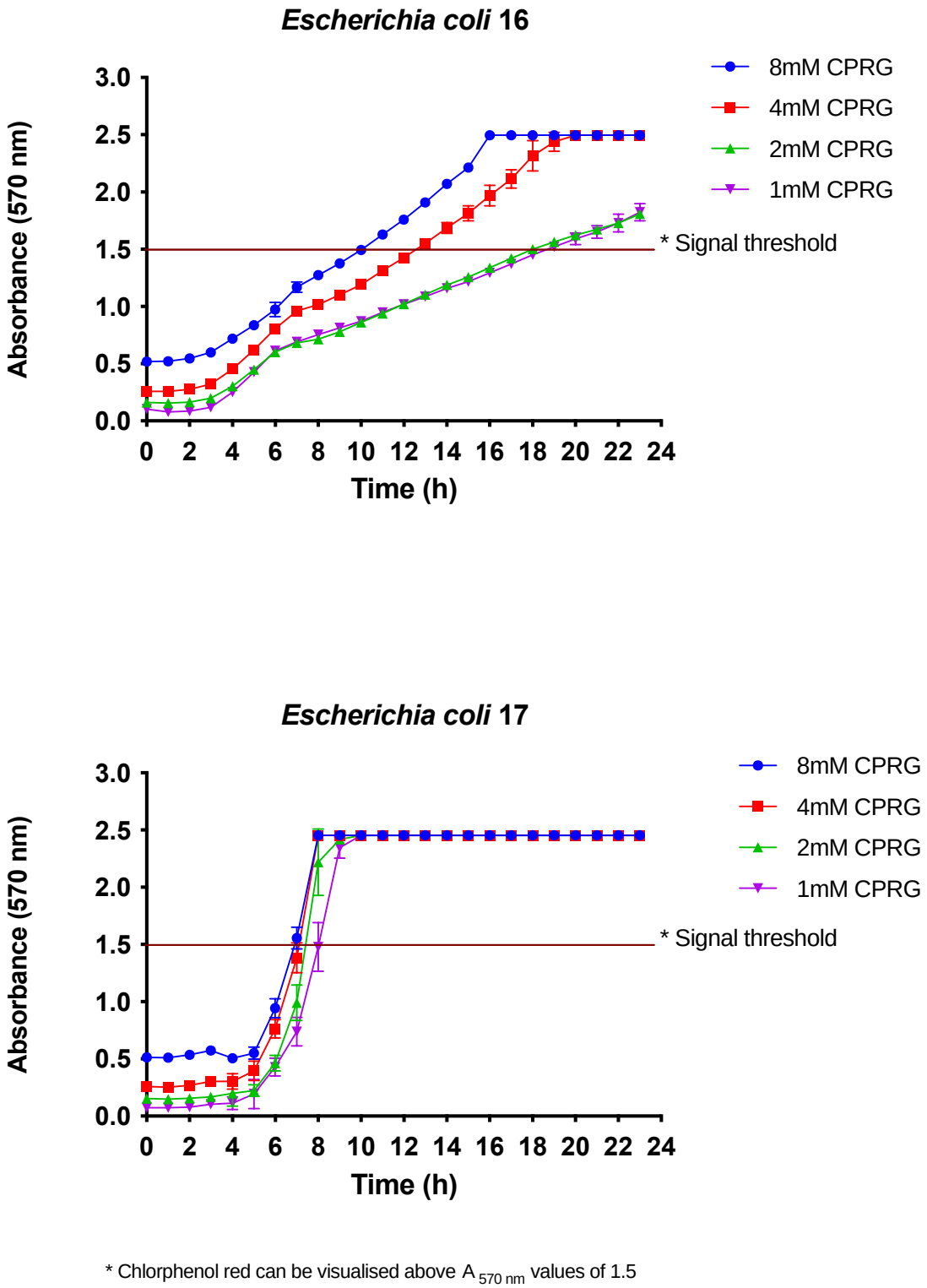


* Chlorphenol red can be visualised above $A_{570\ nm}$ values of 1.5

**Figure 5.3.9** Evaluation of chlorophenol red β-galactopyranoside for detection of *Escherichia coli* using ß-galactosidase activity. Plotted values represent means from 3 independent experiments. Error bars represent SD

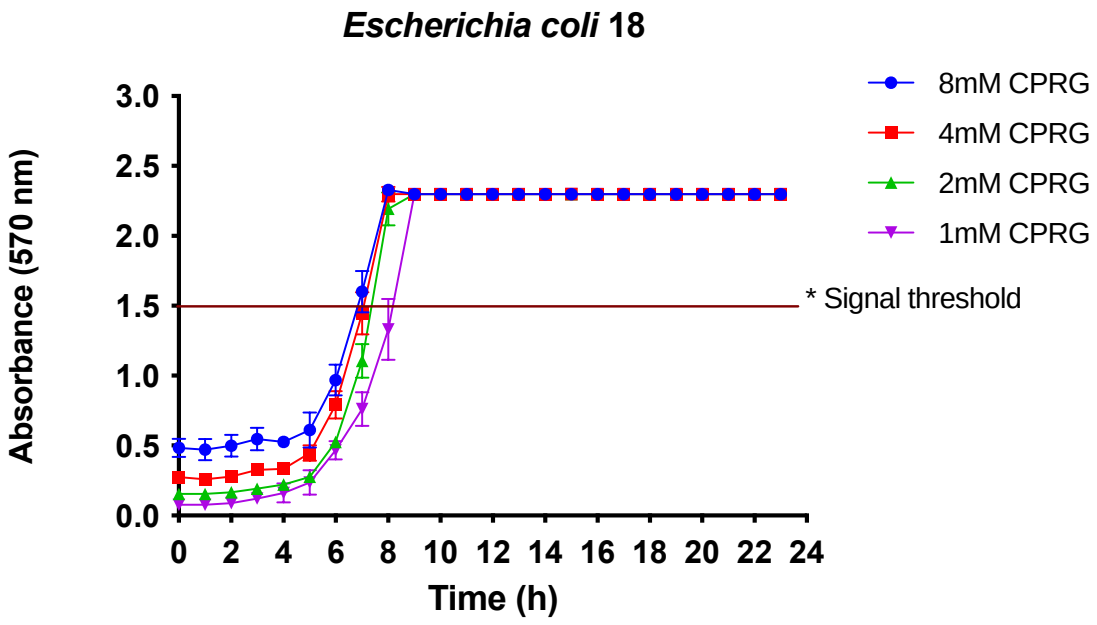


**Figure 5.3.10** Evaluation of chlorophenol red β-galactopyranoside for detection of *Escherichia coli* using ß-galactosidase activity. Plotted values represent means from 3 independent experiments. Error bars represent SD

#### 5.3.1.2 Detection of *E. coli* using 4-methylumbelliferyl-ß-D-glucuronide substrate

Cleavage of the substrate 4-methylumbelliferyl-ß-D-glucuronide (MUG) by β-glucuronidase positive bacteria produces 4-MU that fluoresces blue under UV light. At 340/460nm, fluorescent intensity (FI) above 30 arbitrary units was detectable by eye. Of the 5 *E. coli* strains assessed, only 2 produced strongly visible signals (Figure 5.3.11) The other test strains appeared only weakly detectable at 25 h (Figure 5.3.12 and 5.3.13).

The intensity of the signals produced did not positively correlate with substrate concentration and the optimal substrate concentration appeared to be 2 mM. Of the 2 strains that produced the greatest amounts of florescent product, the detection times were 5.5 h and 17 h, equating to $2.2 \times 10^8$ and $> 9 \times 10^8$ CFU/ml. The strains producing weak signals were detectable between 21 and 25 h with between $8.3 \times 10^8$ to $> 1.1 \times 10^9$ CFU/ml in the cultures at these times.

A fluorescent product was detected for *E. coli* cultures incubated with MUG when viewed under UV light (Figure 5.3.14). Unexpectedly, the *Pseudomonas aeruginosa* also fluoresced under UV light following incubation with MUG for 24 h. The other CAUTI causing microorganisms did not produce a product visible under UV light.

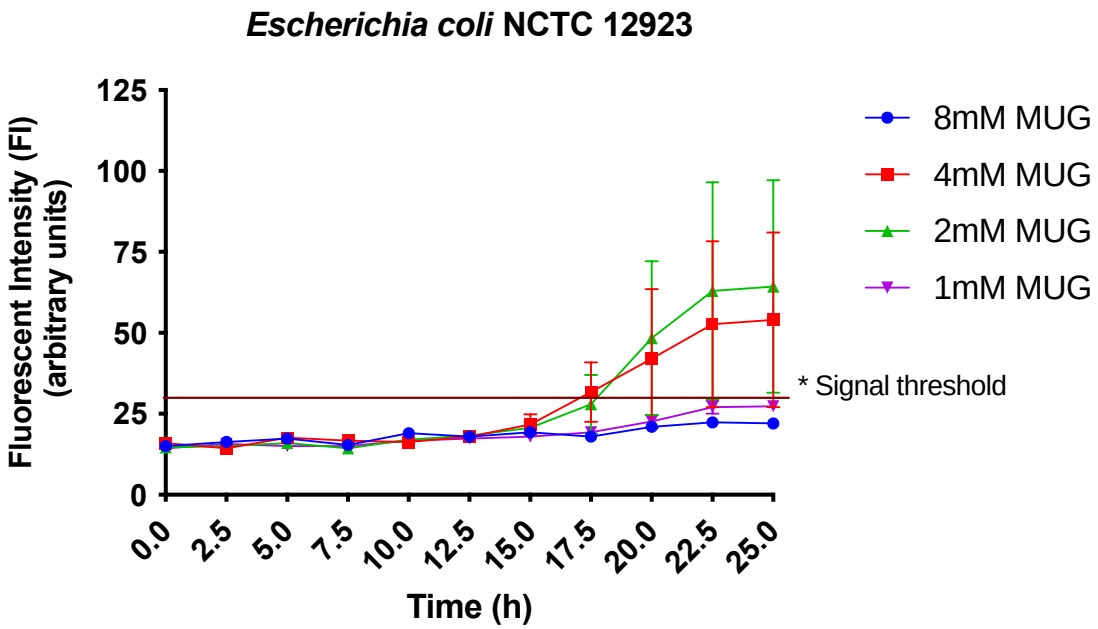


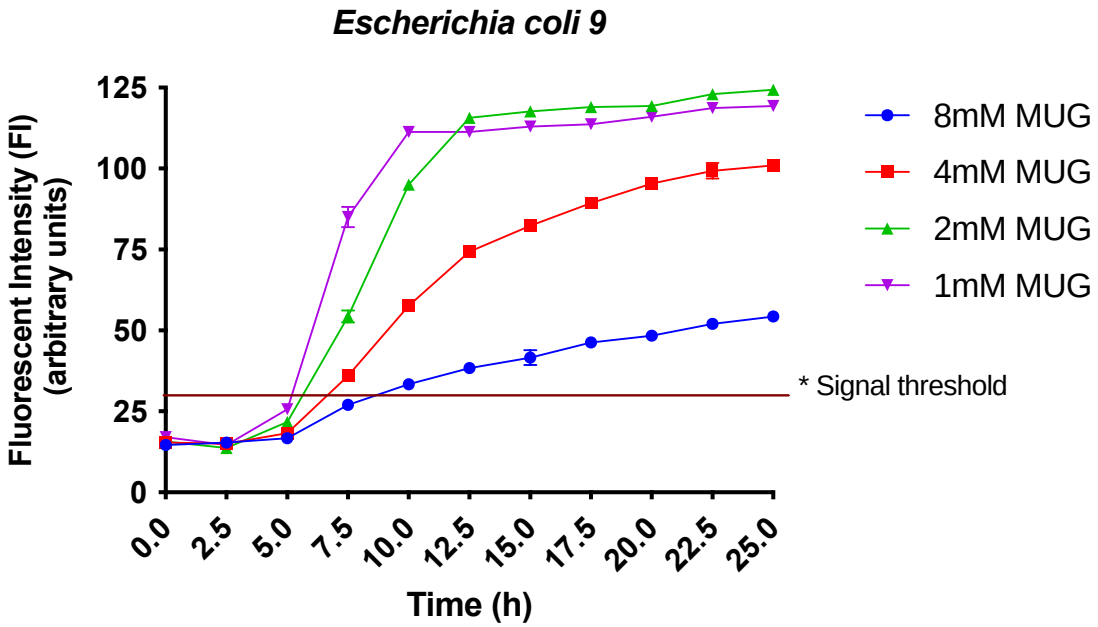


* 4-methyl-umbelliferone can be visualised above FI values of 30

**Figure 5.3.11** Detection of *Escherichia coli* through ß -glucuronidase activity on 4-methylumbelliferyl-ß-D-glucuronide substrate. Plotted values represent means from 3 independent experiments. Error bars represent SD

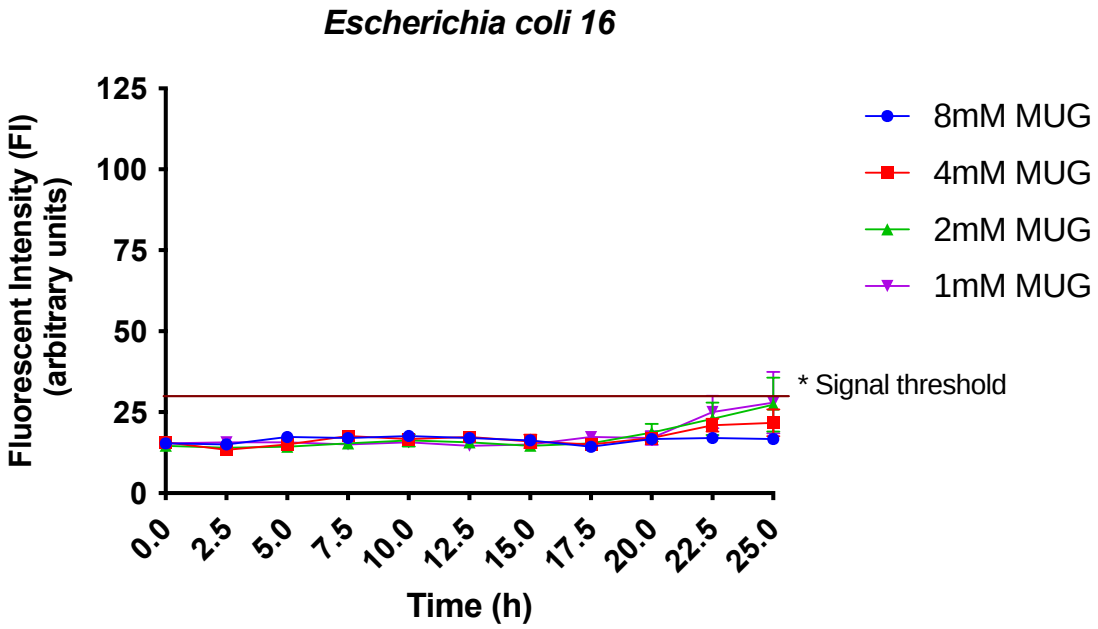


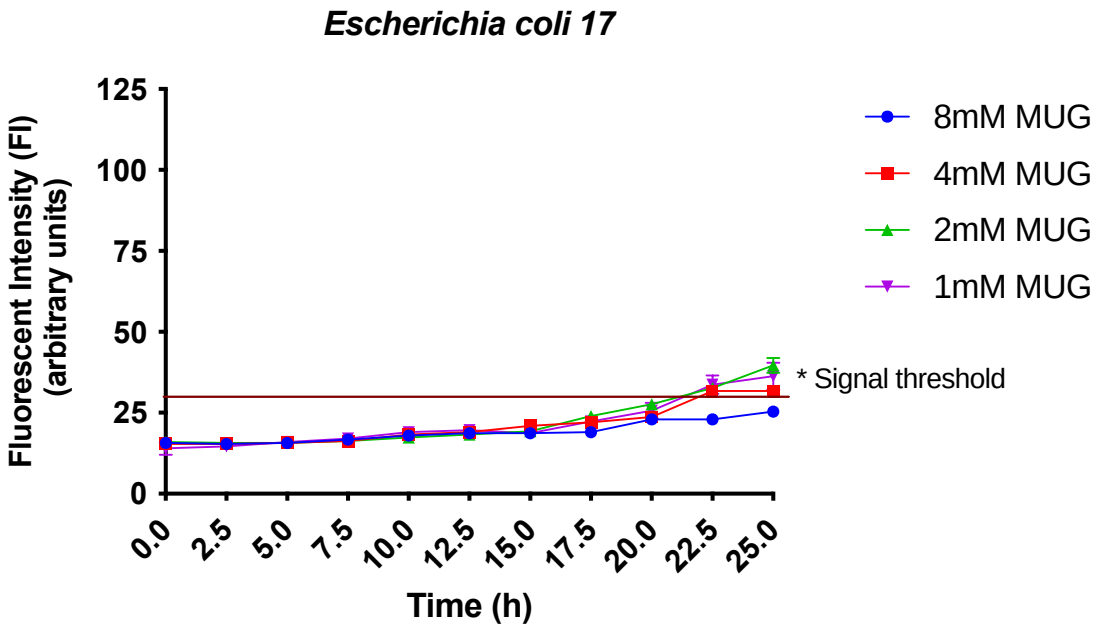


* 4-methyl-umbelliferone can be visualised above FI values of 30

**Figure 5.3.12** Detection of *Escherichia coli* through ß -glucuronidase activity on 4-methylumbelliferyl-ß-D-glucuronide substrate. Plotted values represent means from 3 independent experiments. Error bars represent SD

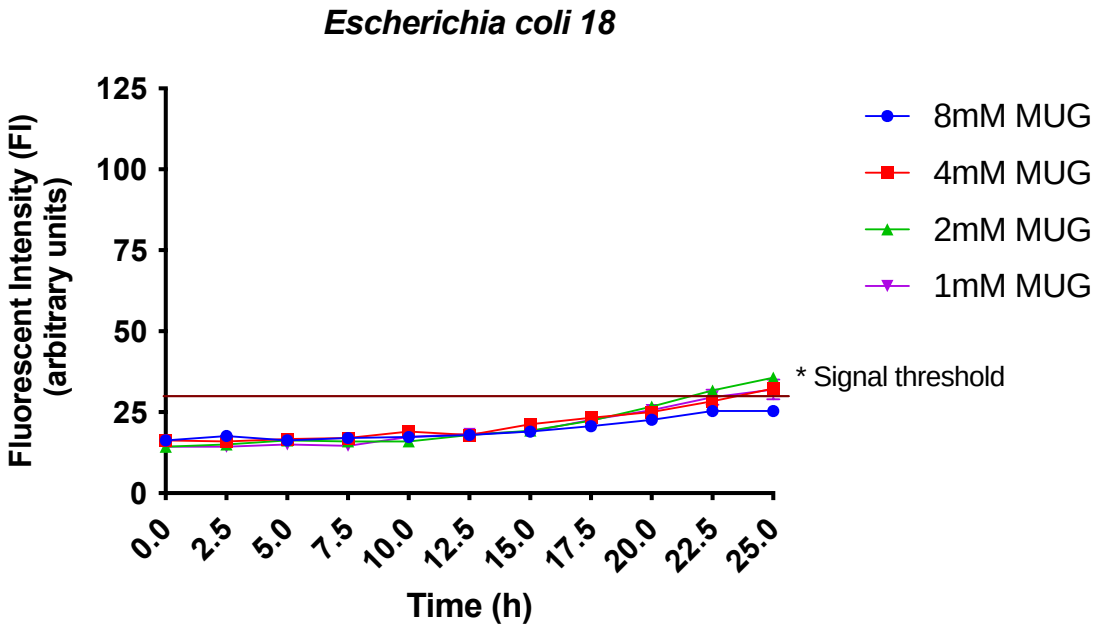


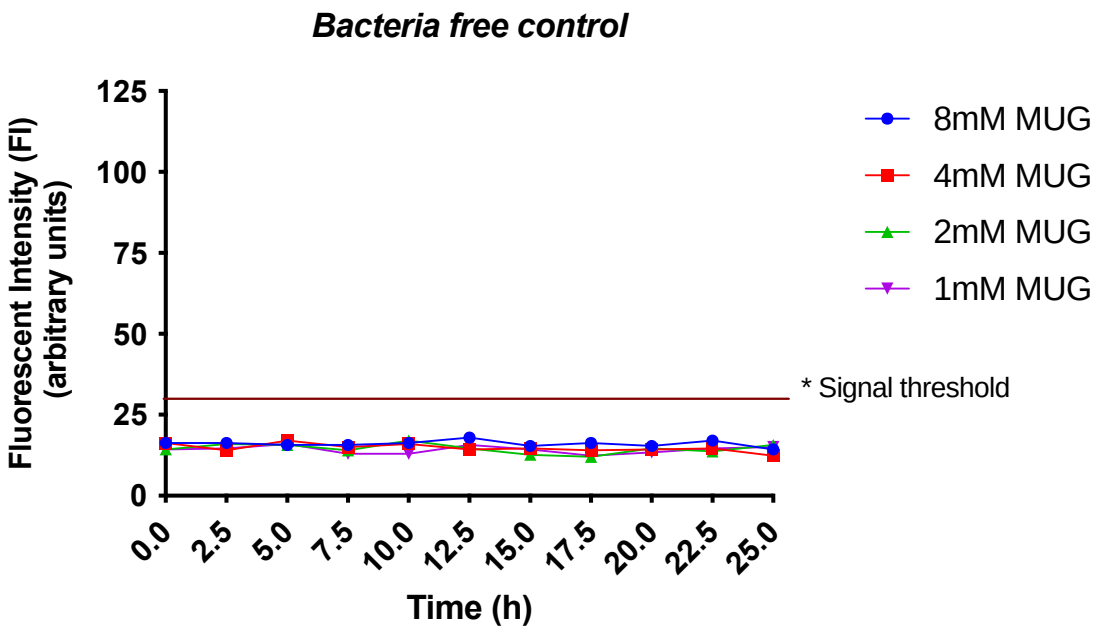


* 4-methyl-umbelliferone can be visualised above FI values of 30

**Figure 5.3.13** Detection of *Escherichia coli* through ß -glucuronidase activity on 4-methylumbelliferyl-ß-D-glucuronide substrate. Plotted values represent means from 3 independent experiments. Error bars represent SD

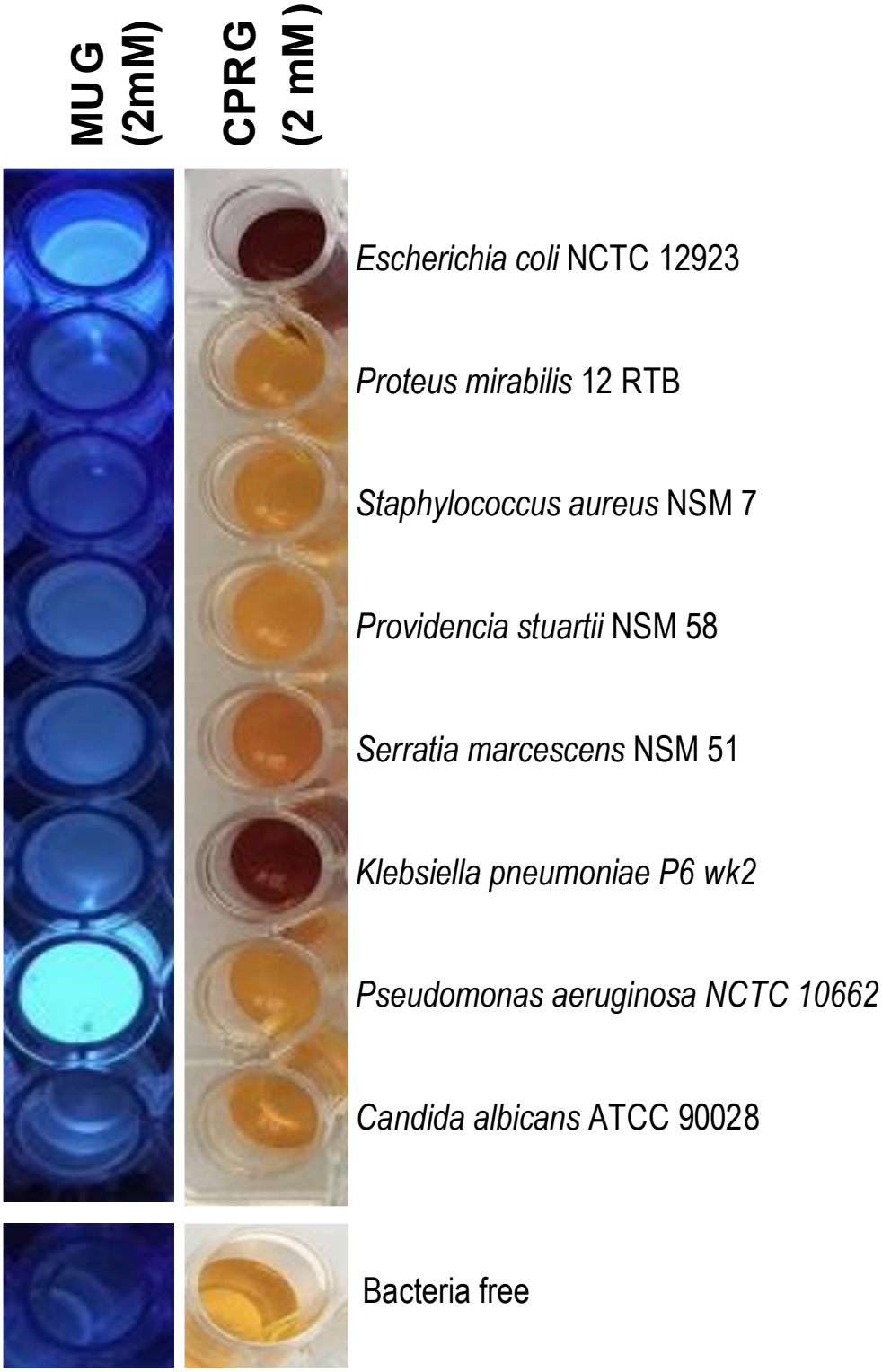


**Figure 5.3.14** Reactions between 8 CAUTI causing microorganisms with the substrates CPRG (2mM) and MUG (2mM). Images were captured after 24 h under bright light (CPRG) and UV light (MUG)

#### 5.3.1.3 Evaluation of bromothymol blue (BTB) as a sensor molecule to detect urease positive bacteria

The use of the pH sensor BTB to detect raised urinary pH of cultures containing urease positive bacteria, including *P. mirabilis,* showed that after a 2.5 h incubation period with 0.05 % BTB, a visible colour change from yellow to blue could be detected by monitoring the absorbance at 590nm (Figure 5.3.15).

From previously generated bacterial growth curves and calibration curves of OD 600nm against CFU, it was estimated that 1 x $10^8$ CFU/ml was present at the time of detection. A reduced BTB concentration of 0.01% (w/v) delayed detection by 1 h. As anticipated, the urease negative *E. coli* cultures did not produce a colour change with either of the BTB concentrations tested.

#### 5.3.1.4 Evaluation of tetrazolium compounds to detect viable bacteria

The commonly used tetrazolium compound, MTT was evaluated for use as a bacterial sensor molecule using two strains of *E. coli*. Positive detection was defined by a visible colour change from yellow to purple, and this occurred between 3 and 5.5 h for the *E. coli* strains evaluated (Figure 5.3.16). Using the previously generated calibration curves as tools to determine CFU counts, the CFU/ml were estimated to be 2.7 x $10^7$ and 8.5 x $10^8$, respectively.

The three novel tetrazolium compounds assessed for use as sensor molecules to detect viable bacteria, were compared using 2 CAUTI causing bacteria, *E. coli* and *P. mirabilis* (Figure 5.3.17). A colour change from colourless to red was indicative of a positive reaction with absorbance values at 490 nm above 2.5 being the threshold for a visible result. Significant lag phases in colour development (up to 8 h) were observed with bacteria for all compounds, although *P. mirabilis* had a lag phase of 17 h when the sensor TTP was used. The sensor compound 2,6-diFTTP produced a visible signal earlier than the other tetrazolium compounds, with detection at 11 h for *E. coli* and 15 h for *P. mirabilis*. At 17 h, a visible colour change was evident using 2,6-diClTTP for both *E. coli* and *P. mirabilis*. TTP took 18 h and 23 h to produce visible signals with *E. coli* and *P. mirabilis* respectively. At the time of detection, the CFU/ ml of *E. coli* was estimated at 1.05 x $10^9$ with 2,6-diFTTP and > 1.05 x $10^9$ for 2,6-diClTTP and TTP. For *P. mirabilis*, the $OD_{600\ nm}$ at the time of detection exceeded those of the calibration curve plotted of OD vs CFU. Therefore, it could only be determined that CFU counts were greater than

$9 \times 10^8$ CFU/ml for all of the novel tetrazolium compounds. No visible signals were detected with the bacteria-free control cultures.

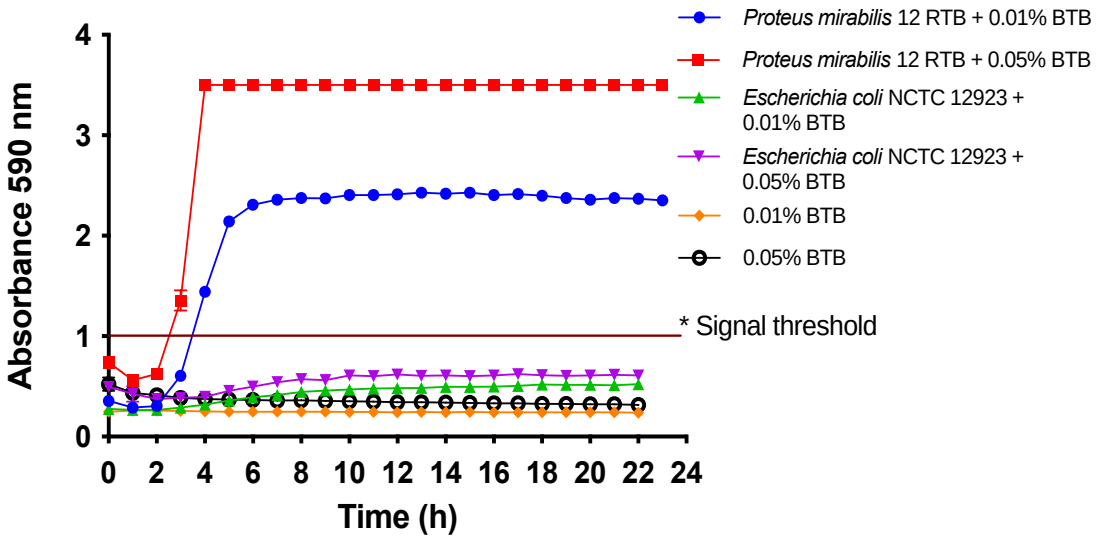


* Colour change from yellow to blue can be visualised above $A_{590\ nm}$ values of 1.0

**Figure 5.3.15** Detection of *Proteus mirabilis* 12 RTB using bromothymol blue (BTB). *Escherichia coli* NCTC 12923 was used as a negative control species. Plotted values represent means from 3 independent experiments. Error bars represent SD

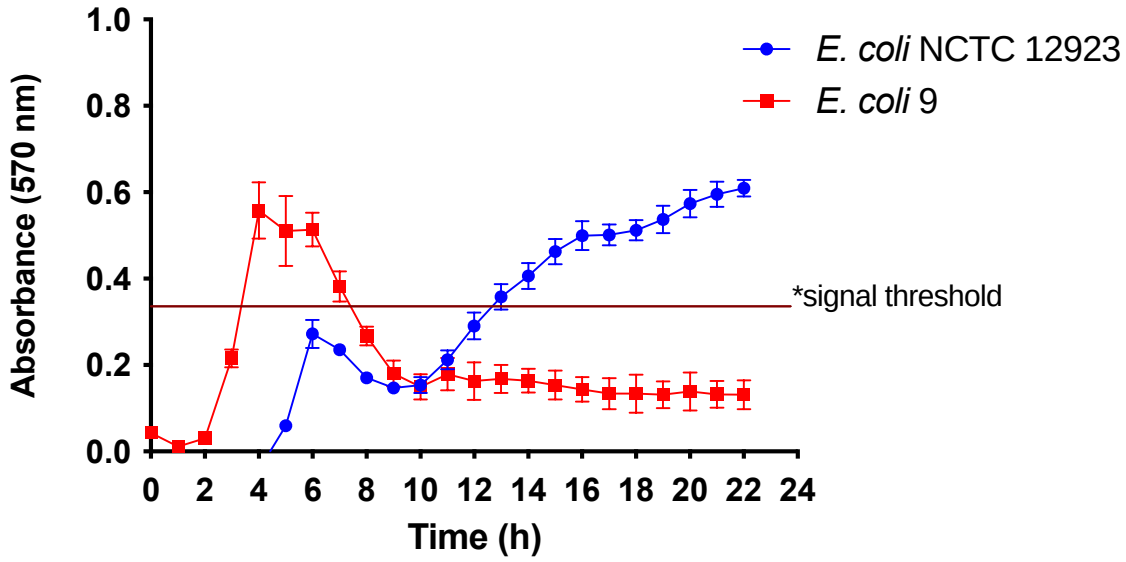


* $A_{570\ nm}$ values above the threshold can be detected by eye

**Figure 5.3.16** Detection of *Escherichia coli* NCTC 12923 and *Escherichia coli* 9 with MTT at a final concentration of 0.1 mM. Plotted values represent means from 3 independent experiments. Error bars represent SD

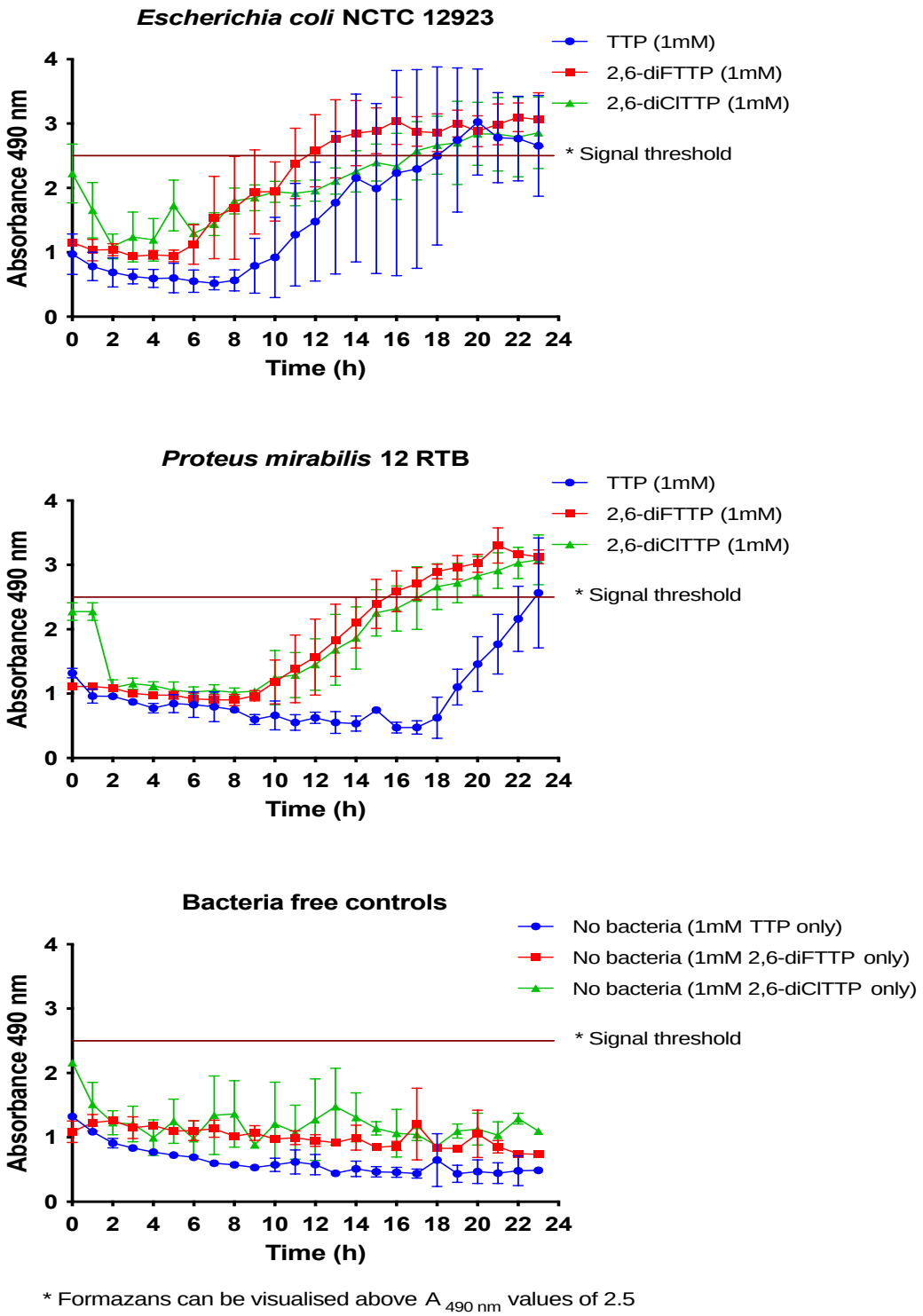


**Figure 5.3.17** Detection of coloured formazan products formed by reduction of the novel tetrazolium compounds triphenyl-tetrazolium phosphate (TTP), 2,6-difluro-triphenyl-tetrazolium phosphate (2,6-diFTTP) and 2,6-dichloro-triphenyl-tetrazolium phosphate (2,6-diClTTP) by *Proteus mirabilis* 12 RTB and *Escherichia coli* NCTC 12923. Plotted values represent means from 3 independent experiments. Error bars represent SD

#### 5.3.1.5 Evaluation of resazurin to detect viable bacteria

Metabolically active bacteria were detected with resazurin using *E. coli* NCTC 12923 and *P. mirabilis* 12 RTB as example species (Figure 5.3.18). Absorbance differences between the blue oxidised resazurin compound and the reduced, pink resorufin product, increased sharply until the 4 or 5 h timepoints before a slight reduction in absorbance differences occurred. These values increased and plateaued after 8 h for *P. mirabilis*, whilst the values gradually increased and plateaued after 17 h for *E. coli*. A visible colour change from blue to pink was determined to have a difference in $A_{570nm}$ and $A_{600nm}$ values of ≥0.4. The times of detection for *E. coli* and *P. mirabilis* were 2.5 h and 3 h, respectively. Extrapolation of the OD 600 nm values from the growth curves at these timepoints against CFU revealed that 2.2 x $10^8$ CFU/ml and 1.8 x $10^8$ CFU/ml were present for *E. coli* and *P. mirabilis*, respectively.

#### 5.3.1.6 Comparison of sensitivity and specificity of the evaluated sensor molecules

Comparing sensor compounds for detecting CAUTI causing bacteria revealed a broad spectrum of sensitivity (Table 5.3.1). For CPRG, sensitivity to detect coliform bacteria ranged between 2.5 x $10^8$ and 1 x $10^9$ CFU/ml, with a large intra-species variation for the *E. coli* strains assessed. Sensitivity of MUG detection was comparable to CPRG, with similar numbers of viable bacteria present at the detection time. As with CPRG, the variation in CFUs detected by MUG differed significantly between strains.

Although only useful to detect urease positive bacteria, BTB proved to be a sensitive compound, signalling the presence of *P. mirabilis* when 1 x $10^8$ CFU/ml were present. The novel tetrazolium compounds (TTP, 2,6-diFTTP and 2,6-diClTTP) and resazurin were evaluated using two test species, *E. coli* NCTC 12923 and *P. mirabilis* 12 RTB. Greater sensitivity was observed with resazurin than the tetrazolium compounds, with 2.2 x $10^8$ and 1.8 x $10^8$ CFU/ml present at the time of detection for *E. coli* and *P. mirabilis*, respectively. The sensitivity of the three novel tetrazolium compounds were all above 9 x $10^8$ CFU/ml for *E. coli* and *P. mirabilis*.

Resazurin and the tetrazolium compounds were universal rather than species specific sensor compounds, with detection based on metabolic activity of the

microorganism. CPRG, MUG and bromothymol blue were all species-specific sensors, detecting products released from the enzymatic breakdown of the substrate, or in the case of BTB, detection of elevated urinary pH due to urease activity of *P. mirabilis*.

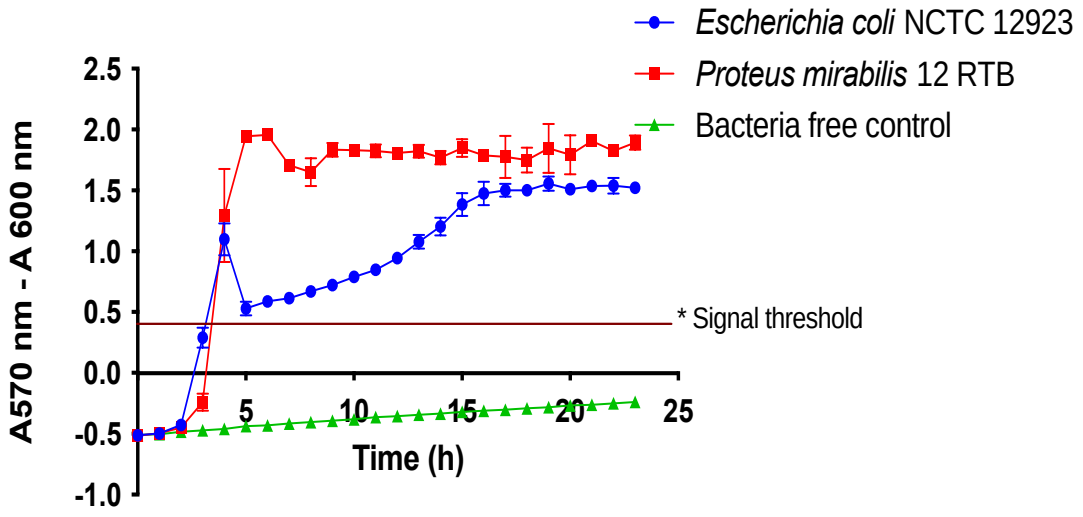


* Differences in reduced ($A_{570\ nm}$) and oxidised ($A_{600nm}$) forms of resazurin above 0.4 represents the visual detection threshold.

**Figure 5.3.18** Exploiting the ability of metabolically active *Proteus mirabilis* 12RTB and *Escherichia coli* NCTC 12923 to reduce resazurin for use as a microbial sensor molecule. Means of three independent experiments plotted with error bars representing SD

### 5.3.2 Evaluation of candidate sensor compounds in a filter paper model

#### 5.3.2.1 Evaluation of 4-methylumbelliferyl-β-D-glucuronide (MUG) and chlorophenol red-β-D-galactopyranoside (CPRG) as filter paper sensor materials

To determine whether *E. coli* NCTC 12923 elicited a reaction with MUG within a solid substrate, filter paper pre-absorbed with MUG was incubated with the bacteria. Under UV light, a blue, fluorescent signal was evident from the MUG filter paper incubated with *E. coli* NCTC 12923 (Figure 5.3.19.).

No reaction was observed in wells containing filter paper with MUG or *E. coli alone*. *Proteus mirabilis 12 RTB* did not emit a fluorescent MU product following incubation with MUG.

Figure 5.3.20 illustrates the ability of *E. coli* NCTC 12923 to yield a positive signal with CPRG within a material, resulting in the CPRG soaked filter paper turning yellow to red over a 24 h period. The colour intensity in the filter paper sensor material did not correlate with the inoculum level added to the material. Two-fold serial dilutions of *E. coli* NCTC 12923 were prepared through rows A-G, yet the red visible products were variable in intensity. The bacteria-free culture remained unchanged in colour.

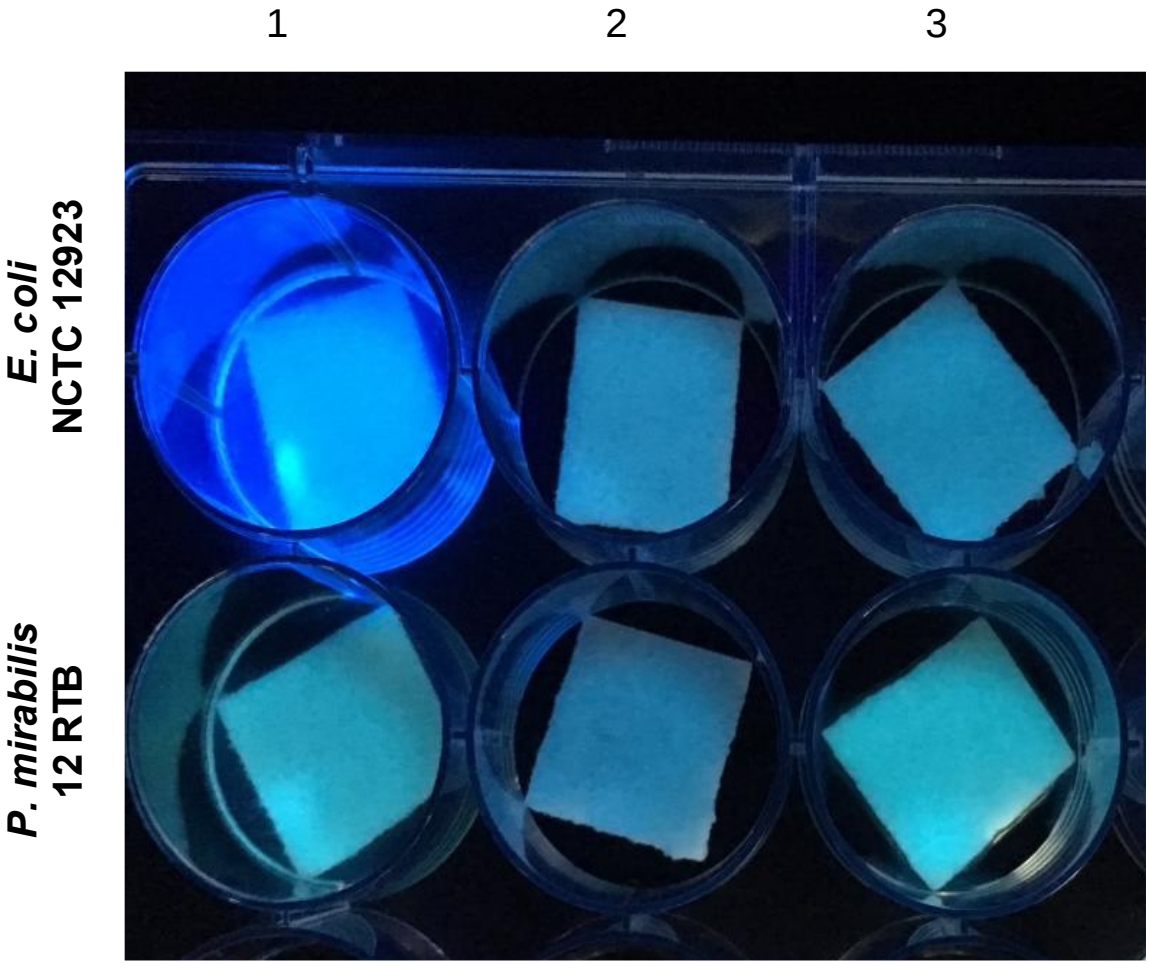


1.Bacteria + 2 mM MUG 2. 2 mM MUG only. 3. Bacteria only

**Figure 5.3.19** Detection of *Escherichia coli* using a filter paper sensor impregnated with 2 mM MUG. Images obtained under UV light following 24 h incubation. *Proteus mirabilis* 12 RTB was used as a negative control strain

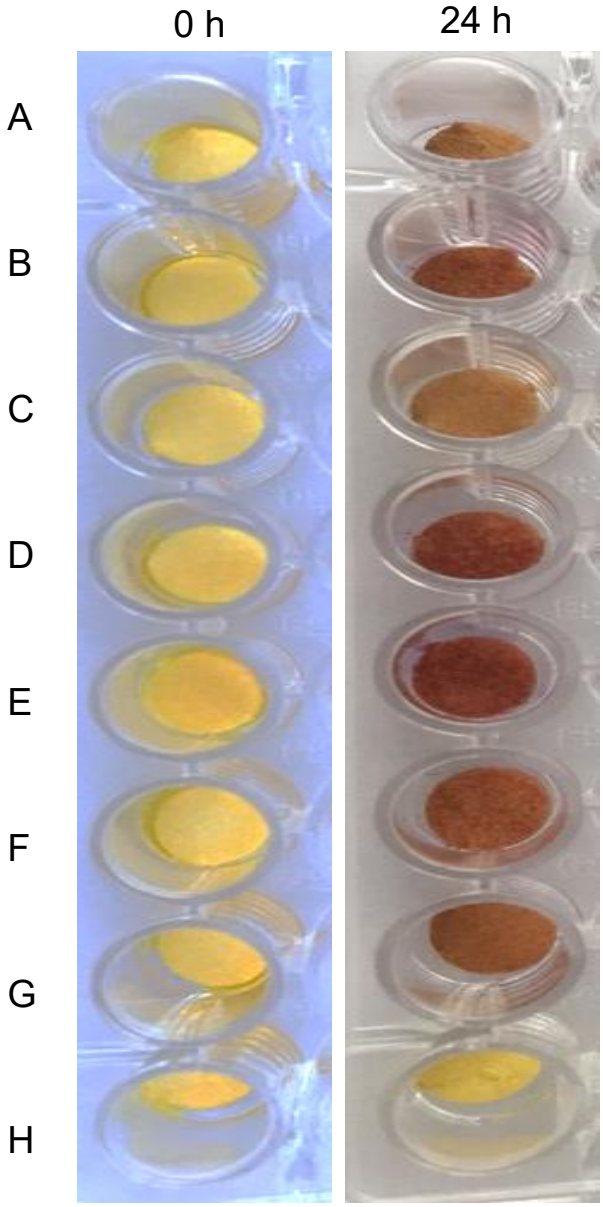


Starting inoculum approximately $1x10^8$ CFUs/ml in well A and decreases two-fold down the column until well G. Well H represents a no bacteria control.

**Figure 5.3.20** Detection of *Escherichia coli* with a CPRG filter paper sensor material. Images captured at t=0 and t=24 h

#### 5.3.2.2 Evaluation of 4-methylumbelliferyl-β-D-glucuronide (MUG) in a dual-species infection model

In dual-species CAUTI assays containing *E. coli* NCTC 12923 plus one other microorganism frequently isolated from urinary catheters and the substrate MUG, *E. coli* produced visible fluorescent signals under UV light in all wells (Figure 5.3.21).

The intensity of the signal produced by *E. coli alone* appeared to be equivalent to that produced in combination with other bacteria. The presence of *Staphylococcus aureus, Candida albicans*, *Pseudomonas aeruginosa*, *Providencia stuartii*, *Klebsiella pneumoniae*, *Proteus mirabilis* or *Serratia marcescens* had no detrimental effect on *E. coli* reaction with the MUG substrate absorbed into the filter paper and production of the fluorescent product. Florescence was not evident when the MUG-soaked filter paper was incubated with the additional 7 CAUTI causing microorganisms alone. The control wells containing only MUG or only bacteria did not produce fluorescent products visible under UV light.

#### 5.3.2.3 Evaluation of tetramethyl-p-phenylenediamine dihydrochloride (Kovac's reagent) as a *Pseudomonas aeruginosa* sensor molecule

Kovac's reagent has long been used as a clinical diagnostic tool to identify bacteria that possess the cytochrome oxidase enzyme. *Pseudomonas aeruginosa* is a CAUTI causing bacteria that produces cytochrome oxidase and thus, was expected to be detectable using this reagent. Figure 5.3.22 illustrates reactions of *Pseudomonas aeruginosa*, *Klebsiella pneumoniae*, *Escherichia coli* and *Proteus mirabilis* with filter paper soaked in Kovac's reagent. As predicted, the cytochrome oxidase produced by *P. aeruginosa* reacted with the Kovac's reagent to produce the purple-coloured indophenol product. The cytochrome oxidase negative species *K. pneumoniae*, *E. coli* and *P. mirabilis* did not yield the indophenol product with Kovac's reagent.

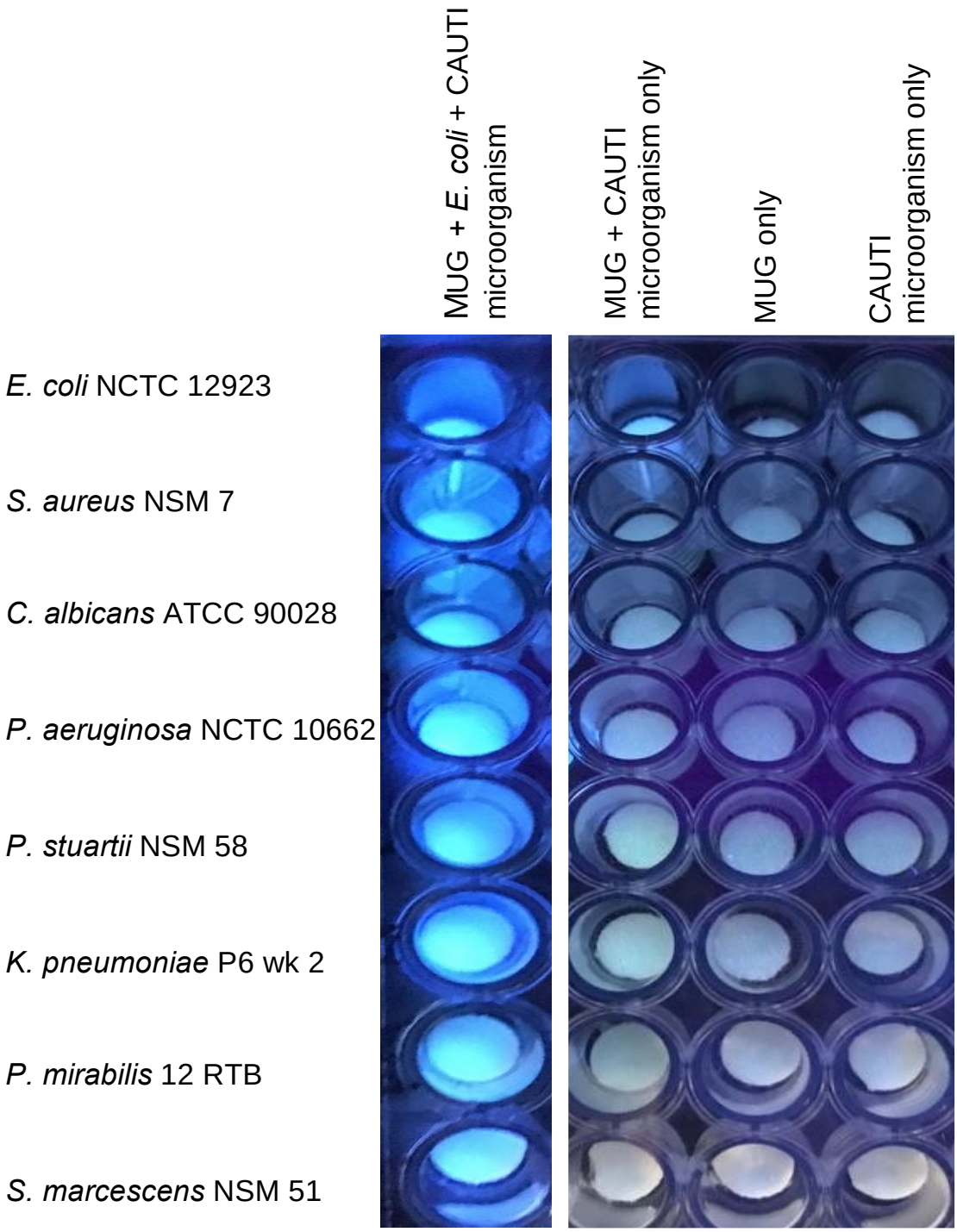


**Figure 5.3.21** Detection of *Escherichia coli* in a dual species test using a MUG filter paper sensor material

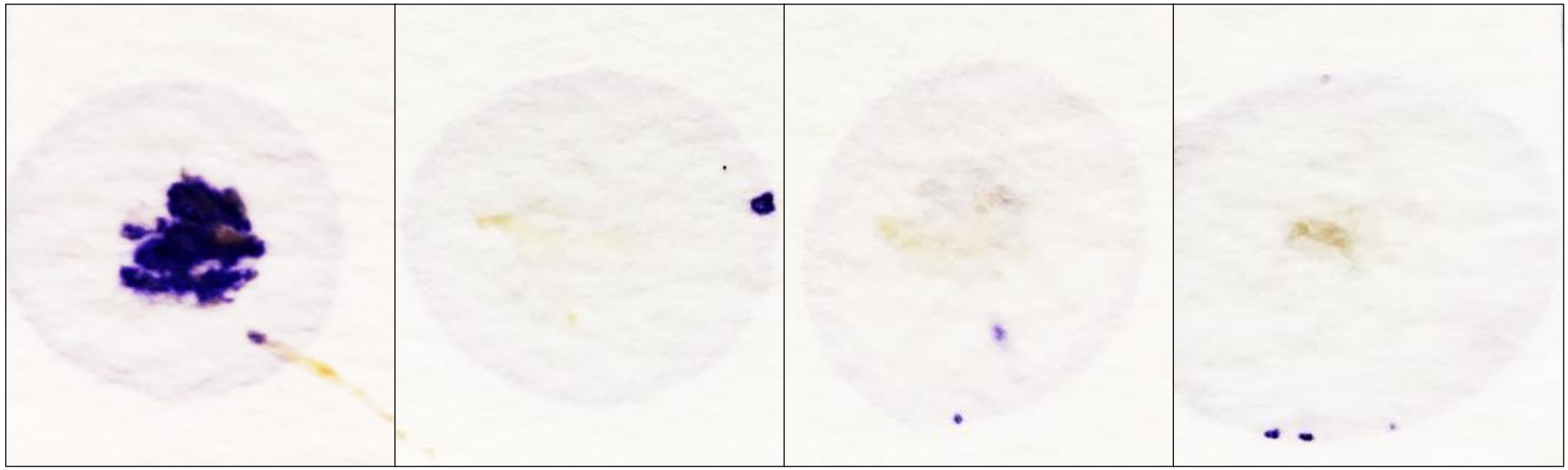

*P. aeruginosa*
NCTC 10662

*E. coli*
NCTC 12923

*K. pneumoniae*
P6 wk2

*P. mirabilis*
12 RTB

**Figure 5.3.22** Reactions of CAUTI bacteria with filter papers soaked with 1% w/v Kovac's reagent (tetramethyl-p-phenylenediamine dihydrochloride

#### 5.3.2.4 Evaluation of MUG, tetrazolium compounds and Kovac's reagent absorbed on to filter paper discs

The suitability of candidate sensor molecules for use in a biomaterial was assessed using filter paper soaked with the compound of interest and incubated with 8 microorganisms commonly associated with CAUTIs. Figure 5.3.23 illustrates the specificity of MUG as a sensor molecule to detect *E. coli* (Figure 5.3.23, column 1). In planktonic cultures, *P. aeruginosa* also led to blue fluorescence under UV light, following incubation with MUG (Figure 5.3.14). This fluorescence was absent in the filter paper model.

*Escherichia coli*, *P. mirabilis*, *P. stuartii*, *S. marcescens* and *K. pneumoniae* all produced detectable coloured formazans after 24 h incubation with novel tetrazolium compounds (TTP, 2,6-diFTTP and 2,6-diClTTP). *Staphylococcus aureus* only produced weakly coloured formazans on the filter papers soaked with TTP. No detectable colour change was observed after 24 h, following addition of *S. aureus* to 2,6-diFTTP and 2,6-diClTTP soaked filter paper (Figure 5.3.23).

A colour change was observed following reaction between *P. aeruginosa* with TTP, but this was barely detected visually. Coloured precipitates were not formed following incubation with 2,6-diFTTP or 2,6-diClTTP. *Candida albicans* failed to reduce any of the novel tetrazolium salt solutions to coloured formazans.

Resazurin was reduced to the vivid pink resorufin by *E. coli*, *P. mirabilis*, *S. aureus*, *P. stuartii*, *S. marcescens* and *K. pneumoniae* within the filter paper biomaterial model. As with the novel tetrazolium compounds, neither *Pseudomonas aeruginosa* nor *C. albicans* reduced resazurin to form the pink resorufin product.

Use of Kovac's reagent in this format to detect cytochrome oxidase positive species was unsuccessful. The colourless solution readily changed to purple as it was absorbed into the filter paper. All samples darkened further to black within 24 h, including bacteria-free controls.

The commonly used tetrazolium salt, MTT, was reduced to a blue formazan product by all of the CAUTI causing microorganisms, although a slight colour change was also observed in the bacteria-free control.

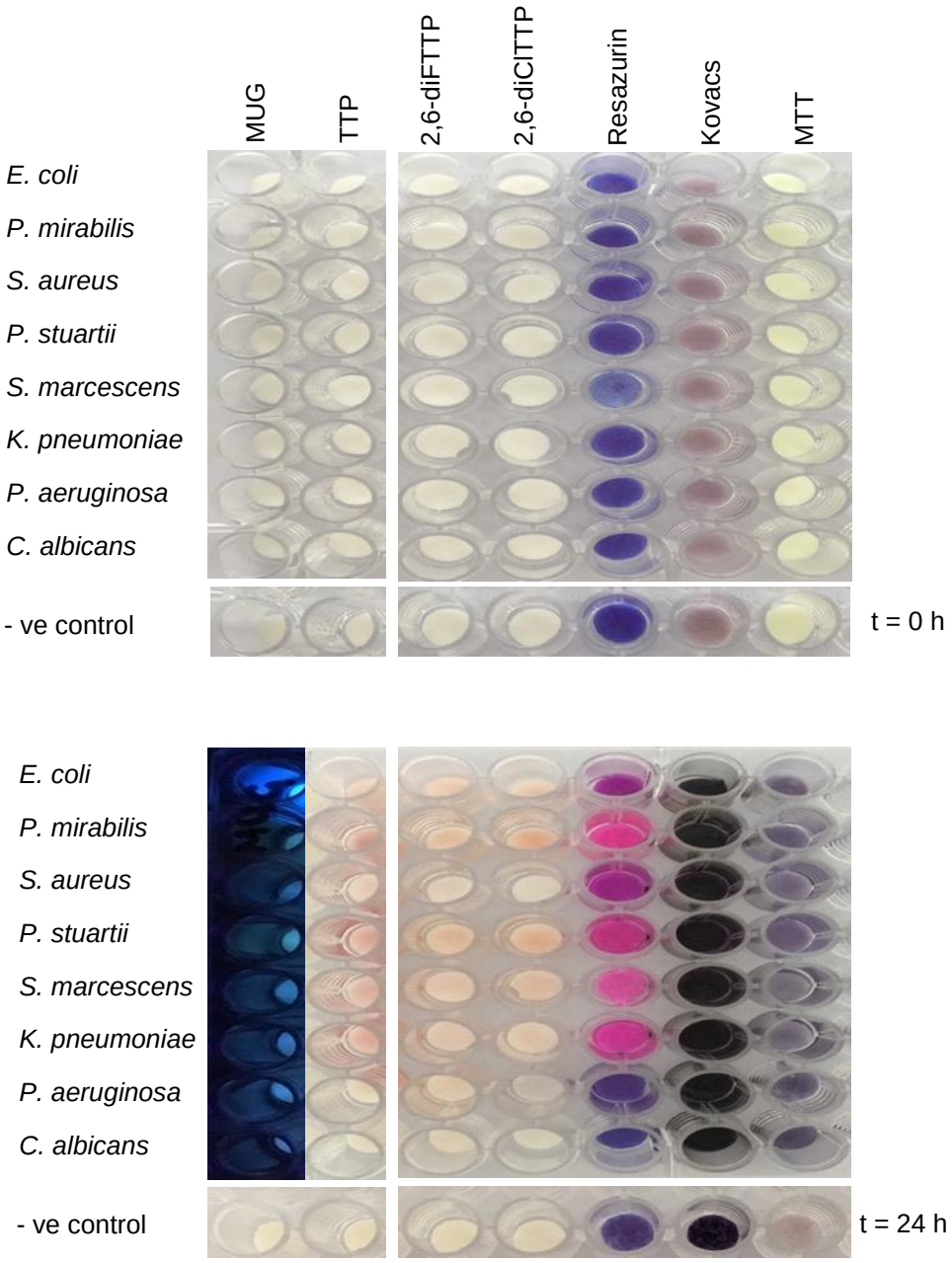


**Figure 5.3.23** Detection of CAUTI causing microorganisms with filter paper sensors. Filter papers were pre-absorbed with the following sensor solutions: MUG (2 mM), TTP (1 mM), 2,6-diFTTP (1mM), 2,6-diClTTP (1mM), resazurin (0.015% w/v), tetramethyl-p-phenylenediamine dihydrochloride (1% w/v), MTT (1mM). CAUTI causing microorganisms added to the sensors were imaged at 0 and 24 h. Plates were viewed under UV light to detect a positive MUG reaction

### 5.3.3 Evaluation of candidate sensor molecules incorporated into polymers

A selection of sensor molecules that performed well in the filter paper assays were chosen for incorporation into silicone polymers, with the aim of developing sensor materials able to detect CAUTI causing organisms.

BTB was successfully incorporated into a silicone polymer using a method developed for commercial sensor production. This method was adapted to create a BTB containing silicone with a porous structure (BTB-P), increasing the surface area, and creating pockets to retain urine and bacteria. Identical methods were also employed to successfully fabricate silicone containing CPRG.

Although resazurin was incorporated into a solid silicone material, the reduction of resazurin to resorufin occurred upon contact with uncured silicone. It was noted that cured silicone did not cause this reduction. Therefore, attempts were made to penetrate cured silicone with resazurin dissolved in various solvents including acetone, xylene, and ethyl acetate. Ultimately, these attempts were unsuccessful (*data not shown*).

Incorporating resazurin into a polyurethane foam did not reduce resazurin, and the resazurin foam was evaluated in subsequent studies.

### 5.3.4 Evaluation of polymer sensor materials in an *in-vitro* batch model

An *in-vitro* batch culture model of *P. mirabilis* infection was used to evaluate the BTB polymer sensor, BTB polymer with an increased surface area (BTB-P) and the polyurethane foam incorporating resazurin.

Increasing the surface area of the BTB polymer reduced the time for a positive signal to occur, as indicated by a colour change from yellow to dark blue, from 6-12 h to 2-4 h (Figure 5.3.24 A). This correlates with the BTB-P sensor triggering at a lower pH (7.6 – 8.4) than the BTB sensor (9.1-9.3) (Figure 5.3.24 B). In this system, the resazurin foam sensor material detected *P. mirabilis* between 2 h and 4 h, as indicated by a colour change from blue to pink, and therefore its performance was equivalent to the BTB-P sensor. The number of bacteria present in the culture system was maximal at 1.7 x $10^8$ CFU/ml at 2 h and then decreased. Resazurin foam was able to detect *P. mirabilis* at a level of approximately 1.7 x $10^8$ CFU/ml.

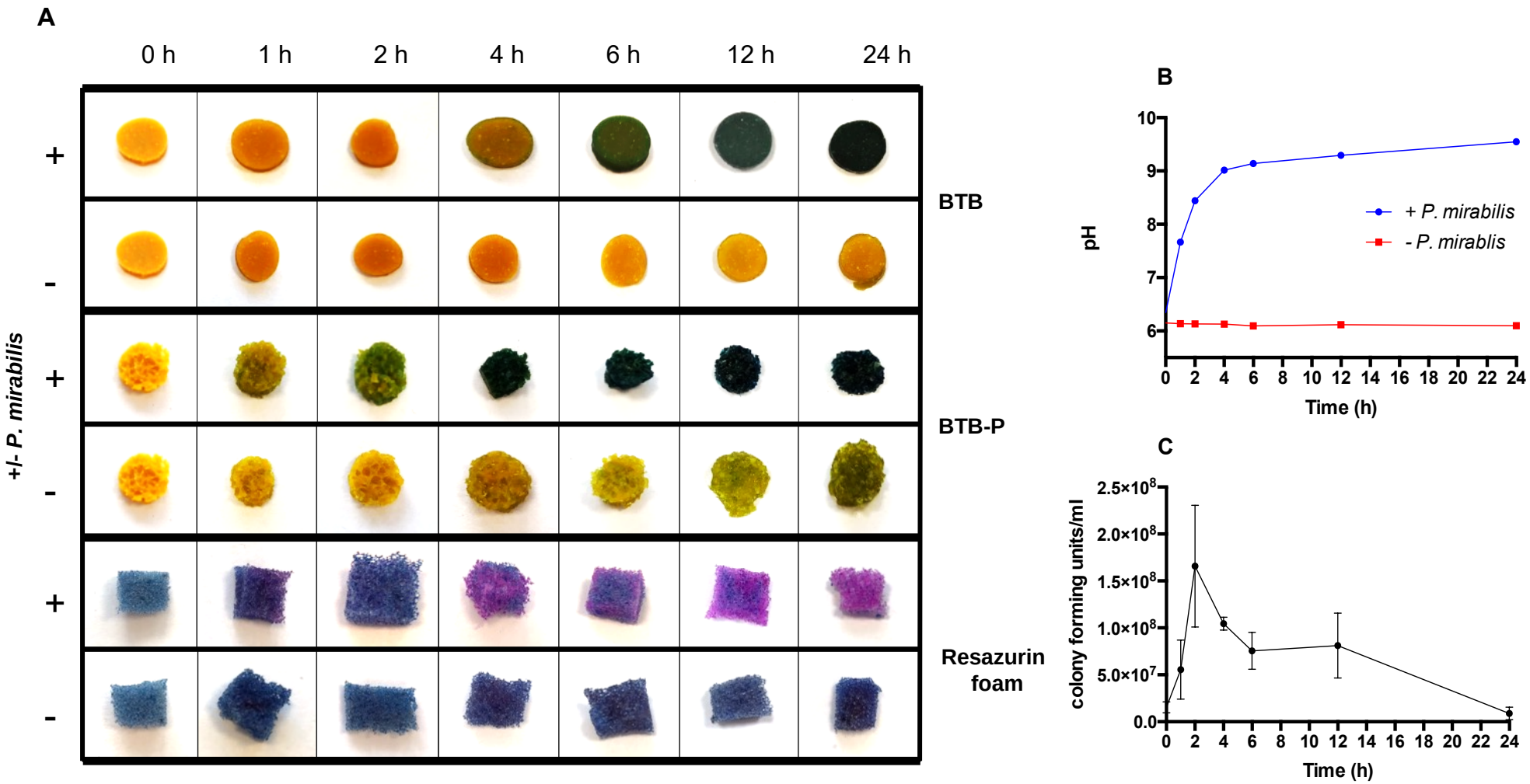


**Figure 5.3.24** Detection of *Proteus mirabilis* with bromothymol blue (BTB) silicone sensor materials and a resazurin polyurethane foam. (A) Appearance of a BTB containing material, porous BTB silicone material (BTB-P) and a polyurethane resazurin foam over 24 h when placed in cultures +/- *Proteus mirabilis* 12 RTB. (B) pH readings of bacterial cultures in artificial urine. (C) colony forming units (CFU) recovered from the cultures at intervals between 0 and 24 h. Error bars represent SD

## 5.4 Discussion

The overarching aim of this research was to identify suitable sensor molecules for bacteria able to cause CAUTIs. The candidate sensor molecules were selected, based on previously reported studies where bacteria were successfully detected. In addition, collaboration with the School of Chemistry, Cardiff University, led to evaluation of novel tetrazolium compounds. The driver behind this research was the need to provide early indication of CAUTIs to clinicians, who in turn, would be able to undertake timely intervention to inhibit infection progress.

The evaluated sensor molecules for urinary pathogens yielded some noteworthy findings. Exploiting β-D-galactosidase (GAL) activity of *E. coli* and other faecal coliforms to produce a chromogenic compound with the substrate CPRG, demonstrated that intensity of the coloured chlorophenol red (CR) product was concentration-dependent, in terms of both chemical and bacteria. Positive correlation occurred between substrate concentration, the number of bacteria and intensity of the signal provided by the coloured product. It was also confirmed that CPRG had specificity for coliform bacteria, yielding positive reactions with *Escherichia coli* (n=3) and *Klebsiella pneumoniae* (n=3) and negative reactions with the non-coliform bacteria (n=3) and *C. albicans*, concurring with findings of previously reported studies (Wutor, Togo, & Pletschke, 2007).

Assessment of CPRG using multiple *E. coli* strains revealed variation in the number of colony forming units required to elicit a positive reaction, suggesting that differences likely existed in β-GAL expression by the strains. In comparison, use of MUG to detect β -D-glucuronidase (β-GUD) positive bacteria, namely *E. coli* (n=3) revealed some unexpected findings. Interestingly, of the eight CAUTI causing pathogens tested, positive signals were generated by *E. coli* and *Pseudomonas aeruginosa*. Previous studies with *P. aeruginosa* demonstrated that some strains produce two pigments, namely pyocyanin and pyoverdin which fluoresce blue/green and yellow/green under UV light, respectively (El-Fouly *et al.*, 2015). It is possible that these fluorescent pigments might have led to a false positive signalling event. However, florescence of *P. aeruginosa* was absent in the filter paper model using MUG. This may be due to lower quantities of bacteria present, which allowed any fluorescence to fall below the threshold of detection.

Detection of *E. coli* using MUG showed that unlike CPRG, strong signals were not detected for all strains investigated. Only 2 out of 5 strains produced fluorescence

under blue light that was immediately visible, suggesting differences in β-GUD expression for the test strains.

In contrast to CPRG, a positive correlation between MUG concentration and fluorescent intensity was not evident. It was evident that the greatest signal responses occurred at lower MUG concentrations. Previous investigations have revealed that fluorescent intensity (FI) between MUG and *E. coli* was pH dependent, with positive correlation between increasing pH and FI (Profeta et al., 2017). As pH was not monitored during this study, it can only be hypothesised that the pH of the MUG stock solutions and culture media affected the FI of the products generated.

Due to CAUTIs often being polymicrobial, MUG was investigated as a sensor in dual-species filter paper models, using *E. coli* plus an additional CAUTI causing microorganism. It was observed that the additional microorganism present in the inoculum did not adversely affect detection, allowing MUG to still be considered as a suitable candidate for detecting CAUTIs.

The enzyme, GUD, has been found in human urine with elevated levels of activity in patients with bladder cancer and other neoplasms (Ho & Kuo, 1995). Additional cellular components of human urine may also exhibit GUD activity and contribute to false positive reactions. Whilst human erythrocytes have been shown to contain little or no GUD activity, blood plasma and exudates from inflamed areas have previously demonstrated high GUD activity (Abul-fadl, 1957). Variable levels of activity have been reported for epithelial cells in urine (Abul-fadl, 1957). However, it has been reported that endogenous mammalian GUD has an optimum pH range of 4-5, whist GUD from *E. coli* operates at a higher pH range of 6.8-7.7 (Paigen & Peterson, 1978). A clinical trial of any CPRG CAUTI sensor would be essential to detect the rate of false positive results.

Ascorbic acid and ammonium salts have both been reported to inhibit GUD activity (Abul-fadl 1957; Young and Kenyon 1990). High levels of dietary vitamin C can ultimately lead to high levels of ascorbic acid excretion in the urine, which may interfere with detection by MUG. The ascorbic acid concentration of urine from healthy patients on diets that contain the recommended levels of vitamin C would need to be determined. Additionally, polymicrobial infection containing *E. coli* and *Proteus mirabilis* could go undetected by MUG due to interference from ammonium salts generated through the urease-dependent breakdown of urea.

β -D-galactosidase (GAL) is also present in human urine at varying concentrations, with significantly higher concentrations reported in patients with renal disease (Dance *et al.*, 1970). As with CPRG, a clinical trial of a MUG-based sensor would be essential for these sensor approaches to ascertain incidences of false-positive or false-negative results.

Both MUG and CPRG yielded positive reactions in filter paper models and could detect *E. coli* in polymicrobial *in vitro* infections. CPRG was selected over MUG for incorporation into the bulk matrix of a silicone elastomer, due to the benefit of being able to visualise a positive reaction by eye and its increased sensitivity compared with MUG. Although the optimal activity of CPRG has been reported at pH 7.8 (Wutor, Togo, & Pletschke, 2007), activity was observed across a broad pH range, adding to the argument that CPRG was preferable to MUG as an *E. coli* sensor in human urine.

Ultimately, although CPRG was successfully incorporated into silicone rubber, the material was unreactive with *E. coli* cultures, possibly due to the impermeable nature of the silicone material. A solution of CPRG released directly into the drainage bag of an *E. coli* infected bladder model may represent a method to detect infection in a catheterised patient and is an area for future study.

Diagnostic laboratories routinely use Kovac's reagent to detect cytochrome oxidase-positive bacteria, including *Pseudomonas aeruginosa*. Although *P. aeruginosa* was successfully detected using this reagent, the light- and time-sensitive nature of the compound deemed it unsuitable to be used within the catheter model or for incorporation into a biomaterial.

Tetrazolium compounds including the commonly used 3-(4,5-dimethylthiazol-2-yl)-2,5-(diphenyltetrazolium bromide (MTT), have been widely used as tools in laboratory assays to detect metabolically active bacteria (Hatzinger et al., 2003; Mshana et al., 1998). Ishiki et al produced an MTT based electrochemical detection system. However, the required incubation steps renders such a device to be unsuitable in a clinical setting (Ishiki et al., 2018).

It was initially envisaged that tetrazolium compounds could be successfully used to detect biofilms on the surfaces of urinary catheters through the visualisation of the coloured formazans. However, use of MTT within the filter paper model highlighted the light sensitive nature of the compound giving rise to false-positive

results. Therefore, further development of the compound into a sensor molecule was halted.

For planktonic cultures of *E. coli* and *P. mirabilis*, the novel tetrazolium compounds, TTP, 2,6-diFTTP and 2,6-diClTTP, produced visible red formazan products, although detection occurred later than with the other compounds assessed and required higher numbers of bacteria present. Of the three novel tetrazolium compounds tested, highest sensitivity occurred with 2,6-diFTTP and the least sensitive was TTP. It was possible that the additional fluorine molecules incorporated into the parent compound, TTP, increased reactivity due to fluorine being a highly reactive group VII element. Although broad spectrum activity was observed for all the tetrazolium filter paper sensors, the formazans produced were only weakly visible. For this reason, along with their lower sensitivity compared with other sensor molecules investigated, the development of further biomaterials incorporating these compounds was discontinued.

Use of resazurin to detect metabolically active cells in planktonic cultures revealed superior sensitivity compared to MUG, CPRG and the tetrazolium compounds. Assessment of resazurin in a filter paper sensor model also highlighted a broad-spectrum activity. The inability of *P. aeruginosa* or *Candida albicans* to reduce resazurin in the filter paper model may be attributed to low metabolic activity on the filter paper substrate, or in the case of *P. aeruginosa*, alginate produced by this mucoid strain may act as a barrier to the tetrazolium compound reaching bacterial cells.

Along with the broad-spectrum activity, the large chromatic shift observed by end users rendered resazurin as a leading candidate for incorporation into further biomaterials for use as a CAUTI sensor device. Unfortunately, reduction of resazurin occurred during incorporation into silicone. Attempts to overcome the problem were unsuccessful, including the use of various solvents to penetrate cured silicone with the compound. However, resazurin was successfully incorporated into a polyurethane foam and was retained in its oxidised state. The compound was subsequently reduced by *P. mirabilis* within an *in-vitro* batch culture model. Resazurin is used widely as a tool for susceptibility testing of microorganisms (Fai & Grant, 2009; Khalifa et al., 2013) and has also been used to monitor environmental contamination (Al-Adhami et al., 2016). However, to

date, its use in clinical settings has not been reported, highlighting the novel nature of such a sensor device.

BTB incorporated into silicone has been described as a CAUTI sensor device, as the compound was assessed against planktonic *P. mirabilis* cultures (Malic et al., 2012). The sensitivity of BTB to detect *Proteus* infections was superior to resazurin and the tetrazolium compounds investigated, based upon time required to detect an infection and CFU/ml present at the detection time. It was also shown that BTB concentration positively correlated with intensity of colour change (signal) observed.

The BTB silicone sensor that had previously been developed between Cardiff University and Technovent Ltd (Malic et al., 2012), was produced and evaluated alongside a porous version (BTB- P) with increased surface area. Although additional BTB-P sensor materials were produced with a range of pore sizes, time constraints prevented their evaluation in an infection model. Use of 3D printing to create a BTB silicone sensor with increased surface area may also be evaluated in future investigations to create sensors of reproducible surface characteristics. Within an *in-vitro* batch culture model of *P. mirabilis* infection, the BTB-P sensor reduced the time taken for an infection to be detected from 6-12 h to 2-4 h. The increased surface area presumably allowed a greater number of ammonium ions and ammonia gas from *P. mirabilis*- infected urine to penetrate the silicone material and elicit the pH dependent colour change from yellow to dark blue.

In a clinical setting, earlier detection of *P. mirabilis* infection would lead to improved patient outcomes through quicker intervention and treatment by care providers.

All the sensor molecules evaluated in this Chapter signalled infection between $10^7$ and $10^9$ CFU/ml. In clinical terms, such Figures would represent established urinary tract infection. The commonly used criterion for diagnosis of a UTI is bacteria present in urine at a level $\geq 10^5$ CFU/ml, although it is recognised that catheterised patients may have low concentrations of bacteria that can progress to higher concentrations. For such patients, the diagnostic criteria may be reduced to $\geq 10^2$ CFU/ml (Wilson & Gaido, 2004).

Although the high CFU counts required to trigger the sensor molecules may appear problematic, infections with bacteria such as *Proteus mirabilis* often remain undetected until advanced stages, once catheter blockage occurs. The developed sensor materials will be evaluated in an *in-vitro* bladder model in the following

chapter and sensor trigger time will be recorded in relation to time taken for catheter blockage to occur.

## 5.5 Conclusions

The aims of this Chapter were to identify a range of chemicals to detect microorganisms commonly associated with CAUTIs. A number of promising compounds were identified and able to detect target organisms using permeable filter paper materials. However, chemical incorporation into silicone proved more difficult, and when achieved, subsequent signalling effects were lost.

Modifying BTB silicone to increase surface area reduced the time taken to detect infection with *P. mirabilis*. Incorporating the redox indicator resazurin into a polyurethane foam also produced a sensor with reduced detection time, compared to the existing BTB sensor in a model of *P. mirabilis* infection. Importantly, the broad spectrum activity of resazurin would lend the foam sensor to be used as a universal sensor material, capable of detecting polymicrobial CAUTIs. These new sensor materials were further assessed in an *in-vitro* bladder model of CAUTI infection (Chapter 6). If successful such new biosensors could represent clinically valuable diagnostic tools.

# Chapter 6

## Assessment of Novel Biomaterials Using an *In-Vitro* Bladder Model

## 6.1 Introduction

*In-vitro* models are important tools in biological and medical research and are often used before progression to *in-vivo* models and clinical trials. The use of such models to study bacterial infection allows activity of biocidal agents to be evaluated against a wide variety of bacterial species in an easily controlled manner, whilst being relatively inexpensive to perform (White, 2001). Furthermore, striking agreement between *in-vitro* models, outcomes in animal models of infection and clinical models have been observed (White, 2001).

Recent focus within the medical science field has been aimed at reducing or replacing *in-vivo* animal models, and as such, the use of *in-vitro* models has become an aspirational target (DeGrazia & Beauchamp, 2019). To adequately replicate a catheterised urinary tract, Stickler et al developed a closed drainage *in-vitro* model (Figure 6.1), that permitted investigation of catheterised bladders, whilst replicating many of the *in-vivo* conditions (David J. Stickler et al., 1999). Stickler states that it was useful to have a simple laboratory model to study urethral catheter biofilms under conditions in which the design features of the catheter and the hydrodynamics of the catheterised bladder were considered (David J. Stickler et al., 1999). This *in vitro* model has been used extensively to study biofilm formation on urinary catheters, with many studies pertaining to the crystalline biofilm formed by *Proteus mirabilis* (Holling et al., 2014; Imani Rad et al., 2019; Jordan et al., 2015). The model was used to determine that catheter materials coated with 2-methacrylol-oxyethylphosphorylcholine co-polymerised with long chain alkyl methacrylate's resisted encrustation by *Proteus* biofilms (D. J. Stickler et al., 2002). Furthermore, Imani et al used the model to determine that allicin, a compound extracted from garlic, could prevent formation *of P. mirabilis*-induced urinary crystals and subsequent catheter blockage, when the compound was added directly to the urine source (Imani Rad et al., 2019).

The bladder model has allowed the efficacies of antimicrobial catheters to be determined and compared (Morris et al., 1997; D. J. Stickler et al., 2002). However, the model fails to account for factors that may affect efficacy in a clinical situation. Factors such as patient handling and poor hygiene, variable urine flow and variances in urine composition could affect the performance of an antimicrobial catheter *in-vivo*. The lack of both bladder and urethral epithelium also prevents the study of the interactions between host tissue and urinary catheters.

Added to this, polymicrobial biofilms are often recovered from the indwelling catheters of patients undergoing long-term catheterisation (Azevedo, Almeida, Melo, et al., 2017), and this may not be considered when designing single-species infection models.

However, the *in-vitro* bladder model still represents a valuable infection model to study factors affecting the catheterised urinary tract. It offers the advantage that sampling of urine from the bladder chamber is simple and non-invasive, whilst the glass bladder chamber allows visualisation of apatite and struvite deposits and encrustation around the catheter eyehole following infection with urease positive bacteria.

### 6.1.1 Design of the *in-vitro* bladder model

Artificial urine (AU) is pumped into a bladder chamber via a peristaltic pump at a flow rate representative of the *in-vivo* situation, *i.e.* approximately 0.5 ml/min (Azevedo, Almeida, Gomes, et al., 2017). An inflated Foley catheter is inserted into the glass bladder chamber, allowing urine to leave the chamber via the catheter eyehole. However, a residual volume of urine remains below the level of the eyehole, representative of the *in-vivo* system.

A Foley catheter connected to a drainage bag collects the output AU and emptying the drainage bag is achieved via an integral tap. To maintain the AU at body temperature, water heated to 37°C may be pumped through the cavity surrounding the bladder chamber, or the entire system can be housed in a 37°C environment. The model can be adapted to study the efficacies of antimicrobial catheter coatings, diffusion of antimicrobials from the catheter balloon or methods to prevent migration of urinary pathogens from the drainage bag into the bladder (Jordan et al., 2015; D. J. Stickler et al., 2002; Williams & Stickler, 2007).

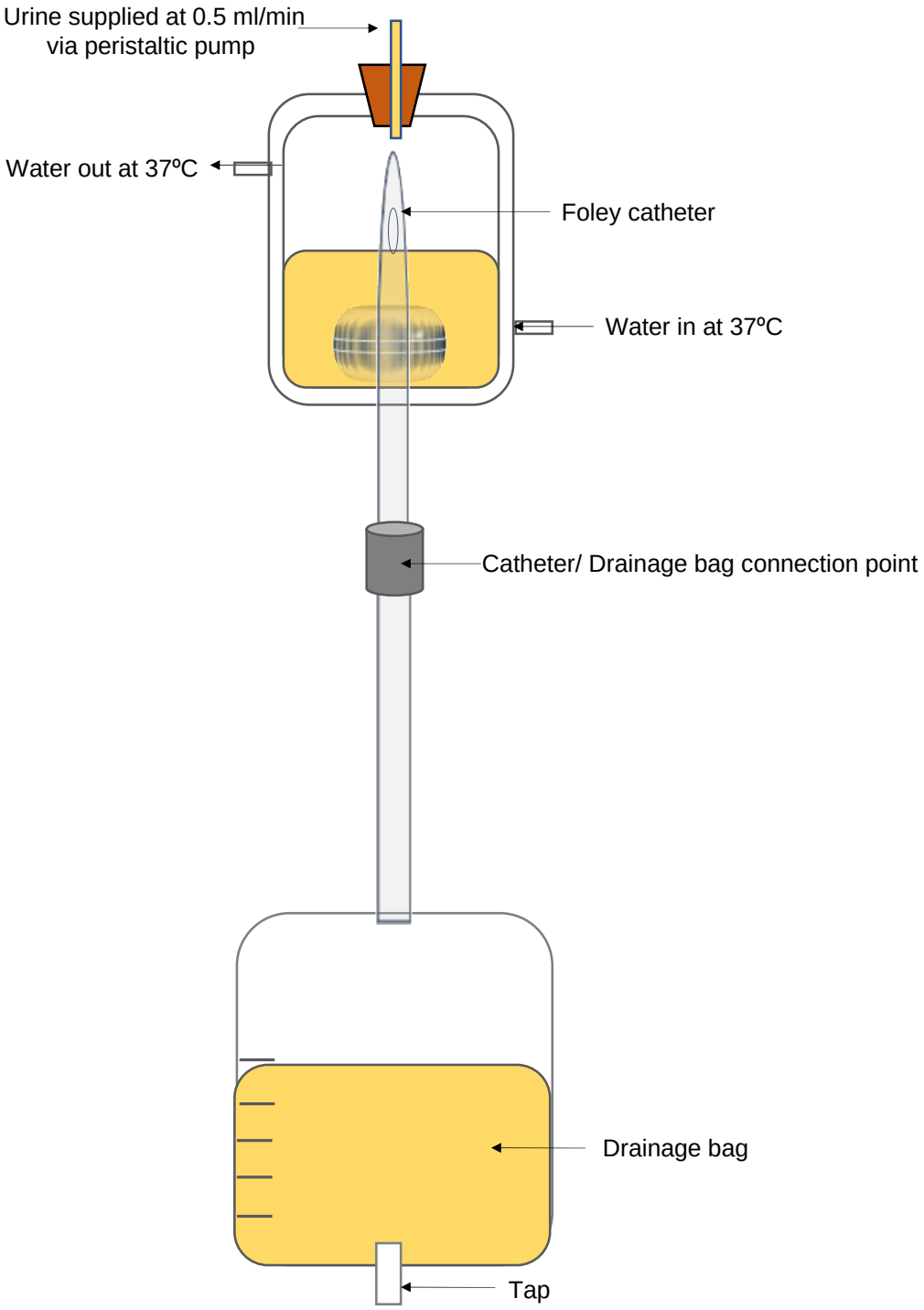


**Figure 6.1** Schematic representation of the *in-vitro* bladder model

### 6.1.2 Aims

The two primary aims of this research Chapter were to:

- Evaluate antimicrobial biomaterial and surfaces developed in Chapter 3, to prevent or delay Foley catheter blockage.
- Determine whether sensors generated in Chapter 5, could provide an early warning detection of biofilm infection in the *in-vitro* model.

To evaluate the antimicrobial biomaterials developed in Chapter 3, the *in-vitro* bladder model was used to assess the ability of silicone elastomer insets, bulk-loaded with triclosan or triclosan acetate, to prevent or delay ascending *Proteus mirabilis* infection from the drainage bag. Jordan et al (Jordan et al., 2015) previously coated urinary catheters with a 0.2% (w/w) triclosan and this approach will be repeated and compared with 0.2% (w/w) triclosan acetate coatings. The coatings were applied to the external and internal surfaces of full-length Foley catheters and delays, or prevention of *P. mirabilis* bladder colonisation determined.

The bromothymol blue (BTB) and resazurin sensor materials developed in Chapter 5 were assessed using the *in-vitro* bladder model. AU from bladder chambers inoculated with *P. mirabilis* were passed over the sensor materials situated between the connectors of the catheters and drainage bags and the time taken for the sensors to trigger recorded. The pH and colony forming units (CFUs) required to trigger the sensors was also determined.

## 6.2 Materials & Methods

### 6.2.1 Production of bulk-loaded antimicrobial cylinders

Silicone slabs of 100 mm x 100 mm x 2 mm depth containing 1% (w/w) triclosan (T2) or triclosan acetate (TA-2) were produced, as described in Section 3.3.2. Coupons were cut from the slabs using 9 mm cork-borers and the centres removed using a 5 mm cork-borer. The resulting silicone rings were bonded using room-temperature vulcanising silicone for 3D printing (Section 4.2) and cured at room temperature to create cylinders 16 mm in length. Control material cylinders were also produced from silicone without antimicrobial (S2).

### 6.2.2 Production of antimicrobial dip-coated catheters

To create dip-coatings containing 0.2% (w/w) triclosan or triclosan acetate, the 1% (w/w) part A and part B formulations described in Section 3.3.3, were diluted 5-fold with silicone based fluid (Probond remover, Technovent, UK) and mixed in a 1:1 ratio for 2 min in a Kenwood stand mixer. Whole size 14 Foley catheters (Bard Medical, UK) were immersed in the dip-coating and the silicone allowed to fill the catheter lumen. The catheters were removed from the dip-coating after 5 min and hung at room-temperature for 12 h, for excess coating to be removed and partial curing to occur. The catheters were autoclaved at 121°C for complete curing and sterilisation.

### 6.2.3 Assessment of bulk-loaded antimicrobial cylinders and dip-coated catheters to prevent ascending *Proteus mirabilis* infection using an *in-vitro* bladder model

The *in-vitro* bladder model was assembled as depicted in Figure 6.2.1. Briefly, reservoirs containing artificial urine at pH 6.1 (as described in Section 5.2.1), were connected via silicone tubing to a glass bladder chamber, with a section of the tubing passing through a peristaltic pump. The AU was delivered to the bladder chamber at a flow rate of 0.5 ml/min. Size 14 all silicone Foley catheters (Bard Medical, UK), were inserted through the tubing at the base of the bladder (urethra) and into the bladder chamber and retained by the catheter balloon inflated with 10

ml of sterile distilled water ($dH_2O$) using a syringe. The catheters were connected to urine drainage bags (Bard Medical, UK) to collect the waste AU.

To assess the ability of silicone bulk-loaded with triclosan and triclosan acetate to prevent ascending *P. mirabilis* infection, cylinders constructed as described in Section 6.2.1 were attached between the base of the catheter and the drainage bag via plastic connectors, leaving a 10 mm bridge of antimicrobial silicone.

*Proteus mirabilis* 12 RTB was cultured in Mueller-Hinton broth (MHB) for 4 h at 37°C and the suspension was centrifuged at 4000 rpm for 5 min. The broth was removed from the pellet which was resuspended in 10 ml of AU. The bacterial suspensions were added to the drainage bags of the bladder models via a strippette, and the bags lifted so that the contaminated AU flowed back down the catheter to levels 1 cm below the base of the silicone inserts. These contamination events were performed at 6 hourly intervals during the first 12 h, followed by a 12 h 'rest period' that occurred overnight. These contamination events occurred daily until the experiment terminated. Drainage bags were emptied daily, leaving 100 ml of residual urine for contamination events.

AU from the bladder chamber was sampled daily and pH recorded using a pH meter (Hanna Instruments, Bedfordshire, UK). The time of *Proteus* infection and catheter blockage was recorded. *Proteus* infection time was determined by growth of *P. mirabilis* colonies on CLED agar from the sampled urine. Each silicone formulation was evaluated over 3 independent experiments. All experiments were conducted in a 37°C warm room.

To determine the effectiveness of catheters dip-coated with triclosan and triclosan acetate, bladder models were set up in a similar way. However, dip-coated catheters (produced in Section 6.2.2), were used without silicone cylinder connections connected between the catheter and drainage bag. Contamination events were performed 3 times daily, but the contamination level was 10 cm above the catheter/drainage bag connection point (depicted in Figure 6.1). The pH of the AU from the bladder chambers was monitored daily along with the time of catheter blockage. Residual volumes of 100 ml of AU were left in the drainage bags following daily emptying. The experiments continued until catheter blockage occurred or for 9 days. Each dip-coating was evaluated 6 times in 6 independent experiments.

Catheters were removed at the end of each experiment and incubated at 37°C to allow crystalline biofilm to dry, before preparation for scanning electron microscopy (SEM).

### 6.2.4 Determination of pH of AU collected from *in vitro* bladder model

Immediately after the AU was collected at each experimental time-point, a portion of the collected AU was passed through a 0.2 μm syringe filter (Sarstedt) to remove microorganisms and the pH measured using a benchtop pH meter (Hanna Instruments). Following calibration of the instrument according to the manufacturer's instructions, the probe was immersed in the sample until the reading stabilised, and the digital reading was recorded. The pH of each sample was measured three times and the average reading recorded. Statistical analysis was conducted using one-way ANOVA with multiple comparisons.

### 6.2.5 Scanning electron microscopy of dip-coated catheters

Low vacuum scanning electron microscopy was used to image biofilm formation in the catheter lumen. Blocked and control catheters were cut into 3 mm cross-sections just below the catheter eye hole and mounted on to aluminium stubs using Leit-C conductive carbon cement (Neubauer Chemikalien, Germany). These were then coated with a thin layer of gold, using a desktop sputter coater (DSR1, VacTechniche, Hastings, UK). Catheter sections were imaged under low vacuum using a scanning electron microscope (Vega, Tescan, Czech Republic).

### 6.2.6 XRMA analysis of crystalline biofilm

Deposits of crystalline biofilm were mounted on to aluminium stubs using adhesive mounts. Stubs for X-ray Micro Analysis (XRMA) were coated in carbon in a Shimadzu Carbon Coater and analysed in the SEM, with the IDFiX microanalysis System (SamX France).

### 6.2.7 Performance of bromothymol blue sensor materials and resazurin in a *Proteus mirabilis*-inoculated, *in vitro* bladder model

The bladder model was assembled as described in Section 6.2.3. *Proteus mirabilis* 12 RTB was cultured overnight in Muller-Hinton broth (MHB) at 37°C and culture

pellets obtained by centrifuging at 4000 rpm (IEC CL10, ThermoFisher Scientific). The broth was replaced with AU and the cultures diluted to 0.3 $OD_{600}$ with additional AU. Five ml of the inoculum was taken up into a stripette and the bladder chamber aseptically inoculated. The solution was left for 1 h, prior to activating the peristaltic pump (Watson Marlow).

Catheters were connected to modules containing silicone sensor materials (described in Sections 5.2.6.1-5.2.6.3), with waste AU passing from the bladder chamber via the catheter, over the sensor material before flowing into the drainage bag (Bard Medical, UK). Multiple sensor units were connected below each other to enable numerous materials to be assessed simultaneously. A bladder model without bacteria was similarly prepared as a negative control. Samples of AU were aseptically collected from the bladder chambers and drainage bags at 1 h, 2 h, 4 h, 6 h, 12 h and 24 h and pH readings taken immediately. The catheters were removed from the bladder model after blockage and stored at 37°C before sectioning and processing for SEM.

A camera (Canon EOS 700D) secured to a tripod and connected to an intervalometer (Qumox, Hong Kong), was set up to take a time-lapse image of the bladder model/sensor every 30 min for 48 h. The time taken for the sensor materials to change to the desired colour and the time of catheter blockage were established by reviewing the captured images of the bladder model and volume of urine in the chamber.

### 6.2.8 Resazurin as an indicator for bladder infection in catheterised models

The *in- vitro* bladder model was set up as previously described and inoculated with *P. mirabilis* 12 RTB. At each time-point ( 1 h, 2 h, 4 h, 6 h,12 h and 24 h) two ml of AU was removed via the drainage port to be used to calculate colony forming units. A 500 μl volume of sterile resazurin solution (0.015 % w/v in $dH_2O$), was delivered into the drainage bag via the same drainage port and mixed with gentle agitation of the bag. The colour of the AU was noted after 20 min and the drainage bag was emptied between timepoints.

## 6.3 Results

### 6.3.1 Assessment of bulk-loaded antimicrobial cylinders and dip-coated catheters to prevent ascending *Proteus mirabilis* infection in an *in-vitro* bladder model

Based on two experiments, the mean number of days for bladder model chambers with non-antimicrobial silicone catheter inserts to be infected by *P. mirabilis* was 8.5 days, confirmed by growth of colony forming units from AU sampled from the bladder chamber. In a third experiment, the bladder chamber was not infected after 9 days.

Silicone cylinders bulk-loaded with triclosan (T2), failed to prevent migration of *Proteus mirabilis* from the drainage bags to the bladder chambers of the *in-vitro* bladder models, with mean infection occurring at 6.3 days. Over the course of the 9 day experiment, catheter blockage only occurred in 1 out of 3 models containing triclosan inserts (Table 6.3.1). Migration of *P. mirabilis* into the bladder chambers was prevented by triclosan acetate silicone inserts in 2 out of 3 experiments.

The pH of AU in the bladder chambers of the models with triclosan and triclosan acetate inserts was not statistically different ($P > 0.05$) from AU from models with non-antimicrobial inserts (fig. 6.3.1).

**Table 6.3.1** Time (days) for ascending *Proteus mirabilis* to reach the bladder using bulk-loaded antimicrobial silicone inserts to prevent migration.

| Silicone formulation | Time for *P. mirabilis* to reach bladder chamber (days) | | |
|---|---|---|---|
| | Experiment 1 | Experiment 2 | Experiment 3 |
| Control (S2) | 8 | 9 | > 9 |
| Triclosan (T2) | 7 (blocked at 9 days) | 6 | 6 |
| Triclosan acetate (TA-2) | > 9 | 7 | > 9 |

S2 = no antimicrobial, T2 = 1% w/w triclosan, TA-2 = 1% w/w triclosan acetate

>9 days define dip-coated bladder chambers that did not become infected with *P. mirabilis* over the 9 day experiment

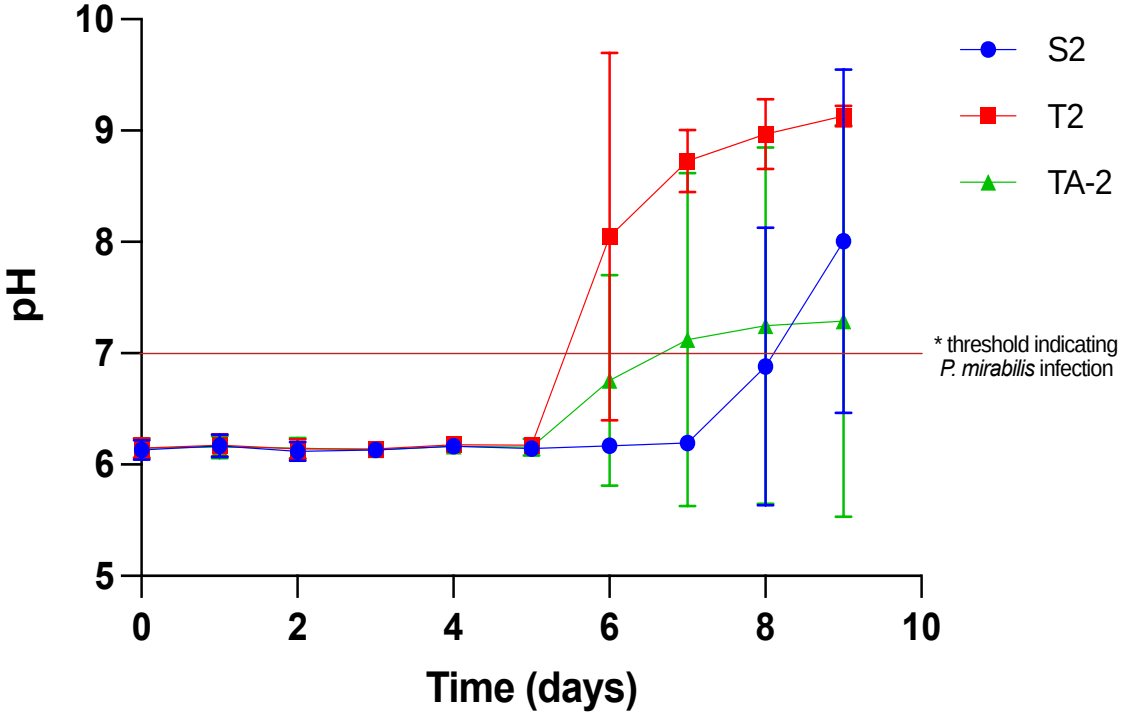


**Figure 6.3.1** Effect of bulk-loaded antimicrobial inserts on AU pH in an *in-vitro* bladder model of ascending *Proteus mirabilis* infection. AU was sampled from the bladder chambers of *in-vitro* bladder models and pH was recorded daily for 9 days. Silicone cylinders bulk-loaded with 1% w/w triclosan (T2), triclosan acetate (TA-2) or without antimicrobial compound (S2), were positioned between the catheters and drainage bags of *in-vitro* bladder models and challenged with AU inoculated with *Proteus mirabilis*. pH readings above 7 indicate *P. mirabilis* infection. Each silicone formulation was assessed 3 times in 3 independent experiments. Mean values plotted +/- SD. Statistical analysis was performed using one-way ANOVA with multiple comparisons

All bladder chambers connected to catheters dip-coated with a non-antimicrobial silicone formulation were infected with *P. mirabilis* during the course of the experiments, with mean infection time of 6.7 days and catheter blockage only occurred in half of these models (Table 6.3.2). The mean pH increased from the baseline of 6.1 – 6.3 to above 7 by day 6 and peaked just below pH 9 at day 8 (Figure 6.3.2). In contrast, all models dip-coated with the triclosan formulation prevented *P. mirabilis* infection over the duration of the experiment, with the pH remaining at a base level of 6.1-6.3. Triclosan acetate dip-coated catheters prevented migration of *P. mirabilis* into the bladder chamber in all but one of the test models (Table 6.3.2).

The pH of AU from the bladder chambers of models with triclosan and triclosan acetate dip-coated catheters *in- situ* were statistically different ($P < 0.05$), to those from the non-antimicrobial coated catheter models (Figure 6.3.2).

**Table 6.3.2** Time (days) for ascending *Proteus mirabilis* to reach the bladder, utilising antimicrobial dip-coated catheters to prevent migration*

| Catheter dip-coating | Time for *P. mirabilis* to reach bladder chamber (days) | | | | | |
|---|---|---|---|---|---|---|
| | Experiment 1 | Experiment 2 | Experiment 3 | Experiment 4 | Experiment 5 | Experiment 6 |
| Control | 5 | 7 (blocked at 9 days) | 8 | 7 | 6 (blocked at 9 days) | 7 (blocked at 9 days) |
| Triclosan (0.2% w/w) | > 9 | > 9 | > 9 | > 9 | > 9 | > 9 |
| Triclosan acetate (0.2% w/w) | > 9 | > 9 | 8 | > 9 | > 9 | > 9 |

> 9 days define dip-coated bladder chambers that did not become infected with *P. mirabilis* over the 9 day experiment.

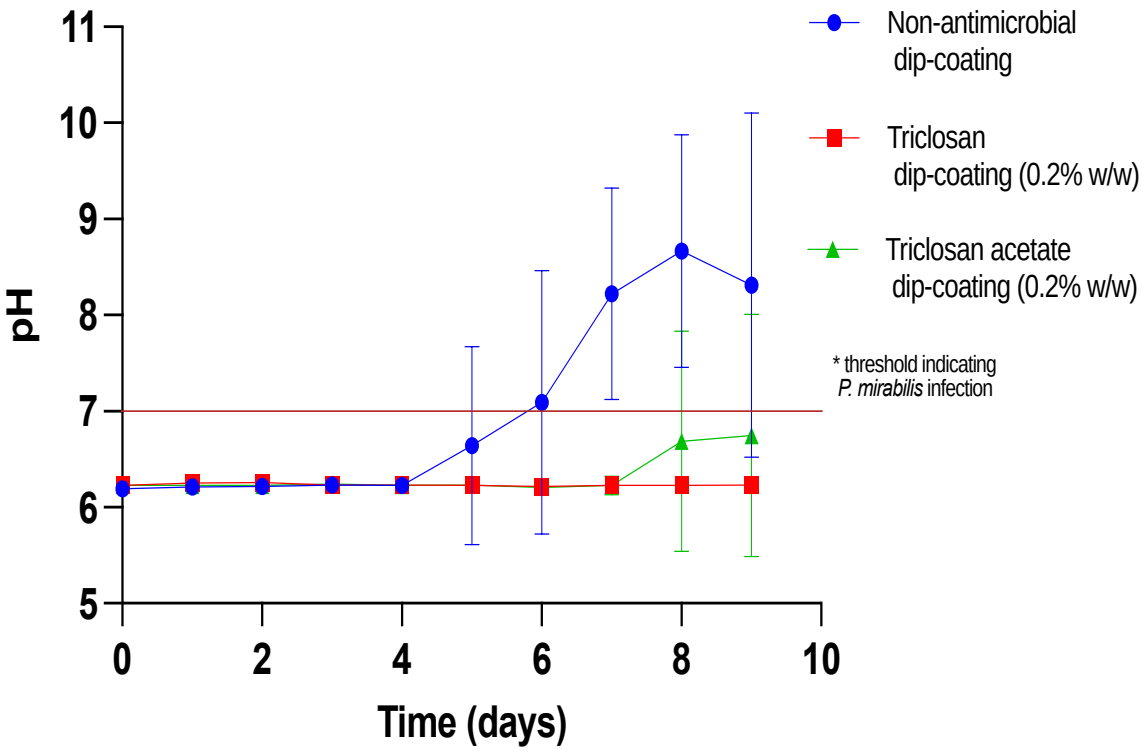


**Figure 6.3.2** Effect of antimicrobial dip-coated catheters on AU pH in an *in-vitro* bladder model of ascending *Proteus mirabilis* infection. Daily pH recordings from AU sampled from bladder chambers of *in-vitro* bladder models over 9 days. All-silicone Foley catheters dip-coated with 0.2% w/w triclosan, triclosan acetate or solvent only were used in *in-vitro* bladder models and challenged with AU inoculated with *Proteus mirabilis*. pH readings >7 indicate *P. mirabilis* infection in the bladder chamber. Each dip-coating formulation was assessed 6 times over 6 independent experiments. Mean values plotted +/- SD. Statistical analysis was performed using one-way ANOVA with multiple comparisons

Scanning electron micrographs of blocked catheters revealed encrustation and blockage around the catheter eye-holes (Figure 6.3.3A). X-ray microanalysis of areas of the catheter without encrustation confirmed the predominant element in the catheter material to be silicon (Figure 6.3.3B). The encrusted biofilm formed on the catheter surfaces appeared to be made up of material with two distinct morphologies. XRMA of the crystalline structures depicted in Figure 6.3.3C were shown to be predominantly comprised of magnesium and phosphorus, with trace elements of silicon, calcium and potassium (Figure 6.3.3D). The major components of the powdered substance shown in Figure 6.3.3E were calcium and phosphorous, with smaller amounts of silicon, sodium, magnesium chlorine and potassium detectable (Figure 6.3.3F).

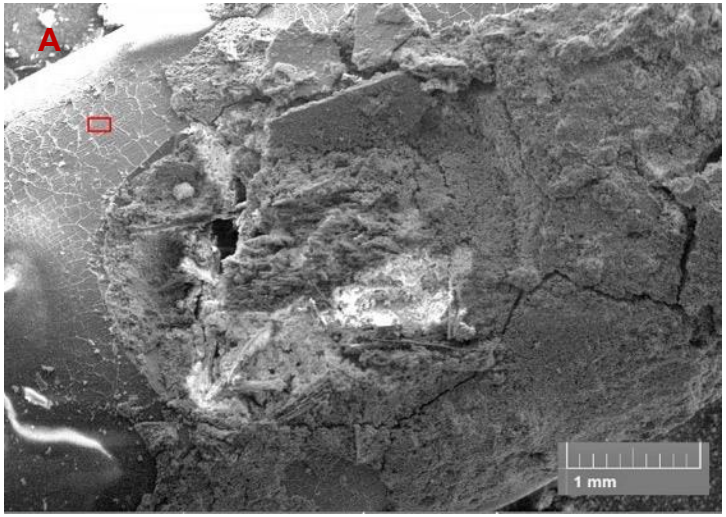
A
1 mm

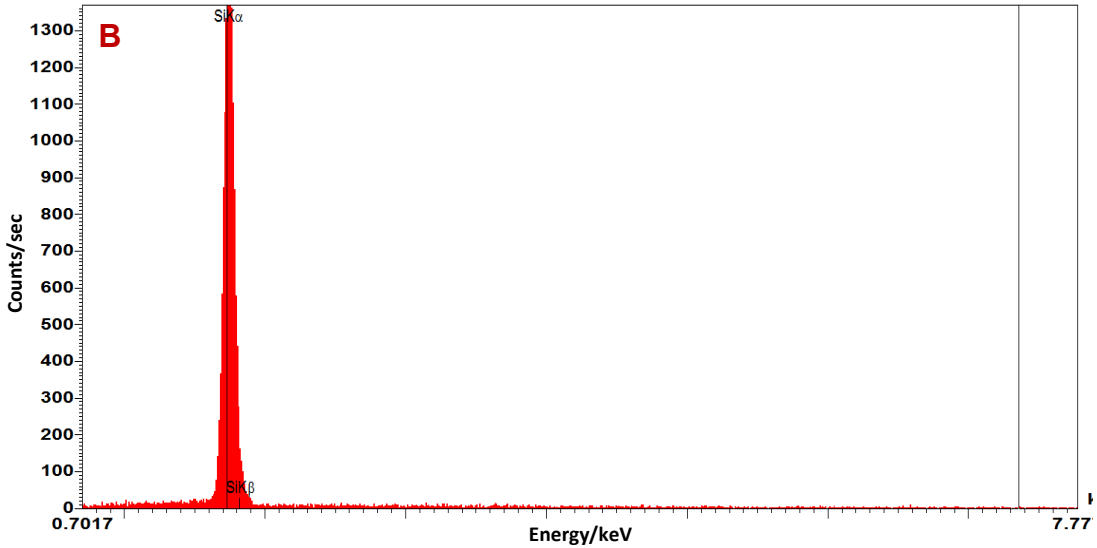
B
SiKα
SiKβ
Counts/sec
Energy/keV
0.7017
7.77

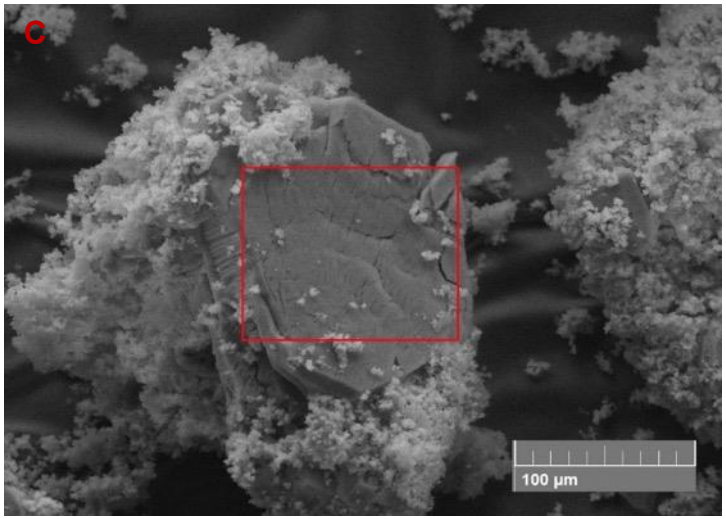
C
100 µm

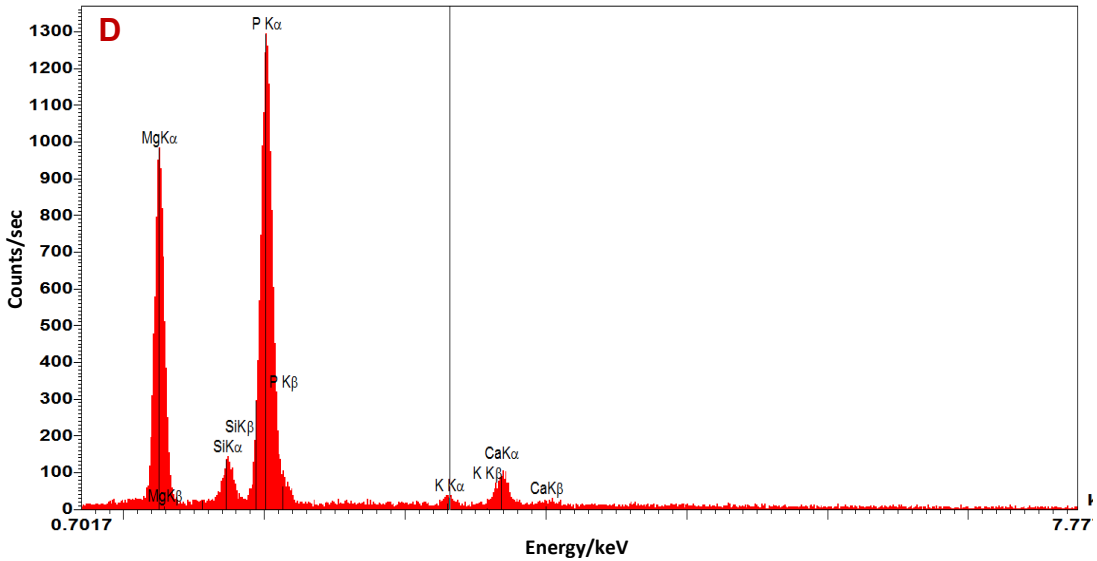
D
P Kα
MgKα
P Kβ
SiKβ
SiKα
MgKβ
K Kα
CaKα
K Kβ
CaKβ
Counts/sec
Energy/keV
0.7017
7.77

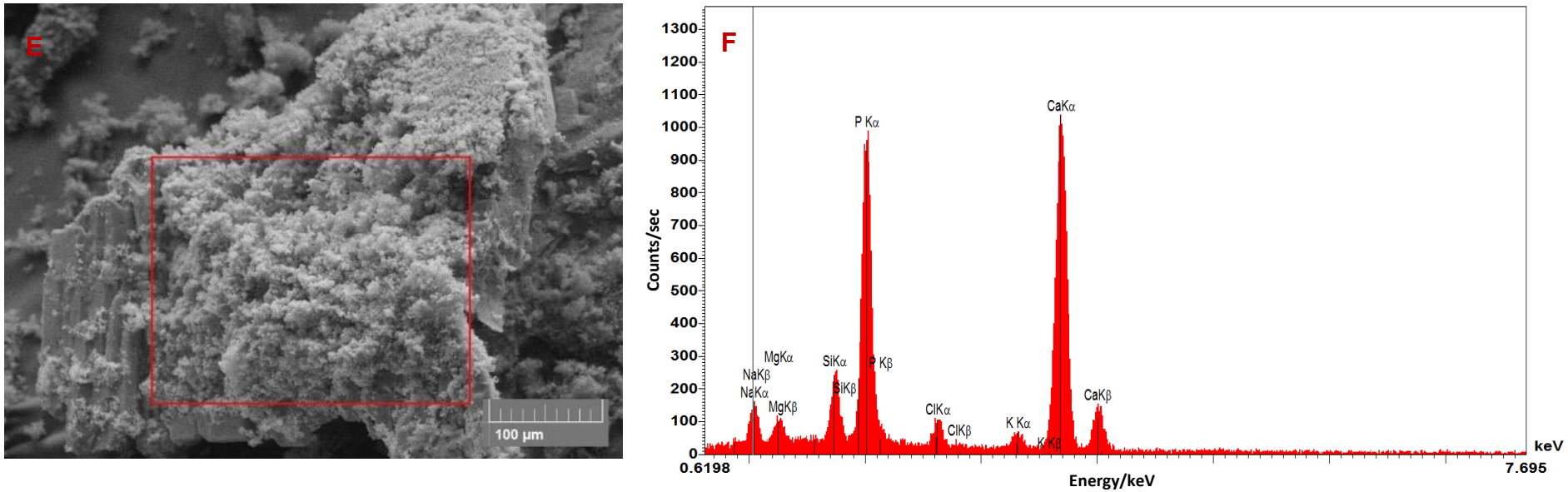


**Figure 6.3.3** Representative scanning electron micrographs and corresponding XRMA of Foley catheter sections taken from a *Proteus mirabilis* encrusted catheter, used in an *in-vitro* bladder model of ascending infection. **A**. An encrusted eye-hole of a catheter used in a bladder model with silicone inserts without antimicrobial compound. **B.** XRMA graph depicting the chemical composition of the area within the marked area of picture A. **C**. A crystalline structure present on the catheter surface. **D** Depicts the chemical composition of the crystalline structure**. E.** Powder material attached to an underlying crystal and **F** represents the corresponding chemical composition.

### 6.3.2 BTB sensor materials and resazurin for *Proteus mirabilis* detection *in vitro* bladder model

Inoculation of *in-vitro* bladder models with *P. mirabilis* 12 RTB, was used to assess the performance of silicone sensor materials containing the pH sensing compound, BTB, and a porous version of the same material (BTB-P). The resazurin foam (produced in chapter 4) was also investigated, but the resazurin was rapidly depleted from the material (*data not shown*) so an alternative was to investigate the release of resazurin solution directly into the drainage bags as a potential microbial detection mechanism. Measurements of pH and CFUs were performed at regular intervals up to 24 h and the time for catheter blockage was also recorded.

The pH of AU collected from the bladder chamber and drainage bags of uninoculated models remained constant at pH 6.3 throughout the 24 h period (Figure 6.6.4). Linear regression analysis performed on the data from the uninoculated bladder and drainage bag samples showed they were not statistically different ($P > 0.05$).

Figure 6.6.4 showed that inoculating the bladder chamber with *P. mirabilis* caused a rapid increase in the pH of AU in the bladder chamber within the first hour, from 6.3 to 7.3. The pH dipped slightly, before steadily increasing to a final pH just below 9 at 24 h. The pH of AU collected from the drainage bag of the inoculated model showed a similar trend to that collected from the bladder chamber with the pH increasing from 6.3 to 9.0 over the 24 h period. Linear regression analysis of the data from the inoculated bladder and drainage bag samples shows they were not significantly different ($P > 0.05$). The pH of AU that had been inoculated with *P. mirabilis* was significantly different to the uninoculated samples, regardless of sample collection point ($P < 0.0001$) (Figure 6.6.4).

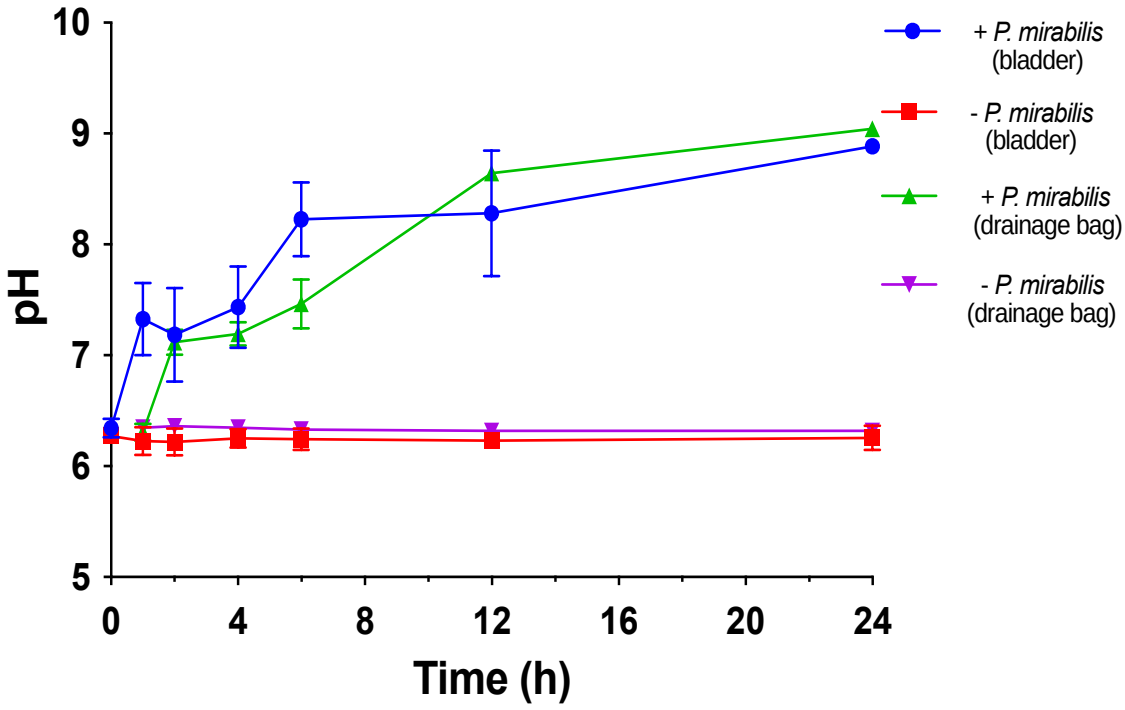


**Figure 6.6.4.** pH of AU collected from the bladder chamber and drainage bags of the *in vitro* bladder model inoculated ± *Proteus mirabilis* 12 RTB. The mean of three separate experiments were plotted with error bars representing SD and linear regression analyses were performed.

AU collected from the bladder chamber of the *in vitro* bladder model showed an initial decrease in *P. mirabilis* CFUs, between 1 and 6 h after the flow of AU commenced. CFU counts subsequently increased up to 1.5 x $10^7$/ml at 24 h (Figure 6.3.5). No CFUs were detected from AU collected from the bladder chambers and drainage bags of uninoculated models at any time-point.

AU collected from the drainage bag of the inoculated bladder model produced lower numbers of CFUs of *P. mirabilis* than the samples collected from the bladder chamber, up to 6 h. There was subsequently a rapid increase in CFU numbers between 6 h and 24 h. However linear regression analysis concludes that the slopes of bladder AU and drainage bag AU samples were not significantly different ($P > 0.05$) (Figure 6.3.5).

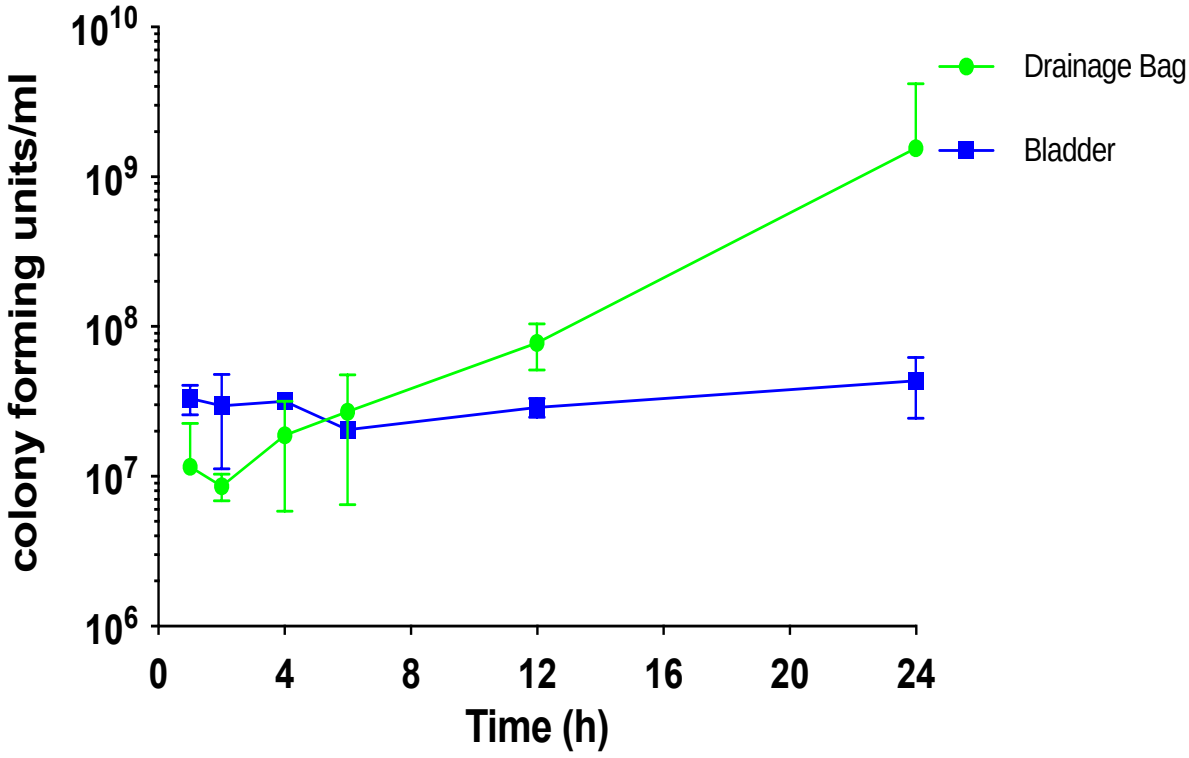


**Figure 6.3.5.** CFUs of *Proteus mirabilis* in AU collected from the bladder chambers and drainage bags of *in vitro* bladder models**.** Data expressed as mean values of 3 independent experiments. Error bars represent SD.

The mean time for the standard BTB silicone sensor to signal a *P. mirabilis* infection occurred at 6.67 h (Table 6.3.3). An increase in sensor surface area created by the introduction of pores within the silicone material (BTB-P), allowed the signal to be detected 3 h earlier than the standard material. The pH of AU at the time of signalling was pH 8.4 for BTB sensor and pH 7.2 for the BTB-P sensor (Figure 6.3.4). Resazurin solution added directly to the drainage bags signalled the presence of proliferating cells within the AU 6 h post infection (Figure 6.3.7 and Table 6.3.3).

Importantly, all three sensor materials or molecules signalled *P. mirabilis* infection over 40 h before catheter blockage occurred, with BTB-P signalling at 43.67h pre-blockage and BTB and resazurin signalling 40h and 40.67h pre-blockage, respectively.

The standard BTB sensor material remained yellow/orange throughout the 48 h period, when AU alone flowed across the surface (Figure 6.3.6, panel A), changing to blue/black once ammonia had been generated in the AU from the breakdown of urea by urease positive *P. mirabilis* (Figure 6.3.6B). The formation of a thick crystalline biofilm over the sensor material is also clearly depicted in Figure 6.3.6B. At the starting pH of 6.2, the porous sensor material (BTB-P) was a yellow/green colour (panel C) and transformed to blue/black (Figure 6.3.6D) once the pH increased above 7.2. As with panel B, a thick biofilm can be observed upon the surface of the BTB-P sensor (Figure 6.3.6D).

**Table 6.3.3** Comparison of the times taken for the porous bromothymol blue sensor material (BTB-P), standard bromothymol blue sensor (BTB) material and resazurin added to the drainage bag, to signal the presence of *P. mirabilis* infection

| Experiment No. | Sensor trigger time (h) | | | Catheter blockage time (h) |
|---|---|---|---|---|
| | BTB-P | BTB | Resazurin | |
| **1** | 3.5 | 7 | 6 | 42 |
| **2** | 4 | 6.5 | 6 | 51 |
| **3** | 3.5 | 6.5 | 6 | 47 |
| **Mean value** | **3.67** | **6.67** | **6** | **46.67** |

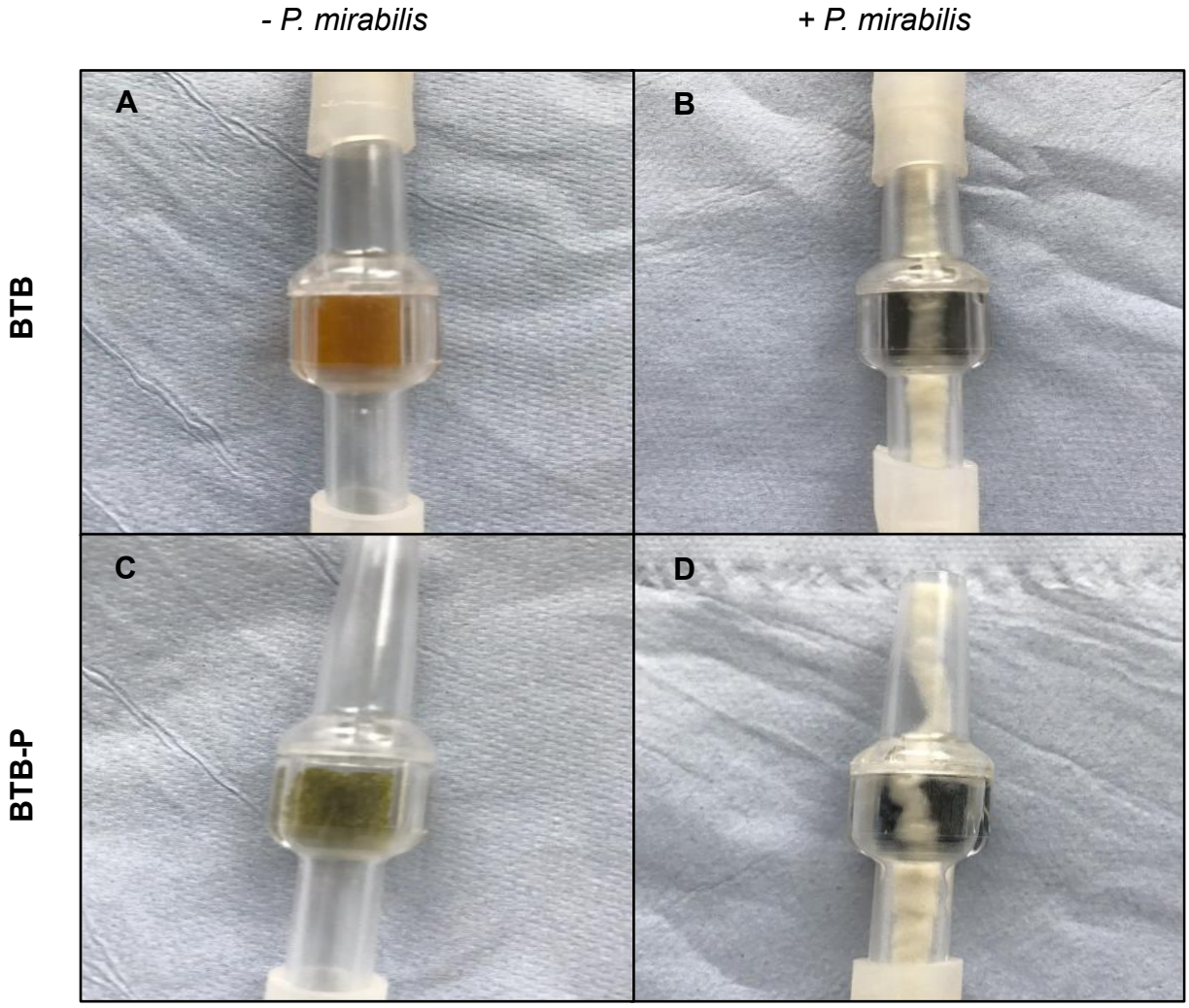


**Figure 6.3.6** Standard bromothymol blue sensor material (BTB) and porous bromothymol blue sensor material (BTB-P) 48 h post-inoculation of the *in-vitro* bladder model with *Proteus mirabilis*. Panels B and D depict the BTB and BTB-P sensor materials, respectively. Panels A and C represent the appearance of the BTB and BTB-P sensor materials without bladder chamber inoculation

Figure 6.3.7 clearly illustrates how the resazurin solution effectively indicated the presence of proliferating bacteria in AU, collected from indwelling urinary catheters. The colour of AU in the drainage bags connected to bladders that had been inoculated with *Proteus mirabilis* showed a change from blue/green to pink colour 4 h after inoculation. Extrapolation from Figure 6.3.5 indicated that the sensitivity of resazurin in this system was at 1.5 x $10^7$ CFU/ml viable cells.

Following resazurin staining of AU in drainage bags connected to uninoculated bladders, the AU changed to a blue/green colour and remained so after the 20 min colour development time. Colour change did not occur at any time-point.

Scanning electron micrographs of urinary catheters removed 48 h after inoculation of the bladder chamber with *P. mirabilis*, revealed the crystalline structure of the biofilm deposited (Figures 6.3.8D-F). Flow of AU into the bladder chamber was stopped once the AU was unable to drain into the drainage bag. Panels C-F of Figure 6.3.8 clearly show a build-up of struvite and hydroxyapatite crystals around the eye-hole and throughout the catheter lumen, preventing drainage of AU. There was no evidence of biofilm formation along the catheter removed from the control bladder (Figure 6.3.8A-C). The catheter eye-hole and lumen were clear of crystalline deposits.

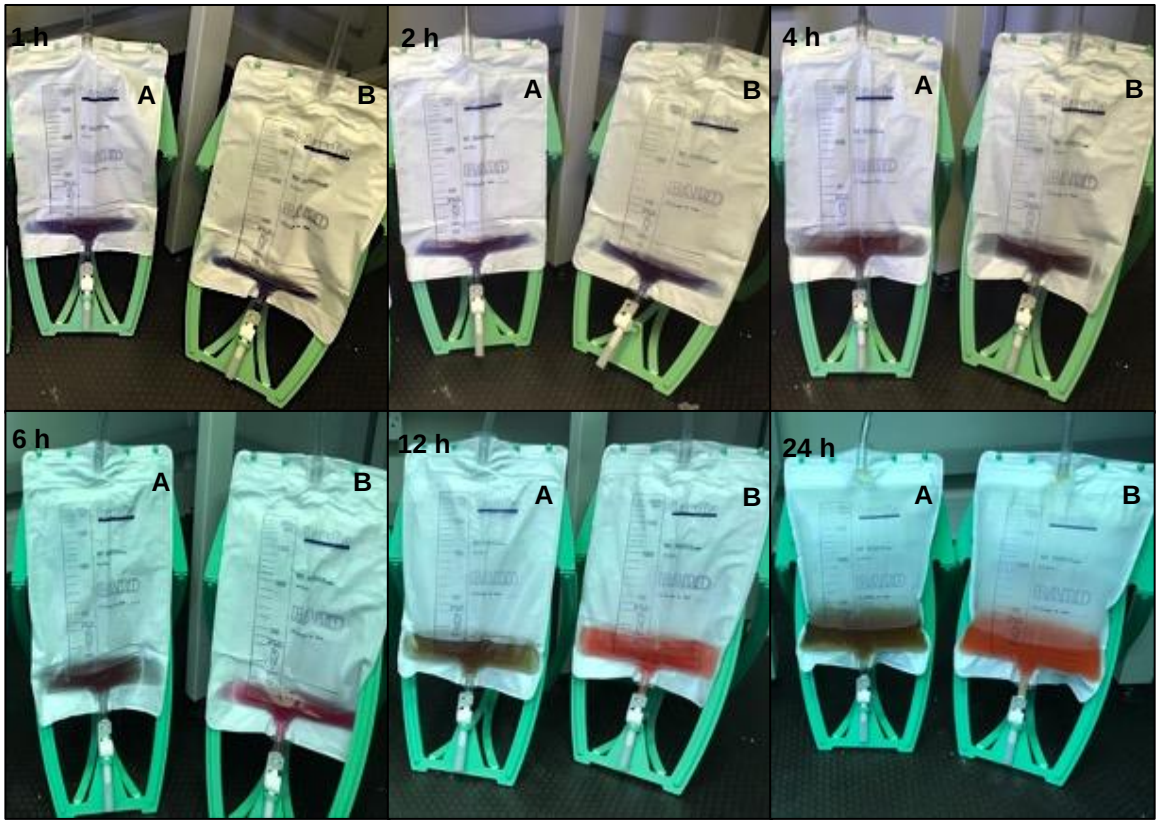


**Figure 6.3.7** Resazurin stained AU collected in drainage bags from an *in-vitro* bladder model, at intervals between 1h and 24 h. Bags A and B represent bladders without and with *Proteus mirabilis 12 RTB*, respectively

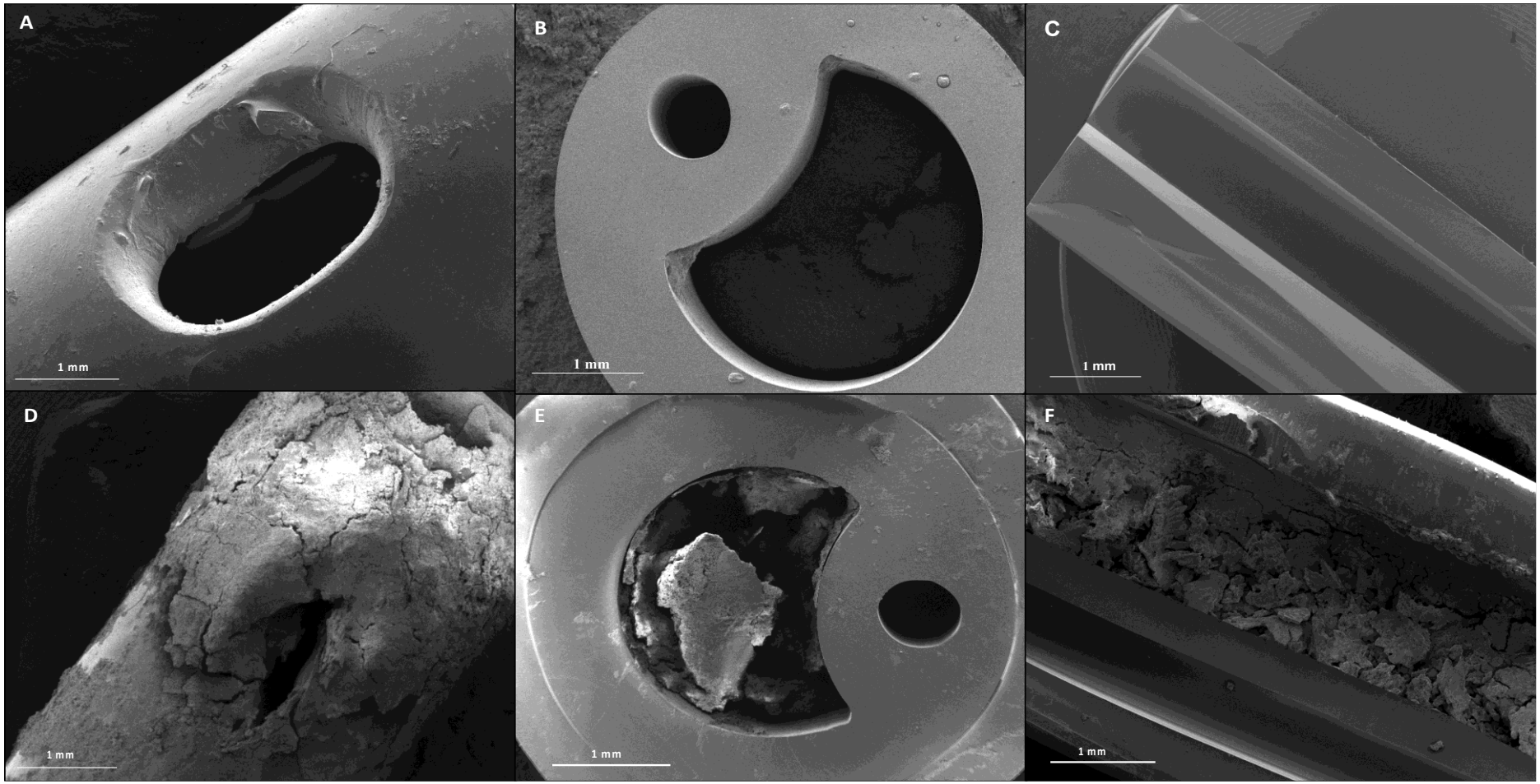


**Figure 6.3.8** Scanning electron micrographs of urinary catheters removed from an *in vitro* bladder model 48 h post-inoculation. Panels A-C represent a catheter from a bladder model without bacteria. Panels D-E show eye-hole, transverse and longitudinal sections through a urinary catheter removed from a *Proteus mirabilis 12 RTB* infected bladder

## 6.4 Discussion

The urinary tract is prone to colonisation by numerous microorganisms, including commensal organisms that colonise the skin and tissue surrounding the urethra, such as *Staphylococcus* species and *Candida* species. Bacteria that normally reside within the digestive tract, including *E. coli*, *P. mirabilis* and *K. pneumoniae* are also able migrate to the urinary tract (Daifuku & Stamm, 1984), with greater incidence of UTIs reported in females, compared to males, due to differences in anatomy, namely shorter urethral lengths and closer proximity of the urethra to the anus (Dund, Durani and Ninama 2015). However, healthy, functioning urinary tracts have systems to mitigate invasion by microorganisms, including removal of microorganisms during voiding, shedding of infected bladder epithelial cells, production of cytokines and initiation of inflammation by the uroepithelium (Lichtenberger & Hooton, 2008; Mulvey et al., 2000).

The introduction of a catheter into the urinary tract disables many of these defence systems and increases the likelihood of bacterial entry into the urinary tract. The force of urine flow from the bladder is reduced and the device provides a direct link between the urinary tract and the external environment (Lichtenberger & Hooton, 2008). A urinary catheter can facilitate entry of microorganisms into the bladder through migration of motile bacteria along extraluminal surfaces or entry can be gained during the catheter insertion process (Lichtenberger & Hooton, 2008). Biofilm formation on the intraluminal surfaces also contributes to CAUTI development, with frequently colonised ‘touch points’, such as drainage taps and connection ports, enabling access of bacteria into the closed drainage system (Lichtenberger & Hooton, 2008).

The formation of crystalline biofilms by urease positive microorganisms along the catheter often leads to catheter blockage, with severe consequences caused by retention of infected urine and reflux into the kidneys. Pyelonephritis and septicaemia can occur, which may prove fatal (Hooton, 2012; D. J. Stickler & Morgan, 2008).

Current approaches to prevent catheter encrustation, include the use of maintenance solutions to irrigate the bladder and catheter, with solutions containing sodium chloride and citric acid commonly used (Paterson et al., 2019). The volume and frequency of administration may vary depending on local policy

(Paterson et al., 2019). However a Cochrane review found insufficient evidence to determine if prophylactic maintenance solutions were beneficial or harmful (Shepherd et al., 2017). Additional approaches to the prevention and management of catheter encrustation, include optimising fluid intake, increasing the acidity of urine through consumption of lemon and prune juice, increased frequency of catheter changes and the use of silver-alloy coated catheters (Paterson et al., 2019).

The use of silver-alloy coated catheters including BARDEX® I.C, (see Table 6, Chapter 1), has been shown to reduce bacteriuria in patients catheterised for a mean of 5 days following radical prostatectomy procedures when compared to a group catheterised with a latex catheter. However this benefit was lost when the catheterisation time increased, with no significant differences observed in bacteriuria after 14 days (Verleyen et al., 1999).

Many research groups have attempted to develop antimicrobial urinary catheters, with mixed success. The incorporation of triclosan, sparfloxacin or rifampicin into the bulk of the silicone catheter matrix has previously been studied (Fisher et al., 2015). The antimicrobial compounds were dissolved in chloroform and the catheters immersed into the antimicrobial loaded solvents to allow penetration into the matrix. This approach successfully prevented catheter colonisation by *P. mirabilis*, *S. aureus* and *E. coli* for 7-12 weeks, when tested in an *in-vitro* flow model. In comparison, commercially available silver-processed and nitrofural coated catheters showed activity of ≤ 2 days in the same study (Fisher et al., 2015). A further clinical trial of a catheter impregnated with all 3 agents involving 30 patients who used long-term catheters (>28 days), revealed that significantly fewer bacterial isolates were attached to the catheter balloons than their original matched catheters. However, there were 84 adverse events recorded amongst the group that were attributed to the antimicrobials or the impregnation process. Furthermore, 82.14% of the participants rated the catheter as no better or different to their usual device.

Despite efforts from researchers and healthcare providers to prevent catheter encrustation, the problem still exists and impacts the well-being of long-term catheter users and the resources of the NHS.

A survey of patients admitted to NHS Trusts between 2016 and 2017, revealed that catheter associated infections, including urinary tract and blood stream

infections, incurred 45,717 excess bed days, 1467 deaths and 10,471 lost quality life adjusted years (QALYs). The total direct hospital costs were estimated at £54.4 million (Smith et al., 2019). To this end, the purpose of this research was to investigate the ability of materials with incorporated biocides to prevent intra-luminal migration of *P. mirabilis* from the drainage bag to the bladder chamber and prevent the associated encrustation and catheter blockage.

The integration of solid inserts constructed from bulk-loaded triclosan and triclosan acetate silicone rubber into the *in-vitro* bladder model was investigated as one approach. A similar strategy was employed by Jordan et al, using shorter inserts of 5 mm in length and inserting them into the fluted end of the catheter, but this approach was unsuccessful (Jordan et al., 2015). It was hypothesised that longer silicone inserts, 16 mm in length, placed between the end of the catheter and drainage bag would create a biocidal bridge that would prevent migrating *Proteus* bacteria from ascending into the catheter and ultimately, into the bladder chamber. Unfortunately, neither of the materials prevented or delayed catheter encrustation over the experimental period. The flow of AU over the antimicrobial silicone sections may have 'washed-away' released antimicrobial agent, maintaining a low surface concentration, and thus negating antimicrobial effects.

To overcome the issues of using short, bulk-loaded sections, entire Foley catheters were dip-coated with triclosan and triclosan acetate containing silicone, providing coatings to the intra and extra-luminal surfaces. All 6 triclosan dip-coated catheters delayed encrustation, by *P. mirabilis,* compared to control catheters, with no infection apparent in the bladder chamber at the experimental end point (9 days). Jordan et al also reported similar findings with 12 of 13 triclosan dip-coated catheters delaying encrustation, compared to controls. However, 4 of these were reported as blocking over the 7 day experimental period (Jordan et al., 2015).

Triclosan acetate dip-coatings also prevented or delayed bladder chamber infection by *P. mirabilis,* compared to controls, with 5 out of 6 bladder chambers remaining infection-free over the test period. The intermittent flow of AU in the bladder model may allow for continued hydrolysis of the triclosan ester to its parent compound, triclosan, and thus delay *P. mirabilis* infection.

Another factor to consider for the improved antimicrobial effects of the dip-coated catheters over the bulk-loaded inserts, is the release of antimicrobial compound from the catheter tip into the AU in the bladder chamber. Such release could allow

a flow of AU containing antimicrobial compound along the urinary catheter, contributing to effects of the compound released lower down the catheter.

*Proteus mirabilis* driven breakdown of urea to ammonia and hydroxyl ions was evidenced by elevated pH of AU. In control catheters, such conditions allowed a crystalline biofilm to form, and SEM and x-ray microanalysis confirmed the presence of crystalline apatite structures formed from large quantities of calcium and phosphate, and powdered struvite formed from magnesium and phosphate.

Whilst the use of triclosan may be controversial, due to reports of cell toxicity and carcinogenicity (Fang et al., 2010; Singha et al., 2017), triclosan use is still permitted in many products with the exception of over-the-counter antiseptic products. To this end, application of triclosan and its derivatives to prevent biofilm development along urinary catheters and reduce CAUTI incidence was determined to be of potential clinical benefit to susceptible patients with long-term indwelling catheters.

Another aim of the research was to produce materials that would signal microbial infection of the catheterised urinary tract, allowing clinicians to implement timely interventions including antibiotic therapy and catheter replacement. Researchers at the University of Bath previously developed a catheter that signalled infection by urease positive organisms and gave a 10-12 h warning of impeding blockage (Milo et al., 2016). However, due to concerns over potential cytotoxic effects of the released carboxyfluorescein dye on the urethra and poor visibility of the dye, a pH responsive lozenge was developed containing a greater concentration of dye that was designed to be situated within the drainage bag (Milo et al., 2018).

The BTB silicone sensor that was previously developed between Cardiff University and Technovent Ltd, was produced and evaluated alongside a porous version (BTB-P) with an increased surface area. In the bladder model, the BTB sensor predicted catheter blockage by *P. mirabilis* 40 h in advance of occurrence, compared to 17-24 h in a similar study by Malic et al (Malic et al., 2012). Small variations in experimental protocols may account for discrepancies in signalling times. The urease activity of the different *P. mirabilis* strains used in the two studies are also factors that may have caused different signalling times.

Early detection of *P. mirabilis* infection would allow for interventions, such as antibiotic therapy to be administered and prevent complications associated with catheter blockage. To this end, it was hypothesised that increasing the surface

area of the BTB sensor would enable higher numbers of ammonium ions from *P. mirabilis* infected AU to penetrate the silicone material and elicit the pH-dependent colour change from yellow to dark blue at an earlier timepoint. This hypothesis was proven when the BTB-P sensor was placed alongside the BTB sensor in the bladder model and signalled *P. mirabilis* infection 43 h before catheter blockage, 3 h earlier than the BTB sensor. The mean AU pH at the time of signalling for the BTB-P sensor was pH 7.2, compared to pH 8.2 for the BTB sensor.

Although the pH range of normal human urine is pH 4.5-8.0 (Nall, 2018), it is anticipated that penetration of the silicone rubber by ammonium ions from *P. mirabilis* infected AU is required to trigger the sensor colour change. A clinical trial of the BTB silicone sensor was previously conducted, with 7 patients completing the trial (Long et al., 2014). The sensor signalled infection in 6 out of the 7 patients who were infected with *P. mirabilis*, *Providencia* and *Morganella* species, with mean signalling time occurring 23 days before catheter blockage. The pH at the time of signalling was reported to be between 5.5 and 9.0, with a mean pH of 7.6 (Long et al., 2014). A clinical trial of the BTB-P sensor would be required to determine if infection with urease positive organisms could be detected at an earlier timepoint, and to determine the incidence of any false-positive signalling events. This study has highlighted that modulating the surface area of the BTB sensor can also alter the signalling time and theoretically, this could be modified further depending on clinical need.

The resazurin foam developed in Chapter 5 failed to signal *P. mirabilis* infection in the bladder model, due to rapid leaching of the sensor agent, likely due to the compound having weak, reversible bonds with the polymer surface. An alternative method was employed that released resazurin solution directly into the drainage bags of infected bladder models, 20 min prior to drainage bag emptying. This approach allowed detection of *P. mirabilis* infection 40 h before catheter blockage occurred and was equivalent in warning time to the BTB sensor. Importantly, a short window existed to detect infection with resazurin, as high numbers of bacteria rapidly reduce the pink resorufin product to the colourless hydroresorufin, and may thus give rise to false negative results. A drawback of this approach was the requirement to manually add the solution to the drainage bag at the time of emptying, increasing the likelihood of introducing microorganisms into the bag from the external environment.

However, it was anticipated that releasing resazurin solution into the drainage bags of catheterised patients would detect infection from other microorganisms and polymicrobial infections and could represent a valuable diagnostic tool. It was envisaged that the use of resazurin solution in catheter drainage bags could be developed further, producing resazurin-filled ‘balloons’ or ‘capsules’ that release their contents prior to bag emptying that would prevent opening of the closed drainage system.

The sensitivity of the three *P. mirabilis* detection methods assessed in this Chapter was similar, at approximately $1.5 \times 10^7$ CFU/ml. Clinically, CAUTIs are categorised as involving bacteria $\geq 1 \times 10^5$ CFU/ml, so there can be confidence that transient colonisation would not cause signalling events using resazurin solution in the drainage bags or using the BTB and BTB-P silicone sensors. This will prevent administration of antibiotic therapies that contribute to antimicrobial resistance.

## 6.5 Conclusions

In conclusion, the aims of the Chapter were met and showed that:

1) The silicone cylinders bulk-loaded with 1% triclosan or triclosan acetate were unable to prevent migration of *P. mirabilis* from the catheter drainage bag into the bladder chamber, likely due to insufficient length of the insert or the loss of released antimicrobial. However, an alternative approach, dip-coating entire Foley catheters with 0.2 % triclosan or triclosan acetate silicone, proved to be effective at preventing bladder infection by *P. mirabilis* over the test period and prevented or delayed catheter blockage.

2) Modifying the structure of a previously developed BTB silicone sensor to increase the surface area allowed earlier signalling of *P. mirabilis* infection, some 43 h before catheter blockage.

The use of resazurin solution added directly into the drainage bags of the bladder model also allowed early detection of *P. mirabilis* infection, and its non-selective mode of action would allow it to be used as a universal microbial sensor.

Crucially, the antimicrobial catheters developed and evaluated in this Chapter provide tools to reduce the incidence of CAUTIs caused by *P. mirabilis*. When used in conjunction with the developed sensor systems, early infection could be detected and reduced, preventing the complications associated with CAUTIs and reduced morbidity and mortality.

# Chapter 7

## General Discussion

## 7.1 General Discussion

Healthcare settings across the globe continue to be blighted by a persistent problem; healthcare acquired infections (HCAIs) (Khan et al. 2017). HCAIs are leading causes of morbidity and mortality, and large numbers can be attributed to the use of indwelling medical devices (Jamal et al. 2015). Prolonged use of such devices often lead to biofilm formation upon their surfaces and these structures can be 1000 times more resistant to antimicrobial compounds than their planktonic forms (Potera 2010).

In the case of the urinary catheter, prolonged usage can lead to catheter-associated urinary tract infection (CAUTIs), mostly through infection with Gram-negative Enterobacteriaceae, including *Escherichia coli*, *Proteus* spp, *Klebsiella pneumoniae* and *Serratia marcescens*, and less commonly through Gram-positive species, including *Staphylococcus aureus*, *Enterococcus faecalis* and *Enterococcus faecium* (Dund JV, Durani K, Ninama RD 2015; Karkee et al. 2018). Although less frequently encountered, the commensal fungi, *Candida albicans*, is also known to play a role in CAUTIs (Guler et al. 2006).

Although all the listed species can form biofilms along the internal and external catheter surfaces, the crystalline biofilm formed by urease producing species, such as *Proteus mirabilis,* are particularly problematic (Jacobsen and Shirtliff 2011). The resulting crystalline structures lead to catheter blockage and retention of infected urine. Without prompt intervention, the urine can reflux into kidneys, causing associated complications, such as pyelonephritis and sepsis, occasionally with fatal outcomes (Stickler and Morgan 2008).

To overcome the issue of biofilm formation upon urinary catheter surfaces, much attention has focussed on modifications to the fabric of the catheter. Modern day catheters are typically manufactured from silicone elastomers, and methods to incorporate antimicrobial agents into the bulk of the silicone matrix have been investigated (Singha et al. 2017), along with modifications to the catheter surfaces aimed at preventing bacterial attachment or through release of biocidal agents from surface coatings (Sankar and Rajalakshmi 2007; Johnson et al. 2012).

The transition from bench to bedside of developed catheters has been fraught with hurdles, either through lack of efficacy in clinical trials, patient discomfort, cytotoxicity, or financial implications. To this end, few of the developed catheters

have progressed to commercial usage. Nitrofurazone impregnated catheters did make the leap to becoming commercially available and were available in NHS settings. However, multi-study reviews showed limited evidence of efficacy in reducing CAUTI incidence and such information, coupled with reports of patient discomfort, led to the withdrawal of nitrofurazone catheters from the market (Johnson et al. 2012; Pickard et al. 2012). The widely reported antibacterial properties of silver led to it becoming the most prevalent agent in antimicrobial urinary catheter development, often through silver-alloy or silver hydrogel coatings (Lederer et al. 2014). Such catheters are widely used for patients undergoing long-term catheterisation, with an aim at reducing the incidence of CAUTIs and associated catheter blockage. These catheters have shown some effectiveness in this regard, but the problem persists (Lederer et al. 2014).

Catheter blockage in long-term catheter users is a widespread issue, and one that contributes to anxiety amongst such patients. Typically, catheter encrustation occurs around the catheter eyehole and in the absence of any symptoms, the encrustation and associated infection can go unnoticed until blockage eventually occurs (Stickler and Morgan 2008). To this end, this project was largely focussed at achieving two main aims; 1) Development of an antimicrobial biomaterial for prevention of CAUTIs and 2) Development of a sensor biomaterial to allow early detection of infection in catheterised patients.

Of the large selection of compounds screened for antimicrobial efficacy against CAUTI causing pathogens, triclosan and triclosan acetate were the leading candidates in terms of spectrum of activity and concentration required to inhibit planktonic growth. Until 2016, triclosan was widely used in a variety of commercially available products including soaps, toothpastes and laundry detergents, but concerns regarding toxicity, carcinogenicity and resistance mechanisms by some bacterial species prompted the US Food and Drug Administration (FDA) to ban its use in over-the-counter antiseptic wash products. An earlier review on triclosan regarding antimicrobial resistance proved to be inconclusive but recommended prudent use of the compound, and in applications where a health benefit can be demonstrated (Scientific Committee on Consumer Products, 2011). Further studies demonstrated no evidence of toxicity, with levels typically found in consumer products. The (FDA) still permits triclosan use in hand sanitisers and in healthcare settings, and therefore,

triclosan was included in this study due to evidence of its ability to provide benefit in clinical applications.

Triclosan solution (0.3%) has previously been used to inflate the balloons of suprapubic catheters and extend the catheter indwelling time (Sperling et al. 2014). The reduced catheter encrustation led to a reduction in pain during catheter changes and improvements in the quality of life of the patients recruited to the clinical study (Sperling et al. 2014). This solution was available for clinical use under the brand name Farco-Fill®, but was withdrawn from the market in July 2021 (NICE 2021).

PDMS elastomers loaded with 1% triclosan have previously demonstrated antimicrobial activity against *E. coli* and *S. epidermidis* for periods up to 49 days (McBride et al. 2009). McBride et al also demonstrated that modifying the elastomer surface with polyethylene glycol (PEG) chains sustained the release of triclosan from the elastomer for at least 70 days (McBride et al. 2009). The study suggested that non-pegylated triclosan silicone may be useful at preventing biofilm formation in short-term catheterised patients (≤30 days) but the pegylated triclosan silicone may provide a prolonged antimicrobial effect and prevent biofilm formation along catheters of long-term catheterised patients (≥30 days) (McBride et al. 2009). Based upon initial screening studies of 13 selected compounds, triclosan and triclosan acetate were the leading candidates to incorporate into silicone elastomers based on their low MICs (≥12.5 μg/ml), obtained against a broad range of microorganisms commonly involved in CAUTI pathogenesis.

Both triclosan and triclosan acetate were successfully bulk-loaded into silicone rubbers and applied in silicone coatings to pre-formed rubbers, with no observed detrimental effects on the physical properties of the rubbers, compared to unloaded controls. Antimicrobial activity of the novel silicones would only be achieved if the compound was delivered in sufficient concentrations to the rubber surface or if the agent could be released from the rubber. Fortunately, our investigations showed that triclosan was released in high enough quantities to inhibit growth of numerous CAUTI pathogens, including *Escherichia coli*, *Proteus mirabilis*, *Providencia stuartii*, *Klebsiella pneumoniae*, *Staphylococcus aureus* and *Candida albicans*. *Serratia marcescens* and *Pseudomonas aeruginosa* were resistant to triclosan, as previously reported (Jones et al. 2006), and growth of

these species were evident on the triclosan silicone rubbers. The dip-coated triclosan silicone was able to sustain release over a 10 week period and this increased to >12 weeks for the bulk-loaded counterpart.

An *in-vitro* bladder model of the catheterised urinary tract was used to assess the developed materials. Whilst the model undoubtably had some limitations, including lack of urethral and bladder epithelium, use of a simplified artificial urine formulation and lack of factors released by the host immune system, it was beneficial at allowing the materials to be assessed with urine flow rates and forces representative of physiological systems. The *in-vitro* bladder model demonstrated that a silicone insert bulk-loaded with 1% triclosan was unable to prevent migration of *P. mirabilis* from the drainage bag to the bladder chamber, likely due to insufficient surface area of antimicrobial silicone. To increase the contact time of the bacteria and antimicrobial silicone, entire catheters were dip-coated in a triclosan silicone coating. Jordan et al had previously demonstrated a delay in catheter blockage in a *P. mirabilis*-infected model using 0.2% triclosan coating (Jordan et al. 2015). Therefore, this concentration was used as a starting point for the investigation. The 0.2% triclosan dip-coating successfully prevented contamination of the bladder chamber over the 9 day test period, and a statistically significant difference was observed between triclosan-coated and control coated catheters. Limited resources prevented the bladder model experiments from being conducted over longer time periods, but if permitted, true differences in blockage times between the control and test catheters may have been observed.

Although numerous investigations have centred around triclosan as an agent to combat CAUTIs and prevent catheter encrustation, the esterified derivative, triclosan acetate (TA), had not been studied for this application. Analysis of artificial urine (AU) that had been co-incubated with TA silicone coupons revealed that TA was retained withing the elastomer, yet triclosan was released. As the pH of AU increased, the hydrolysis of TA to triclosan also increased, resulting in higher levels of triclosan in the surrounding AU.

Zone of inhibition studies also revealed that silicone coupons bulk-loaded with triclosan, produced larger zones than the TA counterparts in the initial weeks, but as the duration of the experiment increased, TA silicone overtook triclosan silicone in terms of diameter of zones produced. The dip-coated TA silicone

provided activity over an 11 week period, compared to 10 weeks for the triclosan dip-coated version. Bulk-loaded TA and triclosan silicone both produced zones > 12 weeks, with larger zones produced by TA silicone. This effectively shows that the use of triclosan acetate within the silicone polymer provides a way to sustain the release of the antimicrobial compound triclosan. The use of triclosan acetate as a way to sustain triclosan release seems to be on-par with the use of pegylated silicone bulk-loaded with triclosan, where release was evident for > 70 days (McBride et al. 2009).

These results also mirror the concepts published in a patent describing TA as an antimicrobial textile coating. The patent describes a method to incorporate TA into textile fibres and impart long-lasting antimicrobial properties (Shulong 1999). Triclosan is highly soluble at elevated pH's and is removed during high pH wash cycles. In contrast TA coated fibres retain their antimicrobial load for longer due to small amounts of TA hydrolysis, and the resulting triclosan release. The patent states "the use of triclosan esters merely provides an effective manner of applying and diffusing triclosan itself within a fabric substrate. It is believed that the antimicrobial properties of a textile treated with triclosan ester are obtained from the triclosan compound itself which is very slowly generated by hydrolysis of the ester in an aqueous or moisture-containing environment" (Shulong 1999).

Translating this application to catheter coatings for long-term catheter users where an indwelling catheter typically remains *in-situ* for a 12 week period, would allow for greater substantivity of the antimicrobial activity and ultimately be of clinical benefit.

As observed for triclosan, bulk-loaded TA silicone inserts failed to prevent migration of *P. mirabilis* from the contaminated drainage bag to the bladder chamber. Again, the approach of dip-coating an entire Foley catheter in 0.2% TA silicone successfully prevented bladder contamination. Had resources and time permitted, extending the duration of the bladder model experiments would have allowed greater comparisons to be made between the two dip-coating formulations, in terms of delay in catheter blockage.

3D printing antimicrobial silicone is a developing area in biomaterial production, with the potential to be applied across vast types of healthcare products and medical devices. The ability to design customisable products makes this

technology attractive for areas such as prosthetic manufacturing, but also for areas where complex geometrical designs are required.

Developing a 3D printable silicone formulation that incorporated triclosan showed promising results, with antimicrobial activity evident against *S. aureus*, *P. mirabilis* and *E. coli*. The mechanical properties of the silicone were also favourable, with high tensile strength and tear resistance observed.

It is hoped that the developed silicone formulation could be used to construct a 3D printable honeycomb-like structure that would be located between the catheter and drainage bag in catheterised patients and prevent migration of motile bacteria into the catheter through a larger biocidal surface area. It is hoped that such a device could contribute to reduced incidences of CAUTIs.

Imidazolium compounds have long been studied as antimicrobial agents, yet their application to prevent medical device associated infection has not been well explored. Ghamrawi et al incorporated two imidazolium compounds (1-octyl-3-methylimidazolium tetrafluoroborate and 1-dodecyl-3-methylimidazolium tetrafluoroborate), into silicone films at concentrations of 2% and 5% and demonstrated release and antimicrobial activity against 13 species, including Gram-negative and Gram-positive species and fungi commonly associated with healthcare-associated infections (Ghamrawi et al. 2017). The antimicrobial activity of such compounds is thought to be largely due to the lipophilic side chains that can disrupt intermolecular interactions and cause the dissociation of the membrane bilayers, leading to leakage of cellular components (Hindi et al. 2009).

Of the three novel imidazolium salts evaluated in the initial screening process, $[HL]^2BR$ was the most promising in terms of minimum inhibitory concentration (MIC), against the broadest range of species, although MICs <50 μg/ml were only evident against *S. aureus* and *C. albicans*. Therefore $[HL]^2BR$ was promoted for incorporation into silicone for development of a novel antimicrobial biomaterial. Although bulk-loading PDMS with the compound was unsuccessful due to inhibition of the curing reaction, an alternative approach that incorporated $[HL]^2BR$ into an acetoxy silicone and applied as a surface coating proved more successful. The antimicrobial silicone inhibited the growth of *Staphylococcus aureus* and *Candida albicans*, but Gram-negative bacteria were resistant to its actions. Although the coating allowed the antimicrobial load to be deposited

rapidly, future investigations could explore ways to provide a long-lasting release that would be beneficial to catheterised patients. Hindi et al suggested that imidazolium salts containing 12–16 carbons in the chain demonstrate the greatest antimicrobial activity (Hindi et al. 2009). Furthermore, it was suggested that their activity is related to the length of the alkyl chain and alkyl chain substituents adversely influence the antimicrobial activity of the imidazolium salts if they are too short or too long (Hindi et al. 2009). With this in mind, although all of the imidazolium salts investigated in this study contained 16 carbon chains, the alkyl side groups may not have been optimal to achieve antimicrobial activity against Gram-negative bacteria.

Due to its spectrum of activity against non-motile pathogens, the $[HL]^2BR$ silicone could not be evaluated in the bladder model using *P. mirabilis* migration as a tool to assess antimicrobial activity. The use of $[HL]^2BR$ coated silicone could have further reaching medical applications, as soft-denture silicone liners to prevent candidiasis, or as coatings for endotracheal tubes where colonisation by Gram-positive bacteria are problematic.

Developing novel antimicrobial biomaterials constitutes a method to prevent biofilm formation and CAUTI incidence in long-term catheterised patients. However, should a CAUTI occur in such patients, early indication of infection would allow healthcare providers to manage the infection, through administration of antibiotics and bladder wash solutions, or scheduling early catheter changes. Such interventions would be aimed at preventing severe complications from arising, most notably catheter blockage due to urease-producing bacteria, or symptoms such as fever, delirium, pyelonephritis and sepsis that may occur with established infections.

Early warning systems have been developed to detect infection by urease positive bacteria, all utilising methods to detect the increase in urinary pH that occurs with such infections.

A pH responsive catheter coating, EUDRDADIT S100®, was developed that degraded when urinary pH was elevated above pH 7 and released a carboxyfluroescein dye from a lower hydrogel layer. The dye was then able to accumulate in the connecting drainage bag (Milo et al. 2016). This technology was later developed and a sensor ‘lozenge’ was produced to be situated in the drainage bag, allowing a higher concentration of dye to be released, thus easier

detection (Milo et al. 2018). The earlier catheter coating detected *P. mirabilis* infection 10-12 h before catheter blockage, but the lozenge allowed earlier detection, some 14.5 h before blockage (Milo et al. 2016; Milo et al. 2018).

An alternative pH responsive sensor utilising the pH indicator bromothymol blue (BTB), was developed by Stickler et al (Stickler et al. 2006). The sensor was produced using BTB covalently bound to cellulose acetate. Placement of the sensor in the drainage bag allowed detection of *P. mirabilis* infection 43 h prior to catheter blockage. Large-scale production of the sensor was problematic so an alternative silicone version was produced (Malic et al. 2012). A clinical trial of the sensor revealed that it signalled infection by *P. mirabilis*, *Providencia* and *Morganella* species 23 days before catheter blockage occurred (Long et al. 2014). The sensor is currently produced and patented by Technovent Ltd, UK, with commercial availability expected in the near future. Working in partnership with Technovent Ltd, a porous version of the BTB silicone sensor was produced that allowed earlier signalling of *P. mirabilis* infection, compared to the standard BTB sensor, when evaluated in an *in-vitro* bladder model. This was due to an increased surface area allowing greater penetration of ammonium ions from infected urine. Evaluation of the new BTB sensor material would be required to determine if any clinical benefit could be achieved. If earlier detection of urease-positive species was achieved in catheterised patients, benefits would include early intervention strategies to minimise complications arising from CAUTIs and prevention of complications associated with catheter blockage. Reducing the financial burden to the NHS associated with CAUTIs would also be of economic benefit.

Microorganisms other than urease producing bacteria are also responsible for significant numbers of CAUTIs, but as yet, no sensors exist to detect their presence in catheterised patients.

Efforts were made during this project to evaluate compounds that could detect some or all of the CAUTI causing pathogens. MUG and CPRG could detect *E. coli* in planktonic cultures and CPRG was selected for incorporation into a silicone elastomer, due to its large chromatic shift from yellow to dark red in the presence of *E. coli* and other coliforms. Unfortunately, the compound was unresponsive when incorporated into a silicone polymer.

A range of novel tetrazolium compounds and MTT were also evaluated but were not deemed suitable for incorporation into silicone due to weak signals or issues with light sensitivity.

Resazurin, a compound commonly used in laboratories to determine cell viability, is reduced from blue to pink to colourless in the presence of live cells. The use of resazurin as a bacterial sensor was explored by Elavarasan et al to determine antibiotic resistance of bacterial clinical isolates (Elavarasan et al. 2013). A portable device containing a microfluid chip and a selection of antibiotic agents were pre-loaded onto the chip and bacterial cultures pre-mixed with resazurin were added. Antibiotic susceptibility was determined by no observed colour change.

Due to reports as a universal cell viability indicator, resazurin was included for evaluation in this study and it was able to signal the presence of 6 out of 8 common CAUTI pathogens when absorbed into filter paper. Contact with uncured silicone caused reduction of the compound, so an alternative approach was explored, adding the compound to a polyurethane foam. The resazurin compound was rapidly depleted from the foam when artificial urine flowed over the material. However, a 0.015% resazurin solution added directly into the drainage bags of *P. mirabilis*-infected bladder models proved effective at signalling infection and allowed detection of this species 46 h before catheter blockage, equivalent to the original BTB sensor. Due to time constraints, the approach of adding resazurin solution directly to drainage bags could not be explored for additional microorganisms, but it is anticipated that signalling would occur in the presence of other viable microorganisms. A resazurin-filled balloon or capsule would be the preferred options to develop the use of resazurin as a sensor tool, and hopefully these could be explored in future studies. Pre-filled balloons or capsules would have advantages over the microfluid device developed by Elavarasan et al (Elavarasan et al. 2013), as the end user would not be required to remove samples and manually add resazurin to cultures.

The use of sensor materials to detect CAUTIs is an underexplored area, and the approaches explored in this project may prove beneficial in allowing early stages of infection to be detected in catheterised patients allowing timely interventions to be implemented.

Using novel antimicrobial catheters in conjunction with sensor systems could not only prevent or delay biofilm formation along catheter surfaces and the associated CAUTIs, but should infection occur, early detection may prevent complications associated with established infections. Ultimately, it is hoped that the number of deaths attributed to CAUTIs would be significantly reduced.

## 7.2 Conclusions

The aims of the PhD were to produce novel biomaterials to be used to reduce the incidence of CAUTI. In this regard, the following aims were achieved:

- Triclosan and triclosan acetate were incorporated into silicone polymers and demonstrated reduced biofilm formation of a broad range of CAUTI causing pathogens. Foley catheters dip-coated in triclosan and triclosan acetate containing polymers were resistant to biofilm formation by *Proteus mirabilis* and the resulting catheter blockage was prevented over the duration of the experiments.

- 3D printed silicone containing 1% triclosan inhibited growth of *S. aureus*, *E. coli* and *P. mirabilis*.

- An acetoxy silicone coating containing 1% of the imidazolium compound $[HL]^2BR$ demonstrated antimicrobial activity against *S. aureus* and *C. albicans.*

- A porous bromothymol blue silicone sensor was developed that allowed earlier detection of *P. mirabilis* infection, when compared to the original version.

- Resazurin solution detects *P. mirabilis* infection within catheter drainage bags and has the potential to detect all viable microorganisms.

Importantly all of these achievements have the ability to reduce incidence of infection in catheterised patients and improve quality of life. The use of agents to prophylactically manage such infections could prevent the emergence of new

antimicrobial resistant strains of bacteria. Antimicrobial resistance is a global concern, and strategies to reduce its prevalence would be beneficial.

# References

Abul-fadl, B. Y. M. A. M. (1957). A note of the b-glucuronidase activity in urine.

J. clin. Path. (1957), 10, 387. 387–389.

Acharya, A., Ackun-Farmmer, M. A., Aggas, J. R., Andersen, P. J., Anderson, J. M., Anseth, K., Archer, P. A., Ashammakhi, N., Avila, J. D., Babensee, J. E., Badylak, S. f., Baek, K., Baker, A. B., Bakht, S. M., Bandyopadhyay, A., Barchowsky, A., Bass, G., Becker, M. L., Belleghem, S. M. Van, … Ziats, N. P. (2020). List of Contributors. In Biomaterials Science. https://doi.org/10.1016/b978-0-12-816137-1.01002-3

Al-Adhami, M., Tilahun, D., Rao, G., & Kostov, Y. (2016). Optical sensor for rapid microbial detection. Advanced Environmental, Chemical, and Biological Sensing Technologies XIII. https://doi.org/10.1117/12.2224132

Asker, D., Awad, T. S., Baker, P., Howell, P. L., & Hatton, B. D. (2018). Non-eluting, surface-bound enzymes disrupt surface attachment of bacteria by continuous biofilm polysaccharide degradation. Biomaterials. https://doi.org/10.1016/j.biomaterials.2018.03.016

Atshan, S. S., Shamsudin, M. N., Karunanidhi, A., van Belkum, A., Lung, L. T. T., Sekawi, Z., Nathan, J. J., Ling, K. H., Seng, J. S. C., Ali, A. M., Abduljaleel, S. A., & Hamat, R. A. (2013). Quantitative PCR analysis of genes expressed during biofilm development of methicillin resistant Staphylococcus aureus (MRSA). Infection, Genetics and Evolution. https://doi.org/10.1016/j.meegid.2013.05.002

Azevedo, A. S., Almeida, C., Gomes, L. C., Ferreira, C., Mergulhão, F. J., Melo, L. F., & Azevedo, N. F. (2017). An in vitro model of catheter-associated urinary tract infections to investigate the role of uncommon bacteria on the Escherichia coli microbial consortium. Biochemical Engineering Journal. https://doi.org/10.1016/j.bej.2016.11.013

Azevedo, A. S., Almeida, C., Melo, L. F., & Azevedo, N. F. (2017). Impact of polymicrobial biofilms in catheter-associated urinary tract infections. In Critical Reviews in Microbiology. https://doi.org/10.1080/1040841X.2016.1240656

Aziz, T., Fan, H., Khan, F. U., Haroon, M., & Cheng, L. (2019). Modified silicone oil types, mechanical properties and applications. In Polymer Bulletin. https://doi.org/10.1007/s00289-018-2471-2

Bagchi, Jaitly, T. (2013). Microbiological evaluation of catheter associated urinary tract infection in a tertiary care hospital. International Journal of Biological and Health Science, 1(2).

Baker, P., Hill, P. J., Snarr, B. D., Alnabelseya, N., Pestrak, M. J., Lee, M. J., Jennings, L. K., Tam, J., Melnyk, R. A., Parsek, M. R., Sheppard, D. C., Wozniak, D. J., & Howell, P. L. (2016). Exopolysaccharide biosynthetic glycoside hydrolases can be utilized to disrupt and prevent Pseudomonas aeruginosa biofilms. Science Advances. https://doi.org/10.1126/sciadv.1501632

Barnes, M., Feit, C., Grant, T. A., & Brisbois, E. J. (2019). Antimicrobial polymer modifications to reduce microbial bioburden on endotracheal tubes and ventilator associated pneumonia. Acta Biomaterialia. https://doi.org/10.1016/j.actbio.2019.04.042

Barrère, F., Mahmood, T. A., de Groot, K., & van Blitterswijk, C. A. (2008). Advanced biomaterials for skeletal tissue regeneration: Instructive and smart

functions. In Materials Science and Engineering R: Reports. https://doi.org/10.1016/j.mser.2007.12.001

Barry, M. A., Craven, D. E., Goularte, T. A., & Lichtenberg, D. A. (1984). Serratia marcescens contamination of antiseptic soap containing triclosan: implications for nosocomial infection. Infect.Control, 5(9), 427–430.

Batista, R. C. S., Arruda, C. V. B., Cassimiro, M., Gominho, L., Moura, A. C., Albuquerque, D. S., & Romeiro, K. (2020). The Role of the Dental Surgeon in Controlling the Dissemination of COVID-19: A Literature Review. In Scientific World Journal. https://doi.org/10.1155/2020/7945309

Behnia, M., Logan, S. C., Fallen, L., & Catalano, P. (2014). Nosocomial and ventilator-associated pneumonia in a community hospital intensive care unit: A retrospective review and analysis. In BMC Research Notes. https://doi.org/10.1186/1756-0500-7-232

Besemer, K. (2015). Biodiversity, community structure and function of biofilms in stream ecosystems. Research in Microbiology. https://doi.org/10.1016/j.resmic.2015.05.006

Bhargava, H. N., & Leonard, P. A. (1996). Triclosan: Applications and safety. American Journal of Infection Control. https://doi.org/10.1016/S0196-6553(96)90017-6

Bibars, A. R. M., Al-Hourani, Z., Khader, Y., & Waters, M. (2018). Effect of thixotropic agents as additives on the mechanical properties of maxillofacial silicone elastomers. Journal of Prosthetic Dentistry. https://doi.org/10.1016/j.prosdent.2017.06.014

Bont, M., Barry, C., & Johnston, S. (2021). A review of liquid silicone rubber injection molding: Process variables and process modeling. In Polymer Engineering and Science. https://doi.org/10.1002/pen.25618

Breijyeh, Z., Jubeh, B., & Karaman, R. (2020). Resistance of gram-negative bacteria to current antibacterial agents and approaches to resolve it. In Molecules. https://doi.org/10.3390/molecules25061340

Broomfield, Robert J., Morgan, S. D., Khan, A., & Stickler, D. J. (2009). Crystalline bacterial biofilm formation on urinary catheters by urease-producing urinary tract pathogens: A simple method of control. Journal of Medical Microbiology. https://doi.org/10.1099/jmm.0.012419-0

Broomfield, Robert James. (2007). Crystalline bacterial biofilm formation on urinary catheters by urease producing urinary tract pathogens.

Browne, N., Hackenberg, F., Streciwilk, W., Tacke, M., & Kavanagh, K. (2014). Assessment of in vivo antimicrobial activity of the carbene silver(I) acetate derivative SBC3 using Galleria mellonella larvae. BioMetals. https://doi.org/10.1007/s10534-014-9766-z

Cakir, I., Dogan, H. B., Halkman, A. K., & Worobo, R. W. (2001). An alternative approach for enumeration of Escherichia coli in foods. International Journal of Food Microbiology, 68(3), 217–223. https://doi.org/10.1016/S0168-1605(01)00488-3

Carter, R. A., Ericsson, S. A., Corn, C. D., Weyerts, P. R., Dart, M. G., Escue, S. G., & Mesta, J. (1998). Assessing the fertility potential of equine semen samples

using the reducible dyes methylene green and resazurin. Archives of Andrology. https://doi.org/10.3109/01485019808987928

Cayton, J., Kennedy, T., O'Dell, B., Stine, M., & Lee, D. (2012). Current market trends of cardiac stents. In Journal of Medical Marketing. https://doi.org/10.1177/1745790411435437

Chabo, R. G., Habana, C. B., & Mosetlhanyane, K. K. (2000). Milk Hygiene in Commercial Dairy Farms in South Eastern Botswana. UNISWA Research Journal of Agriculture, Science and Technology. https://doi.org/10.4314/uniswa-rjast.v3i2.4705

Chene, G., Boulard, G., & Gachie, J. P. (1990). A controlled trial of a new material for coating urinary catheters. Agressologie: Revue Internationale de Physio-Biologie et de Pharmacologie Appliquées Aux Effets de l'agression.

Chiara Morozzi, 1 Fabrizio Pertusati1, Giulia Novelli1, Daniele Giannantonio1, Emily Stoke2, Katrina Duggan3, Serena Vittorio4, Ian Fallis2, David Williams3, L. D. L. and M. S. (2020). A comprehensive investigational study of a small molecule inhibitor of LTA biosynthesis in Gram-positive bacteria (p. Unpublished work).

Colas, A. (2005). Silicones: Preparation, Properties and Performances. Dow Corning, Life Sciences.

Copeland, M. F., & Weibel, D. B. (2009). Bacterial swarming: A model system for studying dynamic self-assembly. Soft Matter. https://doi.org/10.1039/b812146j

Costa, B., Mota, R., Parreira, P., Tamagnini, P., Martins, M. C. L., & Costa, F. (2019). Broad-spectrum anti-adhesive coating based on an extracellular polymer from a marine cyanobacterium. Marine Drugs. https://doi.org/10.3390/md17040243

Costa, B., Mota, R., Tamagnini, P., Martins, M. C. L., & Costa, F. (2020). Natural Cyanobacterial Polymer-Based Coating as a Preventive Strategy to Avoid Catheter-Associated Urinary Tract Infections. Marine Drugs. https://doi.org/10.3390/md18060279

Costerton, J. W., Lewandowski, Z., Caldwell, D. E., Korber, D. R., & Lappin-Scott, H. M. (1995). Microbial Biofilms - Annual Review of Microbiology, 49(1):711. Annual Review of Microbiology. https://doi.org/10.1146/annurev.mi.49.100195.003431

Coulter, F. B., Schaffner, M., Faber, J. A., Rafsanjani, A., Smith, R., Appa, H., Zilla, P., Bezuidenhout, D., & Studart, A. R. (2019). Bioinspired Heart Valve Prosthesis Made by Silicone Additive Manufacturing. Matter. https://doi.org/10.1016/j.matt.2019.05.013

Cramton, S. E., Gerke, C., Schnell, N. F., Nichols, W. W., & Götz, F. (1999). The intercellular adhesion (ica) locus is present in Staphylococcus aureus and is required for biofilm formation. Infection and Immunity. https://doi.org/10.1128/iai.67.10.5427-5433.1999

D'Almeida, M., Attik, N., Amalric, J., Brunon, C., Renaud, F., Abouelleil, H., Toury, B., & Grosgogeat, B. (2017). Chitosan coating as an antibacterial surface for biomedical applications. PLoS ONE. https://doi.org/10.1371/journal.pone.0189537

Daifuku, R., & Stamm, W. E. (1984). Association of Rectal and Urethral Colonization With Urinary Tract Infection in Patients With Indwelling Catheters.

JAMA: The Journal of the American Medical Association. https://doi.org/10.1001/jama.1984.03350150028015

Davenport, E. K., Call, D. R., & Beyenal, H. (2014). Differential protection from tobramycin by extracellular polymeric substances from Acinetobacter baumannii and Staphylococcus aureus biofilms. Antimicrobial Agents and Chemotherapy. https://doi.org/10.1128/AAC.03071-14

Davis, C. (2019). Catheter-associated urinary tract infection: Signs, diagnosis, prevention. British Journal of Nursing. https://doi.org/10.12968/bjon.2019.28.2.96

De Cubber, J. (1998). A silicone elastomer manipulation technique for the production of medical devices. Journal of Facial and Somato Prosthetics.

DeGrazia, D., & Beauchamp, T. L. (2019). Beyond the 3 Rs to a More Comprehensive Framework of Principles for Animal Research Ethics. ILAR Journal. https://doi.org/10.1093/ilar/ilz011

DeZeeuw, J., O'Regan, N. B., Goudie, C., Organ, M., & Dubrowski, A. (2020). Anatomical 3D-Printed Silicone Prostate Gland Models and Rectal Examination Task Trainer for the Training of Medical Residents and Undergraduate Medical Students. Cureus. https://doi.org/10.7759/cureus.9020

Dickson, M. N., Liang, E. I., Rodriguez, L. A., Vollereaux, N., & Yee, A. F. (2015). Nanopatterned polymer surfaces with bactericidal properties. Biointerphases. https://doi.org/10.1116/1.4922157

Dinwiddie, M. T., Terry, P. D., & Chen, J. (2014). Recent evidence regarding triclosan and cancer risk. International Journal of Environmental Research and Public Health. https://doi.org/10.3390/ijerph110202209

Dong, Y. H., Wang, L. H., Xu, J. L., Zhang, H. B., Zhang, X. F., & Zhang, L. H. (2001). Quenching quorum-sensing-dependent bacterial infection by an N-acyl homoserine lactonase. Nature. https://doi.org/10.1038/35081101

Donlan, R. M. (2001). Biofilm Formation: A Clinically Relevant Microbiological Process. Clinical Infectious Diseases, 33(8), 1387–1392. https://doi.org/10.1086/322972

Donlan, R. M., & Costerton, J. W. (2002). Biofilms: Survival mechanisms of clinically relevant microorganisms. In Clinical Microbiology Reviews (Vol. 15, Issue 2, pp. 167–193). https://doi.org/10.1128/CMR.15.2.167-193.2002

Dufour, D., Leung, V., & Lévesque, C. M. (2012). Bacterial biofilm: structure, function, and antimicrobial resistance. Endodontic Topics, 22(1), 2–16. https://doi.org/10.1111/j.1601-1546.2012.00277.x

Dund JV, Durani K, Ninama RD, S. M. (2015). Profile of UTI in Indwelling Urinary Catheterized Patients in Tertiary Care. International Journal of Health Science and Reseach, 5(9), 181–188.

Duquenne, M., Fleurot, I., Aigle, M., Darrigo, C., Borezée-Durant, E., Derzelle, S., Bouix, M., Deperrois-Lafarge, V., & Delacroix-Buchet, A. (2010). Tool for quantification of staphylococcal enterotoxin gene expression in cheese. Applied and Environmental Microbiology. https://doi.org/10.1128/AEM.01736-09

Elavarasan, T., Chhina, S. K., Parameswaran, M., & Sankaran, K. (2013). Resazurin reduction based colorimetric antibiogram in microfluidic plastic chip. Sensors and Actuators, B: Chemical. https://doi.org/10.1016/j.snb.2012.10.011

Fai, P. B., & Grant, A. (2009). A rapid resazurin bioassay for assessing the toxicity of fungicides. Chemosphere. https://doi.org/10.1016/j.chemosphere.2008.11.078

Fang, J. L., Stingley, R. L., Beland, F. A., Harrouk, W., Lumpkins, D. L., & Howard, P. (2010). Occurrence, efficacy, metabolism, and toxicity of triclosan. In Journal of Environmental Science and Health - Part C Environmental Carcinogenesis and Ecotoxicology Reviews (Vol. 28, Issue 3, pp. 147–171). https://doi.org/10.1080/10590501.2010.504978

Farnleitner, A. H., Hocke, L., Beiwl, C., Kavka, G. G., & Mach, R. L. (2002). Hydrolysis of 4-methylumbelliferyl-β-D-glucuronide in differing sample fractions of river waters and its implication for the detection of fecal pollution. Water Research. https://doi.org/10.1016/S0043-1354(01)00288-3

FDA. (2017). Technical Considerations for Additive Manufactured Medical Devices. In Center for Devices and Radiological Health.

Feneley, R. C. L., Hopley, I. B., & Wells, P. N. T. (2015). Urinary catheters: history, current status, adverse events and research agenda. Journal of Medical Engineering & Technology, 39(8). https://doi.org/10.3109/03091902.2015.1085600

Feng, P. C. S., & Hartman, P. A. (1982). Fluorogenic assays for immediate confirmation of Escherichia coli. Applied and Environmental Microbiology. https://doi.org/10.1128/aem.43.6.1320-1329.1982

Fisher, J. F. (2011). Candida urinary tract infections - Epidemiology, pathogenesis, diagnosis, and treatment: Executive summary. Clinical Infectious Diseases, 52(SUPPL. 6). https://doi.org/10.1093/cid/cir108

Fisher, L. E., Hook, A. L., Ashraf, W., Yousef, A., Barrett, D. A., Scurr, D. J., Chen, X., Smith, E. F., Fay, M., Parmenter, C. D. J., Parkinson, R., & Bayston, R. (2015). Biomaterial modification of urinary catheters with antimicrobials to give long-term broadspectrum antibiofilm activity. Journal of Controlled Release, 202, 57–64. https://doi.org/10.1016/j.jconrel.2015.01.037

Flemming, H. C., & Wingender, J. (2010). The biofilm matrix. In Nature Reviews Microbiology (Vol. 8, Issue 9, pp. 623–633). https://doi.org/10.1038/nrmicro2415

Fluckiger, U., Ulrich, M., Steinhuber, A., Döring, G., Mack, D., Landmann, R., Goerke, C., & Wolz, C. (2005). Biofilm formation, icaADBC transcription, and polysaccharide intercellular adhesin synthesis by staphylococci in a device-related infection model. Infection and Immunity. https://doi.org/10.1128/IAI.73.3.1811-1819.2005

Fong, J. N. C., & Yildiz, F. H. (2015). Biofilm Matrix Proteins. Microbiology Spectrum. https://doi.org/10.1128/microbiolspec.mb-0004-2014

Fossati, M., Cappelli, B., Biral, E., Chiesa, R., Biffi, A., Ossi, C., Moro, M., Cirillo, D. M., Clementi, M., Soliman, C., Ciceri, F., Roncarolo, M. G., Fumagalli, L., & Marktel, S. (2010). Fatal vancomycin- and linezolid-resistant Enterococcus faecium sepsis in a child undergoing allogeneic haematopoietic stem cell

transplantation for beta-thalassaemia major. Journal of Medical Microbiology. https://doi.org/10.1099/jmm.0.018598-0

Gale, R. T., & Brown, E. D. (2015). New chemical tools to probe cell wall biosynthesis in bacteria. In Current Opinion in Microbiology. https://doi.org/10.1016/j.mib.2015.07.013

Galvin, S., Boyle, M., Russell, R. J., Coleman, D. C., Creamer, E., O'Gara, J. P., Fitzgerald-Hughes, D., & Humphreys, H. (2012). Evaluation of vaporized hydrogen peroxide, Citrox and pH neutral Ecasol for decontamination of an enclosed area: A pilot study. Journal of Hospital Infection. https://doi.org/10.1016/j.jhin.2011.10.013

Gee, R. H., Charles, A., Taylor, N., & Darbre, P. D. (2008). Oestrogenic and androgenic activity of triclosan in breast cancer cells. Journal of Applied Toxicology. https://doi.org/10.1002/jat.1316

Ghamrawi, S., Bouchara, J. P., Corbin, A., Rogalsky, S., Tarasyuk, O., & Bardeau, J. F. (2020). Inhibition of fungal growth by silicones modified with cationic biocides. Materials Today Communications. https://doi.org/10.1016/j.mtcomm.2019.100716

Ghanwate, N. A., Thakare, P. V, Bhise, P. R., & Tayde, S. (2014). Prevention of Biofilm Formation in Urinary Catheters by Treatment with Antibiofilm Agents. International Journal.

Gök, Y., Akkoç, S., Albayrak, S., Akkurt, M., & Tahir, M. N. (2014). N-Phenyl-substituted carbene precursors and their silver complexes: Synthesis, characterization and antimicrobial activities. Applied Organometallic Chemistry. https://doi.org/10.1002/aoc.3116

Gominet, M., Compain, F., Beloin, C., & Lebeaux, D. (2017). Central venous catheters and biofilms: where do we stand in 2017? In APMIS. https://doi.org/10.1111/apm.12665

Gristina, A. G. (1987). Biomaterial-centered infection: Microbial adhesion versus tissue integration. Science. https://doi.org/10.1126/science.3629258

Grundei, H. (1996). Voice prosthesis. The Journal of the Acoustical Society of America. https://doi.org/10.1121/1.414590

Guler, S., Ural, O., Findik, D., & Arslan, U. (2006). Risk factors for nosocomial candiduria. Saudi Medical Journal.

Ha, H.-J., Park, J.-H., & Kim, M.-H. (2016). Knowledge and Performance Level of Infection Control Guidelines on Indwelling Urinary Catheter, Central Venous Catheter and Ventilator Among Intensive Care Nurses. Journal of the Korea Academia-Industrial Cooperation Society. https://doi.org/10.5762/kais.2016.17.6.113

Haifei Yang. (2012). Mechanisms of antimicrobial resistance in Serratia marcescens. African Journal of Microbiology Research, 6(21). https://doi.org/10.5897/AJMR11.1545

Haley, R. W., Culver, D. H., White, J. W., Morgan, W. M., & Emori, T. G. (1985). The nationwide nosocomial infection rate: A new need for vital statistics. American Journal of Epidemiology. https://doi.org/10.1093/oxfordjournals.aje.a113988

Haque, M., Sartelli, M., McKimm, J., & Bakar, M. A. (2018). Health care-associated infections – An overview. In Infection and Drug Resistance. https://doi.org/10.2147/IDR.S177247

Harmsen, M., Lappann, M., Knøchel, S., & Molin, S. (2010). Role of extracellular DNA during biofilm formation by listeria monocytogenes. Applied and Environmental Microbiology. https://doi.org/10.1128/AEM.02361-09

Harshan, Bahuleyan, A., & Bhai, G. (2019). Identification and antibiogram of gram positive cocci from catheter associated urinary tract infection (CAUTI) in intensive care units of a tertiary care hospital. Indian Journal of Microbiology Research. https://doi.org/10.18231/2394-5478.2019.0016

Hatzinger, P. B., Palmer, P., Smith, R. L., Peñarrieta, C. T., & Yoshinari, T. (2003). Applicability of tetrazolium salts for the measurement of respiratory activity and viability of groundwater bacteria. Journal of Microbiological Methods. https://doi.org/10.1016/S0167-7012(02)00132-X

Hazell, G., Fisher, L. E., Murray, W. A., Nobbs, A. H., & Su, B. (2018). Bioinspired bactericidal surfaces with polymer nanocone arrays. Journal of Colloid and Interface Science. https://doi.org/10.1016/j.jcis.2018.05.096

Heide, C. (1999). Silicone rubber for medical device applications. In Medical Device and Diagnostic Industry.

Heiner, J., Stenberg, B., & Persson, M. (2003). Crosslinking of siloxane elastomers. Polymer Testing. https://doi.org/10.1016/S0142-9418(02)00081-8

Henry, N. D., & Fair, P. A. (2013). Comparison of in vitro cytotoxicity, estrogenicity and anti-estrogenicity of triclosan, perfluorooctane sulfonate and perfluorooctanoic acid. Journal of Applied Toxicology. https://doi.org/10.1002/jat.1736

Hernandez, K., Lopez, T., Saca, D., & Bello, M. (2017). Incidence of eskape pathogens and their antibiotic resistance in patients with invasive devices in the ICU of a public hospital. Critical Care.

Hindi, K. M., Panzner, M. J., Tessier, C. A., Cannon, C. L., & Youngs, W. J. (2009). The medicinal applications of imidazolium carbene-metal complexes. In Chemical Reviews. https://doi.org/10.1021/cr800500u

Ho, K. -J, & Kuo, S. -H. (1995). Urinary beta-glucuronidase activity as an initial screening test for urinary tract malignancy in high risk patients. Comparison with conventional urine cytologic evaluation. Cancer. https://doi.org/10.1002/1097-0142(19950801)76:3<473::AID-CNCR2820760318>3.0.CO;2-6

Hodyna, D., Kovalishyn, V., Rogalsky, S., Blagodatnyi, V., & Metelytsia, L. (2016). Imidazolium Ionic Liquids as Potential Anti-Candida Inhibitors: QSAR Modeling and Experimental Studies. Current Drug Discovery Technologies. https://doi.org/10.2174/1570163813666160510122201

Hodyna, D., Kovalishyn, V., Semenyuta, I., Blagodatnyi, V., Rogalsky, S., & Metelytsia, L. (2018). Imidazolium ionic liquids as effective antiseptics and disinfectants against drug resistant S. aureus: In silico and in vitro studies. Computational Biology and Chemistry. https://doi.org/10.1016/j.compbiolchem.2018.01.012

Hogan, S., Zapotoczna, M., Stevens, N. T., Humphreys, H., O'Gara, J. P., & O'Neill, E. (2016). Eradication of Staphylococcus aureus Catheter-Related Biofilm

Infections Using ML:8 and Citrox. Antimicrobial Agents and Chemotherapy. https://doi.org/10.1128/aac.00910-16

Holá, V., Ruzicka, F., & Horka, M. (2010). Microbial diversity in biofilm infections of the urinary tract with the use of sonication techniques. FEMS Immunology and Medical Microbiology. https://doi.org/10.1111/j.1574-695X.2010.00703.x

Holling, N., Dedi, C., Jones, C. E., Hawthorne, J. A., Hanlon, G. W., Salvage, J. P., Patel, B. A., Barnes, L. M., & Jones, B. V. (2014). Evaluation of environmental scanning electron microscopy for analysis of Proteus mirabilis crystalline biofilms in situ on urinary catheters. FEMS Microbiology Letters, 355(1), 20–27. https://doi.org/10.1111/1574-6968.12451

Hooper, S. J., Lewis, M. A. O., Wilson, M. J., & Williams, D. W. (2011). Antimicrobial activity of CitroxTM bioflavonoid preparations against oral microorganisms. British Dental Journal. https://doi.org/10.1038/sj.bdj.2010.1224

Hooton, T. M. (2012). Uncomplicated Urinary Tract Infection. New England Journal of Medicine, 366(11), 1028–1037. https://doi.org/10.1056/NEJMcp1104429

Hsu, B. M., Huang, C. C., Chen, J. S., Chen, N. H., & Huang, J. Te. (2011). Comparison of potentially pathogenic free-living amoeba hosts by Legionella spp. in substrate-associated biofilms and floating biofilms from spring environments. Water Research. https://doi.org/10.1016/j.watres.2011.07.019

Huang, Y. H., Lin, J. S., Ma, J. C., & Wang, H. H. (2016). Functional characterization of triclosan-resistant enoyl-acyl-carrier protein reductase (fabV) in pseudomonas aeruginosa. Frontiers in Microbiology. https://doi.org/10.3389/fmicb.2016.01903

Hyldgaard, M., Mygind, T., Vad, B. S., Stenvang, M., Otzen, D. E., & Meyer, R. L. (2014). The Antimicrobial Mechanism of Action of Epsilon-Poly-l-Lysine. Applied and Environmental Microbiology. https://doi.org/10.1128/aem.02204-14

Ikeda, T. (2010). Liquid Silicone Rubber Injection Molding System. Seikei-Kakou. https://doi.org/10.4325/seikeikakou.22.654

Imani Rad, H., Peeri, H., Amani, M., Mohammadnia, A., Ogunniyi, A. D., Khazandi, M., Venter, H., & Arzanlou, M. (2019). Allicin prevents the formation of Proteus-induced urinary crystals and the blockage of catheter in a bladder model in vitro. Microbial Pathogenesis. https://doi.org/10.1016/j.micpath.2019.05.016

Isa, H. W. M., Johari, W. L. W., Syahir, A., Shukor, M. Y. A., Nor Azwady, A. A., Shaharuddin, N. A., & Muskhazli, M. (2014). Development of a bacterial-based tetrazolium dye (MTT) assay for monitoring of heavy metals. International Journal of Agriculture and Biology.

Ishiki, K., Nguyen, D. Q., Morishita, A., Shiigi, H., & Nagaoka, T. (2018). Electrochemical Detection of Viable Bacterial Cells Using a Tetrazolium Salt. Analytical Chemistry. https://doi.org/10.1021/acs.analchem.8b02404

Ivanova, K., Fernandes, M. M., & Tzanov, T. (2013). Current advances on bacterial pathogenesis inhibition and treatment strategies. Microbial Pathogens and Strategies for Combating Them: Science, Technology and Education. https://doi.org/10.13140/RG.2.1.3988.7840

Ivanova, Kristina, Fernandes, M. M., Francesko, A., Mendoza, E., Guezguez, J., Burnet, M., & Tzanov, T. (2015). Quorum-Quenching and Matrix-Degrading

Enzymes in Multilayer Coatings Synergistically Prevent Bacterial Biofilm Formation on Urinary Catheters. ACS Applied Materials and Interfaces. https://doi.org/10.1021/acsami.5b09489

Jacobsen, S. M., & Shirtliff, M. E. (2011). Proteus mirabilis biofilms and catheter-associated urinary tract infections. Virulence, 2(5), 460–465. https://doi.org/10.4161/viru.2.5.17783

Jain, A., Ganesh, N., & Venkatesh, M. P. (2018). QUALITY STANDARDS FOR MEDICAL DEVICES. International Journal of Drug Regulatory Affairs. https://doi.org/10.22270/ijdra.v2i4.149

Jain, M., Dogra, V., Mishra, B., Thakur, A., Loomba, S. L., & Bhargava, A. (2011). Candiduria in catheterized intensive care unit patients: Emerging microbiological trends. Indian Journal of Pathology and Microbiology. https://doi.org/10.4103/0377-4929.85091

Jamal, M., Ahmad, W., Andleeb, S., Jalil, F., Imran, M., Nawaz, M. A., Hussain, T., Ali, M., Rafiq, M., & Kamil, M. A. (2018). Bacterial biofilm and associated infections. In Journal of the Chinese Medical Association. https://doi.org/10.1016/j.jcma.2017.07.012

Jamal, M., Tasneem, U., Hussain, T., & Andleeb, and S. (2015). Bacterial Biofilm: Its Composition, Formation and Role in Human Infections. Research & Reviews: Journal of Microbiology and Biotechnology.

Jang, H. J., Chang, M. W., Toghrol, F., & Bentley, W. E. (2008). Microarray analysis of toxicogenomic effects of triclosan on Staphylococcus aureus. Applied Microbiology and Biotechnology. https://doi.org/10.1007/s00253-008-1349-x

Jang, H. J., Nde, C., Toghrol, F., & Bentley, W. E. (2008). Microarray analysis of toxicogenomic effects of Ortho-phenylphenol in Staphylococcus aureus. BMC Genomics. https://doi.org/10.1186/1471-2164-9-411

Jindal, S. (2016). 3D PRINTING OF TWO - COMPONENT RTV SILCONE SUITABLE FOR MAXILLOFACIAL PROSTHESES.

Jindal, S. K., Sherriff, M., Waters, M. G., & Coward, T. J. (2016). Development of a 3D printable maxillofacial silicone: Part I. Optimization of polydimethylsiloxane chains and cross-linker concentration. Journal of Prosthetic Dentistry. https://doi.org/10.1016/j.prosdent.2016.02.020

Jindal, S. K., Sherriff, M., Waters, M. G., Smay, J. E., & Coward, T. J. (2018). Development of a 3D printable maxillofacial silicone: Part II. Optimization of moderator and thixotropic agent. Journal of Prosthetic Dentistry. https://doi.org/10.1016/j.prosdent.2017.04.028

Johnson, J. R., Johnston, B., & Kuskowski, M. A. (2012). In vitro comparison of nitrofurazone- and silver alloy-coated foley catheters for contact-dependent and diffusible inhibition of urinary tract infection-associated microorganisms. Antimicrobial Agents and Chemotherapy, 56(9), 4969–4972. https://doi.org/10.1128/AAC.00733-12

Johnson, N. A., Southerland, M. R., & Youngs, W. J. (2017). Recent developments in the medicinal applications of silver-nhc complexes and imidazolium salts. In Molecules. https://doi.org/10.3390/molecules22081263

Jones, G. L., Muller, C. T., O'Reilly, M., & Stickler, D. J. (2006). Effect of triclosan on the development of bacterial biofilms by urinary tract pathogens on urinary

catheters. J Antimicrob Chemother, 57(2), 266–272. https://doi.org/10.1093/jac/dki447

Jordan, R. P. C., & Nicolle, L. E. (2014). Preventing Infection Associated with Urethral Catheter Biofilms. In Biofilms in Infection Prevention and Control: A Healthcare Handbook (pp. 287–309). https://doi.org/10.1016/B978-0-12-397043-5.00016-5

Jordan, R. P., Malic, S., Waters, M. G., Stickler, D. J., & Williams, D. W. (2015). Development of an antimicrobial urinary catheter to inhibit urinary catheter encrustation. Microbiology Discovery, 3(1), 1. https://doi.org/10.7243/2052-6180-3-1

Junter, G. A., Thébault, P., & Lebrun, L. (2016). Polysaccharide-based antibiofilm surfaces. In Acta Biomaterialia. https://doi.org/10.1016/j.actbio.2015.11.010

Jurásková, A., Møller Olsen, S., Dam-Johansen, K., Brook, M. A., & Skov, A. L. (2020). Reliable Condensation Curing Silicone Elastomers with Tailorable Properties. Molecules (Basel, Switzerland). https://doi.org/10.3390/molecules26010082

Kaliyathan, A. V., Mathew, A., Rane, A. V., Kanny, K., & Thomas, S. (2018). Natural rubber and silicone rubber-based biomaterials. In Fundamental Biomaterials: Polymers. https://doi.org/10.1016/B978-0-08-102194-1.00004-9

Kampf, G., & Kramer, A. (2004). Epidemiologic background of hand hygiene and evaluation of the most important agents for scrubs and rubs. In Clinical Microbiology Reviews. https://doi.org/10.1128/CMR.17.4.863-893.2004

Kanetoshi, A., Katsura, E., Ogawa, H., Ohyama, T., Kaneshima, H., & Miura, T. (1992). Acute toxicity, percutaneous absorption and effects on hepatic mixed function oxidase activities of 2,4,4′-trichloro-2′-hydroxydiphenyl ether (Irgasan® DP300) and its chlorinated derivatives. Archives of Environmental Contamination and Toxicology. https://doi.org/10.1007/BF00226000

Kaper, J. B., Nataro, J. P., & Mobley, H. L. T. (2004). Pathogenic Escherichia coli. In Nature Reviews Microbiology. https://doi.org/10.1038/nrmicro818

Karkee, P., Dhital, D., Madhup, S. K., & Sherchan, J. B. (2018). Catheter Associated Urinary Tract Infection: Prevalence, Microbiological Profile and Antibiogram at a Tertiary Care Hospital. Annals of Clinical Chemistry and Laboratory Medicine. https://doi.org/10.3126/acclm.v3i2.19675

Associated Urinary Tract Infection: Prevalence, Microbiological Profile and Antibiogram at a Tertiary Care Hospital. Annals of Clinical Chemistry and Laboratory Medicine. https://doi.org/10.3126/acclm.v3i2.19675

Kazmierska, K. A., Thompson, R., Morris, N., Long, A., & Ciach, T. (2010). In vitro multicompartmental bladder model for assessing blockage of urinary catheters: Effect of hydrogel coating on dynamics of proteus mirabilis growth. Urology. https://doi.org/10.1016/j.urology.2010.04.039

Khalifa, R. A., Nasser, M. S., Gomaa, A. A., Osman, N. M., & Salem, H. M. (2013). Resazurin Microtiter Assay Plate method for detection of susceptibility of multidrug resistant Mycobacterium tuberculosis to second-line anti-tuberculous drugs. Egyptian Journal of Chest Diseases and Tuberculosis. https://doi.org/10.1016/j.ejcdt.2013.05.008

Khan, H. A., Baig, F. K., & Mehboob, R. (2017). Nosocomial infections: Epidemiology, prevention, control and surveillance. In Asian Pacific Journal of Tropical Biomedicine (Vol. 7, Issue 5, pp. 478–482). https://doi.org/10.1016/j.apjtb.2017.01.019

Khan, I. D., Basu, A., Kiran, S., Trivedi, S., Pandit, P., & Chattoraj, A. (2017). Device-Associated Healthcare-Associated Infections (DA-HAI) and the caveat of multiresistance in a multidisciplinary intensive care unit. Medical Journal Armed Forces India. https://doi.org/10.1016/j.mjafi.2016.10.008

Kowalczuk, D., Ginalska, G., Piersiak, T., & Miazga-Karska, M. (2012). Prevention of biofilm formation on urinary catheters: Comparison of the sparfloxacin-treated long-term antimicrobial catheters with silver-coated ones. Journal of Biomedical Materials Research - Part B Applied Biomaterials, 100 B(7), 1874–1882. https://doi.org/10.1002/jbm.b.32755

Kretschmar, M., Hube, B., Bertsch, T., Sanglard, D., Merker, R., Schröder, M., Hof, H., & Nichterlein, T. (1999). Germ tubes and proteinase activity contribute to virulence of Candida albicans in murine peritonitis. Infection and Immunity. https://doi.org/10.1128/iai.67.12.6637-6642.1999

Król, J. E., Wojtowicz, A. J., Rogers, L. M., Heuer, H., Smalla, K., Krone, S. M., & Top, E. M. (2013). Invasion of E. coli biofilms by antibiotic resistance plasmids. Plasmid. https://doi.org/10.1016/j.plasmid.2013.03.003

Kunin, C. M., Chin, Q. F., & Chambers, S. (1987). Formation of encrustations on indwelling urinary catheters in the elderly: A comparison of different types of catheter materials in “blockers” and “nonblockers.” Journal of Urology. https://doi.org/10.1016/S0022-5347(17)43412-4

Kuriyama, T., Williams, D. W., Patel, M., Lewis, M. A. O., Jenkins, L. E., Hill, D. W., & Hosein, I. K. (2003). Molecular characterization of clinical and environmental isolates of vancomycin-resistant Enterococcus faecium and Enterococcus faecalis from a teaching hospital in Wales. Journal of Medical Microbiology. https://doi.org/10.1099/jmm.0.05123-0

Lambert, J. M., Lee, M. -S, Taller, R. A., & Solomon, D. D. (1991). Medical grade tubing: Criteria for catheter applications. Journal of Vinyl Technology. https://doi.org/10.1002/vnl.730130409

Lederer, J. W., Jarvis, W. R., Thomas, L., & Ritter, J. (2014). Multicenter cohort study to assess the impact of a silver-alloy and hydrogel-coated urinary catheter on symptomatic catheter-associated urinary tract infections. Journal of Wound, Ostomy and Continence Nursing, 41(5), 473–480. https://doi.org/10.1097/WON.0000000000000056

Lewis, K. (2010). Persister Cells. Annual Review of Microbiology. https://doi.org/10.1146/annurev.micro.112408.134306

Lewis, L. N., Stein, J., Gao, Y., Colborn, R. E., & Hutchins, G. (1997). Platinum catalysts used in the silicone industry. Platinum Matals Reviews.

Li, Y. H., & Tian, X. (2012). Quorum sensing and bacterial social interactions in biofilms. In Sensors. https://doi.org/10.3390/s120302519

Liao, Y. H., Muthuramalingam, K., Tung, K. H., Chuan, H. H., Liang, K. Y., Hsu, C. P., & Cheng, C. M. (2020). Portable device for quick detection of viable bacteria in water. Micromachines, 11(12), 1–9. https://doi.org/10.3390/mi11121079

Lichtenberger, P., & Hooton, T. M. (2008). Complicated urinary tract infections. In Current Infectious Disease Reports (Vol. 10, Issue 6, pp. 499–504). https://doi.org/10.1007/s11908-008-0081-0

Limoli, D. H., Jones, C. J., & Wozniak, D. J. (2015). Bacterial Extracellular Polysaccharides in Biofilm Formation and Function. Microbiology Spectrum. https://doi.org/10.1128/microbiolspec.mb-0011-2014

Lin, Y. H., Xu, J. L., Hu, J., Wang, L. H., Leong Ong, S., Renton Leadbetter, J., & Zhang, L. H. (2003). Acyl-homoserine lactone acylase from Ralstonia strain XJ12B represents a novel and potent class of quorum-quenching enzymes. Molecular Microbiology. https://doi.org/10.1046/j.1365-2958.2003.03351.x

Lipovsky, A., Thallinger, B., Perelshtein, I., Ludwig, R., Sygmund, C., Nyanhongo, G. S., Guebitz, G. M., & Gedanken, A. (2015). Ultrasound coating of polydimethylsiloxanes with antimicrobial enzymes. Journal of Materials Chemistry B. https://doi.org/10.1039/c5tb00671f

Livak, K. J., & Schmittgen, T. D. (2001). Analysis of relative gene expression data using real-time quantitative PCR and the 2-ΔΔCT method. Methods. https://doi.org/10.1006/meth.2001.1262

Long, A., Edwards, J., Thompson, R., Lewis, D. A., & Timoney, A. G. (2014). A clinical evaluation of a sensor to detect blockage due to crystalline biofilm formation on indwelling urinary catheters. BJU International. https://doi.org/10.1111/bju.12577

Loveday, H. P., Wilson, J. A., Pratt, R. J., Golsorkhi, M., Tingle, A., Bak, A., Browne, J., Prieto, J., & Wilcox, M. (2014). Epic3: National evidence-based guidelines for preventing healthcare-associated infections in nhs hospitals in england. Journal of Hospital Infection. https://doi.org/10.1016/S0195-6701(13)60012-2

Luis, E., Pan, H. M., Bastola, A. K., Bajpai, R., Sing, S. L., Song, J., & Yeong, W. Y. (2020). 3D printed silicone meniscus implants: Influence of the 3D printing process on properties of silicone implants. Polymers. https://doi.org/10.3390/POLYM12092136

Lukin, R. Y., Kuchkaev, A. M., Sukhov, A. V., Bekmukhamedov, G. E., & Yakhvarov, D. G. (2020). Platinum-catalyzed hydrosilylation in polymer chemistry. In Polymers. https://doi.org/10.3390/POLYM12102174

M., V., R., P., & M., B. (2017). Prevalence of microorganisms causing catheter associated urinary tract infections (CAUTI) among catheterised patients admitted in a tertiary care hospital. International Journal of Research in Medical Sciences. https://doi.org/10.18203/2320-6012.ijrms20172084

Madsen, J. S., Burmølle, M., Hansen, L. H., & Sørensen, S. J. (2012). The interconnection between biofilm formation and horizontal gene transfer. In FEMS Immunology and Medical Microbiology. https://doi.org/10.1111/j.1574-695X.2012.00960.x

Mahmoud Ahmed Abdallah, N., Bendary Elsayed, S., Mohamed Yassin, M., & Metwally El-gohary, G. (2011). Biofilm forming bacteria isolated from urinary tract infection, relation to catheterization and susceptibility to antibiotics. International Journal for Biotechnology and Molecular Biology Research.

Maiti, P. K. (2005). Development of a silicone modified unsaturated polyester varnish for rated electrical insulation application. IEEE Transactions on Dielectrics and Electrical Insulation. https://doi.org/10.1109/TDEI.2005.1453450

Maki, D. G., & Tambyah, P. A. (2001). Engineering out the risk for infection with urinary catheters. Emerging Infectious Diseases. https://doi.org/10.3201/eid0702.010240

Malic, S., Waters, M. G. J., Basil, L., Stickler, D. J., & Williams, D. W. (2012). Development of an “early warning” sensor for encrustation of urinary catheters following Proteus infection. Journal of Biomedical Materials Research - Part B Applied Biomaterials, 100 B(1), 133–137. https://doi.org/10.1002/jbm.b.31930

Mangili, A., Bica, I., Snydman, D. R., & Hamer, D. H. (2005). Daptomycin-resistant, methicillin-resistant Staphylococcus aureus bacteremia. Clinical Infectious Diseases. https://doi.org/10.1086/428616

Matsumoto, K., Zako, M., Shimizu, N., Kanda, T., & Sakurai, H. (1999). Statically indeterminate stress analysis of sport shoes. Nihon Kikai Gakkai Ronbunshu, A Hen/Transactions of the Japan Society of Mechanical Engineers, Part A. https://doi.org/10.1299/kikaia.65.2045

Mayer, H. (1998). The chemistry and properties of silicone resins: Network formers (in paints and renders). In Pigment and Resin Technology. https://doi.org/10.1108/03699429810246953

Mazurek, P., Vudayagiri, S., & Skov, A. L. (2019). How to tailor flexible silicone elastomers with mechanical integrity: A tutorial review. In Chemical Society Reviews. https://doi.org/10.1039/c8cs00963e

McBride, M. C., Karl Malcolm, R., David Woolfson, A., & Gorman, S. P. (2009). Persistence of antimicrobial activity through sustained release of triclosan from pegylated silicone elastomers. Biomaterials, 30(35), 6739–6747. https://doi.org/10.1016/j.biomaterials.2009.08.047

McNamara, P. J., & Levy, S. B. (2016). Triclosan: An instructive tale. In Antimicrobial Agents and Chemotherapy. https://doi.org/10.1128/AAC.02105-16

Melaiye, A., Simons, R. S., Milsted, A., Pingitore, F., Wesdemiotis, C., Tessier, C. A., & Youngs, W. J. (2004). Formation of Water-Soluble Pincer Silver(I)-Carbene Complexes: A Novel Antimicrobial Agent. Journal of Medicinal Chemistry. https://doi.org/10.1021/jm030262m

Mewis, J., & Wagner, N. J. (2009). Thixotropy. In Advances in Colloid and Interface Science. https://doi.org/10.1016/j.cis.2008.09.005

MHRA. (2021). Regulating medical devices in the UK. In Government guidance.

Micek, S. T. (2007). Alternatives to vancomycin for the treatment of methicillin-resistant Staphylococcus aureus infections. In Clinical Infectious Diseases. https://doi.org/10.1086/519471

Miles, A. A., Misra, S. S., & Irwin, J. O. (1938). The estimation of the bactericidal power of the blood. Journal of Hygiene. https://doi.org/10.1017/S002217240001158X

Mills, D., Tappa, K., Jammalamadaka, U., Weisman, J., & Woerner, J. (2018). The use of 3D printing in the fabrication of nasal stents. Inventions. https://doi.org/10.3390/inventions3010001

Milo, S., Acosta, F. B., Hathaway, H. J., Wallace, L. A., Thet, N. T., & Jenkins, A. T. A. (2018a). Development of an Infection-Responsive Fluorescent Sensor for the Early Detection of Urinary Catheter Blockage. ACS Sensors, 3(3). https://doi.org/10.1021/acssensors.7b00861

Milo, S., Acosta, F. B., Hathaway, H. J., Wallace, L. A., Thet, N. T., & Jenkins, A. T. A. (2018b). Development of an Infection-Responsive Fluorescent Sensor for the Early Detection of Urinary Catheter Blockage. ACS Sensors. https://doi.org/10.1021/acssensors.7b00861

Milo, S., Thet, N. T., Liu, D., Nzakizwanayo, J., Jones, B. V., & Jenkins, A. T. A. (2016). An in-situ infection detection sensor coating for urinary catheters. Biosensors and Bioelectronics, 81, 166–172. https://doi.org/10.1016/j.bios.2016.02.059

Modaresifar, K., Azizian, S., Ganjian, M., Fratila-Apachitei, L. E., & Zadpoor, A. A. (2019). Bactericidal effects of nanopatterns: A systematic review. In Acta Biomaterialia. https://doi.org/10.1016/j.actbio.2018.09.059

Mojsiewicz-Pieńkowska, K., Jamrógiewicz, M., Zebrowska, M., Mikolaszek, B., & Sznitowska, M. (2015). Double layer adhesive silicone dressing as a potential dermal drug delivery film in scar treatment. International Journal of Pharmaceutics. https://doi.org/10.1016/j.ijpharm.2015.01.050

Moreira, J. M. R., Teodósio, J. S., Silva, F. C., Simões, M., Melo, L. F., & Mergulhão, F. J. (2013). Influence of flow rate variation on the development of Escherichia coli biofilms. Bioprocess and Biosystems Engineering. https://doi.org/10.1007/s00449-013-0954-y

Morris, N. S., Stickler, D. J., & Winters, C. (1997). Which indwelling urethral catheters resist encrustation by Proteus mirabilis biofilms? British Journal of Urology. https://doi.org/10.1046/j.1464-410x.1997.00185.x

Morrissey, I., Oggioni, M. R., Knight, D., Curiao, T., Coque, T., Kalkanci, A., Martinez, J. L., Baldassarri, L., Orefici, G., Yetiş, Ü., Rödger, H. J., Visa, P., Mora, D., Leib, S., & Viti, C. (2014). Evaluation of epidemiological cut-off values indicates that biocide resistant subpopulations are uncommon in natural isolates of clinically-relevant microorganisms. PLoS ONE. https://doi.org/10.1371/journal.pone.0086669

Morse, D. J., Wilson, M. J., Wei, X., Bradshaw, D. J., Lewis, M. A. O., & Williams, D. W. (2019). Modulation of Candida albicans virulence in in vitro biofilms by oral bacteria. Letters in Applied Microbiology. https://doi.org/10.1111/lam.13145

Mshana, R. N., Tadesse, G., Abate, G., & Miörner, H. (1998). Use of 3-(4,5-dimethylthiazol-2-yl)-2,5-diphenyl tetrazolium bromide for rapid detection of rifampin-resistant: Mycobacterium tuberculosis. Journal of Clinical Microbiology. https://doi.org/10.1128/jcm.36.5.1214-1219.1998

Mulvey, M. A., Schilling, J. D., Martinez, J. J., & Hultgren, S. J. (2000). Bad bugs and beleaguered bladders: Interplay between uropathogenic Escherichia coli and innate host defenses. Proceedings of the National Academy of Sciences, 97(16), 8829–8835. https://doi.org/10.1073/pnas.97.16.8829

Murakami, S., Igarashi, T., Tanaka, M., Tobe, T., & Mikami, K. (1993). Adherence of bacteria to various urethral catheters and occurrence of catheter-induced urethritis. Hinyokika Kiyo. Acta Urologica Japonica.

Nakka, J. S., Jansen, K. M. B., & Ernst, L. J. (2011). Effect of chain flexibility in the network structure on the viscoelasticity of epoxy thermosets. Journal of Polymer Research. https://doi.org/10.1007/s10965-011-9595-5

Nall, R. (2018). Urine pH: Normal ranges and what they mean. Medical News Today.

Naples, J. G., & Ruckenstein, M. J. (2020). Cochlear Implant. In Otolaryngologic Clinics of North America. https://doi.org/10.1016/j.otc.2019.09.004

National Institute for Health and Care Excellence. (2018). Urinary tract infection (catheter-associated): antimicrobial prescribing. Nice.

NICE. (2012). Healthcare-associated infections : prevention and control in primary and community care. Clinical Guidance, cg 139(February). nice.org.uk/giudance/cg139

Nicolle, L. E. (2012). Urinary Catheter-Associated Infections. In Infectious Disease Clinics of North America (Vol. 26, Issue 1, pp. 13–27). https://doi.org/10.1016/j.idc.2011.09.009

Nicolle, L. E. (2015). Infections associated with urinary catheters. In Clinical Infectious Disease, Second Edition. https://doi.org/10.1017/CBO9781139855952.122

Noly, P. E., Pagani, F. D., Noiseux, N., Stulak, J. M., Khalpey, Z., Carrier, M., & Maltais, S. (2020). Continuous-Flow Left Ventricular Assist Devices and Valvular Heart Disease: A Comprehensive Review. In Canadian Journal of Cardiology. https://doi.org/10.1016/j.cjca.2019.11.022

O'Toole, G., Kaplan, H. B., & Kolter, R. (2000). Biofilm Formation as Microbial Development. Annual Review of Microbiology, 54(1), 49–79. https://doi.org/10.1146/annurev.micro.54.1.49

Ohemeng, K. A., Schwender, C. F., Fu, K. P., & Barrett, J. F. (1993). DNA gyrase inhibitory and antibacterial activity of some flavones(1). Bioorganic and Medicinal Chemistry Letters. https://doi.org/10.1016/S0960-894X(01)80881-7

Oldani, C., & Dominguez, A. (2012). Titanium as a Biomaterial for Implants. In Recent Advances in Arthroplasty. https://doi.org/10.5772/27413

Olivares, E., Badel-Berchoux, S., Provot, C., Prévost, G., Bernardi, T., & Jehl, F. (2020). Clinical Impact of Antibiotics for the Treatment of Pseudomonas aeruginosa Biofilm Infections. In Frontiers in Microbiology. https://doi.org/10.3389/fmicb.2019.02894

Orsi, G. B., & Ciorba, V. (2013). Vancomycin resistant enterococci healthcare associated infections. In Annali di igiene : medicina preventiva e di comunità. https://doi.org/10.7416/ai.2013.1948

Ouyang, H., Liu, Z., Li, N., Shi, B., Zou, Y., Xie, F., Ma, Y., Li, Z., Li, H., Zheng, Q., Qu, X., Fan, Y., Wang, Z. L., Zhang, H., & Li, Z. (2019). Symbiotic cardiac pacemaker. Nature Communications. https://doi.org/10.1038/s41467-019-09851-1

Oxidase test. UK Standards for Microbiology. (2019).

Ozbolat, V., Dey, M., Ayan, B., Povilianskas, A., Demirel, M. C., & Ozbolat, I. T. (2018). 3D Printing of PDMS Improves Its Mechanical and Cell Adhesion

Properties. ACS Biomaterials Science and Engineering, 4(2). https://doi.org/10.1021/acsbiomaterials.7b00646

Paganelli, F. L., van de Kamer, T., Brouwer, E. C., Leavis, H. L., Woodford, N., Bonten, M. J. M., Willems, R. J. L., & Hendrickx, A. P. A. (2017). Lipoteichoic acid synthesis inhibition in combination with antibiotics abrogates growth of multidrug-resistant Enterococcus faecium. International Journal of Antimicrobial Agents. https://doi.org/10.1016/j.ijantimicag.2016.12.002

Paigen, K., & Peterson, J. (1978). Coordinacy of lysosomal enzyme excretion in human urine. The Journal of Clinical Investigation. https://doi.org/10.1172/JCI108989

Palza, H., Nuñez, M., Bastías, R., & Delgado, K. (2018). In situ antimicrobial behavior of materials with copper-based additives in a hospital environment. International Journal of Antimicrobial Agents. https://doi.org/10.1016/j.ijantimicag.2018.02.007

Paterson, C., Dalziell, R., Forshaw, T., Turner, A., & Fraser, G. (2019). Prevention and management of urinary catheter blockages in community settings. Nursing Standard. https://doi.org/10.7748/ns.2019.e11431

Patil, S., Deally, A., Gleeson, B., Müller-Bunz, H., Paradisi, F., & Tacke, M. (2011). Novel benzyl-substituted N-heterocyclic carbene-silver acetate complexes: Synthesis, cytotoxicity and antibacterial studies. Metallomics. https://doi.org/10.1039/c0mt00034e

Pelling, H., Nzakizwanayo, J., Milo, S., Denham, E. L., MacFarlane, W. M., Bock, L. J., Sutton, J. M., & Jones, B. V. (2019). Bacterial biofilm formation on indwelling urethral catheters. Letters in Applied Microbiology, 68(4). https://doi.org/10.1111/lam.13144

Percival, S. L., Suleman, L., Vuotto, C., & Donelli, G. (2015). Healthcare-Associated infections, medical devices and biofilms: Risk, tolerance and control. In Journal of Medical Microbiology. https://doi.org/10.1099/jmm.0.000032

Percy, M. G., & Gründling, A. (2014). Lipoteichoic acid synthesis and function in gram-positive bacteria. In Annual Review of Microbiology. https://doi.org/10.1146/annurev-micro-091213-112949

Pickard, R., Lam, T., MacLennan, G., Starr, K., Kilonzo, M., McPherson, G., Gillies, K., McDonald, A., Walton, K., Buckley, B., Glazener, C., Boachie, C., Burr, J., Norrie, J., Vale, L., Grant, A., & N'Dow, J. (2012). Antimicrobial catheters for reduction of symptomatic urinary tract infection in adults requiring short-term catheterisation in hospital: A multicentre randomised controlled trial. The Lancet. https://doi.org/10.1016/S0140-6736(12)61380-4

Piddock, L. J. V. (2006). Multidrug-resistance efflux pumps - Not just for resistance. Nature Reviews Microbiology. https://doi.org/10.1038/nrmicro1464

Poole, K. (2004). Efflux-mediated multiresistance in Gram-negative bacteria. In Clinical Microbiology and Infection (Vol. 10, Issue 1, pp. 12–26). https://doi.org/10.1111/j.1469-0691.2004.00763.x

Potera, C. (2010). ANTIBIOTIC RESISTANCE: Biofilm Dispersing Agent Rejuvenates Older Antibiotics. Environmental Health Perspectives. https://doi.org/10.1289/ehp.118-a288

Profeta, G. S., Pereira, J. A. S., Costa, S. G., Azambuja, P., Garcia, E. S., Moraes, C. da S., & Genta, F. A. (2017). Standardization of a continuous assay for glycosidases and its use for screening insect gut samples at individual and populational levels. Frontiers in Physiology. https://doi.org/10.3389/fphys.2017.00308

Reagent, V. (2004). alamarBlue ® - The Fast , Simple Reliable Reagent to Assess Cell Health How does alamarBlue work ? Toxicol In Vitro.

Reddy, S. T., Chung, K. K., McDaniel, C. J., Darouiche, R. O., Landman, J., & Brennan, A. B. (2011). Micropatterned surfaces for reducing the risk of catheter-associated urinary tract infection: An in vitro study on the effect of sharklet micropatterned surfaces to inhibit bacterial colonization and migration of uropathogenic Escherichia coli. Journal of Endourology. https://doi.org/10.1089/end.2010.0611

Ricco, J. B., & Assadian, O. (2011). Antimicrobial silver grafts for prevention and treatment of vascular graft infection. Seminars in Vascular Surgery. https://doi.org/10.1053/j.semvascsurg.2011.10.006

Richards, M. J., Edwards, J. R., Culver, D. H., & Gaynes, R. P. (1999). Nosocomial infections in medical intensive care units in the United States. In Critical Care Medicine. https://doi.org/10.1097/00003246-199905000-00020

Richter, S. G., Elli, D., Kim, H. K., Hendrickx, A. P. A., Sorg, J. A., Schneewind, O., & Missiakas, D. (2013). Small molecule inhibitor of lipoteichoic acid synthesis is an antibiotic for Gram-positive bacteria. Proceedings of the National Academy of Sciences of the United States of America. https://doi.org/10.1073/pnas.1217337110

Robeyns, C., Picard, L., & Ganachaud, F. (2018). Synthesis, characterization and modification of silicone resins: An “Augmented Review.” In Progress in Organic Coatings. https://doi.org/10.1016/j.porgcoat.2018.03.025

Rosa, R. G., Schwarzbold, A. V., Santos, R. P. D., Turra, E. E., Machado, D. P., & Goldani, L. Z. (2014). Vancomycin-resistant Enterococcus faecium bacteremia in a tertiary care hospital: Epidemiology, antimicrobial susceptibility, and outcome. BioMed Research International. https://doi.org/10.1155/2014/958469

Rudkin, J. K., Edwards, A. M., Bowden, M. G., Brown, E. L., Pozzi, C., Waters, E. M., Chan, W. C., Williams, P., O’Gara, J. P., & Massey, R. C. (2012). Methicillin resistance reduces the virulence of healthcare-associated methicillin-resistant staphylococcus aureus by interfering with the agr quorum sensing system. Journal of Infectious Diseases. https://doi.org/10.1093/infdis/jir845

Russell, J. C., & Stratford, P. (2000). Bacteria, biofilms, and devices: The possible protective role of phosphorylcholine materials. Journal of Endourology. https://doi.org/10.1089/end.2000.14.39

Ryan, C., Hesselgreaves, H., Wu, O., Paul, J., Dixon-Hughes, J., & Moss, J. G. (2018). Protocol for a systematic review and thematic synthesis of patient experiences of central venous access devices in anti-cancer treatment. Systematic Reviews. https://doi.org/10.1186/s13643-018-0721-x

Sabbuba, N., Hughes, G., & Stickler, D. J. (2002). The migration of Proteus mirabilis and other urinary tract pathogens over Foley catheters. BJU International. https://doi.org/10.1046/j.1464-4096.2001.01721.x

Salgado Yepez, E., Bovera, M. M., Rosenthal, V. D., González Flores, H. A., Pazmiño, L., Valencia, F., Alquinga, N., Ramirez, V., Jara, E., Lascano, M., Delgado, V., Cevallos, C., Santacruz, G., Pelaéz, C., Zaruma, C., & Barahona Pinto, D. (2017). Device-associated infection rates, mortality, length of stay and bacterial resistance in intensive care units in Ecuador: International Nosocomial Infection Control Consortium's findings. World Journal of Biological Chemistry. https://doi.org/10.4331/wjbc.v8.i1.95

Salvarci, A., Koroglu, M., & Gurpinar, T. (2015). Evaluation of antimicrobial activities of minocycline and rifampin-impregnated silicone surfaces in an in vitro urinary system model. Journal of the Pakistan Medical Association, 65(2), 115–119.

Sampath, T., Thamizharasan, S., Saravanan, M., & Timiri Shanmugam, P. S. (2020). Materials testing. In Trends in Development of Medical Devices. https://doi.org/10.1016/B978-0-12-820960-8.00006-X

Sanaie, S., Mahmoodpoor, A., & Najafi, M. (2017). Nasogastric tube insertion in anaesthetized patients: A comprehensive review. In Anaesthesiology Intensive Therapy. https://doi.org/10.5603/AIT.a2017.0001

Sandborgh-Englund, G., Adolfsson-Erici, M., Odham, G., & Ekstrand, J. (2006). Pharmacokinetics of triclosan following oral ingestion in humans. Journal of Toxicology and Environmental Health - Part A: Current Issues. https://doi.org/10.1080/15287390600631706

Sankar, S., & Rajalakshmi, T. (2007). Application of poly ethylene glycol hydrogel to overcome latex urinary catheter related problems. BioFactors. https://doi.org/10.1002/biof.5520300403

Santajit, S., & Indrawattana, N. (2016). Mechanisms of Antimicrobial Resistance in ESKAPE Pathogens. In BioMed Research International. https://doi.org/10.1155/2016/2475067

SCCP (Scientific Committee on Consumer Products). (2011). Opinion on triclosan. European Commission.

Schembri, M., Ussery, D., Workman, C., Hasman, H., & Klemm, P. (2002). DNA microarray analysis of fim mutations in Escherichia coli. Molecular Genetics and Genomics. https://doi.org/10.1007/s00438-002-0705-2

Schneewind, O., & Missiakas, D. (2014). Lipoteichoic acids, phosphate-containing polymers in the envelope of gram-positive bacteria. In Journal of Bacteriology. https://doi.org/10.1128/JB.01155-13

Senning, Ä. (1983). Cardiac pacing in retrospect. The American Journal of Surgery. https://doi.org/10.1016/0002-9610(83)90130-7

Shepherd, A. J., Mackay, W. G., & Hagen, S. (2017). Washout policies in long-term indwelling urinary catheterisation in adults. In Cochrane Database of Systematic Reviews. https://doi.org/10.1002/14651858.CD004012.pub5

Shepherd, D. E. T. (2002). Risk analysis for a radio-carpal joint replacement. Proceedings of the Institution of Mechanical Engineers, Part H: Journal of Engineering in Medicine. https://doi.org/10.1243/0954411021536243

Shilling, M., Matt, L., Rubin, E., Visitacion, M. P., Haller, N. A., Grey, S. F., & Woolverton, C. J. (2013). Antimicrobial Effects of Virgin Coconut Oil and Its Medium-Chain Fatty Acids on Clostridium difficile. Journal of Medicinal Food. https://doi.org/10.1089/jmf.2012.0303

SHIMA, S., MATSUOKA, H., IWAMOTO, T., & SAKAI, H. (2012). Antimicrobial action of .EPSILON.-poly-L-lysine. The Journal of Antibiotics. https://doi.org/10.7164/antibiotics.37.1449

Shulong, L. (1999). Esterified triclosan derivatives as improved textile antimicrobial agents. https://patentimages.storage.googleapis.com/c1/d8/b7/e8827b4fccb2cf/US5968207.pdf

Sicard, C., Shek, N., White, D., Bowers, R. J., Brown, R. S., & Brennan, J. D. (2014). A rapid and sensitive fluorimetric β-galactosidase assay for coliform detection using chlorophenol red-β-d-galactopyranoside. Analytical and Bioanalytical Chemistry. https://doi.org/10.1007/s00216-014-7935-0

Singha, P., Locklin, J., & Handa, H. (2017). A review of the recent advances in antimicrobial coatings for urinary catheters. In Acta Biomaterialia (Vol. 50, pp. 20–40). https://doi.org/10.1016/j.actbio.2016.11.070

Skřivanová, E., Molatová, Z., Skřivanová, V., & Marounek, M. (2009). Inhibitory activity of rabbit milk and medium-chain fatty acids against enteropathogenic Escherichia coli O128. Veterinary Microbiology. https://doi.org/10.1016/j.vetmic.2008.09.083

Smith, D. R. M., Pouwels, K. B., Hopkins, S., Naylor, N. R., Smieszek, T., & Robotham, J. V. (2019). Epidemiology and health-economic burden of urinary-catheter-associated infection in English NHS hospitals: a probabilistic modelling study. Journal of Hospital Infection. https://doi.org/10.1016/j.jhin.2019.04.010

Song, P., Ma, Z., Ma, J., Yang, L., Wei, J., Zhao, Y., Zhang, M., Yang, F., & Wang, X. (2020). Recent progress of miniature MEMS pressure sensors. In Micromachines. https://doi.org/10.3390/mi11010056

Sosa Hernández, Ó., Matías Téllez, B., González Martínez, J., Juárez Vargas, R., Estrada Hernández, A., Sánchez Rivas, M. P., & Cureño Díaz, M. A. (2019). Healthcare-associated infections due to ESKAPE pathogens in a hospital of Mexico City 2013-2017. In Enfermedades Infecciosas y Microbiologia.

Soto, S. M. (2013). Role of efflux pumps in the antibiotic resistance of bacteria embedded in a biofilm. Virulence. https://doi.org/10.4161/viru.23724

Sperling, H., Eisenhardt, A., Mumperow, E., Gralla, O., Lümmen, G., Seidali, K., Hinke, A., & Jäger, T. (2014). Investigation of the use of triclosan in patients with indwelling catheters: A randomized, double blind, multicenter, placebo-controlled clinical study. Urologe. https://doi.org/10.1007/s00120-014-3642-x

Srinivasan, A., Karchmer, T., Richards, A., Song, X., & Perl, T. M. (2006). A Prospective Trial of a Novel, Silicone-Based, Silver-Coated Foley Catheter for the Prevention of Nosocomial Urinary Tract Infections. Infection Control & Hospital Epidemiology. https://doi.org/10.1086/499998

Steinbichler, G. (1987). INJECTION MOULDING OF LIQUID SILICON RUBBER. Kunststoffe - German Plastics.

Stickler, D. J., & Morgan, S. D. (2008). Observations on the development of the crystalline bacterial biofilms that encrust and block Foley catheters. Journal of Hospital Infection, 69(4), 350–360. https://doi.org/10.1016/j.jhin.2008.04.031

Stickler, D. J., Evans, A., Morris, N., & Hughes, G. (2002). Strategies for the control of catheter encrustation. International Journal of Antimicrobial Agents. https://doi.org/10.1016/S0924-8579(02)00091-2

Stickler, D. J., Jones, S. M., Adusei, G. O., & Waters, M. G. (2006). A sensor to detect the early stages in the development of crystalline Proteus mirabilis biofilm on indwelling bladder catheters. Journal of Clinical Microbiology, 44(4), 1540–1542. https://doi.org/10.1128/JCM.44.4.1540-1542.2006

Stickler, D., Ganderton, L., King, J., Nettleton, J., & Winters, C. (1993). Proteus mirabilis biofilms and the encrustation of urethral catheters. Urological Research, 21(6), 407–411. https://doi.org/10.1007/BF00300077

Stickler, David J. (2008). Bacterial biofilms in patients with indwelling urinary catheters. In Nature Clinical Practice Urology (Vol. 5, Issue 11, pp. 598–608). https://doi.org/10.1038/ncpuro1231

Stickler, David J., & Jones, G. L. (2008). Reduced susceptibility of Proteus mirabilis to triclosan. Antimicrobial Agents and Chemotherapy. https://doi.org/10.1128/AAC.01094-07

Stickler, David J., & Morgan, S. D. (2006). Modulation of crystalline Proteus mirabilis biofilm development on urinary catheters. Journal of Medical Microbiology. https://doi.org/10.1099/jmm.0.46404-0

Stickler, David J., Jones, S. M., Adusei, G. O., Waters, M. G., Cloete, J., Mathur, S., & Feneley, R. C. L. (2006). A clinical assessment of the performance of a sensor to detect crystalline biofilm formation on indwelling bladder catheters. BJU International. https://doi.org/10.1111/j.1464-410X.2006.06562.x

Stickler, David J., Morris, N. S., & Winters, C. (1999). Simple physical model to study formation and physiology of biofilms on urethral catheters. Methods in Enzymology. https://doi.org/10.1016/S0076-6879(99)10037-5

Suller, M. T. E. (2000). Triclosan and antibiotic resistance in Staphylococcus aureus. Journal of Antimicrobial Chemotherapy, 46(1), 11–18. https://doi.org/10.1093/jac/46.1.11

Surender, E. M., Bradberry, S. J., Bright, S. A., McCoy, C. P., Clive Williams, D., & Gunnlaugsson, T. (2017). Luminescent lanthanide cyclen-based enzymatic assay capable of diagnosing the onset of catheter-associated urinary tract infections both in solution and within polymeric hydrogels. Journal of the American Chemical Society. https://doi.org/10.1021/jacs.6b11077

Talja, M., Korpela, A., & Jarvi, K. (1990). Comparison of urethral reaction to full silicone, hydrogen-coated and siliconised latex catheters. British Journal of Urology.

Tambyah, P. A., Halvorson, K. T., & Maki, D. G. (1999). A prospective study of pathogenesis of catheter-associated urinary tract infections. Mayo Clinic Proceedings. https://doi.org/10.4065/74.2.131

Tenke, P., Riedl, C. R., Jones, G. L., Williams, G. J., Stickler, D., & Nagy, E. (2004). Bacterial biofilm formation on urologic devices and heparin coating as

preventive strategy. International Journal of Antimicrobial Agents. https://doi.org/10.1016/j.ijantimicag.2003.12.007

Thomas, J., Linton, S., Corum, L., Slone, W., Okel, T., & Percival, S. L. (2012). The effect of pH and bacterial phenotypic state on antibiotic efficacy. International Wound Journal. https://doi.org/10.1111/j.1742-481X.2011.00902.x

Thomas, X. (2003). Silicone Adhesives in Healthcare Applications. Dow Corning Corporation.

Thompson, J. S., Hodge, D. S., & Borczyk, A. A. (1990). Rapid biochemical test to identify verocytotoxin-positive strains of Escherichia coli serotype O157. Journal of Clinical Microbiology. https://doi.org/10.1128/jcm.28.10.2165-2168.1990

Timmermans, A. J., Harmsen, H. J. M., Bus-Spoor, C., Buijssen, K. J. D. A., Van As-Brooks, C., De Goffau, M. C., Tonk, R. H., Van Den Brekel, M. W. M., Hilgers, F. J. M., & Van Der Laan, B. F. A. M. (2016). Biofilm formation on the Provox ActiValve: Composition and ingrowth analyzed by Illumina paired-end RNA sequencing, fluorescence in situ hybridization, and confocal laser scanning microscopy. Head and Neck. https://doi.org/10.1002/hed.24014

Tiwari, A. A., & Ghnawate, N. (2017). Detection of Biofilm Forming Bacterial Communities from Urinary Catheter of Patients with Change in Its Antibiotic Susceptibility Pattern and Triclosan Effect from Different Hospitals of Amravati City Maharashtra, India. Open Journal of Medical Microbiology. https://doi.org/10.4236/ojmm.2017.73005

Toh, H. W., Toong, D. W. Y., Ng, J. C. K., Ow, V., Lu, S., Tan, L. P., Wong, P. E. H., Venkatraman, S., Huang, Y., & Ang, H. Y. (2021). Polymer blends and polymer composites for cardiovascular implants. In European Polymer Journal. https://doi.org/10.1016/j.eurpolymj.2020.110249

Townsend, E. M., Moat, J., & Jameson, E. (2020). CAUTI's next top model – Model dependent Klebsiella biofilm inhibition by bacteriophages and antimicrobials. Biofilm. https://doi.org/10.1016/j.bioflm.2020.100038

Trautner, B. W., & Darouiche, R. O. (2004). Role of biofilm in catheter-associated urinary tract infection. In American Journal of Infection Control. https://doi.org/10.1016/j.ajic.2003.08.005

Tsuchiya, H., & Iinuma, M. (2000). Reduction of membrane fluidity by antibacterial sophoraflavanone G isolated from Sophora exigua. Phytomedicine. https://doi.org/10.1016/S0944-7113(00)80089-6

van Hemel, N. M., & van der Wall, E. E. (2008). 8 October 1958, D Day for the implantable pacemaker. Netherlands Heart Journal. https://doi.org/10.1007/bf03086195

Van Houdt, R., & Michiels, C. W. (2005). Role of bacterial cell surface structures in Escherichia coli biofilm formation. In Research in Microbiology (Vol. 156, Issues 5–6, pp. 626–633). https://doi.org/10.1016/j.resmic.2005.02.005

Vardaka, V. D., Yehia, H. M., & Savvaidis, I. N. (2016). Effects of Citrox and chitosan on the survival of Escherichia coli O157: H7 and Salmonella enterica in vacuum-packaged turkey meat. Food Microbiology. https://doi.org/10.1016/j.fm.2016.04.003

Vargas-Cruz, N., Rosenblatt, J., Reitzel, R. A., Chaftari, A. M., Hachem, R., & Raad, I. (2019). Pilot Ex Vivo and in Vitro Evaluation of a Novel Foley Catheter

with Antimicrobial Periurethral Irrigation for Prevention of Extraluminal Biofilm Colonization Leading to Catheter-Associated Urinary Tract Infections (CAUTIs). BioMed Research International. https://doi.org/10.1155/2019/2869039

Vasudevan, R. (2014). Biofilms: Microbial Cities of Scientific Significance. Journal of Microbiology & Experimentation. https://doi.org/10.15406/jmen.2014.01.00014

Veerachamy, S., Yarlagadda, T., Manivasagam, G., & Yarlagadda, P. K. (2014). Bacterial adherence and biofilm formation on medical implants: A review. In Proceedings of the Institution of Mechanical Engineers, Part H: Journal of Engineering in Medicine (Vol. 228, Issue 10, pp. 1083–1099). https://doi.org/10.1177/0954411914556137

Verleyen, P., De Ridder, D., Van Poppel, H., & Baert, L. (1999). Clinical application of the Bardex IC foley catheter. European Urology. https://doi.org/10.1159/000068005

Verleyen, P., De Ridder, D., Van Poppel, H., & Baert, L. (1999). Clinical application of the Bardex IC foley catheter. European Urology. https://doi.org/10.1159/000068005

Villari, P., Iannuzzo, M., & Torre, I. (1997). An evaluation of the use of 4-methylumbelliferyl-β-D-glucuronide (MUG) in different solid media for the detection and enumeration of Escherichia coli in foods. Letters in Applied Microbiology, 24(4). https://doi.org/10.1046/j.1472-765X.1997.00076.x

Wagers, P. O., Shelton, K. L., Panzner, M. J., Tessier, C. A., & Youngs, W. J. (2014). Synthesis and Medicinal Properties of Silver-NHC Complexes and Imidazolium Salts. In N-Heterocyclic Carbenes: Effective Tools for Organometallic Synthesis. https://doi.org/10.1002/9783527671229.ch06

Wang, F., Li, X., Wang, X., & Jiang, X. (2020). Efficacy of topical silicone gel in scar management: A systematic review and meta-analysis of randomised controlled trials. International Wound Journal. https://doi.org/10.1111/iwj.13337

Wang, G., Li, A., Zhao, W., Xu, Z., Ma, Y., Zhang, F., Zhang, Y., Zhou, J., & He, Q. (2021). A Review on Fabrication Methods and Research Progress of Superhydrophobic Silicone Rubber Materials. In Advanced Materials Interfaces. https://doi.org/10.1002/admi.202001460

Wang, T., Flint, S., & Palmer, J. (2019). Magnesium and calcium ions: roles in bacterial cell attachment and biofilm structure maturation. Biofouling. https://doi.org/10.1080/08927014.2019.1674811

Wang, Y., Lee, S. M., & Dykes, G. (2015). The physicochemical process of bacterial attachment to abiotic surfaces: Challenges for mechanistic studies, predictability and the development of control strategies. In Critical Reviews in Microbiology. https://doi.org/10.3109/1040841X.2013.866072

Warren, J. W., Tenney, J. H., Hoopes, J. M., Muncie, H. L., & Anthony, W. C. (1982). A prospective microbiologic study of bacteriuria in patients with chronic indwelling urethral catheters. Journal of Infectious Diseases, 146(6), 719–723. https://doi.org/10.1093/infdis/146.6.719

Whitchurch, C. B., Tolker-Nielsen, T., Ragas, P. C., & Mattick, J. S. (2002). Extracellular DNA required for bacterial biofilm formation. Science. https://doi.org/10.1126/science.295.5559.1487

White, R. L. (2001). What in vitro models of infection can and cannot do. Pharmacotherapy. https://doi.org/10.1592/phco.21.18.292s.33906

WHO. (2020). Global Antimicrobial Resistance and Use Surveillance System (GLASS) Report. Who.

Williams, G. J., & Stickler, D. J. (2007). Some Observations on the Diffusion of Antimicrobial Agents Through the Retention Balloons of Foley Catheters. Journal of Urology, 178(2), 697–701. https://doi.org/10.1016/j.juro.2007.03.091

Wilson, M. L., & Gaido, L. (2004). Laboratory diagnosis of urinary tract infections in adult patients. In Clinical Infectious Diseases. https://doi.org/10.1086/383029

World Health Organization (WHO). (2016). WHO | Antimicrobial resistance: global report on surveillance 2014. Antimicrobial Resistance: Global Report on Surveillance 2014.

Wright, B. D., Shah, P. N., McDonald, L. J., Shaeffer, M. L., Wagers, P. O., Panzner, M. J., Smolen, J., Tagaev, J., Tessier, C. A., Cannon, C. L., & Youngs, W. J. (2012). Synthesis, characterization, and antimicrobial activity of silver carbene complexes derived from 4,5,6,7-tetrachlorobenzimidazole against antibiotic resistant bacteria. Dalton Transactions. https://doi.org/10.1039/c2dt00055e

Wutor, V. C., Togo, C. A., & Pletschke, B. I. (2007). The effect of physico-chemical parameters and chemical compounds on the activity of β-d-galactosidase (B-GAL), a marker enzyme for indicator microorganisms in water. Chemosphere. https://doi.org/10.1016/j.chemosphere.2007.02.050

Wutor, V. C., Togo, C. A., Limson, J. L., & Pletschke, B. I. (2007). A novel biosensor for the detection and monitoring of β-d-galactosidase of faecal origin in water. Enzyme and Microbial Technology. https://doi.org/10.1016/j.enzmictec.2006.10.039

Xin, H., Chen, J., Li, T., Hu, G., Fang, Z., Zhou, H., Guo, K., Wang, L., & Wang, Y. (2021). One-step preparation of the engineered titanium implant by rationally designed linear fusion peptides with spacer-dependent antimicrobial, anti-inflammatory and osteogenic activities. Chemical Engineering Journal. https://doi.org/10.1016/j.cej.2021.130380

Yang, X., Sha, K., Xu, G., Tian, H., Wang, X., Chen, S., Wang, Y., Li, J., Chen, J., & Huang, N. (2016). Subinhibitory concentrations of allicin decrease uropathogenic escherichia coli (UPEC) biofilm formation, adhesion ability, and swimming motility. International Journal of Molecular Sciences. https://doi.org/10.3390/ijms17070979

Yehia, H. M., Elkhadragy, M. F., Al-Masoud, A. H., & Al-Megrin, W. A. (2019). Citrox improves the quality and shelf life of chicken fillets packed under vacuum and protects against some foodborne pathogens. Animals. https://doi.org/10.3390/ani9121062

Yoda, R. (1998). Elastomers for biomedical applications. Journal of Biomaterials Science, Polymer Edition. https://doi.org/10.1163/156856298X00046

Young JC1, Kenyon EM, C. E. (n.d.). Inhibition of beta-glucuronidase in human urine by ascorbic acid (p. Hum Exp Toxicol. 19(3):165-7).

Youngs, W. J., Medvetz, D. A., Hindi, K. M., Panzner, M. J., Ditto, A. J., & Yun, Y. H. (2008). Anticancer activity of Ag(I) N-heterocyclic carbene complexes derived

from 4,5-dichloro-1H-imidazole. Metal-Based Drugs. https://doi.org/10.1155/2008/384010

Yu, B. J., Kim, J. A., Ju, H. M., Choi, S. K., Hwang, S. J., Park, S., Kim, E. J., & Pan, J. G. (2012). Genome-wide enrichment screening reveals multiple targets and resistance genes for triclosan in Escherichia coli. Journal of Microbiology. https://doi.org/10.1007/s12275-012-2439-0

Zare, M., Ghomi, E. R., Venkatraman, P. D., & Ramakrishna, S. (2021). Silicone-based biomaterials for biomedical applications: Antimicrobial strategies and 3D printing technologies. In Journal of Applied Polymer Science. https://doi.org/10.1002/app.50969

Zhu, L., Lin, J., Ma, J., Cronan, J. E., & Wang, H. (2010). Triclosan resistance of Pseudomonas aeruginosa PAO1 is due to FabV, a triclosan-resistant enoyl-acyl carrier protein reductase. Antimicrobial Agents and Chemotherapy. https://doi.org/10.1128/AAC.01152-09

Zuniga, J. M. (2018). 3D printed antibacterial prostheses. Applied Sciences (Switzerland). https://doi.org/10.3390/app8091651

Zuniga, J. M., & Cortes, A. (2020). The role of additive manufacturing and antimicrobial polymers in the COVID-19 pandemic. In Expert Review of Medical Devices. https://doi.org/10.1080/17434440.2020.1756771

# Appendix

Triclosan and triclosan acetate standards of known concentration were run on the HPLC instrument to enable a standard curve to be plotted. This curve was then used to calculate triclosan concentration from solutions where the concentrations of the compound were unknown.

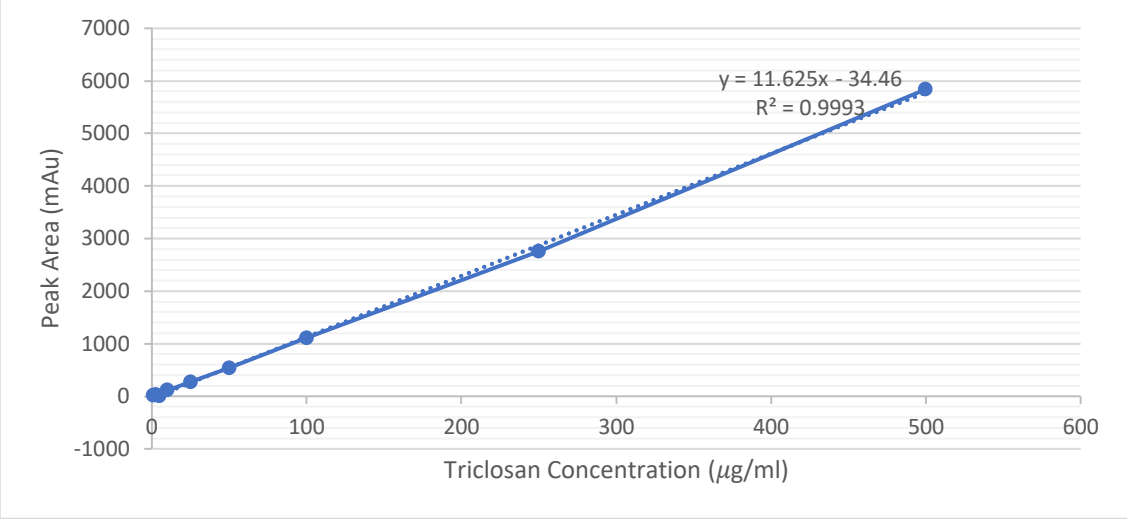


**Figure 1 Calibration curve of triclosan concentration against peak area.** Standard solutions of triclosan were analysed by HPLC. The regression line of peak area observed at 4.2 min for each concentration is plotted.

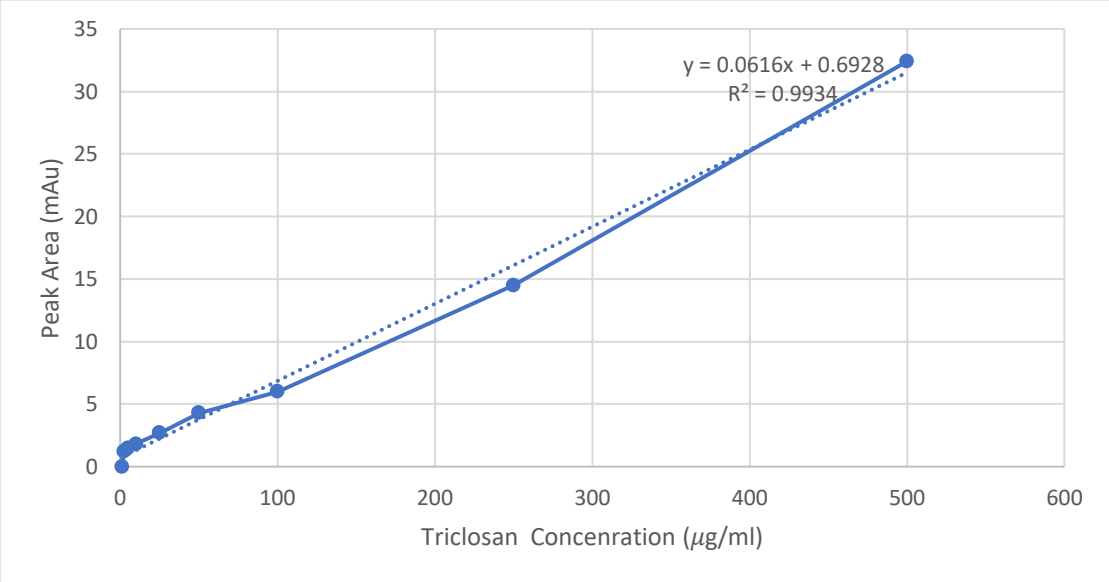


**Figure 2 Calibration curve of triclosan acetate concentration against peak area.** Standard solutions of triclosan were analysed by HPLC. The regression line of peak area observed at 6.3 min for each concentration is plotted.